THE INFLUENCE OF STATE ON THE CAPACITY OF DRIVEN PILES IN SANDS

by

ULRICH KLOTZ

A thesis submitted for the Degree of
Doctor of Philosophy

City University
Department of Civil Engineering

July 2000

CONTENTS

LIST OF TABLES

LIST OF FIGURES

ACKNOWLEDGEDMENTS

The three and a half years I spent at the Geotechnical Engineering Research Centre (GERC) at City University have been exciting, challenging and rewarding. I would like to take this opportunity to thank all the people who I had the pleasure of meeting or working with during this period.

First I would like to express my gratitude to my advisor Dr. Matthew Coop for his guidance, encouragement and support, especially for not asking too many embarrassing questions after yet another centrifuge had gone wrong and for not loosing faith in my ability to succeed.

I would also like to thank Prof. Neil Taylor for his support throughout but in particular during the development of the centrifuge equipment. Special thanks to Prof. John Atkinson for the discussions on soil mechanics, that helped me to understand some fundamental aspect of my project more clearly. Thanks also to Dr. Sarah Stallebrass for providing and maintaining the computer facilities necessary to process the test data and finally to write this thesis.

The Dogs Bay sand used for this study was kindly supplied by Prof. Guy Houlsby from Oxford University and I am grateful for his support. I would also like to thank Dr. Jamie Standing from Cambridge University for sharing his expertise on instrumentation during the development of the instrumented model pile. I also need to thank Mr. Roy Vipond from the Department of Mechanical Engineering at City University, for the support during the interface roughness measurements.

The work described in this thesis would not have been possible without the skills and commitment of the technical staff at the GERC. I would like to thank Mr. Keith Osborne for helping to convert my sometimes obscure ideas into reality especially during the development of the instrumented model pile. Thanks also to Mr. Reg Allen, who skilfully transferred the drawings which were kindly prepared by Mr. Carl Lodge into such a pretty pile driving actuator. Special thanks to Mr. Lloyd Martyka for his commitment to finding and removing all sorts of electrical problems from the centrifuge and triaxial equipment.

The research was funded for three years by the EPSRC and in the closing stages by the GERC and by the Gottlieb Daimler and Carl Benz Stiftung through a maintenance grant. I gratefully acknowledge their support.

Thanks are also due to all the people that were part of the Group during my stay especially Ms. Chiara Martinelli, Mr. Andrea Cavalieri and Mr. Simon Coffey who conducted tests related to this project with dedication and enthusiasm. I would also like to thank all other present and past members of the group as well as the numerous visitors for the time spent together inside and outside the University. Special thanks go to Ms. Claudia Albert and Ms. Alessandra Nocilla, who managed to change many things in my life.

Last not least I would like to thank my family and my friends outside the GERC especially Natascha, Vojkan, Gabi, and Christoph for their encouragement, support and for successfully managing to distract my thoughts from geotechnical research.

DECLARATION

I grant powers of discretion to the University Librarian to allow this thesis to be copied in whole or in part without further reference to me. This permission covers only single copies made for study purposes, subjected to normal conditions of acknowledgement.

ABSTRACT

The prime objective of the thesis was to study the influence of state on the capacity of driven piles in sand. The work was prompted by findings of recent laboratory based research on the mechanics of granular soils (Coop & Lee, 1993 and Jovicic & Coop, 1997) which showed that, as for clays, a principal controlling factor of soil behaviour is the stress-volume state. The work started in November 1996 and was funded buy the EPSRC under contract GR/L16590.

Centrifuge testing was used to investigate the behaviour of driven piles in sands. A new actuator and strongbox package were designed and constructed taking full advantage of the centrifuge facilities. A fully instrumented model pile was developed, which consisted of eleven segments and allowed five independent measurements of shaft friction, four of radial stress and one of end bearing to be taken during installation. The pile was jacked into samples of two sands of varying densities at accelerations of between 50-200g, simulating piles of up to 70 m in length and 3.2 m in diameter.

The two sands used in the investigation were a carbonate sand and a quartz sand, chosen for the diversity of their geological origins and behaviour. A series of triaxial tests was conducted in order to characterise the behaviour of each sand, and in particular to locate precisely their critical state lines in stress-volume space.

The centrifuge model tests showed that neither the end bearing nor the shaft friction could be adequately predicted using methods based on relative density of the sand such as API-RP2A (1993), but that the controlling factor for both was the state of the soil relative to the location of the critical state line, which should be quantified not only by the density of the soil, but also the effective stress level. The radial stress was found to be highest approximately seven pile diameters above the pile tip and not at the pile tip as assumed in recent design methods (e.g. Randolph et al., 1994 and Jardine & Chow, 1996). The friction angles mobilised on the model pile were found to be significantly lower than those that were measured by means of interface shear box tests, and it was found that the correct friction angle could only be measured by interface ring shear tests taken to very large displacements.

An examination of the literature showed clearly that available field data support the new framework, although the data were both very scattered and very limited in extent, particularly because even the most extensive field tests rarely included even the basic laboratory tests required to apply the new method of analysis.

The work therefore highlights severe limitations with many current pile design methods for piles in sands and suggests how new methods should be based on correct quantification of state.

NOMENCLATURE

SYMBOLS

Note: all symbols shown appear in Italic in the text of the thesis and in all the equations.

General Symbols

A	area
D	diameter
F	force
g	gravitational acceleration
H	height
m	mass
V	volume
x, y, z	co-ordinates
Δ	small change of any parameter
ε	strain
ρ	density
σ	stress

Symbols related to Soil Mechanics

B_p	breakage potential
B_r	relative breakage
B_t	total breakage
c'	cohesion
D_{50}	average particle size
ΔP	pressure difference of plate dilatometer (Konrad, 1988)
D_r	relative density
e	current void ratio
E	Young's modulus
e_c	void ratio at critical state (Gudehus, 1996)
e_{c0}	void ratio at critical state at zero pressure (Gudehus, 1996)
e_d	void ratio in densest possible state (Gudehus, 1996)
e_{d0}	minimum void ratio at zero pressure (Gudehus, 1996)
e_i	void ratio on the NCL (Gudehus, 1996)
e_{i0}	maximum void ratio at zero pressure (Gudehus, 1996)
e_λ	void ratio of soil in situ projected to p'=1.0 kPa
e_{max}	maximum void ratio
e_{min}	minimum void ratio
e_o	initial void ratio
e_{ss}	void ratio at steady state (after Been & Jefferies, 1985)
G	tangent shear modulus
G_{max}	tangent shear modulus at very small strains ($G_{max} = G_o$)
G_o	elastic shear modulus at very small strains ($G_o = G_{max}$)
$G_{o(nc)}$	shear modulus at very small strains sands on the NCL
h_s	granular hardness (Gudehus, 1996)
I_1	mean effective stress (Konrad, 1988)
I_D	density index equal to relative density in BS 1377
I_R	corrected relative density (Bolton, 1986)

K	earth pressure coefficient
K_{nco}	earth pressure coefficient at rest for normally consolidated soil
K_o	earth pressure coefficient at rest
M	gradient of critical state line in q:p' space
N	specific volume intercept of NCL at p'=1.0 kPa
n	exponent for hypoplastic model (Gudehus, 1996)
p	mean total stress
p'	mean effective stress
p'_{cs}	mean effective stress defined on CSL
p'_e	equivalent mean effective stress defined on NCL
p'_p	mean effective stress at intersection of swelling line and NCL ($p'_p = p'_\gamma$)
p'_s	mean intergranular pressure (after Gudehus, 1996)
p_a	atmospheric pressure
p_{lim}	limit pressure from cavity expansion theory
q	deviatoric stress (total stress is equal to effective stress)
R_s	stress ratio in v:lnp'- plane
v	specific volume
v_{cs}	specific volume at critical state
v_κ	specific volume of overconsolidated soil projected to p'=1.0 kPa
v_λ	specific volume of soil in situ projected to p'=1.0 kPa
α	angle of wedge failure during cavity expansion (Randolph et al., 1994)
δ	interface angle of friction
δ_{cs}	interface angle of friction at critical state
ϕ'	angle of friction
ϕ'_{cs}	angle of friction at critical state
ϕ'_{max}	maximum angle of friction (peak angle of friction)
Γ	specific volume intercept of CSL at p'=1.0 kPa
κ	slope of swelling line
λ	slope of isotropic normal compression line and critical state line in the v:lnp' plane
ν	Poisson's ratio
σ'_a	axial effective stress
σ'_r	radial effective stress
ψ	state parameter in terms of volume (Konrad 1988)
ψ_A	state parameter in terms of volume (Been & Jefferies, 1985)
ψ_I	Paramter e_{max}-e_{min} to normalise the state parameter (Konrad 1988)
ψ_N	normalised state parameter (Konrad, 1988)

Symbols related to Piles

a, b	parameters to adjust S_t (Randolph et al., 1994)
A,B,C	constants in MTD pile design method
A_b	area of pile base
A_β	value of β for stress ratio R_s equal to one
A_{Nq}	value of Nq for stress ratio R_s equal to one
A_s	area of pile shaft
$_{av}q_s$	average unit shaft resistance of a pile
d_{CPT}	cone diameter of CPT
d_p	pile diameter
dz	relative pile head movement
E_p	Young's modulus of a solid pile
G_{av}	average shear modulus (de Nicola & Randolph, 1993)

G_{op}	operational shear modulus (MTD pile design method)
h	distance between a transducer and the pile tip (MTD pile design method)
I_r	rigidity index (Vesic, 1977)
L	length of burial of a pile
L_{act}	active length of the transducer on the model pile
L_{av}	length for averaging the transducer reading on the model pile
L_p	pile length
m_β	gradient in $\ln\beta$:$\ln R_s$ pile design chart
m_{Nq}	gradient in $\ln N_q$:$\ln R_s$ pile design chart
N_q	bearing capacity factor
p'_o	mean effective stress in the ground before installation of the pile
q_b	unit base resistance of a pile
Q_b	ultimate base capacity of a pile
$q_{b(z)}$	unit base resistance of a pile at depth, z
q_c	cone resistance of CPT
$\bar{q}_c$	average cone resistance in CPT
q_s	unit shaft resistance of a pile
$\bar{q}_s$	average global unit shaft resistance of a pile
Q_s	ultimate shaft capacity of a pile
$\bar{q}_{s-loc}$	average local unit shaft resistance on the model pile
$q_{s(z)}$	shaft resistance of a pile at depth, z
$q_{s,tip}$	local shaft friction at the pile tip
$q_{s\text{-}loc}$	local unit shaft resistance on the model pile
Q_u	ultimate pile capacity
R	pile radius
S_t	ratio of the radial effective stress acting in the vicinity of the pile tip at shaft frictional failure to the end bearing capacity (Randolph et al., 1994)
V_k	correction factor (Kraft, 1990)
z	depth of interest along the embedded length of the pile
β	unit shaft friction normalised with vertical effective stress ($\beta = K\tan\delta$)
βmax	maximum value of β
βmin	minimum value of β
Δ	volume change parameter (Vesic, 1977)
δ_f	interface angle of friction at failure (MTD-Method)
δh	radial movement of the soil (MTD-Method)
$\Delta\sigma'_{rd}$	change in radial effective stress during loading
η	normalised cone resistance in (MTD-Method)
η_p	pile compressibility (de Nicola & Randolph, 19993)
μ	parameter to adjust rate of exponential decay of shaft friction (Randolph et al., 1994)
ν_p	Poisson's ratio of the pile
σ'_{re}	equalised radial effective stress (MTD-Method)
$\bar{\sigma}_{r-loc}$	average radial total stress on the model pile
σ'_{rf}	radial effective stress at shaft friction failure (MTD-Method)
σ'_v	vertical effective stress
σ'_{vo}	initial vertical effective stress before installation of the pile

Symbols related to Laboratory Testing

A_c	current cross sectional area of triaxial sample
A_o	initial cross sectional area of triaxial sample
D_o	initial sample diameter of a triaxial sample

d_o	initial sample diameter of the membrane
E_m	Young's modulus of membrane
G_s	specific gravity
L_e	evaluation length
L_o	initial length of a triaxial sample
p'	mean effective stress
q	deviatoric stress
R_a	roughness average
R_{max}	maximum peak to valley height within the sampling length
R_n	normalised roughness
R_{na}	normalised roughness average
R_p	peak height
R_{st}	radius of stylus
R_t	maximum peak to valley height within the evaluation length
R_v	valley height
t_o	initial thickness of the membrane
u	pore pressure
U_c	uniformity coefficient
v	(current) specific volume
v_i	initial specific volume
V_s	volume of solids
V_t	total volume
w	water content
$_{av}\varepsilon_{a,loc}$	average local axial strain
ε_a	axial strain
$\varepsilon_{a,loc}$	local axial strain
ε_r	radial strain
$\varepsilon_{r,loc}$	local radial strain
ε_s	shear strain
ε_v	volumetric strain
ρ_d	dry density
ρ_{max}	maximum density
ρ_{min}	minimum density
ρ_s	particle density
σ'_3	principal effective stress equal to radial stress in triaxial compression test
σ'_{3corr}	correction due to membrane restraint applied to the radial stress in a triaxial test
σ'_a	axial effective stress
σ'_r	radial effective stress

Symbols related to Centrifuge Modelling

a	acceleration
a_c	Coriolis acceleration
CF_{cor}	corrected calibration factor
CF_{org}	original calibration factor
d_b	distance between pile tip and base of strongbox
d_{sw}	distance between the side wall of the strongbox and the centre of the pile
d_w	diameter of strongbox
G_f	gauge factor of a strain gauge
h_m	model height
h_p	prototype height

L_{SRT}	length of shaft resistance transducer on the instrumented model pile
m_z	reduction of specific volume over depth in centrifuge model
N	scale factor
N_a	number of active arms in a strain gauge circuit
r	radius (of the centrifuge)
R_e	radius at which the scaling factor is accurate
R_t	radius from the centre of the centrifuge to the top of the model
$SPAN_{SRT}$	difference in calibration factor between the less and more sensitive axis on the shaft resistance transducers on the instrumented model piles
v_i	initial specific volume
V_{in}	input voltage (strain gauge bridge circuit excitation voltage)
V_{out}	output voltage of a strain gauged transducer
v_z	specific volume at depth z in a prototype
z_m	depth of centrifuge model
z_p	equivalent prototype depth to the depth in centrifuge model
σ'_{vm}	vertical effective stress in the centrifuge model
σ'_{vp}	vertical effective stress in a prototype structure
v_c	velocity of the particles in the radial direction
ω	radial acceleration

ABREVIATIONS

API	American Petroleum Institute
ASTM	American Society for Testing Materials
BFT	Base Force Transducer
BRE	Building Research Establishment
BS	British Standard
CPT	Cone Penetration Test
CSL	Critical State Line
CUIMP	City University Instrumented Model Pile
DBS	Dogs Bay Sand
DIN	Deutsches Institut für Normungswesen (German Standard Institution)
DMT	Flat Plate Dilatometer
GERC	Geotechnical Engineering Research Centre at City University
IC	Imperial College of Science and Technology, London
LBS	Leighton Buzzard Sand
LVDT	Linear Variable Differential Transformer
MTD	Marine Technology Directorate
NCL	Isotropic (Normal) Compression Line
OCR	Overconsolidation Ratio
PCD	Pitch Cylinder Diameter
PPT	Pore Pressure Transducer
QSS	Quasi Steady State
RST	Radial Stress Transducer
SPT	Standard Penetration Test
SRT	Shaft Resistance Transducer

1. Introduction

1.1 Background

Piles have been used to provide foundations for a variety of structures since the very beginning of civilisation. For example the earliest piles discovered in Europe were constructed almost 4000 years ago. The process of pile design up to the 20th century remained empirical relying mainly on correlations with the observed resistance during pile installation. As a consequence the understanding of the fundamental mechanisms governing the capacity of piles remained poor. This was documented by Terzaghi (1930) who pointed out that neither the term "pile capacity" was properly defined nor the basic concepts of pile-soil interaction or load transfer behaviour were well understood. This lack of understanding caused frequent foundation problems and in a number of cases piles were used in ground conditions that perhaps did not require piles at all.

The development of the first theories to determine the capacity of piles prior to construction, using the results of laboratory tests or in situ soil data started in the 1950s. At first, existing bearing capacity equations for shallow foundations were extended to the deep foundation problem. Later, procedures using cavity expansion theories were introduced. With the further development of in situ testing techniques new methods for estimating pile capacities directly from the results of in situ tests evolved. By the mid 1970s a variety of different methods were available that had in common the underlying assumption that it is the relative density that governs the behaviour of piles in sand. Most procedures were empirical or semi-empirical and relied heavily on the experience of the geotechnical engineer involved.

The onset of the offshore oil production required high capacity piles to provide adequate foundations for the oil platforms. It became apparent that the extrapolation of existing pile capacity equations developed primarily from pile tests on short piles on-shore to the very different off-shore conditions was inadequate (Williams et al., 1997). Additionally, sands of different mineralogy such as carbonate sands were encountered leading to even more uncertainty in using the existing methods that were developed and verified based exclusively on pile tests in silica sands. Consequently Randolph et al. (1994), identified driven piles in sand as being the "area of greatest uncertainty in foundation design" and also that current design methods such as API RP-2A (1993) were "not consistent with the processes that govern capacity".

Recent laboratory investigations into the fundamental mechanics of granular materials carried out at City University (Coop & Lee, 1993, Jovicic & Coop, 1997) have shown that, as for clay

soils, the stress-volume state is the key factor controlling the soil behaviour and expected to equally control the behaviour of engineering structures and in situ tests. The approach has been used to a limited extend for the interpretation of in situ tests such as the CPT (Been & Jefferies, 1985; Konrad, 1998) and the plate dilatometer (Konrad, 1988) with state being quantified by a state parameter. However only a few attempts have been made to utilise state in the analysis of engineering problems. Instead, recent in situ pile research and design methods have only considered the relative density of the soil which is not a true measure of soil state. The lack of appreciation of the potential importance of state has meant that many field tests have been carried out to too shallow depths, so that it is doubtful whether the data are relevant to full scale piles.

1.2 Objectives

The main objective of the current research was therefore to extend the concept of soil state to the analysis of driven piles in sand. Sands of different mineralogy and from a variety of geological origins were used so that a general framework could be established. The importance of the stress state was investigated by conducting tests on a fully instrumented model pile in a geotechnical centrifuge measuring the base resistance, the local shaft resistance as well as the radial stress during pile installation. The centrifuge test data were interpreted with the aid of the results of laboratory element tests. Currently available pile design methods were critically reviewed and the existing data of full scale pile tests will be reinterpreted based on the findings of this research with the aim of establishing a new unifying framework of analysis for driven piles based on state which is applicable to all types of sand.

1.3 Outline of Thesis

This thesis is divided into six chapters that cover different aspects related to the capacity of driven piles in sand. Following this introduction (Chapter 1) the thesis proceeds with Chapter 2 which contains the literature review including literature on the mechanics of granular materials, the application of the state parameter concept to interpret in situ tests, as well as currently available pile design methods. Particular emphasis is given to the techniques that have been developed to identify critical states in the triaxial apparatus.

Chapter 3 covers the laboratory tests carried out to characterise the soils used. First the two sands selected for the research are described. This is followed by a discussion of the equipment used for and results of interface roughness measurements and tests conducted in the direct shear box to study the pile-soil interface behaviour. Finally, details are given of the modifications to

the existing triaxial testing equipment as well as the test procedures adopted. The test results of the triaxial tests are discussed with particular emphasis on identifying the critical state lines of the soil in stress-volume space. The critical state lines identified for both sands form the basis for the normalisation of the centrifuge test data described in Chapter 5.

Chapter 4 on centrifuge modelling starts with a brief outline of basic centrifuge testing techniques and the centrifuge facilities at City University. This is followed by a detailed description of the development and construction of the new equipment needed for the tests to be undertaken for the current research which included a new pile driving actuator and strongbox assembly as well as a fully instrumented model pile. A full account is given of the procedures developed to calibrate the transducers, prepare the samples and conduct the experiments. Finally, the testing programme and configuration of each centrifuge test are described in detail.

In Chapter 5 the results of the centrifuge model tests are presented and discussed. First the procedures are described which were developed to arrive from typical raw data to the final fully corrected and reduced data set. This is followed by sections on the pile behaviour observed during installation and the results of the pile load tests. In addition the effects of creep and particle breakage on pile capacity were investigated and the procedures adopted are described as well as the test results. The final main part of the chapter examines the effect of state on pile capacity by normalising the centrifuge test data with respect to the critical state lines for the sand determined in Chapter 3.

Finally, in Chapter 6 the work undertaken and the results obtained during this project are summarised, the limitations of the investigations are highlighted and recommendations were given as to how further work could enhance the findings presented in this thesis. The thesis closes with some concluding remarks on the implications of the findings of this research for pile design in the future.

2. Literature Review

2.1 Introduction

The literature review will focus on the behaviour of sands and the axial capacity of driven piles in sands. At the beginning the literature on the mechanics of coarse grained soils is reviewed. Particular attention is given to the published work on the large strain behaviour and the position and shape of the critical state line. The second section covers the literature on theories of pile-soil interaction that have led to the static pile capacity formulae currently available. The review includes published material on model tests as well as full scale field tests.

2.2 The Mechanics of Coarse Grained Soils

2.2.1 Introduction

Early work investigating the behaviour of coarse grained soils focused primarily on the strength properties and the behaviour of siliceous sands at large strains (e.g. Bishop & Green, 1965). More recently, improvements of the infrastructure in urban areas, which prompted the construction of deep excavations and tunnels adjacent to or underneath existing buildings, required a better understanding of the behaviour of coarse grained soils at small strains (e.g. Scholey et al., 1995). With the onset of the off-shore oil production an increasing demand for a better understanding of the soil behaviour of carbonate sands evolved (e.g. Golightly & Hyde, 1988). In the Pacific regions of Southern China, Korea and Japan decomposed granite soils are frequently encountered during construction and problems associated with these soils prompted further research (e.g. Nishida, 1990).

Most work has focused on the behaviour of only one particular type of material, typically silica sand. Very few attempts have been made towards establishing a general framework for a greater variety of granular materials considering features such as stress-strain behaviour, stiffness, particle rearrangement and particle crushing. Gudehus (1996) proposed a hypoplasticity model for granular materials such as silica sand, flour, sugar and wheat on the assumption that the particles do not crush during shearing, while Coop & Lee (1993) and Jovicic & Coop (1997) showed that, as for clays, the behaviour of sands of different mineralogies can be described within the framework of critical state soil mechanics despite the particle crushing that dominates their behaviour.

McDowell & Bolton (1998) proposed a framework for crushable aggregates based on micromechanical considerations. They showed that the tensile strength of the soil grains satisfies the Weibull statistics originally developed to characterise brittle ceramics. They concluded that it is the tensile strength of the smallest particle that determines the current yield stress of the aggregate.

As a starting point of the literature review the work of Coop & Lee (1993) will briefly be reviewed. Their observations will then be compared with the work of other researchers.

2.2.2 Introduction to Critical State Soil Mechanics

Soil behaviour will be examined in the following chapters within the framework of critical state soil mechanics as defined by Schofield & Wroth (1968). As this framework has been widely used in the past and is sufficiently documented in the literature only the most fundamental aspects of the framework will be defined here. The definition of the basic parameters in stress-volume space is illustrated in Figure 2-1. The normal compression line (NCL) is the boundary for all possible states and is reached under an isotropic stress condition. The critical state line (CLS) is reached after shearing the soil to large strains (see Section 2.2.6). Both lines are unique reference states for any reconstituted and non-cemented soil.

2.2.3 General Stress-Strain Behaviour of Coarse Grained Soils

The programme of research carried out at City University between 1990 and 1997 focused on three sands of different geological origins, which were tested in the triaxial apparatus over a wide range of pressures, with the aim to establish a general framework of their mechanical behaviour. The soils tested were a carbonate sand from Dogs Bay on the west coast of Ireland, Ham River sand which is a silica sand, and a decomposed granite from Korea. Full details of the soils are given in Coop & Lee (1993).

A number of common features were observed while testing these soils. The behaviour was found to be essentially plastic for initial isotropic loading and shearing while the soil response was much stiffer in unload-reload than during first loading. Both the current density and current stress state were identified as the controlling influences on the behaviour. Finally, particle breakage was shown to be a function of mineralogy.

The macroscopic behaviour observed for these coarse grained soils exhibits many features in common with the behaviour of fine grained soils. However, in spite of their similar macroscopic

behaviour the microscopic mechanisms that govern the stress-strain response of coarse and fine grained soils are quite different. It is generally accepted that main mechanism of plastic deformation for fine grained soils is particle rearrangement, while for coarse grained soils in addition to particle rearrangement the mechanism of particle breakage is of fundamental importance.

2.2.4 Particle Breakage

Hardin (1985) suggested to quantify the amount of particle breakage by the term relative breakage, B_r, which is a measurement of the change in the location of the gradings curve, the definition of which is illustrated in Figure 2-2. He observed that the amount of particle breakage in a coarse grained soil is a function of the initial particle size distribution, particle shape, particle hardness, soil confinement, state of stress and the presence or absence of water.

At the macroscopic scale the soil behaviour is governed by the average effective stresses transferred through the soil skeleton, whereas on the microscopic scale it is the number of particle contacts of each individual particle that determines the magnitude of the contact stresses that govern breakage. The number of particle contacts depends in turn on the particle size and the particle size distribution. The size of particles and the presence of fines in the soil matrix also effects the initial density and therefore the extent of particle breakage. Both the NCL and CSL are only unique for one particular initial grading. Therefore, if a sample is taken out of the apparatus following a test in which there has been significant breakage, reconstituted to the same initial density and reloaded, the position of the NCL and CSL will change (Coop & Atkinson, 1992).

Coop & Lee (1993), showed that the onset of particle breakage at a given stress level is a function of the strength of the particles or, in other words, their mineralogy. This is illustrated in Figure 2-3, where the relatively hard quartz particles of Ham River sand start to show signs of breakage at a stress level of about 1 MPa, whereas for the biogenetic Dogs Bay sand only about 100 kPa is required.

The presence or absence of water may also effect the extent of particle breakage. Coop & Lee (1994) found that the positions of the state boundary surfaces of dry Dogs Bay sand and dry decomposed granite were different from their positions in saturated conditions, while the friction angle remained unchanged. They attributed this effect to an increase in particle strength due to intra-particle suction in the dry condition resulting in a decrease of particle breakage and therefore a reduction in volumetric compression during either isotropic loading or shearing.

The phenomenon of particle breakage and its effect on the compressibility of crushable aggregates was studied by McDowell & Bolton (1998). They proposed a micromechanical framework based on the tensile strength of the particles and found that the successive fracturing of the smallest particles under increasing macroscopic stress defines the current yield stress of the aggregate.

The effect of particle breakage on the validity of conventional soil models has been addressed by Hettler & Vardoulakis (1984). They pointed out that a rigid-granular model is not valid for the analysis of problems involving pressures beyond the limiting intergranular pressure, where grain crushing rather than particle re-arrangement becomes the dominant mechanism. The soil models developed subsequently by Chandler (1985) and Baharom & Stallebrass (1998) distinguish between these two mechanisms and are able to capture the main features of soil behaviour observed experimentally, for example by Coop & Lee (1993).

2.2.5 Behaviour in Isotropic and One-dimensional Compression

Isotropic compression data for the three soils are given in Figure 2-4. The samples were created with a variety of different initial densities. Regardless of the initial density all samples converged towards a unique line, the normal compression line (NCL). The normal compression line may be characterised by :

$$v = N - \lambda \ln p' \tag{2.1}$$

where v is the specific volume, λ the gradient of the NCL, p' the mean normal stress and N the specific volume on the NCL at a p' of 1 kPa. Similar normal compression lines at high pressures for different silica sands have been reported by Miura & Yamanouchi (1975) for Toyoura sand and by Atkinson & Bransby (1978) for Chatahochee River sand, based on data presented by Vesic & Clough (1968). The pressure required to reach the NCL depends on the mineralogy of the sand and its initial density, ranging from approximately 800 kPa for Dogs Bay sand to 10 MPa for Ham River sand. Dense samples require higher pressures than loose samples to reach the NCL, resulting from the greater number of particle contacts and thus lower contact stresses. Large volume changes are associated with increasing pressures as soon as the NCL is reached. Coop & Lee (1993) attributed this phenomenon to particle breakage. They found that the gradual onset of this particle breakage results in a poorly defined yield of the compression curve during first loading. The unload-reload behaviour was found to be very stiff and essentially elastic, emphasising the almost purely plastic behaviour of the soil during first loading.

Further tests in one-dimensional compression showed the K_o compression lines for Dogs Bay sand and Ham River sand to be parallel to the NCL in v:lnp′ space. The values for K_o of 0.5 observed for Dogs Bay sand and 0.57 for Ham River sand did not vary significantly with stress level and were greater than those which would be obtained from the relationship proposed by Jaky (1944):

$$K_o = \left(1 + \frac{2}{3}\sin\phi'\right)\left(\frac{1-\sin\phi'}{1+\sin\phi'}\right) \tag{2.2}$$

where ϕ' is the friction angle of the soil.

The question of the appropriate K_o value for sands is important to the present research as the interpretation of the centrifuge model tests requires knowledge of the mean effective stress in the model. One fundamental question to ask is which friction angle is appropriate for Equation 2.2. Muir-Wood (1994) argued that due to the dependency of K_o on the in situ structure of a sand the peak angle of shearing resistance as measured in a triaxial test should be used. In contrast Bolton (1991) proposed the following modified empirical relationship for the K_o of sands:

$$K_o = 1 - \sin\phi'_{mob} = 1 - \sin(\phi' - 11.5^\circ) \tag{2.3}$$

The reduction of the friction angle in this equation increases the calculated values of K_o. For example, for Dogs Bay sand the value of K_o from Equation 2.3 is 0.52, which is much closer to the measured value of 0.5 than the value of 0.31 predicted by Equation 2.2.

The value of K_o is known to reduce during unloading, the rate of reduction increasing with decreasing stress level (Schmidt,1966). One method used frequently for predicting the stress path in K_o unloading in clays was proposed by Mayne & Kulhawy (1982):

$$K_0 = K_{0nc} OCR^{\sin\phi'} \tag{2.4}$$

where K_{onc} is the K_o in first loading and OCR the overconsolidation ratio. It is clear that depending on the method used to calculate the value of K_o in first loading a variety of stress paths could be predicted.

Because of the uncertainty associated with the methods to predict K_o values it was decided to measure K_o for the relevant stress paths for each soil using a computer controlled triaxial apparatus. The results of this study will be presented in Chapter 3.

2.2.6 Behaviour During Shearing and Critical State of Coarse Grained Soils

The stress-strain behaviour of sands during shearing is highly non-linear (e.g. Bishop & Green, 1965). The volumetric strains can be either contractive or dilative and are controlled by the initial state of the soil and the level of confining stress during shearing. Dense samples tend to dilate when sheared in a drained test, causing a decrease in pore pressure in an undrained test. Loose soils at high stresses contract when sheared in a drained test and consequently the pore pressures increases if the test is undrained.

Provided that shearing is continued to large enough strains the stress ratio as well as the volumetric strain tend towards a constant value. This state known as the "critical" state, was defined by Roscoe et al. (1958) as: "a condition at which the soil continues to deform at constant stress and constant void ratio". The critical state is independent of the initial density, structure, fabric and stress path. This makes it an ideal reference state to interpret soil behaviour. Critical states have thus been identified by a number of researchers for a variety of sands (e.g Bouvard & Stutz, 1986; Coop & Lee, 1993 and Chu & Lo, 1993).

Coop & Lee (1993) identified critical states for all their three sands as shown in Figure 2-4 mainly by shearing the samples under high confining pressures from initial states above the critical state line. They found the critical state line (CSL) to be approximately linear and parallel to the NCL in stress-volume space. The position of the critical state line is given by:

$$v = \Gamma - \lambda \ln p' \tag{2.5}$$

where Γ is the specific volume on the CSL at a mean normal stress p' of 1.0 kPa. The definition of these parameters is illustrated in Figure 2-1. As for isotropic loading, the shearing behaviour and the position of the critical state line was found to be governed by particle breakage. The critical state lines in q′: p′ space were also found to be independent of the stress level being approximately straight with a constant gradient, M. One interesting feature, apparent from Figure 2-4, is the effect of the initial grading curve on the position of the NCL and CSL. The well graded decomposed granite shows much smaller values of N , Γ and λ compared to Dogs Bay and Ham River sands which are poorly graded.

Poulos (1981) defined the term "steady state" of deformation for any mass of particles as: "the state in which the mass is continuously deforming at constant volume, constant shear stress and constant velocity". The term steady state is generally used in conjunction with undrained triaxial tests (e.g. Ishihara, 1993). However, it has been shown (e.g. by Been et al., 1991 and Verdugo & Ishihara, 1996) that the steady state and the critical state are in fact the same and in order to avoid confusion over terminology the term "steady state" should therefore be abandoned.

Ishihara et al. (1975), introduced the concept of a state of phase transformation sometimes also referred to as a quasi-steady state (Been et al., 1991) in which a state of minimum or constant shear stress is encountered at an intermediate strain in an undrained triaxial test. After passing the quasi-steady state the shear stress starts to increase until reaching an ultimate value. The data presented by Verdugo & Ishihara (1996) show that such a quasi-steady state (QSS) only occurs for loose and medium dense specimens at intermediate confining stresses. Furthermore, Coop (1999b) pointed out that the QSS may not occur in sands that are naturally overconcolidated, of different mineralogy to quartz, under drained loading, or for tests conducted at very high pressures. Been et al. (1991) considered the QSS to be the result of developing shear bands. It must therefore be concluded that the concept of QSS is unsuitable as a general reference state for coarse grained soils.

Knowledge of the position and shape of any reference state line is fundamentally important when applying normalisation techniques. Based on experimental observations, researchers have proposed critical state lines of different shapes and positions for a variety of granular materials. Lee & Seed (1967), Bouvard & Stutz (1986), Chu & Lo (1993) as well as Verdugo & Isihihara (1996) proposed critical state lines that were curved in the v:lnp′ plane for a variety of silica sands. Based on tests on Erksak sand, Been et al. (1991) suggested that the curved CSL could be approximated by using a bi-linear function as shown in Figure 2-5. They argued that the change in gradient at higher stresses is due to the onset of particle breakage. The tests conducted on silica sand by Coop & Lee (1993) identify the critical state only at high pressures which following the argument of Been et al. should give the steeper gradient. As can be seen from Figure 2-4 and Figure 2-3 the onset of particle breakage is clearly a function of the mineralogy and for weak grains the assumption of a linear critical state line may hold to pressures as low as 100 kPa. A summary of critical state lines of a variety of carbonate and silica sands was given by Coop (1999b) and is shown in Figure 2-6.

Experimentally observed critical state lines have been incorporated in a variety of soil models. For example, the Nor-Sand model developed by Jeffries (1993) assumes a straight critical state line, whereas the hypoplastic model (Gudehus, 1996; Herle, 1997) assumes an exponential function in the form of:

$$\frac{e_c}{e_{co}} = \frac{e_l}{e_{io}} = \frac{e_d}{e_{do}} = exp\left[-\left(\frac{3p'_s}{h_s}\right)^n\right] \tag{2.6}$$

where e_l is the void ratio along the NCL, e_c the void ratio at critical state, e_d the limiting void ratio representing the densest possible state, e_{io}, e_{co} and e_{do} are the initial void ratios at zero

mean normal stress, p', the mean normal (granular) pressure, h_s the granular hardness and finally n the exponent. A graphical representation of this formulation is given in Figure 2-7. The procedure to determine these parameters for pressures below the onset of significant particle breakage has been described by Herle (1997). Cudmani (2000) has extended the pressure range of the parameters to 2 MPa.

For this study the critical state line will be determined experimentally by means of triaxial tests and will then be used to normalise the data obtained from the centrifuge tests. Therefore, the different techniques adopted by researchers to measure critical states in the triaxial apparatus will be reviewed in detail in Section 2.3.

2.2.7 The Concept of State for Coarse Grained Soil

The geological history of deposition, loading and unloading of a soil determines its current state in terms of in situ stress and density. Historically, the state of a coarse grained material is defined by its relative density, D_r, or density index, I_D:

$$D_r = I_D = \frac{e_{max} - e}{e_{max} - e_{min}} \tag{2.7}$$

where e is the current void ratio and e_{max} and e_{min} the maximum and minimum void ratios determined from standard laboratory tests. However, this definition is not sufficient to define the stress-strain response where elements of soil can exist at the same current specific volume but on different sides of the critical state line as illustrated in Figure 2-8. Shearing the sample in the lower stress region (A) in a drained triaxial test will result in a dilative response, whereas the sample in the higher stress region (B) will contract. This difference in behaviour must be captured in any proper definition of the current state of the soil and therefore such a definition must include both the stress level as well as the volume relative to a well defined reference state, for example the critical state.

Based on experimental investigations on Kogyuk sand, Been & Jefferies (1985) defined a state parameter, ψ_A in terms of the void ratio (Figure 2-9) by comparing the current void ratio, e to that at the steady state, e_{ss} (as defined by Poulos, 1981):

$$\psi_A = e_\lambda - e_{ss} \tag{2.8}$$

They suggest that the state parameter is independent of mineralogy as their correlation between state parameter and large strain properties, such as the drained peak friction angle worked for

sands of different mineralogy. On the other hand, owing to the effects of initial fabric on the small strain properties, they expected the correlations with the volumetric compressibility and shear modulus to work less well.

A different definition of the current state in terms of stress and volume was introduced by Jovicic & Coop (1997), who used a normalisation with respect to the NCL based on a stress ratio at the current volume rather than defining it in terms of a volume at the current pressure, as used by Been & Jefferies. The definition of the normalising parameters, p_p' and p_e' are shown in Figure 2-1. When investigating the influence of isotropic confining pressure on stiffness, as shown in Figure 2-10, the normalisation gave two unique lines for each sand, one for overconsolidated samples and one for those undergoing first loading only. In Figure 2-10 G_o is the elastic shear modulus of the soil and the normalising parameter for the stiffness, $G_{o(nc)}$, is the value of G_o on the NCL at the current p'.

2.2.8 Applications of the State Parameter Approach to Geotechnical Problems

Been et al. (1986 and 1987) applied the concept of state parameter to interpret results of cone penetration tests (CPT) obtained in calibration chambers on samples of Monterey-No.0 and Hokksund sands which are both quartz sands. The steady state line was established by means of undrained triaxial tests. They normalised the cone resistance, q_c by subtracting the mean total stress, p and dividing by the current p'. Plotting this normalised cone resistance, against the state parameter resulted in a well defined correlation as shown in Figure 2.11. The effect of initial fabric seemed to be of only minor importance in this problem, as the penetration of the cone is associated with large strains in a localised zone around the probe.

Konrad (1988), following the work by Been & Jefferies (1985), applied the state parameter concept to interpret results of dilatometer tests (DMT) in Ottawa sand, another quartz sand. Instead of using the void ratio at a reference pressure, e_1, he defined the state parameter, ψ, directly in terms of the current void ratio, e, and the void ratio at steady state at the current p', e_{ss}:

$$\psi = e - e_{ss} \tag{2.9}$$

To reduce the scatter in the data presented by Been et al. (1986), Konrad correlated the peak dilation rate with the state parameter for different sands, introducing a normalised state parameter, ψ_N, by normalising the state parameter in Equation 2.9 with respect to the difference

of the density limits e_{max} and e_{min} to account for the different grain shapes and grain size distributions.

$$\psi_N = \frac{\psi}{e_{max} - e_{min}} = \frac{\psi}{\psi_l} \tag{2.10}$$

Figure 2-12 shows a unique correlation between the DMT pressure difference, ΔP, normalised by the mean normal stress which Konrad called, I_l, and the normalised state parameter obtained from tests on samples of different relative densities. No test data are available for samples on the contractive side of the CSL but by assuming that for a highly compressible soil of ψ/ψ_l equal to one, the ratio of $\Delta P/I_l$ would tend to zero they extrapolated the results from tests in dilative soils as indicated.

A further investigation into the use state parameter which included the grain crushing stress was published by Konrad (1998), who followed the approach of Been et al. (1991) by representing the critical state line as a bi-linear function. However, as the onset of crushing is a progressive process, this bi-linear shape is clearly an idealisation. Konrad found that the correlation between the CPT cone resistance and the normalised state parameter is affected by the stress level and is therefore not unique. He proposed to compare the measured cone resistance at a reference stress state of 100 kPa with that for a reference soil which he chose to be Ticino sand. The resulting improvement of the relationship between the normalised cone resistance and the normalised state parameter is shown in Figure 2-13.

In summary it may be concluded that in using normalisation procedures to characterise the behaviour of soils it is most important to identify a particular unique reference condition. Both the critical state line and the isotropic normal compression line are appropriate unique reference lines and it is the distance of the current stress-volume state from the NCL or CSL which is the principal factor controlling the shearing behaviour of coarse grained soils at small as well as large strains. This distance is affected either by changes in stress or changes in volume, and both must therefore be accounted for. In contrast, an empirical parameter, such as relative density, which considers only the volume of the soil relative to two fixed, but arbitrary, values cannot work as an alternative normalising parameter as it does not account for the stress level.

The position and shape of these reference lines is usually obtained by means of soil element tests, mostly conducted in the triaxial apparatus. The advances in experimental techniques to measure soil properties at large strains will be discussed in the next section.

2.3 The Measurement of Critical State Parameters in the Triaxial Apparatus

Roscoe et al. (1958) concluded that the experimental evidence presented to support the existence of a "critical void ratio line" was less conclusive for tests conducted in the triaxial apparatus in comparison to the results obtained from the simple shear apparatus. They attributed this problem to the limitations of the triaxial testing procedure mainly due to the onset of non-homogeneous deformations and development of shear bands at large strains. Despite these remarks the triaxial apparatus has repeatedly been used to study the large strain behaviour of coarse grained soils and to identify critical states. The experimental techniques to measure stresses and strains have thus evolved substantially over the past forty years. In this section particular emphasis is given to the techniques developed to identify critical states as the proposed normalisation procedure for the centrifuge model pile tests uses the critical state line in stress-volume space as the reference state. Much discussion has centred around the question of the sample shape and mode of deformation during shearing and its effect on the measured friction angle and volume change.

It appears that the critical state friction angle can be determined relatively reliably in the triaxial apparatus. Bishop & Green (1965) showed that the friction angle is not affected by the sample geometry and the end conditions, as long as a sample with non-lubricated ends has an aspect ratio of more than 2:1. The difference in end condition and sample geometry seemed only to affect the overall stress-strain behaviour in the post peak region. The question of which observed behaviour was the true response of the soil has remained unanswered for some time. Consequently Lee & Seed (1967) and Seed & Lee (1967) used standard 2:1 triaxial specimens with non-lubricated end platens. The tests were conducted drained or undrained on saturated samples and the volume changes were measured with a volume gauge. The primary reason for this approach was the simplicity of the procedure in comparison with using dry soil and an inner cylinder as proposed by Bishop & Henkel (1962). The critical state line identified by Lee & Seed for drained tests on Sacramento river sand is shown in Figure 2-14. The undrained tests by Seed & Lee gave much the same critical state line, a fact that was not fully recognised by Poulos (1981).

Based on standard undrained triaxial tests, Been et al. (1991) suggested that the CSL of Erksak sand shown in Figure 2-5 could be approximated as bi-linear. However, Chu & Lo (1993) have argued that due to developing shear bands associated with local drainage, undrained triaxial tests as used by Been et al. (1991) may not be able to bring a dense specimen to a critical state and therefore questioned their results.

The main problem associated with the use of 2:1 samples and non-lubricated end platens is that shear planes are more likely to develop around the peak especially in dense samples and hence the volumetric strains are concentrated in a very small region of the sample. In addition, barrelling leads to a significant error when a volume gauge is used to measure the average strain under the assumption that the sample deforms as a right cylinder. Rowe & Barden (1964) were among the first to address this problem and introduced lubricated ends for their tests on samples of Mersey River sand. They found that the samples with a H/D of 1:1 and lubricated ends developed multiple shear bands and deformed much more uniformly exhibiting a reduced degree of strain softening and a more uniform dilation leading to an increase in the dilative volumetric strain as the samples approached the critical state at about 30 % axial strain. In contrast the samples with non-lubricated ends and an H/D of 2:1 failed with rapid strain softening at 9.5 %, along a single shear band that developed following pronounced barrelling during the earlier stages of the test.

The effect of non-homogeneous deformations leading to strain softening can be observed from Figure 2-15 which shows test data by Chu & Lo (1993), on samples of Sydney sand. Sample #4, with well lubricated ends shows no strain softening at all up to 15% axial strain, whereas the samples #2 and #3 with poorly lubricated ends and sample #1 with non-lubricated ends show significant strain softening. The corresponding volume change of test #4 which was a dense sample was linear with no tendency towards a critical state. Similar difficulties were encountered for drained tests on loose specimens for which a critical state was not reached at shear strains in excess of 20 % as the deviatoric stress was still rising. The tests then had to be terminated as the samples developed non-homogenous deformations. Chu & Lo concluded that, at low pressures drained triaxial tests were unsuitable to reach a critical state within the homogeneous strain regime on either contracting or dilating samples.

Similar difficulties in reaching a critical state were encountered by Lade & Yamamuro (1996) during their high pressure triaxial compression tests on Cambria sand. Volume changes continued to occur at very large shear strains in excess of 40 % for the drained tests whereas in the undrained tests the pore pressures stabilised but the deviator stress kept on decreasing. They attributed this to particle breakage which they believed continued to occur throughout shearing.

Following the work of Rowe & Barden (1964), other researchers have adopted lubricated ends for large strain testing at low pressures. Verdugo & Ishihara (1996) identified a curve shaped critical state line for Toyoura sand using this technique in combination with a 2:1 sample geometry and global measurement of volumetric strains. As shown in Figure 2-16 they obtained a very good agreement between drained and undrained tests, as well as dense and loose samples suggesting that the effect of localisation on the overall volumetric strain is small. Unfortunately

no information was provided regarding the sample shape at the end of the tests nor the visibility of shear bands. The data obtained by Verdugo & Ishihara must be treated with caution, as following the arguments by Chu & Lo (1993), their experimental techniques were not suitable to identify correctly critical states.

As a result of the problems associated with the measurement of critical states from conventional drained and undrained triaxial tests, Chu & Lo (1993) developed a testing technique using strain path rather stress path control. For a dense sample of Sydney sand they started with conventional drained shearing and then imposed a constant volume condition in the post failure region. A critical state could then be achieved within the region of homogeneous deformation. Their critical state line shown in Figure 2-17 is clearly non-linear with a linear p' axis but even re-plotting the data using a logarithmic scale still results in a non-linear relationship with the onset of a steeper gradient at about 1500 kPa. However, their method did not allow the local measurement of radial or axial deformation and hence did not proof the homogeneity or otherwise of the deformations.

The effect of non-homogeneous deformations of the specimen in the radial direction on the calculated volumetric strain was demonstrated by Kolymbas & Wu (1990). They conducted a series of drained triaxial tests on dry specimens of loose and dense Karlsruhe sand using end lubrication, an H/D of 1:1 and three radial strain belts mounted along the sample. In a number of tests the sample expanded more at the base than at the top. The resulting difference in volumetric strain is illustrated in Figure 2-18. This effectively shows that unless the sample retains a rectangular shape throughout the test no unique answer can be obtained for the volume change associated with a particular confining stress. Also evident is the sensitivity of the volumetric strain to changes in radial strain. Another interesting observation is that regardless of the confining pressure, up to an axial strain of 12% hardly any strain softening occurred in the dense samples, an observation also made by Chu & Lo (1993).

A rather different method to measure the volumetric strain was employed by Bouvard & Stutz (1986). They used gamma ray attenuation to obtain density profiles over the height of the sample. Typical distributions are shown in Figure 2-19a for two 1:1 samples with different end conditions. It is apparent that the density profile for the 1:1 sample with lubricated ends is more uniform then for the same geometry with non-lubricated ends. For samples with non-lubricated ends the radial expansion is clearly concentrated in the centre and no global volume variations as measured in a conventional triaxial apparatus cannot provide correct results. Figure 2-19b shows a comparison of the changes in diameter with axial strain for loose samples, with different geometries and end conditions. It is evident that the samples with non-lubricated ends barrel significantly more. Perhaps the most significant observation is that the 2:1 sample with

lubricated ends barrels at an axial strain of about 13%, while the 1:1 sample with the same end condition does not. The authors assumed that the 1:1 sample with lubricated ends gave the "true" radial strain and used this sample geometry to determine the CSL of Hostun sand which is shown in Figure 2-20. However, one could argue that the fact that the 1:1 does not barrel is a sign of restraint at the ends and the radial strain measured is therefore too small. One disadvantage of the gamma ray attenuation may be seen in the fact that the density is assumed to be constant across the plane of measurement. This assumption ignores the existence of shear bands in the sample, which is not compatible with experimental observations for example by Rowe & Barden (1964).

It appears that no suitable method has therefore yet been developed that allows the assessment of the onset of non-homogeneous deformation in triaxial tests and to measure accurately the void ratio at the critical state. Bouvard & Stutz as well as Chu & Lo (1993) have argued that global volumetric strain measurements as used for example by Verdugo & Ishihara (1996) become meaningless as soon as the sample starts to barrel or shear bands start to form. These problems also rule out the use of undrained triaxial tests. The argument that short samples with lubricated ends deform in a more uniform way than 2:1 samples also with lubricated ends has yet to be proven. It has been shown in the discussion so far that the advantage of a 1:1 sample geometry lies in its ability to suppress single shear bands as they would need to go through the end platens. However, this poses the question whether the remaining restraint at the lubricated ends, although small, restricts the radial expansion of the sample in the centre. It could be argued that the fact that short samples do not barrel is an indication of restraint. Or to put it in another way, if there were no restraint at the free ends, the radial strain measured in the centre of a short sample should be the same as in the centre of a 2:1 sample.

The first point regarding the homogeneity of deformation of loose and dense short samples was addressed by Desrues et al. (1996). They introduced the novel technique of computer tomography to obtain images of the samples at various sections and stages during tests on dry Hostun sand. Two images taken of a dense specimen are shown in Figure 2-21a. Whereas the 2:1 sample with non-lubricated ends shows only one well defined shear band that developed at about 7 % axial strain, the pattern of localisation in the 1:1 sample with lubricted ends is much more complex. However, the onset of localisation for the latter specimen was substantially delayed and occurred at around 16%. The multiple shear zones observed are consistent with observations by Rowe & Barden (1964). After the shear bands in the 1:1 sample had developed the globally measured volumetric strain reached a plateau that might have been interpreted as the critical state. By comparing the void ratio in the shear band with the global measurement Desrues et al. (1996) showed that the local volumetric strain kept increasing and a critical void ratio was achieved at the end of the test that was very similar to that measured on loose samples

(Figure 2-21b). It must therefore be assumed that, although not clearly visible from the outside, shear bands also develop in 1:1 samples with lubricated ends and the globally measured volumetric strain is therefore not necessarily the true strain at a particular applied stress.

Another method developed recently (Kuo & Frost, 1996) uses a microscope coupled with a digital image processing system. Originally the method was used to study the distribution of local void ratio for different sample preparation methods. Frost & Jang (2000) went further and applied the method to study the evolution of sand microstructure by means of the local void ratio during shearing. The sample has to be impregnated with epoxy resin prior cutting it into sections to measure the local void ratio. This means that only one value can be obtained per sample at a given strain level and hence Frost & Jang had to use seven samples prepared at identical initial void ratios. The method thus relies heavily on the repeatability of the tests in order to have comparable microscopic deformations. As bifurcation can be triggered by any random local inhomogeneity the chances that the profiles obtained are consistent are clearly limited. Although the method provides a unique insight into microscopic deformations, as illustrated in Figure 2-22, it is complex and obtaining a continuous critical state line in the v:lnp' plane would be very time consuming.

Macari et al. (1997) used a digital imaging technique to measure the volume changes of a specimen externally by placing two digital cameras at 90° to each other on the outside of the triaxial apparatus. This allowed the volume changes to be calculated across two planes which could be extended to three dimensions by assuming a symmetrical shape. Figure 2-23 shows a comparison between the experimentally determined global volumetric strain and the volumetric strains obtained by the image analysis technique. There is generally a good correlation until about 40 minutes. Macari et al. argued that the observed deviation at large strains may be attributed either to non-symmetrical deformations not accounted for in the image analysis or to the formation of shear bands. One positive aspect of the method by Macari et al. is that the volume changes in different sections of the sample can be measured, thus providing a detailed picture of the sample deformation. However, it does not allow measurements inside the sample, hence volumetric strains after localisation cannot be obtained.

Using local instrumentation in both the axial and radial direction provides an alternative way of monitoring the sample deformation and possibly to detect shear planes. By comparison with microscopic strain measurements, Frost & Jang (2000) showed that if the gauges are placed at the centre of a specimen over about one-third of its height they can provide reasonable estimates of the true response of the specimen. As the technology of local transducers was already available at the start of the testing programme this approach was adopted for this study. The radial strain was measured locally at the mid-height of the specimen to avoid problems with end

restraint. At the beginning 1:1 samples with lubricated ends were used for the Leighton Buzzard sand. Later on, mainly for the tests on Dogs Bay sand, the sample geometry was changed to 2:1. Details of the experimental techniques developed, as well as the test results and critical state lines identified, are presented and discussed in Chapter 3.

In summary, despite over 40 years of research into the large strain behaviour of coarse grained soils, identifying critical states in a triaxial apparatus in terms of stress and volume is a very difficult task. Accurate volumetric strain measurements at low pressures are hampered by the adverse effects associated with barrelling and shear bands. These issues become less significant at higher pressures as shown by Coop & Lee (1993). The location of the critical state line determined is very much affected by the technique employed to measure the volumetric strains. For example, Been et al. (1986) and Konrad (1988) used undrained triaxial tests, a technique which according to Chu & Lo (1993) is not suitable to reach critical states. The analysis of CPT and DMT based on a state parameter derived from these critical state lines is therefore equally questionable.

Desrues et al. (1996) used computer tomography to measure the void ratio at critical state. Although this method provides test data of outstanding detail and quality, it is very complex and hardly available for routine testing. One of the aims of this research is to develop a method for pile design based on soil parameters that can be obtained routinely, for example, in a commercial laboratory. Therefore, local axial and radial gauges in conjunction with lubricated end platens will be used for the present study. The interpretation of the results will require great care as shear planes can be expected to develop beyond 10% axial strain.

Given the uncertainty of the shape of the critical state line at low pressures and high specific volumes it appears that there is considerable merit in using a normalisation based on a stress ratio as proposed by Coop & Jovicic (1997) over the method proposed by Been & Jefferies (1985) and Konrad (1998) which uses a difference of specific volumes. This is further reinforced by the fact that most coarse grained soils in the ground (e.g. Coop, 1999b) have specific volumes for which a reference pressure such as p'_e (Figure 2-1) would be within the linear range of the experimentally determined reference lines.

2.4 The Capacity of Driven Piles in Sand

2.4.1 Introduction

The literature review of driven piles in sand will cover the different aspects of pile capacity analysis. Firstly the term pile capacity will be defined and then the methods currently available

for estimating the base and shaft capacity of driven piles in sand will be reviewed. Some remarks on factors affecting pile capacity are included in a separate section. Finally, the literature on pile load tests will be reviewed to apply the state parameter concept as defined in the previous chapter to suitable pile test data.

Due to the very complex nature of this problem, documented in a very large number of publications, a selection is necessary, focusing on static pile capacity equations and on the calculation of the ultimate capacity of closed-ended driven piles in sand. Topics such as determining pile capacities from dynamic pile formulae, open-ended and grouted driven piles are excluded.

Throughout the literature review the term "pile" is used exclusively for a closed-ended driven pile. The term "pile capacity" refers to the ultimate capacity of an, axially loaded single pile.

2.4.2 The Axial Capacity of Driven Piles

The axial capacity of a driven pile is given by Equation 2.11 given the assumption that the pile carries the applied load partly by shear resistance generated along the pile shaft, and partly by normal stress generated at the base of the pile as shown in Figure 2-24. The ultimate capacity, Q_u, of the pile under axial load is then equal to the sum of the base capacity Q_b and the shaft capacity Q_s:

$$Q_u = Q_b + Q_s = A_b q_b + A_s \int_0^z q_s(z)dz \tag{2.11}$$

where A_b is the area of the pile base, q_b the unit base resistance, A_s the area of the pile shaft, q_s is the local unit shaft resistance along the pile and z the embedded length of the pile.

The definition of the ultimate pile capacity has been widely discussed in the past. For example Vesic (1977) has listed no less than nine different criteria to determine the ultimate capacity. The definition is of particular importance for predictions of the pile capacity and the interpretation of pile load tests. Perhaps the most generally accepted one is to define the ultimate capacity as the force corresponding to a pile head settlement equal to 10 % of the pile diameter, for driven piles, unless the load-settlement curve shows a distinct maximum load.

The magnitude of the base resistance as well as the magnitude and distribution of the shaft friction depends on a variety of factors, some of which are interrelated. To quantify these parameters and incorporate them into a comprehensive pile design method has been the focus of

much research on piles over the last fifty years. The aim of the following paragraphs is to review these methods, outlining their underlying assumptions and illustrating the shortcomings of the predictions made.

2.4.3 Predicting the Base Capacity of Driven Piles in Sand

There are generally three different methods currently being used to predict the base capacity of driven piles in sand: bearing capacity theory, cavity expansion theory and empirical correlations with in situ tests. These methods will be reviewed in the following paragraphs.

(a) Bearing Capacity Theory

By extending the bearing capacity equations for shallow foundations to deep foundations, researchers in the 1960s, (e.g Meyerhof, 1951, 1976) proposed that the base resistance of a pile is proportional to the vertical effective stress in the ground:

$$q_b = N_q \sigma'_{vo} \tag{2.12}$$

where N_q is the bearing capacity factor and σ'_{vo} is the initial in situ vertical effective stress at the pile tip prior to pile installation. Traditionally, the N_q is related to the peak angle of friction, ϕ'_{max} which was thought to depend solely on the density of the sand. As shown in Figure 2-25 the values of N_q proposed in the literature vary considerably which is due to different underlying assumptions regarding the governing failure mechanism.

These apparent difficulties led to modifications of the bearing capacity factors that were adopted, for example by the American Petroleum Institute (API-RP2A 1984, 1991 and 1993), for the construction of fixed off-shore platforms. As shown by Bond et al. (1997) the bearing capacity factors used by API gradually evolved as a function of available pile test data and are currently grouped according to soil type and relative density, ranging from 8 for a very loose sand to 50 for a very dense sand. The resulting profile is illustrated in Figure 2-26. There is, however, no account taken of different stress levels in the soil along the pile. Hence the maximum value of the unit end bearing is limited to 1.9 MPa for loose sands and 12 MPa for dense sands. This is equal to an overburden pressure of 240 kPa, or in other words to approximately 20-25 m pile depth in a saturated soil. These limits are arbitrary and have been subject to much criticism and discussion as their existence cannot be explained by physical phenomena.

Commonly, the introduction of limiting values is attributed to Vesic (1967) but was actually proposed earlier by Kerisel (1964) based on tests on instrumented model piles installed at 1g.

However, as Kulhawy (1984) points out, Vesic (1967) adopted the concept only as a preliminary working hypothesis and in his final report (Vesic, 1977) he did not mention it. Instead he proposed a more rational approach based on the results of a study using the theory of cylindrical cavity expansion. Nevertheless the concept of applying limiting values for end bearing capacity has survived in pile design practice today as documented in the API guidelines (1993) or Tomlinson (1995), perhaps mainly on the grounds of obtaining a conservative design.

Coyle & Castello (1981) analysed a series of pile load tests and showed that the approach of relating N_q to the friction angle (Figure 2-25) does not provide reliable predictions, and this is the reason why in some countries (e.g. Germany) the use of static pile capacity formulae is not permitted. Coyle & Castello proposed a new correlation relating the unit base resistance to the relative depth of the pile tip and the friction angle. In the ensuing discussion Zeitlen & Paikowsky (1981) showed that owing to the stress dependency of the friction angle the values of base capacity would increase at a slower rate with increasing depth and no limiting values were therefore required.

The problem associated with the dependency of the friction angle on the stress level and its effect on the bearing capacity of deep foundations has been investigated further by Bolton (1986). He proposed that because of the decreasing peak friction angle of a sand with increasing mean effective stress the bearing capacity factor N_q in Equation 2.12 should decrease with increasing mean normal stress. This idea was first introduced by Randolph (1985) and then developed further by Fleming et al. (1992). In their approach they relate the peak friction angle ϕ'_{max} to the critical state friction angle, ϕ'_{cs} and the corrected relative density of the sand I_R. The correction of the relative density takes the mean effective stress level, p' into acount and is given by:

$$I_R = I_D[5.4 - ln(p'/p_a)] - 1 \qquad (2.13)$$

where I_D is the uncorrected density index (equal to the relative density), and p_a is atmospheric pressure. This empirical relationship is only valid for mean effective stresses above 150 kN/m^2. Bolton suggested that for very high stress levels I_R should be taken as zero and values of I_R greater than four should be treated with caution. The appropriate value of ϕ'_{max} may then be calculated from:

$$\phi'_{max} = \phi'_{cs} + 3I_R \qquad (2.14)$$

The end bearing pressure can then be obtained for given values of I_R, ϕ'_{cs} and σ'_v by an iterative procedure. Figure 2-27 shows a typical design chart. This procedure has the advantage that it is an approach that is physically more sound although still empirical and the pressure

dependency of the peak friction angle is taken into consideration. The resulting reduction in the rate of increase of the bearing capacity factor with depth seems preferable over the earlier methods, as no arbitrary limiting values are suggested.

The main problems with using bearing capacity analyses are that the failure mechanisms assumed do not necessarily coincide with those that occur around the tip of a pile and that the deformations of the soil are neglected. This means that dependence of the pile base resistance on the soil stiffness and compressibility observed in laboratory and field tests (Yu & Mitchell, 1998) cannot be predicted.

(b) Cavity Expansion Theory

A fundamentally different approach to calculate the unit base resistance of a deep foundation, based on the theory of cavity expansion, was proposed by Vesic (1972) following earlier work by Skempton et al. (1953). He suggested that the controlling factor for the magnitude of q_b in Equation 2.12 should be the mean stress level p' (which he denoted σ'_o), rather than the vertical effective stress:

$$p' = \frac{1+2K_o}{3}\sigma'_v \tag{2.15}$$

where K_o is the in situ coefficient of lateral earth pressure. He also introduced a new bearing capacity factor taking into account the rigidity of the load bearing soil strata, using the rigidity index, I_r. The method is based on the representation of the bearing capacity problem for deep foundations as the expansion of a spherical cavity in an infinite soil mass. Vesic considered the soil to be elastic, perfectly plastic, as characterised by the strength parameters c' and ϕ'_{max}, deformation parameters E' (Young's modulus) and ν' (Poisson's ratio) as well as a volume change parameter Δ, representing the average volumetric strain in the plastic zone surrounding the cavity. Vesic suggested typical values for I_r based on in situ soil characterisation using the relative density. However, one apparent problem of the method is associated with estimating values for Δ.

Randolph et al. (1994), combined the effects of mean effective stress level on peak friction angle and the rigidity index in a new semi-empirical model of deep bearing failure. Figure 2-28 shows a schematic diagram of the mechanism of cavity expansion. They defined the end bearing capacity q_b as:

$$q_b = p_{lim}(1+\tan\phi'\tan\alpha) \tag{2.16}$$

where p_{lim} is the limit pressure from cavity expansion theory, ϕ' is the friction angle of the soil and α the angle of failure wedge as illustrated in Figure 2-28.

Assuming that the soil immediately beneath the pile tip has been sheared to its ultimate state, Randolph et al. proposed that the friction angle could be taken as the critical state friction angle, ϕ'_{cs} and the angle of the failure wedge as $(45^o + \phi'_{cs}/2)$. They suggest calculating the limit pressure from a closed form expression such as that proposed by Carter et al. (1986). As these solutions also assume the soil to be elastic, perfectly plastic, with a Mohr-Coulomb failure criterion and a constant rate of dilation, Randolph et al. proposed a correction for the friction angle and the angle of dilation taking the pressure level into account by following the approach by Bolton (1986). The shear modulus is obtained using a correlation with relative density as suggested by Lo Presti (1987) thus avoiding the problem associated with volume changes. Figure 2-29 shows a comparison between the bearing capacities calculated using the methods of Randolph et al. and Fleming et al. (1992) for three different values of relative density. The agreement is quite remarkable. The greater curvature of the line for the cavity expansion method can be attributed to a decrease in the rigidity index with depth.

Yasufuku & Hyde (1995) used a cavity expansion type of approach to predict the bearing capacity of model pile tests in crushable soils. They modified the original cavity expansion equation of Vesic (1972) to account for increased soil compressibility. Predicted and measured bearing capacities are shown in Figure 2-30 for Dogs Bay sand at different relative densities. Using the bearing capacity solution by Terzaghi (1943) developed for quartz sand the bearing capacity is over-predicted mainly because of the high friction angle of this soil. In comparison, the cavity expansion approach models the behaviour of the model pile much more accurately.

The disadvantage of both the bearing capacity and the cavity expansion methods is that the soil is idealised as an homogeneous elastic, perfectly plastic medium and the effect of layering or changes in soil properties within the soil mass cannot be accounted for. Chow (1996) pointed out that the parameters required (e.g. shear modulus, G) also vary with strain level, stress rate, loading history and ageing. It is also possible that failure around the pile tip may not develop according to the mechanisms assumed leading to additional uncertainty. This issue has been addressed by Cudmani (1996) while formulating a cavity expansion solution using a hypoplastic soil model. Finally, the methods assume that the base resistance is related to the relative density, which is an hypothesis not supported by more recent research for example by Jovicic & Coop (1997) who showed that the soil behaviour is actually controlled by the current stress-volume state.

(c) Correlation With In situ Tests

Owing to the uncertainties involved in using the methods described so far, a number of researchers have proposed the use of in situ tests to determine the unit base resistance. This is a

purely empirical procedure and experience and engineering judgement are therefore crucial in the interpretation of the test results for a successful design. The interpretation relies heavily on information about the expected penetration resistance of the CPT-cone in a comparable reference material, which is usually obtained in a calibration chamber (e.g. Baldi et al. 1986).

Most conveniently the results from Cone Penetration Tests (CPT) are used for pile design, because of the similarity between the penetrating cone and a driven pile. However, cone penetrometers were originally developed for clays and consequently penetration of coarse grained soils is often difficult. In some reported case histories (e.g. Chow & Jardine, 1997) the cone did not penetrate further than 6 m. In such cases the design procedure often has to rely on results from Standard Penetration Tests (SPT), which leads to a significant decrease in the number of sampling points with depth. Procedures based on SPT data will not be included in this section.

The unit end bearing resistance, q_b, of the pile is often taken as being equal to the resistance of the cone tip, q_c :

$$q_b = q_c \tag{2.17}$$

Kraft (1990) proposed a more general approach to compute the bearing capacity from the CPT cone resistance. In his approach he introduces a correction factor, V_k, in Equation 2.17 for variability within an "homogeneous" stratum. The values of V_k are related to the relative density of the deposit and range from 0.5 for dense to 0.6 for loose sands. He noted that the probability for larger variations would increase with the size of soil mass under consideration. Furthermore, he stresses that due to the different shape of the cone and different method and speed of installation, the cone resistance from the CPT might not equal the pile resistance of a full scale pile. For example Durgunoglu & Mitchel (1975) found that the resistance of a 60° CPT-cone was 64 % of the resistance of penetrometer with a flat tip, which is more representative of a pile. A comparison of typical results obtained by the methods of Kraft with those of API-RP2A is shown in Figure 2-31.

Another important factor affecting the reliability of in situ pile design procedures is scale effects. Tejchman & Gwizdala (1979) reported that the unit base resistance of 100 cm long model piles tested at 1-g depended strongly on the pile diameter as illustrated in Figure 2-32. This observation is supported by Kraft (1990) who argues that this can be attributed to different patterns of the failure surfaces, which are influenced by the depth to diameter ratio of the probe and the soil compressibility. A second scale effect is associated with the zone of influence around the pile tip and the soil variability within this zone. This issue has been discussed in detail by Meyerhof (1983). A pile tip, because of its larger diameter compared to the cone,

"senses" variation in soil conditions over a larger zone. Nordlund (1963) and Fleming & Thorburn (1983) have suggested the procedure illustrated in Figure 2-33 for averaging the values of q_c over a depth range above and below the tip of the pile to account for this effect.

The latest design method based on the CPT is the "New Design Method for Off-shore Piles" developed at Imperial College (Jardine & Chow, 1996). It evolved from over ten years of research including tests on fully instrumented model piles in sand at the test sites of Dunkirk and Labenne (Lehane et al., 1993) and the analysis of numerous case histories. Although the method was developed based on correlations between field measurements and CPT data, the method has also been applied in cases where no CPT data were available. For example Williams et al. (1997) have recommended obtaining CPT data from SPT data via correlations with the relative density, as proposed by Skempton (1986) and Lunne & Christoffersen (1983).

Experimental evidence (e.g. Jardine & Chow, 1996) has shown that for large diameter piles the ratio of q_f/q_c is less than unity and the ratio tends to fall with pile size. They attributed this effect partly to the development of local shear bands, which limit the influence of peak strength and dilation rates and partly to the reduced relative pile to soil settlement at the pile tip, especially for the very slender piles used off-shore. In the MTD-Method the unit end bearing resistance is defined as:

$$q_b = \bar{q}_c [1 - 0.5 \log(d_p / d_{CPT})] \tag{2.18}$$

where $\bar{q}_c$ is the average cone resistance over an interval 1.5 pile diameters above and below the pile toe, d_p is the pile diameter and d_{CPT} is the cone diameter, which is generally 0.036 m. Equation 2.18 is purely empirical and tends to zero for a pile diameter of 3.6 m. Therefore, Jardine & Chow proposed a lower bound of q_b equal to $0.13q_c$ for d_p >2 m. Compared to the method proposed by Fleming et al. (1992) the MTD-Method is more conservative as q_b decreases rapidly as a function of the pile to cone diameter ratio.

The issue of limiting values for base resistance derived from in situ tests has repeatedly been discussed in the literature. Fleming et al. (1992) do not mention any limit to the base resistance. Instead they recommend comparing values from CPT tests with the results from modified bearing capacity formulae. However, Tomlinson (1995) introduces a concept of limiting values based the OCR of the soil, following the work of te Kamp (1977). The limiting value for the unit end bearing resistance for all "cohesionless" soils is taken as 15 MPa, slightly higher than in API-RP2A.

Generally, the idea of using in situ tests to estimate the base resistance of a pile should be favoured over the other two methods as long as CPT test data are available. The primary

argument here is that a penetrating cone replicates closely the stress and strain paths that are likely to occur during pile installation. The interpretation should, however, be done with an awareness that the cone resistance is controlled by the in situ stress-volume state (e.g. Been & Jeffries, 1985) and not by the relative density alone as is assumed by the MTD-Method. However, there is still considerable uncertainty in predicting the base resistance of a driven pile from in situ tests which is mainly due to scale effects and soil variability.

2.4.4 Predicting the Shaft Capacity of Driven Piles in Sand

(a) Average Unit Shaft Friction and Critical Depth

Early methods were based on back analyses of field tests using a global average unit shaft resistance, q_s, by simply dividing the ultimate shaft capacity of a pile by the surface area of the shaft. This was often due to the difficulty in installing multiple load cells along the pile in order to obtain values of local shaft resistance. Therefore only very limited information on the distribution of local shaft resistance was available and consequently these methods were very unreliable. The unit shaft resistance is generally expressed as:

$$q_s = K\sigma'_{vo} \tan\delta \tag{2.19}$$

where K is an earth pressure coefficient relating the normal effective stress acting around the pile to the initial in situ effective overburden stress σ'_{vo} and δ is the friction angle between the pile and soil. For the average unit shaft friction along the pile shaft the average vertical stress is required. Although Equation 2.19 looks very simple, there has been much debate over the magnitudes of K and δ and the distribution of the unit shaft friction along the pile for different pile geometries, pile materials and installation methods.

The interface friction angle, δ, between the pile and soil can be measured with reasonable accuracy in laboratory direct shear tests. First attempts to quantify δ assumed it to be five degrees less than the peak friction angle of the soil ϕ'_{max}. In the API-RP2A (1993) guidelines values for $\tan\delta$ are given with respect to the density of the soil as quantified by the relative density. Uesugi & Kishida (1986) and Kishida & Uesugi (1987) have reported a detailed laboratory study of the effects of the surface roughness of steel on δ. They showed that the normalised roughness of the surface, R_n as defined as the maximum peak to valley distance, R_{max}, divided by the average grain size, D_{50}, has a pronounced effect on δ. For example, for a given grading of Toyoura sand δ varied between 12° and 30° as a function of R_n. This observation was confirmed in a more recent study by Garnier & Koenig (1998), who conducted

pull out tests on plates in a centrifuge. Their results are illustrated in Figure 2-34. Fleming et al. (1992) point out that for typical pile surfaces, such as oxidized steel or concrete, this normalised roughness coefficient will exceed 0.05 and the coefficient of friction at the interface will therefore lie between 75 % and 100 % of ϕ' for the soil itself. Assuming that there is no dilation to be expected between the sand and the pile wall they suggest to use the critical state fiction angle ϕ'_{cs} instead of δ in Equation 2.19. Jardine et al. (1992) proposed the use of the constant volume interface friction angle δ_{cs} instead of the peak value of δ, and found it to decreases with increasing D_{50} for a given roughness as shown in Figure 2-35. The diagram is essentially the same as that of Kishida & Uesugi. It shows that the interface friction angle reduces significantly with decreasing normalised roughness and this is an important factor to consider when conducting laboratory based pile research.

Owing to the difficulty in measuring the radial stress directly on the pile, numerous suggestions have been made regarding the magnitude of K and consequently q_s . The API guidelines suggest a constant K of 0.8 for a partial displacement (i.e. open-ended) pile and 1.0 for a full displacement (i.e. closed-ended) pile, irrespective of the direction of loading (tension or compression). Limiting values to q_s are applied ranging from 50 kPa for very loose to 115 kPa for very dense sands. Hence the unit shaft friction increases linearily with depth up to the limiting value and remains constant thereafter.

As pointed out by Randolph et al. (1994), the assumptions in the API guidelines, where limiting values of end bearing and shaft friction are reached at an absolute stress level which is independent of the pile diameter, contrasts with the recommendations of Vesic (1967) who expressed the critical depth as a function of the pile diameter. However Altaee et al. (1993) argued that Vesic had possibly neglected residual stresses in the pile. The effect of residual loads on the distribution of local shaft friction determined by Altaee et al. following load tests on two piles is shown in Figure 2-36a and b. The uncorrected distribution (Figure 2-36b) looks rather similar to the data presented by Vesic (Figure 2-36c). It may be concluded that such uncertainties are a result of the limited database of pile load tests and their generally poor quality, due to lack of instrumentation and soil data.

Kraft (1990) has presented an alternative approach for estimating K based purely on the relative density and the effective area ratio of the pile, which is independent of the grain size. The suggested variation of K, shown in Figure 2-37, is based on field test data and a relationship for δ based on the peak angle of friction ϕ'_{max}. A comparison of unit shaft resistance profiles from Kraft's method and API-RP2A is shown in Figure 2-38. No limiting values are applied and the average shaft friction increases with depth at a steady rate. Randolph et al. (1994) point out that the profiles of shaft friction derived from Kraft's approach are not in keeping with experimental

evidence, which shows average shaft friction values approaching a limit at large depths. However, as discussed above the experimental evidence cited by Randolph et al. is in itself questionable.

Kulhawy (1984) has argued that the experimental observation of limiting shaft friction arises from a combination of decreasing peak friction angle with stress level and reducing K values with depth, due to the tendency for the in situ stress ratio K_o to decrease with depth. This effect has been quantified in the approach proposed by Fleming et al. (1992). In their view K depends on the in situ earth pressure coefficient, the method of pile installation and the initial density of the sand. They suggested linking the unit shaft friction to the unit base resistance of the pile by taking K equal to 2 % of Nq. Whilst this approach leads to a good agreement with results of pile tests on short piles (e.g. Vesic, 1970) it tends to overestimate the pile capacity for very long and slender piles, for example in off-shore conditions, which is mainly due to the fact that piles of such geometries are not covered by the database of pile tests used to develop the method. This disagreement results from ignoring another important factor for the magnitude of the unit shaft friction which is the length (i.e. geomerty) of the pile. The discussion in the next section will therefore focus on advances in understanding the distribution of shaft friction along slender piles.

(b) Distribution of Unit Shaft Friction with Depth

The distribution of local shaft friction has been studied by Vesic (1970) using instrumented model piles of different lengths. Typical distributions of shaft friction are shown in Figure 2-36. Similar observations have often been made in later studies (Hanna & Tan, 1973; Lehane et al., 1993). Heerema (1980) has referred to the decay of q_s with distance from the pile tip as friction fatigue.

The concept of friction fatigue was first introduced to pile design by Toolan et al. (1990), who allowed for friction degradation using the β-method as proposed by Burland (1973), where:

$$\beta = K \tan\delta = \frac{q_s}{\sigma'_{vo}} \tag{2.20}$$

Based on back analyses of pile tests, authors such as Bhushan (1982) had suggested using a constant value of β along the pile shaft which varies only with the initial relative density, D_r of the soil using the empirical relation:

$$\beta = 0.18 + 0.0065 D_r \tag{2.21}$$

Toolan et al. (1990) proposed a correlation between β and the penetration depth of a pile accounting also for the relative density. This correlation is illustrated in Figure 2-39. It is valid for full displacement piles and based on back analyses of tests on piles which were mostly between 10 and 30 m long. For piles of up to 10 m in length and for the 10 m above the pile tip of longer piles β can be taken directly from Figure 2-39. Down to 10 m above the pile tip β is either 0.24 or can be taken from Figure 2-39 whichever is lower. As can be seen from Figure 2-40, this approach results in a sharp jump in the shaft resistance profile along the pile, that will certainly not occur in reality. However, the method does differentiate between high friction near the pile tip and a reduced or degraded, shaft friction over much of the length of the pile.

Based on the interpretation of 25 load tests, Lings (1997) proposed an empirical relationship again linking the shaft capacity to the relative density. He argued that experimental observations provide evidence that there is a depth at which the average shear stress reaches a quasi constant value. He assumed a linear distribution of local shaft friction with depth with the maximum value at the tip being twice the average according to:

$$q_{s,tip} = 2\bar{q}_s = 20 * 10^{1.2 D_r^{1.6}} \tag{2.22}$$

Randolph et al. (1994) presented an alternative approach with respect to the magnitude of the peak unit shaft friction and the distribution along the pile shaft. The approach assumes that the shaft friction reaches a maximum (β_{max}) close to the pile tip and than decays exponentially with decreasing depth of burial to a minimum value (β_{min}) at the surface. It is assumed that the magnitude of β_{max} is related to the unit base resistance by:

$$\frac{q_{s,tip}}{q_b} = \frac{\beta_{max}}{N_q} = S_t \tan\delta \tag{2.23}$$

where S_t is the ratio of the radial effective stress acting in the vicinity of the tip at shaft frictional failure to the end bearing capacity. As mentioned earlier, Fleming et al. (1992) suggested a value of S_t of 0.02. Randolph et al. proposed an exponential relationship given by:

$$S_t = a \exp(-b \tan\phi'_{cs}) \tag{2.24}$$

where a and b are parameters used to adjust the function to model field data. The argument for using ϕ'_{cs} rather than ϕ'_{max} is firstly that it is more easily obtainable from disturbed samples in the laboratory and secondly that the soil in the immediate vicinity of the pile will have been sheared to its ultimate condition during installation. The typical values of S_t obtained from back analyses of field tests are in the range of 0.02-0.05. The distribution of the β along the pile shaft then is obtained from:

$$\beta(z) = \beta_{min} + (\beta_{max} - \beta_{min}) exp[-\mu(L-z)/d_p] \quad (2.25)$$

where β_{min} is a suggested limiting value similar to that used by Toolan et al. (1990), and which is linked to the active earth pressure coefficient, μ is the rate of exponential decay, L the embedded length of the pile, z the depth below ground level and d_p the diameter of the pile. Thus $(L-z)/d_p$ is the normalised length of the pile that has been driven past a particular location. It should be noted that Equation 2.25 describes the decay of radial stress at a given location on the pile shaft as the pile tip is driven past.

Figure 2-40 shows a profile obtained by this method compared to that of the Toolan et al. (1990) approach, the API guidlines and the results of a pile test by Vesic (1970). A fairly good agreement with the field data is obtained by the method proposed by Randolph et al. (1994). Methods such as those proposed in the API guidelines do not properly identify the relevant mechanical relationships that govern the distribution of shaft friction of the long piles used off-shore. However, the uncertainty of the effect of residual stresses on the curves presented by Vesic prevent definitive conclusions from being made. A comparison between the pile test data by Altaee et al. (1993) shown Figure 2-36a and the results in Figure 2-40 shows that the method of Randolph et al. captures the general trend reasonably well although the bell shape curvature at the base seems slightly more pronounced than from the field measurements.

(c) Correlation with In situ Tests

As with the base resistance, values of unit shaft resistance can either be obtained directly from the friction sleeve measurements of a CPT, or from correlations with the cone tip resistance, or from the N-values of the SPT.

Meigh (1987) suggests values of q_s ranging from 0.0033 to 0.018 q_c depending on the pile type while Fleming et al. (1992) recommended the direct use of the results from the CPT friction sleeve measurements or, in cases where no such results are available the use of the empirical relationship proposed by Vesic (1977):

$$q_s = 0.11 e^{-\tan\phi'_{max}} q_c \quad (2.26)$$

The above methods fall short on the issue of distribution of the shaft friction along the pile. This was introduced in the latest method based on the CPT, the MTD-Method (Jardine & Chow, 1996). Based on field measurements on instrumented piles it accounts for friction fatigue as well as increases in radial stress due to suppressed dilation during pile installation. The local unit shaft resistance is obtained by considering the simple Coulomb failure criterion:

$$q_s = \sigma'_{rf} \tan\delta_f \tag{2.27}$$

where σ'_{rf} is the radial effective stress at shaft frictional failure and δ_f is the interface friction angle at failure obtained, for example, from Figure 2-35. According to Jardine & Chow (1996), the radial effective stress at failure depends on a number of factors such as the vertical effective stress level, the distance of the pile tip from the point of interest (friction fatigue) and possible dilative effects during pile loading. These effects are quantified by the following set of equations:

$$\sigma'_{rf} = \sigma'_{re} + \Delta\sigma'_{rd} \tag{2.28}$$

$$\sigma'_{re} = 0.029 q_c (\sigma'_{vo}/p_a)^{0.13} (h/R)^{-0.38} \tag{2.29}$$

$$\Delta\sigma'_{rd} = 2G_{op}\delta h / R \tag{2.30}$$

$$G = q_c [A + B\eta + C\eta^2]^{-1} \tag{2.31}$$

$$\eta = q_c / \sqrt{(P_a \sigma'_{v0})} \tag{2.32}$$

where σ'_{re} is the equalised radial effective stress, σ'_{vo} is the free field vertical effective stress $\Delta\sigma'_{rd}$ the change in σ'_r during loading, P_a is atmospheric pressure, h/R the height above pile tip, G_{op} the operational shear modulus, δh the radial movement of the soil, R the pile radius, A,B,C are constants and η is the normalised cone resistance.

The definitions of some of the parameters are illustrated in Figure 2-41. In essence the method is very similar to that proposed by Randolph et al. (1994) as it considers friction fatigue using an exponential decay of the shaft friction from a maximum at the pile tip to a minimum at the ground surface. The effect of a change in radial effective stress during loading due to dilative effects is accounted for by Equation 2.30, which is derived from cavity expansion theory. The term δh/R in Equation 2.30 accounts for the effect of the pile size on the shaft friction. δh is assumed to be constant and approximately equal to two times the roughness average, R_a, for typical offshore pile. As a consequence Equation 2.30 implies that the radial stress and therefore the shaft resistance increases with decreasing pile diameter.

Although the MTD-Method is purely empirical based on the measured CPT resistance and calibrated against observations of recent tests on relatively small and short piles (Lehane, 1992 and Chow, 1996), Bond et al. (1997) concluded that the method is currently the most reliable one to predict the capacity of piles driven off-shore into the silica sands the North Sea.

2.4.5 Factors Affecting Pile Capacity

In the previous paragraphs the different pile design methods have been introduced in general terms. The survey has focused on the fundamental mechanisms that govern the capacity. Most design methods idealise the pile-soil system to a certain extent, hence the effect of various additional factors affecting the capacity of driven piles in sand will be discussed next.

(a) Method of Pile Installation

There are a number of different pile installation methods currently in use. The selection criteria include environmental factors (noise, vibration) and economic criteria (installation speed and pile capacity). Piles are mainly driven using pneumatic or diesel hammers. In some cases vibration techniques in combination with high pressure jetting or grouting may be used as well. The different driving methods will effect the initial state of stress around the pile as well as the soil density. The rate of penetration may also have an effect on the pile capacity. This has been cause of discussion especially with regard to the applicability of cone penetration data to pile design because of the different installation methods and rates of penetration compared to full scale driven piles (Kraft, 1990).

(b) Pile Type and Dimensions

There are a variety of different driven pile types available such as closed-ended and open-ended piles made from either concrete or steel, or piles made from H-sections and sheet piles. Further variety is introduced by the family of tapered piles and driven, cast-in-place piles.

The pile shape will effect the shaft resistance, with for example tapered piles showing a much increased shaft resistance. Large diameter driven piles are usually open-ended. This introduces some uncertainty with respect to the plugging behaviour of the pile and its effect on the pile capacity (Hight et al., 1996). Also in case of H-section piles, there can be uncertainty regarding the base resistance and the effective shaft area. The pile flexibility, especially with long and slender piles also has significant effects on the shaft resistance (Murff, 1980) as the phenomena of friction fatigue has been observed for such piles (Heerema, 1980). Finally the pile material and roughness of its surface affects the interface friction behaviour of the pile (Kishida & Uesugi, 1987).

(c) In situ State of the Soil

This is perhaps the most important factor of all. Most currently available design methods based on laboratory tests characterise the in situ state in terms of relative density (e.g. Toolan et al. 1990). The effects of stress level are only taken into account to correct the strength parameters of the soil. As far as methods using in situ tests are concerned the interpretation also centres

around relative density as the relevant state variable (Jardine & Chow, 1996) even though, as shown for example by Been & Jefferies (1985), the penetration of the cone is governed by the in situ stress-volume state which is best described using a state parameter.

Following work by Coop & McAuley (1993), Coop (1999a) demonstrated that the shaft friction of a variety of piles strongly depends on the in situ stress-volume state of the soil with reference to the critical state. The results from the literature that Coop analysed for a variety of soils types including carbonate, silica and volcanic sands are shown in Figure 2-42 and indicate that there is an approximately linear relationship between soil state as quantified by the mean effective stress at the critical state p'_{cs} (Figure 2-1) divided by the initial p' both at the same specific volume and β. In can be envisaged that such a relationship would also hold for the base resistance but to date no such relationship has been proposed. Hence to develop such a relationship and to verify that for shaft friction will be the focus of this research project.

(d) Soil Type

A number of sands of different mineralogy, particle shape and particle size have been encountered as foundation strata for piles, such as silica sands and carbonate sands. Particle shape and size depend on the age of the sand and depositional environment and typically include angular, sub-rounded and rounded particles of between 0.1 and 2mm.

The soil parameters used to describe the soil strength and stress-strain behaviour include the peak and critical state friction angles, the angle of dilation, relative density, rigidity index, shear modulus and Poisson's ratio. Most methods assume the material to be elastic-perfectly plastic with a Mohr-Coulomb failure criterion and a constant rate of dilation (e.g. Carter et al., 1986). However, more recently the importance of pressure dependent dilation characteristics, non-linear stiffness behaviour and anisotropic frictional strength have been recognised (e.g. Randolph et al., 1994 and Jardine & Chow, 1996).

The particle size directly effects the pile-soil interface friction behaviour (Kishida & Uesugi, 1987). Additionally the grading of the soil affects the stress-strain behaviour of the soil, such as the location of the critical state line, as shown earlier. As it is the distance of the current state of the soil from the critical state line that governs the behaviour of coarse grained soils, different positions of the critical state line will prompt different responses of a pile during installation and subsequent loading.

Semi-analytical methods are generally based on reinterpreting results from field tests on relatively short piles almost all of which were installed in silica sands. However, the effect of different mineralogies on the pile capacity can be extreme. Depending on the stress level

induced during pile installation and subsequent loading, particle breakage with consequent change in volume can have a significant effect on the load-settlement characteristics of a pile. The lack of a general framework based on the fundamental mechanical features of coarse grained soils has led to repeated errors in predicting the pile capacities of long and slender piles driven into silica as well as carbonate sands (e.g. King & Lodge, 1988 and Williams et al., 1996). In particular the experience at Rankin prompted much research into the behaviour of carbonate soils. The updated version of API-RP2A (1993) contains a commentary on carbonate soils noting that the pile capacity in these deposits can be as little as 15% of the capacity in silica sand. However, Coop & McAuley (1993) and Coop (1999a) showed that, contrary to popular belief, the behaviour of these carbonate sands was not fundamentally different from other sands and that there is an approximately linear relationship between soil state and β. Despite the difference in pile type and size a clear trend of increasing β with p'_{cs}/p'_o can be observed from Figure 2-42.

(e) Time Effects

There is substantial experimental evidence that the shaft capacity of driven piles is time dependent (e.g. Lehane et al., 1993 and Chow, 1996). Increases in shaft capacity of up to 250 % have been observed, as is illustrated in Figure 2-43. Chow et al. (1996) attributed this effect to a) chemical processes (particularly corrosion of steel piles), b) changes of the sand properties due to ageing and c) a long term increase in the radial effective stress due to a creep induced reduction of arching effects. None of these effects is currently considered in routine pile design methods.

(f) Type of Loading

There are three main load types to consider in the process of designing piled foundations: a) compression loading, b) tension loading and c) cyclic loading.

There has been considerable discussion about the magnitude of the shaft capacity of a pile subjected to compressive and tensile loading. The experimental data of Lehane et al. (1993) show that there are significant changes in the radial effective stress during loading due partly to the rotation of the principal stress directions and partly to the radial strains occurring in the pile and adjacent soil. De Nicola & Randolph (1993) have shown that the difference is due to two quantities: the slenderness ratio L/d_p for the pile and the dimensionless expression:

$$\eta_p = \nu_p \tan\delta((L/d_p)/(E_p/G)) \tag{2.33}$$

where ν_p is the Poisson's ratio of the pile material, E_p is the equivalent Young's modulus assuming a solid pile, and G_{av} is the average shear modulus. In essence, η_p represents a dimensionless pile compressibility.

According to Jardine & Chow (1996), the cyclic response of piles is governed by the potential losses of radial effective stresses and shear stiffness during cycling. This depends on the ratio of the cyclic to the static load components, pile compressibility, soil type and the in situ stress conditions.

(g) Group Effects

The stress state around a single pile and subsequently its capacity may change due to the installation of additional piles in its vicinity. This effect depends on the distance of the neighbouring piles. For example Lehane et al. (1993) reported a 50 % increase in shaft capacity due to an increase in radial effective stress. The increase in shaft capacity was associated with a decrease in current mobilised base resistance due to overall pile uplift. As a result of the high costs of full scale load tests on pile groups there is still a lack of information regarding the redistribution of shaft and base resistance of piles in pile groups and its effect on the load settlement behaviour of such foundations.

2.4.6 Full Scale Pile Tests and Laboratory Based Pile Research

In this section the literature on full scale tests on driven piles and laboratory based pile research will be reviewed with the aim of identifying good quality test data. Good quality test data requires separate measurements of base resistance and shaft friction as well as corrections for the effects of residual stresses and drift of the instruments. Particular attention is given to the quality of soil test data available for a each pile test. The data need to be sufficient to establish the critical state line in stress-volume space. This information is essential if the pile behaviour is to be examined within the proposed state parameter framework. This review was carried out with the intention of using the data from the literature for a comparison with the data obtained during this project. However due to lack of time this objective was not achieved. The review should therefore be seen as an attempt to identify good quality tests that could be used for re-analyses in the future.

(a) Full Scale Pile Tests

Traditionally, predictions from pile design methods (e.g. API-RP-2A, MTD-Method) are evaluated against case histories of full scale pile load tests. Coyle & Castello (1981) used a database of 34 tests of which only 16 included both compression and tension loading. Chow &

Jardine (1996) validated their method (MTD-Method) against 65 full scale pile tests of which 41 were on closed-ended piles and 21 of those were compression tests. Randolph et al. (1994) found that the soil data accompanying most of the 21 tests in their database to be very limited and in addition that many of the piles had not been loaded to their ultimate capacity, as defined in Section 2.4.2.

One of the most comprehensive studies on driven piles was conducted by Vesic (1970). His results have subsequently been referred to by numerous researchers (e.g. Randolph et al., 1994). However, as discussed in Section 2.4.4 there has been some doubt in recent years over the quality of Vesic data regarding the effect of residual stresses (e.g. Altaee et al., 1993). The data will therefore not be used for this study.

Hunter & Davisson (1969) accounted for residual stresses in their tests on the Arkansas River site. However, the accompanying soil data do not permit critical states to be identified, hence the data cannot be used within the proposed framework. The same is true for many other tests prior to 1990 (e.g. Beringen et al., 1979).

Lehane (1992), reported tests on two instrumented piles at Labenne. Measurements included load and displacement at the pile head, end bearing as well as local shaft friction and effective radial stresses at discrete locations along the pile shaft. Laboratory tests were conducted including shear box, triaxial and interface shear box tests. The penetration of the 100 mm diameter pile was limited to about 6 m. The interpretation focused on the shaft friction and the h/R friction fatigue effect. The base resistance at the final depth was found to be 4.5 MPa, and was similar to the cone resistance. Even though some laboratory tests have been carried out on this soil the data available again does not permit identification of critical states and the pile data cannot be interpreted within the proposed state parameter framework.

During the EURIPIDES pile testing programme (Zuidberg, 1996) 12 load tests were performed on a fully instrumented pile 762 mm in diameter and open-ended. These were carried out in two locations at depths of between 30 and 47 m. This programme, in terms of quality of the test data and similarity to off-shore piles, represents the most comprehensive so far. Unfortunately the soil data were not included in the above reference and most of the pile data remain confidential until the middle of the year 2000 and cannot therefore be used for this study.

Chow (1996) conducted three tests in dense marine sand at Dunkirk using the same instrumented model pile as Lehane (1992). The depth of penetration varied between 6.0 and 7.5 m. The soil properties were investigated by means of in situ tests (CPT, DMT) and laboratory tests (triaxial, shearbox and interface shear box tests). The profiles obtained of base resistance and average shaft resistance during pile installation are shown in Figure 2-44a and b.

There is good agreement between the measured cone and base resistances indicating that scale effects and soil variability for the given pile geometry are marginal. However, the base resistance mobilised during the load tests following installation reached only 72% at a normalised pile head displacement of 0.4 associated with peak shaft friction and a maximum of 90% for larger displacements. Shown on Figure 2-44b is the mobilised shaft resistance during two compression (L1C) and one tension load tests (L1T) for the piles. Chow observed an increase in shaft friction from installation to the load test between 7 and 10% and attributed this to equalisation of the radial stress and the slower rate of shearing during the load test. Again, the soil data accompanying the pile tests are insufficient to identify critical states and the data again cannot be re-interpreted using the proposed state parameter approach.

Coop (1999a) has collected full scale test data from pile load tests in a variety of sands, where sufficient soil laboratory data were available. The resulting profile of β against state parameter was shown in Figure 2-42. Most of the data were obtained from tension tests on piles off-shore and no equivalent data for base resistance could be obtained.

(b) Calibration Chamber Tests

These tests are mainly undertaken with the aim of calibrating in situ testing devices such as cone penetrometers and cone pressuremeters. The similarity of the penetrating cone to the penetration of a pile makes these tests particularly suitable.

Baldi et al. (1986) calibrated their CPT in Ticino sand. This material is a well known sand for laboratory soil element studies and a bi-linear critical state line has been suggested by Konrad (1998). Cudmani (2000) determined the input parameters for the hypoplastic model and the CSL computed from Equation 2.6 can be used to normalise the data obtained by Baldi et al. (1986).

Evans (1987) and Yasufuku & Hyde, (1995) conducted tests on model piles in a calibration chambers using Dogs Bay sand. Nutt (1993) conducted experiments on a cone pressuremeter in the same soil. As the grading used for their studies is similar to that selected for the present research, both data sets, in combination with the critical state data given in Chapter 3 could be used and interpreted within the state parameter concept.

(c) Centrifuge Model Tests

A number of researchers have conducted studies on driven model piles or cone penetrometers in the centrifuge (e.g. Ko et al., 1984, Phillips & Valsangkar, 1987, Fioravante, 1994 and de Nicola & Randolph, 1999). Mostly well known "laboratory" soils such as Leighton Buzzard and Toyoura sand were used. However, critical state data are available only for a limited number of soils.

Fioravante (1994) used an instrumented model pile at different g-levels and studied the effect of the method of installation on the pile behaviour in Toyoura sand. Axial load cells were mounted at different heights along the pile, thus allowing local measurements of shaft resistance. Typical penetration profiles are shown in Figure 2-45. The critical state line for this soil was identified by Verdugo & Ishihara (1996) and an approximation to this line using Equation 2.6 can be used to normalise the centrifuge test data.

Phillips & Valsangkar (1987) conducted centrifuge cone penetrometer tests in 14/25 Leighton Buzzard sand. Additional cone penetrometer test data from calibration chamber tests are also available (Houlsby & Hitchman, 1988). The critical state line for the material has been identified by Stroud (1971). An approximation to the CSL by Stroud (1971) using Equation 2.6 in combination with the parameters determined by Cudmani (2000) could again be used to normalise the test data.

In summary it may be concluded that the vast majority of the full scale pile tests published in the literature are of limited quality and almost all lack basic but good quality information about the large strain soil behaviour. Consequently only a very limited database can be obtained for silica sands which is restricted to short, small diameter piles. For carbonate sands no high quality data for base resistance could be found. One general problem of full scale field tests is that the soil conditions cannot be controlled and the pile behaviour is additionally affected by factors such as soil variability, depositional history, layering, bonding and possibly ageing effects.

Laboratory based pile research projects can provide alternative sources of high quality data as a number of experiments can be performed under carefully controlled conditions. Particularly suitable are calibration chamber tests on cone penetrometers due to their similarity to driven piles as well as centrifuge model tests. The variation of the level of acceleration in the centrifuge while using the same model pile allows observations of scaling effects. Due to lack of similarity of stress levels (Craig & Sabagh, 1994), conventional 1-g laboratory tests are not suitable to study the behaviour of full scale piles.

2.5 Summary and Conclusions

The review of the literature on the mechanics of coarse grained soils has shown that for sands as for clays the current in situ state in terms of stress and volume is the key factor controlling the soil behaviour. Coarse grained soils of different mineralogies, particle shapes and particle sizes

behave in essentially identical ways and their behaviour can be described within the critical state framework.

When applying normalisation procedures to soil test data it is important to use a unique and well defined reference condition. It was shown that both the isotropic compression and the critical state line are such unique reference lines and that it is the distance of the current stress-volume state from the NCL or CSL which is the principal factor controlling the shearing behaviour at small as well as large strains. This distance is affected either by changes in stress or changes in volume, and both must therefore be accounted for.

Experimental identification of critical states especially in stress-volume space has been shown to be a difficult task. This is mainly due to errors in the measured volumetric strain due to non-homogeneous deformations and shear bands. The recently developed methods for measuring volume changes locally by computer tomography (Desrues et al., 1996) and digital image analysis (Kuo & Frost, 1996) are very promising but at present are unsuitable for routine testing. It was demonstrated that local gauges, although limited to monitoring the deformations in fixed locations, can provide an alternative solution and this technology was hence selected for the present study.

With respect to piles, it can be summarised that the predictions of pile capacity based on currently available design methods are highly variable and that the semi-analytical methods such as API-RP2A are the least reliable. The variability is mainly due to the assumptions made in the derivations of the methods such as failure modes, soil compressibility and stress-strain behaviour of the soil. Methods based on in situ tests, especially on cone penetration tests, such as the MTD-Method, although equally empirical, tend to be more reliable. However, these methods are strongly affected by scale effects and soil variability. The method by Randolph et al. (1994) seems particularly affected by this problem as it assumes the pile base resistance to be equal to the cone resistance. On the other hand the MTD-Method relies heavily on high quality field tests conducted on relatively small and short piles. An extrapolation to long and large diameter piles as used frequently off-shore requires caution especially if no CPT-data are available.

All pile design methods tend to use the relative density as the key parameter to characterise the soil state and subsequently the pile response during loading. Although it has been recognised that pile behaviour is affected by the stress level as well as initial density, the stress level is taken into consideration only to correct the strength and stiffness properties of the soil. All methods have been developed for and evaluated against pile tests in silica sands and their semi-empirical nature prohibits a general use for other soils types without verification by means of

full scale load tests. The effects of particle breakage shown by Yasufuku & Hyde (1995) to control the bearing capacity and load-settlement behaviour of piles in crushable soils are currently not considered in conventional pile design methods.

Recent research into the fundamental mechanisms that govern the behaviour of coarse grained soils has shown that a more thorough approach should include the in situ stress state in the description of the initial state of a coarse grained soil. A first attempt to apply this principle to pile design has been made by Coop & McAuley (1993) and Coop (1999a) with encouraging results. To advance further in this direction is the central point of interest within this research project. The soil element tests and centrifuge model tests conducted to provide the high quality test data needed to establish a more general framework will be described in the next two chapters.

3. Laboratory Soil Testing Programme

This chapter focuses on the laboratory testing programme undertaken for this research project. First the two sands tested are introduced and details given of their geographical and geological origin along with a description of their engineering characteristics. This is followed a description of the surface roughness measurements carried out on the pile and on the shear box interface plates. Direct shear box tests were undertaken to study the behaviour of the soils when sheared along the pile surface. Additionally, a series of interface ring shear tests was carried out towards the end of the project. These will be discussed separately in Chapter 5. The main part of the chapter covers the triaxial testing equipment, procedures used and test results obtained. The aim of these tests was to identify the position of the critical state line for each soil over a wide range of pressures. The chapter closes with a short summary and conclusions of the test results presented.

3.1 Origin and Characteristics of the Soils Tested

3.1.1 Silica Sand (Leighton Buzzard Sand)

The silica sand used for this project is known in the literature as Leighton Buzzard sand. More precisely, in geological terms, it is a Lower Greensand from the Leighton Buzzard Beds in the UK. The deposits were formed in a shallow marine environment during the Cretaceous period some 65 to 146 million years ago. In the literature it is usually described as a natural, uncrushed silica sand (SiO_2) light brown to pale silver to brown in colour, with rounded to sub-rounded particles. The behaviour of Leighton Buzzard sand has been studied in the past at Cambridge University (e.g. Roscoe, 1967 and Stroud, 1971) and elsewhere. It has also frequently been used in centrifuge model tests (e.g. Springman et al., 1991 and Ng & Springman, 1994). From now on Leighton Buzzard sand will be referred to by the abbreviation LBS.

For this study a commercially available standard LBS, Class D was used and was supplied by the David Ball Corporation, Cambridge. Figure 3-1a shows a picture of some typical sand grains under the microscope. The material delivered consists of angular to sub-angular particles rather than rounded to sub-rounded ones as stated in the general geological description of Leighton Buzzard sand. The particle sizes of this material range between 0.15 mm and 0.30 mm. The sand is poorly graded as 85 % of the particles are within the stated range. Grains of this size were considered small enough to eliminate particle size effects in the centrifuge model tests. The grading curve of the material is given in Figure 3-2. On delivery the sand is washed, dried and free of silt, clay and organic matter.

3.1.2 Carbonate Sand (Dogs Bay Sand)

Carbonate deposits are most commonly found on the ocean floor of the Atlantic, the Indian Ocean and the Pacific Ocean. The deposits are formed at a very slow rate and consist mainly of carbonate organisms such as molluscs, corals and eclinoids. The material used in this study was identified and retrieved by Evans (1987) from Dogs Bay situated on the west coast of the Republic of Ireland. The behaviour of Dogs Bay sand is well documented in the literature. Golightly & Hyde (1988) as well as Coop (1990) investigated its large strain behaviour. Jovicic (1997) documented the behaviour of the soil in terms of stiffness at small strains. Model pile tests using Dogs Bay sand were carried out by Evans (1987). Carbonate sands similar to Dogs Bay sand have also been used for centrifuge model tests (e.g. Nunez et al., 1988b). From now Dogs Bay sand will be referred to as DBS.

For this study some of the original soil retrieved by Evans was borrowed from Oxford University. According to Houlsby et al. (1988), DBS consists mainly of foraminifera and mollusc shells, has a high calcium carbonate content (88-94 %) and is poorly graded. Figure 3-1b shows a microscopic view of some typical sand grains. As can be observed the sand particles are relatively unbroken and their open angular nature gives rise to a high void ratio. Coop (1990) determined a particle density for the material of 2.71 g/cm^3 which, compared to a silica sand, is relatively high. The grading curve of the natural material is given in Figure 3-2.

3.1.3 Results of Index Tests on Both Sands

A series of different index tests was carried out according to BS 1377 (1990) to classify the soils. These tests have been described in detail by Klotz (1998) and included selection of appropriate particle size distributions, and measurements of the particle density and the density limits. The index properties for both sands are summarised in Table 3-1.

Since the behaviour of sands is grading dependent, a careful control of the initial grading is essential to obtain repeatable high quality test data. It was therefore decided to reduce the range of particle sizes between a limited number of the BS 1377 standard sieve sizes available. The natural water content of the Dogs Bay varied between 10 and 20 %, and it was therefore dried in the oven at 110 °C for four days prior to dry sieving.

Filling the centrifuge model container requires a substantial amount of material, for example about 30 kg of LBS if the initial density is 1.6 g/cm^3. For this reason it was decided to use the sieving machine shown in Figure 3-3 capable of shaking 450 mm diameter sieves. It was found from a study of the time dependency of sieving that sieving 2500 g of soil for about 90 minutes

resulted in changes in the mass of sand retained on each sieve of less than 0.25%. A typical change of grading with time for LBS is shown in Figure 3-4.

The grading chosen for the tests on LBS contained only those particles that passed through the 212 μm aperture sieve and were retained on the 150 μm sieve. The soil is therefore poorly graded. The grading curve is assumed to be a straight line between the two aperture sizes, since the intermediate size distribution is not known. For the DBS a similar grading to that used by Coop and Lee (1993) was selected. The range of particle sizes is from 0.063 to 1.0 mm, but most of the sand is between 0.15 and 0.3 mm, and it is therefore poorly graded. The grading curves for the two sands as tested are presented in Figure 3-5.

The particle density of each of the materials used has previously been determined by other authors. Therefore, only a limited number of tests were carried out for this study in order to verify the values reported in the literature. The procedures adopted followed BS 1377 (1990). For the LBS ten tests were carried out. The particle density obtained varied between 2.63 and 2.66 g/cm^3, the average value being 2.65 g/cm^3. The average value determined is the same as that commonly reported in the literature (e.g. Stroud, 1971). Based on this good agreement for LBS no tests of the particle density were carried out for DBS and the value measured by Golightly & Hyde (1988) of 2.71 g/cm^3 has been used instead.

Most frequently the current state of a granular material is characterised in terms of its relative density, D_r , according to Equation 2.7 (Chapter-2). This parameter is often used to interpret laboratory and field test data. As has been shown in previous studies (Tavenas & La Rochelle, 1972), the relative density is greatly affected by the methods used to determine the limiting reference densities. This can lead to variations in the computed values of D_r of the order of ±10-20 %. Within this study the methods of BS 1377 (1990) were compared with those in the American ASTM code (D-4253-83 and D-4254-83) as well as in the German code (DIN 18126). The procedures adopted were described in detail by Klotz (1998). The limiting void ratios obtained for the different soils are summarised in Table 3-1. The scatter observed for the maximum void ratio was considerably less than for the minimum void ratio. In general, the relative density is of minor importance to this study as it will only be used to compare conventional design methods based on this parameter with the proposed new method using a state parameter type of approach.

3.2 Surface Roughness Measurements

The importance of the roughness characteristics of metal surfaces in understanding the shearing behaviour of soil-metal interfaces has been recognised for some time (e.g. Potyondy, 1961). More recently Kishida & Uesugi (1987) have suggested to relate the measured roughness to the average grain size of the soil. This approach has been adopted for the present study. A series of surface roughness measurements has been made on sections of the model pile and metal plates for the shear box and ring shear tests. The roughness of both the shear box and ring shear interface plates was adjusted to match the roughness of the model pile sections in order to obtain similarity in shearing behaviour for both.

This section starts with a definition of the different parameters that are commonly used to characterise the roughness of a surface. This is followed by description of the equipment and procedures used for the measurements. Finally, the test results will be presented and discussed.

3.2.1 Definition of Roughness and Normalised Roughness

The focus in this section will be on machined surface textures as this process was used to manufacture all the components of the model pile. Later on in Section 5.3.5, changes of the initial roughness due to pile installation and its effect on the interface behaviour will be discussed.

A simple model of a rough surface is shown Figure 3-6 and illustrates the common parameters used to describe surface texture (e.g. BS1134, 1972). Roughness refers to the small scale peaks and valleys whereas waviness describes the larger scale features of the surface. Roughness height, is defined as the maximum distance between the peak and the valley of a surface profile. The roughness spacing is the distance between peak or valleys. Similar definitions are made for the waviness. In reality the surface texture is very much more complex featuring irregular waves, irregular non-symmetric roughness profiles and other imperfections. For example the roughness height is rarely constant and cannot therefore be expressed as a single number. Additionally most devices used to obtain the roughness profile have a limited evaluation length and it is difficult to obtain a complete three dimensional surface model. The standard procedure therefore is to take measurements at different locations perpendicular to direction of machining (the lay) and to take an average of the readings.

The most commonly used parameters for characterising surface texture is by means of the roughness average, R_a. The graphical derivation of this parameter is illustrated in Figure 3-7a.

The horizontal line through the profile is called the centreline. It is positioned such that, within the sampling length, the sum of the areas enclosed by the profile above the centre line equals the sum of those below it. One problem with the definition of the roughness average, R_a is that it gives no information on the shape of the irregularities or profile as illustrated in Figure 3-7b. Some additional parameters characterising peaks and valleys are illustrated in Figure 3-8. The value of R_{max} refers to the maximum peak to valley height within the sampling length L. These are still not all the possible measurements that might be of interest when studying the surface texture but are those most frequently used in the context of soil-metal interface studies.

Yoshima & Kishida (1981) proposed to normalise the roughness by dividing the measured value of R_{max} by the average particle size, D_{50} of the soil:

$$R_n = \frac{R_{max}}{D_{50}} \tag{3.1}$$

where R_n is the normalised roughness. The sampling length in standard tests is usually about 2.5 mm. Kishida & Uesugi (1987) showed that this procedure produces considerable scatter mainly due to the effect of waviness on R_{max}. In order to improve the quality of their data they reduced the sampling length for R_{max} in Equation (3.1) to the average particle size, D_{50} . This approach has also been adopted more recently by Garnier & Koenig (1998). The refinement tends to reduce the effects of irregular surface patterns such as scratches and generally reduces the value of R_{max}. Alternatively a normalised roughness average, R_{na}, may be defined by substituting R_a into Equation 3.1 instead of R_{max}. Both normalising procedures were used in this study and are discussed in the following section.

3.2.2 Equipment and Procedures

The roughness measurements were carried out by the author in collaboration with Roy Vipond from the Department of Mechanical Engineering at City University. The most frequently used technique to measure surface roughness employs a stylus that travels across the surface. Other methods are based on optical or electrical techniques. For this study a computerised Talysurf-4 unit which is a stylus type device was used and will be described briefly.

The experimental set-up of the Talysurf-4 unit is illustrated in Figure 3-9. The stylus is mounted on a beam connected to the pick-up unit. Its dimensions greatly affect the characteristics of the information which the pick-up can obtain from the surface. The skid, positioned on the left of the stylus, supports the weight of the pick-up. It thus allows the pressure at which the stylus acts on the surface to be adjusted very precisely. Different skid

sizes are available to match individual surface characteristics. The pick-up converts the vertical and horizontal movements into an electrical signal which is then amplified and transferred to the data acquisition unit. The software available on the data acquisition PC allows the selection of different amplifications and filter configurations to improve the clarity of the signal. The test data are stored on hard disc and can also be printed out.

Roughness measurements on model pile CUIMP-3 were carried out in axial direction (at 90° to the direction of machining) on five aluminium and on four titanium sections. This set-up is illustrated in Figure 3-10. A further six measurements were taken on the aluminium and three on the titanium interface plates for the shear box tests. The parameters measured included the roughness average, R_a, the maximum roughness, R_{max} as well as the peak height, R_p and valley height, R_v. The sampling length was set to 2.6 mm. A correction for the stylus sizes is applied to R_a (Dagnall, 1980). The stylus radius of 25 μm used for this study caused a potential error of about 10% given the measured roughness average R_a of 1.13 μm. The corrected averages of the values for each material and section were taken to calculate the normalised roughness from Equation 3.1.

3.2.3 Test Results and Discussion

The results of the measurements on the model pile are summarised in Table 3-2 and for the interface plates in Table 3-3. Figure 3-11 shows a typical roughness profile as measured on the model pile.

Due to the similarities in surface finish of the model pile sections, the measured values of R_a show less scatter in comparison with the interface plates. Although both materials were turned on a lathe using the same tool the titanium sections are still slightly smoother. There is a clear influence of the material characteristics on the surface roughness.

The surface texture of the aluminium plate varies quite substantially. There are two distinct irregularities in the locations of tests Al-I1 and Al-I5 leading to very high values of R_a. These two tests were subsequently ignored as the irregularities were of local nature and not representative of the general surface texture. The titanium plate shows a more uniform surface texture apparent in the smaller scatter of the R_a values. It can be observed that owing to the different surface finish the titanium interface is slightly smoother than the aluminium interface.

It appears that the roughness averages of the model pile are slightly, but not significantly, higher than those for the interface plates. One would therefore expect the shearing behaviour along the surface of the model pile to be similar to that observed in the interface direct shear tests.

The normalised interface roughness data are presented in Table 3-4 for each interface type, material type and soil type. It can be seen that, following the definition by Garnier & Koenig (1998), the normalised roughness values R_n based on R_{max} for the shear box interface plates as well as the pile surface fall into the category of smooth to intermediate roughness (see Figure 2-34). The interface friction angle likely to be mobilised for the LBS, which is similar to the Fontainebleau sand used by Garnier & Koenig (1998), should be in the order of 14° to 27°.

3.3 Shear Box Tests

The shear box tests described in this section were carried out by Simon Coffey for his final year B.Eng. project between October 1998 and May 1999. The project was supervised by Dr. M.R. Coop and the author. This section only provides a short summary of the tests conducted. For further details on the experimental procedures the reader is referred to Coffey (1999).

The tests were aimed at studying the soil behaviour as the soil particles are sheared along titanium and an aluminium plates of similar roughness to the model pile. Particular attention was given to the initial density of the soils and the stress level at which the shearing stage was conducted. These were chosen to cover the ranges that were likely to occur during the centrifuge model pile tests.

3.3.1 Equipment and Procedures

(a) Equipment

A computer controlled direct shear box apparatus was used for the study. The original hardware was manufactured by Wykeham Farrance but subsequently modified by adding a computer control (Coop & McAuley, 1993). In its present configuration it allows full control of stress paths and displacements during shearing.

The forces in the axial and vertical directions are measured by Wykham Farrance Type 4958 load cells. Strain-gauged displacement transducers (Type MPE-HS) measure the horizontal and vertical displacements during shearing. The shear force is generated by a variable feed motor-drive system, that allows different speeds to be selected by choosing the appropriate gear-box ratio. A maximum normal stress of 1 MPa can be applied through a 10:1 lever arm by means of pressurising a pneumatic cylinder. Besides providing greater ease of use over the traditional dead weight system, this configuration allows accurate control of the applied normal stress.

The transducer signals can be amplified prior to data-logging. The data are then transferred to an IBM compatible PC via an A/D converter card. Data-logging as well as control intervals can be selected as appropriate for each test. The applied normal stress is controlled by adjusting the pressure delivered by a pressure converter controlling the air-pressure to the pneumatic cylinder. The applied pressure is adjusted depending on the reading of the vertical load cell or vertical displacement transducer as required.

The shear box consists of two rigid 16 mm thick, 125 mm square plates with a 100 mm diameter hole drilled into the centre accommodating the interface plate. Two locating bolts are incorporated to assist in positioning the plates. Additionally, two spacing bolts are added on opposite sides to allow the top plate to be raised prior to shearing. The assembly sits in a water tight shear box carriage which, in order to reduce friction, travels on two strips of ball bearings. Details of this set-up are shown in Figure 3-12. Both interface plates were 100 mm in diameter and 30 mm thick. The aluminium plate which has a turned surface finish consisted of a solid section whereas for the titanium a composite arrangement was used consisting of a 27 mm thick steel plate with a 3 mm thick titanium plate bonded on top. The finish of the titanium plate was originally rolled but then ground with grades 400 and 800 sanding paper.

(b) Procedures

The tests were performed at constant normal stress with the two different sands being sheared along either a titanium or an aluminium plate. The roughness of the plates was similar to the roughness the model pile surface. Details of the roughness profiles were given in the previous section. The normal stress varied between 100 and 1000 kPa. Samples in wet and dry conditions were tested at different initial densities. A summary of all the tests undertaken is given in Table 3-5. For more detailed information on the sample preparation and calibration procedures the reader is referred to Coffey (1999).

Before starting the shearing stage the shear force load cell was connected and pre-tensioned to reduce the slack present in the system. The box was then split using the spacing bolts by about 0.5 to 1 mm following recommendations by other researchers (e.g Shibuya et al., 1993 and Standing, 1998). The samples were sheared under strain control at speeds of between 0.0045 and 0.009 mm/min. Each shearing stage took about four hours to complete. The experimental set-up prior to shearing is illustrated in Figure 3-13.

3.3.2 Test Results and Discussion

Thirteen interface shear box tests were carried out. The configurations of each test as well as the measured interface friction angles are summarised in Table 3-5. The original intention to

conduct the centrifuge tests on partially saturated samples led to series of similar interface tests (SBLBS-3 to SBLBS-6). To obtain the damp samples of LBS the soil was first saturated and then drained to an equilibrium water content of about 20%. For comparison, one saturated test (SB-LBS7) and two dry tests were performed (SBLBS-1 and SBLBS-2) with the same soil and interface material. This allows conclusions to be made on the effect of the presence of water on the interface friction behaviour. Two tests were carried out using the titanium interface plate, one on Leighton Buzzard sand (SBLBS-10) and the other on DBS (SBDBS-1). Both sands were placed dry, compacted to a dense state and sheared at a normal stress of 500 kPa. Finally, the last two tests were on dense samples of DBS (SBDBS-2 and SBDBS-3), again compacted to a dense state and sheared along the aluminium interface at normal stresses of 100 and 1000 kPa respectively.

Figure 3-14 shows the volumetric strain data plotted against the shear strain for all tests. The volumetric strain is the ratio of the change in height over the original sample height and the shear strain the ratio of the horizontal displacement over the original sample height. Both definitions are somewhat simplistic, as in reality the strains in the sample are localised. It can be observed that, with the exception of tests SBLBS-7, all samples compressed during shearing. Test SBLBS-6 initially compressed and then started to dilate. Comparing tests SBLBS-1 and -2, SBLBS-3 and -4 as well as SBDBS-2 and -3 shows that the samples of both soils prepared at similar void ratios compress more during shearing as the confining pressure increases. It is interesting to note that even the dense silica sand samples did not dilate during shearing. This is consistent with observations by Garnier & Koenig (1998) for smooth interface plates and silica sand. Similar behaviour has been reported by Lemos (1986), who showed that increasing the confining stress from 100 to 200 kPa was sufficient to suppress dilation even in very dense samples of LBS. Most samples reach a constant volume at between 10 and 20% shear strain which for the given sample geometry is equivalent to about 16 to 32 mm horizontal displacement. This is consistent with observations by other researchers (e.g. Jardine et al., 1993). Coffey (1999) noted that his volumetric measurements were significantly affected by loss of sand through the gap beyond a shear strain of about 20% leading to a gradual increase in volumetric strain at larger shear strains.

Figure 3-15 shows that no significant peak interface friction angle develops in either sand in a dry condition. The response of the carbonate sand tests is slightly stiffer. The carbonate sand reaches a constant stress ratio at about 5% shear strain compared to 10% for the silica sand. There is a small effect of confining pressure on the mobilised friction angle with the higher pressures yielding slightly higher values. Test SBDBS-3 is somewhat different as the stress ratio is briefly constant between 5% and 10% shear strain and then starts to increase again. As can be seen from the stress path plot shown in Figure 3-18, the critical state interface friction angle for

both soils in a dry condition is around 26.5°. This is a rather surprising result as the critical state friction angle for the soils measured in the triaxial apparatus is 32.5° for the silica and 43° for the carbonate sand. The values measured for the LBS compare well with values obtained by other researcher for similar silica sands and steel interfaces of comparable normalised roughness (Jardine et al., 1993). However, they are in the upper range of values reported by Garnier & Koenig (1998). The values for DBS compare well with the 27° obtained by Coop and McAuley (1993) on a smooth steel interface of comparable normalised roughness.

The stress-strain behaviour of the tests on damp and saturated silica sand is illustrated in Figure 3-16. Compared to the tests on dry sands a significantly higher stress ratio and therefore interface friction angle was measured. The measured values of about 33° are similar to the critical state friction angle of the soil measured in the triaxial apparatus. This implies that the presence of water on the aluminium interface changes the interface characteristics leading to a higher friction angle. In contrast, Lehane (1992) observed no such change in interface shearing behaviour between steel plates and silica sand in dry and wet conditions. The mobilised friction angle of the damp silica sand samples reduces slightly with increasing confining pressure. The looser samples are again softer in their initial response resulting in lower friction angles.

Figure 3-17 shows the stress-strain response of the tests on the titanium interface. Both soils have a very stiff response and show no distinct peak. The final friction angle of 25° is almost identical for both soils and about 1.5° lower than the friction angle measured on the aluminium plate. The lower friction angle for the titanium corresponds to its slightly smoother surface finish resulting in a smaller normalised roughness. The stress paths followed by these tests are also shown in Figure 3-18.

In summary it can be concluded that the results of the soil-metal interface tests performed in the direct shear box are consistent with results reported by other researchers under similar conditions (e.g. Coop & McAuley, 1993 and Jardine et al., 1993). With regard to the friction angle along the pile-soil interface, the critical state friction angle is the important parameter due to the large strains that occur during pile installation. The measured friction angles on dry soil were independent of the soil mineralogy and varied little for the two interface materials due to their similar normalised roughness. One limitation of direct shear tests lies in the relatively small displacements that can be applied. Furthermore, the magnitude of strain and the remoulding of the soil around the pile tip and its effect on the particle orientation and particle size cannot properly be modelled. The "true" interface behaviour could therefore be somewhat different, especially if there is substantial particle breakage. The measured interface friction angles should therefore be viewed as a guide for the interpretation of the model pile tests.

diameter split mould was modified to accommodate the enlarged polished stainless disk during sample preparation.

The Bishop & Wesley triaxial cell used had been set-up for samples with a height and diameter of 120 and 60 mm respectively. The introduction of lubricated end platens required additional *changes to be made with regard to the sample geometry.* For the present study, the use of local instrumentation prohibited using samples with an aspect ratio less than 1:1, hence a ratio of 1:1.5 was chosen at the beginning of the test series with the additional option of samples with an aspect ratio of 1:1. The experimental set-up is shown in Figure 3-21. From tests TLBS-14 sample geometry was changed once more back to an aspect ratio of 2:1.

Obtaining volumetric strains as accurate as possible at large strains was considered to be of fundamental importance to identify critical states. However, the conventional way of measuring the volumetric strain directly using a volume gauge could not be utilised, since the samples were either dry or partially saturated. There are a number of alternative ways of measuring the volumetric strains under such conditions which have been discussed in Chapter 2. The more complex methods such as computer tomography and digital image processing were not considered as the aim of the project was to apply laboratory testing techniques that can also be performed routinely in a commercial environment. This reduces the suitable methods to either measuring the volume change externally using a second chamber as described by Bishop & Henkel (1962) and Lee (1991), or by calculation from locally measured axial and radial strains. Both methods were used for this study and will be described in the following sections.

The second option was adopted for the majority of tests conducted for the present study. The volumetric strains are calculated from both locally measured radial and axial deformations of the sample. The calculations required are described in Section 3.4.2. It is of importance to retain a sample geometry as close as possible to a right cylinder throughout the test as the radial strain is measured only at the mid-height of the sample. This is ensured by the use of lubricated end platens.

Submersible LVDTs with a linear range of 10 mm were used in the present study to measure the local axial compression of the sample. This technique was developed at City University by Cuccovillo & Coop (1997). The details of the local axial transducer arrangement are shown in Figure 3-22. The maximum distance between the centres of the LVDT pads was chosen to be 40 mm allowing axial strains of 25 % to be measured. Additionally, a global axial LVDT was used for comparison with the local transducer readings and for measurements at large strains

beyond 25%, for which bedding errors and compression of the grease layer can be neglected (Goldscheider, 1982).

A radial belt was used to determine the local radial strain. The first such device was developed at City University by Coop (1996) using only one submersible miniature LVDT for the measurement of the radial displacement. Given the linear range of the LVDT of about 10 mm the maximum measurable radial strain on a 60 mm diameter sample is about -10%. To overcome this problem, the *radial strain belt was modified by adding a second submersible miniature LVDT*, thus increasing the range of measurable radial strain to about -20%. A schematic sketch of the radial strain belt is shown in Figure 3-23. Even though two LVDTs are mounted on the belt, they measure the displacement with respect to the same diameter. In contrast to the two local axial gauges the two measurements of radial strain are therefore not truly independent. This is slightly unfortunate, as the radial strain is twice as important for the calculation of the volumetric strain as will be shown in Equation 3.4. Therefore the chosen design of the radial strain belt, although robust and reliable, is not perfect. The fully assembled set-up for a typical test with local instrumentation is shown in Figure 3-21.

The results of an extensive test series on both soils with the local gauges were inconclusive and the author was forced to resort to *using an inner-chamber*. This required substantial modifications to the apparatus. It was decided to adopt and improve the set-up of Lee (1991) using a water filled inner-chamber. The main components of the system are shown schematically in Figure 3-24. A picture of the fully assembled unit is shown in Figure 3-25. The sample is surrounded by a 6 mm thick, 90 mm diameter steel tube, which is connected at both ends to aluminium plates. The use of steel instead of perspex avoids the problem reported by Lee (1991) associated with the absorption of water in the walls of the inner-chamber which led to errors in the volumetric strain measurements. Externally placed tie bars hold the top plate in position and the chamber is sealed by compressing O-rings placed between the steel tube and the aluminium plates. The top platen and pedestal pass through the plates via centrally placed holes which are again sealed with O-rings. The diameters of both pedestal and top platen were designed to minimise the friction but retain water tightness. Top and bottom drainage were provided to the sample by means of PVC tubes connected to the pedestal and top platen. The pressure in the inner-chamber is measured by the pressure transducer originally used to measure the pore pressure and the pressure can be controlled independently from the outer cell pressure. This allows accurate control of the pressure in both chambers, an improvement over the design of Lee (1991). The amount of water leaving or entering the inner-chamber is measured with a 50 cc capacity Imperial College type volume gauge. The volumetric strain measurements needed to be calibrated to take into account the effects of the axial ram movement, deformations

of the inner-chamber and the connecting pipes as well as the compression of the membrane surrounding the sample. These issues will be addressed in Section 3.4.2.

The *computer control program was first modified* to accommodate the additional local LVDTs. Further modifications included changes in the calculation procedure for the stresses and strains. The average local axial and the local radial strain readings are used to calculate the volumetric and shear strains using the equations given in the Section 3.4.2. The calculation of the current sample area was also modified to use the measured local radial strain rather than the external volume and axial strain readings. The final modifications concerned the layout of the computer screen and changing the data storage procedure.

(c) Instrumentation of the Bishop & Wesley Triaxial Apparatus

For the triaxial tests undertaken for this study, eight transducers have been used. These included a load cell measuring the deviatoric force, one pore pressure transducer, one cell pressure transducer, one global axial LVDT, two local axial LVDTs and two LVDTs on the radial strain belt.

The deviatoric force is measured inside the cell with a submersible load cell. This load cell, built by Wykeham Farrance, has a capacity of 5 kN. The pore pressure as well as the cell pressure is measured by Druck pressure transducers with a pressure range of 0-1000 kPa. The global axial strain is obtained from the displacement of the axial ram measured externally with an LVDT manufactured by RDP, the linear range of which is 25 mm. The submersible local LVDTs used to measure the local axial and radial strain respectively are also manufactured by RDP and have a linear range of 10 mm. Signal conditioning of these devices prior to data logging is achieved by means of RDP-S7AC amplifiers located outside the cell.

For the inner-chamber tests the local gauges were removed and a 50cc Imperial College type volume gauge connected to the drainage line of the inner-chamber. An LVDT similar to the global axial LVDT was attached to the volume gauge to determine the volume changes.

(d) High Pressure Triaxial Apparatus

The stresses generated in the centrifuge model tests, in combination with the dense initial states of the samples, required some high pressure tests to determine the position of the critical state line at pressures in the order of 5 to 10 MPa. For this purpose a high pressure system capable of applying cell pressures of up to 10 MPa was used. The main characteristics of this apparatus were described by Cuccovillo & Coop (1999a). A schematic diagram of the system is given in Figure 3-26. The cell is configured for samples of 50 mm diameter and an H/D ratio of 2:1.

Owing to the high cell pressures the triaxial cell is made from a 12.5 mm thick steel tube and hydraulic oil is used instead of water for the cell fluid. The standard 800 kPa air pressure is multiplied by hydraulic pumps up to ten times to provide the high pressures for the axial and cell pressures. An hydraulic cylinder attached to the loading frame at the top of the cell allows tests to be carried out under axial stress control. Additionally, shearing stages can be performed under strain control by using the motorised 5 tonne loading frame. The latter technique was used exclusively for this study. Control of the pressures as well recording and storing of the test data is achieved by the same BBC and Spectra-ms systems as for the standard apparatus.

The standard instrumentation comprises a 25kN internal load cell of the Surrey University type to measure the deviatoric force, two Druck pressure transducers with a range of 6 MPa, a standard 50 cc volume gauge of the Imperial College type, one global axial LVDT fixed to the ram, two local axial LVDTs, and bender elements for small strain stiffness measurements. For this study a radial strain belt equipped with one LVDT was added. Further modifications included the introduction of lubricated end platens. These were chosen to be the same diameter as the sample as little radial expansion was expected owing to the high confining stresses applied.

3.4.2 Calibration, Accuracy of Measurements and Inherent Errors

(a) Calibration of the Transducers

The transducers were calibrated whilst connected to the control and data acquisition system of the triaxial cell, to minimise errors. Precision supply voltage regulators were used to adjust the transducer supply voltage to precisely 8 V for the Bishop & Wesley system and 10 V for the high pressure system. Maintaining a constant supply voltage is important, as fluctuations adversely effect the transducer output. The linear ranges of the transducers are determined by applying either known forces, pressures or displacements. Subsequently the calibration factors were determined by linear regression and were stored in the calibration file of the control program. The transducers were re-calibrated at regular intervals following procedures described in detail by Lau (1988) for the standard transducers and Fearon (1998) for the local LVDTs. A typical calibration curve for local axial LVDT-2 on the Bishop & Wesley cell is shown in Figure 3-27.

Additional considerations were required for the inner-chamber tests for which the local instrumentation was removed. As the axial ram moves into the inner-chamber the water is displaced into the volume gauge. This leads to an apparent negative volumetric strain (i.e. dilation) which needs to be taken into account. To calibrate for this effect the cell was assembled without a sample and a cell pressure of 100 kPa applied. The ram was then slowly

moved into the inner-chamber while monitoring the axial and volumetric strains. The procedure was repeated at a cell pressure of 700 kPa. The theoretical volumetric strain can be calculated based on the diameter of the pedestal and the stroke of the ram. A comparison of the theoretical and measured values is shown in Figure 3-28. As can be seen there is an excellent agreement. The correction was incorporated in the computer control program as a function of the ram displacement measured by the global axial LVDT.

One additional effect while using the inner-chamber was a sensitivity of the volumetric strains to the level of confining stress. This resulted in compressive volumetric strains as the pipes in the inner-chamber and the membrane compressed with an increase in confining pressure. To calibrate for this effect a steel dummy sample covered with a standard 0.7 mm thick membrane was tested. The cell was assembled and the pressure increased simultaneously in both inner and outer chamber to 700 kPa over four hours. Figure 3-29 shows the resulting volumetric strain. This correction was also incorporated into the control program. The pressure was then kept constant for 4 hours and subsequently reduced back to zero. Holding the pressure constant revealed a sensitivity of the volumetric strain to time. This effect which was much smaller was considered individually for each test depending on the test duration and the corrections were applied after the test was completed.

(b) Accuracy of the Transducers

The accuracy of measurements is defined as the closeness with which the readings approach the true value. The values of transducer accuracy given in Table 3-6 were quoted by Jovicic (1997) for a similar Bishop & Wesley cell and Spectra Micro-ms system and are typical for this kind of triaxial apparatus. For the high pressure system the accuracy as a percentage of the current reading is comparable to that of the Bishop & Wesley cell (Cuccovillo & Coop 1997). For the present study the required level of accuracy is lower than that required for the measurement of small strain stiffness, which was the focus of the research by both Jovicic and Cuccovillo & Coop. The reason for using these very accurate transducers was their availability at the start of this research rather than their high accuracy. For further details on transducer accuracy and the different system related errors the reader is referred to Jovicic (1997). In addition to the errors due to transducer inaccuracy further errors occur in the triaxial test which are related to the performance of the apparatus, sample preparation as well as the calculation procedures used. These errors are described in the next section.

(c) Inherent Errors in Triaxial Testing

Baldi et al. (1988) identified several sources of measurement errors in triaxial testing. Their notation followed a definition given by Jardine et al. (1984) and is illustrated in Figure 3-30.

Seating errors are due to manufacturing or alignment imperfections between the load cell, top platen and filter stone as well as between the filter stone and the pedestal. Alignment errors may result from a lack of co-axiality or perpendicularity in the equipment or from a tilt of the specimen. Bedding errors mainly result from the difficulty of trimming a sample so that its end faces are flat and perpendicular to the vertical axis of symmetry. Compliance might occur due to extension of the tie bars at increasing pressures, deformation of the load cell and, as is the case for the present study, compression of the lubricated end platens.

The errors due to bedding and compliance can be eliminated by using local axial instrumentation as will be shown later on. The errors due seating and mis-alignment may cause non-uniform strains that might be apparent from differences in the two measured local axial strains at small strains primarily during isotropic compression. It is assumed that the non-uniformity of strains inside the sample at small strains, is of secondary importance to the behaviour of the soil at large strains. Hence the average of the two local axial strain measurements will be used to calculate the volumetric and shear strains. Overall the use of local instrumentation provides the highest quality strain measurement data currently obtainable in triaxial testing.

For the inner-chamber tests the effects of these inherent errors had to be considered as no local instrumentation was used. As will be shown in Section 3.4.3, the effect of compression of the grease layer and compliance of the apparatus are insignificant for the magnitude of strains necessary to reach the critical state. Given the self aligning nature of the mould used to create the samples the effects of alignment error as well as the seating error are also very small (see Section 3.4.3).

A further source of error is associated with the membrane surrounding the sample. In the case of radial expansion of the soil the membrane provides a restraint. This restraint may be interpreted as an increase in confining pressure and is most significant for tests at low confining pressures as reported by Fukushima & Tatsuoka (1984). For the tests in this study corrections to the radial stress were applied where necessary following a procedure proposed by Kolymbas & Wu (1990). This issue is discussed further in Section 3.4.6c.

3.4.3 Sample Preparation, Testing and Calculation Procedures

Samples of both DBS and LBS were tested at a variety of initial specific volumes paying special attention to tests at low pressures and high initial specific volumes. The methods adopted during sample preparation and testing as well as the calculation procedures will be outlined in this section.

(a) Sample Preparation Procedure

The dense and medium dense samples were prepared by dry or wet compaction. In a preliminary study it was found that preparing the samples at a water content of 8 % using the wet compaction method (Bishop & Henkel, 1962) yielded samples with the highest specific volumes. The method is especially suitable to obtain samples that compress during shearing even at very low stresses. At a later stage in the programme the method was changed to dry deposition (e.g. DIN 18126), following problems with the centrifuge model pile tests under partially saturated conditions.

Preparation of the sample started by selecting the appropriate grading of the sand, weighing the air dried material and mixing it thoroughly. For the wet compacted samples water in the proportion of 8% of the dry weight was added during the mixing process. The mixture was then covered with a cling film and left for one hour. In the meantime the triaxial cell was prepared.

The 0.2 mm thick lubricant layer was applied to the top and bottom stainless steel discs using a specially designed aluminium ring. A 0.3 mm membrane was then placed on top of the grease layer. The two discs were then attached to the top platen and base pedestal respectively. Afterwards the 60 mm diameter membrane was passed over the bottom enlarged disc and attached to the pedestal. The split-mould was assembled using two sets of jubilee clips, adding talcum powder on the inside of the mould to prevent adhesion between the membrane and the mould. The membrane was than stretched over the top of the mould and fixed in place at the top of the mould with an O-ring. Subsequently a vacuum of 30 kPa was applied to the inside of the mould via the suction tube using an adjustable vacuum pump.

For samples prepared by the dry deposition method, the soil was passed through a funnel occupying the whole sample area, that first rested at the bottom of the mould and was then lifted up continuously until the mould was filled to the top. The dry compacted samples were prepared in five layers and the sand placed in the mould with a small spoon. A surcharge was then placed on top of the soil while vibrating the mould. The wet compacted samples were prepared in eight to ten layers. The soil was again placed with a small spoon and then for the loose samples compacted lightly with a wooden tamping rod. For the medium and dense samples the tamping energy was increased by using a metal rod and an increased drop height. For further details on the sample preparation procedures the reader is referred to Jovicic (1997) and Klotz (1998).

After placing the soil in the mould the top surface was carefully flattened using a steel ruler. During the entire procedure care was taken not to spill any soil, since the specific volume was calculated from the difference in mass between original material and excess material after

sample preparation. The top platen with enlarged plate was then placed taking care of its alignment and the membrane was pulled over it and secured using an O-ring. The vacuum was then released and re-applied also at 30 kPa but now internally via the base drainage path to the sample. The mould was then finally removed and the membrane cleaned carefully. A rubber suction cap (Atkinson & Evans, 1985) was placed on top of the top platen. The initial dimensions of the sample were determined from an average of several measurements, the initial diameter being calculated by deducting twice the thickness of the membrane. These measurements were then transferred as initial dimensions into the control program at the start of the test and were subsequently used as reference dimensions to calculate the global axial strains as well as the local radial strains.

Attaching the local displacement transducers was a very delicate task. The mounting pads of the local axial gauges were placed at a spacing of 40 mm on opposite sides of the sample. The radial strain belt was mounted at the mid-height of the sample. Great care was taken to ensure that the mounts of the radial strain belt were placed opposite one another to minimise non-uniformity of readings between the two LVDTs on the belt. All the mounting pads were glued to the sample using an instant high strength glue. The distances between the pads holding the local axial LVDTs were measured in four locations and the averages taken as the initial gauge lengths for the calculation of the local axial strains. Finally the cell body was placed and the cell filled with de-aired water. The fully assembled sample is shown in Figure 3-31. The sample preparation procedure for the high pressure tests was essentially similar.

The sample preparation procedure for the inner-chamber system followed that described above except that no local transducers were fitted. After measuring the sample dimensions the steel tube was place around the sample and the top plate slid over the top platen. The position of the top platen was measured before and after placing the top plate to account for changes in height that might occur during this operation. The inner-chamber was filled with de-aired water after carefully de-airing all the connecting tubes.

(b) Testing Procedures

Following sample preparation all but one transducer readings were set to zero. The exception was the pore pressure transducer which at this stage measured the vacuum applied to the sample. The cell pressure was then increased to 30 kPa whilst simultaneously reducing the vacuum applied to the sample to zero, thus keeping the effective stress in the sample constant. The disturbance of the sample during this operation was monitored with the local instrumentation. The next step was to connect the suction cap following the procedure described by Lau (1988). The use of local instrumentation again allowed the monitoring of any disturbance. Before the start of the isotropic compression stage all strains were reset to zero and

new sample dimensions were declared taking into account any prior disturbance of the sample. The samples were then isotropically compressed using computer control and applying a constant rate of both axial and radial stress increase of between 5 and 25 kPa per hour.

A series of K_o compression tests on both soils has been carried out to an axial stress of up to 2 MPa. The reading of the radial strain belt was used to control the radial stress in order to maintain a condition of zero radial strain. Subsequently a K_o unloading stage back to an axial stress of 100 kPa was undertaken. This was either followed by an isotropic loading stage to a desired stress level for the subsequent shearing stage or by a K_o re-loading stage followed by a shearing stage.

Prior to shearing the strains were re-zeroed once more and new sample dimensions declared. In the Bishop & Wesley cell the samples were sheared at a constant rate of strain using the Bishop ram in combination with a timed relay at speeds of about 0.5 mm/h. For some tests shearing at small strains was carried out under stress control at a rate of 5-10 kPa/h, by increasing the pressure delivered to the axial loading cylinder. Shearing was then switched to strain control at large strain levels. In the high pressure apparatus shearing was carried out form the start under strain control using the motorised loading frame.

For the large strains required to reach the critical state, the maximum effective stroke of the axial loading ram on the Bishop & Wesley cell became a critical factor. Some of the total stroke of 25 mm was consumed during connection of the suction cap and during isotropic compression. The remaining stroke for the shearing stage proved insufficient to reach a critical state and it was therefore necessary to reset the position of the axial ram by turning the screw at the top of the cell, which positions the axial load cell. Prior to rewinding, the deviator stress was reduced by about 10% to minimise sample disturbance as rewinding tends to increase the axial stress applied to the sample. In cases were the axial stress prior to rewinding was expected to be higher than the maximum mains air pressure, a 2:1 pressure multiplier was connected to the axial ram. The rewinding was then carried out under a constant axial stress. This pushes the sample downwards, lowering the axial loading ram to its original position. Using this procedure required great care, since the sample might have been sheared at the top by accidentally applying a torsional shear stress. It was another advantage of the local instrumentation that any disturbance of the sample at this stage could be monitored. Finally, the shearing stage was resumed until either reaching the critical state or the end of the linear range of the transducers was reached.

At the end of the test the suction cap was disconnected from the load cell and the cell pressure gradually decreased to 100 kPa. A suction of 30 kPa was then applied to the sample whilst

reducing the cell pressure to zero. The final sample dimensions were determined and thereafter the local instrumentation dismantled. The sample was removed quickly from the pedestal and for the partially saturated samples its final water content was measured. The membrane was weighed before and after cleaning it thoroughly so that the material left on it could be taken into account in determining the final dry weight of the sample. The specific volume calculated using the final mass of the soil was always within 1.5 % of the value obtained using the original mass.

(c) Calculation Procedures

The standard set of formulae are based the assumption that the sample retains its cylindrical shape throughout the test and that the volumetric strain is measured with an external volume gauge (e.g. Jovicic, 1997). As the degree of barrelling increases the volumetric strain measured by the volume gauge starts to deviate significantly from the volumetric stain calculated from the axial strain and the radial strain measured at the mid-height of the sample. This becomes a crucial point in evaluating the test data if both methods are used simultaneously. Therefore, at the end of each test the shape of the sample was carefully evaluated and, as will be explained later, corrections have been applied to the volumetric strains where necessary.

The data have been evaluated in terms of ordinary strains. The average local axial strain, $_{av}\varepsilon_{a,loc}$, is calculated using Equation 3.2 and the local radial strain from Equation 3.3:

$$_{av}\varepsilon_{a,loc} = \frac{1}{2}(\varepsilon_{a,loc1} + \varepsilon_{a,loc2}) \tag{3.2}$$

$$\varepsilon_r = \frac{1}{2}(\varepsilon_{r,loc1} + \varepsilon_{r,loc2}) \tag{3.3}$$

where ε_{loc1} and ε_{loc2} are either the local axial or local radial strains. Considering the quadratic terms the volumetric strain, ε_v, can be expressed as an ordinary strain in terms of measured axial and radial strains using:

$$\varepsilon_v = \varepsilon_a + 2\varepsilon_r - 2\varepsilon_r\varepsilon_a - \varepsilon_r^2 + \varepsilon_r^2\varepsilon_a \tag{3.4}$$

where ε_a is the average local axial strain as defined by Equation 3.2 and ε_r the radial strain given by Equation 3.3. The shear strain, ε_s, is then calculated from the measured average local axial strain and volumetric strain calculated from Equation 3.4 using:

$$\varepsilon_s = \varepsilon_a - \frac{1}{3}\varepsilon_v \tag{3.5}$$

The current cross-sectional area, A_c, of the sample is calculated from:

$$A_C = A_0(1-\varepsilon_r)^2 \tag{3.6}$$

where A_0 is the initial cross sectional area at the mid-height of the sample and ε_r the radial strain calculated from Equation 3.3. Finally, the axial stress is calculated from:

$$\sigma_a = \sigma_r + \frac{F}{A_c} \tag{3.7}$$

where F is the deviatoric force measured by the load cell and σ_r is the radial stress messured by the cell pressure transducer.

The calculations of the current specific volume of the sample are based on the initial specific volume, the measured volume change during the test and also the final specific volume at the end of the test. The initial specific volume, v_i, is calculated as the ratio of the total volume of the sample, V_t, to the volume of the solids V_s.

$$v_i = \frac{V_t}{V_s} \tag{3.8}$$

The volume of the solids is calculated from:

$$V_s = \frac{m_s}{\rho_s} \tag{3.9}$$

where m_s is the dry mass of the solids and ρ_s is the particle density of the solids. Finally the current specific volume of the sample, v, is calculated using:

$$v = v_i(1-\varepsilon_v) \tag{3.10}$$

For the inner-chamber tests the volumetric strain was measured directly and the radial strain and current area of the sample calculated following the standard procedure described, for example, by Jovicic (1997). The current area is given as:

$$A_c = A_0 \frac{(1-\varepsilon_v)}{(1-\varepsilon_a)} \tag{3.11}$$

where ε_v is the volumetric strain measured by the volume gauge and ε_a the global axial strain.

The raw data files had first to be converted from BBC-format into ASCII code and were then imported in a spreadsheet program for further analysis and graphical representation. At first the

transducer readings were evaluated for consistency and their continuity between various stages checked. Corrections to the average axial strain were sometimes used in cases where one axial transducer apparently gave a wrong output, for example when it had gone out of its linear range.

Data collected and recorded by transducers that went out of their linear range were also eliminated. If the local axial LVDTs went out of their range before the radial strain transducer reached its limit, the change in displacement of the global axial LVDT was used from that point onwards. This assumes that that the compliance, seating and alignment errors are insignificant at this late stage of the test, which is a reasonable as the strains were typically greater than 15% and the deviatoric stress practically constant. The limited linear range of the LVDTs on the radial belt determined the end of meaningful data as no further volumetric strains could be calculated beyond this point.

All test data were routinely treated according to the procedures outlined so far. Further sources of error are related to compliance, zero drift, membrane compression, membrane stiffness and deformations of the sample that deviated significantly from a right cylinder. Their importance is linked to effect of the inherent errors caused by imperfections of the apparatus, the data logging system or by inaccuracy of the transducers. As a consequence a final assessment was made after all the data had been processed and corrections applied when necessary. This will be described later on.

3.4.4 Testing Programme

A total of forty-four triaxial tests was carried out for this study in order to investigate the behaviour of the soils used over a wide range of stresses and most importantly to determine the position of their critical state lines. The original intention to conduct the centrifuge tests on partially saturated samples led to series of similar triaxial tests (TLBS-1 to TLBS-10 and TBDS-1 to TDBS-4). As this idea was subsequently abandoned, dry samples were used exclusively during the later part of the triaxal testing programme. While for silica sands there is no significant difference in behaviour between wet and dry samples, for DBS the position of the CSL is a function of the presence or absence of water (Coop & Lee, 1994). Therefore, none of the data on the partially saturated samples of DBS were used to determine the critical state line of the dry soil. For the LBS, data from both partially saturated and dry tests were used.

Sixteen tests were carried out on LBS and ten tests on DBS using the locally instrumented Bishop & Wesley triaxial apparatus. Details of the configuration and testing procedure for each test are given in Table 3-7 for the LBS and in Table 3-8 for the DBS. A further eight tests, summarised in Table 3-9, were undertaken in the same apparatus with the aim of measuring the

value of K_o of both soils. All of these tests were conducted by the author between July 1997 and July 1999. Seven additional tests using the inner-chamber configuration in the Bishop & Wesley triaxial apparatus were undertaken; three on LBS and four on DBS. A summary of these tests is given in Table 3-10. The tests were carried out by Chiara Martinelli, an MEng. student from the University of Brescia, under the supervision of the author, between August and December 1999.

The test series was completed by a series of three high pressure tests in the 10 MPa triaxial apparatus. The primary aim of the tests was to measure the value of K_o of both soils over a larger range of stresses necessary to determine the in situ stress in the centrifuge model tests on overconsolidated sand and to add a few additional points to the critical state line database. These tests were also carried out by Chiara Martinelli under the supervision of Dr. Matthew Coop and the author between January and March 2000.

In the following two sections the test data will be presented and discussed first for the DBS and then for the LBS. Even though high quality data were obtained during all stages of the tests the discussion will focus on the behaviour during one-dimensional compression and during shearing to large strains which includes the measurement of the critical state parameters. Therefore, neither the measurements made during isotropic compression nor the small strain stiffness data will be presented in this thesis. Where possible, the test results will be compared to measurements reported in the literature.

3.4.5 Results and Discussion for Dogs Bay Sand

Coop & Lee (1994) showed that the behaviour of carbonate sands in general, and the position of the critical state line in particular, is affected by the presence or absence of moisture. Therefore tests TDBS-1 to TDBS-4 conducted on wet samples are not considered in the discussion on the position of the critical state line as all the good quality centrifuge tests were performed on samples of dry DBS. The initial configuration of all tests is summarised in Tables 3-8 to 3-11.

(a) Behaviour in One-Dimensional Compression

The soil behaviour of DBS during one-dimensional compression in v:lnp′ space is shown in Figure 3-32. Also shown are the two compression curves during preparation of the centrifuge model tests CDBS-13 and CDBS-14. The latter two tests cross over the one-dimensional compression line determined by Coop (1990). Both high pressure triaxial tests TDBS-Ko3 and TDBS-Ko4 seem to converge towards the K_o compression line of Coop. One possible cause for the difference in behaviour between the triaxial tests and the tests on the centrifuge model in the consolidometer could be friction along the side walls of the centrifuge strongbox. This would

increase the measured axial force and hence the calculated value of mean normal stress. The consequences of this problem for the stress state inside the centrifuge model will be discussed in more detail in Chapter 5.

The measured K_o values as well as the stress paths followed during one-dimensional compression of dry DBS are shown in Figure 3-33*a* and Figure 3-33*b* respectively. The value of K_o is fairly constant with an increase in stress level and is not sensitive to changes in initial density. The average K_o value was determined by linear regression as 0.54 which is slightly higher than the 0.51 measured by Coop (1990) on saturated DBS. However, the measured value is substantially higher than the 0.27 predicted using Equation 2.2 proposed by Jaky (1944). The relationship proposed by Bolton (1991) given in Equation 2.3 yields a K_o value of 0.47 which is significantly closer to the measured values. The predicted unloading curve shown in Figure 3-33*b* was obtained by combining the relationship of Bolton with the relationship proposed by Mayne & Kulhawy (1982) for clays given in Equation 2.4. The unloading curve based on an initial K_o from Bolton captures the features of the experimentally determined stress path fairly well.

(b) Behaviour During Shearing

Coop (1990) identified the critical state line of the material in a wet condition as being approximately straight over a range of pressures between 100 and 10000 kPa. The tests within this study therefore focused on the lower end of the pressure range between 50 and 400 kPa.

Following a constant p' stress path during shearing at low stresses (for example TLBS-7) required a reduction of the radial stress to as little as 30 kPa. This potentially increases the error due to membrane restraint. Figure 3-34 shows the uncorrected and corrected stress-strain curves for test TLBS-7. The correction for membrane restraint was applied to the radial stress only, following a procedure proposed by Kolymbas & Wu (1990):

$$\sigma_{3corr} = -\frac{2t_o E_m}{d_o}\varepsilon_r \tag{3.12}$$

where σ_{3corr} is the correction for the radial stress, t_o the thickness of the membrane, E_m the Young's modulus of the membrane, d_o the initial diameter of the membrane and ε_r the radial strain.

As expected, the difference is significant only for shear strains above 8%. The maximum error in stress ratio for a 0.3 mm thick membrane is about 4% which is equivalent to a change in the friction angle of about 1.5°. The correction was applied to all constant p′ tests on both soils at

pressures of 100 kPa and below as well as for all the inner-chamber tests, for which a 0.7 mm thick membrane was used.

The stress paths for each test are shown in Figure 3-35. The standard stress paths with constant radial stress and a gradient of 3:1 indicate the tests conducted with the inner-chamber set-up. The stress-strain relationships during shearing are illustrated in Figure 3-36a and Figure 3-36b respectively. The tests at 700 kPa confining stress have a very soft response and had to be stopped at a stress ratio of 1.2, substantially short of their critical state. Tests TDBS-Ko2, TDBS-5 and TDBS-14 seem to approach the critical state in terms of stress ratio at shear strains of about 28%. The low pressure constant p' tests develop a peak at about 10% shear strain but then, with the exception of TDBS-6, tend towards a similar stress ratio as the other tests at larger strains. Judging from the stress ratios at the end of shearing the critical state stress ratio is about 1.7.

Typical stress-dilatancy data for dry DBS are presented in Figure 3-37. The trend of the data indicates a critical state stress ratio of about 1.66, which is in good agreement with the M of 1.65 measured by Coop (1990) and also agrees well with the value interpreted from Figure 3-36a. Another interesting feature in the stress-dilatancy diagram is the constant value of $d\varepsilon_v/d\varepsilon_s$ of 1.5 measured for tests TDBS-Ko1 and TDBS-5 up to stress ratios of about 0.9. By calculating the value of $d\varepsilon_v/d\varepsilon_s$ from Equations 3.4 and 3.6 for the case of zero radial strain a value of exactly 1.5 is obtained. This means that the radial strain belt measures no strain at all and the sample more or less follows a K_o compression path. This is also evident from the strain data presented in Figure 3-36 which, for small strains, are essentially straight with a gradient of one. It can therefore be concluded that either the radial strains at the start of shearing are truly close to zero or alternatively, that the friction between the core and the body of the LVDT restrains the movement of the radial strain belt.

Published data using volume gauge measurements (e.g. Lee, 1991) indicate that there is a negative component of radial strain even at small strains, as the volumetric strain is less than the axial strain. Similar observations were made by Kolymbas & Wu (1990), who used three radial belts but of a more flexible design. However, zero radial strains at small strain levels have been observed by Hettler and Vardoulakis (1984) on samples of Karlsruhe sand in a large triaxial apparatus. There therefore seems to be some disagreement in the literature regarding this issue. As far as the measurements with the radial belt used in this study are concerned, further tests would be required to answer the question whether the strain data are correct or affected by the friction between LVDT core and LVDT body. This is beyond the scope of this thesis as it only affects the small strain region which is not of interest here.

Figure 3-38 shows the points reached in q:p′ space for all tests at the end of shearing. The critical state line presented is based on measurements by Coop (1990) on the same material in a saturated condition. This critical state line will be used later to estimate the mean normal stress at the critical state for the tests at 700 kPa confining pressure.

From Figure 3-36b it can be observed that the constant p′ tests dilate very strongly showing no sign of reaching a critical state within the achievable range of axial strain. This extreme dilation contradicts the behaviour observed by other researchers (e.g. Coop, 1990) who used saturated samples and measured the volume changes externally with a volume gauge. It is also incompatible with the behaviour observed by the author for tests using the inner-chamber. For example test TLBS-5, a constant p′ test at 300 kPa, starts to dilate at 10% strain whereas TLBS-14 conducted with the inner-chamber compresses throughout even if the mean normal stress at the end of shearing was less than for test TDBS-5. As a consequence of these observations the readings from the local gauges in tests TDBS-5 to TDBS-7 as well as TDBS-Ko1 and TDBS-Ko2 were examined in more detail.

Figure 3-39 shows the local axial strains plotted against the global axial strain for each test. It is clear that non-homogeneous axial deformations axial occurred in all tests. It is also evident that the onset of the non-homogeneous deformations is a function of the confining pressure, as most samples had similar specific volumes at the start of shearing. The dilatant response of samples at low pressures and the associated formation of shear bands that is evident from Figure 3-39 is an indication that the critical state line lies at specific volumes above the specific volume of the specimen at the start of shearing.

Figure 3-40 illustrates the shape of the sample at the end of test TDBS-7. A set of two shear planes inclined at about 56° to the horizontal can clearly be identified. It can be seen that both local axial gauges as well as the radial belt are located on wedges that have been displaced almost as rigid bodies after the formation of the planes. This explains the decreasing rate of local axial strain. It also explains the almost constant rate of dilation, as the radial strain simply increases as a function of the axial displacement, for the given angle of the shear planes, under a rigid body motion. For test TDBS-7 the inclination of the shear plane to the horizontal (Figure 3-36b) is about 46°, which is not too far from the theoretical angle of 56° associated with the rigid body motion mechanism.

The developing shear bands violate the most important assumption for the calculation of stresses and strains in triaxial tests, that the soil sample can be idealised as a continuum. Therefore, all data beyond the onset of non-homogeneous deformation have been ignored. The resulting stress-strain data are then presented in Figure 3-41a and Figure 3-41b.

A closer look at Figure 3-41b reveals that, regardless of the consideration of non-homogeneous deformations, there is a further incompatibility of the strain data for tests TDBS-5 and TDBS-14. The explanation of this incompatibility is the barrelling of the sample during shearing that occurs despite lubricating the end platens as illustrated in Figure 3-42. The lubrication is effective in that the sample expands at both ends, but the expansion in the centre is always more indicating the presence of some friction. Hence in the locally instrumented tests the measured radial strain is larger than the average radial strain calculated with the assumption that the sample retains its cylindrical shape. This in turn leads to more apparent dilation for the locally instrumented tests than for those using an inner cylinder. Because of the friction on the end platens it is believed that the locally measured radial strain is probably more representative of the true strain than the average radial strain. Therefore the average global radial strains will be corrected for the effect of barrelling.

The procedure for correcting the radial strain is illustrated in Figure 3-43. If it is assumed that the sample barrels while retaining a shape that can be described by an arc, an expression for the equivalent average diameter can be derived. The average change of diameter over the full height of the sample is approximately 2/3 of the measured change of mid-height diameter. However, as the axial strain measured represents an average strain between the mounts of the axial gauges it was decided to average the radial strain over the same length of the sample.

This approach was applied to the strains measured for the inner-chamber tests TDBS-11 to TDBS-14. The average radial strain was first multiplied by a factor of 3/2 to obtain the radial strain at the mid-height of the sample and then reduced by a factor of 0.96 representing the difference between the average radial strain between the axial gauge mounts and the estimated central radial strain. Similarly, the locally measured radial strain of the 2:1 samples was reduced by a factor of 0.96 and for the 1:1 samples of LBS by 0.85 to take into account the barrelling between the mounts of the local axial gauges. The higher reduction factor for the shorter samples results from the increased curvature due to the closer proximity of the mounts to the ends of the sample. This procedure appears to contradict the observation of reduced curvature of the shorter samples but was nevertheless applied for consistency. The final corrected volumetric strain curves are shown in Figure 3-44. As can also be seen, the data obtained by the two testing methods are now much more consistent. The low pressure tests still dilate but for pressures above 250 kPa the behaviour during shearing is purely compressive. This is consistent with observations by Coop (1990). These corrected data were then used to calculated the specific volume at the end of shearing and subsequently to determine the critical state line in v:lnp' space.

The test data and the proposed critical state line are illustrated in v:lnp′ space in Figure 3-45. Also shown is the maximum specific volume of 2.84 determined from the index tests and an extrapolated critical state for test TDBS-12. For this extrapolation the stress at the critical state was obtained from Figure 3-38 and the volumetric strain extrapolated from Figure 3-44. It appears that the critical state line is slightly to the right of that determined by Coop (1990) for saturated samples as had been suggested by Coop & Lee (1994) even though they did not have sufficient data to locate the precise position of the CSL for dry DBS. The assumption of a linear relationship in v:lnp′ space seems to hold for pressures above 200 kPa. For the lower pressures a continuation of the straight line would require substantial dilation of the soil which, given the measurements conducted in this study, seems unlikely. It is therefore proposed to adopt a similar procedure as will be discussed in detail for the LBS (Herle, 1997) and use the maximum specific volume as the limiting or critical state volume at atmospheric pressure. An exponential function is best suited to describe mathematically the shape of the critical state line at low stresses. The proposed shape also leaves some room for further dilation of the low confining pressure tests, which is consistent with the observed behaviour in Figure 3-44. The critical state parameters are summarised in Table 3-13.

The observation of dilation during shearing of DBS at low pressures gave rise to a study of the role of particle breakage. Figure 3-46 shows the grading curves of some typical tests. There is no apparent particle breakage for TDBS-5, a constant p′ test conducted at 100 kPa, which shows a dilative response during shearing. For TDBS-6 and TDBS-12 particle breakage was observed and both tests show a compressive response.

This relationship between particle breakage and mean normal stress can be illustrated using relative breakage, B_r, as proposed by Hardin (1985), as discussed in Section 2.2.4. Figure 3-47 shows values of B_r plotted against the logarithm of mean effective stress at the end of shearing. There is an approximately linear relationship and the onset of breakage for dry DBS is at about 90 kPa. A comparison with the relationship proposed by Coop & Lee (1993) for the saturated soil shows that the dry particles are generally stronger and there appears to be a different gradient for the saturated and dry samples of DBS, again confirming the observations of Coop & Lee (1994).

In summary, it can be concluded that the measurement of volumetric strains in a triaxial apparatus for specimens of dry DBS at low pressures and high initial specific volumes is very difficult with conventional instrumentation owing to the formation of shear bands. Applying a computer tomography technique as described by Desrues et al. (1996) could provide some improvement. However, given the steep gradient of the critical state line in v:lnp′ space and the specific volumes achieved in the centrifuge models, the proposed normalisation for the pile test

data would not be significantly affected if the critical state line were assumed to be straight rather than curved, and this assumption will be made in Chapter 5 for the DBS for simplicity.

3.4.6 Results and Discussion for Leighton Buzzard Sand

Not all the tests summarised in Tables 3-7 to 3-11 will be presented and discussed. For example, tests TLBS-1 and TLBS-2 were of preliminary nature and did not have lubricated ends. Furthermore the original, single LVDT, radial strain belt was used which did not allow sufficiently high strains to be measured due to the limited linear range of the transducers.

With the exception of tests TLBS-11 to TLBS-13 all other tests were conducted on samples with a water content of 8 %. The suction due to this partially saturated condition is of the order of 1 kPa, which is very small compared to the applied stresses. No correction to the measured total stress was therefore applied. Following observations by Coop & Lee (1994), who found that the behaviour of wet and dry samples of quartz sand is essentially the same, the data obtained from all of the tests TLBS-5 to TLBS-19 will be used to determine the CSL of LBS.

(a) Effect of Inherent Errors

The combined effect of apparatus compliance, compression of the lubricated ends, and bedding error can be observed from the difference between the global axial and local axial strains in Figure 3-48 obtained during isotropic compression of sample TLBS-10. A summary of this effect on the other test data is given in Table 3-12. The error due to compliance and compression of the lubricated ends is clearly a function of the stress level and amounts to about 1% axial strain at 700 kPa confining stress. It is also apparent that the relationship is non-linear and for higher pressures the system becomes stiffer, perhaps as the error is reduced to compliance only, as the bedding error is eliminated. This is consistent with observations by Goldscheider (1982). The differences in the local axial strain readings are due to the effects of misalignment and seating errors. As can be seen from Table 3-12, the maximum error is about ±0.25% and the behaviour is independent of the stress level and the density, which confirms earlier observations by Sarsby et al. (1980). Based on these observations, corrections for the bedding, seating and compliance errors were applied to the tests with the inner-chamber, where no local instrumentation could be used.

(b) Behaviour During One-Dimensional Compression

Figure 3-49 shows the data for the one-dimensionally compressed samples TLBS-Ko1 to TLBS-Ko4 in the v:lnp'-plane. Additionally, the one-dimensional compression data from the centrifuge model test CLBS-21 are presented. The pressure available in the low pressure triaxial

tests was too low to reach yield. The centrifuge test data seem to approach yield in the proximity of the isotropic NCL determined by Cuccovillo & Coop (1999b). Due to the limited data available it is not possible to arrive at conclusions regarding the friction along the boundaries of the centrifuge strongbox during compression of test CLBS-21, as was possible for the DBS.

The stress paths in terms of axial and radial stress for the triaxial tests are presented in Figure 3-50. The precise K_o values for each test were determined by linear regression from the data and are given in Table 3-9. There is an effect of density on K_o with the loose samples giving higher values. For comparison with the measured values, the predicted stress paths using the methods of Jaky (1944) and Bolton (1991) are shown as well. It appears that the equation proposed Jaky, which uses the peak friction angle is more suitable for the dense samples, whereas the method by Bolton, where the peak friction angle is reduced by 11.5° to account for a lower degree of mobilised friction works well for the looser samples.

Figure 3-51 shows the measured and predicted stress paths in q:p′ space for first loading and subsequent unloading. It can be observed that combining both the Jaky and Bolton expressions with the unloading stress path equation for clays by Mayne & Kulhawy (1982) results in a good agreement between the predicted and the measured stress paths.

The experimentally determined K_o values were used to estimate the in situ stresses in the centrifuge model taking into account the effect of density on K_o. No separate re-loading stage was performed for LBS. Following the observations on DBS it was assumed that the same K_o value would apply in re-loading as was measured in first loading.

(c) Behaviour During Shearing

Figure 3-52 shows a comparison of the local axial strains with the global axial strains for tests TLBS-4 and TLBS-7. Both tests have a similar specific volume and were sheared at 400 kPa confining pressure. The main difference between the samples is the grease used for the lubricated ends. During TLBS-4 the increase of local axial strain starts to decay rapidly at about 12%, which may be defined as the onset of non-homogeneous deformation. Sample TLBS-7, however shows no such decay in the rate of local axial strain. In this test the local axial strains are very close to the global axial strains indicating no localisation and that the effect of compliance and bedding errors were also small.

The grease UNISILCONE TK44-N3 used for TLBS-7, was found to be more suitable than the standard silicone grease and was therefore applied to all triaxial tests on both soils from test TLBS-5 onwards. The behaviour of test TLBS-7 shown in Figure 3-52 is representative for all

of the good quality tests on the LBS. Unlike the behaviour of DBS, there was no clear indication of localisation in the local axial strain measurements, possibly the results of the 1:1 sample geometry predominantly used for the tests. However, following observations by Desrues et al. (1996) there is the possibility that non-homogeneous deformations developed in other areas of the sample that are not monitored by the local instrumentation. Therefore, the tests results, especially those of the dilative samples, were examined very carefully.

The stress paths followed by the individual tests are shown in Figure 3-53a. With the exception of tests TLBS-Ko3 and TLBS-16, which were constant p′ tests, all other tests were carried out at a constant radial stress. Figure 3-53b shows the critical state line in stress space estimated from the data for the maximum strain achieved in each test, the gradient is 1.3, corresponding to a ϕ'_{cs} of 32.5°.

Figure 3-54 shows the stress-strain behaviour for all of the good quality tests. The test details are summarised in Table 3-7 to Table 3-11. It may be observed that the dense and medium dense samples exhibit a stiffer response than the loose samples. Also the slightly overconsolidated sample Ko-3, sheared along a constant p′ stress path has a particularly stiff response. The loose samples, as well as the dense sample TLBS-8, do not quite reach a constant stress ratio at the final shear strain of around 24%. Although showing quite substantial dilation, with the exception of tests TLBS-8 and TLBS-Ko3, none of the tests develops a significant peak in the stress stain curve. This confirms earlier observations, for example by Kolymbas & Wu (1990), who found that lubricating the ends in triaxial tests reduces the magnitude of the peak. This has implications for the observed stress-dilatancy relationship as will be discussed later.

Typical stress-dilatancy data are shown in Figure 3-55. As for the tests on DBS the radial strain belt often does not respond up to stress ratios as high as 0.4 (TLBS-5) leading to the constant value of $d\varepsilon_v/d\varepsilon_s$ equal to 1.5 observed for some tests. The trend of the stress-dilatancy data indicates a critical state stress ratio of 1.17, which is substantially lower than the value of 1.3 determined from Figure 3-53. Furthermore, the absence of large peaks in the stress-strain curve while the sample is dilating means that during the latter stages of each test the rate of dilation increases at an almost constant stress ratio until a maximum is reached and then decreases along the same line until a condition of zero volume change is reached. This behaviour does not comply with conventional stress-dilatancy relationships and was most noticeable in tests TLBS-11 and TLBS-12. These observations will be discussed later.

The strain data given in Figure 3-54 as well as the v:lnp′ diagram presented in Figure 3-56 show some interesting features that are worth exploring in more detail. The very loose samples

TLBS-5, TLBS-7, TLBS-14 and TLBS-15, where local instrumentation was used, originally compress but start to dilate at a shear strain of about 8%. There is a strong difference in the volumetric strain between the inner-chamber tests TLBS-17 and TLBS-10, which was similar but carried out with local instrumentation. Test TLBS-17 indicates that the soil reached a critical state at a specific volume of about 1.85 whilst TLBS-10 dilates strongly at a constant rate towards a specific volume of more than 2.0. As for the DBS this difference is due to the effect of barrelling and a correction was therefore applied to all the test data as has been described for the tests on DBS. However, given the uncertainty involved in applying these corrections one could draw a straight CSL through the uncorrected data at pressures above 800 kPa, as indicated in Figure 3-56.

Also remarkable and illustrated in Figure 3-57 is the difference between the local and global measurements of volumetric strain for tests TLBS-11 and TLBS-12. Both 1:1 samples were saturated, had similar specific volumes at the start of shearing and the global volumetric strain was measure with a volume gauge. It appears that the local radial strain measurements, although more accurate, are much more vulnerable to changes in sample shape and irregularities compared to the global measurements. Test TLBS-12 expanded much more at the base than at the top and was therefore omitted for subsequent analysis of the CSL location as the global and local strains did not agree even after the correction. Test TLBS-11 barrelled symmetrically during the test and after applying a correction to the local radial strain both the local and global volumetric strains are in fairly close agreement.

Figure 3-58 illustrates the difference in the measured local radial strains due to barrelling between samples with an H/D of 1:1 and 2:1. All the samples were loose and were prepared by wet compaction to similar specific volumes. Tests TLBS-6 and TLBS-15 were sheared at a constant radial stress of 100 kPa, and the other two tests at 400 kPa. There is a clear trend that for larger strains the end restraint on the 1:1 sample reduces the radial strain. The shorter samples thus appear less barrelled, which is often interpreted as a sign of more uniform strains (e.g. Bouvard & Stutz, 1986). It appears therefore that using loose 1:1 samples tends to over-estimate the amount of compression during shearing, especially at large strains thus leading to a critical state line in stress-volume space that would be too low. Unfortunately no tests on dense samples were carried out and the effect of initial density on the error in radial strain cannot be addressed. No correction for this effect was therefore applied. However, the test results have shown that the much promoted use of 1:1 samples is in need of a critical review.

The final strain data corrected for the barrelling effect are shown in Figure 3-59. The correction factors applied were the same as for the DBS. As discussed above, there was no need to account for localisation effects for the loose samples. Following the correction of the data there is a

much more consistent pattern in comparison to Figure 3-54, with all loose samples compressing and the dense samples still dilating but at a reduced rate. There is also much better agreement between tests TLBS-10 and TLBS-17. The two tests shown in Figure 3-52 were on loose samples and there is a greater potential for localisation in the denser samples. Following suggestions by Desrues et al. (1996) the test data for the tests on dense samples were therefore terminated arbitrarily between 8 and 16 % shear strain to account for the onset of non-uniform deformation even though in the examples given in Figure 3-52 there was no indication of localisation from the two local axial LVDTs. However, there is a possibility that shear bands may have developed on planes that were not intercepted by the two local gauges. The sensitivity of the test results to the radial strain measurements is clearly visible and the good agreement mainly results from the corrections applied to the measured radial strain which themselves bear some uncertainty. In retrospect, measuring the radial strain at more than one location on the sample would have been advantageous.

Figure 3-60 shows the stress-dilatancy relationship produced using the corrected shear and volumetric strains from Figure 3-59. The stress ratio remained unchanged, as the error in the stresses due to the change in area is less than 2%. The corrections applied to the radial strain for barrelling, predominately for the inner-chamber tests and the tests on the 1:1 samples leads to a much improved plot. The intercept at zero dilation, which is equivalent to the critical state stress ratio, M, is now 1.29, which is very close to the value of 1.3 obtained from the q:p′ plot. The corrected set of data are also more consistent with conventional stress-dilatancy relationships.

The final v:lnp′ diagram is presented in and Figure 3-61. Following the corrections of the radial strain the data are again more consistent than in Figure 3-56. It appears that tests TLBS-5 and TLBS-11 are close to a critical state. Test TLBS-10 was at the same confining pressure as TLBS-5 but did not reach a critical state. However, examining the v:lnp′ diagram shows that at the end of test TLBS-10 the specific volume is still lower than that of TLBS-5 and hence there is room for more dilation. Similar observations can be made for the other tests. The use of the wet compaction method allowed the creation of samples that compressed during shearing. Consequently the critical state was approached from initial states below and above the critical state line. This gives additional confidence in the measurements and the corrections applied.

Judging from the corrected test data the critical state line gradient at low and intermediate pressures appears to be very flat in comparison to that at higher pressures as determined by, for example Coop (1999b) for Thanet sand. Also shown in Figure 3-61 is the critical state line obtained by Verdugo & Ishihara (1996) for Toyoura sand. Their critical state line seems to agree nicely with that of Thanet sand for larger pressures. This confirms the observation by

Coop (1999b) that the critical state lines of silica sands at large pressures can be approximated as straight lines and generally have a very similar gradient and location.

Based on the measurements taken, the position of the critical state line for the LBS is assumed to be curved in the region of low to intermediate stresses and roughly parallel to that determined by Verdugo & Ishihara for Toyoura sand. Following Herle (1997) the v_{max} of 2.01 determined from the index tests is used as a starting point for the line at very low pressures which is in very good agreement with the test data. One data point at a pressure of 4.5 MPa was obtained from test HPLBS-1 conducted in the high pressure apparatus. From this it appears that the gradient of the CSL in this region is similar to that of Thanet sand.

The difficulty in obtaining reliable volumetric strain measurements at low pressures provides a strong argument for using a state parameter defined as a stress ratio as opposed to a state parameter based on the specific volume as has been used for example by Been & Jefferies (1985). The maximum specific volume in the centrifuge test was about 1.97 at a mean normal stress of 100 kPa which is just in the area where the critical state line starts to become steeper. The onset of the steeper gradient seems to be more gradual than for the DBS and affects the normalisation much more. As a consequence of the uncertainty in the volumetric strain measurements and hence in the location of the CSL the centrifuge model test data will be normalised using both a straight CSL as indicated in Figure 3-56 as well as the exponential CSL shown in Figure 3-61. The critical state parameters for both normalisations are summarised in Table 3-13.

The main conclusion for the tests on LBS is the same as for the tests on DBS. It was found that measuring volumetric strains accurately on dry or partially saturated samples in a triaxial apparatus is very difficult. The main difficulty arises from the effect of barrelling and the onset of non-homogeneous deformation on the local measurements. By applying appropriate corrections to the test data a critical state line has been identified that was surprisingly consistent in shape and position to observations by other researchers even though they had used less accurate volumetric strain measurements.

3.5 Summary

This chapter has focused on the laboratory testing programme undertaken within this research project. A silica sand, Leighton Buzzard sand, and a carbonate sand, Dogs Bay sand, were selected for testing. Although the two sands have similar grading curves the difference in mineralogy and particle shape gave rise to a difference in index properties.

Direct shear box tests were undertaken with the aim of studying the behaviour of the soils when sheared along the pile surface. In order to achieve similarity between the shear box interface and the model pile surface, the roughness of both surfaces was measured in representative locations using a Talysurf-4 unit and the roughness of the interface plates subsequently adjusted. The measurements were interpreted using the approach of relative roughness as defined by Kishida & Uesugi (1987). During the shear box tests it was found that the mobilised interface friction angle for both soils in a dry condition was very similar despite their different soil-soil friction angles. Wet and saturated samples sheared along the aluminium interface had significantly higher friction angles compared to the dry samples. The slightly smoother surface finish of the titanium interface over the aluminium had little effect on the mobilised friction angle. Therefore, the mobilised shaft friction along the model pile should be unaffected by the change in material for different pile sections.

Bishop & Wesley and high pressure triaxial apparatus were used to determine the shape and position of the critical state line for each sand over a wide range of pressures. Lubricated end platens as well as local instrumentation were introduced to enhance the quality of the test data. The grease used for lubrication had a significant effect on the efficiency of the lubricated end platens. It was found that the error due to compression of the lubricated ends, bedding and compliance was a function of the applied stress, whereas the magnitude of alignment and seating errors was independent of the applied stress and was a function of the procedure used for sample preparation.

One fundamental advantage of the local measurements is the ability to observe the "true" strains of the sample. This allows non-homogeneous deformations to be detected during shearing at large strains if the shear bands develop on planes that include the mounts of the local LVDTs. Such behaviour was observed for all low pressure tests on Dogs Bays sand but was not observed in similar tests on LBS, although it is suspected that localisation may have occurred.

The values of K_o measured during one-dimensional compression were significantly different from the values predicted by the methods of Jaky (1944) and Bolton (1991). For the LBS the value of K_o was found to depend on the initial specific volume of the sample. However, this effect was very small for the DBS.

Measuring volumetric strains in triaxial tests was found to be very difficult. An incompatibility between locally and globally measured strains was observed. Despite using lubricated ends the samples barrelled during shearing at large strains possibly due some residual friction at the ends. The radial strain measured at the mid-height of the sample was therefore larger than the average

radial strain calculated by assuming the shape of a right cylinder. As a consequence the locally measured volumetric strains are larger and the resulting critical states in v:lnp′ space differ significantly from values measured by other researchers (e.g. Verdugo & Ishihara, 1996) who used conventional global measurements. A correction for the effect of barrelling on the locally instrumented tests as well as the global measurments of radial strain was therefore introduced. This procedure, although convenient, is rather crude and does not answer the question as to which observed behaviour is the "true" response of the soil. To find an answer to this fundamental question would have required an extension of the testing programme, which was beyond the scope of this research project. The difficulty in obtaining reliable volumetric strain measurements at low pressures and consequent difficulty in locating the CSL provides a strong argument for using a state parameter defined as a stress ratio as opposed to a state parameter based on the specific volume as has been used for example by Been & Jefferies (1985).

The critical state line in q:p′ space was easier to determine than in v:lnp′ space. The former was found to be a straight line whereas the latter may be curved at low pressures and straight at higher pressures. The onset of the steeper gradient of the critical state line is a function of the mineralogy and occurs at a mean normal stress of around 200 kPa for DBS and 2000 kPa for LBS. Given the in situ states of the centrifuge tests it was considered appropriate to use a straight critical state line for DBS to normalise the centrifuge model test data. For the LBS the in situ states of the centrifuge tests fall within the curved part of the CSL. Due to the uncertainty in the volumetric strain measurements in this region two critical state lines, one a straight line and the other an exponential function will be used to normalise the centrifuge model test data.

Based on the experience gained during the soil testing programme the following conclusions with respect to measurements of critical states by other researchers as reviewed in Chapter-2 can be drawn. The procedure adopted, using local gauges in combination with lubricated end platens has been shown to be robust and gave satisfactory results, although it would have been beneficial to use more than one radial strain measurement. Given the problems encountered with respect to shear bands, undrained triaxial tests as used for example by Been et al. (1991) and drained tests with only one global volumetric strain measurement (Verdugo & Ishihara, 1996) must generally be considered unsuitable and therefore normalisations based on such tests (e.g. Been et al., 1986 and Konrad, 1998) should be treated with caution. Ideally one should use computer tomography such as developed by Desrues et al. (1996). However, this method is very complicated to use and not suitable for routine laboratory testing. As an alternative it is recommended to apply the procedure adopted in this study but adding additional radial strain sensors.

4. Centrifuge Modelling

The aim of this research was to establish a basic framework relating the capacity of driven piles in sand to the in situ state of the sand prior to pile installation. This was achieved by means of centrifuge testing, a technology widely used today to study problems from every area of geotechnical and geoenvironmental engineering (Taylor, 1995). Phillips & Valsangkar (1987), Cyran et al. (1991) and de Nicola & Randolph (1993) have used centrifuge modelling to investigate the behaviour of piles with respect to different installation methods, pile types and soil types.

This chapter outlines the fundamental concepts of centrifuge modelling and their relevance to this research project. This is followed by the description of the equipment developed (Figure 4-1) as well as the procedures adopted for preparing the centrifuge models, calibrating the transducers and performing the actual tests. Finally, the different test series conducted are described. The test results will be discussed separately in Chapter 5.

4.1 Fundamental Concepts of Centrifuge Model Testing

The advantage of using the centrifuge over field tests is that a much greater variety of prototype scenarios can be investigated repeatedly at appropriate in situ stress levels and under controlled laboratory conditions, thus leading to better quality test data. This, however, requires careful planning of the tests and appropriate procedures to minimise the errors inherent in centrifuge model testing as outlined in the following sections.

4.1.1 Principles of Centrifuge Modelling

The principle of centrifuge modelling is based on Newton's law of motion. A payload (model) is placed on a platform at a distance, r from the centre of rotation and accelerated to a constant angular velocity, ω during the test (Figure 4-2). This condition is known as uniform circular motion and imposes a radial acceleration, a, onto any item attached to the centrifuge arm where:

$$a = \omega^2 r \tag{4.1}$$

In uniform circular motion, the acceleration is always directed towards the centre of the circle (the centre of rotation) and hence is always perpendicular to the vector of the angular velocity. The radial acceleration imposed by a centrifuge is usually related to a scaling factor, N, and expressed as a multiple of the earth's gravitational acceleration, g, as:

$$N = \frac{a}{g} \tag{4.2}$$

Thus by adjusting the angular velocity at a given radius to a certain scaling factor allows modelling of any prototype stress distribution in a geotechnical centrifuge. This is illustrated in Figure 4-2. The procedure, however, is not as straightforward as these two governing equations suggest. For example, different physical quantities such as length, stress and time obey different scaling laws. Furthermore, as can be seen from Equations 4.1 and 4.2, the scaling factor, N, is not a constant but a function of the radius, a fact that can lead to scaling errors. Before embarking on the development of a centrifuge model, careful consideration of the appropriate scaling laws and the possible scaling errors is therefore required. Both are of equal importance for the successful development of a centrifuge model and the interpretation of the results.

4.1.2 Scaling Laws and Scaling Errors

Scaling laws are either derived by dimensional analysis or by considering the governing equations of a particular problem. The most important scaling relationship for this project is the correlation of the stress field between the prototype and model scale. The procedure to obtain the appropriate scaling relationship for this case is by dimensional analysis and will be outlined briefly. Table 4-1 which is adapted from Ko (1988) summarises the most common scaling relationships for geotechnical problems. Scaling errors result mainly from the geometrical discrepancy between the earth's gravitational field relative to the scale of engineering applications and the nature of the acceleration field created in the centrifuge relative to the model size.

For most engineering applications it may be assumed that the earth's gravitational acceleration is constant with depth and the in situ vertical total stress in the prototype, σ_{vp}, will therefore increase linearly with depth:

$$\sigma_{vp} = \rho g h_p \tag{4.3}$$

where ρ is the soil density and h_p the prototype height. In contrast, at any given radius, the vertical total stress, σ_{vm}, in a centrifuge model of height, h_m, and soil density, ρ, is given by:

$$\sigma_{vm} = \rho N g h_m \tag{4.4}$$

Thus, for σ_{vm} equal to σ_{vp} the prototype height, h_p can be expressed as Nh_m. Therefore, the scale factor (model to prototype) for length or any other linear dimension is 1/N. However, as can be seen from Equation 4.1 the radial acceleration varies with the radius, thus the scale factor is only

correct at one particular location in a model. This problem turns out to be minor if care is taken to select the radius at which the gravity scale factor N is determined. The aim of this procedure is to minimise the areas of under- and over-stress (Figure 4-3) and hence to reduce the inherent error in the stress field. Taylor (1995) quantified the error as generally being less than 3 % for most geotechnical centrifuges if the level of acceleration is chosen at the radius R_e defined on Figure 4-3. This approach was adopted for all centrifuge tests reported.

Besides the error associated with the stress field along the centreline of the model, there is a further error induced in the stress field due to a lateral acceleration caused by the geometry of most centrifuges and the shape of the model containers. Centrifuges usually have a flat platform oriented perpendicular to the radius passing through its centroid. Researchers frequently use rectangular or cylindrical containers with a flat base and build models with a flat surface. During rotation of the centrifuge there will therefore be a component of lateral acceleration, the effect of which needs to be recognised. The radial acceleration varies with the radius and consequently there is an increased over-stress in the bottom corners of the model and a different stress gradient along the boundary of the container compared to the centre line. Taylor (1995) points out that for model containers of 200 mm half-width and an effective radius of 1.6 m the lateral acceleration is about 12.5% of the radial acceleration. For the tests conducted in this research programme, an effective radius of 1.5 m was used. Given the model half-width of 150 mm and an average model height of 440 mm this results in an lateral acceleration at the soil surface of approximately 11% of the radial acceleration. This error seems large at first but given the cylindrical shape of the strongbox it occurs only in a very limited area of the model. Furthermore, the pile is driven into the soil in the centre of the strongbox and the area of interest is therefore even less effected by this problem.

A further fundamental problem of centrifuge modelling is related to the effect of Coriolis acceleration which develops when there is movement of the model in the plane of rotation such as the horizontal movement of a base shaking earthquake simulator or the in-flight raining of sand to build an embankment. In the present study this error can only effect the movement of the particles around the pile during installation. The effect may be quantified using the relationship:

$$a_c = 2v_c\omega \tag{4.5}$$

where a_c is the Coriolis acceleration, v_c is the velocity of the particles in the radial direction (m/s) and ω the angular velocity of the centrifuge (rad/s). Taylor (1995) suggests that for relatively slow events where the velocity of the particles in the radial direction, v_c is less than $0.05\omega r$, the error is not significant. The maximum angular velocity induced during a 200-g test is 36 rad/s at a radius of 1.6 m this amounts to a velocity of around 2.9 m/s which is orders of

magnitude faster then the maximum speed of penetration of the pile of 0.5 mm/s. Thus for the present study any errors due to Coriolis acceleration can be considered insignificant.

With respect to the model to be developed for this project the following additional sources of error have to be assessed:

- Scaling effects due to grain size
- Proximity of boundaries
- Arching and friction inside the container
- Roughness of the pile surface
- Pile flexibility

The problem of *scaling effects due to grain size* is most significant if one attempts to model a certain prototype condition. According to the scaling laws described earlier the average grain size diameter of the soil in the model should be reduced by 1/N for correct representation of the prototype grain size. Therefore, a sand in the field with an average grain size, D_{50}, of 1 mm should be scaled in a 1:100 model to a D_{50} of 10μm. This particle size is already in the range of silt particles or of flour. As has been shown in the literature review, the behaviour of coarse grained soils depends on the stress level, the mineralogy, the average grain size as well as the grain size distribution. Reducing the grain size as indicated above would have a significant effect on the response of the soil. As this study is not primarily concerned with accurately reproducing a prototype condition it was decided to use sand particles as fine as possible and to use the same soil in the soil element tests as well as in the centrifuge model tests.

With regard to experiments on piles, the ratio between the pile diameter, d_p, and the mean particle size, D_{50}, can have an effect on the failure mechanisms and hence ultimately govern the behaviour of the pile. In addition the shaft resistance is significantly affected by changes in the ratio of the pile roughness to the average particle size. It has been shown by various researchers who have investigated the problem of grain size related errors in the centrifuge modelling of pile capacity problems (e.g. Ovesen, 1979), that for a ratio of d_p/D_{50} larger than 30, scaling effects due to particle size are negligible. For this study the average particle size was reduced as much as possible. The ratio d_p/D_{50} is around 90 for the Leighton Buzzard sand (LBS) and 65 for the Dogs Bay sand (DBS).

In recent years a number of authors have been investigating the *boundary effects* during pile or penetrometer tests in granular soils on the centrifuge (Phillips & Valsangkar, 1987; Corte et al., 1991; Gui, 1994; Fioravante et al., 1994; Renzi et al. 1994). Their observations varied depending on the soil type, the level of acceleration and the initial density of the soil.

Summarising these studies it can be concluded that a ratio of the distance, d_b, between the pile tip and the base of the container to the pile diameter, d_p, of greater than 10-12 eliminates boundary effects at the base of the container. A ratio of the distance from the side walls to the centre of the pile, d_w to d_p of greater than 5 will prevent boundary effects resulting from the side walls of the container. Based on this, ratios of $d_b/d_p \geq 5$ and $d_w/d_p \geq 10$ were chosen for the design of the strongbox. The decision to choose a smaller than recommended ratio of d_b/d_p can be justified on the grounds that the penetration depth could easily be decreased if boundary effects were found to occur.

The phenomenon of *arching and friction at the container boundaries* in model testing has been observed by a number of researchers. For example Chin & Poulos (1996) found that the stresses along the boundaries of their 1.4 m diameter CPT calibration chamber did not increase linearly with depth, nor was the stress distribution uniform across the base. They attributed the decrease of horizontal stress to friction on the side walls and held arching across the base to be responsible for the increased vertical stress in the corners of the container. However, it has been recognised that directly measuring total stresses in granular materials is very difficult since any deflection of the measuring device required to obtain a signal will automatically reduce the stress to be measured due to arching across the transducer. Lubrication of the container walls and encapsulation of the soil within a latex membrane similar to a triaxial test is good practice to reduce the effects of friction on the boundaries. However, if the in situ radial stresses along the container boundaries are to be measured, as was intended for this study, this technique becomes unsuitable. In any case, care must be taken to account for potential experimental errors resulting from friction and arching effects on the boundaries of the container.

Scaling the roughness of a relatively smooth prototype steel pile would require special polishing techniques to be used in centrifuge model testing. Rather than modelling an actual prototype pile the present study aims to establish a fundamental framework for the influence of the stress-volume state on the capacity of piles and therefore does not rely on an accurate scaling of details such as pile roughness. It is considered more important to conduct the tests at the appropriate stress level using a reasonably smooth pile surface and a small, but not too small, average grain size, thus allowing for a good contact ratio of particles along the pile and therefore a continuous response of the pile during loading. In addition, as described in Section 3.2, the average surface roughness of the model pile was measured and interface shear box tests were performed using metal interfaces of similar roughness, thus correctly modelling the pile-soil interaction along the shaft.

Murff (1980) showed that for very long piles the *pile-soil flexibility* has a significant effect on the pile capacity. Piles commonly used in offshore conditions have diameters up to 3.60 m and

can be over 100 m long. They are also open-ended. For the instrumented model pile, there are several constraints regarding the pile geometry. Firstly the pile must be large enough to accommodate the necessary transducers. Manufacturing and instrumentation must also be possible at moderate cost. The material chosen to build the pile must also be strong enough to sustain the high forces imposed while jacking it into the soil. For this research project is was therefore decided to use a pile of 16 mm diameter and 375 mm length. At a scaling factor N of 200 this is equivalent to a prototype of 3.2 m diameter and 75 m length. The pile is closed-ended and made in some parts from solid sections and in others from individual sleeves attached to a solid core. The pile flexibility is therefore somewhat different from an equivalent prototype pile.

4.1.3 Conversion from Model to Prototype Scale

When presenting results of centrifuge tests conducted at different accelerations it is helpful to convert the measured quantities such as in situ stresses, pile penetration and pile capacity to the prototype scale. This poses the question regarding the appropriate scaling factor to be used, since as discussed in Section 4.2.1 it varies with the radius. For this study the scaling factor was set according to the procedures described in Section 4.2.2 to be correct at 1/3 of the model depth measured from the top. As shown by Taylor (1995) the stress at any point in the model is given by:

$$\sigma_{vm} = \int_0^z \rho\omega^2 (R_t + z)dz = \rho\omega^2 z_m \left(R_t + \frac{z_m}{2} \right) \tag{4.6}$$

where z_m is the depth of the model measured from the top and R_t the radius from the centre of the centrifuge to the top of the model. This relationship was used to determine the in situ vertical stress in the equivalent prototype for a given depth in the model.

Owing to the stress gradient in the model there is a possibility that an initially homogeneous model might compress to some non-uniform density profile at the target g-level. This in turn will affect the stress calculation in Equation (4.6). For the present study the settlement of the soil was monitored at four different depths during the test thus allowing the density to be determined for four discrete layers of soil. The effect of inhomogeneity of density with depth will be discussed further in Chapter 5.

The current penetration depth scales by 1/N as it is a quantity of length. Following the argument presented for the stress calculation the variation of scaling factor with depth was also considered for converting the pile penetration from model to the prototype scale. Using Equations 4.3 and 4.6 and solving for the prototype height, h_p gives:

$$h_p = \frac{\omega^2 z_m}{g}\left(R_t + \frac{z_m}{2}\right) \tag{4.7}$$

This is then the appropriate relationship for converting the model dimensions to the prototype scale. Equation 4.7 can be expressed in terms of the scaling factor, N, for each centrifuge test at the radius R_e by substituting Equation 4.2 into Equation 4.1 and further substituting the new expression into Equation 4.7:

$$h_p = \frac{Nz}{R_e}\left(R_e + \frac{z}{2} - \frac{h_m}{3}\right) \tag{4.8}$$

Equation 4.8 has been used for all conversions of model depth and pile penetration to the prototype scale, as discussed in Chapter 5. For the prototype pile capacities presented at prototype scale the scaling relationship $1/N^2$ from Table 4-1 was used.

Centrifuge model tests, or physical model tests in general, can only be successful if the experimenter is aware of the errors associated with the testing techniques employed. The potential sources of error identified as well as the dissimilarities between model and prototype condition which were highlighted in this section will therefore be considered carefully while analysing the results from the model tests before extrapolating them to prototype conditions.

4.2 Equipment

For the present study a new centrifuge model was developed with the aim to maximise the penetration depth of the model pile for the given the geometrical restraints of the centrifuge. Both the centrifuge facilities at City University as well as all the steps involved in designing and commissioning the centrifuge model will be described.

4.2.1 Centrifuge Facilities at City University

The London Geotechnical Centrifuge Centre at City University was established in 1989 and is equipped with a purpose built Acutronic 661 geotechnical centrifuge. Since commissioning, the system has been upgraded a number of times, including the replacement of the slip rings and data acquisition system. The main characteristics of this centrifuge are described in detail by Schofield & Taylor (1988). The more recent modifications, including the 2D and 3D image analysis capability are described by Grant (1998). The following therefore gives only a brief

introduction of the main features of the centrifuge facility. Its current configuration is shown schematically in Figure 4-4.

The centrifuge has a radius between the centre point and the swing platform, during flight, of 1.8 m. The capacity of the centrifuge is 40 g-tons and it can achieve a maximum angular velocity of 345 rpm. A dead weight which is guided and positionable on a continuous thread acts as counterweight to balance the payload during flight. The system shuts down automatically if the out-off-balance cells mounted in the frame of the centrifuge base register, on average, measures more than 15 kN. In the tests reported, the average out-off-balance force monitored rarely exceeded 5 kN.

To increase aerodynamic performance the platform is protected with an aerodynamic shield and the centrifuge is contained within an aerodynamic shell. There is no air-conditioning available, but water supplied from a hydraulic slip ring can be evaporated in the centrifuge chamber and this was found to stabilise the temperature during long-term tests. This feature will be discussed in more detail in Section 5.2.3. For safety reasons the whole centrifuge is enclosed in a protective barrier consisting of 0.8 m thick sandwiched reinforced concrete walls.

The signals from the data control room as well as power and excitation for the instrumentation and signal feedback are transferred to the swing through slip rings above the rotor arm on the axis of the centrifuge. There are 130 electrical and 5 fluid slip rings, the latter having a capacity of 5 bar. Sixty-four of the electrical slip rings are used for transducer signal transmission; the others for power supply, CCTV or to trigger solenoid valves. There is also an RS232 link to an amplifier control rack that drives a two-axis actuator used for low capacity model tests such as penetrometers or shallow foundations.

The new data acquisition system, installed in 1995, features onboard signal amplification for the 64 data-logging channels using a variable gain of up to 1000. Power to the transducers can be supplied at 3 to 10 V and the output range for the signals from the transducers after amplification is ± 5 V. The amplifier unit is located close to the centrifuge axis together with an on-board PC, converting the analogue transducer signals to digital. It employs a multiplexing technique to transfer the data through the slip rings as a continuous data stream. The range of ± 5 V is converted to 2^{16} bits resulting in a theoretical resolution of 0.15 mV/bit. The noise level in general operation is approximately ± 1 bit. The rate of screening the required set of data channels can be specified within a range of 1 to 300 s. The data-logging PC is located in the remote control room outside the centrifuge containment. The data-logging software allows test data to be displayed in real time either numerically or graphically. The data are then stored in ASCII file format for subsequent analysis.

4.2.2 Development of a New Pile Driving Actuator and Strongbox

The study of the behaviour of driven piles over a considerable depth requires a high acceleration. For example, at 200-g a 400 mm model pile would be equivalent to a prototype pile of 80 m in length, a pile length frequently used in off-shore applications. This in turn results in high forces required to push the pile into the soil during flight, a procedure necessary to achieve similarity in stress condition between model and prototype (Craig, 1988). In order to achieve the maximum penetration of 400 mm allowed by the geometry of centrifuge, and to cater for a design force of 50 kN, a new pile driving actuator had to be developed. This new device, shown schematically in Figure 4-5, can operate at up to 200-g and will be described in the following sections.

(a) Boundary Conditions for the Mechanical Design

There are several boundary conditions of either a geometrical or mechanical nature that have to be considered in the design process of any centrifuge equipment. The main conditions related to this research project are:

- Geometry of the centrifuge.
- Desired level of acceleration.
- Payload restrictions of the centrifuge.
- Soil type.
- Maximum pile driving resistance.
- Speed of pile penetration.
- Limits on the deformation of the experimental set-up.

The *geometrical boundary conditions* for the size of a model package are defined by dimensions of the platform and the centrifuge arm. The available volume above the platform, over its full area, is 700 x 500 x 500 mm. The maximum height of the model is limited to 960 mm and the volume at the maximum height to 200 x 350 x 960 mm. The aim in the design was to maximise the effective penetration to be as close as possible to 400 mm. In addition the actuator was designed for model pile diameters of between 10 mm and 30 mm, the smaller size being typical for centrifuge penetrometer probes.

For this research project a *maximum acceleration of 200-g* was chosen in order to create a sufficiently high stress field for modelling a variety of different prototype piles. For the Acutronic 661 centrifuge the *maximum permissible payload* at this acceleration is 200 kg, which includes the weight of the soil, the strongbox and the actuator.

The *type of soil* used has a very significant effect on the driving resistance. Depending on the hardness of the granular particles and their initial state in terms of stress and volume, the required penetration force may vary by orders of magnitude. For this study the LBS, consisting of rounded silica particles provided the greatest driving resistance. This soil has been used in many previous centrifuge model tests (e.g. Phillips & Valsangkar, 1987; Nunez et al., 1988a; and Springman et al., 1991).

The estimation of the *driving resistance* was based on published data of penetration tests considering stress level, average particle size, initial density, pile diameter and penetration depth. The most significant problem was that, to the author's knowledge, nobody has undertaken penetration tests in a centrifuge at 200-g over a depth of 400 mm. The penetration resistance had therefore to be extrapolated from published test data. This proved to be very difficult, since there were only limited similarities between the tests proposed for this research project and the configuration of the tests reported in the literature. As a result, the estimates of maximum driving resistance for the silica sand at the maximum acceleration ranged from 10 kN to 200 kN. A comparative investigation was carried out using static pile capacity formulae. The results obtained were in the order of 10 kN to 60 kN, depending on the method used. It was therefore concluded that an average value for the driving resistance should be taken for the design of the actuator. Since forces above 70 kN proved to be critical for the design of the driving system, the actuator was finally designed to allow for a maximum penetration resistance of 50 kN.

The effect of *penetration speed* on the pile or penetrometer resistance in coarse grained silicious soils has been investigated by Ferguson and Ko (1985), Phillips and Valsangkar (1987) as well as Corte et al. (1994). The penetration speeds ranged between 0.5 mm/s and 20 mm/s. It was observed that the penetration resistance was independent of the penetration speed. With respect to the design of the actuator the penetration time could therefore be optimised in terms of the test time required to push the 400 mm long pile into the soil. The time span had to be long enough to allow for sufficient data to be collected, but for practical reasons, not be too long either in order to minimise the effects of temperature change on the strain-gauged instrumentation. A range of design penetration speeds between 0.25 mm/s and 1 mm/s was therefore chosen, giving test times of between 6.5 minutes and 27 minutes.

Deformations of the actuator had to be limited in order to ensure sufficient accuracy of verticality of the pile during penetration and to prevent unnecessary friction or any other types of mechanical problem during operation. The maximum permissible deformation of the base plate of the actuator was chosen to be not greater than 0.5 mm.

(b) Design of the Driving System

There are many different arrangements that can be envisaged to drive a model pile into a box of sand during centrifuge operation. Devices similar to pile hammers, dropping a dead weight onto to top of the pile have been developed for example by Nunez et al. (1988a), Cyran et al. (1991) and by Zelikson et al. (1994). The more common designs uses either an electrical or hydraulic/pneumatic jacking system. Such devices have been developed for example by Sabagh (1984), Phillips & Valsangkar (1987), Fioravante et al. (1994) and Yet et al. (1994). After evaluating carefully all the advantages and disadvantages of the different systems (Klotz, 1998) the electrically driven screw type was selected.

The driving system shown in Figure 4-1 consists of the following main components: a servo-controlled motor to allow remote operation, a gear box to increase the motor torque and adjust the speed and a screw system to translate the rotary motion of the motor into a linear motion required for the pile. Figure 4-5 shows the fully assembled unit on top of the strongbox.

The ball screw selected for the actuator was 40 mm in diameter and had a 5 mm pitch and was driven via a set of three gears (100mm PCD) by the servo-controlled motor. The chosen design force of 50 kN required a drive-unit capable of delivering a torque of 44 Nm. A pancake shaped servo disc motor, type U9D-D, of 0.53 Nm average torque was selected connecting to a 1:160 ratio Harmonic Drive gearbox of a zero backlash type (model HFUC-2UH-20). This unit has a continuous output torque of 51 Nm assuming a 60 % efficiency of the gearbox. The 100 line encoder fitted to the end of the motor shaft gives 400 quadcounts output per input revolution which converts to 5,120,000 counts over the stroke of the actuator of 400 m. This allows very accurate positioning of the pile. The driving speed can be varied between 0.05 and 0.8 mm/s. To prevent the crosshead linking the pile to the ball screw from rotating two fixed shafts made of 20 mm diameter case hardened steel and of are used, the crosshead being guided by two FRELON-Bushings.

The drive unit is connected to a controller mounted near the centre of the centrifuge which houses the power supply unit, servo amplifier as well as the two axis programmable motion controller (type EuroServo/3). The controller can be programmed using any IBM or compatible PC via an RS232 communication line. A series of programs for the controller were written in the programming language MINT (Motion INTerpreter) which essentially is a modified version of BASIC. The drive unit including the motor, gearbox, controller and control software was supplied by Heason Technologies Group, Chichester.

(c) Design of the Actuator Housing and the Strongbox

Following the selection of the mechanical components for the driving system, the actuator housing and the strongbox could finally be designed. Given the available dimensions for models on the centrifuge, the strongbox was designed in a cylindrical shape with an external height of 469 mm and an internal diameter of 300 mm. This allows placing a 439 mm thick layer of soil while keeping a clearance of 20 mm at the top. The available height for the actuator is therefore 491 mm. Assuming 12.5 mm thick plates for the housing, a height of the gears and the bearings for the ball screw of about 32 mm and the height of the ballnut of 56 mm yields an effective stroke of the actuator of 378 mm. A clearance between the pile tip and the soil surface of 5 mm before the test then yields a maximum penetration depth of 373 mm which is close to the 400 mm originally envisaged. At 200-g this is equivalent to a prototype pile length of 74.6 m. The axis of the pile is positioned on the centreline of the strongbox.

Criteria such as sufficient strength, rigidity, minimum weight and corrosion resistance are important for selecting the most suitable material to manufacture the centrifuge modelling hardware. It was decided to use high strength aluminium for the side walls of the actuator and high strength stainless steel for its base plate. The strongbox was divided into two parts. A circular stainless steel tube forms the side walls to achieve maximum rigidity with an aluminium base plate in order to minimise the weight. The mechanical properties of the materials used for the actuator and the strongbox are summarised Table 4-2.

The structural analysis of the actuator comprised simple calculations using beam equations as well as more sophisticated 3D finite element analyses in order to model the behaviour of the actuator housing and the crosshead in the centrifuge at 200-g (Klotz, 1998). The circular tube section used for the side walls of the strongbox has a wall thickness of 8 mm. Based on "Hoop Stress Theory" the required thickness for the stresses generated at the maximum acceleration was only 1.6 mm. However, the thickness was increased to 8 mm to limit the deformations. The circumferential strains were estimated to be less than 0.02%. A solid rectangular flange was welded to the top of the tube to provide additional stiffness and to act as a mounting platform for the actuator.

Instrumenting the actuator and the strongbox was of major concern in the design process. Limit switches are provided at both ends of the mechanical stroke of the actuator. In addition, the actuator is fitted with two linear potentiometers, model CFL400 supplied by Techni Measure, Studley. They have an electrical stroke of 400 mm and a resistance of between 5 kΩ and 20 kΩ and operate on a 5 Volt power supply. The use of two potentiometers was to prove very valuable as one of the transducers occasionally malfunctioned. The strongbox is fitted with

three series of five circular steel plates each 20 mm thick and placed at equal spacings vertically along the side wall of the strongbox. These allow further instrumentation such as stress transducers or pore pressure transducers to be mounted if required. The base plate of the strongbox is fitted with two drainage holes to allow for partially saturated or saturated test conditions, again if required.

This section has provided an overview of the development of a new single axis actuator and a strongbox. For further details on the design process for the actuator and strongbox assembly, as well as technical details of the individual components, the reader is referred to Klotz (1997 and 1998). The development of the actuator started in February 1997 and the fully assembled prototype was first tested on the centrifuge in November 1997. Figure 4-6 shows the fully assembled strongbox and actuator unit on the centrifuge platform.

4.2.3 Development of the City University Instrumented Model Pile (CUIMP)

In this section the various model piles built for this research project will be described. The model piles developed, for example by de Nicola and Randolph (1993) and Fioravante et al. (1994) were successfully jacked into the sands at accelerations of between 30 and 100-g. To the authors knowledge nobody has to date undertaken centrifuge model tests on instrumented model piles pushed into silica sands at 200-g. The aim of the design was to develop a pile system offering some degree of redundancy and sufficient robustness suitable for the harsh testing environment.

The development of the instrumented model pile comprised the following four steps:

- Development of CUIMP-1, a solid pile with one global load cell
- Development of CUIMP-2, housing ten transducers
- Modification of the model pile, CUIMP-2, leading to CUIMP-3
- Production of a new pile CUIMP-4 based on CUIMP-3

(a) Development of CUIMP-1

As discussed in Section 4.2.2 (a) some difficulties were anticipated with respect to the range of mobilised pile resistance for the variety of g-levels and soil types used in this study. It was therefore decided to use a simple solid pile, CUIMP-1, connected to a global load cell in order to establish the magnitude of base and shaft resistances before embarking on the development of the fully instrumented version. The solid model pile was built in two sections from a 5/8'' diameter rod of high strength stainless steel. The flat tip of the pile can be replaced by a conical pile tip for modelling a penetrometer.

(b) Development of CUIMP-2

The development of model pile CUIMP-2 was based on the results from the tests performed with CUIMP-1. The data from test LBS-1 conducted at 100-g suggested that the maximum force required to push the pile into a sample of dense LBS at 200-g was likely to be as high as 40 kN. Allowing for a total shaft friction deduced from the tension test of 10 kN, the base load transducer could be subjected to a force of up to 30 kN

The predictions of the shaft friction distribution and the magnitude of radial stress along the pile proved difficult. For simplicity it was assumed that the unit shaft friction would increase linearly with depth. The length of the different friction sleeves was then adjusted to give a similar magnitude of transducer output. In order obtain some redundancy in the system it was considered necessary to have at least five friction sleeves and similar number of radial stress transducers placed along the pile shaft. This led to the final design of the pile shown in Figure 4-7 that features one base force transducer (BFT), five shaft friction sleeves (SRT) and four radial stress transducers (RST). In total the pile consists of 15 individual components. A summary of the materials used for the piles and their properties is given in Table 4-2. The geometry and position of the individual transducers is summarised in Table 4-3.

Given the high base force it was decided to uncouple the BFT from the SRTs and in addition to separate each shaft friction section. This approach is significantly different from previous designs of instrumented piles (e.g. de Nicola & Randolph, 1993 and Fioravante et al., 1994) and should allow better quality test data to be obtained as the force measured at the base is not transmitted through all the other transducers. A detail of the base section of the pile is shown in Figure 4-8. The chosen diameter of the pile of 16 mm meant that the base force needed to be transmitted over a 10 mm diameter section to allow for the wall thickness of the friction sleeve of 1.5 mm and a gap of 1.5 mm. For a base force of 40 kN this gives an axial stress of 610 MPa which is far in excess of the yield stress of mild steel. It was therefore decided to use titanium Ti-6.4 as material for the pile core. The gap between the friction sleeve and the core section provided protection for the strain gauges for the BFT which were bonded to the core on opposite sides, close to the pile tip.

The anticipated stress level in the SRTs was in the order of 70 MPa at full-scale and allowed the use of an aluminium-alloy. A detail of a typical sleeve section is shown in Figure 4-8. The sleeve is attached to the core section at the top by means of a short M12 thread. The gap of 1.5 mm between the core and the sleeve allows the reminder of the sleeve to compress freely as the pile is pushed into the soil. Four flats are provided at the top of each sleeve to accommodate both the strain gauges and the terminals for balancing the strain gauge circuits. The strain

gauges, which are bonded onto flats on opposite sides register the accumulated force along the active length of each sleeve. The reduction in cross sectional area at the location of the gauges also increases the sensitivity. After the gauges had been placed they were covered with a layer of epoxy resin which was then trimmed to the correct pile diameter.

The RSTs shown in Figure 4-9 were designed in a dog bone or dumb-bell shape and inserted into 9 mm diameter holes drilled through the pile core. This design was chosen in response to the tests reported by Standing (1997). His segmental beam type sections measured the radial stress in three locations along an 8 mm diameter nail in a calibration chamber. Standing (1997) encountered severe problems with his original design, that he subsequently abandoned. The final design still showed unsatisfactory behaviour such as unacceptable non-linearity and hysteresis. The design of the new instrumented pile is unique compared to previous instrumented piles for centrifuge tests (e.g. de Nicola & Randolph, 1993 and Fioravante et al., 1994) in that none of these designs included radial stress transducers.

The RSTs are made from a solid rod of aluminium that is first turned to the final outer dimensions. The outside diameter at the ends is just under 9 mm, and 6.2 mm in the centre section. A 5.2 mm hole was then drilled through the centre, reducing the wall thickness to just 0.5 mm, which was required for good sensitivity. The ends of the hole were then blocked and the ends of the transducer turned to match the circumference of the pile. A small hole is provided at the top of the dumb-bell for the electrical lead wires. A locating pin prevents the transducer from rotating. The strain gauges were bonded onto the outside of the hollow cylinder, in the centre and on opposite sides. These parts were extremely difficult to machine and strain gauging was also a major challenge.

The next steps in the development were the design of the individual transducers, the selection of the most suitable configuration of the strain gauge circuits, consideration of bridge balance and temperature compensation, and finally the design of a suitable wiring scheme given the very limited space available. These are discussed under the following separate headings.

(c) Strain Gauge Selection and Excitation Voltage for CUIMP-2

The use of semiconductor strain gauges was ruled out due to the fact that the gauges for the RSTs and BFT had to be bonded onto curved surfaces. In addition there is far more flexibility in using foil gauges so far as gauge sizes, backing material and resistance are concerned. Furthermore the supplier of the gauges, Measurements Group UK, offered a full bonding service despite the anticipated difficulties caused by the curved surfaces and geometrical constraints. The strain gauges selected were transducer class T-rosettes type N2A-13-S064L-350, with a gauge factor of two (Measurements Group, 1992). They were arranged as full

Wheatstone bridge circuits in order to enhance the sensitivity and provide compensation for temperature (Measurements Group, 1998). The T-rosettes were placed on opposite sides of each transducer to cancel the effects of any potential eccentricity of load. In order to reduce the power consumption and so the amount of heat dissipated by the strain gauges, a gauge resistance of 350 Ω in combination with a power supply of 3 Volts was chosen.

The output, V_{out}, of a strain-gauged transducer is given by:

$$V_{out} = \frac{G_f V_{in} \varepsilon N_a}{4} \tag{4.9}$$

where G_f is the gauge factor, V_{in} is the bridge excitation in Volts, ε is the strain in the spring element in microstrain, and N_a the number of active arms in the bridge. The chosen full bridge configuration has four active arms. The anticipated full-scale outputs calculated from Equation 4.9 for each transducer on CUIMP-2 to CUIMP-4 are summarised in Table 4-4. With the exception of the BFT the full-scale strain level in the spring element is less than the 1700 με recommended by leading manufacturers (e.g. Measurements Group, 1998). The output signals were therefore amplified on the centrifuge using a gain of 1000. The maximum strain level of the base force transducer is within the limit of 5000 με specified by Göpel et al. (1994) for foil gauges subjected to a limited number of load cycles.

(d) Wiring Scheme for CUIMP-2

Each transducer on the pile is connected with four wires: two supply the power to the bridge circuit and the other two transmit the output signal. To allow for redundancy it was decided to use individual power supply lines for each transducer instead of a common power rail. This meant a total of forty wires had to be accommodated. As the centre section is subjected to very high stresses and could not be weakened further, the only option left was to route the wires along the outside of the pile. The aim was not to increase the pile diameter by applying an additional coating for wire protection (e.g. de Nicola & Randolph, 1993) as this would have caused problems with the radial stress transducers. Therefore the wires were routed through four channels slotted into the skin of the pile all the way from the tip to the top. This arrangement is shown in Figure 4-10. The rectangular channels were 0.75 mm deep and 2 mm wide and each accommodated up to twelve wires. This meant that the only type of wire that could be used was a single strand 0.16 mm diameter copper wire coated with polyimide enamel. Additional channels of similar dimensions were created around the circumference at the top of each friction sleeve to allow the routing of the interconnecting bridge wires. All lead wires are connected to a terminal at the top of the pile. From there onwards 0.254 mm diameter stranded tinned copper

wires insulated with vinyl were used and soldered to a forty pin connector attached to the crosshead of the actuator. The arrangement is shown in Figure 4-11.

(e) Assembly of CUIMP-2

A picture of the fully assembled pile is shown in Figure 4-12. The individual parts of the pile were manufactured in the workshop of the GERC. The core sections and friction sleeves were first assembled starting from the tip. At this stage the holes for the RSTs were drilled and all the channels for the wires as well as the flats for the strain gauges on the friction sleeves were cut. The base section was then taken off again to allow the strain gauges to be placed.

Strain gauging of the pile, balancing of the bridges, compensation for temperature effects as well as wiring the transducers was carried out by Measurements Group UK, in Basingstoke. The RSTs were both strain-gauged and temperature compensated outside the pile and then subsequently pushed into place. The gaps between the RSTs and the pile were filled with the elastic compound M-Bond-600. The terminal connector was then fitted and all the channels and flats filled with an epoxy resin compound consisting of the resin MY750 and the hardener HY951 mixed at a mass ratio of 10:1. This material though originally quite viscous cures within 24 hours and is then extremely hard providing sufficient protection for the wires and strain gauges on the pile. It reached a yield strength of 120 MPa and had a Young's Modulus of around 4 GPa. The entrance of the gap between the friction sleeves and the core section was filled with an elastic silicone compound to prevent entrapment of sand particles during pile installation. Finally all excess resin and silicone was carefully removed and the pile was then ready for calibration.

(f) Modifications to CUIMP-2 Leading to CUIMP-3 and CUIMP-4

Following the calibration of the pile and a series of preliminary tests in the centrifuge, the design of CUIMP-2 was slightly modified resulting in CUIMP-3. One point of concern was the wire terminal at the top, which proved too weak, as wires became disconnected during operation of the centrifuge. It was decided to reduce the pile diameter in this area by 1.5 mm over a length of 30 mm and route the wires in different way.

A second point of weakness was the connection of the lead wires to the RSTs. On exiting the RST the wires need to be bent by 90 degrees to fit into the lead wire channel. The edges were found to be too sharp and were cutting through the insulation of the wires leading to shorts in the transducer circuit. This problem occurred on two out of four RSTs on CUIMP-2. To improve the situation the diameter of the holes was increased and counter-sunk on the outside. Additionally, all the corners were carefully rounded.

Following the calibration of CUIMP-2 a strong cross-sensitivity between the base force transmitted through the core and the output of the SRTs was observed. This could partially be explained by the possibility that the wire channels filled with epoxy resin transmitted some force. However, the magnitude of cross-sensitivity seemed to vary for the different sleeves. One other possible cause was thought to lay in the proximity of the strain gauges on the sleeves to the point connecting the sleeve and core. Therefore, the locations of the strain gauges on the sleeves of CIUMP-3 and CUIMP-4 were lowered by 5 mm. The new positions of the transducers are given in Table 4-3.

A further problem was the chosen wiring scheme for the BFT. Originally the lead wires were left long enough and just routed around the tip of the friction sleeve into the appropriate channel. During calibration of the RSTs on CUIMP-3 the base section started to move as the pile had to be twisted to remove it from the calibration chamber. At this point one of the lead wires broke. To overcome this problem a slot was machined into the sleeve above the terminal strip of the BFT. This provided access to the terminal and allowed the wire the be reconnected. The slot was then covered with a small plate. The arrangement is shown in detail in Figure 4-13.

The implementation of all these rather small changes increased the pile reliability dramatically. In particular the final pile, CUIMP-4, performed in an outstanding way. It seemed that all those involved in the design, manufacturing and strain gauging of the pile improved the quality of their work from one pile to the next thus allowing the experimental programme of pile tests to be completed successfully.

4.2.4 Additional Instumentation of the Centrifuge Model

Additional instrumentation of the centrifuge model included a load cell attached to the top of the model pile, three Linearly Variable Differential Transformers (LVDTs) measuring the soil settlement and three temperature sensors. The locations of these transducers are illustrated in Figure 4-1. Their technical details are summarised in Table 4-5.

A purpose built compression-tension load cell of 50 kN capacity was connected to the top of the pile and was supplied by Applied Measurements Ltd., Aldermaston. It is a solid cylinder type transducer instrumented with conventional foil strain gauges connected in a full Wheatstone bridge. The sensitivity is 1.617 mV/V resulting in a full-scale output of 16.17 mV for the 10 V supply voltage chosen. The non-linearity and hysteresis errors, as a percentage of the full-scale output, are less than 0.012 % and 0.006 % respectively. The first device manufactured (Serial number 115546) did not satisfy the specifications with respect to the alignment of the main axis. The longer section connecting to the crosshead was slightly bent leading to an eccentricity at the

pile tip of about 5 mm. A technically identical new load cell (Serial number 15832) was therefore supplied which in Table 4-8 to 4-11 is referred to as the "new load cell". The shaft of the old load cell was bent back until the eccentricity was less than 1.7 mm. This load cell then called the "old load cell" and was also used for a number of pile tests as the performance of the transducer was not affected by the bending operation. Depending on the expected maximum force for each test the amplifier was set to either 500 or 1000 gain.

Two different types of LVDTs were used depending on the expected settlement. For highly compressible samples (e.g. loose DBS) ±15 mm stroke LVDTs were used with ±5 mm stroke LVDTs for the less compressible samples. Both transducer types were manufactured by Schlumberger and supplied by RS Components Ltd. They have an output of ±3.5 V at the limits of their displacement range. Due to this high output voltage and the expected displacements the transducer signals were not amplified. The core of each of the LVDTs was attached to an M2 threaded rod which had a 20 mm diameter plastic disc screwed onto its tip to reduce the bearing pressure, thus preventing the rod from penetrating the soil under its own weight. The rods were surrounded by 3 mm ID perspex tubes supporting the soil, thus allowing the rod to move freely. This ensured that only the displacement of the tip of the rod was measured and the measurement was not affected by the compression of the adjacent soil. The position of each LVDT is shown in Figure 4-1.

Both types of temperature sensors were supplied by RS Components Ltd. For the early Tests (CLBS-9 to CLBS-13 and CDBS-2 to CDBS-6) low cost temperature sensors of a three pin integrated circuit type (model LM-35 CZ) were used. These have an accuracy at 25 °C of ±0.4 °C and a sensitivity of 10 mV/ °C for a 10 V power supply. Unfortunately they responded rather slowly to changes in temperature and were difficult to calibrate. From tests CLBS-14 and CDBS-7 onwards they were replaced by platinum resistance temperature sensors. The sensing element of type Pt 100 which operates on a 10 V power supply is inserted into the tip of a 3 mm diameter, 100 mm long stainless steel probe. The accuracy of these probes is better than ±0.06 °C at 0 °C. Two of the sensors were integrated into the side walls of the strongbox thus measuring the temperature in the soil. The third one was attached to the actuator as shown in Figure 4-1. The output signal of these temperature sensors was amplified by a gain of 10.

4.3 Procedures

This section deals with the procedures and experimental techniques used for the centrifuge model tests in this study. Performing centrifuge model tests is a very complex and difficult task that requires great care as each task is critical to the success of the test. In order to highlight the

individual steps involved this section is divided into three subsections. Firstly the procedures and results of the calibrations of the transducers are described. This is followed by details of the adopted sample preparation methods. Finally the testing procedures employed for the different centrifuge tests are introduced.

4.3.1 Calibration of the Transducers

One basic assumption in centrifuge model testing regarding the transducers is that a calibration performed at 1-g does not change during the test regardless of the level of acceleration. Generally, it is important that the transducers used during centrifuge testing are calibrated in the appropriate data-logging channels on the centrifuge and not with any other source of amplification or signal conditioning. In general, the calibration procedure followed similar procedures as outlined in Chapter 3 on triaxial testing. The transducers were powered up for at least three to four hours prior to calibration to allow the temperature of the gauge circuits to reach a stable condition; for the model pile this period was extended to twelve hours. Calibrating the instrumented model piles was by far the most time consuming calibration exercise and will therefore be discussed in some detail. The accuracies of the transducers as well as the accuracy of the calibrations are summarised in Table 4-5 for the additional instrumentation and in Table 4-6 for the model piles.

(a) Linear Potentiometers

These two devices were calibrated only once before they were mounted in the actuator and connected to the crosshead. The potentiometers were clamped to a plate and a steel ruler used to apply incremental displacements of 20 mm in both directions. The sensitivity of the potentiometers is 82 bits/mm. Given the noise level of the centrifuge data-logging system of about ±1 bit, displacements as little as 0.02 mm can be resolved. The accuracy of the calibration is about 0.1%, which over the maximum penetration depths of 350 mm results in an error of the order of 0.4 mm, equivalent to about 8 cm at prototype scale for an acceleration of 200-g. The calibration was regularly checked by moving the crosshead over a certain distance and comparing the manually measured displacement with the output of the potentiometers. The agreement was always within ±0.1 mm.

(b) Global Load Cell UCE-50 kN

The 50 kN compression-tension load cells were calibrated over their full range in compression using the Budenberg device shown in Figure 4-14. The oil pressure in the system is adjusted manually by turning the wheel until it is equal to the pressure required in the piston to lift an assembly of steel discs of known mass. This pressure is simultaneously applied to the load cell mounted on another piston. As the area of the hydraulic piston is known the applied force can

be calculated. A correction for the weight of the Budenberg piston and the load cell is required in order to obtain the force truly applied. For the calibration in tension a different apparatus was used. The load cell was attached to the short end of a lever arm assembly (50 mm long) and a maximum force of 14 kN applied by adding up to 129 kg mass to a hanger on the other side (560 mm long). The output of both load cells was found to be very linear and repeatable in both tension and compression. A typical calibration record is shown in Figure 4-15. The accuracy of the calibration was better than 0.5 % of the current reading. The load cells were re-calibrated twice confirming that the calibration was repeatable.

(c) LVDTs

Both types of LVDTs were calibrated individually over their full range in steps of 2 to 4 mm using a screw micrometer attached to a specially designed clamping block. The accuracy of the calibration is about 0.1%. In addition to calibrating each LVDT the whole LVDT system was calibrated in the centrifuge in order to investigate the amount of deflection of the rods and the LVDT rack at various g-levels. This was thought necessary since the transducers could not simply be re-zeroed at the target g-level, a practice commonly adopted in centrifuge tests (e.g. Grant, 1998). It was observed that there was not just relative movement between of the cores and the LVDT body, but that the LVDTs themselves were "settling in" as the g-level increased. It was concluded that the overall accuracy of the measured displacements of the LVDT system at 200-g is of the order of ±0.2 mm.

(d) Temperature Sensors

The temperature probes were calibrated in a water bath over a range of 0 to 80 °C. Two conventional thermometers were employed to monitor the water temperature. This fairly crude method resulted in a calibration accurate to about ±2.0%.

(e) Model Piles CUMP-2 to CUIMP-4

Following the strain gauging of the pile, the bridges were balanced to better than ±0.05mV/V and then compensated for temperature effects between 10-40°C to better than ±0.1μV/V/°C. Subsequently each transducer was calibrated over the anticipated stress range.

The base force transducer (BFT) was only calibrated in compression between 0 to 10 kN using the Budenberg device. A picture of this set-up is shown in Figure 4-14. The effect of any possible eccentricity on the calibration was investigated by turning the pile through 90° and repeating the same load cycle. The difference in output was less than ±0.02%. The calibration was generally very linear and repeatable reaching an accuracy of better than ±1% of the current reading. A typical calibration record for CUIMP-3 is shown in Figure 4-16. During the calibration of the BFT it was discovered that the friction sleeves were cross sensitive to the base

load. Interestingly there was no such sign for the radial stress transducers. The effects of cross-sensitivity on the output of the individual transducers will be discussed separately in Chapter 5.

The Budenberg device was again used to calibrate the shaft resistance transducers (SRTs) over a range of 0 to 1000 N. For this exercise the device had to be modified to allow the force to be applied with two brackets that could fit into the gap between the friction sleeve and the core section. The set-up is illustrated in Figure 4-17. Three load cycles were applied prior to the actual calibration to crack the contacts in the epoxy resin covering the lead wire channels and any epoxy connecting the sleeve to the core section. Four calibration cycles were subsequently performed. Generally some hysteresis was observed in the friction sleeve output during the calibration leading to an accuracy of the order of ±15 % of the current reading.

SRT-1 was calibrated on both axes, the more sensitive axis "in line" with the strain gauges and then at 90° in the less sensitive direction. The observed difference in sensitivity is due to the relatively short length of the sleeve, insufficient to create a homogeneous strain field as the force is applied only at two discrete points around the circumference of the sleeve. This problem is illustrated in Figure 4-18 for a typical calibration record of SRT-1 on pile CUIMP-3. For the shortest friction sleeve, SRT-1, the difference in output between the two directions was about 45%. The average value between the two calibration constants was chosen and entered in the calibration file. Unfortunately, due to lack of space to place the brackets this procedure could not be applied to any of the remaining sleeves. These were consequently calibrated in the more sensitive direction only. To take into account the effect of inhomogeneity of strains, the calibration of each sleeve was adjusted proportionally to its length according to:

$$CF_{cor} = \frac{CF_{org}}{1 + \left(\frac{SPAN_{SRT-1}}{2}\right)\left(\frac{L_{SRT-1}}{L_{SRT}}\right)} \tag{4.10}$$

where CF_{cor} is the corrected calibration factor of the sleeve that is calibrated, CF_{org} is the original calibration factor determined along the more sensitive axis, $SPAN_{SRT-1}$ is the difference between the calibration factors of SRT-1 for the more and less sensitive axes, L_{SRT-1} is the length of SRT-1 and L_{SRT} the length of the friction sleeve under consideration. The correction was in the order of 20% for the next shortest sleeve (SRT-2) and about 5% for the longest sleeve (SRT-5).

The observed effect of cross-sensitivity between the friction sleeve calibrated and the readings from friction sleeves located above its position on the pile was identical to that observed for the BFT. Additionally, the calibration of the radial stress transducers revealed a cross-sensitivity of

the friction sleeves to radial stress. The magnitude and methods of correcting for these cross-sensitivities will be discussed separately in Chapter 5.2.6. Fortunately, there was no cross-sensitivity of the RSTs to axial load.

All radial stress transducers (RSTs) were calibrated simultaneously in a purposed built calibration chamber which is shown in Figure 4-19. The chamber consisted of a 400 mm long, 27 mm diameter thick, walled steel tube connected to the pressure outlet of the Budenberg device. The pile was covered with a thin sleeve of low temperature heat shrink and inserted through the O-ring seal from one end. Before pushing the pile through to the second O-ring seal the chamber was filled with hydraulic oil. The pile was then pushed through the O-ring to its final position, thus sealing the chamber. The pressure for the original calibration was applied over a range of 0-1000 kPa.

As can be observed from the typical calibration records for CUIMP-3, shown in Figure 4-20, the calibrations are fairly linear over the full range and the accuracy at pressures above 400 kPa is of the order of ±5% for RST-1, RST-2 and RST-3, and ±15% for RST-4 owing to the more significant hysteresis of this transducer. The cause of this hysteresis of RST-4 is not clear, but is most likely due to a defect of the transducer as it was not observed for RST-4 on CUIMP-4. For the latter transducer the accuracy was also within ±5% of the current reading. On closer inspection a slight non-linearity is revealed at the beginning of the calibration between 0 and 400 kPa. This issue will be discussed in more detail in Chapter 5. As the data acquisition software did not allow for non-linear calibration coefficients a linear calibration was assumed for the tests and any non-linearity was taken into account in the subsequent analysis of the test data.

In addition to calibrating the individual transducers the effect of temperature changes and the operation of the actuator on the output signals, as well as the change in signals over time, were investigated. However, it was considered more appropriate to study these effects under increased gravity as would be the case during a centrifuge test and these aspects will be discussed further in Chapter 5. Following the calibration of the transducers on the model pile, the gaps between the friction sleeves and the core sections were re-filled with silicone sealant. The pile was then carefully cleaned and connected to the load cell ready for testing.

4.3.2 Sample Preparation

All samples for the data presented here were prepared using dry condition. Prior to placing the sand in the strongbox the temperature sensors and the LVDT-rods were installed and the

package weighed to the nearest 0.1 kg. The set-up is illustrated in Figure 4-21. Particular methods were developed for each sand type to obtain the required densities.

The first dense samples of LBS (CLBS-1 and CLBS-4) were prepared on a shaking table with no surcharge. This did not allow accurate control of the final density and the application of this procedure was consequently restricted to the preliminary tests with CUIMP-1. From test CLBS-13 onwards a raining system was introduced. This device, illustrated in Figure 4-22, has previously been used by other researchers at the GERC and was described by Grant (1998). A conical piece of Styrofoam coated with tape was placed at the top flange of the box to deflect the sand. The sand was rained at a very slow flow rate of around 3.0E-5 m3/s in order to minimise the effect of air entrapment in the box (Azouri, 1998). The raining of one sample took almost 30 minutes.

The loose samples of LBS were prepared by air pluviation with a minimum constant drop height. The set-up for this method is shown in Figure 4-23. The barrel at the top of the fork-lift acted as a reservoir containing sufficient soil for one sample. The forklift was then raised slowly at a speed similar to that of the rising soil surface. The soil passed through the pipe and a series of sieves at the outlet before reaching the strongbox. The tip of the pipe was moved in a circular fashion allowing the sand surface to rise evenly until reaching the top. This procedure is similar to the method described in BS 1377 and is known to produce very loose samples.

Prior to the first test on DBS, the soil was reconstituted to the grading specified in Section 3.1.2 and mixed thoroughly in an industrial mixer shown in Figure 4-24. The method developed for preparation of the loose samples of LBS was found to be not suitable for the loose samples of DBS. Owing to the larger band of particle sizes and their angular shape there was a degree of segregation of different particle sizes. The soil was therefore placed manually after mixing using a medium sized beaker. Although this may sound primitive and prone to human error, resulting in non-uniform samples and a larger scatter of densities, the pattern of driving resistance observed in these tests was very satisfactory and consistent with the other tests.

The dense samples of DBS were created using a dry compaction technique. Originally the soil was placed in the strongbox in the same way as for the loose samples and the box filled to the top. After scraping the surface a wooden plate was placed on the surface and loaded with dead weights of 20 kg resulting in a surcharge of about 3 kPa. The box was then struck with a hammer until the soil settlement ceased under the given load. Subsequently the weights were removed and the box refilled. The dead weight was then increased to 37 kg or 6 kPa and the compaction continued until no further settlement occurred. This procedure is similar to a method described in DIN 18126 to produce dense samples. Samples of intermediate initial

density were originally prepared in a loose condition and then compacted using the method described above until the desired density was reached.

Two partially saturated samples (CLBS-9 and CLBS-10) were used during the preliminary testing stage with CUIMP-3. These were prepared in a dry condition and then saturated with distilled water from the bottom upward using the drainage lines provided in the base of the box (see Figure 4-1). On saturation the soil was allowed to drain to an equilibrium water content before placing the sample on the centrifuge swing. Further drainage occurred during the spin-up of the centrifuge.

The overconsolidated samples produced from both soils (CLBS-21, CDBS-13 and CDBS-14) were initially prepared in a loose condition. The strongbox was then placed under a computer controlled consolidation press (Grant, 1998) and a maximum vertical stress of 3 MPa applied. This arrangement is shown in Figure 4-25. The vertical stress and displacements were recorded manually during compression. By adding a known mass of soil and compressing to a predetermined sample height it was possible to achieve very similar initial densities of the overconsolidated samples compared to the denser compacted samples of either sand. The significance of this will be discussed in Chapter 5.

Following the placement of the sand the surface was flattened carefully without densifying the sample. This was best achieved by using a scraper and removing the excess soil with a low suction hoover. After completing the sample preparation procedure the package was weighed to the nearest 0.1 kg and carefully placed on the centrifuge platform. All settlements between sample preparation and placing the model on the swing were recorded and taken into account in the calculation of the initial specific volume.

4.3.3 Centrifuge Testing Procedures

This section is divide into three sub-sections which deal with the procedures adopted to perform the centrifuge tests. The first section covers the pre-testing procedures, the second the procedures during the tests and the third the post-testing procedures. Overall, setting up a sample and connecting all the transducers took between half a day and one day. The actual test duration depended on the chosen sequence and varied between one hour and four hours. The post-testing procedures, ignoring the time of data-analysis, took up to another 4 hours. Therefore up to three tests could have been performed each week but on average the more realistic frequency was about two tests per week.

(a) Pre-Testing Procedure

Following the preparation of the sample, the strongbox was carefully transferred to the centrifuge and placed on the swing. To achieve accurate positioning of the model for each test, the strongbox was attached to the centrifuge swing by four locating bolts. At this stage a steel ruler was used to determine the position of the soil surface relative to the top of the strongbox at different points to the nearest 0.2 mm. A pile guide was slid over the pile and the latter together with the load cell and connector terminal, were then attached to the crosshead. The crosshead was then moved to its highest position and the guide firmly pushed into the baseplate of the actuator. Before placing the actuator on top of the strongbox, the distance between the baseplate and the tip of the pile was measured in order to calculate the displacement necessary for the pile to touch the top of the soil. The actuator was securely fastened to the strongbox by means of five high tensile steel bolts.

The LVDT rack was placed and the LVDTs positioned at the upper end of their linear range. The temperature sensors were installed and all the transducers were then connected to the junction boxes and the appropriate gains set on the amplifiers. The actuator was connected to the power supply and controller and cables were securely tied to the centrifuge container and the swing.

A CCD camera (Grant, 1998), mounted on the aerodynamic shield and directed towards the ballscrew and gear system, was used to monitor the actuator during centrifuge operation. To enhance the quality of the image, three low energy lights were mounted in the vicinity of the model. Two pipes were connected to the hydraulic slip rings carrying water to be sprayed to allow the temperature to be kept constant during the test (Section 5.2.3). Finally, the counterweight was set to the distance required to balance the centrifuge. The set-up was then kept in this condition for at least two hours allowing the transducers to reach an equilibrium operating temperature.

(b) Procedures During the Centrifuge Tests

Following the set-up of the model, the calibration constants were entered in the data acquisition program and the effective radius and target g-level set in the centrifuge control program. The motor control program was started and the motor moved over a short distance to establish accurate response. At this stage the aerodynamic shell of the centrifuge was closed, the data-logging sequence started at an interval of 5 s and, following final safety checks, the centrifuge accelerated towards the target g-level. During spin-up the output of all transducers as well as the out-off-balance load cells were carefully monitored. After arriving at the target g-level the data-logger was restarted and all readings except the temperature sensors and the LVDTs re-zeroed. The output was then monitored over a period of 20 minutes to allow the transducers to stabilise

prior to the test. The actual test was performed in several stages which are described in detail in the next section. The data-logging interval during pile driving was set to 1s. After the crosshead had arrived back at the top, another resting period of about five minutes was allowed before the centrifuge was stopped.

(c) Post-Testing Procedures

After the centrifuge had stopped the transducers were disconnected and the actuator taken off. Before removing the strongbox the position of the soil surface was measured again as described above. This measurement served as a reference to determine the position of the soil surface during the test. The strongbox was subsequently removed and the soil taken out carefully while monitoring the soil for signs of particle breakage. Depending on the test g-level and the soil type, the soil was either re-sieved and reconstituted or just re-mixed prior to the next test. The pile was taken out of the actuator and all transducers except the SRTs were re-calibrated following the procedures described in Section 4.3.1. The recorded test data were then transferred to a different computer for further data analysis using conventional spreadsheet software.

4.4 Test Programme

The aim of the test programme was to study the influence of state on the behaviour of driven piles in sand. To achieve a range of initial conditions as varied as possible two different soils were used to prepare samples at mainly three different densities; loose, medium dense and dense, that were tested at accelerations of 50, 100 and 200-g. For the given pile geometry of 16 mm diameter and a penetration of 355 mm this represents prototype piles of between 0.8 and 3.2 m in diameter and 17.5 to 71 m in length.

The first test (CLBS-1) with the fully assembled model and CUIMP-1 was performed in January 1998. The twenty-three tests that emerged with good quality data were carried out between June and December 1999 over seventeen months after test CLBS-1. In this intermediate period forty-four additional tests, which are now considered preliminary were carried out. Twenty-one of them were necessary to find a suitable motor for the high acceleration of 200-g, while the results obtained from further twelve tests assisted in the design of the fully instrumented model pile. The eleven tests summarised in Table 4-9 and discussed in Section 5.2.2, were required to study the effect of gravity on the output of the pile while it was pushed into the strongbox but without soil. The following discussion of the test programme will include all the tests performed, as each test was important in developing and refining the experimental procedures, thus contributing to the success of the project.

4.4.1 Commissioning of the Driving Unit and Preliminary Tests

A total of twelve preliminary tests were carried out which are summarised is in Table 4-8. Two tests, CLBS-1 and CDBS-1, were undertaken on samples of dry LBS and DBS respectively to establish the magnitude of driving resistance in tension and compression using CUIMP-1. This was particularly aimed at assisting in the development of the fully instrumented model pile CUIMP-2 as discussed in Section 4.2.3(b).

A string of problems with the driving unit during commissioning and the preliminary test series caused concern. As a consequence three different motor and encoder configurations had to be used during the test programme. The characteristics of each system are summarised in Table 4-7. At the start, the communication to the controller broke down during flights above 150-g due to power failure. This problem was solved by strengthening the controller rack and by tightening down all components. The local transformer was also moved to a lower gravitational field within the rack. One other problem occurred with regard to the encoder of the motor. Communication with the pancake shaped motor ceased at 200-g due to failure of the encoder. The tests resumed after its replacement. However, the replacement encoder was of a 500 line type and allowed only a maximum penetration of 125 mm at any one time. This meant that the full penetration could only be achieved in a stepwise fashion of three intervals of 125 mm.

During test CLBS-3 it became apparent that the pancake motor selected was unsuitable to drive the pile into the soil at 200-g as an overflow frequently occurred due to excessive following errors during operation above 150-g. This problem could only be resolved by replacing the entire motor with a cylindrical shaped motor that was more powerful and of conventional brushed type. This drive unit (Type MDA-10-2H2), which also has a 500 line encoder was first used for CLBS-4 on a sample of dense LBS at 200-g. Due to an error in assembling the gear on the motor shaft causing an eccentricity in the gear arrangement, the shaft of the centre gear bent at the maximum axial force of 14 kN. The test was abandoned and a considerable interruption of the test programme occurred due to the time required to repair the actuator. As the brush motor was only given on a loan basis it had to be replaced once more.

A new S19-1A cylindrical servo-motor, equipped with a 100 line encoder was purchased with similar operating characteristics to the brushed motor and was introduced for CLBS-5. This unit lasted considerably longer, until test CLBS-13, when the problem of insufficient motor capacity reappeared. It was replaced by the previous MDA-10-2H2 unit, was then used for all subsequent tests.

The maximum axial force that could be achieved even with this motor was 13 kN (test CLBS-20), which was not sufficient to push the pile over the full stroke into dense LBS at 100 and 200-g. The cause of this problem was related to the gearbox, which started to slip. This was rather unexpected as theoretically the gearbox should have been capable of delivering a peak torque equivalent to well over the design 50 kN axial force. The discrepancy was possibly due to distortions of the driving system and a drop in efficiency so that the required torque to move the ballscrew might have been significantly higher than anticipated leading to this rather disappointing result. Due to lack of time no further attempts were made to overcome the problem.

The series of tests that then followed with the model pile CUIMP-2 were equally unsuccessful. Model pile CUIMP-2 was abandoned following test CLBS-8 when six out of the ten transducers had developed faults. The test series resumed with the new pile CUIMP-3. During the next two tests CLBS-9 and CLBS-10 the pile was pushed into samples of partially saturated soil. This caused electrical shorts in the strain gauge circuits of four out of the ten transducers as the moisture penetrated through the micro-pores of the epoxy resin protecting the gauges and lead wires. Partially saturated samples had originally been introduced because of the availability of good quality soil element test data for the soil in this state (Coop & Lee, 1993) but because of the electrical problems all subsequent tests were on dry soil. CUIMP-3 was used for two more tests, CLBS-11 and CLBS-12. During test CLBS-12 the RST closest to the tip (RST-1) and that located in the middle (RST-3) broke. Transducer RST-1 is especially important for two reasons: firstly it allows interpretation of the distribution of the radial stress along the pile shaft and secondly it is necessary to apply the cross-sensitivity corrections to friction sleeves SRT-1 and SRT-2. It was therefore decided to abandon CUIMP-3 and continue with the new and improved model pile, CUIMP-4. The use of CUIMP-4 marked the turn in the fortunes of the research project. Fifteen successful centrifuge tests were then performed within only three months which form the core of the good quality tests that will now be described.

4.4.2 Good Quality Tests on Leighton Buzzard Sand

Ten good quality test were carried out on this soil using CUIMP-3 and CUIMP-4. The main characteristics of these tests are summarised in Table 4-10. The speed of pile installation varied between 0.1 and 0.2 mm/s during push-in and was generally 0.5 mm/s during pull-out. The strategy adopted following the problems with drive unit was to carry out the low g-level tests and tests on loose samples first before finally attempting the tests on the dense samples.

The use of the two different piles for similar soil conditions and stress levels (e.g. tests CLBS-12 and CLBS-16) allowed a study to be made of the effects of differences in manufacturing on the pile behaviour. Tests CLBS-12 and CLBS-19 were both carried out on loose samples at 100-g using CUIMP-3, thus allowing observations on test repeatability. For test CLBS-21 the soil was placed loose and then compressed under the consolidation press (Section 4.3.2) to an initial density similar to test CLBS-12 which had been normally consolidated. This allowed observations on the effect of overconsolidation on the pile behaviour.

Two 50-g tests were conducted on samples of initially loose (CLBS-14) and dense (CLBS-15) states using CUIMP-4. Two pile load tests were performed during each test, one at a penetration of 125 mm the other one at 240 mm. The pile was pushed into the soil until the desired depth was reached and then, following a short resting period, pulled out by about 2 mm in order to mobilise the full tensile shaft capacity. The load test was conducted on re-loading at a constant rate of 0.1 mm/s over a displacement of 10 mm. Thereafter the penetration resumed at 0.2 mm/s until either the position for the next load test or the final penetration was reached.

Six 100-g tests were conducted at various initial densities using CUIMP-3 and CUIMP-4. These included three loose samples (CLBS-12, CLBS-14 and CLBS-19), one medium dense sample (CLBS- 17), one dense sample (CLBS-20) and one overconsolidated sample (CLBS-21). With the exception of test CLBS-20, where the pile penetration ceased at 280 mm, the pile could be pushed to the full penetration depth of 350 mm for all tests. One load test similar to that described for the 50-g tests was performed during test CLBS-12. The load tests carried out during tests CLBS-20 and CLBS-21 followed a slightly different procedure. The pile was pulled out only as far as was required to reduce the head load to zero, thus simulating more closely the procedure during a conventional field load test and preventing stress relaxation around the pile tip. Prior to re-loading at the final penetration depth during test CLBS-21 a resting period of 6 minutes was allowed to study the effect of creep, after which and the pile was pushed into the soil for 3 mm at a speed of 0.1 mm/s. The pile was then unloaded again to zero head load and the resting period extended to 20 minutes. A final cycle was then performed including a resting period of 120 minutes. These three stages are referred to as creep stages and are discussed in detail in Chapter 5.

Finally, two 200-g tests were conducted using CUIMP-4, test CLBD-18 on a loose sample and test CLBS-22 on a dense sample. One load test was performed during CLBS-22 following the modified procedures described in the previous paragraph. In test CLBS-22 the pile penetrated only 150 mm.

4.4.3 Good Quality Tests on Dogs Bay Sand

Thirteen good quality test were carried out on this soil using CUIMP-3 and CUIMP-4. The main characteristics of these tests are summarised in Table 4-11. The speed of pile installation was essentially the same as for the tests on LBS. In general the driving resistance was significantly less compared to the LBS so no problems with respect to driveability occurred in this test series.

Two different piles were used once more in similar soil conditions and stress levels (tests CDBS-2 and CDBS-11) allowing the investigation of the effect of differences in manufacturing tolerances on the pile behaviour. Tests CDBS-3 and CDBS-4 were both carried out on medium dense samples at 200-g using CUIMP-4, thus allowing observations on the repeatability of behaviour for this pile. For the 100-g test, CDBS-13, the soil was placed loose and then compressed using the consolidation press to a dense state similar to test CDBS-8, which had reached its state by compaction and which was also tested at 100-g. This allowed observations on the effect of overconsolidation on the pile behaviour. Similar observations were possible between the compacted 200-g test CDBS-12 and the overconsolidated 200-g test CDBS-14.

Two 50-g tests were conducted on samples of initially loose (CDBS-5) and dense (CDBS-6) states using CUIMP-4. Two pile load tests were performed during each test at intermediate penetrations of 125 and 240 mm depth. Prior to the load test the pile was again pulled out by about 2 mm in order to mobilise the full tensile shaft capacity.

Four 100-g tests were conducted at various initial densities using CUIMP-3 and CUIMP-4. These included one loose sample (CDBS-7), one medium dense sample (CDBS-9), one dense sample (CDBS-8) and one overconsolidated sample (CDBS-13). Five load tests and three creep stages were performed during test CDBS-13. Prior to the load tests the pile was pulled out only as far as was required to reduce the head load to zero. The creep stages included three cycles of loading-unloading with resting periods of 6, 20 and 120 minutes. The load tests were carried out at a constant speed of 0.1 mm/s.

Finally seven successful 200-g tests were conducted using both CUIMP-3 and CUIMP-4. These included two loose samples (CDBS-2, CDBS-11), three medium dense samples (CDBS-3, CDBS-4 and CDBS-10), one dense sample (CDBS-12) and one overconsolidated sample (CDBS-14). Two load tests similar to those for the 50-g tests were performed during tests CDBS-2 and CDBS-4. The load tests carried out during tests CDBS-11 to CDBS-14 again followed the modified procedure of zero head load prior to loading. In addition, the effect of creep on the pile behaviour was studied by means of three creep stages between 6, 20 and 120 minutes during test CDBS-11 and one creep stage of 45 minutes during CDBS-14.

4.5 Summary

Details have been given of all the processes involved in using centrifuge modelling for modelling the behaviour of an instrumented model pile pushed into sand. The background and the principles of centrifuge model testing have been introduced, including the scaling laws and potential sources of error related to this research study. A new actuator and strongbox assembly was then described that allows a model pile of 400 mm in length to be pushed into the soil at a maximum acceleration of 200-g. Following a series of preliminary tests with an un-instrumented pile, three versions of a fully instrumented model pile were developed that allowed the base force, shaft friction and radial stresses to be measured during pile installation. The experimental methods developed for the centrifuge tests, including sample preparation, calibration of the transducers and testing procedures were described in detail. Most problems occurred during operation of the motor and its encoder at the high gravity levels. The first version of the instrumented model pile was also unreliable and it was not until the introduction of the third fully instrumented pile, CUIMP-4, that the testing programme could finally be completed successfully.

5. Centrifuge Model Test Results

The main aim of the research was to establish a basic framework relating the capacity of driven piles in sand to the in situ state prior to pile installation. The results of the centrifuge tests undertaken to achieve this aim will be presented in this chapter. A fully instrumented model pile was pushed into the soil at constant speed while carefully monitoring the mobilised base resistance, shaft resistance and radial stresses. In order to arrive at the final data set a number of corrections were necessary which will be described in detail. Finally, the centrifuge test results will be combined with the results from the triaxial tests presented in Chapter 3 allowing the new framework to be established.

Besides studying the penetration resistance and stress distribution during pile installation, a series of pile load tests was conducted for a number of tests at different depths with the aim to investigate the effect both of stress relief around the pile tip and of time on the mobilised shaft and base resistances. For these tests the pile was first unloaded either to a condition of zero head load or fully mobilised tensile shaft capacity and then re-loaded at constant speed. The effects of soil creep on the pile capacity was studied by introducing waiting periods following the unloading of the pile, prior to the onset of re-loading. Particle breakage has been identified as a major contributing factor to the volumetric deformation of sands (Coop & Lee, 1993). In order to examine the role of this with respect to piles the grading before and after each test was carefully examined.

5.1 Typical Raw Test Data

During pile installation in the centrifuge, readings from all channels are stored on the hard disc of the data-logging computer at a selected rate. Generally the rate of logging was chosen in relation to the speed of testing and the anticipated change in transducer output, in order to collect sufficient data for subsequent data smoothing procedures to be applied without changing significantly the measured characteristics of the pile response. On average, five readings per millimetre penetration were taken during the installation of the pile. This rate was increased to seventeen readings per millimetre during the pile load tests, owing to the much more rapid increase in pile resistance during re-loading.

After each test the data were transferred from the data-logging PC to another PC for data analysis. The data were loaded into a commercially available spreadsheet package and first checked for consistency. A typical penetration curve using the raw data is shown in Figure 5-1 for test CDBS-12 on Dogs Bay sand. The data presented show three unload-re-load cycles at

125, 240 and 340 mm penetration. After reaching the final penetration of 360 mm the pile was pulled out in one continuous movement. The data during spin-up and spin-down of the centrifuge are not included on the plot.

The high frequency of data-logging resulted in around 6000 data sets (with 19 transducer readings each) being collected for each test. This is indicated in Figure 5-1 by the high density of data points especially during the penetration and pull-out phase. The number of data sets proved far too high for the efficient use of the available spreadsheet software.

5.2 Data Reduction and Corrections

This section outlines all the steps involved to arrive at the final data from the raw test data set. First the amount of data was reduced to a more manageable level. Then the data were corrected for the effects of gravity and drift. This was followed by further corrections to account for the non-linearity in transducer output and the effect of cross-sensitivities between individual transducers. The fully corrected set of data was then smoothed before subsequent analysis and interpretation. At the end of this section an assessment is made on the overall accuracy of each transducer on the model pile. This will be important for the discussion of the results presented in Sections 5.3 to 5.7.

5.2.1 Procedure of Data Reduction

The aim of the procedure is to reduce the number of data sets and as a consequence the level of noise while maintaining their characteristics. This was achieved by taking an average over five consecutive data sets. No reduction was carried out for the data of the load tests. The data instead were smoothed by the means outlined in Section 5.2.7. On average the procedure adopted reduced the number of data sets from about 6000 to 1700, a far more manageable number.

The effect of the data reduction process is illustrated in Figure 5-2, again for test CDBS-12. In both Figure 5-1 and Figure 5-2 each symbol represents one data point. In comparison with the raw data from Figure 5-1 the data reduction method reduces the number of data points only during pile installation and the final pull-out stage, which is indicated by the reduced number of data in Figure 5-2. The load-displacement curve using the reduced data set is also smoother but its shape is unchanged, so the method chosen meets the requirements specified earlier.

5.2.2 Gravity Effects on the Measurements

There are generally three gravitational effects which influence the measurements in the centrifuge.

The first effect is due to the increase in the gravitational force due to the acceleration of the centrifuge that leads to a change in output of the transducers. For example, in the model the global load cell will measure a negative or tensile force as the pile tries to accelerate away from it. This effect was taken into account by re-zeroing all the readings on the model pile prior to pile penetration.

The second effect occurs during pile installation and is due to a change in acceleration with radius at a given angular velocity, as shown by Equation 4.1. For example, the global load cell will register an increasing tensile force with increasing pile penetration which is not related to the true penetration resistance and therefore needs to be taken into account. The problem was solved by pushing the pile into the empty strong box during a centrifuge flight and monitoring the output of all transducers. These readings were then used to correct the test data. An example of the magnitude of correction required is given in Figure 5-3 for the global load cell during test Gravity-4 conducted at 200-g on pile CUIMP-4. As predicted by Equation 4.1 the tensile force increases linearly with depth and reaches a maximum of 120 N at the final penetration. The gravity corrections for the shaft resistance transducers (SRTs) and the base force transducer (BFT) were significantly less due to their smaller mass, compared to the total mass of the pile which affects the global load cell. The radial stress transducers (RSTs) were generally insensitive to changes in radial acceleration as they are fully embedded in the pile and have little mass.

The third possible effect is related to the calibration of the transducers. All the equipment was usually calibrated at 1g under the assumption that the increase in acceleration has no significant effect on the calibration. The only possible, although not entirely satisfactory way to verify this assumption was to cross check the output of the global load cell while penetration the pile into the empty strongbox against predictions from a theoretical solution. The theoretical solution was derived by considering the mass of the pile and calculating the resulting force under increased gravity based on Equations 4.1 to 4.8. The result, shown in Figure 5-3, indicates that there is no significant change in calibration. The measured and calculated tensile forces generally agree to within 5%.

5.2.3 Temperature Effects on the Measurements

As mentioned in Section 4.3.1, the centrifuge at City University is not equipped with an air conditioning system, thus the temperature tends to rise with time as a function of the heat dissipated by the motor and the aerodynamic resistance during centrifuge rotation. Changes in ambient temperature affect the transducer output in two ways. Firstly it causes a shift in zero and secondly a change in calibration (span-shift). For the current study only the effect of zero shift was considered. A comparison of the specifications on temperature compensation of the model pile with commercial foil gauge transducers (Entran, 1995) showed, that the error due to span shift is generally similar in magnitude to the error due to zero shift.

The first aim was to establish the temperature regime during a typical 200-g test. Two samples of dry and loose Leighton Buzzard sand were used and the temperature was monitored in the soil as well as in the air over two hours. Figure 5-4 shows the temperature changes with time during one of these tests. The motor temperature almost doubles during the test leading to a steady rise in air temperature, while due to the poor thermal conductivity of the dry silica sand the temperature inside the strongbox remains largely unchanged. At the end of the test the temperature gradient between air and soil is about 10°C. It is interesting to note that the temperature at the actuator housing is about 4°C less than at the ceiling of the chamber.

For the specified temperature compensation of the model pile to better than ±0.1μV/V/ °C and the chosen excitation voltage of 3V, the 10°C temperature gradient would have resulted in a zero shift equal to ±3 μV. Given the relatively low output of some of the transducers, for example of approximately 43 μV for RST-4 in loose Dogs Bay sand at 50-g, this would have been equivalent to an error of ±7 %. It was therefore decided to reduce the temperature change by feeding water through two hydraulic slip-rings and evaporating it inside the centrifuge chamber. The water was sprayed against the side walls of the chamber from two pipes attached to the base of the swing.

The resulting temperature changes during test CDBS-11 are shown in Figure 5-5. At the start of the test all the temperatures are fairly similar. The water was turned on soon after the centrifuge started to accelerate. This led to an immediate drop in temperature in the chamber as the temperature sensor is mounted close to the point of water discharge. The temperature close to the actuator started to rise continuously from 23 to 25 °C, while the temperature in the soil increased at a much slower rate. The temperature gradient between air and soil is therefore reduced to about 2°C and the error due to zero shift consequently to about ±1.5%, which was considered acceptable. After arriving at the target g-level, which took between 10 and 20 minutes, another 25 minute resting period was allowed to stabilise the transducer outputs before

the readings were re-zeroed and the pile driven into the soil. As can be seen, this time interval corresponds to the steepest change in temperature.

5.2.4 Drift Corrections

Drift in the transducer output is identifiable as a change in the zero output between two well defined reference conditions, for example, the position of the pile before and after the test. In terms of the model pile this meant that the readings of the transducers did not return to zero after the pile had returned to its initial position after extraction from the soil. Drift in this sense does not include any zero shift due to the temperature gradient between air and soil as discussed before. At both start and end of the test the pile is in the air, hence the shift in zero that occurs when the pile enters the soil is not considered by this correction and remains an independent source of error. However, any zero shift due to changes in the ambient air temperature were eliminated by this correction.

The drift correction applied to the data assumed that the drift in transducer output is a linear function of the test time. Hence the difference between the first and last reading of each transducer on the model pile was taken and the value obtained split into time steps equal to the logging rate and then subtracted or added to the measured value in order to obtain the correct zero transducer output at the end of the test. The effect of this correction is illustrated in Figure 5-6 for the shaft resistance transducer SRT-2 on CUIMP-4 during test CDBS-9. The magnitude of drift shown is typical for the friction sleeves. The observed drift as a percentage of the maximum output was less for the RSTs and the BFT.

5.2.5 Changes in Calibration and Non-Linearity of Transducer Output

(a) Changes in Calibration

It is good practice in centrifuge testing (e.g. Grant, 1998) to check the original calibration at regular intervals. Owing to the delicate nature of the transducers on the model pile and the harsh testing environment, the pile was re-calibrated after each test. For practical reasons the re-calibration was restricted to the base force transducer (BFT) and the radial stress transducers (RST). The shaft resistance transducers (SRT) were re-calibrated only once at the end of the test series, as this operation involved the removal of the silicone sealant between the SRTs and the pile core. Figure 5-7 shows a typical re-calibration sequence for the BFT on CUIMP-4. It can be seen that the repeatability is excellent with a change of gradient of less than 0.5%. The repeatability for the RSTs was less good as is shown in Figure 5-8. At full-scale the span increased between test CDBS-4 and CDBS-10 by a voltage equivalent to 20 kPa or 8%.

However, this did not affect the overall accuracy significantly, as the transducer output was corrected routinely after each test, to account for the non-linearity that can also be observed in Figure 5-8. This procedure will be discussed in more detail in the next section.

(b) Non-Linearity of Transducer Output

As indicated in Section 4.3.1e the RSTs exhibited some non-linearity in the low stress range due to friction between the transducer and the side walls of the pile. No significant non-linearity was observed for the other transducers on the model pile.

The non-linearity of the RSTs was accounted for by re-calibrating the pile after each test and using the non-linear calibration obtained to correct the data obtained during the test. The range of pressures applied during re-calibration was adjusted to the pressures measured during the test in order to obtain the most accurate correction. Typical calibration curves are shown in Figure 5-9 for the RSTs on CIUMP-4 obtained after test CDBS-10. The maximum radial stress during this test was measured by RST-2 at 180 kPa, hence the pressure range during re-calibration was set to 200 kPa. The minimum radial stress of 60 kPa was registered by RST-4. A series of small pressure increments was therefore applied in the range between 0 and 50 kPa to identify properly the non-linearity of the calibration in this region. Above a pressure of 100 kPa the calibration for the transducers becomes fairly linear. There was very little hysteresis for any of the RSTs.

The error due to non-linearity very much depends on the current output of the transducer. In case of RST-3 the error due to the assumed linear calibration is 65 kPa or 30% for an applied pressure of 200 kPa. However, if the applied pressure is only 40 kPa the error reduces to 1.4 kPa or 3.5%. A polynomial least squares regression was chosen for the non-linear calibration curves and that function was then used to correct the readings of each transducer. This procedure reduced the error to about 2% throughout the entire range of pressures.

5.2.6 Cross-Sensitivity Effects

During calibration of the model pile a series of cross-sensitivities between different transducers was discovered (see Section 4.3.1e). These fall broadly into three categories:

- Cross-sensitivity of the SRTs to the applied base force
- Cross-sensitivity between adjacent SRTs
- Sensitivity of the SRTs to the applied radial stress

The magnitude of these cross-sensitivities for the transducers on CUIMP3 and CUIMP-4 are summarised in Table 5-1.

The first cross-sensitivity is the most significant due to the expected high base forces, especially in the silica sand. It appeared that the cross-sensitivity was due to a combination of a Poisson's ratio effect caused by the stress in the pile core and force transmission through the epoxy filled wire channels. The first effect arises if for example a compressive axial force is transmitted through the pile core which causes the SRT to expand circumferentially thus changing the resistance of the gauges aligned in this direction. The longitudinal channels accommodating the wires connecting the strain gauge bridges to the terminal at the top of the pile were re-filled with epoxy resin (see Chapter-4). As up to 12 wires were bonded and coated in any one channel some axial resistance was introduced between the sleeves and the pile core that could have allowed some of the base force to be transmitted through the friction sleeves rather than through the core section only. Typical cross-sensitivities obtained during the re-calibration of pile CUIMP-4 after test CDBS-10 are shown in Figure 5-10. The base force in this test reached 2100 N at the final penetration.

As can be seen, the RSTs are not sensitive to the base force. However, there is a strong cross-sensitivity between the base force and the SRTs, especially SRT-4 and SRT-5. The strong hysteresis is possibly due to a hysteretic or time dependent response of the epoxy resin used to fill the wire channels. This made it difficult to use a single correction. However, as the reduction in base force during unloading of the pile was usually very rapid and of little interest it was decided to use the same correction for both loading and unloading. This correction was determined from the loading data for each SRT.

The cross-sensitivity between the SRTs is due to the same mechanism as described for the base force. However, due to the much smaller forces in the sleeves the magnitude of these errors is less. Correction factors were obtained following the same procedure as outlined for the BFT with the difference that the calibration was performed only once at the start of the test series. The overall correction was then applied under the assumption that the individual cross-sensitivities can be superimposed. Mathematically, this can be described by:

$$\Delta SRT(n+1) = \sum_{i=0}^{n} F(i)_T \, CF(i)_{cross} \tag{5.1}$$

Where $\Delta SRT(n+1)$ is the change in output due to cross-sensitivity of the shaft resistance transducer considered, $F(i)_T$ is the applied force on any SRT below the friction sleeve under consideration and $CF(i)_{cross}$ the cross-sensitivity calibration factor of the sleeve under

consideration due to $F(i)_T$. The case of n equal to one refers to the calibration of the base transducer. This definition does not take into account the contributions by the uninstrumented sections of the pile shaft, which are small.

The cross-sensitivity of the SRTs to radial stress is a significant factor as in some cases the correction made can exceed the value measured prior to applying the correction. The cross-sensitivity is due to the arrangement of the strain gauges on the sleeves. A Poisson's ratio gauge is mounted at 90° next to the active gauge which is in line with the pile axis (Figure 4.8). Both gauges have the same sensitivity and are integrated into a fixed backing. As the radial stress is applied the pile is strained circumferentially thus changing the resistances of predominantly the Poisson's gauges and consequently the resistance of the bridge circuit. The resulting cross-sensitivities for all SRTs are fairly linear with little hysteresis, and fall into a narrow range as illustrated in Figure 5-11 for CUIMP-4 after test CDBS-10.

The cross-sensitivity correction for the radial stress is, however, more difficult to apply than is apparent from the calibration. As the pile penetrates the soil the radial stress varies with depth. Therefore, an assumption about the distribution of the radial stress along the pile is required. For the corrections applied to the data presented in Sections 5.3 to 5.7 the average reading was taken of the two RSTs above and below the friction sleeve considered. In cases where only one RST was available, for example at SRT-1 and SRT-5 the reading of the RST closest to the friction sleeve was taken directly. The correction thus relies on all the RSTs functioning properly in order to obtain the best possible correction. Unfortunately, as will be discussed later, this was not always the case.

All the possible sources of experimental error related to the measurements with the model pile as identified in this section are in addition to those stated in Section 4.2.4 which were observed during the "ideal" calibration at 1-g. An assessment of the overall accuracy is therefore required, taking into account all possible sources of error related to measurements with CUIMP-3 and CUIMP-4. This will be discussed further in Section 5.2.8.

5.2.7 Data Smoothing Procedure

Following the correction of the test data a final smoothing procedure was applied. Figure 5-12 illustrates the effect of two different techniques on a typical profile of radial stress obtained from RST-1 during test CLBS-16. As can be seen there is no significant gain in using a smoothing procedure of more than a 5-point running average. In addition smoothing by averaging over a wider interval tends to cut out useful data particularly from the base transducer at the start of penetration of the pile, where the resistance increases quickly. As the data had

already been smoothed during the data reduction procedure (compare Figure 5-1 and Figure 5-2) the technique of taking a running average of every five consecutive data points was used. All the test data presented in Sections 5.3 to 5.7 were smoothed with this procedure.

5.2.8 Overall Accuracy of the Transducers on the Model Piles

The assessment of the overall accuracy must include all the issues discussed in the previous sections as well as the results of the original calibrations presented in Section 4.3.1. The assessment of accuracy made in this section covers both model piles, CUIMP-3 and CUIMP-4 and is stated as a percentage of the current reading.

It can be concluded that the BFT provides the most accurate measurement as it is neither cross-sensitive to the radial stress nor any friction sleeve. In addition the calibration was found to be extremely linear, repeatable and only marginally effected by the increase in gravity, hence the measured unit base resistance is accurate to within about ± 2%. The total shaft capacity has been obtained by subtracting the measured base force from the overall penetration force measured by the global load cell on top of the pile. The global load cell was also found to be extremely reliable and the calibration was very linear and repeatable. However the output was found to be affected by gravity. Hence, the average global unit shaft friction can be considered accurate to within ±5%. The RSTs come second in accuracy owing mainly to their non-linearity and changes in calibration for subsequent calibration cycles. The accuracy of the radial stresses measured is believed to be within about ±10%. The SRTs are least accurate, mainly due to their cross-sensitivities to the base force, other SRT forces and radial stresses. The accuracy is additionally hampered by difficulties during calibration due to the geometry of the pile as discussed in Section 4.4. The overall accuracy is of the order of ±25 %.

The estimated level of accuracy may appear rather poor in comparison to commercial transducers. However, the confidence in the measurements made is significantly improved by:

- the high degree of redundancy in the measurements made on the pile.
- the consistency between tests conducted with the same pile on similar samples.
- the consistency between tests conducted with two different piles on similar samples.
- the consistency between the global and local shaft friction data.
- the large number of tests and the consistency between them.

5.3 Pile Behaviour During Installation

This section deals with the behaviour of the model pile during installation. First the data of the global penetration resistance are presented and discussed. This is followed by two sections, on the magnitude and distribution of the base resistance and shaft resistance during pile installation. Following current engineering practice the relative density is first used to quantify state and the deficiencies of this procedure will be highlighted where appropriate. The measured values of both base and shaft resistance will then be compared to recommended design values for similar conditions as well as to results of other experimental studies in both types of sand. The aim of these comparisons is the verification of the experimental results. Section 5.3.4 covers aspects of the magnitude and distribution of radial stress. Finally, in Section 5.3.5 the shaft friction and radial stress measurements will then be combined to obtain profiles of interface friction angle with depth. These will be compared both to the interface friction angles measured in the direct shear box (as described in Section 3.3.2) and to results of ring shear tests.

The centrifuge test data are presented in prototype units. The conversion from model to prototype scale is achieved by applying the procedures outlined in Section 4.2.3. This allows direct comparison between tests conducted at different g-levels as far as stresses are concerned. In terms of overall resistance there will still be a difference between the tests which is due to the different prototype pile geometries as a result of using the same pile in tests at different g-levels. The data obtained during the unload and re-load cycles illustrated in Figure 5-1 are not included in this section and will be discussed separately in Section 5.4.

Each of the following sections will be divided into two sub-sections. The first covers the results of the tests on Leighton Buzzard sand (LBS) and second the results of the tests on Dogs Bay sand (DBS). For convenience these abbreviations will be used to refer to the two sands. The configuration and testing procedures for all tests were outlined previously in Section 4.5 and will not be repeated here. The reader is also referred to Tables 4.8 to 4.11 for full details of each test.

5.3.1 Penetration Resistance

(a) Penetration Resistance in Leighton Buzzard Sand

Figure 5-13 shows the distribution of penetration resistance with pile tip penetration for tests CLBS-12 to CLBS-22. The penetration resistance increases monotonically with depth. With the

exception of tests CLBS-20 and CLBS-22, where the increase is almost linear with depth, the resistance increases more quickly at shallow penetrations and at a slightly reduced rate at deeper penetrations. This behaviour is most visible for test CLBS-18 and is consistent with observations by other researchers (e.g. de Nicola & Randolph, 1999). Generally, the shape of the curves suggests that the sample preparation methods chosen were suitable to create fairly homogeneous specimens. There is no indication of layering or significant variations of density within any sample.

A comparison between tests CLBS-12, CLBS-16 and CLBS-19 demonstrates the excellent repeatability of the tests using different model piles. All of these tests were carried out at 100-g on loose samples.

The effect of changes in density on the penetration resistance is rather dramatic. For example, at a penetration of 20 m the resistance in CLBS-19 is about 16 MN while for CDBS-20 it is about 90 MN. Both tests were carried out at 100-g. This increase by a factor of 5.6 corresponds to a difference in specific volume of 0.24. Similar observations can be made for tests CLBS-18 and CLBS-22 conducted at 200-g as well as the 50-g tests CLBS-14 and CLBS-15.

An increase in penetration resistance due to overconsolidation is apparent from tests CLBS-19 and CLBS-21. The difference in soil state between these two tests will be discussed in Section 5.7.1. Even though the densities of both samples are similar, the penetration resistance for CLBS-21 is twice as high as for CLBS-19 and is similar in magnitude to that for CLBS-17, which was a medium dense sample.

There appears to be a small boundary effect for a number of tests as the pile tip approaches the base of the strongbox. For example in test CLBS-18 the resistance starts to increase at a higher rate at about 45 m penetration. Given the model dimensions this corresponds to a ratio between the distance of the pile tip from the base, d_b, and the pile diameter, d_p, of 12. This confirms results reported by other researchers (e.g. Corte et al., 1991, see Section 4.2.2), who observed boundary effects during cone penetrometer tests in a silica sand at ratios of d_b / d_p in the order of 10-12. However, the increase in resistance at larger depths could also be the result of changes in density within the sample due to the higher stress field. The data will therefore not be deleted at this point, but the issue kept in mind until the discussion of data normalisation in Section 5.7.

(b) Penetration Resistance in Dogs Bay Sand

Figure 5-14 shows the distribution of penetration resistance with pile tip penetration for tests CDBS-2 to CDBS-14. As for the samples of LBS the penetration resistance on the normally consolidated samples increases rapidly at shallow penetrations and at a reduced rate at deeper

penetrations. Again, the shape of the curves suggests that the sample preparation methods were suitable to create homogeneous specimens, with no indication of layering or variations of density within any sample.

Some peculiar behaviour was observed below a penetration of 50 m during test CDBS-2, where the resistance remained essentially constant. As this behaviour was not observed for any of the other tests at similar densities and penetrations, the data were subsequently deleted. A comparison between tests CDBS-2 and CDBS-11 above a penetration of 40 m otherwise demonstrates the excellent repeatability of the tests using different model piles. Both tests were carried out at 200-g on loose samples of similar densities.

While for the LBS the resistance between a loose and a dense sample increased by a factor of 5.6, the increase in resistance for DBS, for example between tests CDBS-7 and CDBS-8 (both 100-g tests), at 20 m penetration, is only a factor of 1.7. In general, for similar values of relative density and g-level, the penetration resistance in DBS is only about 20% of the resistance in LBS. It is therefore obvious that design methods based on relative density alone will not capture the fundamental mechanisms that govern the behaviour of piles. A method capable of explaining this difference in pile behaviour will be proposed and discussed in Section 5.7.

The effect of overconsolidation on the penetration resistance for DBS is quite dramatic as illustrated by tests CDBS-8 and CDBS-13 as well as CDBS-12 compared to CDBS-14. The initial states of these samples are described in Section 5.7.1. Even though the densities of all four samples are similar, the penetration resistance in the overconsolidated samples increases much more rapidly and shows a distinct peak. The penetration resistance at the peak is roughly twice the resistance in the compacted sample at the same depth. Beyond the peak the resistance decreases to a similar value as for the compacted sample at the final penetration. A similar behaviour was observed by McDowell & Bolton (1999) during centrifuge penetrometer tests on samples of Quiou sand, also a carbonate sand. They observed a peak resistance even for compacted samples but did not test oversonsolidated samples. Their micromechanical explanation for this phenomenon will be discussed further in Section 5.6.

Again there appears to be a boundary effect for the dense samples as the pile tip approaches the base of the strongbox. For example in test CDBS-12 the resistance starts to increase at a higher rate at about 30 m penetration or a ratio d_b / d_p of 17. In this test significant settlements occurred during acceleration of the centrifuge leading to a reduction in specific volume with depth. This changed the state of the soil, which could explain the change in penetration resistance, so as for the LBS the data will not be deleted at this point, but the issue kept in mind until the discussion in Section 5.7.

5.3.2 Base Resistance

(a) Base Resistance in Leighton Buzzard Sand

Figure 5-15 shows the distribution of measured pile base resistance with depth for the tests in LBS. A comparison with Figure 5-13 indicates that 65-80% of the penetration resistance is due to the base resistance.

The distribution of unit base resistance with depth is illustrated in Figure 5-16. The values of unit base resistance were obtained from the measured total base capacity taking an average diameter of the model pile of 15.96 mm. The unit base resistance increases rapidly at shallow penetrations and at a slightly reduced rate at deeper penetrations. There is however, no indication of a limiting value as suggested, for example by API-RP2A (1993) or Tomlinson (1995). The base resistance at the final penetration of CLBS-18 is about 17 MPa, which is about five times the limiting values suggested in API-RP2A for a loose silica sand.

The measured values of q_b are similar to results of centrifuge pile tests reported by Fioravante (1994) on samples of Toyoura sand, a sand similar in grading and mineralogy to LBS. They also compare favourably with results from calibration chamber tests on cone penetrometers as reported by Baldi et al. (1982) on Ticino sand and Houlsby & Hitchman (1988) on LBS.

There is excellent agreement between the readings of the BFTs on piles CUIMP-3 and CUIMP-4 in tests CLBS-12, CLBS-16 and CLBS-19. There appears to be a slightly looser layer between 16 and 26 m depth in tests CLBS-12 and CLBS-16 leading to a constant value of unit base resistance over this interval. In comparison, CLBS-19 exhibits this behaviour over a very much reduced depth.

The overconsolidation of sample CLBS-21 which was initially loose leads to an increase in unit base resistance to a value more typical for a medium dense sample. Thus, if a cone penetrometer were to be driven into this sample, it would probably be classified as medium dense, similar to sample CLBS-17, although the density measurement would reveal a loose state.

A comparison of tests CLBS-14, CLBS-18 and CLBS-19, all of which were conducted on samples of similar initial density shows an apparent increase in unit base resistance with prototype pile diameter. For example, the unit base resistance at 20 m penetration for test CLBS-18 (prototype pile diameter 3.2 m) is 8 MPa, whereas for test CLBS-14 (prototype pile diameter of 0.8 m) it is only 5.5 MPa. This apparently contradicts current pile design methods such as the MTD-Method (Jardine & Chow, 1996) where the unit base resistance is thought to

decrease with increasing pile diameter (Equation 2.18). There is also no evidence that the unit end bearing for a pile of 3.6 m diameter is equal to zero as implied by Equation 2.18. However, it is not entirely clear which diameter should be used in Equation 2.18 for centrifuge model tests. The fact that the base resistance does not scale seems to indicate that the model pile diameter should be used. The experimental results presented are supported by observations of Fioravante (1994), who measured similar increases in base resistance with increasing prototype pile diameter. It is not entirely clear whether the observed increase in unit base resistance could be due to a boundary effect or changes in mean normal stress due to friction along the side walls, as no stress sensors were embedded in the walls of the strong box to monitor the radial stresses during pile installation.

Tests CLBS-15, CLBS-20 and CLBS-21 which were conducted on dense samples at different g-levels show very close agreement in unit base resistance up to a depth of about 5 m. For deeper penetrations the unit end bearing of the 50-g test reduces while the other two tests show an almost identical increase to about 30 m. It appears, therefore that the question regarding a possible boundary effect is not easily answered. However, the test data are consistent in that the denser samples which are further away from the critical state line have a higher unit base resistance compared to the loose samples. The sensitivity of the pile behaviour to changes in specific volume with depth, discussed previously, makes a direct comparison between the tests difficult. This problem can be resolved by normalising the data with respect to a suitable reference state taking into account both the current stress and the volumetric state of the soil. A suitable approach is presented and discussed in Section 5.7.

Figure 5-17 shows values of bearing capacity factor, N_q, plotted against relative density. The bearing capacity factor was calculated using Equation 2.13 from the unit base resistance data presented in Figure 5-16 and the vertical stress in the centrifuge model the calculation of which will be discussed in Section 5.7.1. The relative density was obtained from the current specific volume at a given depth, the calculation of which will also be discussed later. It can be observed that due to the compression of the soil with increasing stress the relative density in the centrifuge model is not constant. This change in density, and consequently in soil state, becomes especially significant for highly compressible soils and/or tests at high accelerations. However, in practice, it is frequently ignored (e.g. Fioravante, 1994, de Nicola & Randolph, 1999).

Figure 5-17 indicates that N_q is a function of the pile penetration. Very high values are obtained for shallow penetrations which decay rapidly with increasing depth. Strictly speaking the N_q values calculated from the base resistance curve during a centrifuge test are not the same as those obtained from back analysing a pile load tests. However, as will be shown later for the tests conducted in this study they are very similar. A comparison to values published in the

literature for silica sand, for example the chart by Bond et al. (1997) (Figure 2.27) shows that the measured N_q values at the final penetration fall somewhere between Terzaghi (1943) and Berezantzev et al. (1961). It is evident that there is no unique relationship between the bearing capacity factor N_q and relative density.

(b) Base Resistance in Dogs Bay Sand

Figure 5-18 shows the base resistance during pile installation. Again the general trend is very similar to the global penetration resistance presented in Figure 5-14. On average 70-90% of the global resistance is due to base resistance which is slightly more than observed during the tests on LBS.

The profiles of unit base resistance with depth are presented in Figure 5-19. At shallow penetrations below 8 m the unit base resistance increases rapidly to very similar values as for LBS. Thereafter the unit base resistance continues to increase but at a markedly reduced rate leading to a distinct "knee" like shape of the curves. This feature is thought to be related to the increasing dominance of particle breakage in DBS at higher pressures (Coop & Lee, 1993). A comparison of the q_b-values at final penetration between LBS and DBS, for example of test CLBS-18 and CDBS-11, reveals that for a similar relative density the base resistance in LBS is 90% higher than in DBS. This clearly illustrates the deficiency of the relative density to characterise the behaviour of piles. There is no indication of a limiting value of unit end bearing even for a depth of 70 m. The measured values are similar to those reported by Chin & Poulos (1996) and Yasufuku & Hyde (1995) on a carbonate sand from the Bass Straights, Australia, and Dogs Bay sand respectively. They are also similar to the results of cone penetrometer tests obtained in Dogs Bay sand in a calibration chamber by Nutt & Houlsby (1991).

There is good agreement between the readings of the BFTs on piles CUIMP-3 and CUIMP-4 in tests CDBS-2 and CDBS-11, both conducted at 200-g on loose samples of similar specific volume. This adds further to confidence in the quality of the measurements obtained, especially for the calculation of the average unit shaft friction.

A comparison of tests CDBS-5, CDBS-7 and CDBS-11, all of which were conducted on loose samples of similar initial density, again shows an apparent increase in unit base resistance with prototype pile diameter. For example, the unit base resistance at 20 m penetration for test CDBS-5 (prototype pile diameter 0.8 m) is 4.8 MPa, whereas for test CDBS-11 (prototype pile diameter 3.2 m) it is 6.8 MPa. Similar observations can be made for the dense samples CDBS-6 and CDBS-8. However, as for the tests on LBS the phenomenon is not as apparent for the tests conducted on dense samples at 100-g and 200-g (CDBS-8 and CDBS-12). It is therefore not clear whether the observed increase in unit base resistance with prototype pile diameter is real

or alternatively due to boundary effect, changes in mean normal stress due to friction along the side walls or due to a scale effect of centrifuge modelling.

Again the test data are consistent in that the denser samples which are further below the critical state line have a higher unit base resistance than the loose samples. Further investigations of these effects are carried out in Section 5.7 after normalising the data.

The effect of overconsolidation on the unit base resistance is similar to that described for the overall penetration resistance as can be seen by comparing tests CDBS-8 and CDBS-13 as well as CDBS-12 and CDBS-14. It is interesting to note that peak in each curve corresponds to the same penetration depth at model scale. This issue will be discussed further in Section 5.6.

Figure 5-20 shows the distribution of N_q plotted against relative density. There is a much larger change in relative density with depth than for LBS due to the higher compressibility of DBS. The bearing capacity factor, N_q , again depends on the pile penetration and is not uniquely related to relative density.

5.3.3 Shaft Resistance

The shaft resistance is obtained using Equation 2.11 by subtracting the base resistance from the ultimate pile resistance. The average global unit shaft friction is then calculated by dividing the shaft resistance by the embedded shaft area of the pile. The distribution of average global unit shaft friction will be presented first for both sands, before local values are examined .

The local unit shaft friction along each friction sleeve is obtained by dividing the measured force by the active area of the friction sleeve, given in Table 4.3. The comparison of the readings from the different sleeves allows observations to be made of the distribution of the shaft friction along the pile during penetration.

The values of unit shaft friction from the individual sleeves can be integrated along the pile shaft in proportion to their length again using Equation 2.11. This allows a value of average local unit shaft friction to be obtained which can then be compared directly to the average global unit shaft friction. Figure 5-21 illustrates the integration procedure adopted for calculating the average local unit shaft friction.

(a) Shaft Resistance in Leighton Buzzard Sand

Figure 5-22 shows the distribution of average global unit shaft friction with depth for pile penetration in LBS. As for the base resistance the unit shaft friction increases with depth and

shows no sign of reaching a limiting value. This is contrary both to recommendations in pile design codes such as API-RP2A (1993) and to opinions expressed more recently, for example by Lings (1997), but is in keeping with results of recent research presented by Randolph et al. (1994) and Jardine & Chow (1996). The measured values are generally similar to those reported by Fioravante (1994) and de Nicola & Randolph (1999).

There is some scatter in the data for the 100-g tests on loose samples (CLBS-12, CLBS-16 and CLBS-19) but the consistency in general is good. As for the base resistance the unit shaft friction is again affected by the prototype pile diameter (CLBS-14, CLBS-16 and CLBS-18), although no significant difference is apparent between the unit shaft friction for the dense samples tested at 100 and 200-g (CLBS-20 and CLBS-22). This g-level effect is thought to be either due to changes in stress due to friction on the side walls or due to a scale effect. Overconsolidation generally increases the unit shaft friction compared to a compacted sample of similar specific volume (CLBS-21 and CLBS-16).

The shaft friction coefficients β (from Equation 2.20) are plotted against pile penetration in Figure 5-23, where β represents an average value and was calculated using the average global unit shaft friction and the average vertical stress. The diagram effectively reproduces the type of relationship proposed by Toolan et al. (1990), which was shown in Figure 2.38. The tests on the loose samples plot to the left, the dense ones further to the right, although the decay in β with pile penetration is much more rapid then assumed by Toolan et al.. Again it should be noted that the β values calculated from the average global shaft resistance curve during a centrifuge test are not the same as those obtained from back analysing a pile load tests. However, as will be shown later for the tests conducted in this study they are very similar. There appears to be a boundary effect for the high g-level tests CLBS-20 and CLBS-22 on dense samples in comparison to CLBS-15 at 50-g. Judging from CLBS-15, there is a tendency to overpredict the shaft resistance of long piles driven into dense sand using the Toolan et al. chart. However, the measurements of β in the centrifuge tests are likely to be affected by differences in interface roughness compared to prototype piles. This issue will be discussed in more detail in Section 5.3.5. The general observation is that no unique relationship exists between β, pile penetration and relative density.

Figure 5-24 shows the measurements of local unit shaft friction made with the five SRTs during penetration for test CLBS-16. The h/R ratio is the distance between the centre of the transducer and the pile tip, h, normalised by the pile radius, R. In general the shaft friction is highest closest to the pile tip as indicated by the reading of SRT-1 and with the exception of SRT-4 decays with increasing h/R along the pile shaft. This broadly confirms observations reported by Jardine & Lehane (1992).

The measurements of average local unit shaft friction during penetration are illustrated in Figure 5-25. The stepwise variation, for example during test CLBS-18, is due to the adopted integration procedure. It is interesting to note that the effect of the prototype diameter is less pronounced compared with the global average. Figure 5-25b, shows the ratio of global to local average unit shaft friction. The measurements fall within a band of ±25%, reflecting the accuracy estimated during calibration.

(b) Shaft Resistance in Dogs Bay Sand

Figure 5-26 to 5-29 show the distribution of average global and local unit shaft friction, individual readings of local unit shaft friction as well as β for pile penetration in Dogs Day sand. As for the shaft resistance in LBS the unit shaft friction in DBS is again affected by the prototype pile diameter (CDBS-5, CLBS-7 and CDBS-2), which is thought to be either due to changes in stress due to friction on the side walls or due to a scale effect.

There are some peculiarities in the average global unit shaft friction measured in tests CDBS-4 and CDBS-5. In both tests there is a marked decrease in shaft friction starting at about 200 mm penetration at the model scale. Such a decay was neither observed in the average local readings (Figure 5-29) nor in the other tests of comparable density and stress level (e.g. CDBS-10) and will therefore be ignored in the subsequent analyses.

Figure 5-27 shows the shaft friction coefficient, β, plotted against pile penetration. Compared to Figure 5-23 the decay in β with depth is similar but the overall values are only 50% of those for the quartz sand. This is in agreement with observations by Coop (1999b) from a back analysis of full-scale pile tests in a variety of carbonate sands and demonstrates that an extrapolation to carbonate sands of design charts based on relative density and a pile test database of silica sand can be very dangerous, as the pile shaft resistance is significantly overestimated. The general observation is again that no unique relationship exists between β, pile penetration and relative density.

Figure 5-28 shows the local unit shaft friction for individual SRTs during penetration with depth for test CDBS-10. In general the shaft friction is highest closest to the pile tip as indicated by the reading of SRT-1. As for the LBS the shaft friction decays generally with increasing h/R ratio along the pile shaft.

As shown by Figure 5-29b, the agreement between the average global and local values of unit shaft friction in DBS is fairly good and within a band of -25 to +50%. There appears to be a greater variation in the locally measured values especially during the 200-g tests, and for the

100-g tests on loose samples the local values are slightly low compared to the global ones. The effect of overconsolidation on the shaft resistance is similar to that observed for the unit base resistance with the exception that the peak occurs at a greater penetration. In general, the magnitude of shaft friction observed is similar to results reported by other researchers (e.g. Chin & Poulos, 1996).

5.3.4 Radial Stress Distribution During Pile Installation

The radial stresses are measured at four positions along each model pile. The positions of each radial stress transducer (RST) are given in Table 4.3. In a similar way to the average local shaft friction an average value of radial stress has been calculated along the embedded length of the pile by integration of the locally measured profile. The procedure adopted is illustrated in Figure 5-30.

(a) Distribution of Radial Stresses During Pile Installation in Leighton Buzzard Sand

The radial stresses during pile penetration in LBS are illustrated in Figure 5-31 for tests CLBS-16 and CLBS-18. In both tests the maximum radial stress occurs at RST-2 at an *h/R* of 12.7. The measured values of radial stresses are generally higher than the estimated earth pressure at rest. At a depth of about 5 m, there is "knee" like feature in the radial stress profile. For larger penetrations the increase in radial stress then occurs at a much slower rate.

In order to investigate the *h/R* effect, the data for tests CLBS-16 and CLBS-18 are re-plotted in Figure 5-32 for three snapshots of different pile penetrations. As can be seen the radial stress increases at first up to a maximum which may be slightly above RST-2 at an *h/R* of around 14. Soon after RST-2 has passed a point in the ground the radial stress starts to decay. This leads to a bell-shaped curve which is somewhat different to distributions of radial stress proposed by Randolph et al. (1994) or Jardine & Chow (1996), who assume that the maximum radial stress occurs adjacent to the pile tip. The distribution in Figure 5-32 is, instead, rather similar to those reported by Vesic (1970) and Altaee et al. (1993). However, the stress state in the lower part of the centrifuge model might have been affected by the friction on the side walls of the strongbox which would have reduced the stresses below those calculated.

Figure 5-33 shows the profiles of average radial stress calculated during pile penetration in LBS. Note that the first RST is approximately 50 mm above the pile tip which leads to the stepwise increase in average radial stress at the start of penetration. In theory all the curves should start from the origin. This for example would have resulted in much better agreement between CLBS-15, CLBS-20 and CLBS-22 which are at different gravity levels. There were some problems with RST-1 and RST-2 on CUIMP-3 during test CLBS-19. As a consequence

the measured average radial stress is much lower compared to CLBS-16. It can be concluded that the RSTs on CUIMP-4 were more reliable compared to those on CUIMP-3. There is good agreement in the profile of average radial stress with depth between the tests on dense samples at various g-levels, and as expected from the unit shaft friction profile, the radial stresses in the dense samples increase almost linearly with depth. The effect of overconsolidation on the average radial stress is less pronounced compared to the average global unit shaft friction.

(b) Distribution of Radial Stresses During Pile Installation in Dogs Bays Sand

Figure 5-34 shows the measured radial stress during penetration for tests CDBS-9 and CDBS-10 respectively. As for LBS, transducer RST-2 yields the highest value, but the magnitude of the radial stresses is generally less than for LBS. The values are again higher than the estimated earth pressure at rest soon after the transducers enter the soil but appear to reach a constant value after a particular depth has been reached.

Figure 5-35 illustrates the *h/R* effect for three snapshots of different penetrations for tests CDBS-9 and CDBS-10. There is a general decay of radial stress with increasing *h/R*. However, as for the LBS, the maximum radial stress does not seem to occur closest to the pile tip as proposed by Randolph et al. (1994) and Jardine & Chow (1996), but reaches a maximum at an *h/R* of around 14.

The profiles of average radial stress calculated for the tests on DBS are shown in Figure 5-36. As can be seen by comparing CDBS-2 conducted with CUIMP-3 and CDBS-12 (CUIMP-4), there is some inconsistency between the readings from both piles with the radial stresses in the dense sample (CLBS-12) being less than in the loose one. The average radial stress measured in CDBS-2 appears to be high in comparison to the other tests while in CDBS-12 it appears to be low. For all samples prepared by dry deposition and subsequent compaction the measured radial stresses fall within a relatively narrow range between 80 and 130 kPa. At depths below 30 m the average radial stress is essentially constant.

The effect of compressing and unloading a loose sample prior to testing (overconsolidation) on the average radial stress reflects the distribution of the unit shaft friction. There is an increase in radial stress by a factor of about 2.7 in test CDBS-14 compared to CDBS-12. This is consistent with the unit shaft friction and adds confidence to the radial stress measurements. It is interesting that the peak average radial stress occurs at a similar depth to the unit shaft friction, but much deeper than the peak in unit base resistance. A possible cause of this could be the change in microstructure during pile installation. This will be discussed further in Section 5.6.

5.3.5 Interface Friction Angles

Measuring the local shaft friction and radial stress directly during pile installation allows the interface friction angle, δ, to be calculated either at particular locations or as an average over the embedded length of the pile. The latter approach will be used exclusively in this study.

The interface friction angles calculated can then be compared to measurements made in laboratory tests such as the direct shear box, as described in Section 3.3 or the ring shear apparatus, as will be discussed later. This allows a much improved assessment of the pile behaviour compared to the conventional procedure of estimating the interface friction angle from the soil-soil friction angle as suggested by Fleming et al. (1992) or simply by assuming a value from experience as suggested in API-RP2A (1993).

(a) Interface Friction Angles in Leighton Buzzard Sand

Figure 5-37 and Figure 5-38 show the interface friction angles calculated from the average global and average local unit shaft resistance and the average radial stress. Both the global and local interface friction angles are essentially constant with depth and vary between 12° and 20°, which is quite low compared to the values recommended in current design methods such as API-RP2A. The mobilised friction angles in the dense samples are generally higher than those in the loose samples. The higher values at the start are not reliable and are the result of the model pile geometry and the problems this caused for averaging the radial stresses at shallow penetrations, as discussed in Section 5.3.4.

There appears to be an effect of g-level, or in other words equivalent prototype pile diameter, on the interface friction angle calculated from the global unit shaft resistance. However no such effect is observed for the local readings. This is consistent with observations on the unit base resistance and the global unit shaft resistance as discussed in Sections 5.3.2 and 5.3.3. As was illustrated in Figure 5-25b, for the unit shaft friction, there is good agreement between the global and local interface friction angles. Using the same radial stress for both local and global friction angles results in an agreement within a band width of ± 25%.

The measured values of interface friction angle along the pile shaft are much lower than the values of 26.5° measured in the shear box, as described in Section 3.3.2, even though the normalised roughness, as well as the stress level, were similar. The friction angles measured in the shear box were more or less independent of the initial sample density, which was an observation also made by Lehane (1992), but for the pile data the evidence is contradictory as to whether density has an effect.

The difference in friction angle between the pile and shear box could in part be due to differences in testing conditions, as the stress state in the shear box is one of plane strain while the pile is an axi-symmetric condition. Wroth (1984) presented the following relationship between the plane strain friction angle, ϕ'_{ps} and the for axi-symmetric friction angle, ϕ'_{tc}:

$$8\phi'_{ps} = 9\phi'_{tc} \tag{5.2}$$

For the interface friction angle measured in the shear box the equivalent value for the pile would then be about 23°, still significantly higher than the average value measured along the pile shaft.

Garnier & Koenig (1998) demonstrated the dependence of the interface friction angle on the normalised roughness of the interface. They obtained friction angles between 14° and 30° on a silica sand-steel interface (see Figure 2.34). This band width is similar to that obtained in the centrifuge tests and could be one explanation for the observations made here. Other possible causes of this phenomenon could be the difference in the stress paths followed due to pile installation of a soil element sheared along the pile interface compared to that in a shear box test, or the difference in the magnitude of the displacements. Both issues will be discussed further after examining the data for the tests on DBS.

(b) Interface Friction Angles in Dogs Bays Sand

The interface friction angles for DBS for both average global as well as average local unit shaft resistance are plotted in Figure 5-39 and Figure 5-40. Both the global and local interface friction angles are essentially constant with depth and vary between 7° and 20°. The friction angle generally increases with increasing density. The higher values at the start are again the result of the model pile geometry as discussed in the previous section. The values obtained for the overconsolidated samples fall within the range of the other 200-g tests.

As for the LBS, the values of interface friction angle along the pile shaft are much lower than the 26.5° measured in the shear box (Section 3.3.2). The effect of g-level, or in other words equivalent prototype pile diameter, on the interface friction angle is also present in DBS. This time the effect is apparent for both global and local readings. As for the LBS there is generally good agreement between both means of calculating δ, although the values calculated from the local shaft friction for the 50 and 100-g tests are slightly less than for the global shaft friction. There is also some discrepancy between the friction angles obtained for test CDBS-10 compared to the other data, which is mainly due to the lower local unit shaft resistance.

(c) Ring Shear Tests

As no suitable explanation for the phenomenon of the low friction angles on the pile-soil interface could be found in the literature it was decided to perform an additional series of interface ring shear tests on both soils using the Bromhead ring shear apparatus. The tests are still being carried out by Mr. Andrea Cavalieri, a visitor from the University of Trento. Normal stresses between 100 and 1000 kPa have been used, which covers the range of radial stresses measured along the pile shaft in the tests on LBS (see Figure 5-33). Already the first test series for each sand sheared along an aluminium interface, the data for which are in Figure 5-41, have given some interesting results. The interface friction angles obtained vary between 8° and 20°, which is very similar to the values measured on the model pile and very different to the measurements in the shear box. The results indicate that the important factor controlling the mobilisation of the interface friction angle is the displacement, as the applied stresses were the same both in the ring shear and shear box tests.

The interface roughness was carefully measured before and after each ring shear test, as described for the shear box tests in Section 3.2, in order to discover changes in roughness that might effect the friction angle of subsequent tests. The two numbers of roughness average, R_a, given in Figure 5-41 refer to measurements taken before and after each test. This information, in combination with the observed mobilised friction angles, reveals some interesting features that are worth noting. At low normal stresses (130-140kPa) the mobilised friction angle in the ring shear tests remains very low for both soils and the roughness tends to reduce slightly during the test. At the higher normal stresses (1000kPa) the mobilised friction angle is much higher, and the roughness increases. If the normal stress is reduced during the tests the mobilised friction angle reduces slightly but not to the values recorded for the lower stress tests which is the result of the increased roughness. At the intermediate stresses (300kPa) a transitional behaviour is seen and the friction angle increases during the tests, but quite slowly and the roughness again increases. It appears from these tests that the hardness of the interface may therefore be as important as its initial roughness.

Following these observations the roughness of model pile CUIMP-3 was measured again at the end of the tests series. Comparing the results of these new measurements with the original values both of which are shown in Table 5-2 reveals that the roughness reduced slightly. This is also evident in from the roughness profiles in Figure 5-42 compared to that in Figure 3.12a which indicates that the peaks of the profile and consequently the R_{max} value are reduced due to abrasion during pile installation. Hence the surface has become smoother. However, looking at a magnified aluminium sleeve section (Figure 5-43) reveals that there is a series of longitudinal scratches, which were carved by the grains passing along the pile. These could not have been

present prior to testing, as the sleeves were machined on the lathe creating a radial surface texture. No such scratches were visible on the titanium sections. This is evident from the values of roughness measured in tests Ti-3/1 and Ti-3/2 which are very similar to Ti-2/1. However, test Ti-3/1 was carried out along a circumferential direction, while test Ti-3/2 was performed in the same location but in a longitudinal direction. One general problem with measuring the surface roughness with a stylus type of instrument is that the measurements are usually taken perpendicular to the direction of machining (along the pile axis) hence all the longitudinal features associated with abrasion along the pile cannot be captured. The scratches that occur in the aluminium section clearly change the surface texture of the pile.

The tests carried out so far have shown that the choice of materials and the initial roughness of any model surface in interface roughness tests is key to achieving good repeatability. It could be concluded that although aluminium was chosen for the friction sleeves of the pile because of its convenience of machining and the sensitivity it gives to the frictional load measurements, in retrospect using a rough interface texture and hard materials, such as titanium and steel, would have given more consistent and repeatable shaft friction measurements. A stylus type instrument only allows a crude assessment of the surface characteristics and it would be beneficial to use more sophisticated techniques for future research in this area. However, as the ring shear tests are not yet fully conclusive no final discussion is possible at this point.

5.4 Results of Pile Load Tests

As described in Section 4.5 load tests in tension and compression were performed at a variety of different depths in both sands. The presentation and discussion of the results will focus on the compression load tests. Full details of the test configurations are provided in Table 5-3 and Table 5-4. At the end a brief comparison will be made between the mobilised shaft resistance in compression and tension.

The data are presented in terms of normalised pile head displacement plotted against normalised shaft or base resistance. The normalised pile head displacement is the relative pile head movement, dz, divided by the pile diameter, d_p. The normalised values of shaft friction and base resistance are the values of the current readings of either divided by the value of shaft or base resistance immediately before stopping and unloading the pile prior to the load test. For the load tests the pile was first unloaded either to a condition of zero head load or fully mobilised tensile shaft capacity, and then re-loaded at constant speed. The condition of zero head load prior to loading resembles more closely a load test in the field.

In the region of small displacements the data were not reduced as described in Section 5.2.1 in order to have a higher number of points. Especially in the early tests the speed on re-loading was a little high, leading to a limited number of data points. In these early tests the pile was pulled out a fixed amount of between 1.4 and 1.8 mm in order to mobilise the full tensile pile capacity. This was also sufficient to have zero base resistance and a negative global force. Some stress relief underneath the pile tip therefore occurred, with soil grains possibly moving into the cavity below the pile tip. As a consequence, upon re-loading the response of the base of the pile was soft at small strains. The final values were, however, similar to those for the load tests starting from a zero head load condition i.e. without the initial stress relief, but larger relative displacements were required for mobilisation of the ultimate capacity.

There are a few problems in the data for some tests at very small displacements as the potentiometers used were operating at their limiting resolution, which is about ±0.02 mm. This gives a d_z/d_p ratio of 0.001. An increase in capacity was sometimes observed with the penetration staying almost constant or even reducing, leading to some scatter in the data. For these tests the data have been smoothed with a five point average while retaining the general trend.

5.4.1 Pile Load Tests in Leighton Buzzard Sand

Figure 5-44 and Figure 5-45 show the mobilisation of unit end bearing and shaft resistance respectively during the pile load tests on LBS. As discussed in Section 2.4.2 a normalised pile head settlement of 0.1 would give the ultimate pile capacity according to most current pile design methods. For the load tests conducted from zero head load initial condition only 90% of the unit base resistance is mobilised at this settlement, the full value being reached at around 0.4. A value of unit shaft resistance equal to that immediately prior to unloading is mobilised at a d_z/d_p of 0.04 and exceeded by about 12% at the end of the compression load test. This is in good agreement with observations by Chow (1996), who attributed the effect to an increase in radial stress (equalisation) and slower shearing rates. The mobilisation of the capacity for the load tests conducted from a full tensile initial condition was delayed. In general only 50% of the unit base resistance was mobilised at 0.1 relative pile head settlement, while the 100% level is again reached at around 0.4. The full unit shaft resistance prior to unloading is mobilised at a normalised displacement of 0.1 and exceeded again by about 12% at a relative settlement of 0.15. There is generally very good agreement between the tests. The minor variations in the mobilisation curves of the tests with an initial zero head load are possibly due to differences in the initial stress state around the pile tip, as unloading of the pile prior to the load test was performed using manual control of the actuator motor. The increase in shaft friction is mainly due to changes in radial stress during the load test. This can be observed for example for test

CLBS-21 in Figure 5-33 at a depth of 24 m, where the radial stress increases from about 200 to 250 kPa. This build up of radial stress decays once the penetration is continued to larger depths. The observation is also significant for the cyclic response of the pile as will be discussed later. The rate of loading considered by Chow (1996) to be a factor contributing to the increase in shaft friction seems to be of secondary importance for the tests conducted in this study. This can be observed from Figure 5-45 by comparing for example test TLBS-12 which was carried out at a speed of 0.2 mm/s with TLBS-20 conducted at 0.05 mm/s. The difference in unit shaft friction between these tests is within the general scatter of the data.

Figure 5-46 shows a comparison of the tensile and compressive shaft capacities obtained from the load tests plotted against the embedded length of the pile. The tensile shaft capacity is between 20 and 70% of the shaft capacity in compression which is much lower than the 90% suggested in the MTD-Method and the 80% proposed by de Nicola & Randolph (1993). The ratio of tensile and compressive shaft capacity appears to be independent of the embedded length of the pile. An alternative plot using state rather than depth will be presented later.

Table 5-3 shows the initial vertical stress in the soil at the depth of the pile tip which was used to calculate the N_q. Half of this vertical stress was taken to calculate β for each load test at a normalised pile head displacement of 0.1. As for the pile penetration data presented earlier, there is a clear trend that both N_q and β reduce with increasing pile penetration, a feature not accounted for in current pile design methods such as API-RP2A. In comparison to API-RP2A the measured values of N_q are high, but they are in good agreement with those measured by Fioravante (1994). The β values obtained are low in comparison to Toolan et al. (1990) and also Fioravante. The latter effect may be explained by differences in pile surface roughness and its effect on the interface friction angle in comparison to piles in the field.

5.4.2 Pile Load Tests in Dogs Bay Sand

Figure 5-47 and Figure 5-48 show the mobilisation of unit end bearing and shaft resistance respectively during the pile load tests in DBS. For the load tests conducted from a zero head load initial condition, 95% of the unit base resistance prior to unloading is mobilised at a settlement of 0.1 pile diameters. Between 0.1 and 0.4 normalised pile head displacement there is no significant increase in unit end bearing. The unit shaft resistance is again mobilised faster and reaches 100% of the previous value at a normalised displacement of 0.04 for CLBS-12 and exceeds it by about 12% at a relative displacement of 0.4. The load mobilisation for the load tests conducted from a tensile initial condition was again delayed with only 50% of the unit base resistance prior to unloading being mobilised at 0.1 normalised pile head displacement, while

the 100% level was reached at around 0.2, which is a smaller displacement than for the tests on LBS. The unit shaft resistance prior to unloading in these tests is mobilised fully at a normalised displacement of 0.1 and exceeded by about 12% at a value of 0.15. The increase in shaft friction during the load tests is again due to changes in radial stress. This is not very obvious from Figure 5-36 but could be observed during data processing from the individual transducer readings for example for test CDBS-12.

Figure 5-49 shows a comparison of the tensile and compressive shaft capacities obtained from the load tests as a function of depth. The tensile shaft capacity is between 20 and 70% of the shaft capacity in compression which is similar to LBS. There appears to be no relationship between the ratio of tensile and compressive shaft capacity and the embedded length of the pile.

There is again some scatter in the data, particularly for the shaft friction. As pointed out in the discussion for LBS this is due to the manual control of the unloading of the pile prior to the load tests. The calculated values of N_q and β are shown in Table 5-4. As for the LBS both N_q and β reduce with increasing pile penetration. The measured β values are similar to results obtained by Coop (1999a) from a back analysis of published field data on piles in a variety of carbonate sands.

The main conclusion from the load tests on LBS and DBS is that the base resistance observed during a pile load test is similar to the resistance during penetration while the shaft resistance was found to increase by 12%. Hence using a slightly conservative approach with respect to the shaft resistance, the calculated N_q and β profiles presented in Section 5.3.2 and 5.3.3 for penetration could be interpreted as design parameters derived from pile load tests at any given depth. They can thus be used as a basis for developing a design method based on soil state, a concept that will be introduced in Section 5.7. It was found that both N_q and β decrease with increasing pile penetration, which is not considered by current pile design methods such as API-RP2A. The shaft friction ratio β seems to be affected by the normalised roughness of the model pile, which may hamper comparisons of the results of model tests with full-scale field tests.

5.5 Effect of Creep on Pile Capacity

In recent years the effect of creep on the capacity of driven piles has been investigated by a number of researchers (e.g. Lehane et al., 1993 and Chow et al., 1996). The pile capacity was found to increase by up to 50% per log cycle of time (see Figure 2.43). The investigations were carried out over a duration of as much as five years.

In order to extend the database on the time dependent behaviour of driven piles it was decided to carry our a number of creep tests in each soil. This was achieved by introducing waiting periods following the unloading of the pile prior to the onset of re-loading for the load test. In contrast to the time required for consolidation, the time during creep events is not scaled during a centrifuge test. Therefore, only relatively short creep stages could be modelled. The maximum time span was limited to two hours in order to keep the temperature in the centrifuge at an acceptable level (see Section 5.2.3). Two additional load cycles at intermittent waiting periods of approximately 6 and 20 minutes were added to achieve about one test per log cycle of time. The details of these tests have been given in Tables 4-10 and 4-11.

The data obtained during the load tests following a creep stage are presented in terms of total, base as well as shaft pile capacity. The total capacities of the pile, $Q_t(t)$, the base resistance, $Q_b(t)$, as well as the shaft resistance, $Q_s(t)$, used here again represent the measurements taken at a normalised pile head settlement d_z/d_p of 0.1 during load test following a particular creep stage. These capacities have again been normalised with respect to the value immediately before the end of penetration prior to the load test, $Q_s(t=0)$.

Figure 5-50 and Figure 5-51 show the results of the creep tests on LBS and DBS respectively. For the first load cycle there is generally an overall increase in the shaft capacity for both soils, as was observed for the load tests above. However, this build up in shaft friction decays with time and an increasing number of load cycles and may not be a creep related phenomenon. This shows the limitations of the adopted testing procedure as the effect of creep which increases the pile capacity (Chow, 1996) is counteracted by the effect of repeated load cycles. Separating both effects would have require additional tests that were beyond the scope of this project. In contrast to the shaft capacity, the base capacity increases slightly with increasing time and number of load cycles. Both effects counteract each other and as a consequence there is no significant increase in total pile capacity within the test period. Generally, the data obtained are of limited use due to the restrictions in test time imposed by the centrifuge.

5.6 Investigation of Particle Breakage

As was shown in Figure 5-16 and Figure 5-19 the stress level underneath the tip of the pile during penetration can be quite considerable. In cases were the stress level exceeds the crushing strength of the grains particle crushing occurs. The micromechanical processes involved have been described by McDowell & Bolton (1998). If there is substantial breakage in then the grading of the soil will gradually change for subsequent tests resulting in a shift in the critical

state line location (Coop & Atkinson, 1992). This was avoided in the centrifuge tests by carefully examining the amount of breakage after each test, especially in the DBS.

No measurable particle breakage occurred in LBS prior to pile installation. The particle breakage was limited to areas around the pile in tests CLBS-4, CLBS-20 and CLBS-22 on dense samples at 50, 100 and 200-g. Crushed particles were visible in the vicinity of the pile tip mainly in the form of little lumps and bands of fine particles of lighter colour. Figure 5-52 shows a small cone of crushed and interlocked particles recovered from the depth of the pile tip at maximum penetration during test CLBS-22. Particles taken from this cone were photographed under a microscope and are shown in Figure 5-53. A comparison with Figure 3.1a clearly shows a change in particle size with a larger proportion of fines. Unfortunately not enough soil could be collected to quantify accurately the amount of particle breakage.

DBS is much more crushable than LBS owing to the lower crushing strength of its particles. Particle breakage already occurred prior to pile penetration simply due to the stress increase in the centrifuge. As a consequence, the entire soil sample was re-sieved on average after every third centrifuge test in order to retain the original grading. The change in overall grading between CDBS-7 and CDBS-10 is illustrated in Figure 5-54. As can be seen the grading remained essentially unchanged. Thorough re-mixing before each test ensured an effectively constant grading curve. Addition breakage occurred during pile installation. Figure 5-55 shows a small cone of crushed and interlocked particles recovered at the depth of the pile tip at maximum penetration during test CDBS-12. Such cones were recovered from every test. The angle of the cone is approximately 85°, which is about 20° more than the angle suggested by Randolph et al. (1994) for a cavity expansion formulation.

For the compacted samples of DBS the soil could be removed easily with a little shovel after each test, regardless of the initial density and the g-level at which the test had been carried out. The situation was rather different for the overconsolidated samples. Figure 5-56 shows a picture taken during the excavation of the soil after test CDBS-13. The dry sand could be excavated at a slope angle of 90° with the exception of the central section which the pile had penetrated. In this zone, approximately 3-4 pile diameters wide, the soil was completely remoulded and the original structure created during compression had been destroyed. In a way, the pile appears to have "punched" through the centre part of the sample leaving the soil structure outside the zone of influence virtually undisturbed. The hole created by the pile collapsed as the pile was removed in flight.

Particles recovered from the centre part of CDBS-13 were photographed under a microscope and are shown in Figure 5-57. A comparison with the original particles shown in Figure 3.1b

clearly demonstrates the magnitude of particle crushing. A series of samples was collected in both the remoulded and intact area of sample CDBS-13. Figure 5-58 shows the average gradings before and after the test. The soil in the undisturbed part of the sample had already crushed to some extent during compression. This is consistent with observations in the triaxial tests as was shown in Figure 3.50. Far more crushing occurred in the "punching" zone around the pile. Similar observations were made after test CDBS-14. The behaviour observed in both tests is similar to results reported by McDowell & Bolton (1999) on dense samples of Quiou sand that had been prepared using a vibration technique.

McDowell & Bolton (1999) have suggested that the peak in resistance seen during penetration (Figure 5-14) is caused by the onset of heavy destructuration due to particle breakage below this depth. They collected a series of samples along the pile shaft and found that little breakage had occurred in the zone above the peak. Unfortunately within this study no such detailed analysis of the particle breakage was possible. However, it is interesting to note that McDowell & Bolton while using a different carbonate sand to DBS observed a peak in the penetration curve for piles pushed into dense samples but no such observation was made in this study, where peaks only occurred in the two overconsolidated samples. Before a final attempt will be made to explain the pile behaviour in the overconsolidated samples of DBS, the data will be normalised with respect to the in situ state as this might account for the observed response during pile installation.

5.7 Normalised Pile Behaviour

So far, the discussion of the results of the centrifuge model tests has highlighted the shortcomings of current pile design methods such as API-RP2A. The data obtained from the centrifuge model tests have been shown to be of good quality and consistent with results reported by other researchers. Figures 5-17, 5-20, 5-23 and 5-27 have shown that there is no unique relationship between relative density and the pile design parameters N_q and β. It was argued that this is because relative density is not a suitable measure of soil state as it does not account for the influence of stress.

All these observations point towards the need to establish a more realistic framework for pile capacity analysis that takes into account both the stress and volumetric state of the soil. In Sections 2.2 and 2.4 of the literature review the framework of critical state soil mechanics and in particular the use of a state parameter have been identified as the most promising option and will now be pursued.

In the following section the in situ state of each centrifuge test will be identified first. Owing to the difficulties with identifying critical states at low pressures in the triaxial tests (see Chapter 3) a stress state parameter will be used to interpret the centrifuge tests rather than a volume state parameter as defined by Been & Jefferies (1985). For simplicity this stress state parameter will be called state parameter although it should be emphasised that it is fundamentally different from the state parameter defined by Been & Jefferies. The state parameter is calculated for each sand as a stress ratio between the in situ stress and the stress at the critical state at the same specific volume. The CSLs determined in Section 3.4 will be used. The behaviour of the model piles will then be re-examined in Section 5.5.2 using this state parameter concept.

5.7.1 Soil State During Centrifuge Tests

The use of the proposed stress state parameter concept requires knowledge of the in situ specific volume and stress prior to pile penetration. During acceleration of the centrifuge, the stress level in the model at a given depth, z, increases as a function of the angular velocity according to Equation 4.6. As a consequence the soil compresses and the specific volume reduces. The magnitude of the compression depends on the specific volume achieved during sample preparation and on the compressibility of the material. This reduction in specific volume can have a significant effect on the pile behaviour and must be taken into account. For this reason three LVDTs were incorporated in the centrifuge model and their probes embedded at different depths in the soil, thus dividing the sample into four layers the change in thickness of which could be measured. The position of the LVDTs is shown in Figure 4.1 and their configuration was described in detail in Section 4.3.4.

The procedures adopted to arrive from the LVDT settlements to the in situ state for each sample will be outlined in detail for the tests on LBS. The in situ states for the Dogs Bays sand have been calculated using the same procedure.

(a) In Situ State During Tests on Leighton Buzzard Sand

Figure 5-59 shows typical settlements measured during test CLBS-18, conducted at 200-g on an initially loose sample of LBS. The settlement increases rapidly during the spin-up phase but changes little during pile penetration. There is some swelling during spin-down towards the end of the test. The surface settlement profile during the test was estimated from the measured surface settlement at the end of the test and the settlement profiles of the three LVDTs during the test.

The specific volume of each layer was then calculated from the original specific volume and the volumetric strain at the target g-level using Equation 3.10. The average density of each layer was then re-calculated using Equation 5.4 in order to obtain the average vertical stress at the centre of the layer from Equation 4.6. Finally, the mean normal stress at the centre of each layer was obtained using the K_o values presented in Section 3.4.6. It was assumed that the friction mobilised on the side walls of the strong box had no significant effect on the vertical and horizontal stresses in the centre of the strong box, and theses stresses ultimately control the behaviour of the pile.

The in situ states of the LBS centrifuge samples are shown in Figure 5-60 together with the two possible critical state lines proposed in Section 3.4.6. The sets of four data points correspond to the four layers. For each test there is one set in the low pressure range represents the in situ state at 1-g while the set at the higher pressures represents the in situ state at the target g-level. The most important aspect to notice in Figure 5-60 is that all the in situ states are below the critical state line. Due to the relatively flat gradient of the CSL the dense samples have a much larger value of the state parameter than the loose samples at the same in situ stress.

Based on Figure 5-60 the normalisation will be performed in two ways: firstly with respect to the linear critical state line given by Equation 2.5 and secondly with respect to the curved critical state line defined by Equation 2.6. The relevant parameters for these equations were presented in Table 3-13. The difference between these two normalisation techniques should be most significant for the loose samples where the two possible CSLs diverge most.

Only four data points for the in situ state, as shown in Figure 5-60, is not sufficient to obtain a continuous profile, for example, of normalised unit base resistance with depth. Therefore, a linear regression was applied to the data. Figure 5-61 shows the distribution of specific volume at target g-level with prototype depth. As can be seen, the specific volume increases approximately linearly with depth according to :

$$v_z = v_i + m_z z_p \tag{5.3}$$

where, v_z is the specific volume at any prototype depth, v_i the initial specific volume at the top of the sample, m_z is the gradient and z_p the prototype depth. The values of m_z shown in Table 5-5 were obtained by linear regression from Figure 5-61 and are listed according to the initial density and g-level. As can be seen, the assumption of a linear relationship is not unreasonable within the range of depths used. The correlation coefficient for tests LBS-20 and CLBS-22 are somewhat lower than for the other tests, which is due to the small overall volume change within the sample, which was reaching the accuracy level of the experimental set-up. It is worth noting

that the gradients for the overconsolidated samples were less than those for the comparable compacted samples at a similar specific volumes. This is consistent with observations by for example Coop & Lee (1993).

This continuous profile of specific volume was then used to calculate the current dry density, ρ_d, at any given depth in the sample using:

$$\rho_d = \frac{\rho_s}{v_z} = \frac{\rho_s}{v_i + m_z z_p} \tag{5.4}$$

where ρ_s is the particle density. The vertical stress in the centrifuge model at any given depth, z_m, can be obtained by substituting this expression into Equation 4.6 for ρ and further substituting for ω^2 as described for Equation 4.8, which yields the relationship:

$$\sigma_{vm} = \frac{\rho_s N g z_m}{(v_i + m_z z_p) R_e}\left(R_e + \frac{z_m}{2} - \frac{h_m}{3}\right) \tag{5.5}$$

where σ_{vm} is the vertical stress in the model, N the scaling factor, R_e is the radius at which the scaling factor is accurate and h_m is the height of the model. The current specific volume at a given depth will be used to calculate an equivalent mean normal pressure at critical state, p'_{cs}, using Equation 5.6 for the linear CSL and Equation 5.7 for the non-linear CSL.

$$p'_{cs} = e^{\frac{\Gamma - v_z}{\lambda}} \tag{5.6}$$

$$p'_{cs} = \frac{h_s}{3}\left(-ln\frac{e_c}{e_{co}}\right)^{\frac{1}{n}} \tag{5.7}$$

where Γ is the specific volume on the CSL for a p' of 1 kPa, λ the gradient of the CSL in v:lnp' space, h_s the granular hardness, e_c the void ratio at the CSL, e_{co} the void ratio at critical state at zero p' and n the exponent of the hypoplastic model. The pressures are then taken to calculate the stress state parameter, R_s:

$$R_s = \frac{p'_o}{p'_{cs}} \tag{5.8}$$

where p'_o is the mean normal stress in the centrifuge model prior to pile installation. The definition of R_s as a stress ratio is different from the state parameter defined by Been & Jefferies (1985) in terms of void ratio, which represents a volume state parameter. For simplicity R_s will

be referred to as state parameter from now on. The centrifuge model data for LBS that were presented in Section 5.3 will now be re-analysed using Equation 5.8. The normalised profiles will be presented in Section 5.7.2. For all calculations involving the shaft friction, the depth in Equations 5.3 and 5.5 will be taken as half the pile tip penetration. Thus the in situ stress as well the pressure at critical state represent average values at this depth.

(b) In Situ State for Tests on Dogs Bay Sand

Figure 5-62 shows typical settlements measured for test CDBS-10 conducted at 200-g. Even though this sample is medium dense, the settlement at the soil surface is 1.4 times that of a loose sample of LBS. This is consistent with the results of the triaxial tests as well as observations by other researchers (e.g. Coop & Lee, 1993).

The in situ states of the DBS centrifuge samples are presented in Figure 5-63. Also shown is the CSL proposed in Section 3.4.5. As can be seen, for this material in situ states exist on both sides of the critical state line, a fundamental difference to LBS and a fact that cannot be accounted for by using relative density as a state variable. The gradient of the critical state line is much steeper than for the LBS and therefore the stress state parameter, R_s, for the dense samples will generally be larger, meaning that the samples are closer to the critical state line, so that the difference in pile behaviour between dense and loose samples of DBS on the left side of the CSL should be less pronounced compared to LBS. As the linear CSL covers the entire range of in situ volumes for the calculation of p'_{cs} there is little merit in introducing a non-linear CSL into the normalising procedure for DBS. Therefore only the shown linear CSL will be used.

Figure 5-64 shows the distribution of specific volume in the samples with prototype depth. Equation 5.3 has again been used to obtain a continuous profile of specific volume with depth. The values for the gradient, m_z, shown in Table 5-6 were obtained by linear regression from Figure 5-64. As can be seen from the coefficients of correlation the assumption of a linear relationship is not unreasonable within the range of depths considered. The gradients for the medium dense tests are slightly greater than for other tests, which means that they compressed more compared to the loose tests. This is slightly surprising, but the changes in specific volume are generally very small and the difference in specific volume is therefore not large. The gradient for the overconsolidated samples is also less than for the comparable compacted samples at the same specific volume. This is consistent with observations by Coop & Lee (1993).

At the end of this section it is appropriate to consider briefly the effect of overconsolidation on the in situ state of the soil. Figure 5-65 shows profiles of OCR with depth for tests CLBS-21, CDBS-13 and CDBS-14. The OCR reduces rapidly with increasing depth from values up to

sixty near the top to around three close to the base. Compression of CDBS-13 and CDBS-14 created a firm interlocking structure in the sand, and scraping the excess soil from the top of the model required some force. This was very different from the behaviour of the dense compacted samples CDBS-8 and CDBS-12 for which no force was required. As can be seen from Figure 5-63 these four samples have very similar in situ states. The change in structure due to overconsolidation is therefore not reflected in the value of state parameter.

It should be noted that Figure 5-65 was produced making the assumption that the vertical stress in the model during compression in the consolidometer is constant throughout the sample depth. The vertical stress was calculated by subtracting an estimated friction along the vertical container boundary from the global axial force measured by the load cell on top of the platen (see Section 3.4.5a). The friction present along the container boundary is apparent from Figure 3-32 as the difference between the K_o-compression curves in the consolidometer and the triaxial tests. The maximum vertical stress in the model during the compression of CLBS-13 is estimated therefore to be was approximately 1300 kPa instead of the 3000 kPa calculated from measured axial force. Following the observations during the one-dimensional triaxial compression tests on Dogs Bays sand (see Section 3.4.5a) the K_o values for first loading were used for both sands to calculated the horizontal in situ stresses during re-loading of the samples in the centrifuge.

5.7.2 Effects of State on the Pile Capacity

In this section the influence of soil state on the pile capacity will be demonstrated. The soil state is defined by the stress state parameter, R_s derived from Equation 5.8. From the centrifuge test data presented in Section 5.3, the profiles of the bearing capacity factor, N_q , and the shaft friction ratio, β, have been selected to illustrate the merit of the new method in comparison with the methods discussed in Section 5.3.2 and 5.3.3.

(a) Effect of State on the Pile Capacity in Leighton Buzzard Sand

Figure 5-66 shows the relationship between the bearing capacity factor, N_q and the state parameter, derived from the linear CSL. The data for shallow penetrations of the pile plot in the left upper corner and the values of N_q continuously reduce as the pile penetrates the soil. The graph has been produced with the same centrifuge data as Figure 5-17, which plotted the data in terms of relative density. As can be seen, the meaningless graph presented in Figure 5-17 is changed into one that clearly shows the dependency of N_q on the state parameter. This is a striking result. There appears to be an approximately linear relationship between N_q and R_s when using logarithmic axes. The further the in situ state is to the left of the CSL the larger is the

bearing capacity factor. For in situ states on the CSL, R_s is equal to 1. Both dense and overconsolidated samples appear to plot slightly above the other test data, possibly due to a boundary effect or the linear CSL chosen. But these issues will be addressed again later.

The relationship between the shaft friction ratio, β, and the state parameter for the linear CSL is presented in Figure 5-67. This graph has been produced with the same centrifuge data as Figure 5-23 which interpreted the data in terms of relative density. The in situ stress was taken as the average mean effective stress along the embedded length of the pile prior to pile penetration. The values of β reduce continuously as the pile penetrates the soil. Again, by simply changing the normalising parameter a unique and approximately linear relationship between β and the state parameter can be found. The value of β reduces with increasing proximity of the in situ state to the CSL. This time the dense samples plot only slightly above the other tests for larger penetrations and the data for the overconsolidated sample are within the scatter of the other data.

Figure 5-68 and Figure 5-69 show the relationship between N_q as well as β and the state parameter determined from the non-linear CSL for LBS. As expected, the loose samples have smaller values of state parameter and are shifted further to the right and now plot close to the test on the overconsolidated sample (CLBS-21) in case of N_q and even further to the right in case of β.

The most likely cause of the almost constant values of N_q and β observed in both normalised graphs for tests on the dense samples (CLBS-20 and CLBS-21) is a boundary effect. Gui et al. (1998) in a study on cone penetrometers in the centrifuge observed a boundary effect in dense samples of silica sand with a ratio of container diameter to pile diameter (d_w/d_p) of less than 21. However, their samples were slightly looser than the ones used in this study and hence it is even more likely that boundary effects are the cause of this increase in N_q and β, as the d_w/d_p ratio of the model was approximately 19. It is interesting to note, that no boundary effect seems to occur in test CLBS-15 also conducted on a dense sample but at only 50-g. In retrospect the use of a larger diameter chamber would have been advantageous.

Figure 5-70 shows the relationship between the bearing capacity factor, N_q and the state parameter, ψ as defined by Konrad (1988). The graph shows two interesting features. Firstly the relationship obtained is rather similar to that presented in Figure 5-17 for relative density with the difference that the dense samples which are further from the CSL and thus have a higher value if state parameter plot to the left rather than the right. Secondly the state parameter remains essentially constant with pile penetration. This reflects the CSL presented in Figure 5-60, which for pressures below 100 kPa is essentially horizontal thus giving a constant value of ψ. It can therefore be concluded that the use of a stress state parameter, R_s, it is not only more

suitable than using the state parameter ψ as defined by Been & Jefferies (1985) and Konrad (1988) because of the difficulty in identifying the CSL at low pressures as discussed in Chapter 3 and its effect on ψ, but also because the decrease in N_q and β with pile penetration can be accounted for when using R_s.

(b) Effects of State on the Pile Capacity in Dogs Bay Sand

Figure 5-71 shows the relationship between the bearing capacity factor, N_q and the stress state parameter, R_s. The graph has been produced with the same centrifuge data as Figure 5-20 in which relative density was used. There again appears to be an approximately linear relationship between $\log N_q$ and $\log R_s$ for the compacted samples. The value of N_q decreases with increasing proximity to the CSL and continues to decrease for the states on the right hand side of the CSL ($R_s > 1$). This is of fundamental importance as such behaviour cannot be taken into account in design methods based on relative density.

The data for the overconsolidated samples originally plot above the data for the compacted samples but then towards the end of penetration fall back in the range of the other tests. The relationship also seems to be non-linear. There is also some scatter in the data for tests CDBS-2 and CDBS-11 which also plot slightly high. There were some problems with the LVDTs in these tests, mainly during CDBS-2, where they went out of range due to the large settlements. It is possible that the estimated in situ specific volume is slightly too high thus increasing the value of R_s.

The relationship between the shaft friction ratio, β, and the state parameter is plotted in Figure 5-72. This graph has been produced with the same centrifuge data as Figure 5-27, which uses relative density. Again, the in situ stress, p', was taken as the average mean effective stress along the embedded length of the pile prior to pile penetration. The values of β continuously reduce as the pile penetrates the soil. There again appears to be an approximately linear relationship between $\log\beta$ and $\log R_s$ with the value of β reducing with increasing proximity of the in situ state to the CSL. The value of β continues to decrease for the states on the right hand side of the CSL ($R_s > 1$).

The data for CDBS-2 are significantly higher than the other tests. It appears that the error associated with the measurement of the specific volume is amplified by the generally high value of average unit shaft friction for this test evident in Figure 5-26. The test data will therefore be excluded during the final discussion. The relationship for the overconsolidated samples is again non-linear. The shape of the curve is consistent with Figure 5-26, where β starts to increase to a peak towards the middle of the penetration and subsequently decays. For test CDBS-14 particularly the value at peak is significantly higher than for all the other tests.

(c) New Pile Design Equations Considering the In Situ State of the Sand

It can be concluded that the data presented for the compacted samples of LBS and DBS provide strong experimental evidence that for piles driven into both materials, the bearing capacity factor N_q as well as the shaft friction ratio β are uniquely related to the stress state parameter, R_s. There are approximately linear relationships in log-log space between N_q or β and the state parameter. Mathematically the relationships obtained can be expressed as:

$$ln\, N_q = m_{Nq}\, ln(R_s) + ln\, A_{Nq} = m_{Nq}\, ln\left(\frac{p'_o}{p'_{cs}}\right) + ln\, A_{Nq} \tag{5.9}$$

$$ln\, \beta = m_\beta\, ln(R_s) + ln\, A_\beta = m_\beta\, ln\left(\frac{p'_o}{p'_{cs}}\right) + ln\, A_\beta \tag{5.10}$$

where m_{Nq} is the gradient of the line for the N_q plot, A_{Nq} is the value of N_q for an R_s equal to one, m_β is the gradient of the line for the β plot and A_β is the value of β for an R_s equal to one. These parameters, for both soils tested, are summarised in Table 5-7. The interpreted lines are illustrated in Figure 5-73 and Figure 5-74. It can be seen that the lines for DBS lie above those of LBS and have a slightly steeper gradient. This means that for the same in situ state of the soil the capacity of a pile driven into DBS will be higher. This is rather interesting given the common argument (e.g. API-RP2A, 1993) based on the consideration of relative density that the pile capacity in carbonate sands is less than in silica sands. It can be concluded that the argument presented in API-RP2A results from a wrong interpretation of pile load tests using relative density and that using state as reference parameter provides a more rigorous framework. In addition by considering state as shown brings the values of β for the two sands much closer together compared to Figure 5-23 and Figure 5-27 where the relative density was used.

A comparison of Figure 5-73 and Figure 5-74 with the stiffness-state relationships obtained by Jovicic & Coop (1997) shown in Figure 2-10 reveals very similar characteristics for both sands. The high values of N_q and β at small values of R_s are equivalent to the high stiffnesses for the test data for the compacted samples at small values of p'/p'$_c$. The effect of overconsolidation is also very similar. For example for LBS test CLBS21 plots above the trend line for N_q determined for the tests on the compacted samples (Figure 5-66) which is similar to the behaviour observed by Jovicic & Coop. Similar observations can be made for N_q in DBS from Figure 5-71. This adds further confidence to the validity and suitability to this new approach to analyse the capacity of driven piles.

Substituting Equations 5.9 and 5.10 into Equation 2.13 and 2.20 respectively yields the following two new equations that may be applied to pile design:

$$q_b = \left(A_{Nq} \left(\frac{p'_o}{p'_{cs}} \right)^{m_{Nq}} \right) \sigma'_v \tag{5.11}$$

$$q_s = \left(B_\beta \left(\frac{p'_o}{p'_{cs}} \right)^{m_\beta} \right) \sigma'_v \tag{5.12}$$

In order to demonstrate the applicability of this framework to prototype piles the data of shaft friction ratio, β, obtained by Coop (1999a) from pile load tests in a variety of sands has been re-plotted in terms of R_s (Figure 5-75) and the interpreted line added to Figure 5-74. As shown in the literature review there are very few high quality soil test data available for most pile load tests. As a consequence Coop (1999a) could not distinguish different lines for different sands. The line of the field data has a gradient similar to that determined from the centrifuge tests on DBS but plots further to the right. Possible causes of this discrepancy could lie in the lower interface friction angle of the model pile compared to typical piles in the field and scale effects. The MTD-Method (Jardine & Chow, 1996) assumes that the shaft resistance increases with decreasing pile size and one would therefore expect the shaft resistance of the centrifuge model tests to be larger than that of the field data. However, it appears that if such an effect would be present it is not as significant as the difference in roughness.

Unfortunately no pile test data could be found in the literature that would have allowed a similar comparison for the bearing capacity factor N_q and state again mainly due to the lack of good quality soil test data. It appears that undertaking a soil testing programme on the soils for the good quality pile load test as identified in Chapter 2 would allow a more detailed analysis. These tests should be carried out with the aim to establish the position of the CSL. This would then allow the results of this laboratory based research to be verified using all available high quality field data and this new method of designing piles using a state parameter to be firmly established.

One additional point to be discussed concerns the observed behaviour of the overconsolidated samples mainly in DBS (Figure 5-71 and Figure 5-72). It has been shown that the higher values of N_q and β for the larger values of R_s are similar to observations by Jovicic & Coop (1997) of higher stiffnesses. The interesting feature is the increase in β from smaller values to a peak and the subsequent reduction. One explanation for the initially low values of β during tests CDBS-13 and CDBS-14 is that the interlocking structure of the sand initially reduces the radial stress

on the pile. This is most evident for test CDBS-13 in Figure 5-36. The gradual braking down of the structure initially increases the radial stress but as the overconsolidation ratio decreases with depth (see Figure 5-65) the increase stops and the ongoing remoulding finally reduces the radial stress to the levels seen in the compacted soil. As a consequence this also reduces the shaft friction of the pile. It is interesting to note that the required pull-out force in both test CDBS-13 and CDBS-14 was similar to tests in the compacted samples CDBS-8 ad CDBS-12 indicating that the effect of overconsolidation and initial structure was removed completely. Unfortunately, the limited amount of test data available prohibits more general conclusions and it appears that more research is required to understand fully the load transfer behaviour of piles driven into overconsolidated deposits of sands.

The results from the pile load tests in tension and compression presented in Section 5.4 were re-plotted with respect to state as quantified by R_s and are presented in Figure 5-76 for LBS using the linear CSL and Figure 5-77 for DBS. For both soils there is considerable scatter in the data and no unique relationship seems to exist. For some tests the ratio of tensile shaft capacity, $q_{s,t}$, to the compressive shaft capacity, $q_{s,c}$, seems to decrease with increasing R_s (e.g. CDBS-12) but for others the opposite is true (e.g. CLBS-12).

5.8 Summary

The results of ten centrifuge model pile tests on LBS and thirteen on Dogs Bay sand have been presented and discussed in this chapter. The variation in centrifuge acceleration enabled modelling of closed-ended prototype piles between 0.8 m and 3.2 m in diameter and 15 to 70 m in length, allowing a very comprehensive assessment of the behaviour of driven piles in sand. The idea of modelling of models was abandoned mainly due difficulties in producing the required fully instrumented piles of different diameters within the time frame of this project.

During pile installation in both sands the unit base resistance as well as the average unit shaft friction were found to increase rapidly at shallow penetrations but at a reduced rate at deeper penetrations. With the exception of the average shaft friction in Dogs Bays sand no evidence was found in support of the existence of limiting values. Contrary to assumptions in the new MTD pile design method, the value of unit end bearing increased with increasing prototype pile diameter. This is thought to be due to friction along the side walls of the strongbox which affects deeper penetrations (50-g) more than shallower ones (200-g). Good agreement was achieved between the locally and globally measured values of average unit shaft friction. Generally, the average radial stress also increased rapidly at shallow penetrations and at a slower rate with increasing penetration. The radial stress was found to reduce along the pile

shaft, but contrary to assumptions of Randolph et al. *1994 and the MTD-Method the maximum* value occurred not at the pile tip but around the position of RST-2, *about 14 pile diameters* above the pile tip. The distribution of radial stress observed along the pile was therefore found to be similar to results presented by Vesic (1970). However, the results might have been affected by friction along the side walls of the centrifuge model. Due to the lower accuracy of the measurements of the SRTs compared to the RSTs, no such distributions of local unit shaft friction along the pile have been plotted. It was then demonstrated that, contrary to assumptions made in most current design methods, there is no meaningful relationship between relative density and the pile design parameters N_q and β. Both N_q and β were found to vary significantly with pile penetration for a given relative density.

The interface friction angles calculated from the measured shaft friction and radial stress readings were essentially constant with depth and similar for both sands, varying between 7° and 20°, significantly lower than the values measured in the direct shear box. The fact that the interface friction angles in both soils were similar is surprising as the critical state friction angles differ by about 8°. An ongoing study in the Bromhead ring shear apparatus has so far confirmed the range of measured friction angles on the model pile. The roughness, especially of the aluminium sections, was found to increase as a function of the applied normal stress causing an increase in friction angle. The sand grains appeared to have carved longitudinal scratches into the aluminium sections that were clearly visible under the microscope. As the pile surface was machined on the lathe the roughness measurements were carried out along the pile axis and it was therefore possible that with the stylus type instrument employed these scratches remained undetected. It can therefore be concluded that stylus type instruments are of limited use to study the complex surface texture created while shearing sand along metal interfaces.

The main conclusion drawn from the load tests on LBS and DBS is that the observed resistance during penetration is similar to the resistance during a pile load test. Hence the calculated N_q and β profiles presented in Sections 5.3.2 and 5.3.3 could be interpreted as design parameters derived from pile load tests at any given depth. They could therefore be used as a basis for developing a design method based on soil state. For both LBS and DBS the ratio between the tensile and compressive shaft capacities varied between 20 and 70% which is lower than recommendations in current pile design methods.

The creep tests had to be limited to a maximum of two hours to avoid excessive increases in ambient air temperature during the test. The pile capacity did not increase significantly over this time interval. Particle breakage was observed mainly in DBS, especially in the overconsolidated samples. Overconsolidation of these samples resulted in an interlocked micro-structure that was subsequently destroyed in a zone of about three to four pile diameters during pile installation.

This gradual destructuration in combination with the decreasing overconsolidation ratio with depth is thought to have caused the peak in the pile capacity curve.

The data presented for the compacted samples of LBS and DBS provide strong experimental evidence that for piles driven into both materials the bearing capacity factor N_q as well as the shaft friction ratio β are uniquely related to the stress state parameter R_s. No such unique relationship was obtained for the state parameter, ψ, as defined by Konrad (1988). The use of a non-linear CSL in LBS resulted in a shallower gradient and larger values of both N_q and β for a given value of R_s. For small values of R_s (0.01) the difference is small but increases to approximately 100% as R_s approaches unity. For simplicity it is suggested to use a linear critical state line, which for LBS would lead to a more conservative design. The trends of decreasing values of N_q and β with increasing R_s identified in both sands are similar to observations by Jovicic & Coop (1997) for sand stiffness. The distinctly different behaviour of the dense samples of LBS was attributed to boundary effects. The values of N_q and β in the overconsolidated samples were generally higher at smaller values of R_s compared to the results on the compacted samples but approached similar values as R_s approached unity. This is again consistent with observations by Jovicic & Coop.

Based on the experimental results, two new equations to calculate the unit base and unit shaft resistance were proposed introducing the concept of state parameter to pile design. The state parameter used was defined in terms of stress rather than void ratio as suggested by Been & Jefferies (1985). It was found that the data obtained from the centrifuge tests (β-values) were lower than those obtained by Coop (1999a) from back analysis of pile tests in the field in mainly carbonate sands. The difference is thought to be due to the lower interface friction angle of the model pile in comparison to prototype piles and possibly scale effects. There is however a need for more high quality laboratory tests to be undertaken in soils for which good quality pile test data are available (see Chapter 2) with the aim of establishing the CSLs and to allow more comparative analyses of field data to support the proposed framework. Given the encouraging results obtained in this study and further verification in the future gained from by re-analysing field tests it is expected that applying this new method will significantly increase the reliability of pile capacity predictions for driven piles in sand.

6. Summary, Conclusions and Further Work

The work undertaken within this project aimed at establishing a framework based on soil state to assess the capacity of driven piles in sand. The purpose of this final chapter is to summarise the methods used, draw conclusions on the different aspects of the project, highlight the limitations of the research, give suggestions as to how future work could enhance the findings obtained and to consider implications of the research for engineering practice.

6.1 Methodology

Centrifuge testing was used to investigate the behaviour of driven piles in sands. A new actuator and strongbox package was designed and constructed taking full advantage of the centrifuge facilities. Following a series of preliminary tests with an un-instrumented pile, three versions of a fully instrumented model pile were developed and constructed, which consisted of eleven segments and allowed five independent measurements of shaft friction, four of the radial stress and one of the end bearing to be taken during installation. The accuracy of the measurements was estimated to be in the order of ±2% for the base resistance, ±5% for the average global unit shaft friction, ±10% for the radial stresses and of the order of ±25 % for the local shaft friction sleeves (SRTs). The piles were jacked into samples of two sands of varying densities at accelerations of between 50-200g, simulating piles of up to 70 m in length and 3.2 m in diameter. In total, ten centrifuge model pile tests in Leighton Buzzard and thirteen in Dogs Bay sand were successfully completed and have been presented and discussed in detail.

The two sands used in the investigation were a carbonate sand and a quartz sand, chosen for the diversity of their geological origins and behaviour. A series of thirty-three triaxial tests in a Bishop & Wesley cell as well as three in a high pressure apparatus were conducted in order to characterise the behaviour of each sand, and in particular to locate precisely their critical state lines in stress-volume space. Lubricated end platens as well as local instrumentation were introduced to enhance the quality of the test data. Further to these tests eight triaxial K_o-compression tests were performed and the measured K_o values used to estimate the horizontal stress in the centrifuge model. In addition, a series of nineteen interface ring shear tests and thirteen direct shear box tests were undertaken to investigate the behaviour of the pile-soil interface. In order to ensure similarity between the interface plates and the model pile surface, their roughness was measured in representative locations using a Talysurf-4 unit and the roughness of the interface plates was then subsequently adjusted.

The centrifuge test data generated were first compared with results reported in the literature. This also included a comparison with assumptions made in currently available pile design

methods. Finally, the centrifuge data were normalised with respect to the critical state line in stress-volume space determined from the triaxial tests in order to assess the influence of the in situ stress-volume state prior to pile installation on the pile capacity.

6.2 Conclusions

The review of the literature on the mechanics of coarse grained soils revealed that identifying critical states and establishing the critical state line in stress-volume space experimentally is difficult. This is mainly due to errors in the measured volumetric strain due to barrelling and the onset of non-homogeneous deformations due to developing shear bands. Recently developed methods for measuring volume changes locally by computer tomography (Desrues et al., 1996) and digital image analysis (Kuo & Frost, 1996) are very promising but at present unsuitable for routine testing. It was demonstrated that local gauges, although limited to monitoring the deformations in fixed locations, can provide an alternative solution and this technology was therefore selected for the present study.

With respect to the literature on piles, it can be concluded that the predictions of pile capacity based on currently available design methods are highly variable and that the semi-analytical methods such as API-RP2A (1993) are the least reliable. The effects of particle breakage shown by Yasufuku & Hyde (1995) to control the bearing capacity and load-settlement behaviour of piles in crushable soils are mostly ignored. Most pile design methods tend to use the relative density as the key parameter to characterise the soil state and subsequently the pile response during loading. Although it has been recognised that the pile behaviour is affected by the stress level as well as initial density, the stress level in the soil is taken into consideration only to correct the strength and stiffness properties of the soil. All methods have been developed for and evaluated against pile tests in silica sands and their semi-empirical nature currently prohibits a general use for other soils types without verification by means of full scale load tests. In addition the lack of appreciation of the potential importance of state has meant that many field tests have been carried out to too shallow depths, so that it is doubtful whether the data are relevant to full scale piles.

During the shear box tests it was found that despite their different soil-soil friction angles the mobilised interface friction angle for both soils in a dry condition was very similar. Wet and saturated samples sheared along the aluminium interface had significantly higher friction angles compared to the dry samples. The slightly smoother surface finish of the titanium interface over the aluminium had little effect on the mobilised friction angle. Therefore, the mobilised shaft friction along the model pile should be unaffected by the change in material.

During the triaxial tests it was observed that the grease used for lubricating the end platens had a significant effect on their efficiency. It was found that the error due to compression of the lubricated ends, bedding and compliance was a function of the applied stress, whereas the magnitude of alignment and seating errors was independent of the applied stress and was a function of the procedure used for sample preparation.

One fundamental advantage of the local measurements of strain is the ability to observe the "true" strains of the sample. This allowed non-homogeneous deformations to be detected during shearing at large strains in cases were the shear bands developed on planes that included the mounts of the local LVDTs. Such behaviour was observed for all low pressure tests on dry Dogs Bays sand but was not observed on the wet compacted samples of Leighton Buzzard sand.

The values of K_o measured during one-dimensional compression were significantly different for the values predicted by the methods of Jaky (1944) and Bolton (1991). For the Leighton Buzzard sand the value of K_o was also found to depend on the initial specific volume of the sample. However, this difference was very small for the Dogs Bay sand.

As expected after studying the literature measuring volumetric strains in the triaxial tests was found to be very difficult. An incompatibility between locally and globally measured strains was observed. Despite using lubricated ends the samples barrelled during shearing at large strains possibly due some residual friction at the ends. The radial strain measured at the mid-height of the sample was therefore larger than the average radial strain calculated by assuming the shape of a right cylinder. As a consequence the locally measured volumetric strains are larger and the resulting critical states in v:lnp′ space are apparently significantly different from the values measured by other researchers (e.g. Verdugo & Ishihara, 1997) who used conventional global measurements. A correction for the effect of barrelling on the locally instrumented tests as well as the global measurements of radial strain was therefore introduced. This procedure, although convenient, is rather crude and does not really answer the question as to which observed behaviour is the "true" response of the soil and where is the precise position of the critical state line at low stress levels. To find an answer to this fundamental question would have required an extension of the testing programme, which was beyond the scope of this research project.

The critical state line in q:p′ space was easier to determine in comparison with the critical state line in v:lnp′ space. The former was found to be a straight line whereas the latter may be curved at low pressures and is approximately straight at higher pressures. The onset of the curvature of the critical state line was found to be a function of the mineralogy. Given the in situ states of the centrifuge tests it was considered appropriate to use a straight critical state line for Dogs Bay sand to normalise the centrifuge model test data. For the Leighton Buzzard sand the in situ

states of the centrifuge tests fall within the curved part of the critical state line. Due to the uncertainty in the volumetric strain measurements in this region caused by barrelling and developing shear bands two critical state lines, one a straight line and the other an exponential function were used to normalise the centrifuge model test data.

Based on the experience gained during the soil testing programme the following conclusions with respect to the critical states proposed by other researchers can be drawn. Given the problems encountered with respect to shear bands, undrained triaxial tests and drained tests with only one global volumetric strain measurement must generally be considered unsuitable and therefore normalisations based on such tests (e.g. Been et al., 1986 and Konrad, 1998) should be treated with caution. Ideally one should use computer tomography such as developed by Desrues et al. (1996). However, this method is very complicated to use an not yet suitable for routine laboratory testing. As an alternative it is recommended to apply the procedure adopted in this study using local strain measurements, perhaps and adding additional radial strain sensors. The difficulty in obtaining reliable volumetric strain measurements at low pressures provides a strong argument for using a state parameter defined as a stress ratio as opposed to a state parameter based on the specific volume as has been used for example by Been & Jefferies (1985).

The equipment developed for the centrifuge model tests caused many problems mainly due to insufficient reliability during the tests at the high accelerations. In retrospect the use of a more powerful motor and gearbox arrangement would have been an advantage. Overdesigning the components by a factor of 500% with respect to stated torque ratings at 1-g appears appropriate to ensure reliability at 200-g. Additionally, the components selected should be of a heavy duty type especially the optical encoder used to control the motor, as this component was a weak link in the configuration. Another significant problem was that during preparation of the overconsolidated samples friction developed along the container boundaries during compression of the sand in the consolidometer the effect of which on the stress state in the sample is unknown due to the lack of stress transducers in the model. In retrospect it would have been beneficial to introduce total stress transducers into the container boundaries and into the soil although lack of time prohibited this.

The first instrumented model pile developed also lacked reliability but this was overcome by improving the design and strain gauging process leading to a high number of successful tests with CUIMP-4. Perhaps the weakest part of the design was the use of polyimide enamel coated wires to connect the strain gauges to the wire terminals at the top of the pile. The insulation of these wires fractures very easily resulting in short circuits that were almost impossible to locate or remove.

During pile installation in both sands the unit base resistance as well as the average unit shaft friction were found to increase rapidly at shallow penetrations but at a reduced rate at deeper penetrations. With the exception of the average shaft friction in Dogs Bays sand no evidence was found in support of the existence of limiting values. Contrary to assumptions in the new MTD pile design method (Jardine & Chow, 1996), the value of unit end bearing increased with increasing prototype pile diameter. This is thought to be due to friction along the side walls of the strongbox which for a given nominal vertical stress affects deeper penetrations at lower g-levels more than shallower ones at higher g-levels. Good agreement was achieved between the locally and globally measured values of average unit shaft friction. Generally, the average radial stress also increased rapidly at shallow penetrations and at a slower rate with increasing penetration. The radial stress was found to reduce along the pile shaft, but contrary to assumptions of Randolph et al. (1994) and made in the MTD-method the maximum value occurred not at the pile tip but about seven pile diameters above the pile tip. The distribution of radial stress observed along the pile was found to be similar to results for shaft friction presented by Vesic (1970). However, the vertical stress in the lower part of the model might have been reduced by the friction along the side walls, thus leading to the observation that the maximum radial stress does not occur at the pile tip. It was also demonstrated that, contrary to assumptions made in most current design methods, there is no meaningful relationship between relative density and the pile design parameters N_q and β. Both N_q and β were found to vary significantly with pile penetration for a given relative density.

The interface friction angles calculated from the measured shaft friction and radial stress readings were essentially constant with depth and similar for both sands, varying between 7° and 20°, significantly lower than the values measured in the direct shear box. A still ongoing study in the Bromhead ring shear apparatus has confirmed the range of measured friction angles on the model pile. The roughness, especially of the aluminium sections, was found to increase as a function of the applied normal stress causing an increase in friction angle. It can therefore be concluded that although aluminium is a suitable material for manufacturing transducers, the main reason for selecting it to build the friction sleeves on the pile, the use of a harder metal such as titanium should give more consistent results.

The main conclusion drawn from the load tests on Leighton Buzzard and Dogs Bay sand is that the observed resistance during driving is similar to the resistance during a pile load test. Therefore the N_q and β profiles obtained during pile installation may be interpreted as design parameters derived from pile load tests at any given depth. For both Leighton Buzzard and Dogs Bay sand the ratio between the tensile and compressive shaft capacities varied between 20 and 70% which is lower than recommendations in current pile design methods. The creep tests had to be limited to a maximum of two hours to avoid excessive increases in ambient air temperature during the test. The pile capacity did not increase significantly over this time

interval. Particle breakage was observed mainly in Dogs Bay sand, especially in the overconsolidated samples. Overconsolidation of these samples resulted in an interlocked micro structure that was subsequently destroyed in a zone of about three to four pile diameters in extent during pile installation. This gradual destructuration in combination with the decreasing overconsolidation ratio with depth is thought to have caused the peak in the pile capacity profile.

The data presented for the compacted samples of Leighton Buzzard and Dogs Bay sand provide strong experimental evidence that for piles driven into both materials the bearing capacity factor N_q as well as the shaft friction ratio β are uniquely related to the stress state parameter R_s. No such unique relationship was obtained for the state parameter, ψ, as defined by Konrad (1988). The use of a non-linear critical state line in Leighton Buzzard sand resulted in larger values of both N_q and β for a given value of R_s. For small values of R_s the difference is small but increases to approximately 100% as R_s approaches unity. For simplicity it is suggested to use a linear critical state line, which for LBS would lead to a more conservative design. The trends of decreasing values of N_q and β with increasing R_s identified in both sands are similar to observations by Jovicic & Coop (1997) for the stiffness of sands. The distinctly different behaviour of the dense samples of LBS was attributed to boundary effects. The values of N_q and β in the overconsolidated samples were generally higher at smaller values of R_s compared to the results on the compacted samples but approached similar values as R_s approached unity. This is again consistent with observations by Jovicic & Coop for the stiffness of sands.

Based on the experimental results two new equations to calculate the unit base and unit shaft resistance were proposed introducing the concept of stress state parameter to pile design. It was found that the (β-values) obtained from the centrifuge tests were lower than the values obtained from back analysis of pile tests in the field in a variety of carbonate and other crushable sands (Coop, 1999a). This difference is thought to be partially due to the smaller normalised roughness and thus the reduced friction angles of the model pile-soil interface in comparison with piles in the field.

6.3 Limitations and Future Work

The triaxial tests conducted for this project were limited to tests mainly in the Bishop & Wesley triaxial apparatus which, given the time constraints, could only undergo modest redesign during this project. The ideal triaxial apparatus for large strain testing of coarse grained soils should allow for axial strains of up to 40% without rewinding the axial loading system. The quality of the measurements could be improved by adding more sensors to measure the radial strain at different points along the sample.

The pile tests conducted during this research project were restricted to centrifuge model tests on an instrumented pile that was jacked into two different sands under controlled conditions. The idea of modelling of models, which requires model piles of different diameters to be tests at g-levels appropriate to obtain the same prototype pile dimensions, was abandoned mainly due to the difficulties in producing the required fully instrumented piles of different diameters within the time frame of this project. No attempt has also been made to model installation effects, group effects and cyclic loading. Mainly due to lack of sufficient soil test data to establish the critical state lines of the soil involved only one attempt has been made to compare the proposed new design procedure to data from pile tests in the field other than those identified by Coop (1999a). Consequently, future work should focus on re-analysing field data and other laboratory based pile research within the new framework. Particularly the latest pile testing programmes conducted at Imperial College (Lehane, 1992 and Chow, 1996) and within the EURIPIDES project (Zuidberg, 1996) appear to be most promising. Also of interest are laboratory based studies on piles in the centrifuge as carried out, for example, by Fioravante (1994) and cone penetrometer test in the calibration chamber (e.g. Nutt, 1993). This, however, requires high quality laboratory tests to be undertaken in the soils in which these tests have been carried out, with the aim of establishing their critical state lines.

6.4 Implications of the Results

The work conducted in this study has shown that the stress-volume state is the key factor controlling the behaviour of a model pile jacked into samples of a silica and a carbonate sand. It was demonstrated that the current practice of using the relative density as a state variable is inadequate as it considers only the volume of the soil and not the effect of the mean normal stress. This lack of appreciation of soil state is thought to be the cause of the uncertainties currently inherent in the design of pile foundations highlighted by Randolph et al. (1994).

It was argued that these uncertainties can only be reduced if the importance of state on the behaviour of piles is recognised. A new method has been developed that accounts for soil state in the design of driven piles. To apply the method requires knowledge of the position of the critical state line of the sand in v:lnp' space as well as its in situ state. At present only a limited number of field tests have been re-examined using this new approach. To continue further in this direction would lead to more realistic pile design procedures possibly for all types of coarse grained soils. Given the encouraging results obtained in this study it is expected that applying this new method will significantly increase the reliability of pile capacity predictions for driven piles in sand.

LIST OF REFERENCES

Altaee, A., Fellenius, B.H. and Evgin, E. (1993). Load transfer for piles in sand and the critical depth. Canadian Geotechical Journal, Vol. 30, pp. 455-463.

Allman, M.A. (1992). Development and operation of the centrifuge actuator. Geotechnical Engineering Research Centre Report GE/92/08. The City University, London.

API-RP2A (1984). Recommended Practice for Planning, Designing and Constructing Fixed Offshore Platforms. Publication of the American Petroleum Institute, 15th edition, Washington.

API-RP2A (1991). Recommended Practice for Planning, Designing and Constructing Fixed Offshore Platforms-Working Stress Design. Publication of American Petroleum Institute, 19th edition, Washington.

API RP-2A-WSD (1993). Recommended Practice for Planning, Designing and Constructing Fixed Offshore Platforms-Working Stress Design. Publication of American Petroleum Institute, 20th edition, Washington.

Arthur, J.R.F. and Dalili, A. (1979). On the lubrication of rubber surfaces. Technical Note, Geotechnique, 29, No. 1, pp. 96-98.

ASTM-D 4253-83 (1983). American Standard for Testing Materials. Determination of the maximum density index. ASTM-publication.

ASTM-D 4254-83 (1983). American Standard for Testing Materials. Determination of the minimum density index. ASTM-publication.

Atkinson, J.H. and Bransby, P.L. (1978). The mechanics of soil: an introduction to Critical State Soil Mechanics, McGraw-Hill.

Atkinson, J.H. and Evans, J.S. (1985). Discussion on: The measurement of soil stiffness in the triaxial apparatus by Jardine et al., Geotechnique, 35, No.3, pp. 378-382.

Azouri, J. (1998). Preparation of sand models for centrifuge tests. BEng. final year project report, City University, London.

Baharom, B. and Stallebrass, S.E. (1998). A constitutive model combining the microscopic and macroscopic behaviour of sands in shear and volumetric deformation. Proc. 4th Europ. Conf. on Numerical Methods in Geot. Eng., Udine (Italy).

Baldi, G., Bellotti, R., Ghionna, V., Jamilkovsky, M. and Pasqualini, E. (1982). Design parameters for sand from CPT. Proc. 2nd Europ. Symposium on Penetration Testing, Amsterdam. pp. 425-432.

Baldi, G., Bellotti, R., Ghionna, V., Jamilkovsky, M. and Pasqualini, E. (1986). Interpretation of CPTs and CPTUs 2nd part: drained penetration of sands. 4th International Geotechnical Seminar: Field Instrumentation and In-Situ Measurements. Singapore, pp. 143-155.

Baldi, G., Hight, D.W. and Thomas, G.E. (1988). A re-evaluation of conventional triaxial test methods. ASTM publication STP 977, pp. 219-263.

Been, K. and Jefferies, M.G. (1985). A state parameter for sands. Geotechnique, 35, No. 2, 99-112.

Been, K., Crooks, J.H.A., Becker, D.E. and Jefferies, M.G. (1986). The cone penetration test in sands: part I, state parameter interpretation. Geotechnique, 36, No. 2, pp. 239-249.

Been, K., Crooks, J.H.A., Becker, D.E. and Jefferies, M.G. (1987). The cone penetration test in sands: part II, general inference of state. Geotechnique, 37, No. 3, pp. 285-299.

Been, K., Jefferies, M.G. and Hachey, J. (1991). The critical state of sands. Geotechnique, 41, No. 3, pp.365-381.

Berezantzev, V.C., Khristoforov, V. and Golubkov, V. (1961). Load bearing capacity and deformation of piled foundations. Proc. 5th ICSMFE, Vol. 2, pp. 3-58.

Beringen, F.L, Windle, D. and Van Hooydonk, W.R. (1979). Results of loading tests on driven piles in sand. Proc. Conf. Recent Developments in Design and Costruction of Piles, ICE, London, pp. 213-225.

Bhushan, K. (1982). Discussion: New design correlations for piles in sand. J. Soil Mech. Found. Div., ASCE, 108, GT-11, pp. 1508-1510.

Bishop, A.W. and Green, G.E. (1965). The influence of end restraints on the compression strength of a cohesionless soil. Geotechnique, 15, No. 3, pp. 243-266.
Bishop, A.W. and Henkel, D.J. (1962). The measurement of soil properties in the triaxial test. Edward Arnold, London.
Bishop, A.W. and Wesley, L.D. (1975) A hydraulic triaxial apparatus for controlled stress path testing. Geotechnique, 25, No. 4, pp. 657-670.
Bolton, M.D (1986). The strength and dilatency of sands. Geotechnique, 36, No.1, pp. 65-78.
Bolton, M.D (1991). Geotechnical stress analysis for bridge abutment design. Transport and Road Research Laboratory Contractor Report 270. London: HMSO.
Bond, A.J., Hight, D.W. and Jardine, R.J. (1997). Design of piles in sand in the UK sector of the North Sea. Report OTH-94-457, prepared by GCG for the Health and Safety Executive. London.
Bouvard, D. (1982). Rheologie des Milieux Pulverulents: Etude Experimentale et Identification d'une Loi de Comportement. These de Docteur-Ingenieur, Grenoble.
Bouvard, D. Stutz, P. (1986). Experimetal study of rehological properties of a sand using a special triaxial apparatus. Geotechnical Testing Journal, ASTM, Vol. 9, No.1, pp. 10-18.
Bowles, J.E. (1988). Foundation analysis and design. 4th Edition, McGraw-Hill, New York.
BS 1134 (1972). British Standard Method for the assessments of surface texture. British Standard Institution Parts 1 and 2.
BS 1377 (1990). British Standard Methods of tests for soils for civil engineering purposes, British Standard Institution Parts 1-9.
Burland, J.B. (1973). Shaft friction of pile in clay - a simple fundamental approach. Ground Engineering, 6(3), pp. 30-42.
Carter, J.P., Brooker, J.R. and Yeung, S.K. (1986). Cavity expansion in cohesive frictional soils. Geotechnique, 36, No. 3, pp. 349-353.
Cavalieri, A. (2000). Personal communication.
Chandler, H.W. (1985). A plasticity theory without Drucker's postulate, suitable for granular materials. J. Mech. Phys. Solids, 33, pp.215-216.
Chin, J.T. and Poulos, H.G. (1996). Tests on model jacked piles in calcareous sand. Geotechnical Testing Journal, ASTM, Vol. 19, No. 2, pp.164 - 180.
Chow, F. C. (1996). Investigation into displacement pile behaviour for off-shore foundations. Ph.D. Thesis, Univ. of London (Imperial College).
Chow, F.C. and Jardine, R.J. (1997). Applying the new Imperial College pile design method to large open ended piles in clay and sand. BASS-Conference proceedings.
Chow, F.C., Jardine, R.J. Brucy, F. and Nauroy, J.F. (1996). The effects of time on the capacity of pipe piles in dense marine sand. Proc. 28th Offshore Technology Conference, OTC 7972, pp. 147-160.
Chu, J. and Lo, S-Ch.R. (1993). On the measurement of critical state parameters of dense granular soils. Geotechnical Testing Journal, ASTM, Vol. 16, No.1, pp. 27-35.
Clinton, D.B. (1987). The determination of soil parameters from stress path tests. PhD Thesis, City Univesity, London.
Coffey, S. (1999). The interaction of soils and metals in shear box tests. B.Eng. final year project report, City University, London.
Coop, M.R. (1990). The mechanics of uncemented carbonate sands. Geotechnique, 40, No. 4, pp. 607-626.
Coop, M.R. (1996). Personal communication.
Coop, M.R. (1999a). The influence of in situ state an the behaviour of carbonate sands. 2nd Int.Conf. on Calcareous Soils, Bahrain, Vol. 2, K.A.Al-Shafei ed., Balkema, pp. 379-400.
Coop, M.R. (1999b). The influence of particle breakage and state on the behaviour of sand. 2nd Intl. Workshop on crushable soils, Yamaguchi, Japan, 39 pages in press.
Coop, M.R. and Atkinson, J.H. (1992). The mechanics of cemented carbonate sands. Geotechnique, 42, No.1, pp. 53-68.
Coop, M.R. and Lee, I.K. (1993). The behaviour of granular soils at elevated pressures. Proc.

Wroth memorial symposium: predictive soil mechanics, Thomas Telford, London, pp. 186-198.
Coop, M.R. and Lee, I.K. (1994). The influence of water on the mechanics of granular soils. Proc. XI ECSMFE, Vol. 1, pp. 1.63-1.72.
Coop, M.R. and McAuley, J.D. (1993). Shaft friction of piles in carbonate soils. Vol. 28, Int. Conf. Offshore Site Inv. and Found. Behaviour (Kluwer-publ.), pp. 645-659.
Corte, J.-F., Garnier, J., Cottineau, L.M. and Rault, R. (1991). Determination of the model soil properties in the centrifuge. Centrifuge 91, pp. 607-614.
Coyle, H.M. and Castello, R.R. (1981). New design correlations for piles in sand. J. Soil Mech. Found. Div., ASCE, 107, GT-7, pp. 965-986.
Craig, W.H. (1988). Installation studies for model piles. Application of Centrifuge Modelling to Geotechnical Design, W.H. Craig editor, Balkema, Rotterdam.
Craig, W.H. and Sabagh, S.K. (1994). Stress-level effects in model tests on piles. Canadian Geotechnical Journal. Vol. 31, pp. 28-41.
Craig, W.H. (1995). Geotechnical centrifuges: past, present and future. Chapter 1, Geotechnical Centrifuge Technology, R.N.Taylor editor, Blackie Academic & Professional.
Cuccovillo, T. (1995). Shear behaviour and stiffness of naturally cemented sands. PhD Thesis, The City University, London.
Cuccovillo, T. and Coop, M.R. (1997). The measurement of local axial strains in triaxial tests using LVDTs. Geotechnique, 47, No.1, pp. 167-171.
Cuccovillo, T. and Coop, M.R. (1999a). An automated triaxial apparatus for elevated pressures. In non-destructive and automated testing of soil and rock properties, ASTM STP 1350. Philadelphia. Amer. Soc. for Test. and Materials, pp. 231-245.
Cuccovillo, T. and Coop, M.R. (1999b). On the mechanics of structured sand. Geotechnique, 49, No. 6, pp. 741-760.
Cudmani, R. (1996). Anwendung der Hypoplastizität zur Interpretation von Drucksondierwiderständen in nichtbindigen Böden. Geotechnik, 1996/4, pp. 266-273.
Cudmani, R. (2000). Quasi-statische, zyklische und dynamische Penetration nichtbindiger Böden. Dissertation, Universität Karlsruhe, in preparation.
Cyran, T.C, Mehle, J.S., and Goble, G.G. (1991). Centrifuge modelling of piles. Centrifuge 91, Boulder, Balkema, pp. 377-384.
Dagnall, H. (1980). Exploring surface texture. Rank Taylor Hobson, Leicester, UK.
de Nicola, A. and Randolph, M.F. (1993). Tensile and compressive shaft capacities of piles in sand. J. Geotech. Engng. Div., ASCE 119, No.12, pp. 1952-1973.
de Nicola, A. and Randolph, M.F. (1999). Centrifuge modelling of pipe piles in sand under axial loads Geotechnique, 49, No.3, 295-318.
Desrues, J., Chambon, R., Mokni, M. and Mazerolle, F. (1996). Void ratio evolution inside shear bands in triaxial sand specimens studied by computer tomography. Geotechnique, 46, No.3, 529-546.
DIN 18126 (1989). Deutsches Instiut für Normung e.V. Untersuchung von Bodenproben: Bestimmung der lockersten und dichtesten Lagerung. DIN-publication.
Durgunoglu H.T. and Mitchel, J.K. (1975). Static penetration resistance in soils: I-Analysis. Proc. In Situ Measurements of Soil Properties, ASCE, 1, pp 151-171.
Eid, K.M. (1987). Scaling effects in cone penetration testing in sand. PhD Thesis, Virginia Polytechnic and State University, Blacksburg, Virginia, USA.
Entran (1995). Load cell catalogue, June 1995 edition.
Evans, K.M. (1987). A model study of the end bearing capacity of piles in layered carbonate soils. PhD Thesis, Oxford University.
Fearon, R. (1998). The behaviour of a structurally complex clay from an Italian landslide. PhD Thesis, City University, London.
Feda, J., Bohac, J. and Herle, I. (1993). End restraint in triaxial testing of soils. Acta Technica CSAV 38, pp. 197-220.
Fellenius, B.H.and Altaee, A. (1995). Critical depth: how it came into being and why it does not exist. Proc. Instn. Civ. Engng. Geotech. Engng, 113, Apr., pp. 107-111.

Ferguson, K.A., and Ko, H.Y. (1985). Application of centrifuge modelling to cone pentrometer technology. Application of Centrifuge Modelling in Geotechnical Design, Manchester, Balkema, pp. 67 - 86.

Fioravante,V. (1994). Centrifuge modelling of axially loaded piles in sand. Proc. Pile Foundations, Exper. Investigations Analysis and Design, Naples, pp. 125-163.

Fioravante,V., Jamiolkowski, M. and Pendroni, S. (1994). Modelling the behaviour of piles in sand subjected to axial load. Centrifuge 94, pp. 455 - 460.

Fleming, W.G.K and Thorburn, S. (1983). Recent piling advances, state of the art report. Proc. Conf. on Advances in Piling and Ground Treatment for Foundations. ICE, London.

Fleming, W.G.K., Weltman, A.J., Randolph, M.F. and Elson, W.K. (1992). Piling Engineering. 2nd edition, Blackie and Son Ltd. London.

Frost, J.D. and Jang, D.J. (2000). Evolution of sand microstructure during shearing. Journal of Geotechnical and Geoenvironmental Engineering, Vol. 126, No. 2, pp.116-130.

Fukushima, S. and Tasuoka, F.(1984). Strength and deformation characteristics of saturated sand at extremely low pressures. Soils and Foundations, Vol. 24, No. 4, pp. 30-48.

Garnier, J. and Koenig, D. (1998). Scale effects in piles and nails loading tests in sand. Centrifuge 98, Balkema, Rotterdam, pp. 205-216.

Goldscheider, M. (1982). Results of the international workshop on constitutive relations for soils. Balkema, Rotterdam, pp. 11-54.

Golightly, C.R. & Hyde, A.F.L. (1988). Some fundamenal properties of carbonate soils. Proc. Int. Conf. Calcareous Sediments, Perth, Vol. 1, pp. 118-132.

Göpel, W., Hesse, J. and Zemel, J.N. (1989). Sensors, a comprehensive survey, Volume-1 VCH-Verlagsgesellschaft mbH, Weinheim.

Göpel, W., Hesse, J, and Zemel, J.N. (1994). Sensors, a comprehensive survey, Volume-7 VCH-Verlagsgesellschaft mbH, Weinheim.

Goto, S. and Tatsuoka, F. (1988).Effects of End Conditions on the Triaxial Compressive Strength for Cohesionless Soil. Advanced Triaxial testing of Soil and Rock. ASTM publication STP 977, pp. 692-705.

Grant, R.J. (1998). Ground movements due to tunnelling in layered ground. PhD-Thesis, City University, London.

Gudehus, G. (1996). A comprehensive constitutive equation for granular materials. Soils and Foundations, Vol. 36, No. 1, pp.1-12.

Gui, M.W. (1994). Centrifuge and numerical modelling of pile and penetrometer in sand. PhD-Thesis. Cambridge University.

Gui, M.W., Bolton. M.D., Garnier, J., Corte, J.F., Bagge, G., Laue, J and Remzi, R. (1998). Guidelines for cone penetrations tests in sand. Centrifuge 98, Balkema, Rotterdam, pp. 155-160.

Hanna, T.H. and Tan, R.H.S. (1973). The behaviour of long piles under compression loads in sand. Canadian Geotechnical Journal 10, No. 3, 311-340.

Hardin, B.O.(1985). Crushing of soil particles. Journal of Geotechnical Engng., ASCE, 111, No. 10, pp. 1177-1192.

Head, K.H. (1985). Manual of soil laboratory testing. Pentech Press, London, Vol. 3, Chapter 22, pp. 1054-1061.

Heerema, E.P. (1980). Predicting pile driveability: Heather as an illustration of the fatigue theory. Ground Engng. 13 (4), pp.15-37.

Herle, I. (1997). Hypoplastizität und Granulometrie einfacher Korngerüste. Dissertation, Universität Karlsruhe.

Hettler, A. and Vardoulakis, I. (1984). Behaviour of dry sand in a large triaxial apparatus. Geotechnique, 34, No.2. pp. 183-198.

Hight, D.W., Lawrence, D.M., Farquhar, G.B., Milligan, G.W.E. and Potts, D.M. (1996). Evidence for scale effects in the end bearing capacity of open ended piles in sand. Proc. 28th Offshore Technology Conference, OTC 7975, pp. 181-192.

Hossain, M.K. and Briaud, J.L. (1993). Improved soil characterisation for pipe piles in sand.

Proc. 25th Offshore Technology Conference, Houston, OTC 7193, pp. 637-654.
Houlsby, G.T., Evans, K.M. and Sweeney, M. (1988). End bearing capacity of model piles in layered carbonate soils. Proc. Int. Conf. on Calcareous Sediments. Perth, Australia, Vol. 1, pp. 209-214.
Houlsby, G.T. and Hitchman, R. (1988). Calibration chamber tests of a cone penetrometer in sand. Geotechnique, 38, No.1. pp. 39-44.
Hunter, A.H. and Davisson, M.T (1969). Measurement of pile load transfer. Proc. Conf. Performance of Deep Foundations, ASTM STP 444, pp. 106-117.
Hyde, A.F.L., Yasufuku, N. and Hyodo, M. (1994). Effect of relative density and crushability of sands on pile end bearing capacity. Proc. Int. Conf. on pre-failure deformations of geomaterials. Hokaido, Japan, Vol. 1, pp. 265-270.
Ishihara, K. (1993). Liquefaction and flow failure during earthquakes. 33rd Rankine Lecture, Geotechnique, 43, No. 3, pp. 351-415.
Ishihara, K., Tatasuoka, F. and Yasuda, S. (1975). Undrained deformation and liquefaction of sand under cyclic stress. Soils and Foundations, Vol. 15, No. 1, pp. 29-44.
Jaky, J. (1944). The coefficient of earth pressure at rest. J.Soc. Hungarian Archit. Engnrs, Vol. 22, pp. 355-358.
Jamilkovsky, M., Ghionna, V.N., Lancellotta, R. and Pasqualini, E. (1988). New correlations of penetration tests for design practice. Proc. of Int. Conf. on Penetration Testing, De Ruiter editor. Balkema, Rotterdam, pp. 263-296.
Jardine, R.J. and Chow, F. C. (1996). New Design Methods for Offshore Piles. Publication MTD 96/103 of the Marine Technology Directorate Ltd, London.
Jardine, R.J., and Lehane, B.M. (1992). Field experiments with instrumented piles in sand and clay. Proc. Conf. Piling: European practice and worldwide trends. Thomas Telford, London. pp. 50-66.
Jardine, R.J., Lehane, B.M. and Everton, S.J. (1993). Friction coefficients for piles in sands and silts. Vol. 28: Offshore Site Investigation and Foundation Behaviour, Society of Underwater Technology. (Kluwer-publ.), pp. 147-180 and 661-677.
Jardine, R.J., Symes, M.J. and Burland, J.B. (1984). The measurement of soil stiffness in the triaxial apparatus. Geotechnique, 34, No. 3, pp. 323-340.
Jefferies, M.G. (1993). Nor-Sand: a simple critical state model for sand. Geotechnique, 43, No. 1, pp. 91-103.
Jovicic, V. (1997). The Measurement and Interpretation of Small Strain Stiffness of Soils. PhD Thesis, City University, London.
Jovicic, V. and Coop, M.R. (1997). Stiffness of coarse grained soils at small strains. Geotechnique, 47, No. 3, pp. 545-561.
Kerisel, J. (1964). Deep foundations, basic experimental facts. Proc. Conf. on Deep Foundations. Mexico, Vol. 1, pp. 5-44.
King R. and Lodge, M., (1988). North-West shelf development - foundation engineering challenge. Proc. Int . Conf. Calcareous Sediments, Perth, Vol.2, pp. 333-342.
Kishida, H. and Uesugi, M. (1987). Tests of the interface between sand and steel in the simple shear apparatus. Geotechnique, 37, No. 1, pp.45-52.
Klotz, E.U. (1997). Development and Operation of a 50 kN, 200-g capacity single axis pile driving actuator. Internal report, City University, London.
Klotz, E.U. (1998). The capacity of driven piles in sands. First year report , City University, London.
Ko, H.Y., Atkinson, R.H., Goble, G.G. and Ealy, C.D. (1984) Centrifugal modelling of pile foundations. ASCE-Symposium on pile foundations, San Francisco, pp. 21-40.
Ko, H.Y. (1988) Summary of the state-of-the-art in centrifuge model testing. Centrifuges in Soil Mechanics, Balkema, pp. 11-18.
Kolymbas, D. & Wu, W. (1990). Recent results of triaxial tests with granular materials. Powder Technology, No. 60, pp. 99-119.
Konrad, J.M. (1988). Interpretation of flat plate dilatometer tests in sands in terms of the state parameter. Geotechnique, 38, No. 2, pp. 263-277.
Konrad, J.M. (1998). Sand state from cone penetrometer tests: a framework considering grain

crushing stress. Geotechnique, 48, No. 2, pp. 201-215.
Kraft, L.M. (1990). Computing Axial Pile Capacity in Sands for Offshore Conditions. Marine Technology, Volume 9, pp. 61-92.
Kulhawy, F.H. (1984). Limiting tip and side resistance: Fact or fallacy? Proc. ASCE Symp. Analysis and Design of Deep Foundations, San Fransisco, pp. 80-98.
Kuo, C.Y. and Frost, J.D. (1996). Uniformity evaluation of a cohesionless specimens using digital image analysis. J. of Geotech. Engng, ASCE, 122, No.5, pp. 390-396.
Kuwano, R. (1996). Laboratory tests on Dunkirk sand. Imperial College, Internal Report.
Kuwano, R. (1999). The stiffness and yielding anisotropy of sand. PhD-Thesis, University of London, Imperial College.
Lade, P.L. and Yamamuro, J.A. (1996). Undrained sand behaviour in axisymmetric tests at high pressures. J. of Geotech. Engng, ASCE, 122, No.2, pp. 120-129.
Lau , W.H.W. (1988). The behaviour of clay in the simple shear and triaxial tests. Ph.D. Thesis. The City University, London.
Lee, I.K. (1991). Mechanical behaviour of decomposed granite soil. PhD thesis, The City University, London.
Lee K.L. and Seed, H.B. (1967). Drained strength characteristics of cohesionless soils. J. Soil Mech. and Found. Division, ASCE, 93, SM6, pp. 118-140.
Lee, K.L. (1978). End restraint effects on undrained static triaxial strength of sand. Journal GE Division Proceedings, ASCE, 104, No. GT 6, pp. 687-704.
Lehane, B.M. (1992). Experimental investigations in pile behaviour using instrumented piles. PhD Thesis, University of London (Imperial College).
Lehane, B.M., Jardine R.J. Bond, A.J. and Frank, R. (1993). Mechanisms of shaft friction from instrumented model pile tests. J. Geotech. Eng. ASCE, 119 (1), pp. 19-35.
Lemos, L.J.L (1986). The effect of rate of shear on residual strength of soil. PhD Thesis, University of London (Imperial College).
Lings, M.L. (1997). Predicting the shaft resistance of driven pre-formed piles in sand. Geotechnical Engineering, 125 (4), pp. 71-84.
Lion, K.S. (1969). "Transducers: Problems and Prospects". IEEE Transactions IECI-16, 2-5.
Lo Presti, D. (1987). Mechanical behaviour of Ticino sand from resonant column tests. PhD thesis, Politechnico di Torino.
Lunne, T. and Christoffersen, H.P. (1983). Interpretation of cone penetrometer data in off-shore sands. Proc. 15th OTC, Houston, Texas, Vol. 1, pp. 181-192.
Macari, E.J., Parker, J.K. and Costes, N.C. (1997). Measurment of volume changes in triaxial tests using digital imaging techniques. Geotechnical Testing Journal, GTJODJ, Vol. 20, No. 1, pp.103-109.
Mansur, C.I., Hunter, A.H. (1970). Pile tests - Arkansas River Project. J. Soil Mech. Found. Engng., ASCE, 96, No. SM5 pp. 1545-1582.
Mayne, P.W. and Kulhawy, F.H. (1982). Ko-OCR relationships in clay. Journal of Geot. Engng., ASCE, 108, GT6, pp. 851-870.
McDowell, G.R. and Bolton, M.D. (1998). On the micromechanics of crushable aggregates. Geotechnique, 48, No. 5, pp. 667-679.
McDowell, G.R. and Bolton, M.D. (1999). Effect of particle size distribution on pile penetration in calcareous sand in the geotechnical centrifuge. 4th Int. Conf. On Deep Foundation Practice, Singapore, pp.327-334.
Measurements Group UK, (1992). Transducer class strain gauge catalogue, Basingstoke.
Measurements Group UK, (1998). Course notes for transducer workshop, Basingstoke 14/05/98.
Meigh, A.C. (1987). Cone penetration testing. CIRIA-Butterworth, 1987.
Meyerhof , G.G. (1951). The ultimate bearing capacity of foundations. Geotechnique, 1, pp. 301-332.
Meyerhof, G.G. (1976). The Eleventh Terzaghi Lecture, Journal of Geot. Engng., ASCE, 102, GT3, pp. 197-227.
Meyerhof, G.G. (1983). Scale effects of ultimate pile capacity. Journal of Geot. Engng., ASCE, 109, No. 6, pp. 797-806.

Miura, N. and Yamanouchi, T. (1975). Effect of water on the behaviour of quartz-rich sand under high stresses. Soils and Foundations, No.4, pp. 23-34.
Muir-Wood, D. (1994) Soil behaviour and critical state soil mechanics, Cambridge University Press.
Murff, J.D. (1980). Pile capacity in softening soil. Int. Journal Num. and Anal. Methods in Geomech., 4, pp. 185-189.
Ng, C.W.W. and Springman, S.M. (1994). Uplift resistance of buried pipelines in granular materials, Centrifuge 94, Balkema, pp. 753-758.
Nishida, K. editor (1990). Residual soils in Japan. Publ. of reasearch committee on Physical and Mechanical Properties of Residual Soil Ground, Japan. Soc. of Soil Mechn. And Found. Engng., 186 p.
Nordlund, R.L. (1963). Bearing capacities of piles in cohesionless soils. J. Soil Mech. Found. Engng. Div., ASCE, 89, SM3, pp. 1-35.
Nunez, I.L, Hoadley, P.J, Randolph, M.F. and Hulett, J.M, (1988a). Driving and tension loading of piles in sand on a centrifuge. Centrifuge 88, Paris, Balkema, pp. 353-362.
Nunez, I.L., Phillips, R., Randolph, M.F., and Wesselink, B.D. (1988b). Modelling laterally loaded soils in calcareous sand. Centrifuge 88. Balkema, pp. 371-381.
Nutt, N.R.F. and Houldby, G.T. (1991). Calibration tests on the cone pressuremter in carbonate sand. Proc. 1st Int. Conf. Calibration Testing, Potsdam, New York, pp. 265-276.
Nutt, N.R.F. (1993). Development of the cone pressuremeter. PhD Thesis, Oxford University.
Ovesen, N.K. (1979). Discussion on "The use of physical models in design". Proc. of the 7th ECSMFE, Brighton, Vol. 4, pp. 310-323.
Pelletier, J.H., Murff, J.D. and Young, A.C. (1993). Historical development and assessment of the current API Design Methods for axially loaded pipes. Proc. 25th Offshore Technology Conference, Houston, OTC 7157, pp. 253-282.
Pestana, J.M. and Whittle, A.J. (1995). Compression model for cohesionless soils. Geotechnique, 45, No. 45, pp. 611-631.
Phillips, R. and Valsangkar, A.J (1987). An Experimental Investigation of Factors Affecting Penetration resistance in Granular Soils in Centrifuge Modelling. Report CUED/D - Soils TR 210. Cambridge University.
Pickles, A.R. (1989). The application of critical state soil mechanics to predict ground deformations below an embankment constructed on soft alluvium. PhD Thesis, City University, London.
Ponce, V.M., Bell, J.M.(1971). Shear strength of sand at extremely low pressures. J. Soil Mech. Found. Engng. Div., ASCE, 97 , SM4, pp. 625-638.
Poorooshasbs, H.B. (1989). Description of flow of sand using state parameters. Computer and Geotechnics, Vol. 8, No. 3, Elsevier Science Publications pp. 195-218.
Potyondy, J.G. (1961). Skin friction between various soils and construction materials. Geotechnique, 11, No. 4, pp. 339-353.
Poulos, S.J. (1981). The steady state of deformation. J. Geotech. Engng., ASCE, 17, GT5, pp. 553-562.
Randolph, M.F. (1985). Capacity of piles driven into dense sand. Report Soils TR 171, Cambridge University Engineering Department.
Randolph, M.F., Dolwin, J. and Beck, R. (1994). Design of driven piles in sand. Geotechnique, 44, No. 3, pp. 427-448.
Renzi, R., Corte, J.F., Rault, G., Bagge, G., Gui, M. and Laue, J. (1994). Cone penetration tests in the centrifuge: Experience of five laboratories. Centrifuge 94. pp. 77 - 82.
Richardson, D. (1984). The importance of natural strains in soil mechanics. Research report GE/84/23, The City University, London.
Roscoe, K.H. (1967). Discussion on shear strength of soil other than clay. Proc. Geotechnical Conf. 2, pp. 188-192.
Roscoe, K.H., Schofield, A.N. and Wroth, C.P. (1958). On the yielding of soils. Geotechnique, 8, No.1, pp. 22-52.

Rowe, P.W. and Barden, L. (1964). Importance of free ends in triaxial testing. Journal of Soil Mechanics and Foundations Division, ASCE, 90, No. SM1, pp. 1-27.
Sabagh, S.K. (1984). Cyclic axial load tests on piles in sand. Application of centrifuge modelling to geotechnical design. Manchester, Balkema, pp. 103-120.
Sarsby, R.W, Kalteziotis, N. and Haddad, E.H. (1980). Bedding error in triaxial tests on granular media. Geotechnique, 30, No. 3, pp. 302-309.
Schmidt, B. (1966). Discussion: Earth pressures at rest related to stress history. Canadian Geotechnical Journal, Vol. 3(4), pp. 239-242.
Schofield, A.N. (1980). Cambridge Geotechnical Centrifuge Operations. 20th Rankine Lecture, Geotechnique, 30, No. 3, pp. 227-268.
Schofield, A.N. and Taylor, R.N. (1988). Development of standard geotechnical centrifuge operations. Centrifuge 88, pp. 29 - 32.
Schofield, A.N., and Wroth, C.P. (1968). Critical State Soils Mechanics, McGraw-Hill, London.
Scholey, G.K., Frost, J.D., Lo Presti, D.C.F. and Jamiolkowski, M. (1995). A review of instrumentation for measuring small strains during triaxial testing of soil specimens. Geotech. Testing Journ., ASTM, Vol.18, No. 2 , pp. 135-156.
Seed, H.B. and Lee K.L. (1967). Undrained strength characteristics of cohesionless soils. J. Soil Mech. Found. Div., ASCE, 93, SM6, pp. 333-360.
Shibuya, S., Mitachi, T., Kitajima, A. and Takadam, M.(1993). Strength of sands as observed in a newly developed direct shear box apparatus. Internal report, Hokkaido Univ., Bulletin No. 166.
Simpson, B. (1992). 29th Rankine Lecture: Retaining structures: displacement and design. Geotechnique, 42, No. 4, 541-576.
Skempton, A.W. (1986). Standard penetration test procedures and the effects in sands of overburden pressure, relative density, particle shape, ageing and overconsolidation. Geotechnique, 36, No.3, pp. 425-447.
Skempton, A.W., Yassin, A.A. and Gibson, R.E. (1953). Théorie de la force portante des pieux dans le sable. Annales de l'Institut technique du Bâtiment et des travaux Publics, Nos. 63-54.
Springman, S.M., Bolton, M.D. and Randolph, M.F. (1991). Modelling the behaviour of piles subjected to surcharge loading. Centrifuge 91, Boulder , Balkema, pp.-253-260.
Standing, J. R. (1997). Studies on the interface resistance of soil nails. Ph.D. Thesis, Univ. of London (Imperial College).
Stroud, M.A. (1971). Sand at low stress levels in the S.S.A. PhD thesis, Cambridge University.
Tatsuoka, F. (1988). Some recent developments in triaxial testing systems for cohesionless Soils. ASTM publication STP 977, pp. 7-67.
Tatsuoka, F. and Haibara, O. (1985). Shear resistance between Smooth or Lubricated Surfaces. Soils and Foundations, Vol. 25, No. 1, pp. 89-98.
Tatsuoka, F., Molenkamp, F., Torii, T., and Hino, T. (1984). Behaviour of Lubrication Layers of Plattens in Element Tests. Soils and Foundations, Vol. 24, No. 1, pp. 113-128.
Tavenas, F. and La Rochelle, P. (1972). Accuracy of relative density measurements. Geotechnique, 22, No. 4, pp. 549-562.
Taylor, R.N. (1995). Centrifuges in modelling: Principles and scale effects. Chapter 2, Geotechnical Centrifuge Technology, R.N.Taylor editor, Blackie Academic & Professional.
Tejchman, A. and Gwizdala, K. (1979). Analysis of safety factors of bearing capacity for large diameter piles. Design parameters for geotechnical engineering, Vol.1, BGS, London, pp. 293-296.
te Kamp, W.C. (1977). Sondern end funderingen op palen in zand, Fugro Sounding Symposium, Utrecht.
Terzaghi, K. (1930). Die Tragfähigkeit von Pfahlgründungen, Die Bautechnik 8, Heft 31, pp 475-478 and Heft 34, pp. 517-521.
Terzaghi, K. (1943). Theoretical soil mechanics, J. Wiley & Sons (publ.), New York.
Tomlinson, M.J. (1995). Foundation Design and Construction. 6th edition, Longman Scientific

& Technical, England.
Toolan, F.E., Lings, M.L., and Mirza, U.A. (1990). An appraisal of API-RP2A recommendations for determining skin friction of piles in sand. Proc. 22nd Offshore Technology Conference, OTC 6422, 4, pp. 33-42.
Ueng, T.S., Tzou, Y.M. and Lee, C.J. (1988). The effect of end restraint on volume change and particle breakage of sands in triaxal tests. ASTM publ. STP 977, pp. 679-691.
Uesugi, M., and Kishida, H. (1986). Influential factors of friction between steel and dry sands. Soils and Foundations, Vol. 26, No. 2, pp. 32-46.
Verdugo, R. and Ishihara, K. (1996). The steady state of sandy soils. Soils and Foundations, Vol. 36, No. 2, pp. 81-91.
Vesic, A.S. (1967). A study of bearing capacity of deep foundations. Final Report, Project B189, Georgia Institute of Technology, Atlanta, GA, 279 pp. 25-31
Vesic, A.S. (1970). Tests on instrumented piles, Ogeechee River Site. J. Soil Mech. Found. Engng Div. ASCE, 96, SM2, pp. 561-584.
Vesic, A.S. (1972). Expansion of cavities in infinite soil mass. J. Soil Mech. Found. Div., ASCE, 96, SM3, pp.561-584.
Vesic, A.S. (1977). Design of pile foundations. Synthesis of Highway Practice No. 42, Transport Research Board, Washington, DC, 68 p.
Vesic, A.S. and Clough, G.W. (1968). Behaviour of granular materials under high stresses. J. Soil Mech. Found. Div., ASCE, 94, No. 3, pp. 661-688.
Viggiani, G. (1992). Small Strain Stiffness of fine grained soils. PhD Thesis, City University London.
Williams, R.E., Chow, F.C. and Jardine, R.J. (1997): Unexpected Behaviour of Large Diameter Tubular Steel Piles. Proc. Int. Conf. on Foundation Failures, Singapore.
Wroth, C.P. (1984). An interpretation of in situ soil tests. 24th Rakine Lecture. Geotechnique, 34, No. 3, pp. 449-489.
Yasufuku, N. and Hyde, A.F.L. (1995). Pile end-bearing capacity in crushable sands. Geotechnique, 45, No. 4, pp. 663-676.
Yet, N.S., Leung, C.F. and Lee, F.H. (1994). Behaviour of axially loaded piles in sand. Centrifuge 94, Singapore, Balkema, pp. 461-466.
Yoshima, Y and Kishida, T. (1981). A ring torsion apparatus for evaluating friction between soil and metal surfaces. Geotechnical Testing Journal No. 4 , pp. 145-152.
Youd, T. (1972). Compaction of sands by repeated shear straining. J. Soil Mech. Found. Div., ASCE, 98(7), pp. 276-287.
Yu, H.S. and Mitchell, J.K.(1998). Analysis of cone resistance: review of methods. Journal of Geotechnical and Geoenvironmental Engineering, Vol. 124, No. 2, pp. 140-149.
Zelikson, A., Raines, R.D. and Malalel, P. (1994). Design and limitations of a pile driving robot. Centrifuge 94, Singapore, Blakema, pp. 467-472.
Zeitlen, J.G. and Paikowsky, S. (1982). Discussion: New design correlations for piles in sand. J. Soil Mech. Found. Div., ASCE, 108, GT-11, pp. 1515-1518.
Zhang, H.Z. and Garga, V.K. (1997). Quasi-steady state: a real behaviour? Canadian Geotechnical Journal, Vol. 34, pp. 749-761.
Zuidberg, H.M. (1996). EURIPIDES; Tests at large scale driven piles in dense silica sands. Proc. 28th Offshore Technology Conference, Houston, OTC 7977, pp. 193-206.

	Leighton Buzzard sand	Dogs Bay sand	method
mineralogy	silica	calcium carbonate	
particle shape	rounded-sub-rounded	shell fragments, angular	
d_{50}	0.18 mm	0. 20 mm	BS 1377
d_{60}	0.19 mm	0. 22 mm	BS 1377
d_{10}	0.16 mm	0. 15 mm	BS 1377
$U_c = d_{60} / d_{10}$	1.20	1.47	BS 1377
ρ_s	2.65 g/cm^3	2.71 g/cm^3	BS 1377
e_{max}	1.01	2.84	ASTM 4253-83
e_{min}	0.72	1.37	ASTM 4254-83

Table 3-1: Index properties of Leighton Buzzard and Dogs Bay sands.

test	position	interface material	R_a µm	R_{max} µm	R_p µm	R_v µm	R_{st} / R_a µm	error %	*corr* R_a µm
AL-P1	C RatG	Al	1.39	10.62	5.79	4.83	18.01	-6.0	1.47
AL-P2	C RatG	Al	1.34	10.18	4.25	5.93	18.67	-6.1	1.42
AL-P3	C RatG	Al	1.10	8.64	3.73	4.91	22.69	-8.5	1.20
AL-P4	C RatG	Al	0.99	7.62	2.71	4.91	25.35	-11.0	1.09
AL-P5	C RatG	Al	1.87	12.16	4.91	7.25	13.38	-3.0	1.93
AL-P5a	B RatG	Al	1.94	13.84	6.52	7.32	12.92	-2.9	1.99
		average:		10.51					1.52
Ti-P1	C RatG	Ti	1.14	10.99	4.61	6.37	21.93	-8.2	1.23
Ti-P2	C RatG	Ti	0.97	7.69	2.49	5.20	25.67	-11.1	1.08
Ti-P3	C RatG	Ti	0.80	6.67	3.52	3.15	31.10	-19.0	0.96
Ti-P4	C RatG	Ti	1.01	8.42	3.66	4.76	24.83	-10.6	1.11
		average:		8.44					1.10

Note: C = centre, B = bottom, RatG = right angle to grid, Ti = titanium, Al = aluminium, R_{st} = radius of stylus.

Table 3-2: Summary of roughness measurements on model pile CUIMP-3.

test	position	interface material	R_a µm	R_{max} µm	R_p µm	R_v µm	R_{st} / R_a µm	error %	*corr* R_a µm
AL-S1	C RatG	Al	3.75	22.41	11.87	10.55	6.66	-0.9	3.79
AL-S2	CM RatG	Al	1.39	10.11	3.66	6.45	18.00	-6.0	1.40
AL-S3	PM RatG	Al	1.13	10.25	4.54	5.71	22.16	-8.3	1.22
AL-S4	P RatG	Al	0.73	7.03	2.20	4.83	34.2	-22	0.89
AL-S5	C PtG	Al	4.48	23.66	13.84	9.81	5.58	-0.6	4.51
AL-S6	CM PtG	Al	1.55	10.11	4.32	5.79	16.1	-4.5	1.62
	ignore Al-S1 and S5	average:		9.38					1.28
Ti-S1	C	Ti	0.76	5.93	2.20	3.74	33.11	-21	0.91
Ti-S2	M	Ti	0.73	7.25	2.2	5.05	34.20	-22	0.89
Ti-S3	P	Ti	0.85	7.03	2.34	4.69	29.45	-18	1.00
		average:		6.74					0.94

Note: C = centre, M = middle, P = perimeter, RatG = right angle to grid. PtG = parallel to grid, Ti = titanium, Al = aluminium, R_{st} = radius of stylus.

Table 3-3: Summary of roughness measurements on interface plates.

interface	interface material	soil type	D_{50} µm	$R_{max(L=2.6mm)}$ µm	R_n	R_a µm	R_{na}
shear box	aluminium	LBS	180	9.38	0.052	1.28	7.2E-3
shear box	titanium	LBS	180	6.74	0.037	0.94	5.3E-3
shear box	aluminium	DBS	200	9.38	0.047	1.28	6.4E-3
shear box	titanium	DBS	200	6.74	0.034	0.94	4.7E-3
pile	aluminium	LBS	180	10.51	0.058	1.52	8.4E-3
pile	titanium	LBS	180	8.44	0.047	1.10	6.1E-3
pile	aluminium	DBS	200	10.51	0.053	1.52	7.6E-3
pile	titanium	DBS	200	8.44	0.042	1.10	5.5E-3

Note: DBS = Dogs Bay sand, LBS = Leighton Buzzard sand.

Table 3-4: Normalised roughness data for CUIMP-3 and shear box interface plates.

test	date	sand type	initial condition	interface material	σ_v' [kPa]	rate of shearing [m/h]	friction angle, δ_{cs} [°]
SBLBS-1	26/10/98	silica	D-D	Al	1000	0.0045	26.6
SBLBS-2	04/11/98	silica	D-D	Al	100	0.0045	24
SBLBS-3	12/11/98	silica	L-Da	Al	1000	0.009	30
SBLBS-4	20/11/98	silica	L-Da	Al	100	0.009	35
SBLBS-5	01/12/98	silica	L-Da	Al	1000	0.009	31
SBLBS-6	09/12/98	silica	D-Da	Al	1000	0.009	35
SBLBS-7	15/12/98	silica	D-Sat	Al	100	0.009	33
SBLBS-10	19/05/99	silica	D-D	Ti	500	0.009	24.5
SBDBS-1	15/01/99	carbonate	D-D	Ti	500	0.009	24.5
SBDBS-2	21/01/99	carbonate	D-D	Al	100	0.009	26.5
SBDBS-3	27/01/99	carbonate	D-D	Al	1000	0.009	31

Note: D-D = dense -dry, L-Da = loose-damp, D-Da = dense-damp, D-Sat = dense saturated, Ti = Titanium, Al = Aluminium.

Table 3-5: Summary of interface shear box tests conducted (data from Coffey, 1999).

transducer	working range	output voltage at full scale	resolution	noise	error due to hyst., drift and non-lin.[1)]
Wykeham Farr. Load cell	5 kN	20 mV	0.15 kPa	±1 kPa	±0.8 %
Druck PPT and RST	1000 kPa	100 mV	0.03 kPa	±0.03 kPa	±0.6 %
RDP global LVDT	25mm	±2V	0.001%	±0.001%	±0.3 %
RDP local ax.+ rad. LVDT	10mm	±3V	5.0E-6%	±5.0E-5%	±0.05 %

Note: [1)] Error as a percentage of current transducer output, PPT = pore pressure transducer, RST = radial stress transducer, LVDT = linear variable differential transformer.

Table 3-6: Details of calibration and transducer accuracy for triaxial apparatus (after Jovicic, 1997).

test	date	H/D	condition of soil	w_c [%]	lubricant for free ends	v_i	radial stress at the end of isotropic compression [kPa]	v_s	v_f	shearing procedure	comments
TLBS-1	29/07/97	2:1	W-L	8	none	2.13	400	2.08	1.93	d-εc	radial belt with 1 LVDT
TLBS- 2	11/08/97	2:1	W-L	8	none	2.15	600	2.06	2.00	d-εc	radial belt with 1 LVDT
TLBS- 3	10/12/97	1.5:1	W-L	8	silicon grease	2.14	400	2.09	2.39	d-εc	new radial belt with 2 LVDTs, strong barrelling, wrong grease?
TLBS- 4	05/01/98	1.5:1	W-L	8	silicon grease	2.13	400	2.10	2.15	d-εc	strong barrelling, wrong grease?
TLBS- 5	10/09/98	1:1	W-L	8	TK44-N3	2.16	700	2.07	1.99	d-εc	new grease reduced barrelling
TLBS- 6	28/10/98	1:1	W-L	8	TK44-N3	2.21	100	2.18	2.13	d-εc	
TLBS- 7 (TLBS-4a)	29/11/98	1:1	W-L	8	TK44-N3	2.20	400	2.13	1.98	d-εc	little barrelling
TLBS- 8	08/12/98	1:1	W-D	8	TK44-N3	1.87	100	1.87	2.01	d-εc	little barrelling
TLBS- 9	15/12/98	1:1	W-D	8	TK44-N3	1.93	400	1.92	2.07	d-εc	little barrelling
TLBS- 10	18/12/98	1:1	W-D	8	TK44-N3	1.87	700	1.84	1.98	d-εc	little barrelling
TLBS- 11	08/01/99	1:1	S-MD	100	TK44-N3	2.04	100	2.08	2.04	d-εc	elephant foot shape
TLBS- 12	12/01/99	1:1	S-MD	100	TK44-N3	2.04	100	2.03	2.11	d-εc	elephant foot shape
TLBS- 13	20/01/99	1:1	S-MD	100	TK44-N3	2.02	100	2.00	2.13	d-εc	elephant foot shape
TLBS- 14	24/02/99	2:1	W-L	8	TK44-N3	2.11	400	2.08	2.04	d-εc	large diff between 2 loc. axial gauges, little barrelling
TLBS- 15	08/03/99	2:1	W-L	8	TK44-N3	2.15	100	2.12	2.03	d-σc/εc	stress controlled at start,
TLBS- 16	16/03/99	2:1	W-L	8	TK44-N3	2.17	100	2.15	2.21	d-σc/εc constant p'	stress controlled at start, stress control problem

Note: W-D = wet - dense, W-L = wet - loose, S-MD = saturated medium dense, w_c = water content, d-εc = drained strain controlled, d-σc = drained stress controlled
v_i = initial specific volume, v_s = specific volume at start of shearing, v_f = specific volume at the end of the test

Table 3-7: Summary of the low pressure triaxial tests on Leighton Buzzard sand with local instrumentation.

Test	date	H/D	condition of soil	w_c [%]	lubricant for free ends	v_i	radial stress at the end of isotropic compression [kPa]	v_s	v_f	shearing procedure	comments
TDBS-1	19/11/98	1:1	W-L	8	TK44-N3	2.97	100	2.92	2.87	d-εc	barrelling about 2-3 mm
TDBS- 2	26/11/98	1:1	W-L	8	TK44-N3	3.02	50	3.00	3.10	d-εc	
TDBS- 3	29/03/99	2:1	W-L	8	TK44-N3	2.89	100	2.86	3.01	d-σc/εc	constant p'
TDBS- 4	06/04/99	2:1	W-L	8	TK44-N3	2.81	100	2.80	2.98	d-σc/εc	constant p', barrelling + shear band
TDBS- 5	02/06/99	2:1	D-MD	0	TK44-N3	2.66	300	2.62	2.64	d-σc/εc	constant p', barrelling + shear band
TDBS- 6	05/06/99	2:1	D-L	0	TK44-N3	2.73	100	2.72	2.96	d-σc/εc	constant p', barrelling 2.5 mm, membrane correction
TDBS- 7	11/06/99	2:1	D-L	0	TK44-N3	2.74	50	2.73	3.13	d-σc/εc	constant p', barrelling 2.8 mm, 2 layers of lubrication, shear band
TDBS- 8	15/06/99	2:1	D-L	8	TK44-N3	2.89	100	2.87	---	d-σc/εc	slight barrelling 1 mm, 2 layers of lubrication, catastrophic failure
TDBS- 9	18/06/99	2:1	D-L	8	TK44-N3	2.95	100	2.92	---	d-σc/εc	test abandoned
TDBS- 10	02/07/99	2:1	D-L	8	TK44-N3	2.80	100	2.78	2.78	d-ud-σc/εc	constant p' - constant ε_v=0 test, little barrelling, stress path below CSL

Note: D-L = dry - loose, W-L = wet - loose, D-MD = dry medium dense, w_c = water content, d-εc = drained strain controlled, d-σc = drained stress controlled
v_i = initial specific volume, v_s = specific volume at start of shearing, v_f = specific volume at the end of the test, d-ud = drained undrained

Table 3-8: Summary of the low pressure triaxial tests on Dogs Bay sand with local instrumentation.

test	date	H/D	condition of soil	w_c [%]	lubricant for free ends	v_i	K_o	radial stress at the end of isotropic re-loading [kPa]	v_s	v_f	shearing procedure	comments
TLBS-Ko1	15/04/99	2:1	W-L	8	TK44-N3	2.16	0.63	--	--	--	--	k_o compr. only, no shearing stage
TLBS-Ko2	21/04/99	2:1	D-L	0	TK44-N3	1.94	0.54	--	--	--	--	k_o compr. only, no shearing stage
TLBS-Ko3	25/04/99	2:1	D-D	0	TK44-N3	1.82	0.38	300	1.81	1.83	d-σc	shearing constant p' stress control
TLBS-Ko4	01/05/99	2:1	D-D	0	TK44-N3	1.77	0.38	335	1.76	1.90	d-σc/εc	shearing constant p'
TDBS-Ko1	14/05/99	2:1	D-L	0	TK44-N3	2.74	0.56	150	2.57	2.94	d-σc/εc	shearing constant p'
TDBS-Ko2	24/05/99	2:1	D-MD	0	TK44-N3	2.53	0.59	500	2.42	2.31	d-σc/εc	shearing constant p'
TDBS-Ko3	21/03/00	2:1	D-L	0	none	2.70	0.53	-	2.27	-	--	k_o compr. only, no shearing stage
TDBS-Ko4	02/04/00	2:1	D-L	0	none	2.69	0.52	-	2.30	2.08	d-σc/ εc	shearing constant σ_r'

Note: D-D = dry - dense, D-L = dry - loose, W-L = wet - loose, D-MD = dry medium dense, w_c = water content, d-εc = drained strain controlled, d-σc = drained stress controlled
v_i = initial specific volume, v_s = specific volume at start of shearing, v_f = specific volume at the end of the test

Table 3-9: Summary of the low pressure K_o compression tests on Leighton Buzzard and Dogs Bay sands with local instrumentation.

test	date	H/D	condition of soil	w_c [%]	lubricant for free ends	v_i	radial stress at the end of isotropic compression [kPa]	v_s	v_f	shearing procedure	comments
TLBS-17	19/11/99	2:1	D-L	0	TK44-N3	1.97	700	1.94	1.85	d-εc	problem unloading-reloading membrane correction
TLBS-18	02/12/99	2:1	D-MD	0	TK44-N3	1.89	100	1.87	1.95	d-εc	membrane correction 5 kPa
TLBS-19	14/12/99	2:1	D-L	0	TK44-N3	1.95	100	1.94	1.88	d-εc	membrane correction 4.4 kPa
TDBS-11	30/08/99	2:1	D-L	0	TK44-N3	2.71	700	2.53	2.15	d-εc	manual correction
TDBS- 12	20/09/99	2:1	D-L	0	TK44-N3	2.71	700	2.51	2.10	d-εc	similar to TLBS-12
TDBS- 13	01/11/99	2:1	D-L	0	TK44-N3	2.75	700	2.59	2.22	d-εc	similar to TLBS-12
TDBS- 14	12/11/99	2:1	D-L	0	TK44-N3	2.75	100	2.71	2.53	d-εc	membrane correction 3.3 kPa

Note: D-L = dry - loose, D-MD = dry medium dense, w_c = water content, d-εc = drained strain controlled
v_i = initial specific volume, v_s = specific volume at start of shearing, v_f = specific volume at the end of the test.

Table 3-10: Summary of the low pressure triaxial tests on Leighton Buzzard and Dogs Bay sands using the inner-chamber configuration.

test	date	H/D	condition of soil	w_c [%]	lubricant for free ends	v_i	radial stress at the end of isotropic compression [kPa]	v_s	v_f	shearing procedure	comments
HPDBS-1	08/03/00	2:1	D-L	0	TK44-N3	2.77	2600	2.50	2.23	d-εc	shearing constant σ_r'
HPLBS-1	21/03/00	2:1	D-L	0	TK44-N3	1.81	2280	1.79	1.75	d-εc	shearing constant σ_r'
HPLBS-2	02/04/00	2:1	D-L	0	TK44-N3	1.84	4600	1.82	1.57	d-εc	shearing constant σ_r'

Note: D-L = dry - loose, d-εc = drained strain controlled
v_i = initial specific volume, v = specific volume at start of shearing, v_f = specific volume at the end of the test.

Table 3-11: Summary of the high pressure triaxial tests on Leighton Buzzard and Dogs Bay sands with local instrumentation.

test	H/D	condition of soil	radial stress at the end of isotropic compression [kPa]	alignment error (%-strain)	error due to compliance and bedding (%-strain)
TLBS- 4	1.5:1	W-L	400	± 0.25	0.45
TLBS- 5	1:1	W-L	700	± 0.8	1.0
TLBS- 7	1:1	W-L	400	± 0.15	0.2
TLBS- 9	1:1	W-D	400	± 0.15	0.5
TLBS- 10	1:1	W-D	700	± 0.2	0.8
TLBS- 14	2:1	W-L	400	± 0.2	0.7

Note: W-D = wet - dense, W-L = wet - loose.

Table 3-12: Typical errors due to alignment, compliance and bedding for Leighton Buzzard sand during isotropic compression.

sand type	function of CSL	M	ϕ'_{cs} deg.	Γ	λ	h_s MPa	n	e_{co}
Leighton Buzzard sand	linear	1.305	32.4	3.02	0.152			
Leighton Buzzard sand	non-linear	1.305	32.4			80	0.72	1.01
Dogs Bay sand	linear	1.65	40.3	4.45	0.340			
Dogs Bay sand	non-linear	1.65	40.3			9	0.75	1.84

Table 3-13: Critical state parameters determined for Leighton Buzzard and Dogs Bay sands.

quantity	prototype	model	quantity	prototype	model
length	N	1	stress	1	1
area	N^2	1	strain	1	1
volume	N^3	1	mass density	1	1
velocity	1	1	energy density	1	1
acceleration	1	N	time (dynamic)	N	1
mass	N^3	1	time (diffusion)	N^2	1
force	N^2	1	time (creep)	1	1
energy	N^3	1	frequency	1	N

Table 4-1: Scaling relations for centrifuge modelling (adopted from Ko, 1988).

	location	material	E [MN/m^2]	ν	ρ [g/cm^3]	UTS /YS [2 %] [MN/m^2]
actuator	side walls base plate	AL - HE 15 SST - 316	70,000 196,000	0.33 0.3	2.85 7.85	385 / 310 515 / 205
strongbox	side walls base plate	SST - 316 AL - HE 15	196,000 70,000	0.3 0.33	7.85 2.85	515 / 205 385 / 310
bolts	general	steel 10.9	210,000	0.3	7.85	1200/950
CUIMP-1	core	steel 431-S29	210,000	0.3	7.85	1000 / 850
CUIMP-2 to CUIMP-4	core section	titanium Ti-6-4	105,000-120,000	0.3	4.48	1100 / 1000
CUIMP-2 to CUIMP-4	sleeves and dumb-bells	AL-Speedal BS4300/5	70,000	0.33	2.85	310 / 225

UTS = ultimate tensile strength, YS = yield stress, AL = aluminium, SST = stainless steel

Table 4-2: Material properties for actuator, strongbox and model piles.

transducer	distance from pile tip to centre [mm]	distance from pile tip to base of sleeve [mm]	distance from pile tip to top of sleeve [mm]	active length of SRT / diameter of RST [mm]	active area [mm^2]
BFT	0				200
SRT-1	17.5/15 [1)]	4.3	30.8/25.8	26.5/21.5	1329/1078
RST-1	47			9	81
SRT-2	70.5/68	56.3	84.8/79.8	28.5/23.5	1429/1178
RST-2	101.5			9	81
SRT-3	133/130.5	111.5	154.5/149.5	43/38	2156/1905
RST-3	171.5			9	81
SRT-4	210.5/208	181.5	248.5/243.5	58/53	2908/2657
RST-4	255			9	81
SRT-5	312.5/310	265	360/355	95/90	4764/4513

1) Note: 17.5/15 mm indicates 17.5 mm for CUIMP-2 and 15 mm for CUIMP-3 and CUIMP-4.

BFT = Base force transducers, SRT = Shaft resistance transducer, RST = Radial stress transducer.

Table 4-3: Geometry and positions of the transducers on CUIMP-2 to CUIMP-4.

transducer	FS applied force or pressure	stress level in metal [MPa]	strain level in metal [με]	FS output at 3V PS [mV]
BFT	40,000 N	610	5100	9.9
SRT-1	3900 N	95	1300	2.6
RST-1	4250 kPa	70	1000	4.0
SRT-2	4050 N	95	1400	2.7
RST-2	3550 kPa	60	800	3.3
SRT-3	4550 N	110	1500	3.0
RST-3	2650 kPa	45	600	2.5
SRT-4	4000 N	95	1400	2.7
RST-4	1550 kPa	25	400	1.5
SRT-5	2300 N	55	800	1.5

BFT = Base force transducers, SRT = Shaft resistance transducer, RST = Radial stress transducer.

Table 4-4: Theoretical full-scale sensitivity (FS) of transducers on CUIMP-2 to CUIMP-4.

transducer	range	sensitivity	error due to noise	error due to non-linearity hysteresis+drift [1)]
load cell UCE-50kN	-20 to 50 kN	1.58 mV/V	± 1 N	0.5 %
LVDT DFG-5	±5 mm	350 mV/mm	± 0.0005 mm	± 0.1 %
LVDT DFG-15	±15 mm	120 mV/mm	± 0.0015 mm	± 0.1 %
potentiometer CFL-400 in actuator	±200 mm	12.5 mV/mm	± 0.02 mm	± 0.1 %
temperature sensor LM35-CZ	±0-100 °C	10 mV/°C	±0.01 °C	± 2 %
temperature sensor PT100	±0-100 °C	10 mV/°C	±0.01 °C	± 2 %

Note: [1)] Error as percentage of current transducer output as estimated following the calibration.

Table 4-5: Characteristics of additional transducers in centrifuge model.

transducer	FS applied force or pressure	FS output at 3V PS CUIMP-2	estimated error due to noise CUIMP-2	estimated error due to non-linearity hysteresis+drift CUIMP-2 [1)]	FS output at 3V PS CUIMP-3	estimated error due to noise CUIMP-3	estimated error due to non-linearity hysteresis+drift CUIMP-3 [1)]	FS output at 3V PS CUIMP-4	estimated error due to noise CUIMP-4	estimated error due to non-linearity hysteresis+drift CUIMP-4 [1)]
BFT	40,000 N	19 mV	± 1.0 N	± 0.4 %	19 mV	± 1.0 N	± 0.4 %	19 mV	± 1.0 N	± 0.5 %
SRT-1	3900 N	6.9 mV	± 0.1 N	± 8 %	5.7 mV	± 0.1 N	± 9 %	5.9 mV	± 0.1 N	± 8 %
RST-1	4250 kPa	0.3 mV	± 2 kPa	± 5 %	3.7 mV	± 0.2 kPa	± 2.5 %	5.2 mV	± 0.2 kPa	± 2.5 %
SRT-2	4050 N				5.7 mV	± 0.1 N	± 14 %	7.6 mV	± 0.1 N	± 12 %
RST-2	3550 kPa	2.6 mV	± 0.2 kPa	± 2 %	4.7 mV	± 0.1 kPa	± 1.5 %	4.0 mV	± 0.2 kPa	± 1.5 %
SRT-3	4550 N	8.8 mV	± 0.1 N	± 13 %	8.9 mV	± 0.1 N	± 8 %	8.3 mV	± 0.1 N	± 7 %
RST-3	2650 kPa				2.8 mV	± 0.1 kPa	± 2.6 %	3.8 mV	± 0.1 kPa	± 2.6 %
SRT-4	4000 N	7.1 mV	± 0.1 N	± 5 %	7.5 mV	± 0.1 N	± 2 %	6.4 mV	± 0.1 N	± 11 %
RST-4	1550 kPa	1.8 mV	± 0.2 kPa	± 2.5 %	4.3 mV	± 0.05 kPa	± 15 %	3.8 mV	± 0.1 kPa	± 4 %
SRT-5	2300 N	3.0 mV	± 0.1 N	± 8 %	3.8 mV	± 0.1 N	± 2 %	3.6 mV	± 0.1 N	± 11 %

Note: [1)] all percentages with respect to current transducer reading, PS = power supply, FS = full scale.

Table 4-6: Characteristics of transducers on CUIMP-2 to CUIMP-4.

unit no	motor type	encoder line No	rated motor torque [Nm]	gearbox ratio	output torque η=0.6 [Nm]	max. axial force [kN]
1	Servo U9D-D	100/500	0.53	160:1	51	57
2	Brush MDA-10-2H2	500	0.95	160:1	91	102
3	Servo S19-1A	100	0.66	160:1	64	72

Table 4-7: Characteristics of drive configurations for the centrifuge tests.

test	date	g-level	initial condition of soil Dr [%] (1g) / (max-g)		pile- type	spec. volume vi(1g)/vi (max-g)	wc [%]	speed push / pull [mm/s]	comments
CLBS-1	19/01/98	100	D-D	Dr = 88 / ---	CUIMP-1	1.75 / --- shaking-table	0	1.0 (0.5) / 1.0	motor problem-speed variation no LVDT in soil, original grading
CLBS- 2	20/01/98	100	D-L	Dr = 23 / ---	CUIMP-1	1.94 / --- funnel	0	1.0 / 1.5	no motor problem, no LVDT in soil, original grading
CLBS- 3	06/03/98	200	D-L	Dr = 23.5	CUIMP-1	1.94 / --- funnel	0	0.75 / 0.75	motor stopped-loose cable, no LVDT in soil, original grading
CLBS- 4	10/03/98	200	D-D	Dr = 106.5 / --	CUIMP-1	1.70 / --- shaking table	0	1.0-0.5-0.1 / 1.0	motor problem, gears worn out, shaft bent no LVDT in soil, original grading
CLBS- 5	13/10/98	100	D-L	Dr = 11 / 21	CUIMP-2	1.97 / 1.95 funnel	0	0.5 / 1.0	no motor problem, RST-1, SRT-2, and SRT-5 with problems, LVDTs in soil, selected grading
CLBS- 6	18/10/98	200	D-L	Dr = 12 / 26	CUIMP-2	1.97 / 1.94 funnel	0	0.5 / 1.0	no motor problem, RST-1, RST-3 and SRT-5 with problems, LVDT, selected grading
CLBS- 7	26/10/98	100	D-L	Dr = 31 / 36	CUIMP-2	1.92 / 1.91 sand rainer	0	0.5 / 1.0	no motor problem, RST-1, SRT-2, RST-2, RST-3, SRT-5 with problems, LVDTs , selected grading
CLBS- 8	13/11/98	200	D-L	Dr = 33 / 44	CUIMP-2	1.91 / 1.88 sand rainer	0	0.5 / 0.5	motor problem pull out, BFT-1, RST-1, SRT2, RST-2, RST-3, SRT-5 problems, LVDTs , selected grading
CLBS- 9	03/03/99	100	W-L	Dr =12 / 23	CUIMP-3	1.97 / 1.94 new funnel	4.43	1.0 / 1.0	no motor problem, SRT-1, RST-2 and RST-3 problems, LVDTs, selected grading, constant temperature, old TS
CLBS- 10	25/03/99	200	W-L	Dr = 12.5 / 28	CUIMP-3	1.97 / 1.93 new funnel	4.68	2.4 / 2.2	constant torque drive, SRT-1, SRT-2, RST-2 and RST-3 prob., LVDTs , selected grading, constant temperature, old TS
CLBS- 11	29/04/99	100	D-L	Dr = 9 / 19	CUIMP-3	1.98 / 1.95 new funnel	0	2.4 / 2.2	constant torque drive, SRT-1, SRT-2, RST-2 and RST-3, LVDTs , selected grading, constant temperature, old TS
CLBS- 13	05/07/99	100	D-L	Dr = 105 / 107	CUIMP-4	1.70 / 1.68 sand rainer	0	0.1 / 0.2 / 0.5	constant speed drive, Motor broken, penetration. 130 mm, selected grading, old TS, test aborted
CDBS- 1	20/01/98	100	D-L	Dr = 10 / --	CUIMP-1	2.79 / --- funnel	0	1.0 / 1.5 no load test	no motor problem, no LVDTs, original grading, no TS

Note: D-D = dry dense, D-L = dry - loose, W-L = wet loose, wc = water content, max-g = target g-level in test, TS = temperature sensor.

Table 4-8: Summary of the preliminary centrifuge tests

test	date	g-level	pile-type	test conducted
Gravity-1	19-01-98	100	CUIMP-1	
Gravity-2	08-10-98	100, 200	CUIMP-2	
Gravity-3	09-06-99	100	CUIMP-3	after CLBS-12
Gravity-4	20/07/99	200	CUIMP-4	for CDBS-2
Gravity-5	03/08/99	200	CUIMP-4	after CDBS-4
Gravity-6	18/08/99	50	CUIMP-4	after CDBS-6
Gravity-7	01-09-99	50	CUIMP-4	after CLBS-14
Gravity-8	07/09/99	100	CUIMP-4	after CDBS-7
Gravity-9	13-09-99	100	CUIMP-4	after CLBS-16
Gravity-10	15/11/99	100	CUIMP-3	after CLBS-19+20
Gravity-11	15/11/99	200	CUIMP-3	for CDBS-11+12

Table 4-9: Tests investigating the effect of gravity on the output of CUIMP-2 to CUIMP-4.

test	date	g-level	initial condition of soil Dr [%] (1g) / (max-g)		pile- type	spec. volume vi(1g) / vi(max-g)	wc [%]	speed push / pull [mm/s] [1)]	comments
CLBS- 12	09/06/99	100	D-MD	Dr = 19 / 29	CUIMP-3	1.95 / 1.92 funnel	0	0.2 / 0.5 / 0.5 two load tests	constant speed drive, no problem with motor, LVDT , SG, CT, old TS, db-1+db3 broken
CLBS- 14	01/09/99	50	D-L	Dr = 7 / 14	CUIMP-4	1.989 / 1.972 funnel	0	0.2 / 0.5 / 0.5 two load tests	constant speed drive, no problems with motor, LVDT, SG, CT, new TS
CLBS- 15	03/09/99	50	D-D	Dr = 92 / 93	CUIMP-4	1.745 / 1.74 sand rainer	0	0.2 / 0.5 no load test	constant speed drive, problems with motor, two reversals, SG, CT, new TS
CLBS- 16	13/09/99	100	D-L	Dr = 11 / 22	CUIMP-4	1.978 / 1.947 funnel	0	0.2 / 0.5 no load test	constant speed drive, no problems with motor, LVDT, SG, CT, new TS.
CLBS- 17	21/09/99	100	D-MD	Dr = 56 / 57	CUIMP-4	1.848 / 1.845 hammer	0	0.2 / 0.5 no load test	constant speed drive, no problems with motor, LVDT, SG, CT, new TS
CLBS- 18	14/09/99	200	D-L	Dr = 8 / 23	CUIMP-4	1.986 / 1.942 funnel	0	0.2 / 0.5 no load test	constant speed drive, no problems with motor, LVDT, SG, CT, new TS
CLBS- 19	23/10/99	100	D-L	Dr = 6 / 18	CUIMP-3	1.99 / 1.95 funnel	0	0.05 / 0.2 / 0.5 three creep stages, 3 LT	constant speed drive, no problems with motor, LVDT, SG, CT, new TS
CLBS- 20	15/11/99	100	D-D	Dr=102 / 104	CUIMP-3	1.71 / 1.71 hammer	0	0.05 / 0.2 / 0.5 three load tests (LT)	constant speed drive, motor/gear box stopped at 280mm, LVDT , SG, CT, new TS
CLBS- 21	27/11/99	100	D-MD-OC	Dr = 29 / 31	CUIMP-4	1.927 / 1.923 consolidometer	0	0.05 / 0.2 / 0.5 three creep stages, 3 LT	constant speed drive, no problems with motor, LVDT, SG, CT, new TS
CLBS- 22	02/12/99	200	D-D	Dr = 105 / 107	CUIMP-4	1.706 / 1.704 sand rainer	0	0.05 / 0.2 / 0.5 two LT, no creep	constant speed drive, motor/gear box stopped at 150mm, LVDT , SG, CT, new TS

Note: D-D = dry dense, D-L = dry - loose, MD = medium dense, OC = overconsolidated, wc = water content, max-g = target g-level in test, SG = selected grading, CT = constant temperature, TS = temperature sensor, LT = load test.

[1)] in cases were there are three values e.g. 0.1/0.2/0.5, 0.1 refers to the speed during the load test, 0.2 to the speed during installation and 0.5 to the speed during pull out.

Table 4-10: Summary of good quality tests conducted on samples of Leighton Buzzard sand.

test	date	g-level	initial condition of soil Dr [%] swing / target-g		pile- type	spec. volume vi(1g) / vi(max-g)	wc [%]	speed push / pull [mm/s]	comments
CDBS- 2	23/07/99	200	D-L	Dr = 1 / 28.5	CUIMP-4	2.83 / 2.71 funnel	0	0.1 / 0.2 / 0.5 two load tests	no motor problem, LVDT-5 out of range, SG, freshly sieved + mixed soil, old TS
CDBS- 3	27/07/99	200	D-MD	Dr = 56 / 67	CUIMP-4	2.58 / 2.54 hammer	0	0.2 / 0.5 no load test	no motor problem, LC drop of at 233 mm, LVDT-15, same soil as in CDBS-2, cable disaster at start, old TS
CDBS- 4	03/08/99	200	D-MD	Dr = 64.5 / 73	CUIMP-4	2.54 / 2.50 hammer	0	0.1 / 0.2 / 0.5 two load tests	no motor problem, LVDT-15, SG, "old LC", freshly re-sieved + re-mixed soil, old TS
CDBS- 5	17/08/99	50	D-L	Dr = 8 / 19	CUIMP-4	2.81 / 2.75 funnel	0	0.1 / 0.2 / 0.5 two load tests	no motor problem, LVDT-15, SG, "old LC", same soil as in CDBS-4, old TS
CDBS- 6	18/08/99	50	D-D	Dr = 80 / 82	CUIMP-4	2.47 / 2.45 hammer	0	0.1 / 0.2 / 0.5 two load tests	no motor problem, LVDTs - mixed, SG, "new LC", same soil as in CDBS-4, old TS
CDBS- 7	07/09/99	100	D-L	Dr = 6 / 24	CUIMP-4	2.82 / 2.72 funnel	0	0.2 / 0.5 no load test	motor problem during pull out, LVST-15, SG, "new LC", soil re-sieved + re-mixed, no RST-3+SRT-4, new TS
CDBS- 8	10/09/99	100	D-D	Dr = 89 / 94	CUIMP-4	2.42 / 2.393 hammer	0	0.2 / 0.5 no load test	no motor problem, LVDTs-mixed, SG, "new LC", same soil as CDBS-7, new TS
CDBS- 9	16/09/99	100	D-MD	Dr = 50 / 61	CUIMP-4	2.60 / 2.532 hammer	0	0.2 / 0.5 no load test	no motor problem, LVDTs-mixed, SG, "new LC", same soil as CDBS-7, new TS
CDBS- 10	17/09/99	200	D-MD	Dr = 49.5 / 66	CUIMP-4	2.61 / 2.52 hammer	0	0.2 / 0.5 no load test (LT)	no motor problem, LVDTs-mixed, SG, "new LC", same soil as CDBS-7, new TS
CDBS- 11	26/10/99	200	D-L	Dr = 11 / 33	CUIMP-3	2.79 / 2.69 funnel	0	0.05 / 0.2 / 0.5 3 creep stages, 3 LT	no motor problem , LVDT-15, SG, freshly re-sieved + re-mixed soil, new TS
CDBS- 12	30/10/99	200	D-D	Dr = 90 / 98	CUIMP-3	2.42 / 2.39 hammer	0	0.05 / 0.2 / 0.5 three LT, no CS	no motor problem, LVDT-15, SG, "new LC", same soil as CDBS-11, new TS
CDBS- 13	09/11/99	100	D-D-OC	Dr =96 / 96	CUIMP-3	2.39 / 2.39 consolidometer	0	0.05 / 0.2 / 0.5 five LT, three CS	no motor problem, LVDT-5, SG, "new LC" , freshly re-sieved + re-mixed soil, new TS
CDBS- 14	20/11/99	200	D-D-OC	Dr = 106 / 106	CUIMP-3	2.34 / 2.34 consolidometer	0	0.05 / 0.2 / 0.5 three LT, one CS	no motor problem, LVDT-5, SG, freshly re-sieved + re-mixed soil, new TS

Note: D-D = dry dense, D-L = dry - loose, MD = medium dense, OC = overconsolidated, wc = water content, max-g = target g-level in test, SG = selected grading, CT = constant temperature, TS = temperature sensor, LVDT-5 = LVDT with a linear range of 5 mm, LT = load test, CS = creep test,
[1)] in cases were there are three values e.g. 0.1/0.2/0.5, 0.1 refers to the speed during the load test, 0.2 to the speed during installation and 0.5 to the speed during pull out.

Table 4-11: Summary of good quality tests conducted on samples of Dogs Bay sand.

transducer	cross-sensitivity when a force or pressure is applied to one of these transducers					
	BFT [%] [1)]	SRT-1 [%] [1)]	SRT-2 [%] [1)]	SRT-3 [%] [1)]	SRT-4 [%] [1)]	RST-1 to RST-4 [%] [2)]
BFT	100 / 100	-	-	-	-	-1 / -1
SRT-1	±3 / ±2	100 / 100	-	-	-	-33 / -35
SRT-2	-3 / ±1	-6 / +2	100 / 100	-	-	-25 / -25
SRT-3	+2 / +3	+2 / +5	+2 / +5	100 / 100	-	-18 / -25
SRT-4	+5 / +6	+9 / +15	+8 / +15	+8 / +7	100 / 100	-18 / -28
SRT-5	+6 / +10	+11 / +16	+10 / +16	+11 / +15	+11 / +20	-17 / -30

Note: +6 / +10% indicates +6% for CUIMP-3 and +10% for CUIMP-4.
BFT = base force transducer, SRT = shaft resistance transducer, RST = radial stress transducer.

1) cross-sensitivity as percentage output of transducer due to applied force
   e.g output SRT-2 = -3 N for 100 N on BFT
2) cross-sensitivity as percentage output of transducer due to applied radial stress
   e.g output base = 3 N for 100 kPa on RST-1

Table 5-1: Typical cross-sensitivities of transducers on CUIMP-3 and CUIMP-4.

test	interface material	average original roughness		final roughness	
		$R_{max(L=2.6)}$ µm	R_a µm	$R_{max(L=2.6)}$ µm	R_a µm
Ti-2/1	titanium	8.44	1.10	5.35	0.43
Ti-3/1	titanium	8.44	1.10	7.40	0.80
Ti-3/2	titanium	8.44	1.10	5.71	0.58
Al-3/1	aluminium	10.51	1.52	7.47	1.15
Al-4/1	aluminium	10.51	1.52	7.98	1.40
Al-4/2	aluminium	10.51	1.52	5.35	0.54

Note: Ti-3/1= measurement number 1 on titanium section 3 from base.

Table 5-2: Comparison between the original roughness at the start and the final roughness at the end of the centrifuge test series of model pile CUIMP-3.

test	g-level	time before loading [min]	depth of pile tip [mm]	depth of pile tip [m]	v_{tip}	D_r [%]	$\sigma'(v)_{tip}$ [kPa]	p'_{tip} [kPa]	p'_{cs} linear CSL [kPa]	p'_{cs} non-linear CSL [kPa]	p'/p'_{cs} linear CSL	p'/p'_{cs} non-linear CSL	$q_b(z)$ [MPa]	$q_s(z)$ [MPa]	q_b [MPa]	q_s [MPa]	N_q	β
CLBS12-1	100	2.0	105	9.9	1.94	25	132	79	1240	740	0.06	0.11	4.5	0.023	3.3	0.024	25	0.36
CLBS12-2	100	0.8	205	19.9	1.93	26	268	159	1263	781	0.13	0.20	6.4	0.027	3.7	0.028	14	0.21
CLBS14-1	50	1.2	118	5.6	1.97	12	73	49	963	258	0.05	0.19	2.6	0.011	1.8	0.013	24	0.36
CLBS14-2	50	1.1	229	11.2	1.97	13	148	100	971	272	0.10	0.37	3.6	0.018	2.1	0.017	14	0.23
CLBS19-1	100	7.8	333	33.8	1.96	16	448	302	1039	386	0.29	0.78	8.9	0.039	8.4	0.046	19	0.21
CLBS19-2	100	23.3	335	34.1	1.96	16	451	304	1039	387	0.29	0.78	8.7	0.047	8.4	0.048	19	0.21
CLBS19-3	100	46.0	338	34.3	1.96	16	455	306	1040	388	0.29	0.79	8.7	0.050	8.7	0.050	19	0.22
CLBS20-1	100	1.8	119	11.2	1.71	104	171	101	5504	6273	0.02	0.02	23.8	0.086	21.3	0.091	125	1.07
CLBS20-2	100	1.7	227	22.2	1.71	104	338	200	5512	6280	0.04	0.03	39.9	0.172	35.1	0.168	104	0.99
CLBS21-1 OC	100	1.8	123	11.6	1.92	31	157	93	1383	994	0.07	0.09	9.3	0.031	8.3	0.035	53	0.45
CLBS21-2 OC	100	1.2	231	22.6	1.92	32	307	183	1394	1013	0.13	0.18	12.9	0.051	11.6	0.057	38	0.37
CLBS21-3 OC	100	8.9	340	34.5	1.92	32	468	278	1405	1033	0.20	0.27	15.0	0.069	13.6	0.073	29	0.31
CLBS21-4 OC	100	20.0	343	34.9	1.92	32	473	281	1406	1034	0.20	0.27	14.2	0.077	13.6	0.072	29	0.31
CLBS21-5 OC	100	63.0	345	35.1	1.92	32	476	282	1406	1034	0.20	0.27	14.1	0.077	13.5	0.070	28	0.29
CLBS22-1	200	2.1	120	22.6	1.70	107	346	205	5857	6606	0.04	0.03	41.3	0.156	36.0	0.160	104	0.92

Note: OC = overconsolidated, CSL = Critical State Line, $q_b(z)$ = unit base resistance before unloading, $q_s(z)$ = average global unit shaft resistance before unloading, N_q = bearing capacity factor, β = shaft friction ratio calculated using the average vertical stress.

Table 5-3: Summary of load tests in Leighton Buzzard sand.

test	g-level	time before loading [min]	depth of pile tip [mm]	depth of pile tip [m]	v_{tip}	D_r [%]	$\sigma'(v)_{tip}$ [kPa]	p'_{tip} [kPa]	p'_{cs} linear CSL [kPa]	p'/p'_{cs} linear CSL	$q_b(z)$ [MPa]	$q_s(z)$ [MPa]	q_b [MPa]	q_s [MPa]	N_q	β
CDBS2-1	200	1.2	103	19.3	2.73	28	189	131	142	0.92	6.6	0.030	3.3	0.030	18	0.32
CDBS2-2	200	1.6	215	42.0	2.71	31	411	285	147	1.93	7.4	0.033	3.1	0.034	7	0.17
CDBS4-1	200	1.8	112	21.1	2.52	74	223	154	261	0.59	7.8	0.028	6.3	0.029	28	0.26
CDBS4-2	200	0.9	221	43.2	2.50	78	460	319	277	1.15	9.1	0.031	8.4	0.034	18	0.15
CDBS5-1	50	1.1	115	5.4	2.76	21	52	36	129	0.28	3.2	0.009	2.4	0.011	47	0.40
CDBS5-2	50	1.0	224	11.0	2.75	21	106	73	130	0.56	4.0	0.010	3.2	0.009	30	0.18
CDBS6-1	50	1.3	119	5.6	2.46	87	61	42	310	0.14	5.3	0.011	4.0	0.013	66	0.43
CDBS6-2	50	3.2	228	11.2	2.46	87	121	84	313	0.27	5.9	0.013	4.6	0.014	38	0.23
CDBS12-1	200	0.6	115	21.7	2.39	102	241	167	380	0.44	9.8	0.026	9.4	0.028	39	0.23
CDBS12-2	200	0.6	224	43.9	2.38	105	490	340	393	0.87	11.1	0.033	10.8	0.038	22	0.16
CDBS12-3	200	0.0	332	67.4	2.37	107	757	525	408	1.29	14.1	0.032	13.7	0.035	18	0.09
CDBS13-1 OC	100	1.0	117	11.0	2.40	100	122	85	369	0.23	16.1	0.029	15.2	0.029	124	0.47
CDBS13-2 OC	100	1.3	227	22.3	2.40	100	247	171	370	0.46	12.7	0.039	11.9	0.038	48	0.31
CDBS13-3 OC	100	9.1	337	34.2	2.40	101	380	263	372	0.71	10.3	0.033	9.8	0.030	26	0.16
CDBS13-4 OC	100	30.7	340	34.6	2.40	101	383	266	372	0.71	9.9	0.034	9.7	0.032	25	0.17
CDBS13-5 OC	100	135	342	34.8	2.40	101	386	268	372	0.72	9.8	0.033	9.6	0.032	25	0.17
CDBS14-1 OC	200	1.14	118	22.3	2.34	114	253	176	446	0.39	18.2	0.082	17.4	0.083	69	0.65
CDBS14-2 OC	200	2.24	227	44.5	2.33	115	507	351	452	0.78	15.0	0.099	14.1	0.089	28	0.35
CDBS14-3 OC	200	29.8	339	68.9	2.33	116	787	546	458	1.19	11.2	0.050	10.6	0.049	14	0.12

Note: OC = overconsolidated, CSL = Critical State Line, $q_b(z)$ = unit base resistance before unloading, $q_s(z)$ = average global unit shaft resistance before unloading, Nq = bearing capacity factor, β = shaft friction ratio calculated using the average vertical stress.

Table 5-4: Summary of load tests in Dogs Bay sand.

test	g-level	state	v_l	m	R
CLBS- 14	50	L	1.98	-0.00022	0.988
CLBS- 12	100	L	1.94	-0.00027	0.986
CLBS- 16	100	L	1.96	-0.00038	0.983
CLBS- 19	100	L	1.97	-0.00032	0.988
CLBS- 18	200	L	1.97	-0.00048	0.997
CLBS- 21	100	OC-MD	1.92	-0.00011	0.988
CLBS- 17	100	MD	1.85	-0.00030	0.949
CLBS- 15	50	D	1.74	-0.00012	0.913
CLBS- 20	100	D	1.71	-0.000019	0.138
CLBS- 22	200	D	1.70	-0.000029	0.715

Table 5-5: Selected parameters for LBS for linear distribution of specific volume with depth.

test	g-level	state	v_l	m	R
CDBS- 5	50	L	2.76	-0.00063	0.980
CDBS- 7	100	L	2.75	-0.00061	0.861
CDBS- 2	200	L	2.74	-0.00056	0.959
CDBS- 11	200	L	2.73	-0.00063	0.944
CDBS- 9	100	MD	2.58	-0.00084	0.854
CDBS- 3	200	MD	2.56	-0.00083	0.972
CDBS- 4	200	MD	2.54	-0.00093	0.996
CDBS- 10	200	MD	2.56	-0.00083	0.972
CDBS- 6	50	D	2.46	-0.00050	0.825
CDBS- 8	100	D	2.41	-0.00053	0.947
CDBS- 12	200	D	2.40	-0.00053	0.937
CDBS- 13	100	D-OC	2.40	-0.00014	0.991
CDBS- 14	200	D-OC	2.34	-0.00019	0.994

Table 5-6: Selected parameters for DBS for linear distribution of specific volume with depth.

Soil	function of CSL	base capacity		shaft capacity	
		m_{Nq}	A_{Nq}	m_β	A_β
Leighton Buzzard sand	linear	-0.45	11	-0.65	0.045
Leighton Buzzard sand	non-linear	-0.40	17	-0.51	0.09
Dogs Bay sand	linear	-0.72	22	-0.84	0.07

Table 5-7: Summary of parameters for pile design using the state parameter approach.

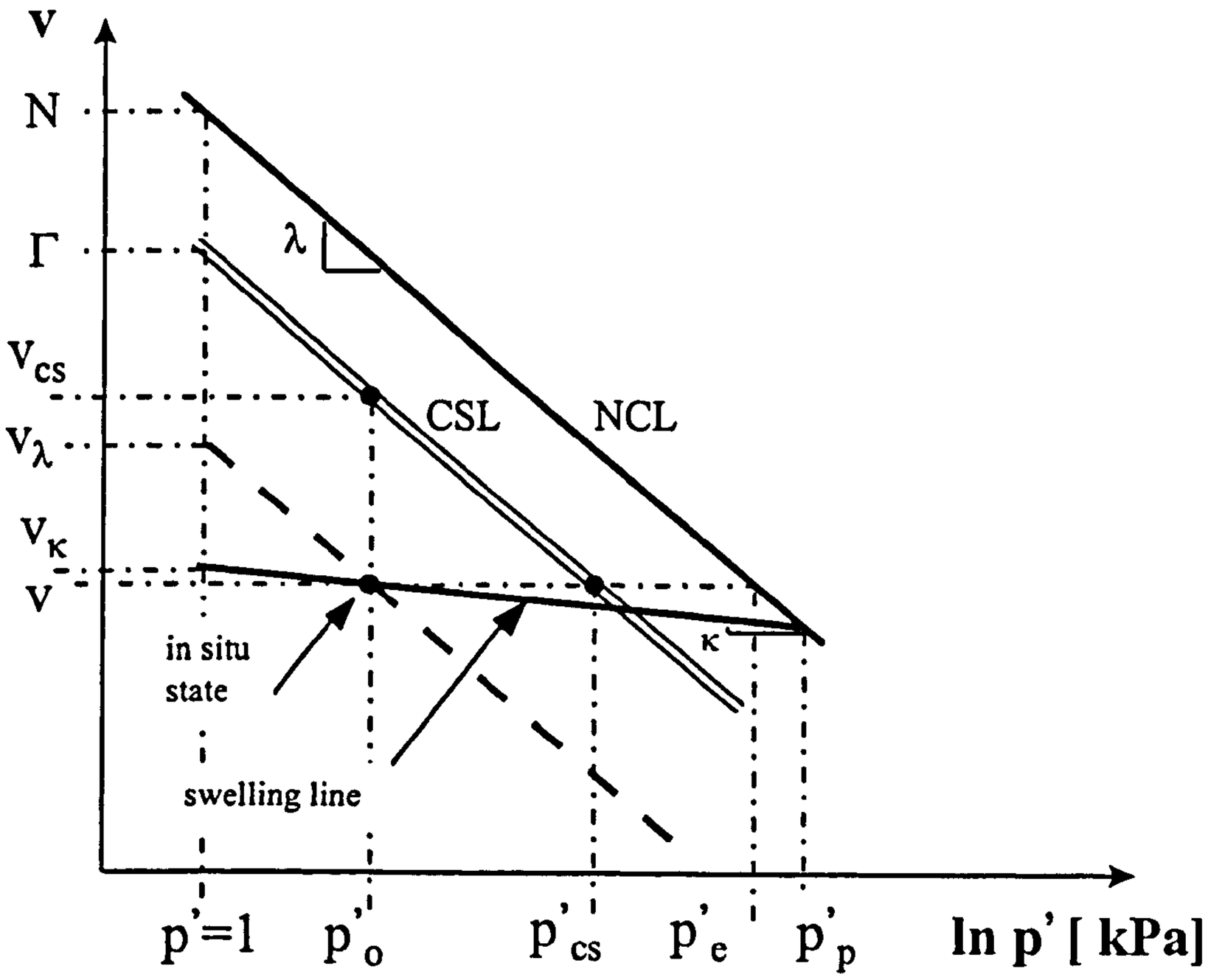

Figure 2-1: Definition of some critical state and normalising parameters.

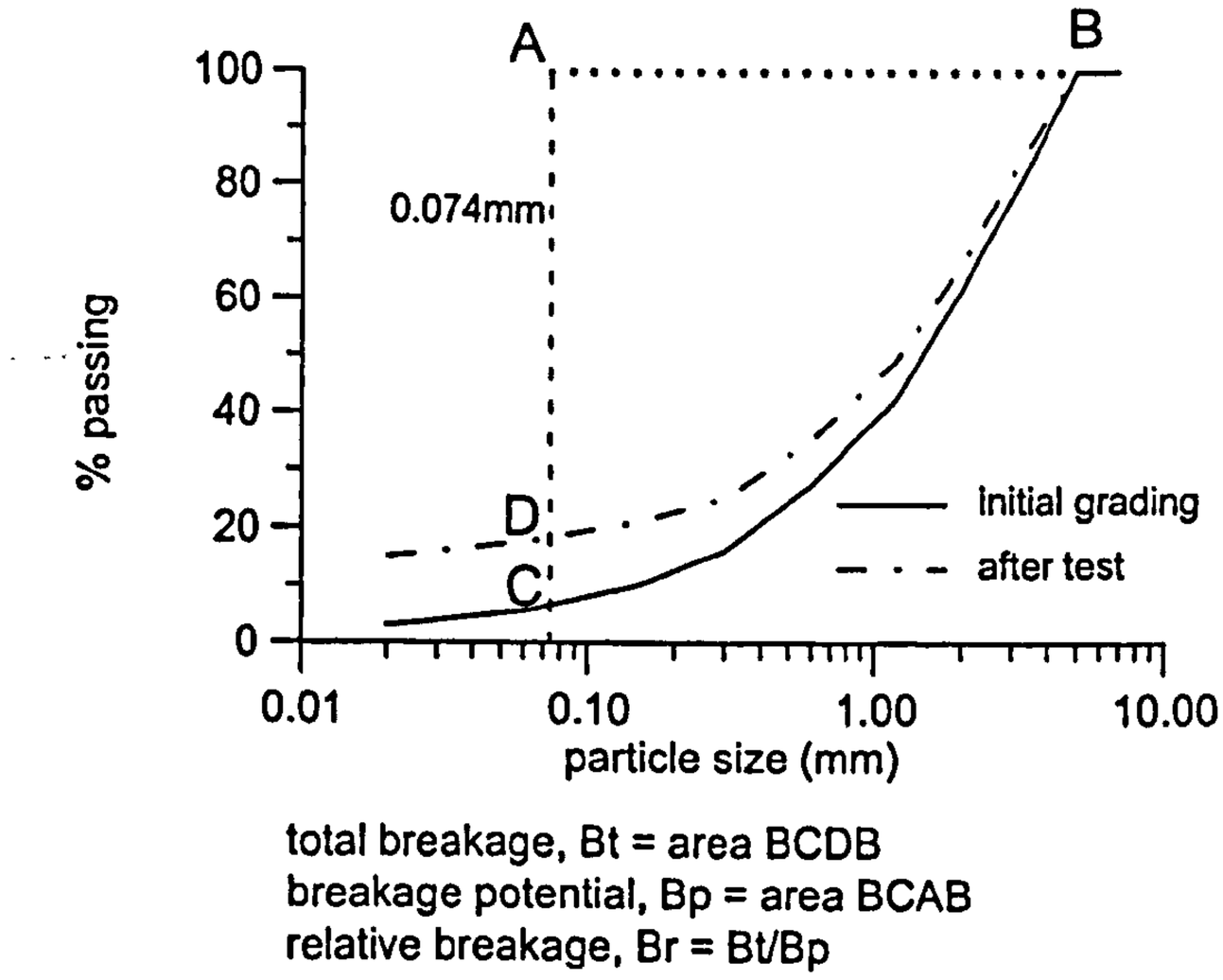

Figure 2-2: Definition of relative breakage, B_r (after Hardin, 1985).

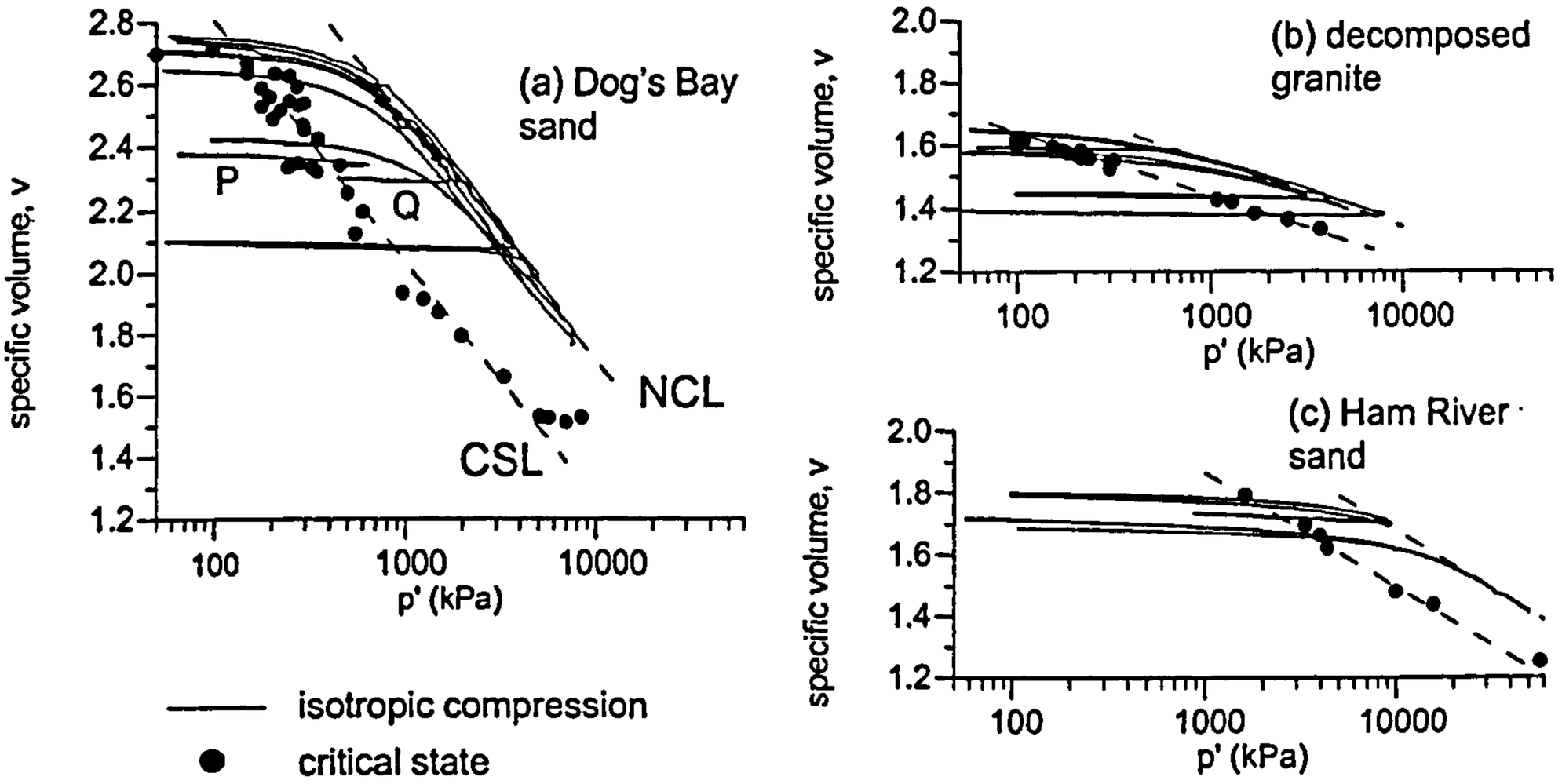

Figure 2-3: Isotropic compression and critical state data for three sands (after Jovicic & Coop, 1997).

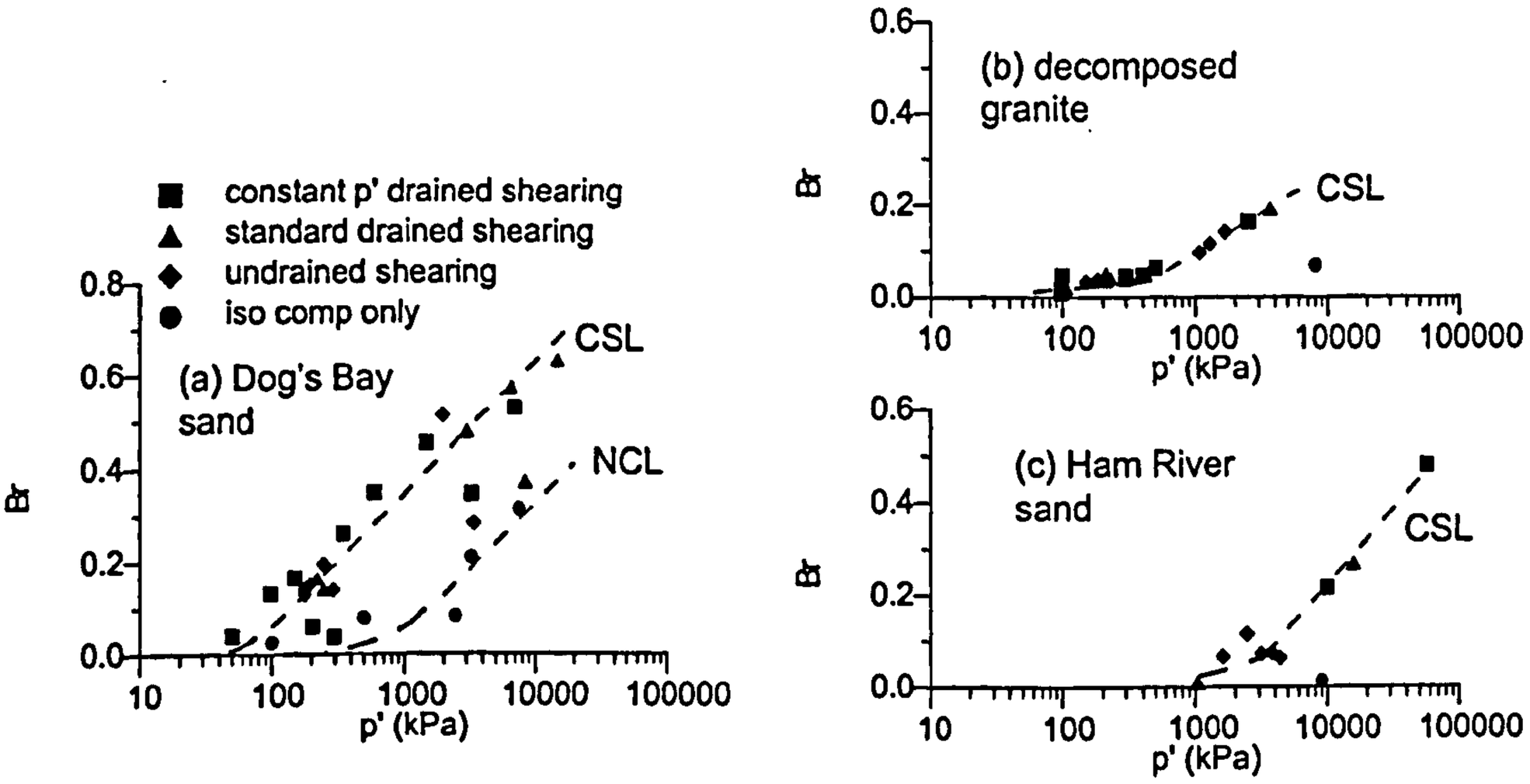

Figure 2-4: Particle breakage for isotropically compressed and sheared samples of three different coarse grained soils (after Coop & Lee, 1993).

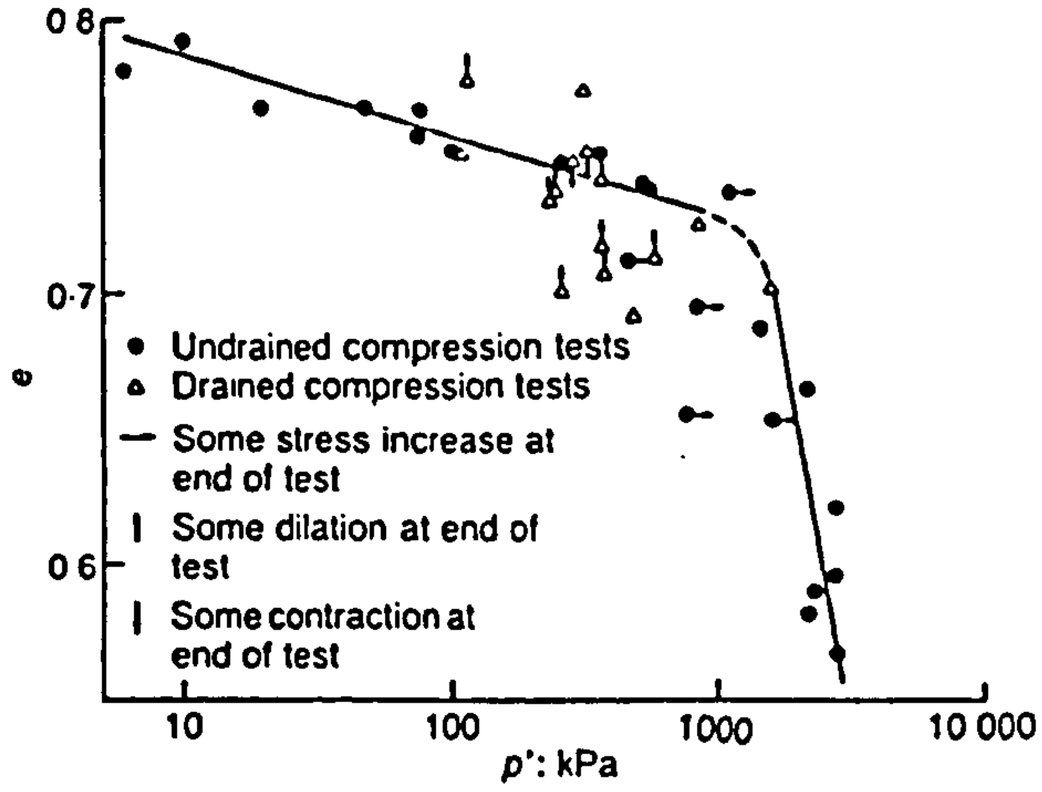

Figure 2-5: Critical state line for Erksak sand (after Been et al., 1991).

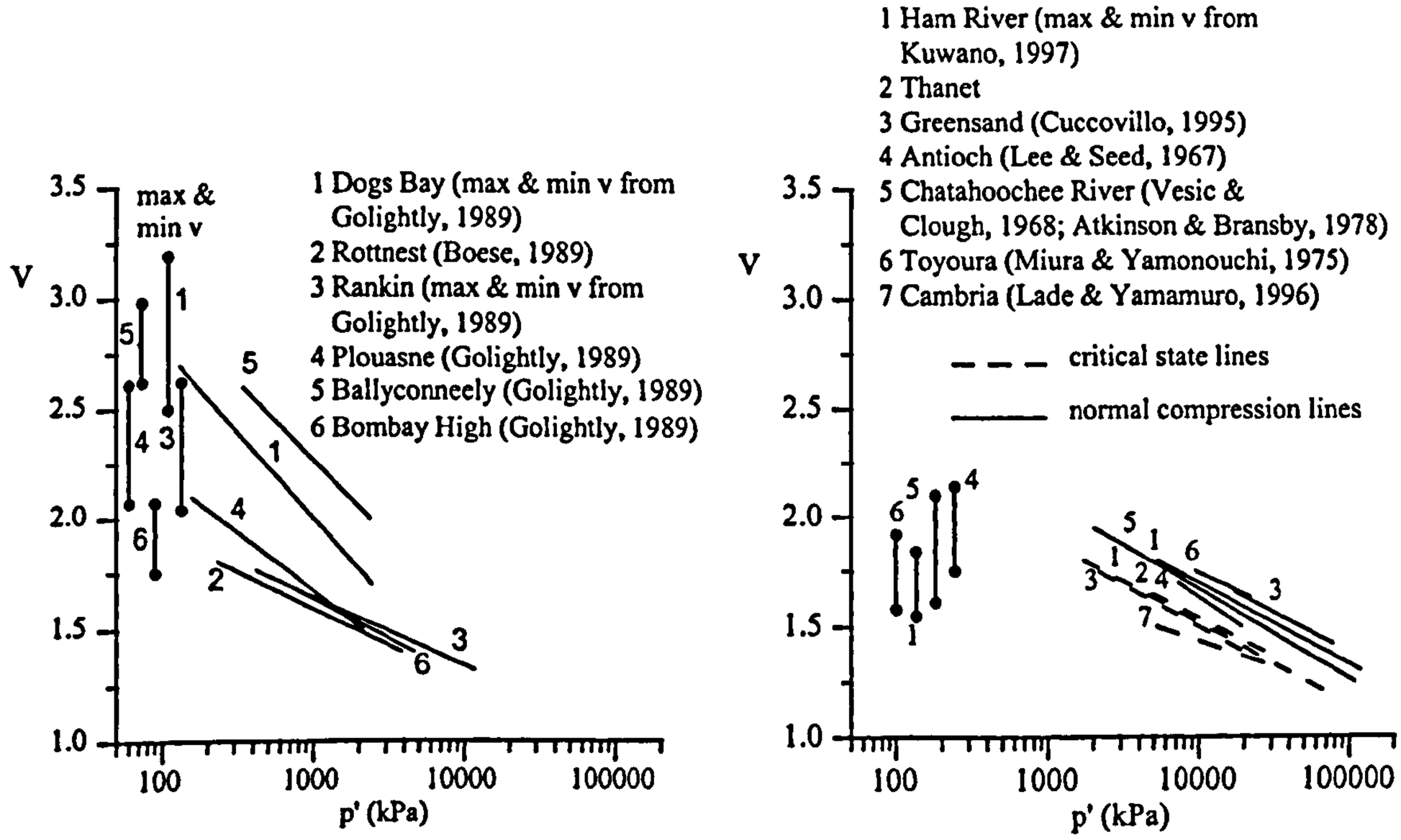

(a) carbonate sands (b) silica sands

Figure 2-6: Critical state lines for a variety of carbonate and silica sands (after Coop, 1999b).

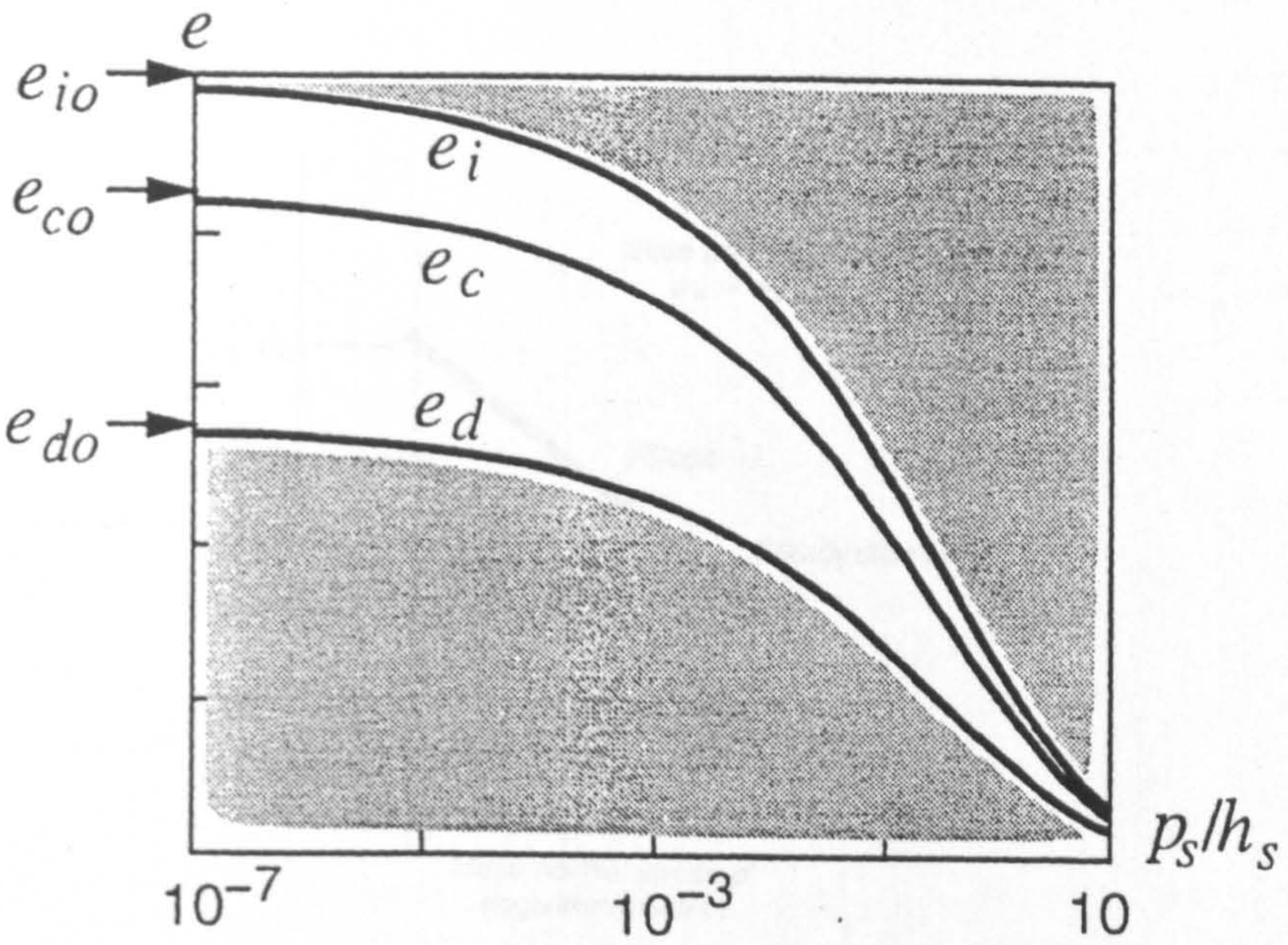

Figure 2-7: Definition of the critical state line in the hypoplastic model (after Gudehus, 1996).

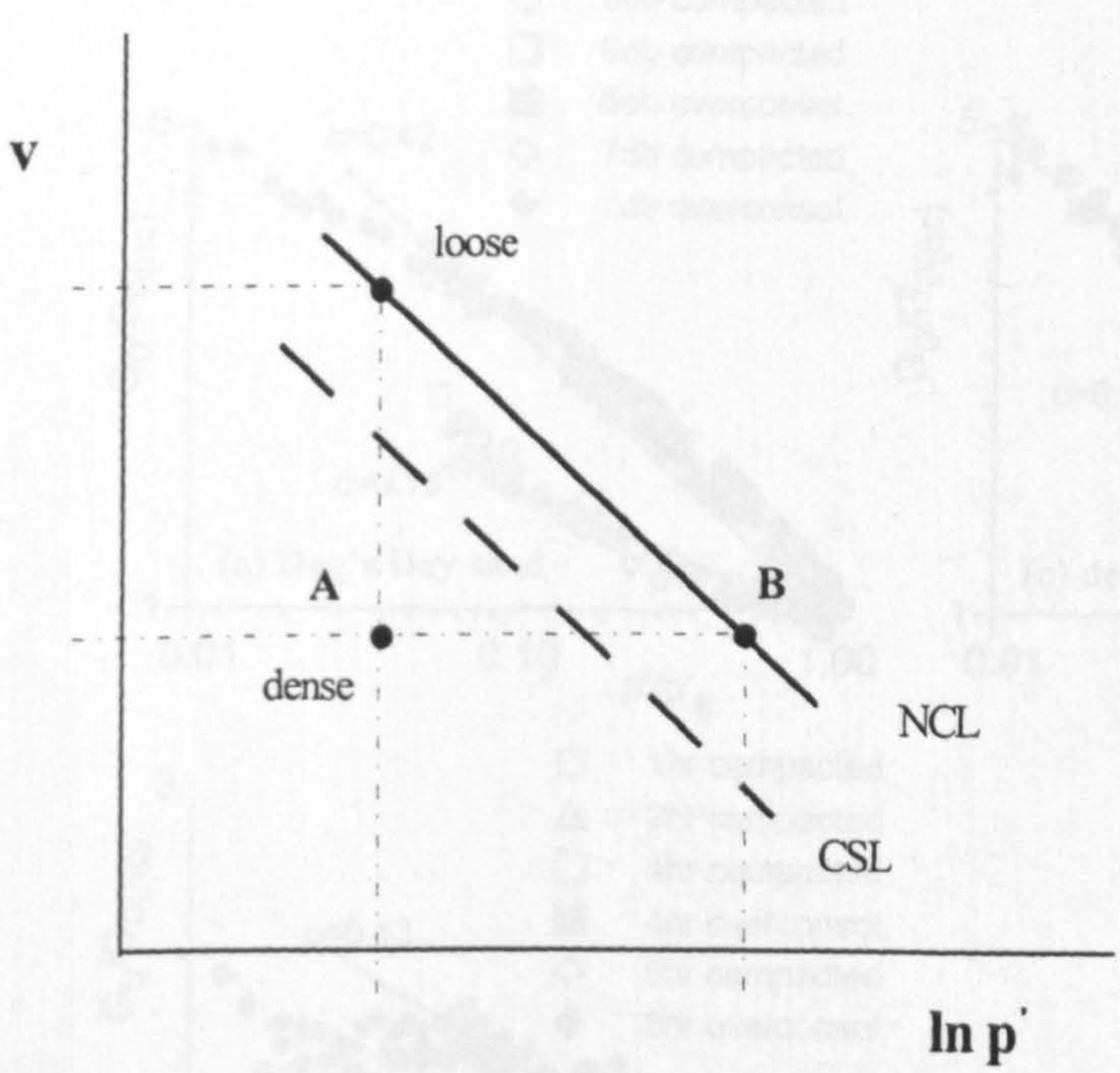

Figure 2-8: Illustration of the importance of the current state.

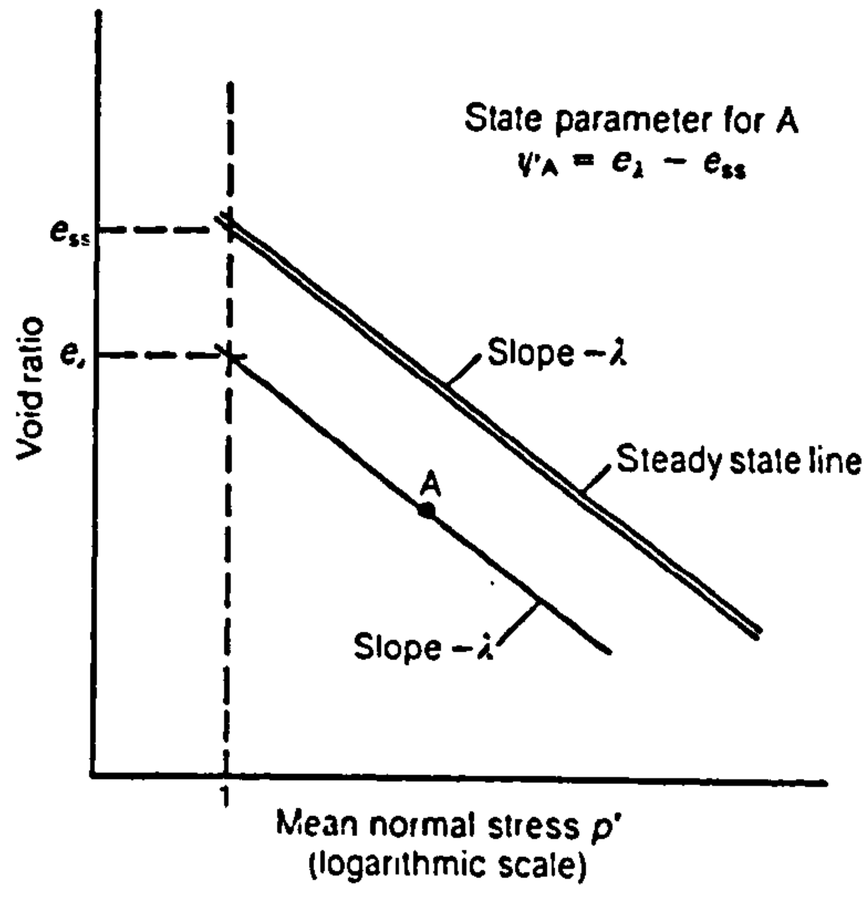

Figure 2-9: State parameter as defined by Been & Jefferies (1985).

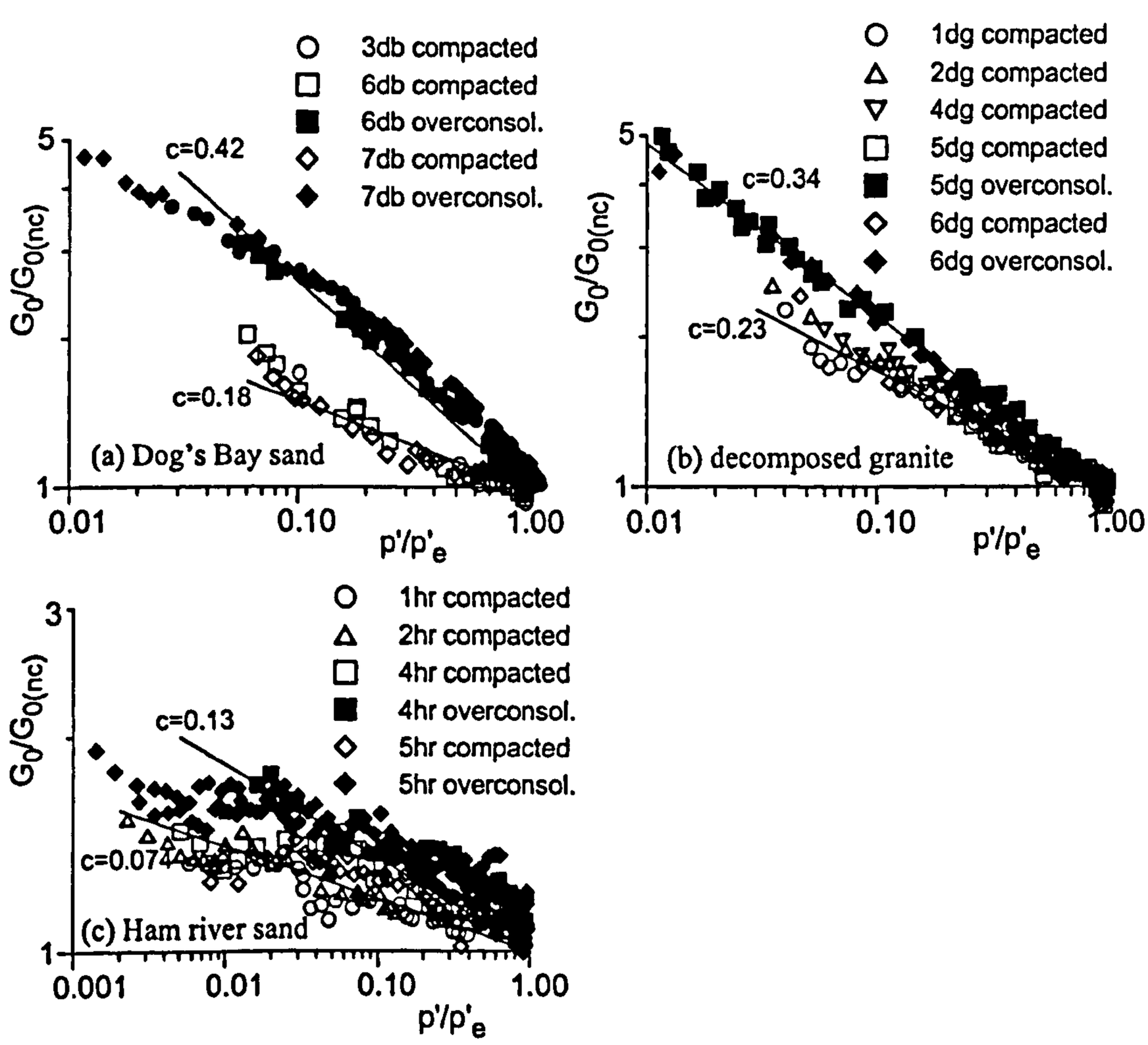

Figure 2-10: Variation of normalised G_o with normalised volumetric state (after Jovicic & Coop, 1997). 1dg, 5hr etc. indicate test numbers.

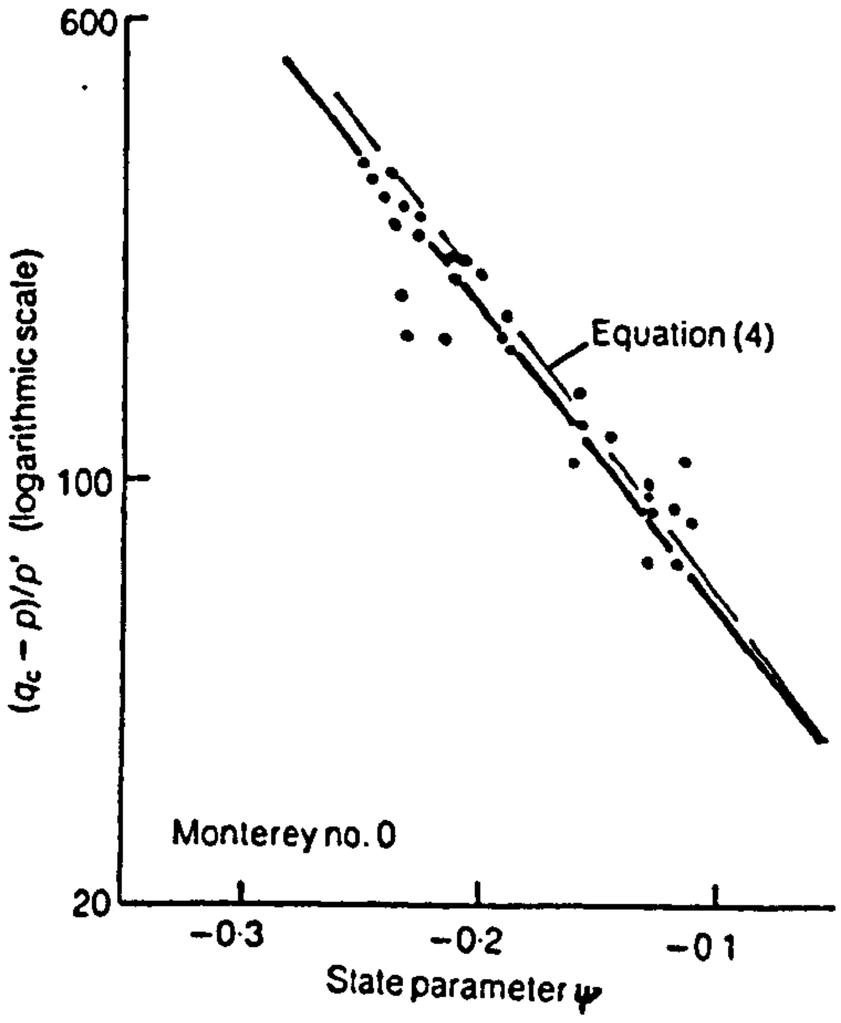

Figure 2-11: Interpretation of CPT data using the state parameter concept for Monterey No. 0 sand (after Been et al., 1987).

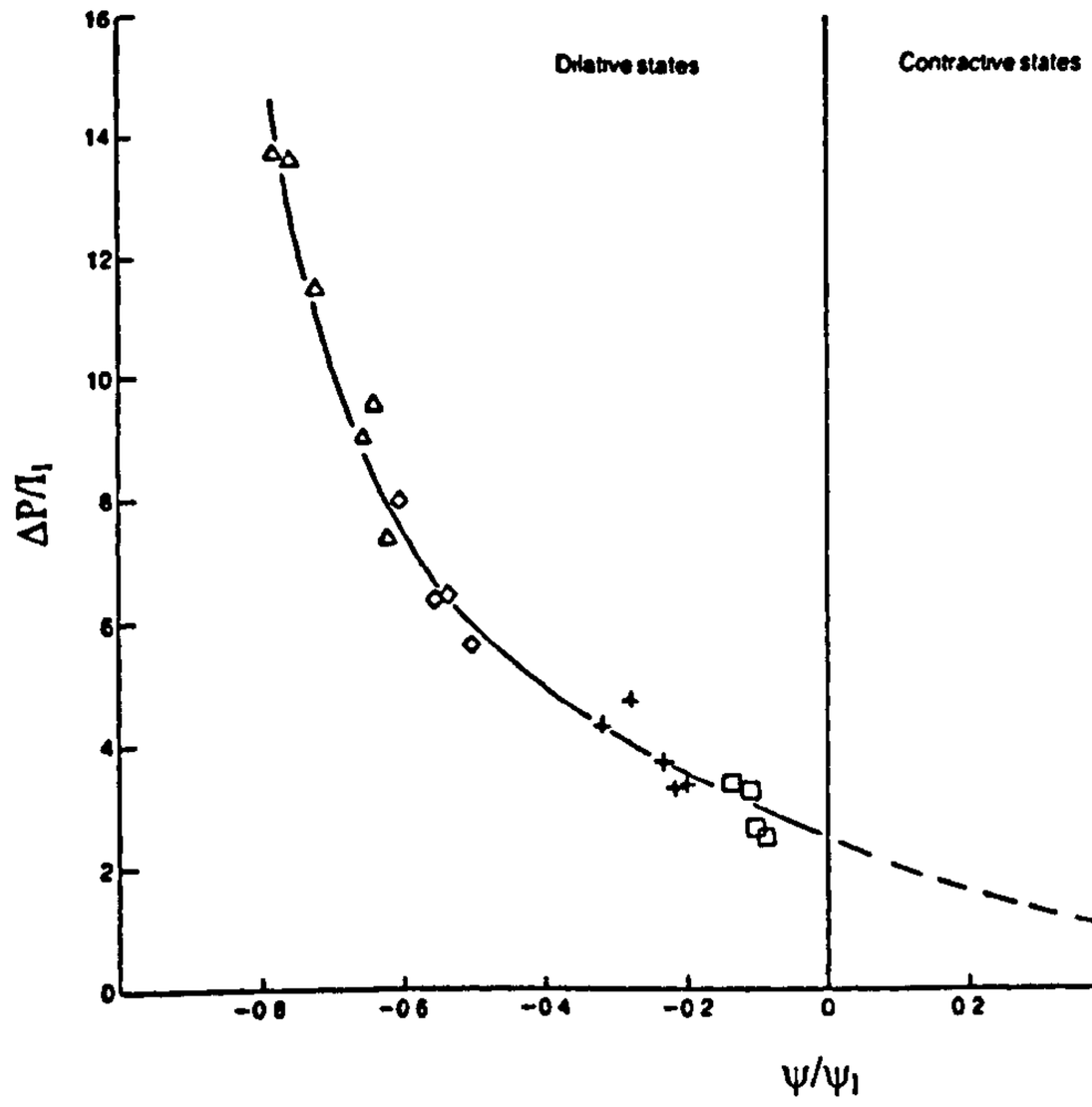

Figure 2-12: DMT test results on Ottawa sand analysed in terms of a normalised state parameter (after Konrad, 1988).

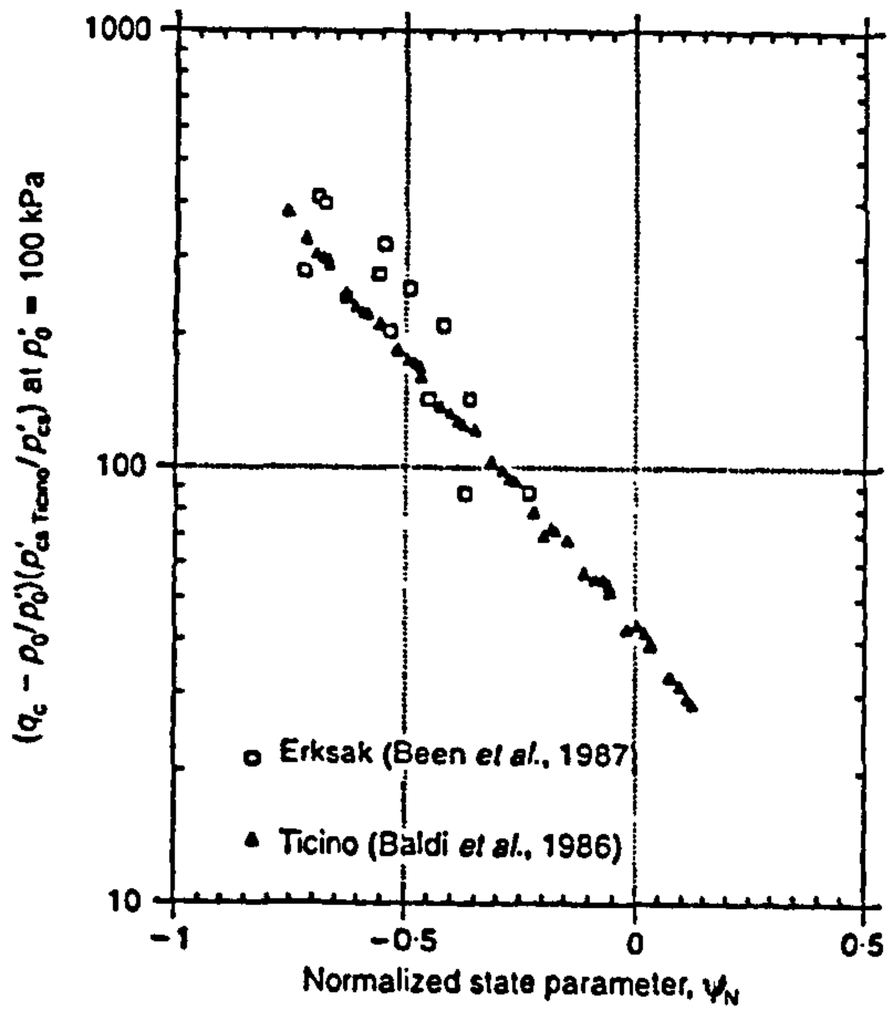

Figure 2-13: Improved correlation between cone resistance and state parameter (after Konrad, 1998).

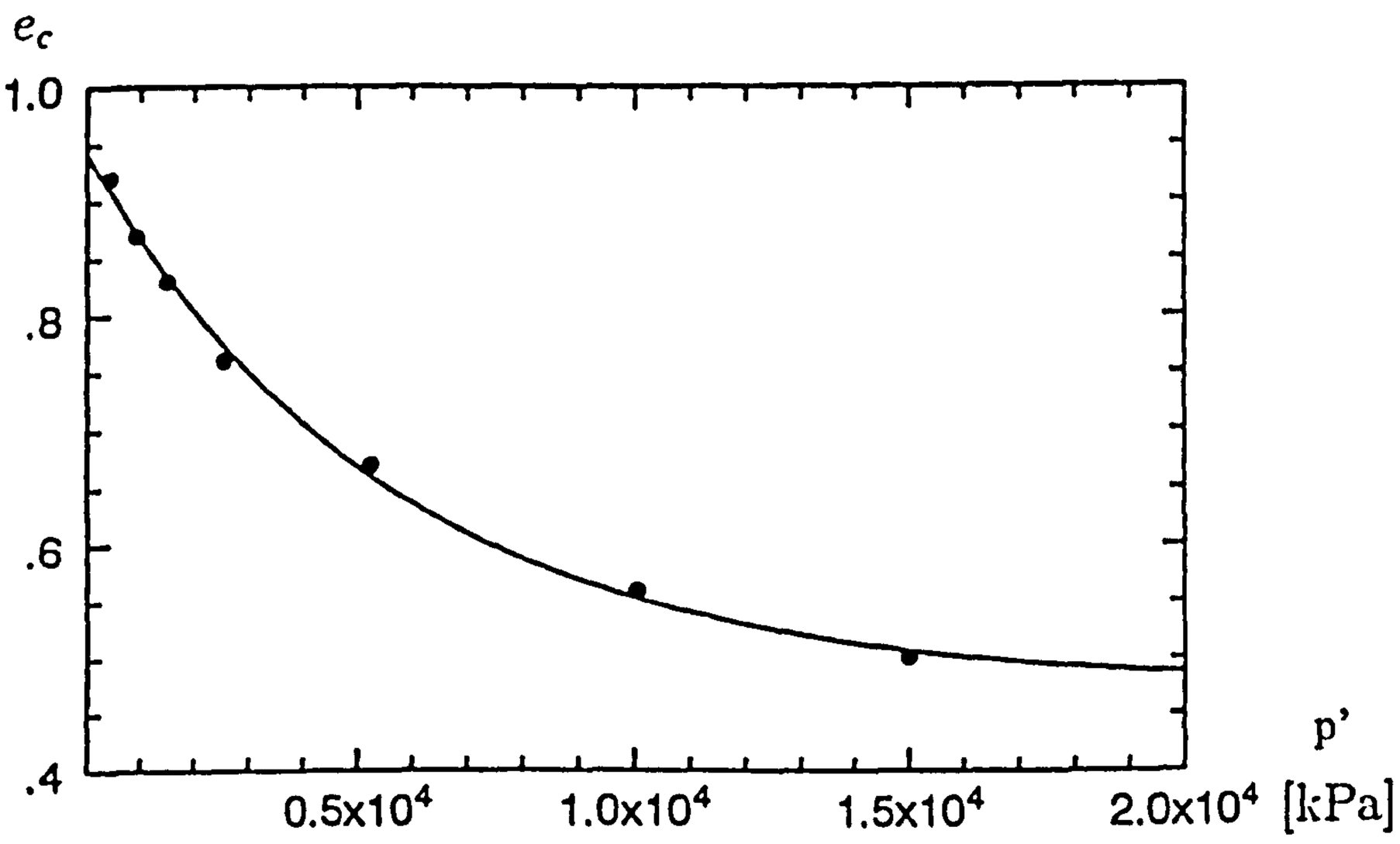

Figure 2-14: Critical state line by Lee & Seed (1967) for Sacramento River sand.

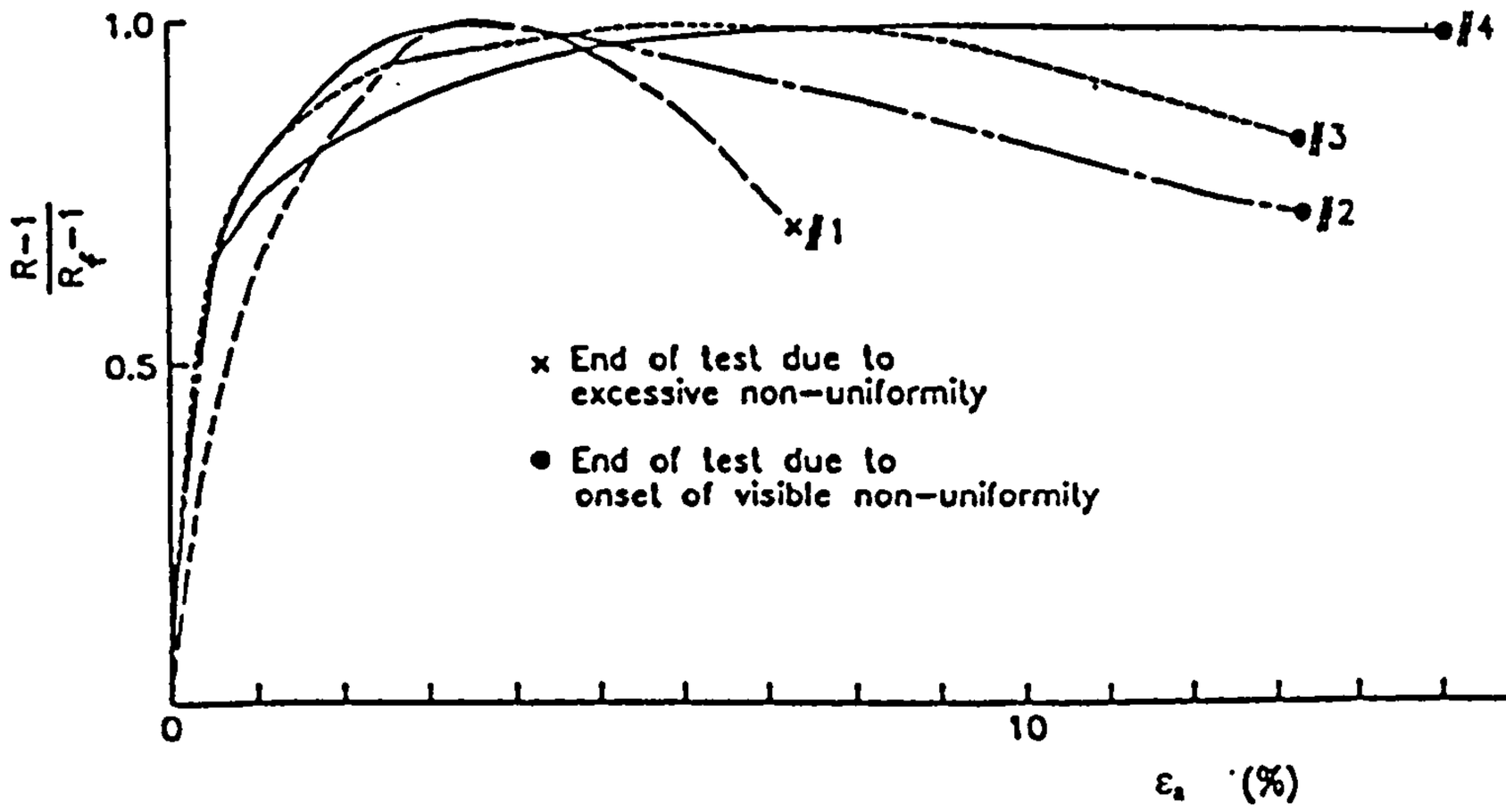

Figure 2-15: Drained triaxial test results with different end conditions (after Chu & Lo, 1993). R represents the current stress ratio and R_f the stress ratio at failure (peak).

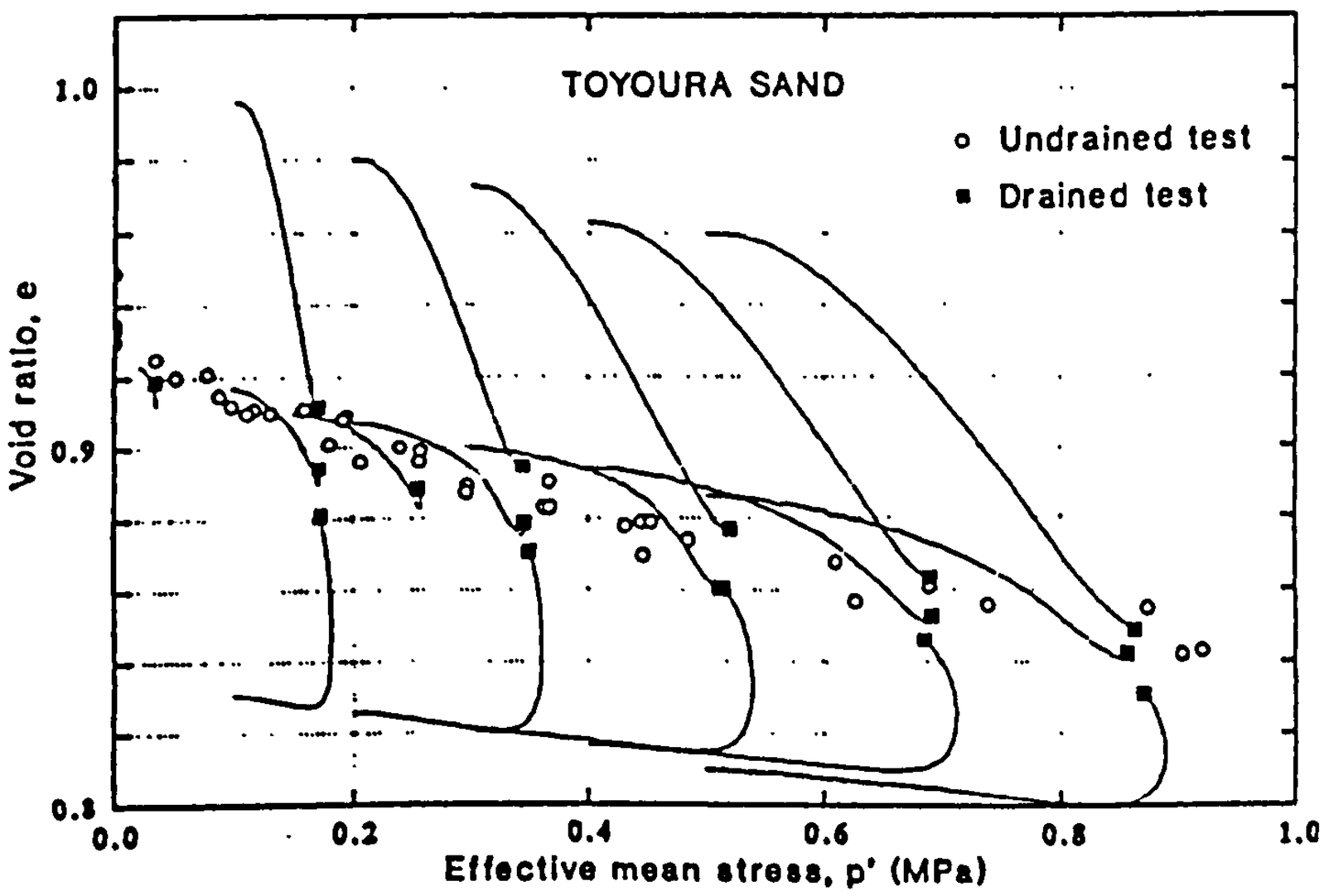

Figure 2-16: Critical states for drained and undrained triaxial tests on Toyoura sand (after Verdugo & Ishihara, 1996).

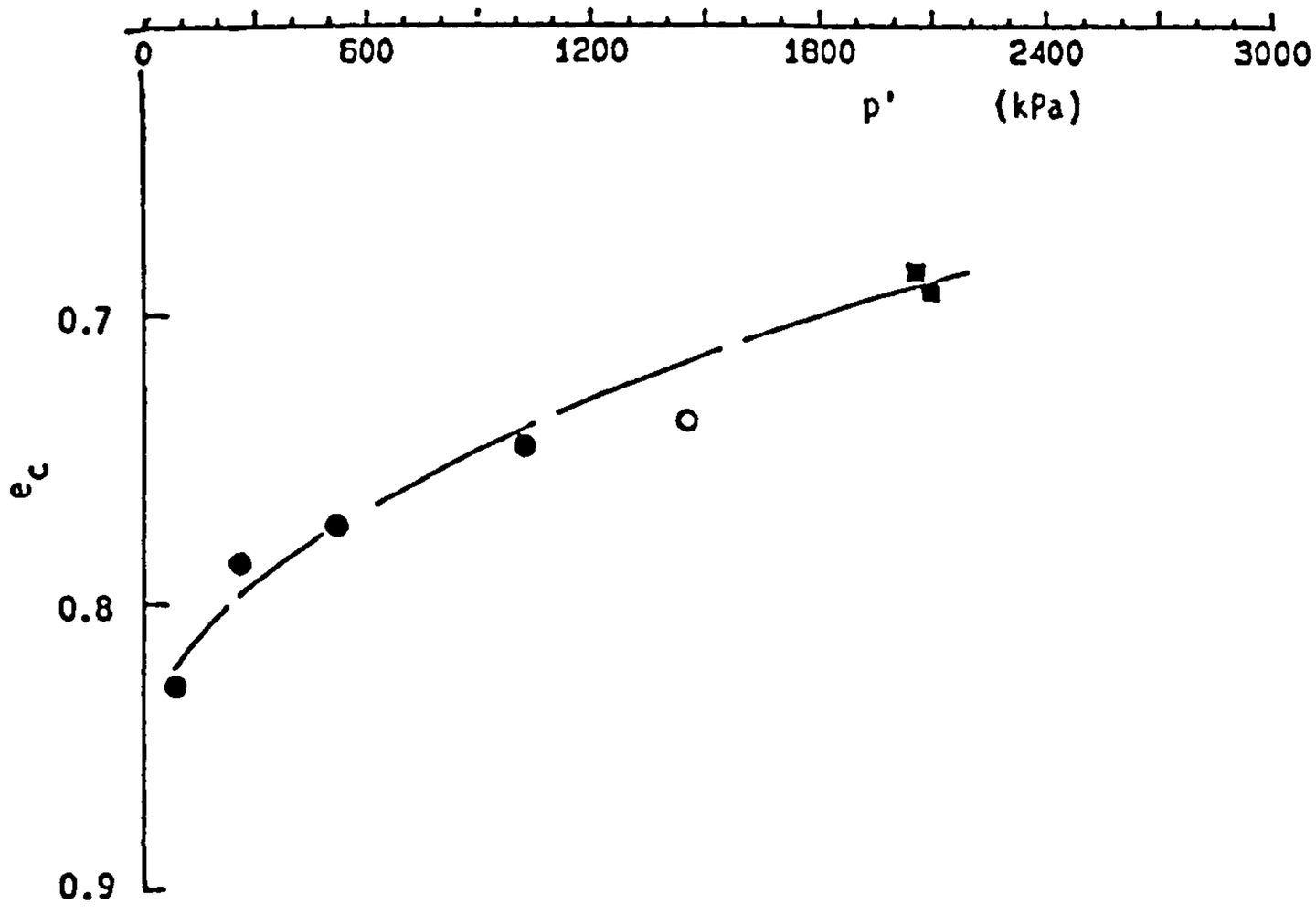

Figure 2-17: Critical states for Sydney sand (after Chu & Lo, 1993).

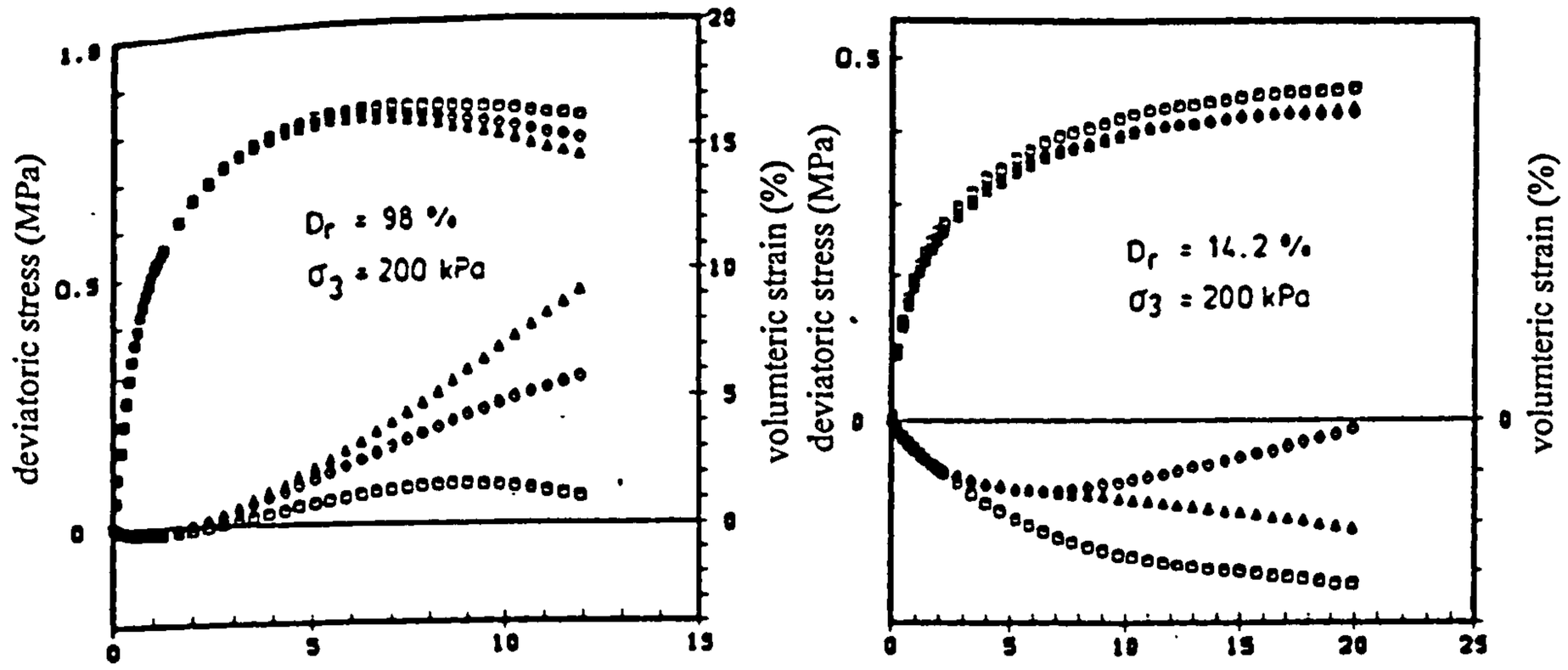

(a) Samples of dense Karlsruhe medium sand

(b) Samples of loose Karlsruhe medium sand

Figure 2-18: Effect of non-homogeneous radial strain on calculated volumetric strain (after Kolymbas & Wu, 1990).

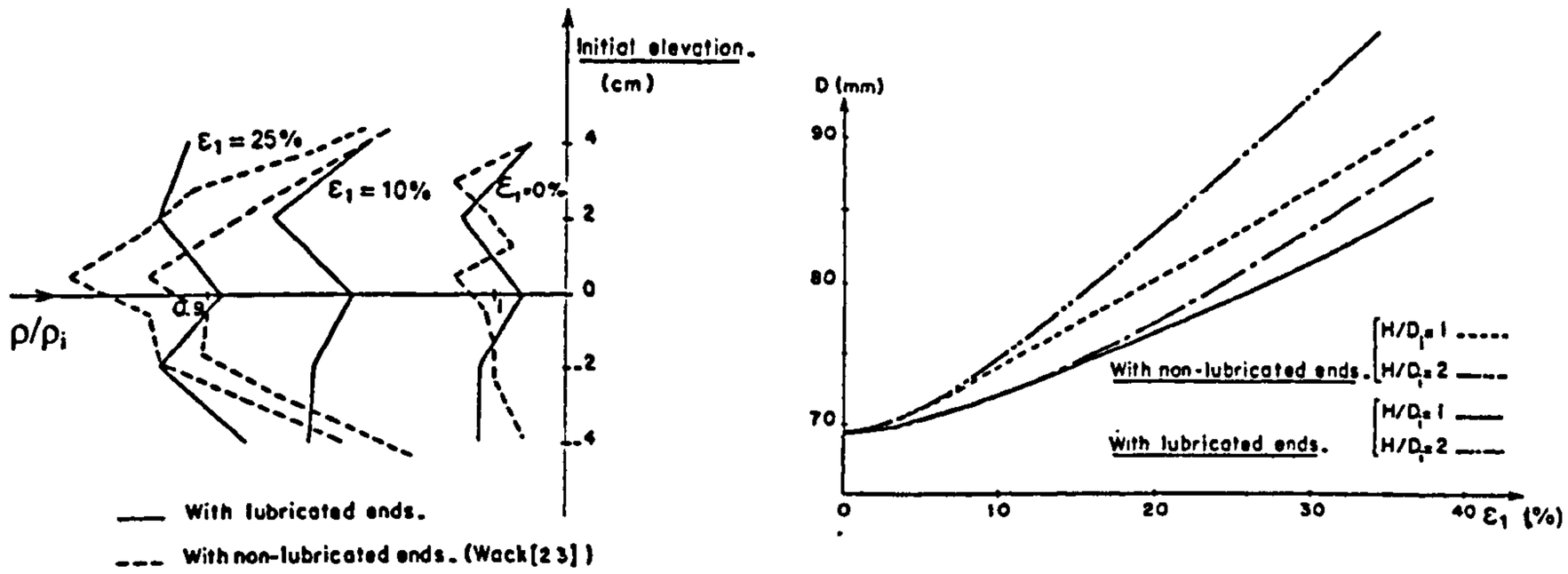

(a) change of density with axial strain

(b) change in mid-height diameter with axial strain

Figure 2-19: Change of density and mid-height diameter with axial strain in samples of Hostun sand (after Bouvard & Stutz, 1986). ε_1 refers to the axial strain, D to the sample diameter, ρ to the density and i to the initial condition.

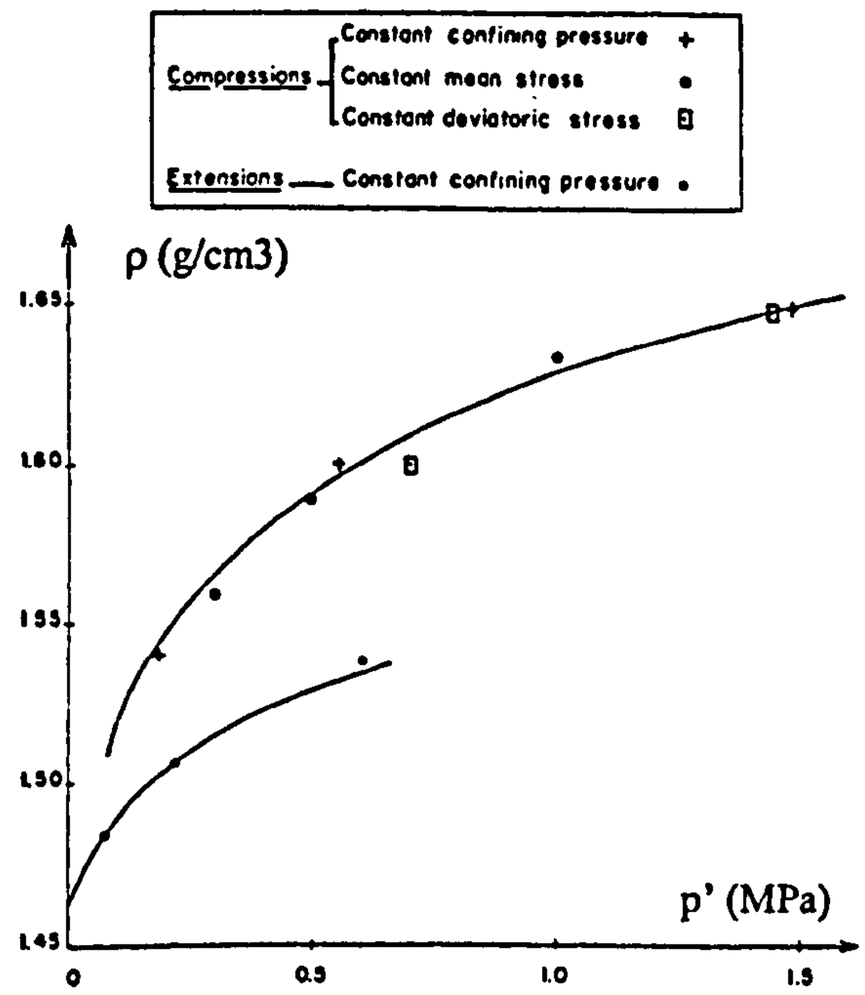

Figure 2-20: Critical states of Hostun sand (after Bouvard & Stutz, 1986).

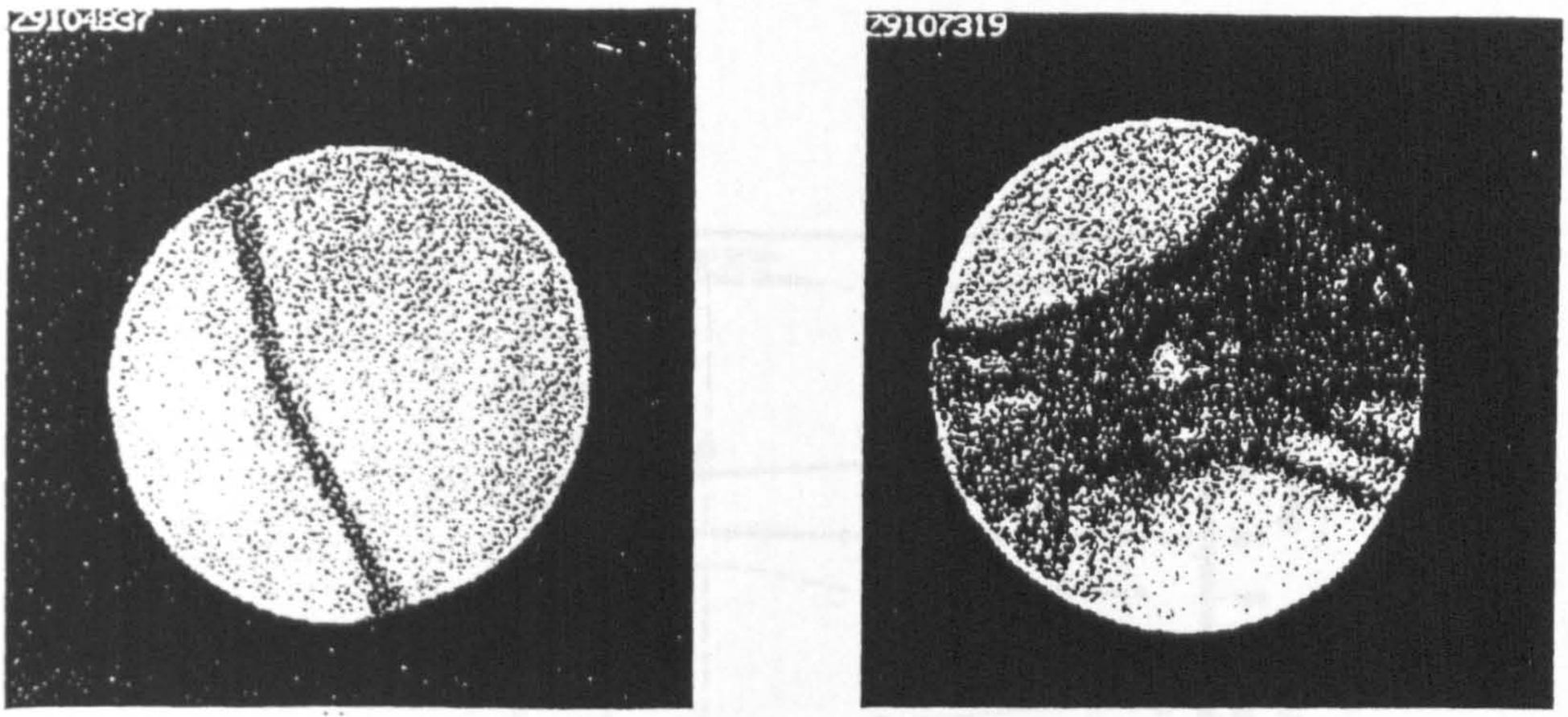

Figure 2-21: Localisation in 2:1 and 1:1 samples and void ratio measurements on 1:1 samples of dry Hostun sand (after Desrues et al. 1996).

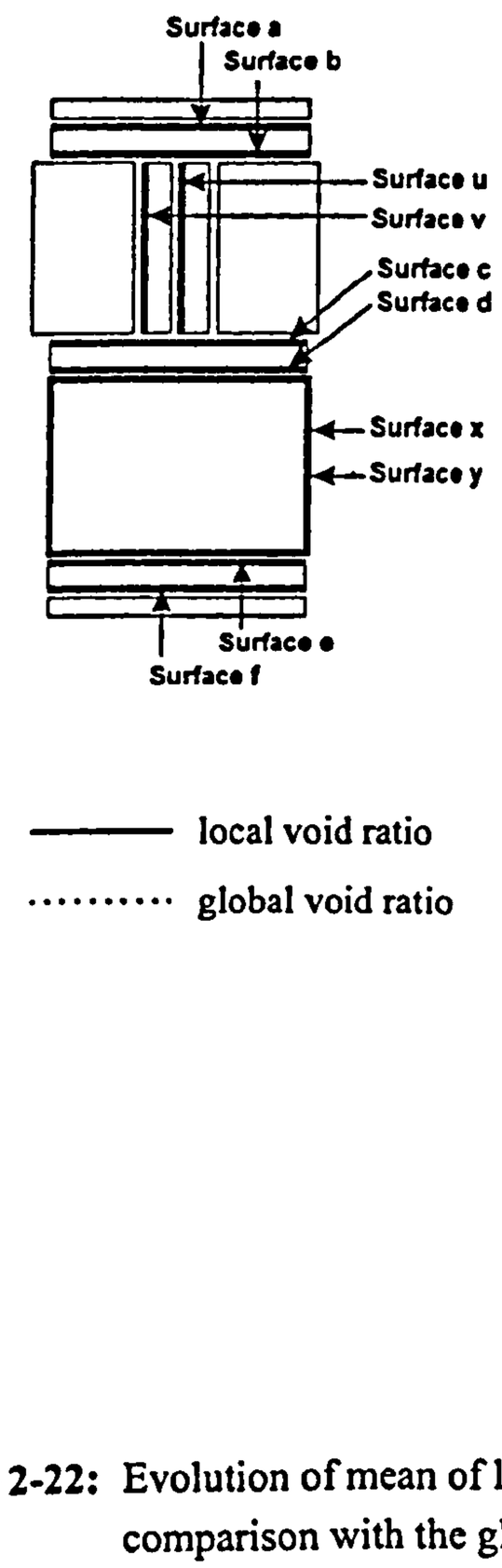

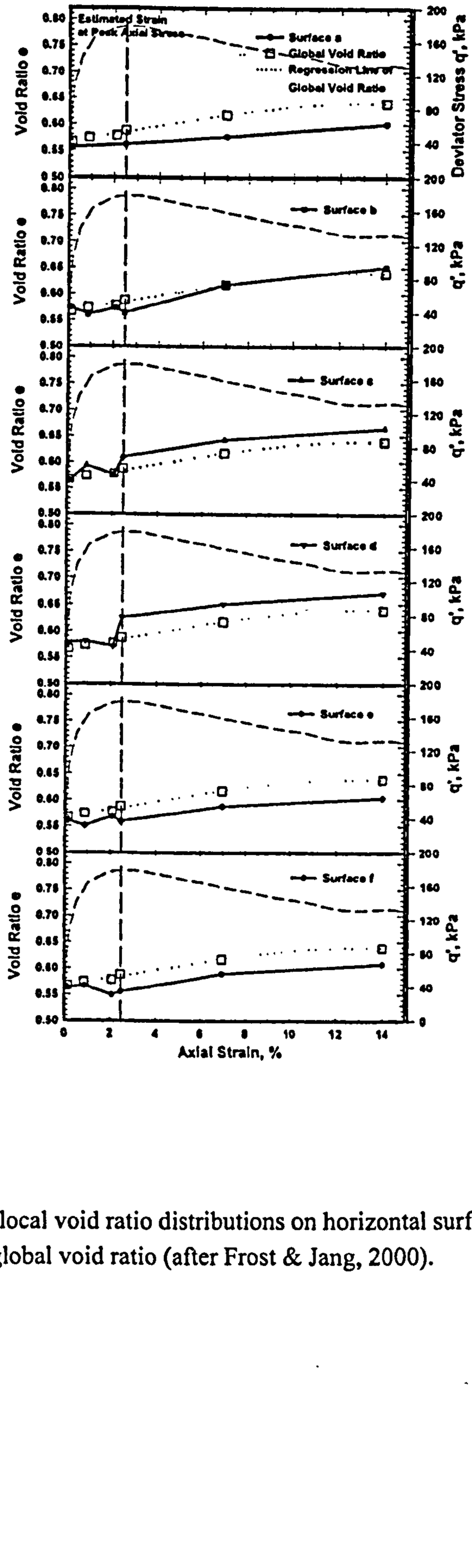

Figure 2-22: Evolution of mean of local void ratio distributions on horizontal surfaces in comparison with the global void ratio (after Frost & Jang, 2000).

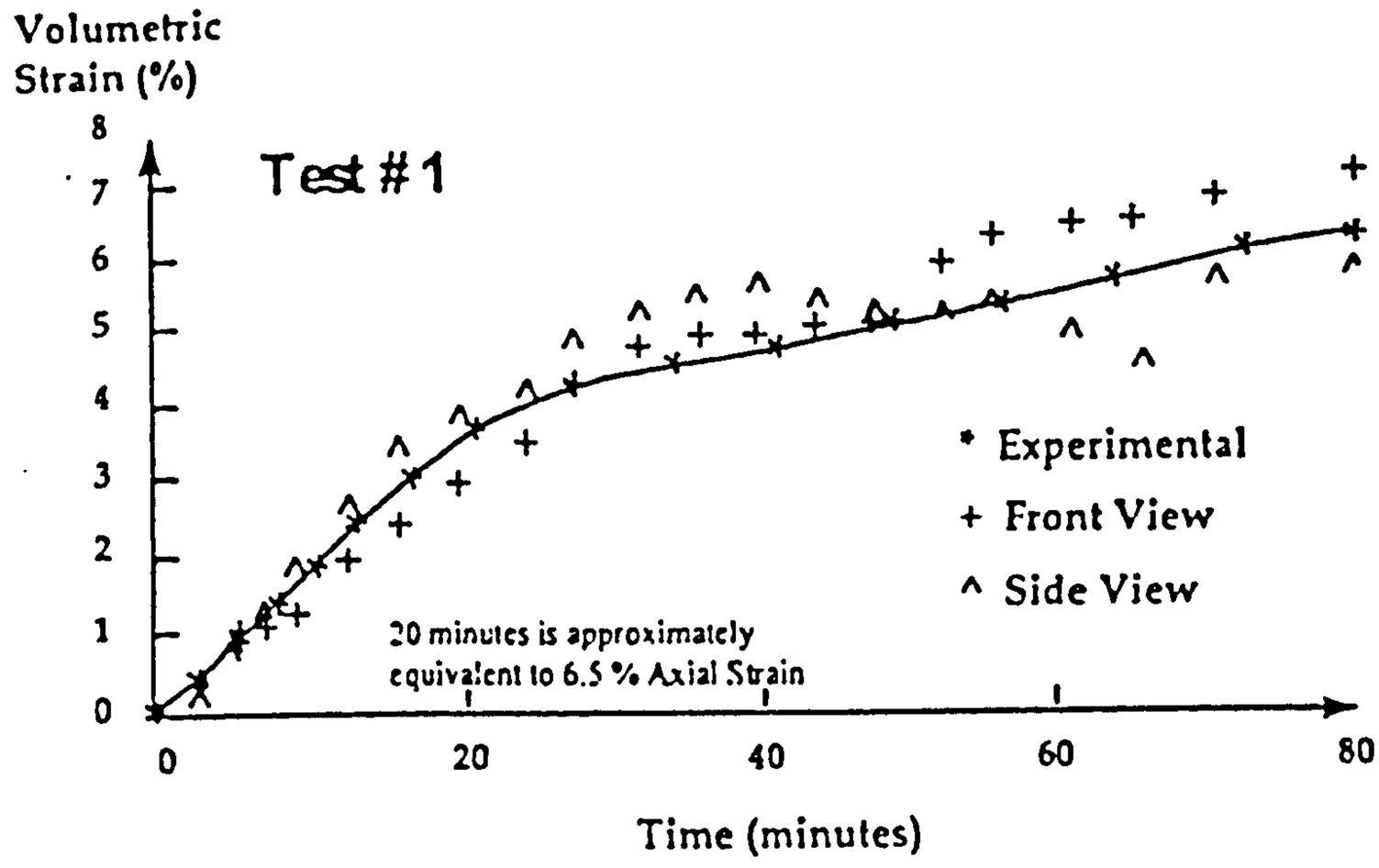

Figure 2-23: Comparison of volume changes measured by a conventional volume gauge and digital image analysis during a drained triaxial test (after Macari et al., 1997).

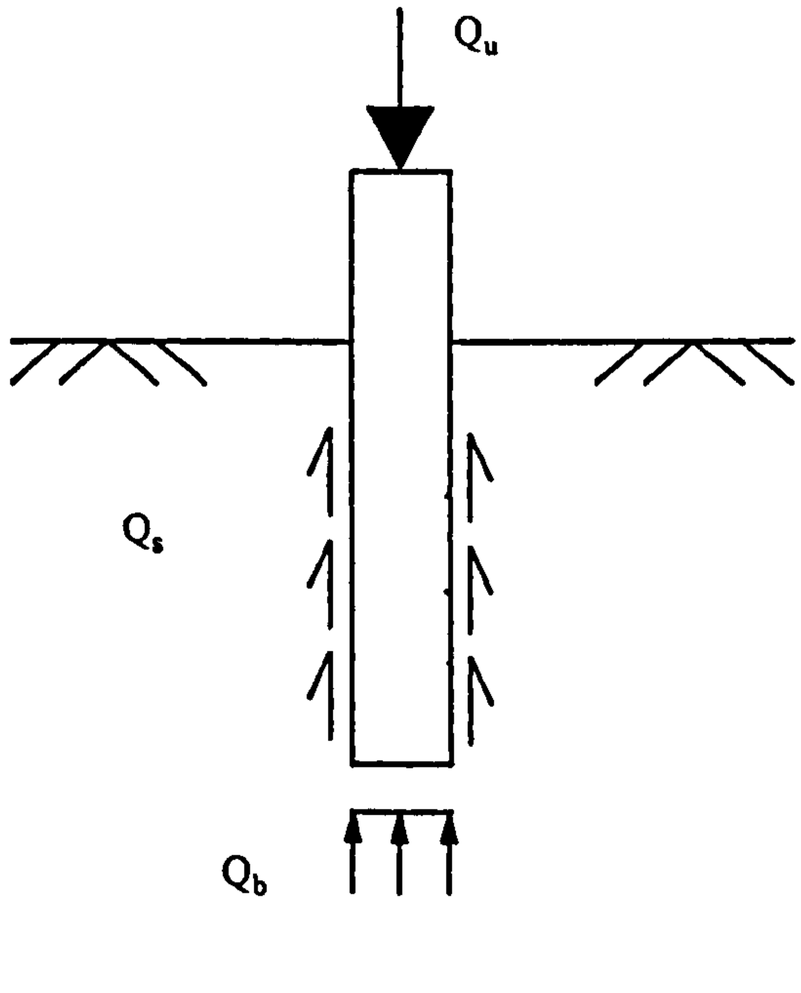

Figure 2-24: Stress transfer of an axially loaded pile.

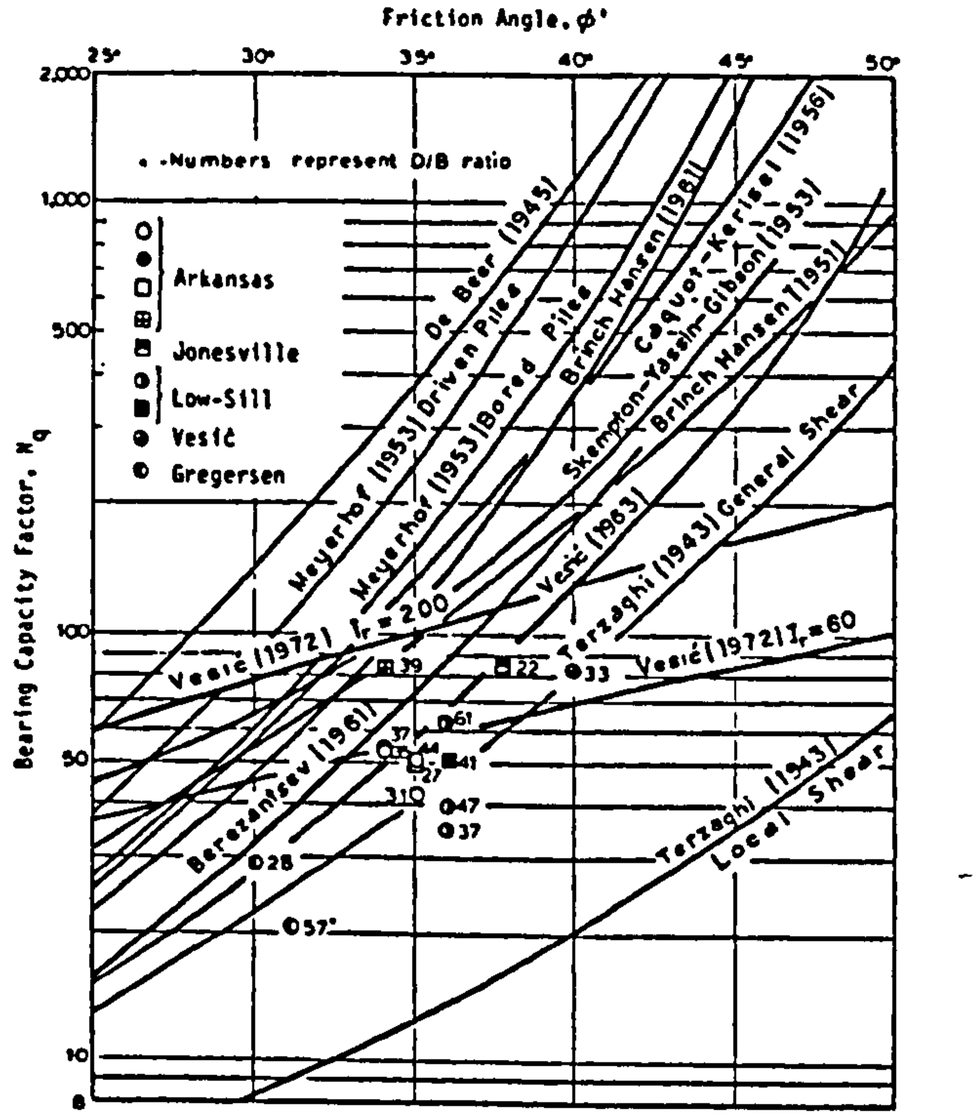

Figure 2-25: Bearing capacity factors (after Coyle & Castello, 1981).

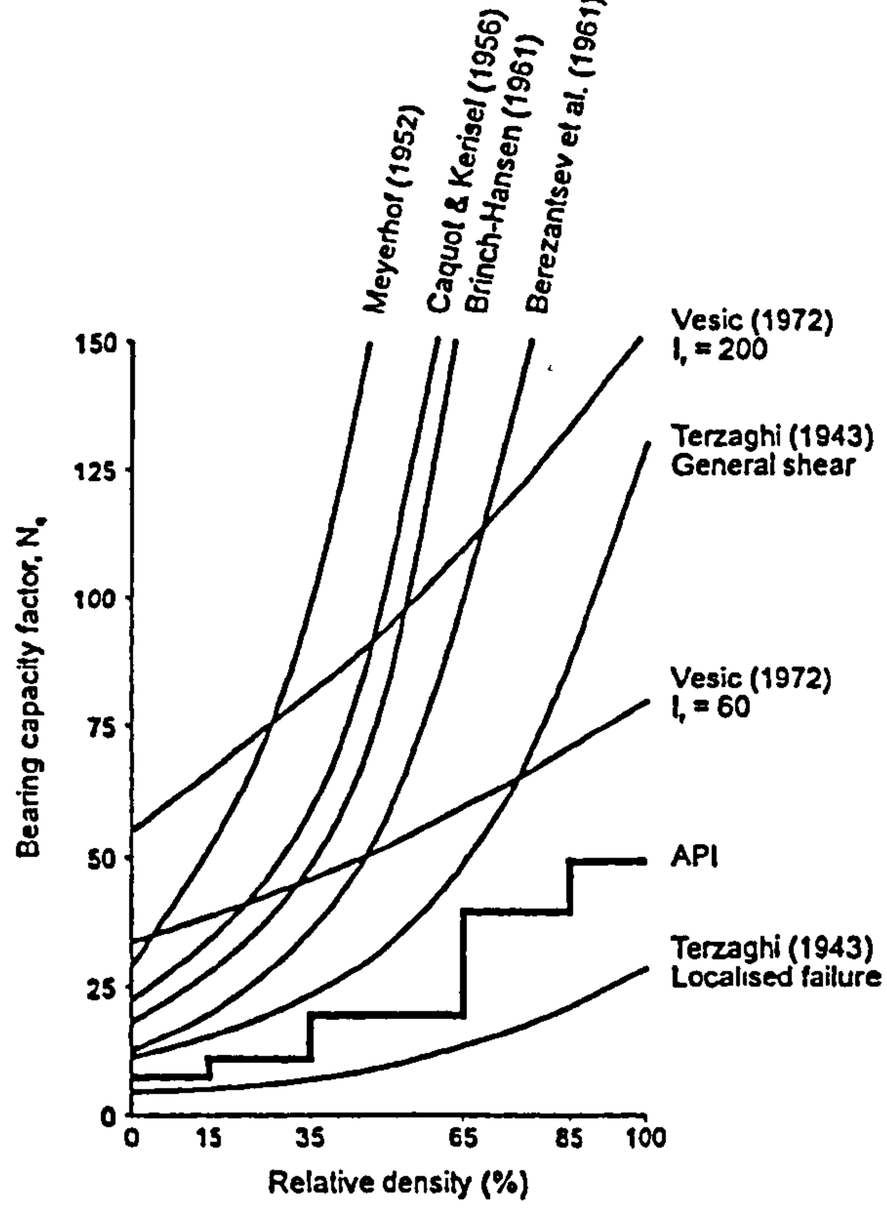

Figure 2-26: Bearing capacity factors according to various authors in comparison with recommendations of API-RP2A (after Bond et al., 1997).

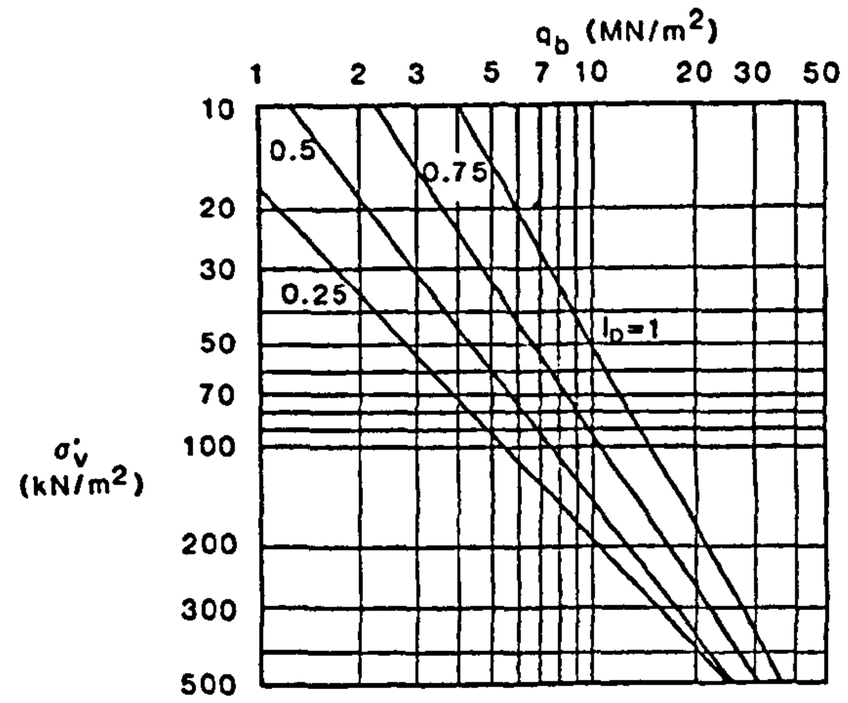

$$\phi'_{cs} = 33^\circ$$

Figure 2-27: Design chart for end bearing capacity (after Fleming et al., 1992).

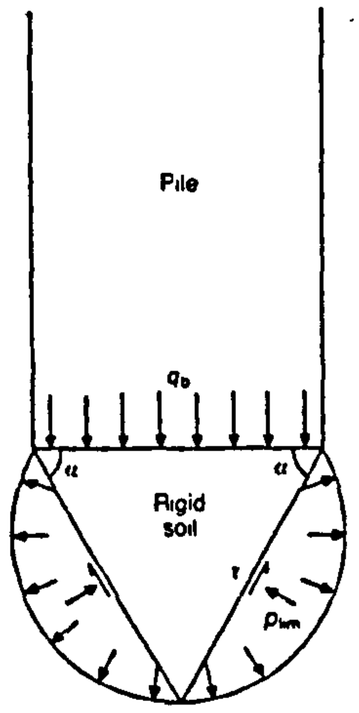

Figure 2-28: Schematic diagram of the mechanism of cavity expansion (after Randolph et al., 1994).

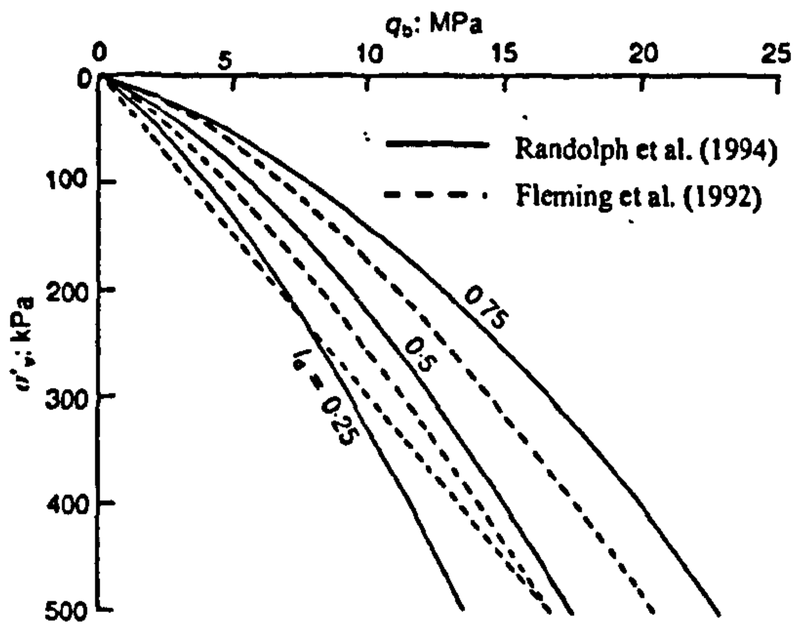

Figure 2-29: Profiles of end bearing capacity for the methods of Randolph et al. (1994) and Fleming et al. (1992).

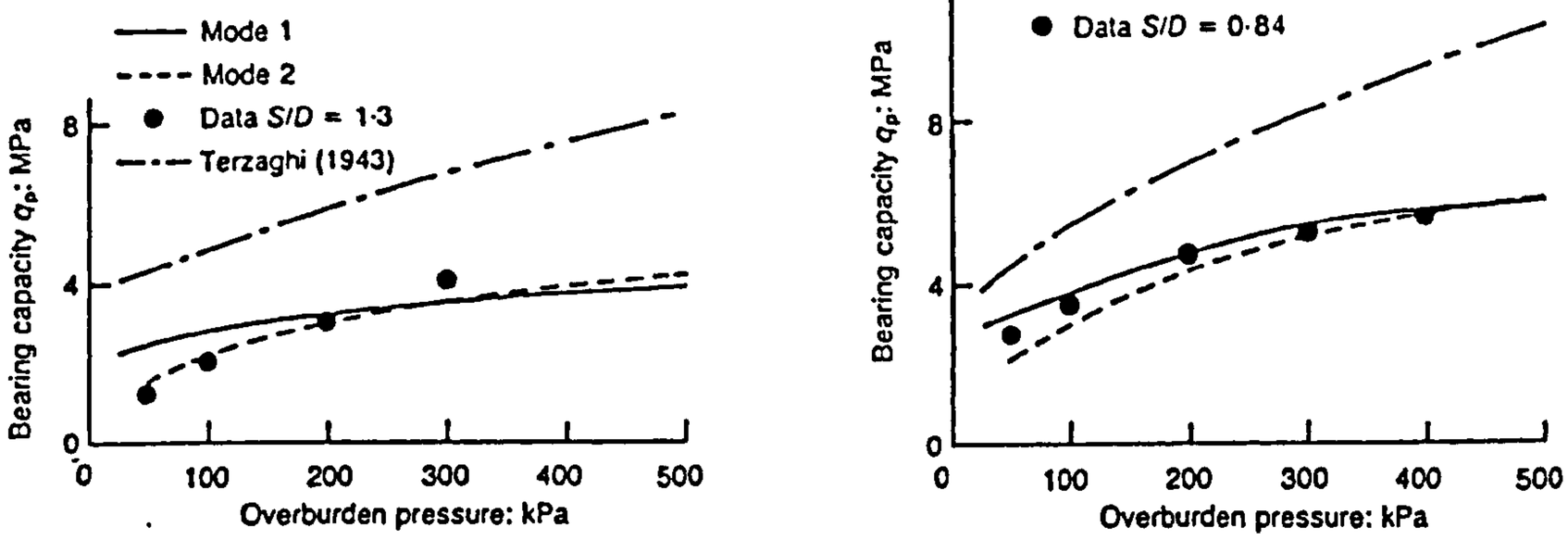

$D_r = 40\%$

$D_r = 75\%$

Figure 2-30: Predicted and measured bearing capacities of model piles in Dogs Bay sand (after Yasufuku & Hyde, 1995). Modes 1 and 2 refer to different analyses, S to the pile head settlement and D to the pile diameter.

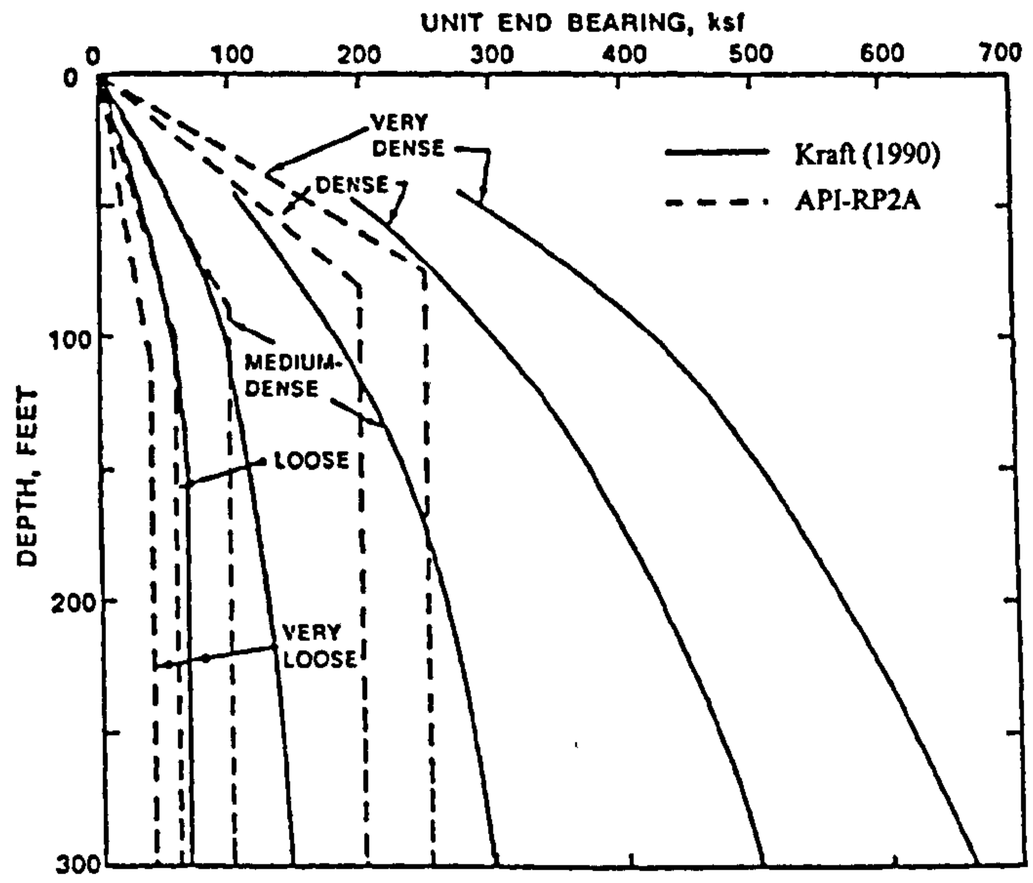

Figure 2-31: Comparison of unit end bearing profiles between Kraft's (1990) method and API-RP2A (1984).

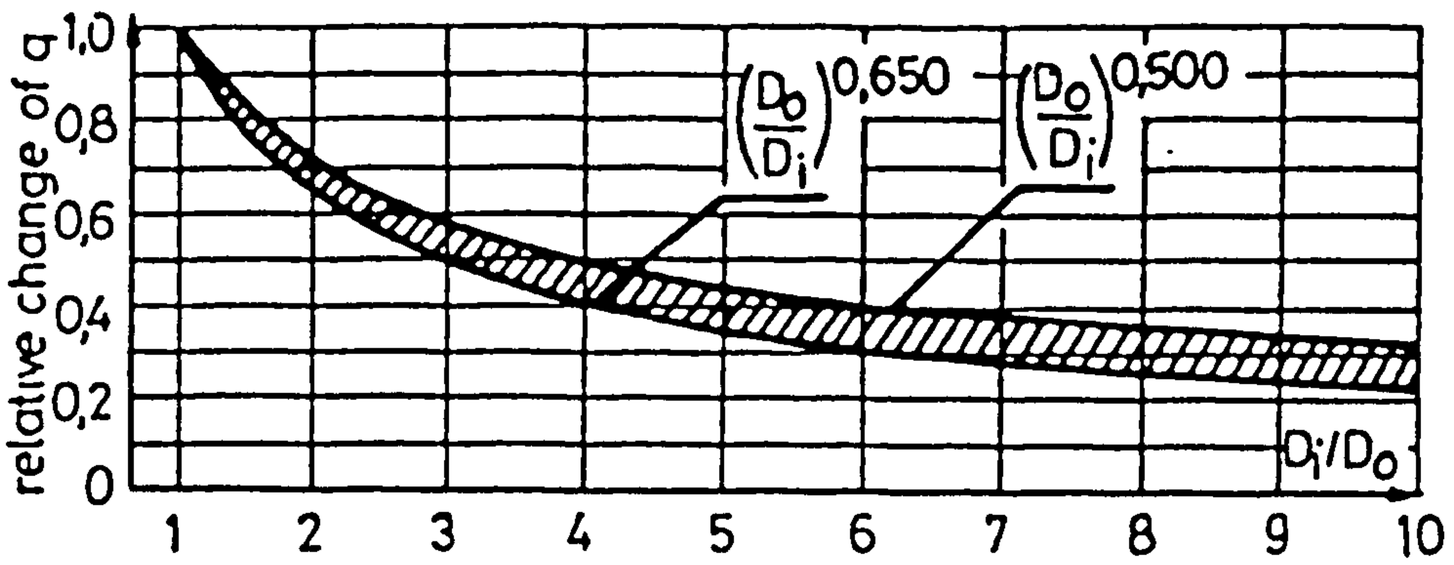

Figure 2-32: Scale effects of pile diameter on unit end bearing (after Tejchman & Gwizdala, 1979). *q* refers to the unit end baring, a relative change of q = 1 to the reference pile of diameter D_o and D_i = piles of different diameter in test series.

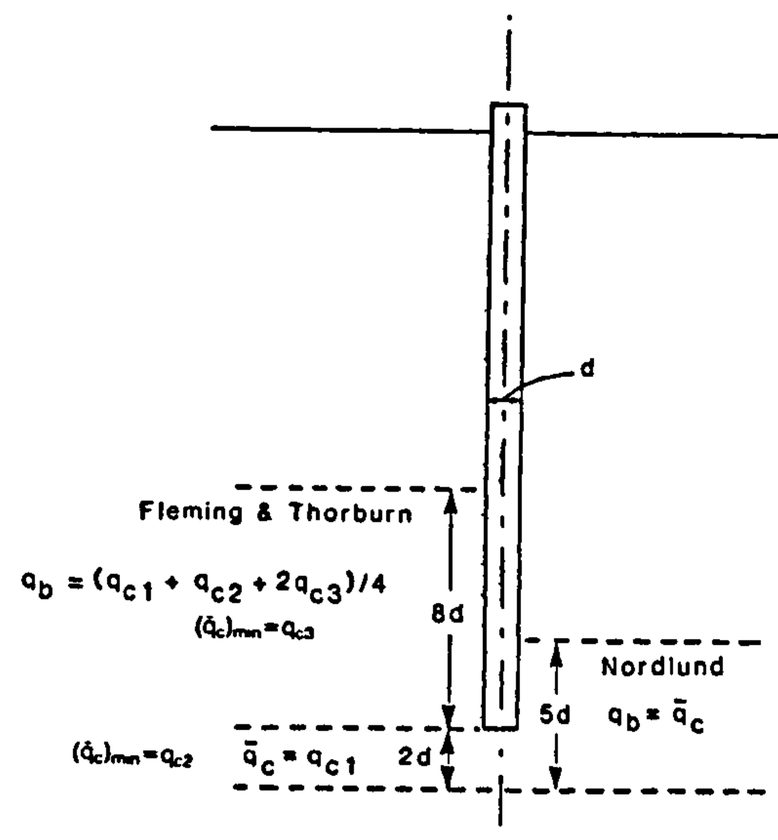

Figure 2-33: Averaging of cone data to give end bearing resistance (after Fleming et al. 1992) where q_{c1} = average cone resistance over 2 diameters below the pile base, q_{c2} = minimum cone resistance over 2 diameters below pile base, q_{c3} = average of minimum values lower than q_{c1} over 8 diameters above the pile base.

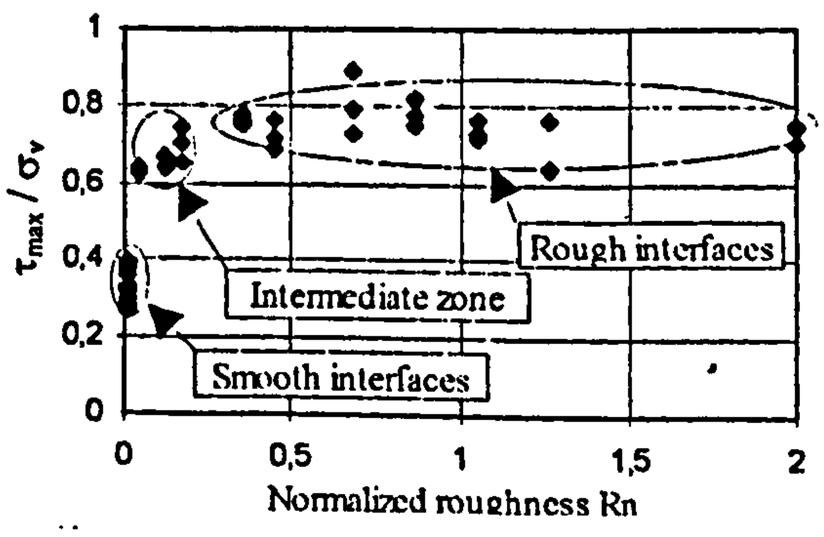

Figure 2-34: Effect of changes in normalised roughness on the measured interface friction angle (after Garnier & Koenig, 1998).

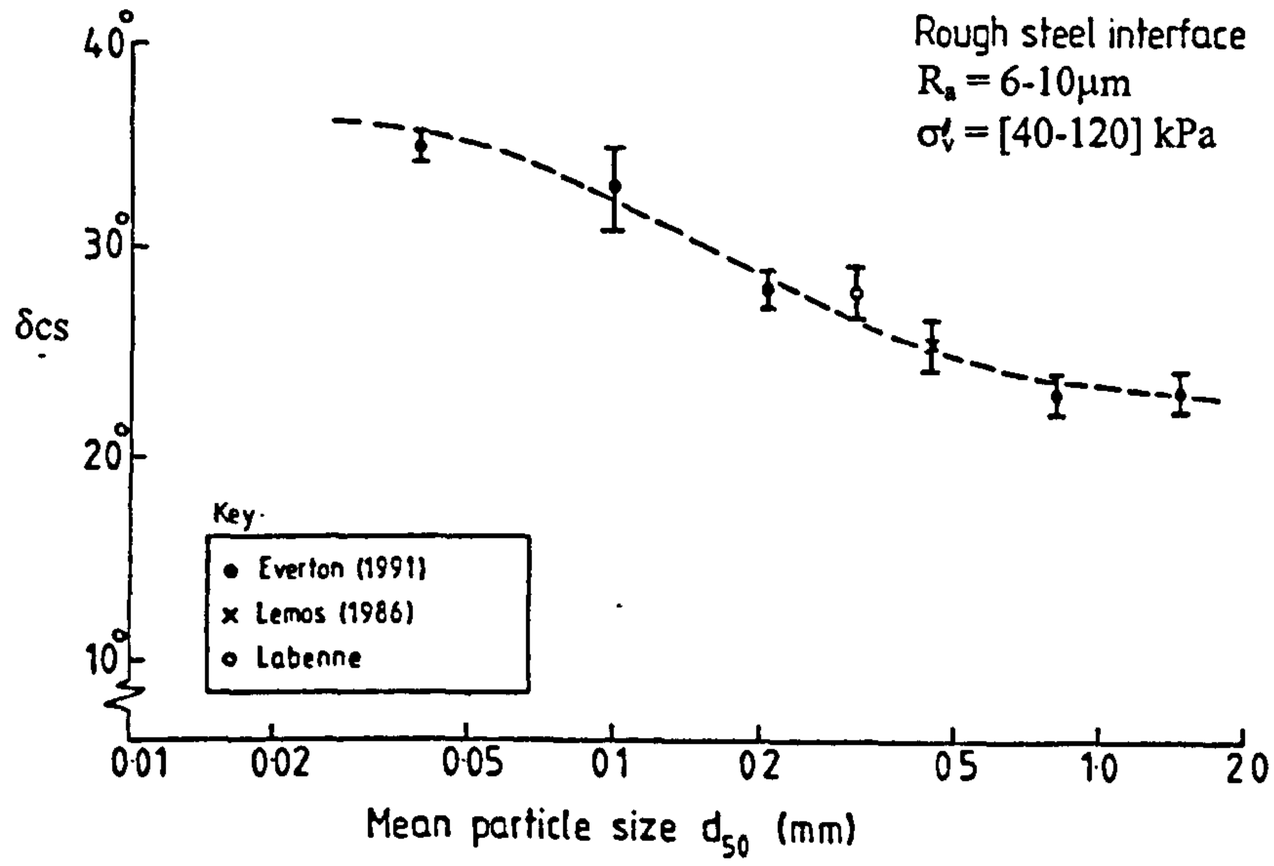

Figure 2-35: Trends for interface friction angle, δ_{cs} (after Jardine et al., 1992).

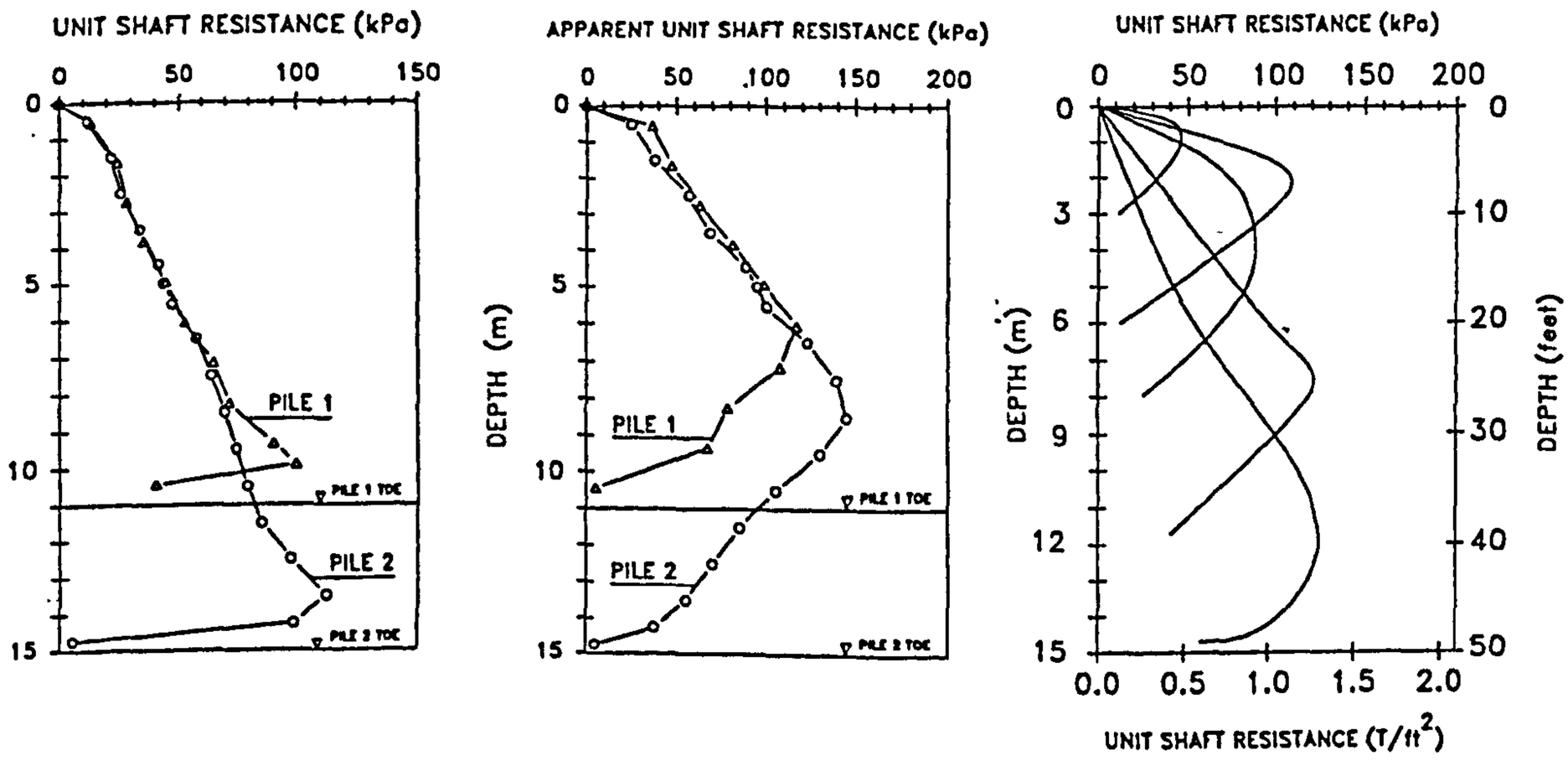

(a) pile data corrected for residual stresses.

(b) data not corrected for residual stresses.

(c) test data presented by Vesic (1970)

Figure 2-36: Effect of residual stresses on distribution of local unit shaft friction along piles (after Altaee et al. 1993).

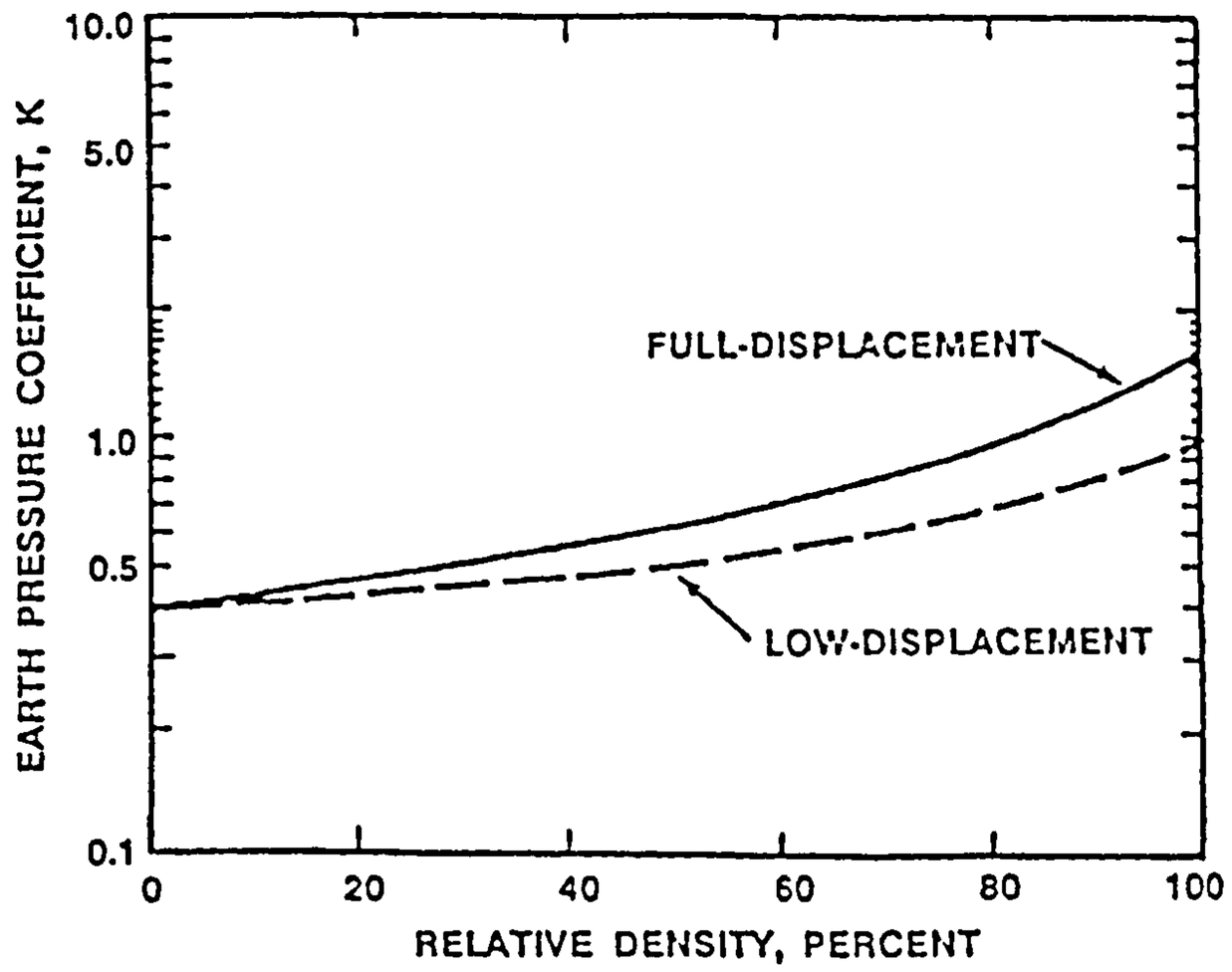

Figure 2-37: Variation of earth pressure coefficient, *K*, with relative density (after Kraft, 1990).

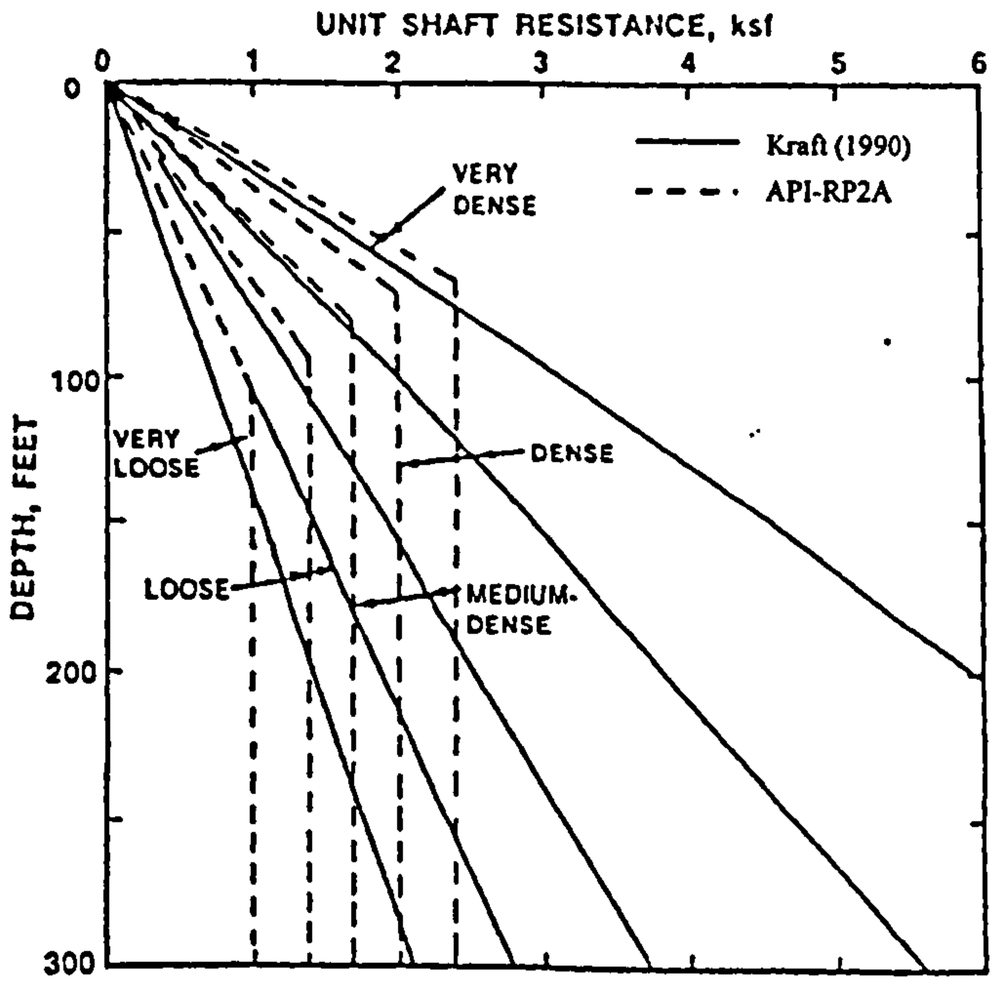

Figure 2-38: Comparison of unit shaft resistance profiles (after Kraft, 1990).

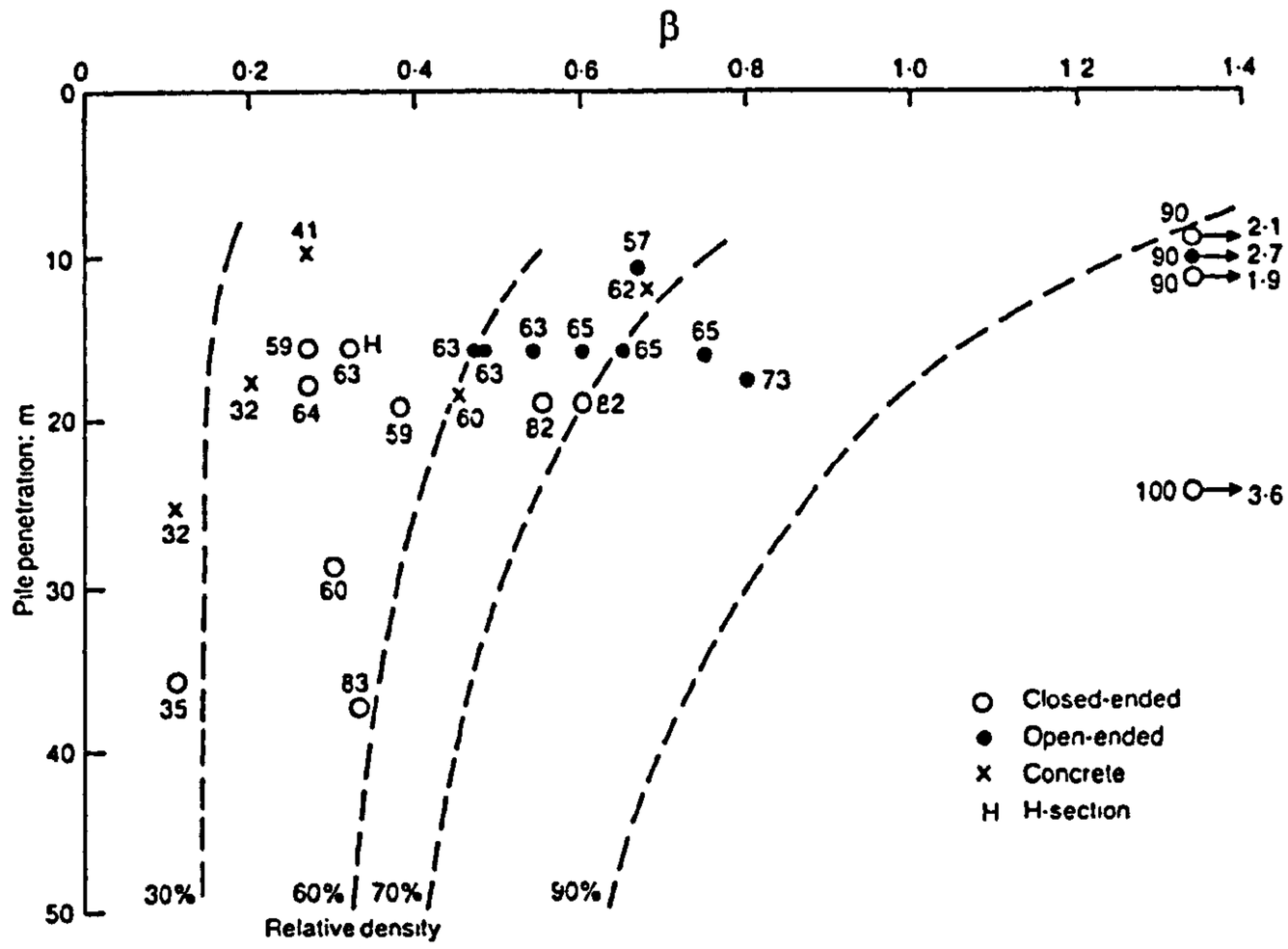

Figure 2-39: Proposed β values over the bottom 10 m of a pile (after Toolan et al., 1990).

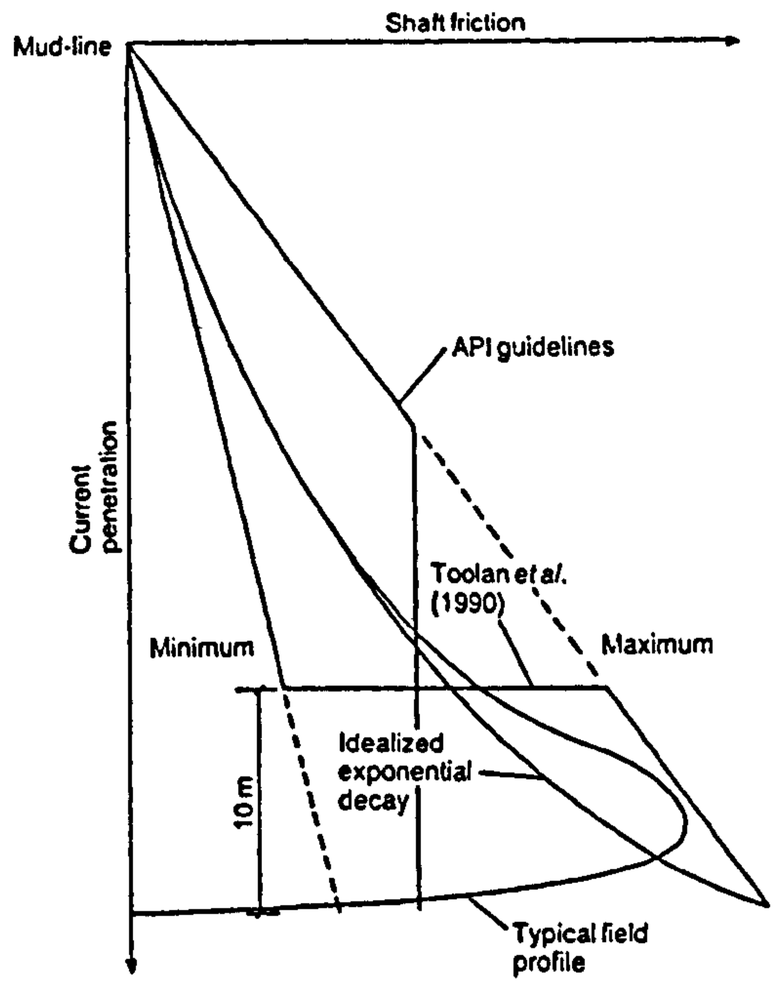

Figure 2-40: Comparison of shaft friction profiles (after Randolph et al., 1994).

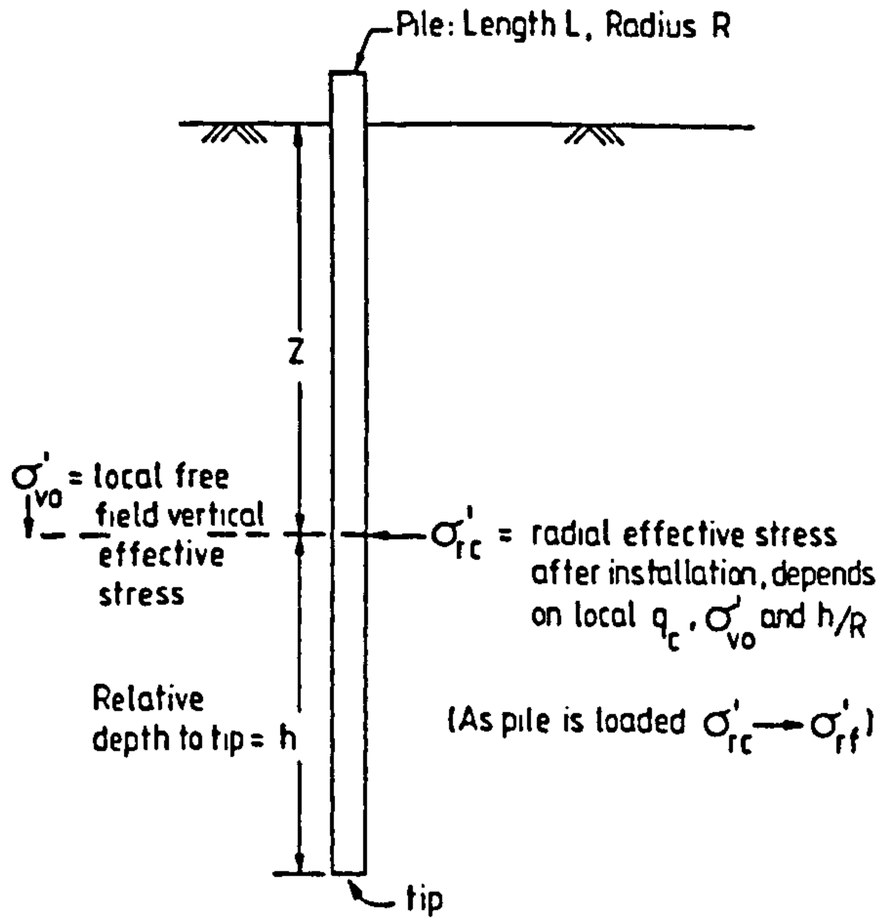

Figure 2-41: Definitions of parameters for the radial effective stress expression (after Jardine & Chow, 1996).

Legend:

	Reference	Location/ Pile Type	Soil
◇	Renfrey et al. (1988)	Rankin driven section	uncemented carbonate/ weak calcarenite
■	Renfrey et al. (1988)	Rankin grouted sections	uncemented carbonate/ weak calcarenite
○	Khorshid et al. (1988)	Rankin steel model pile (SFT)	uncemented carbonate/ weak calcarenite
●	Ripley et al. (1988)	Rankin conductor load test	uncemented carbonate/ weak calcarenite
⊕	Dolwin et al. (1988)	Rankin redrive of foundation pile	uncemented carbonate/ weak calcarenite
◆	Nauroy & Le Tirant (1985)	Plouasne, grouted section	uncemented carbonate/ weakly cement carbonate
▽	Cotecchia et al. (1998)	Naples, grouted pile	volcanic sand
△	Lehane et al. (1993)	Labenne, jacked steel pile	silica sand
✡	Yasufuku et al. (1997)	Japan, grouted pile	"Shirasu" volcanic sand

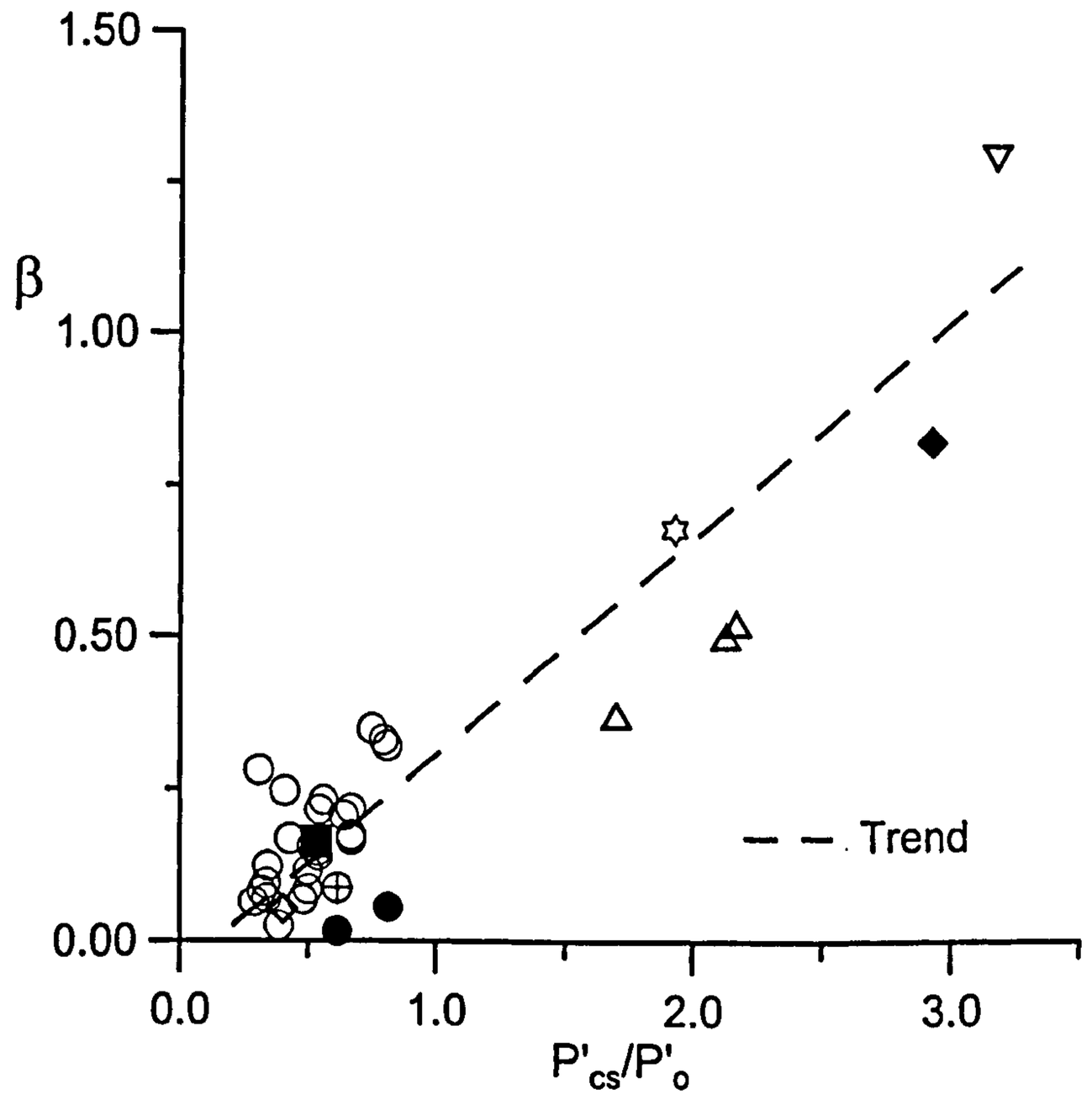

Figure 2-42: Dependence of unit shaft friction (β) on in situ state for a variety of pile and sand types (after Coop, 1999a).

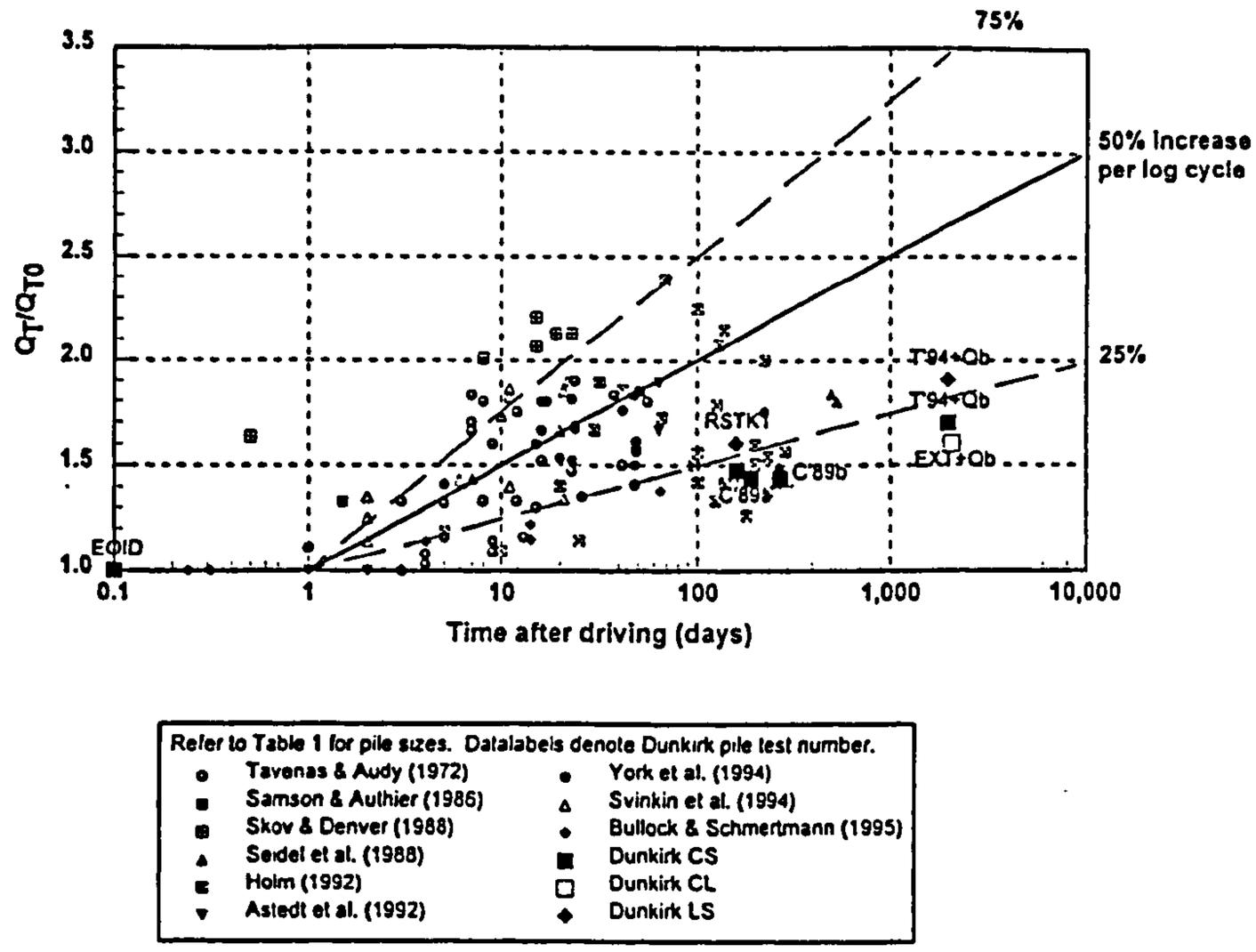

Figure 2-43: Increase in total pile capacity with time (after Chow et al., 1996). Q_T refers to the total capacity at time, T and Q_{T0} the total pile capacity after installation.

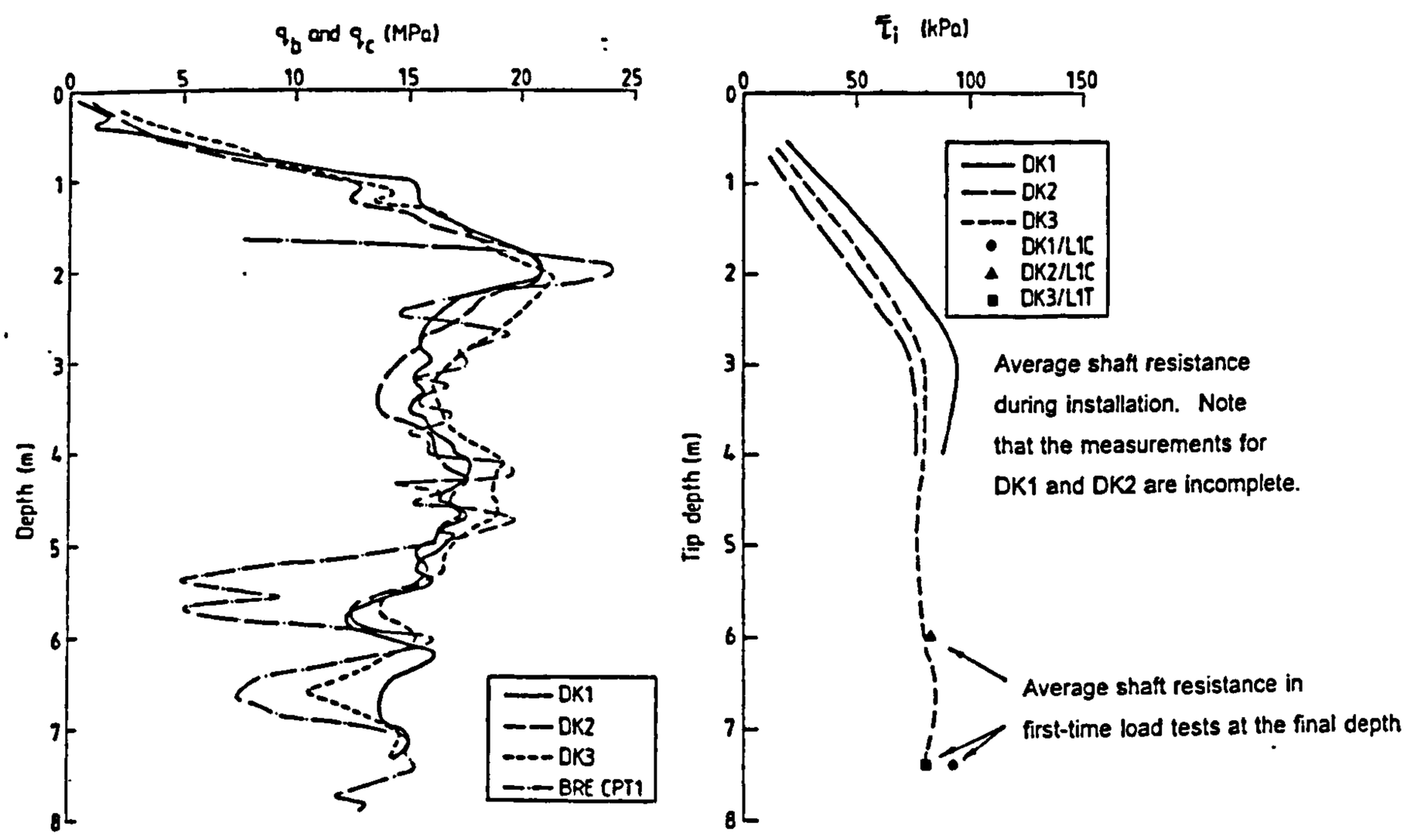

(a) base resistance

(b) shaft resistance

Figure 2-44: Penetration profiles and load tests for pile tests in Dunkirk (after Chow, 1996). DK refers to piles at Dunkirk site, L1C to a compression load test and L1T to a tension load test.

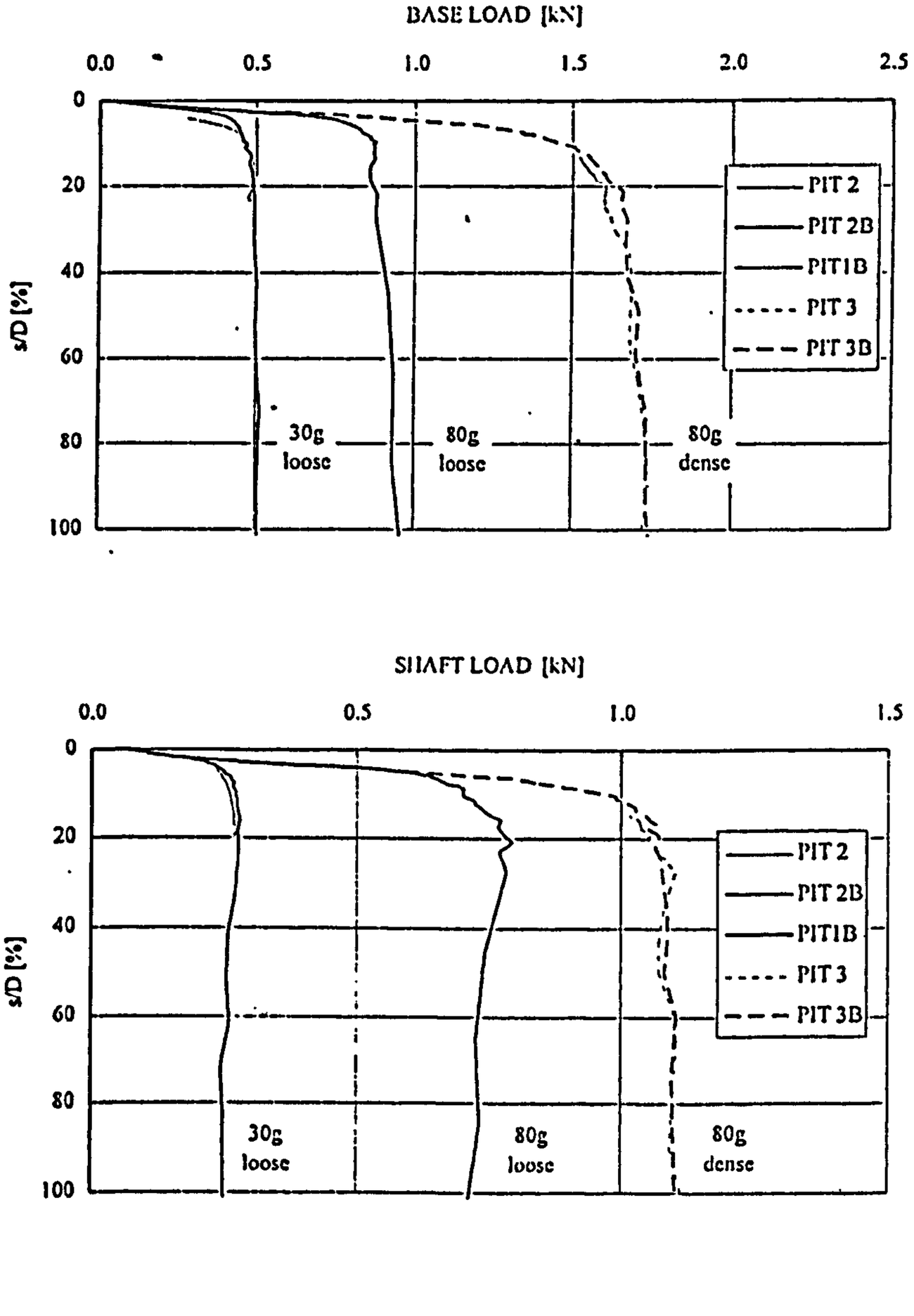

Figure 2-45: Penetration profiles of a pile driven into Toyoura sand in the centrifuge (after Fioravante (1994). PIT refers to the pile test, s to the pile head displacement and D to the pile diamter.

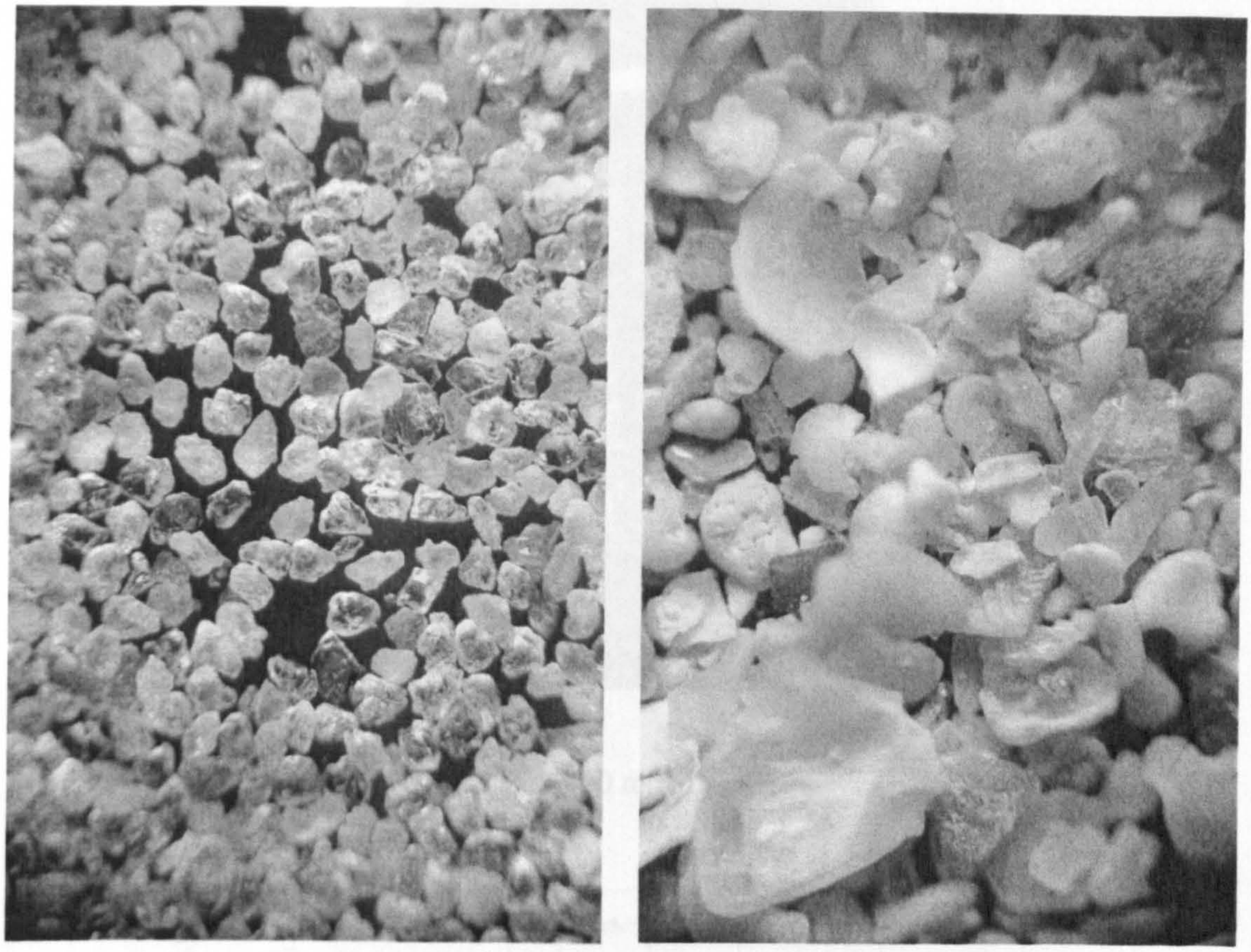

Figure 3-1: Microscopic view of particles: (a) Leighton Buzzard sand (b) Dogs Bay sand.

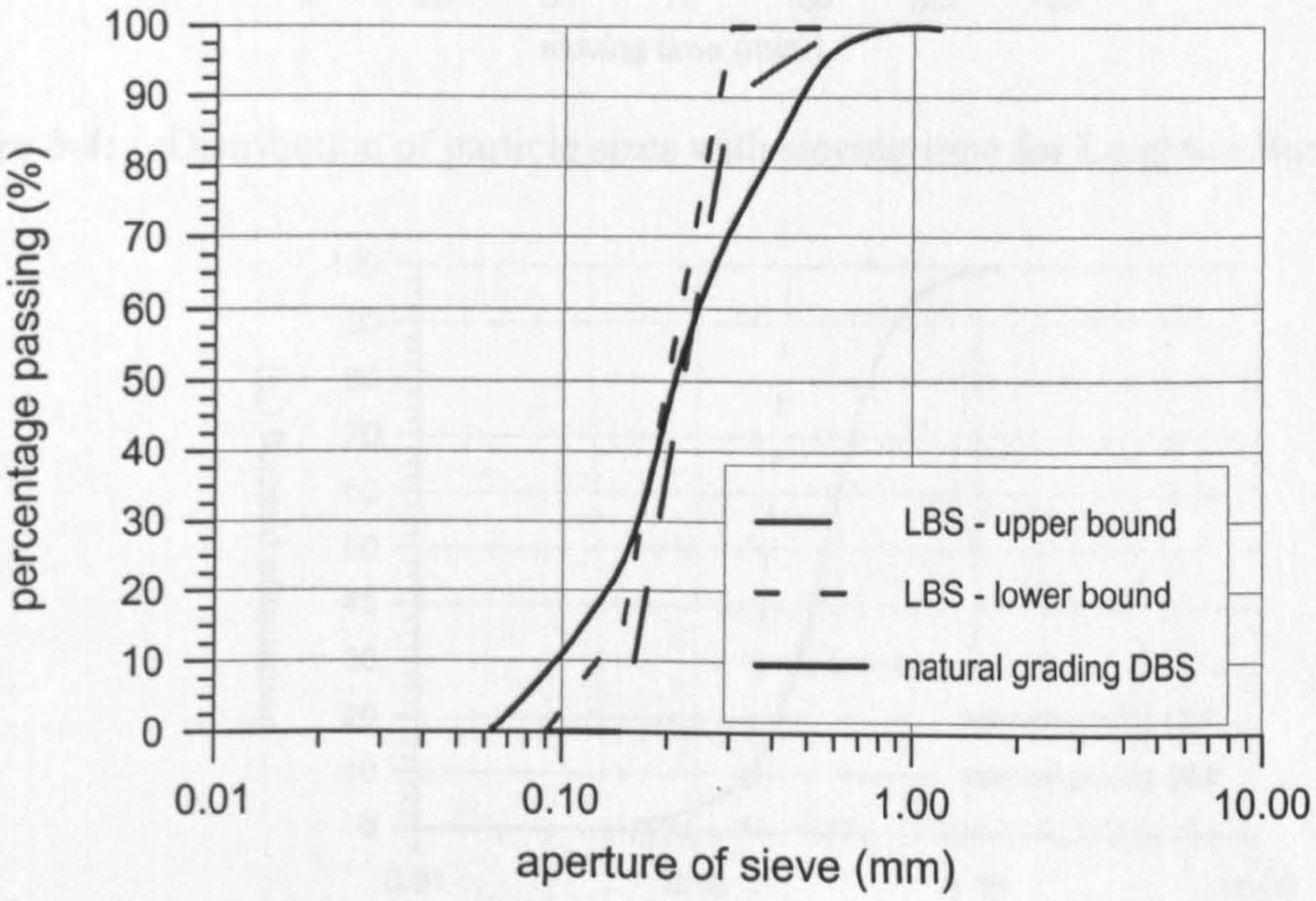

Figure 3-2: Original grading curves of Class D Leighton Buzzard and Dogs Bay sand.

Figure 3-3: Mechanical sieve shaker for 450 mm diameter sieves.

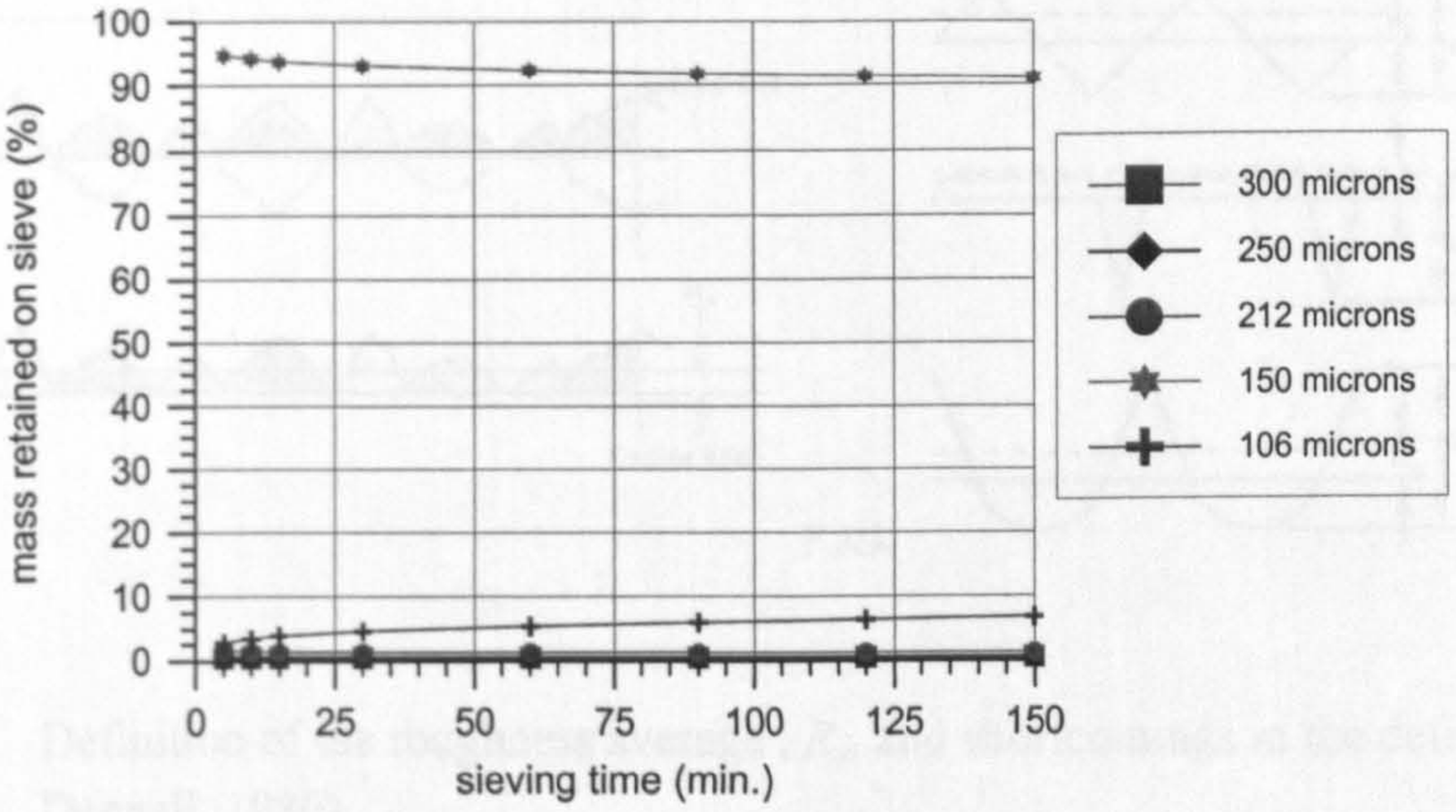

Figure 3-4: Distribution of particle sizes with sieving time for Leighton Buzzard sand.

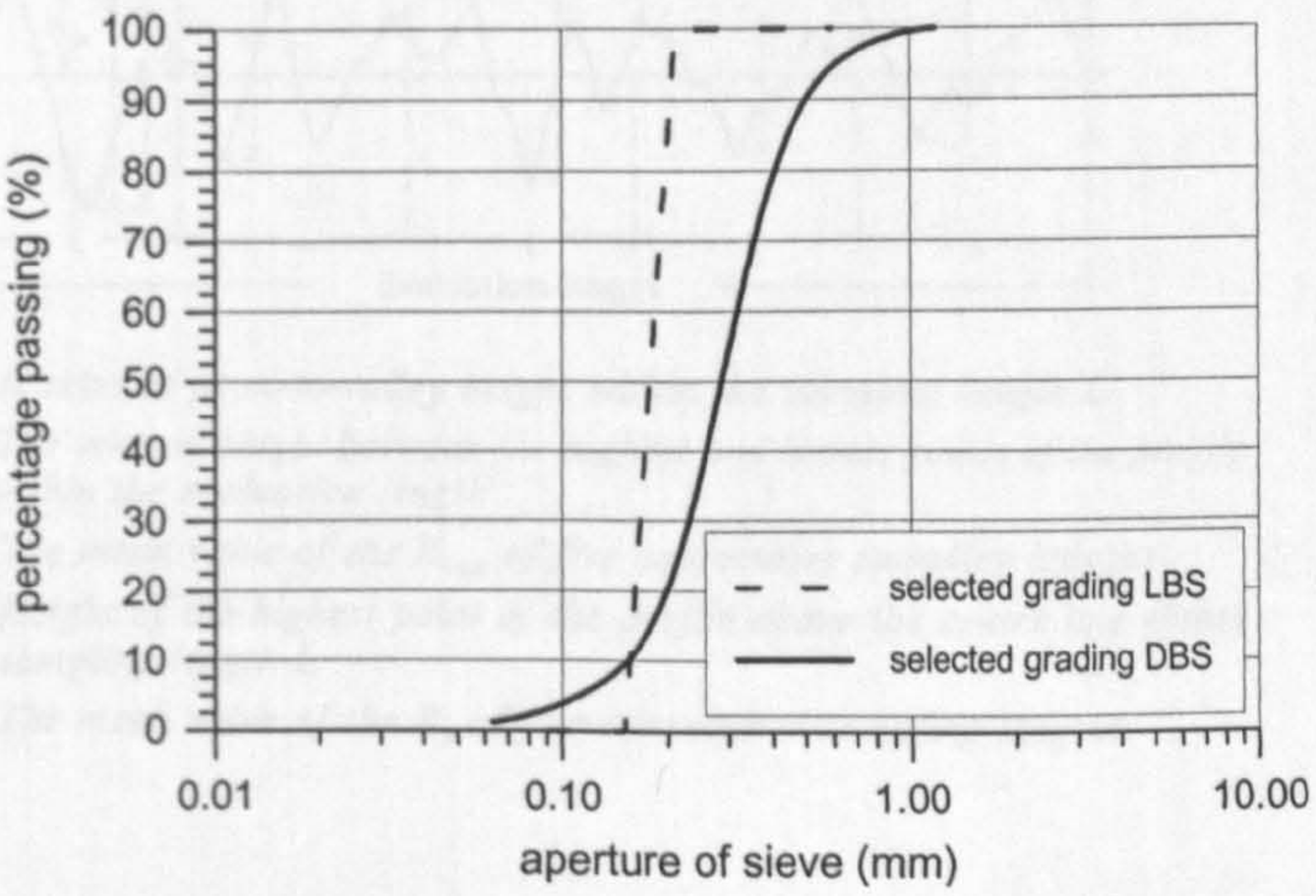

Figure 3-5: Selected grading curves for Leighton Buzzard and Dogs Bay sand.

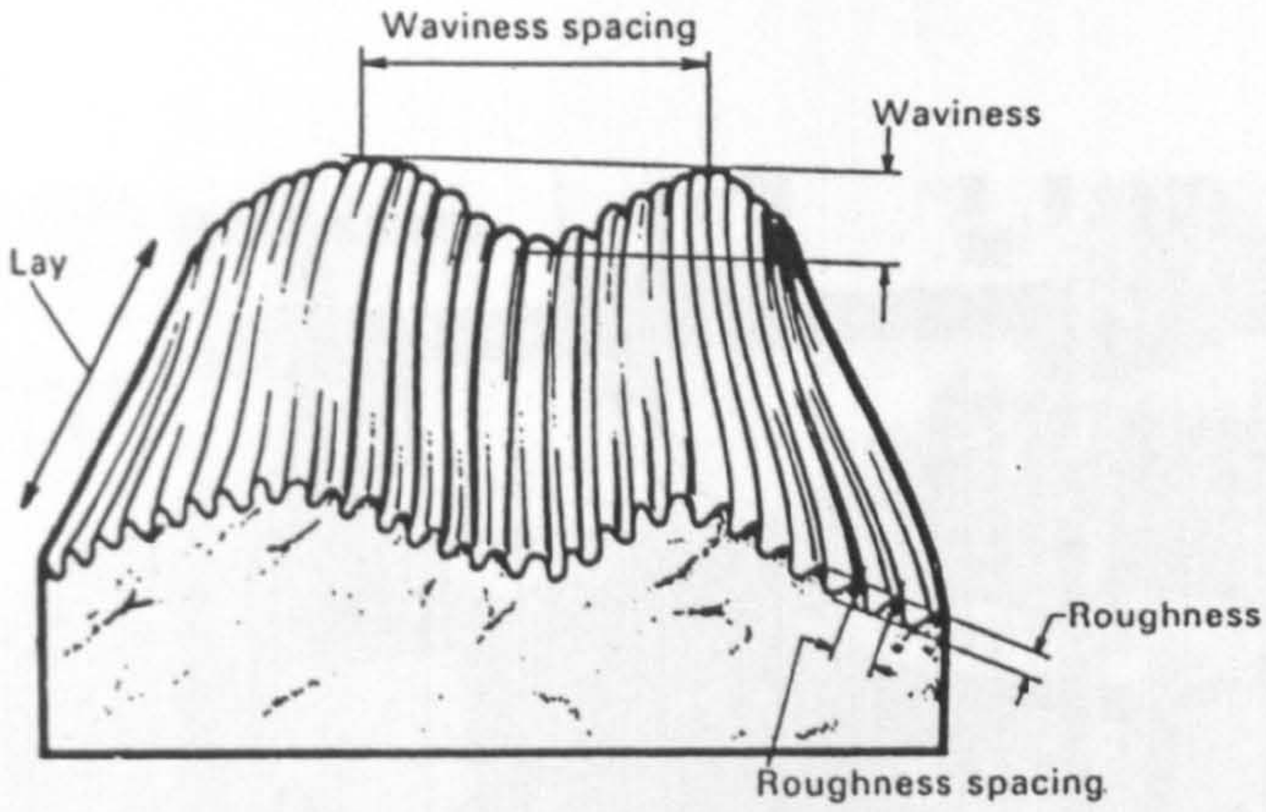

Figure 3-6: Illustration of roughness and waviness (after Dagnall, 1980).

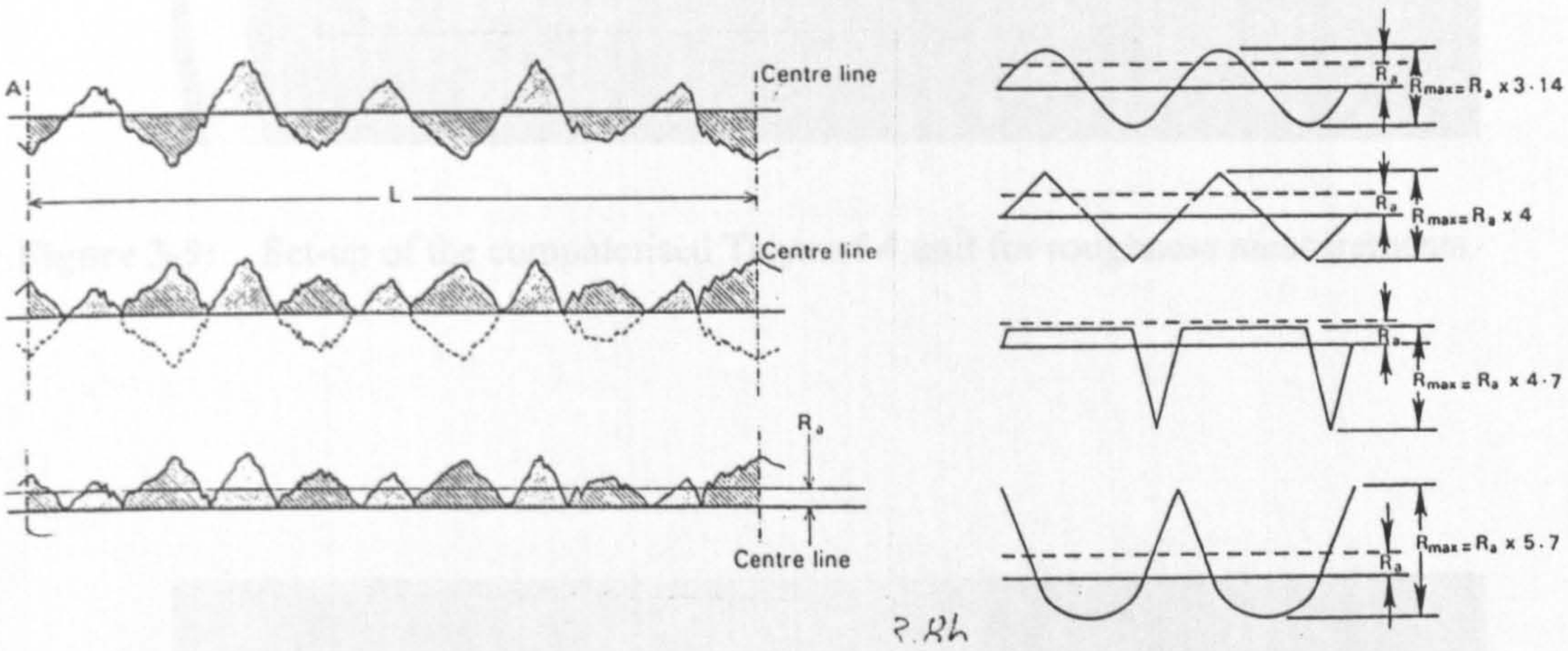

Figure 3-7: Definition of the roughness average , R_a, and shortcomings in the definition (after Dagnall, 1980).

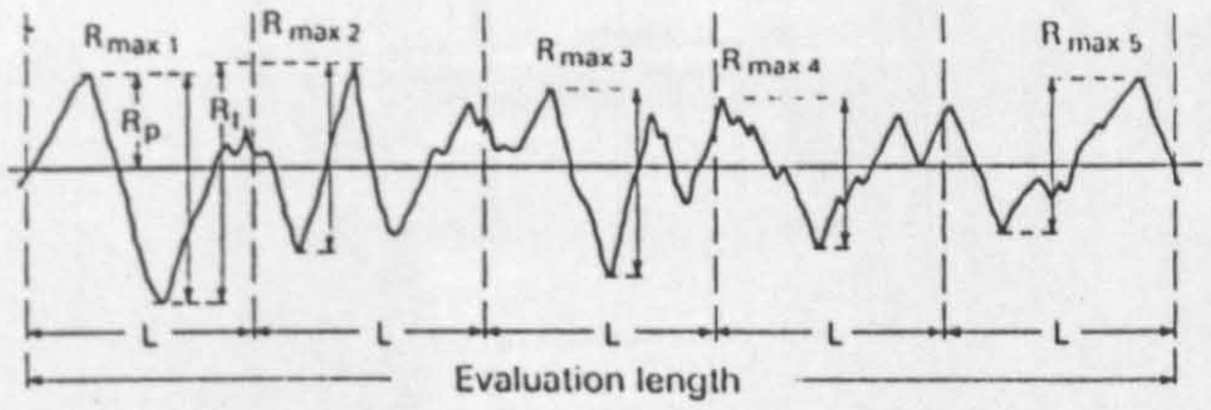

R_{max} = Maximum peak-to-valley height within the sampling length L

R_t = The vertical height between the highest and lowest points of the profile within the evaluation length

R_{tm} = The mean value of the R_{max} of five consecutive sampling lengths

R_p = Height of the highest point of the profile above the centre line within sampling length L

R_{pm} = The mean value of the R_p of five consecutive sampling lengths

Figure 3-8: Definition of some roughness peak parameters (after Dagnall, 1980).

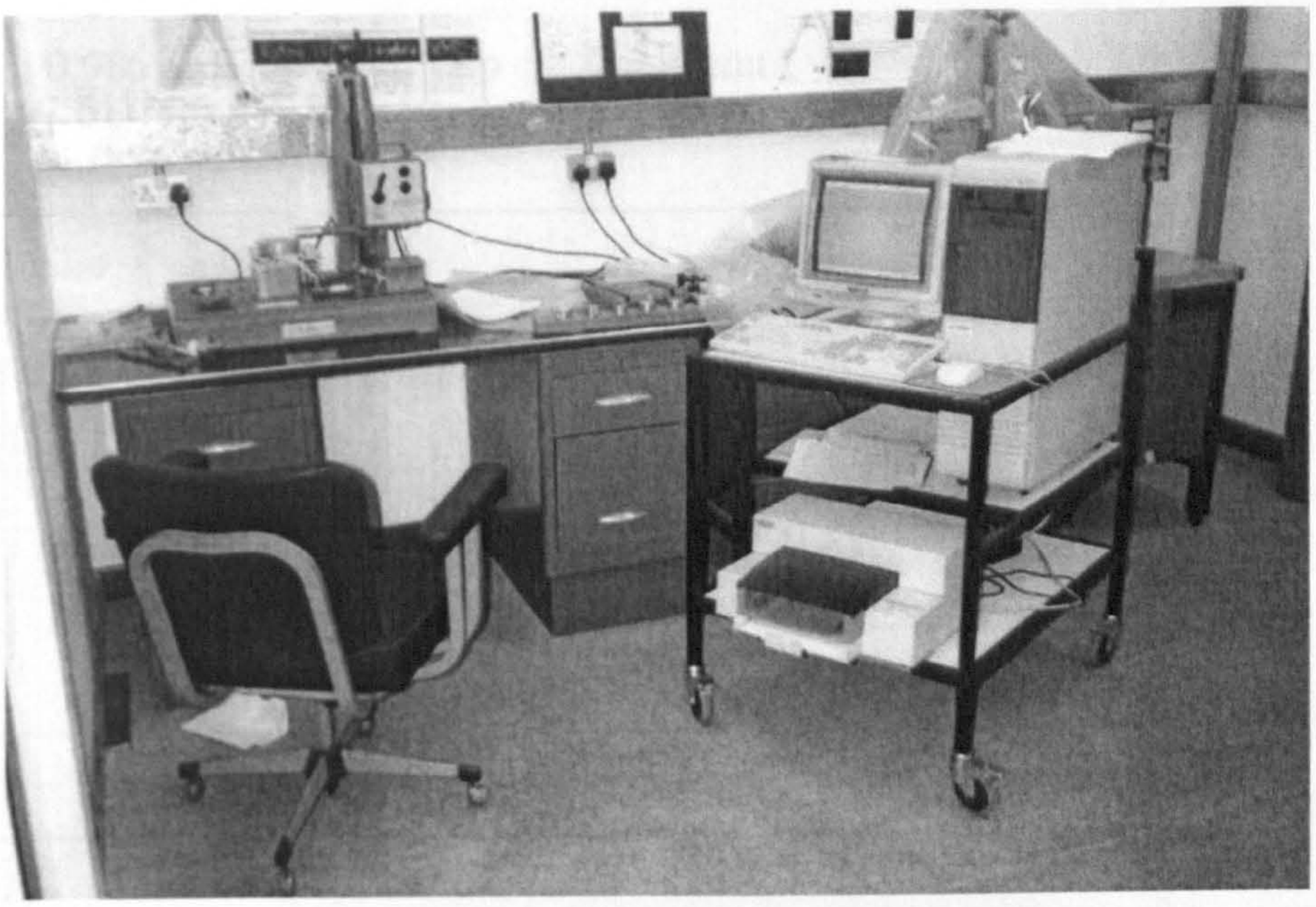

Figure 3-9: Set-up of the computerised Talysurf-4 unit for roughness measurements.

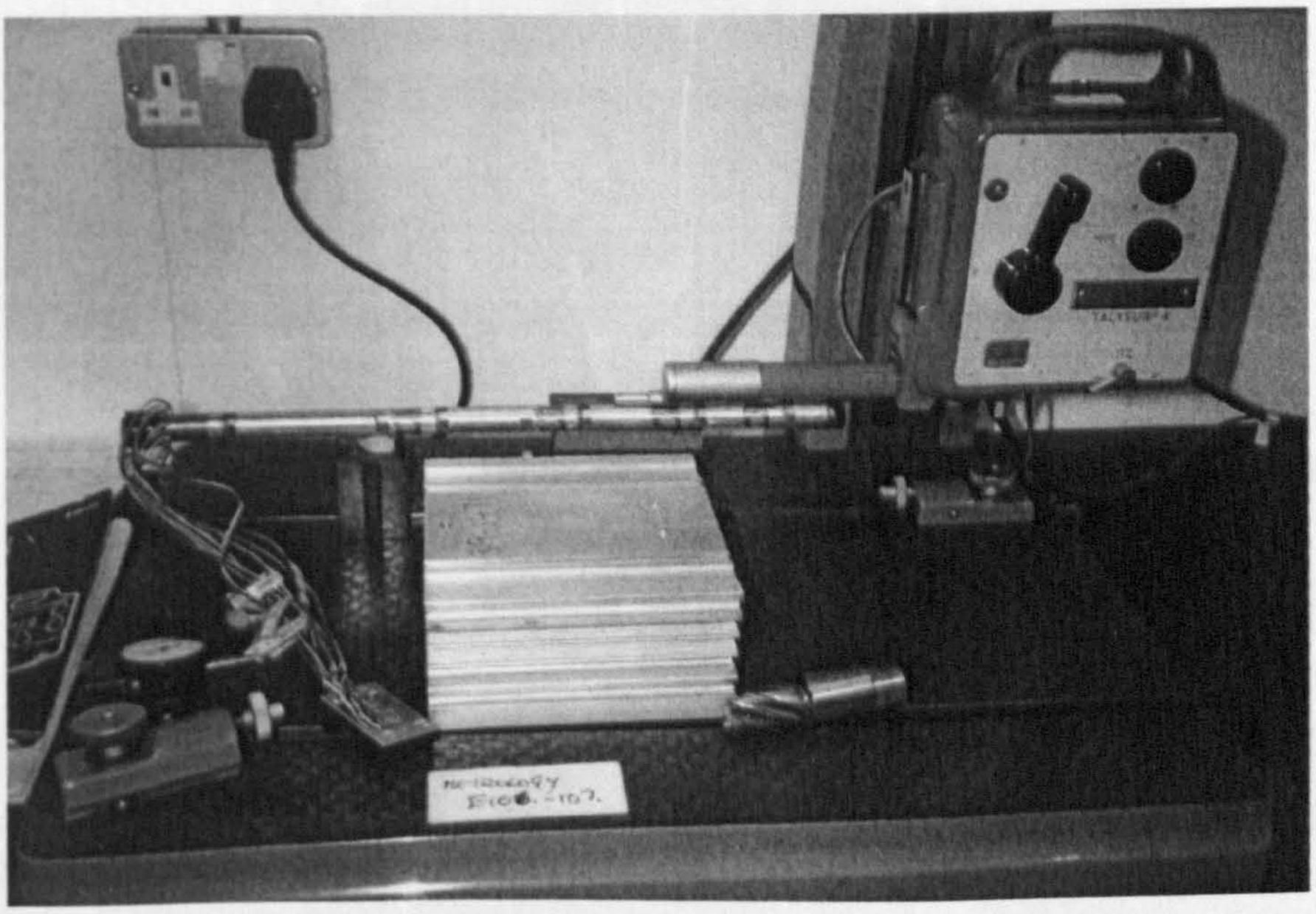

Figure 3-10: Set-up for measuring the surface roughness of the model pile CUIMP-4.

MEASUREMENT SETTINGS

Vv: 5000 **Vh**: 50 **Filter cut-off**: n/a **Date**: 16-2-1999

UNFILTERED PARAMETER RESULTS

Ra	0.986 μm	Rp	2.710 μm	Rv	4.907 μm
Rt	7.617 μm				

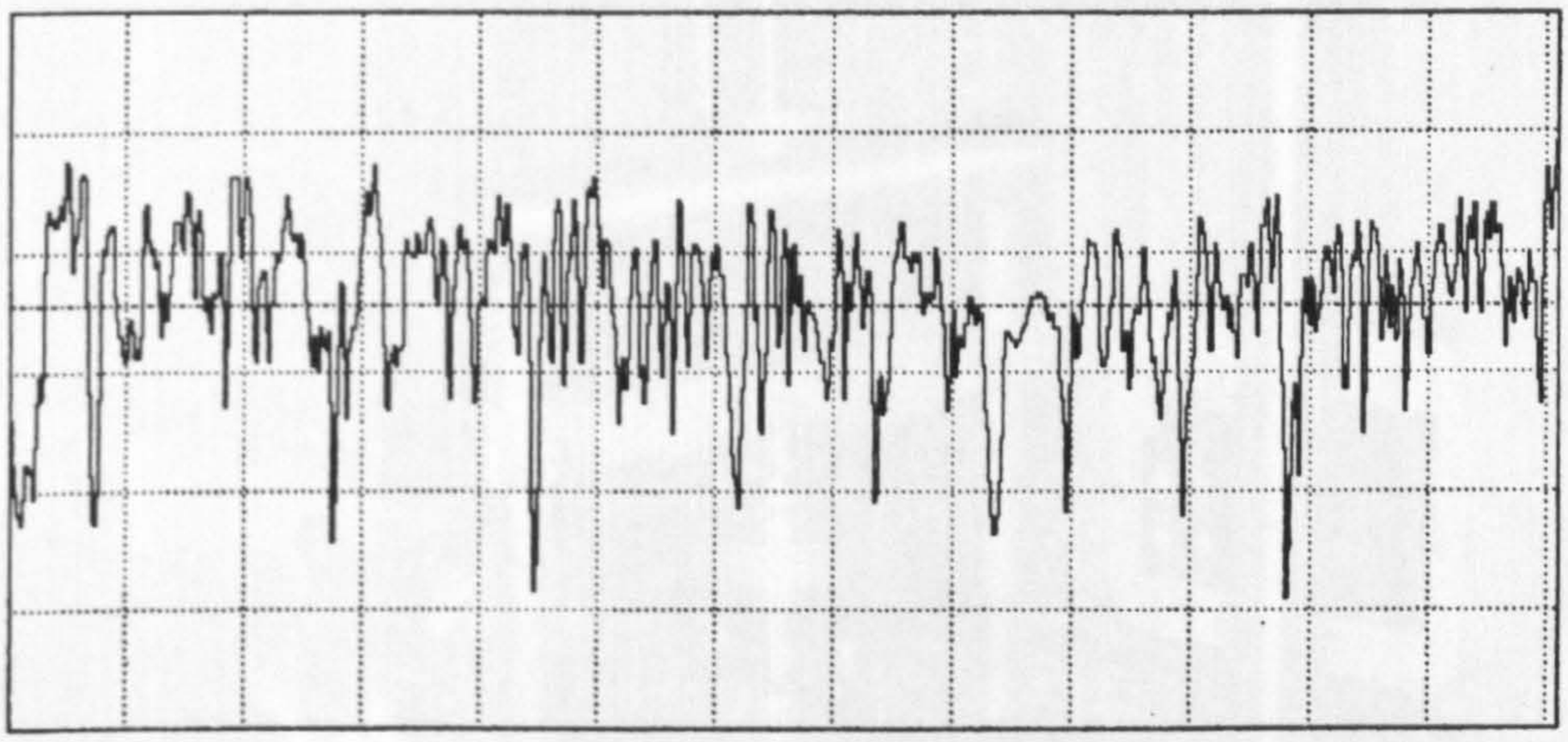

Vertical scale = 2.00 μm/div Horizontal scale = 0.20 mm/div

Figure 3-11: Typical surface roughness profile of CUIMP-3.

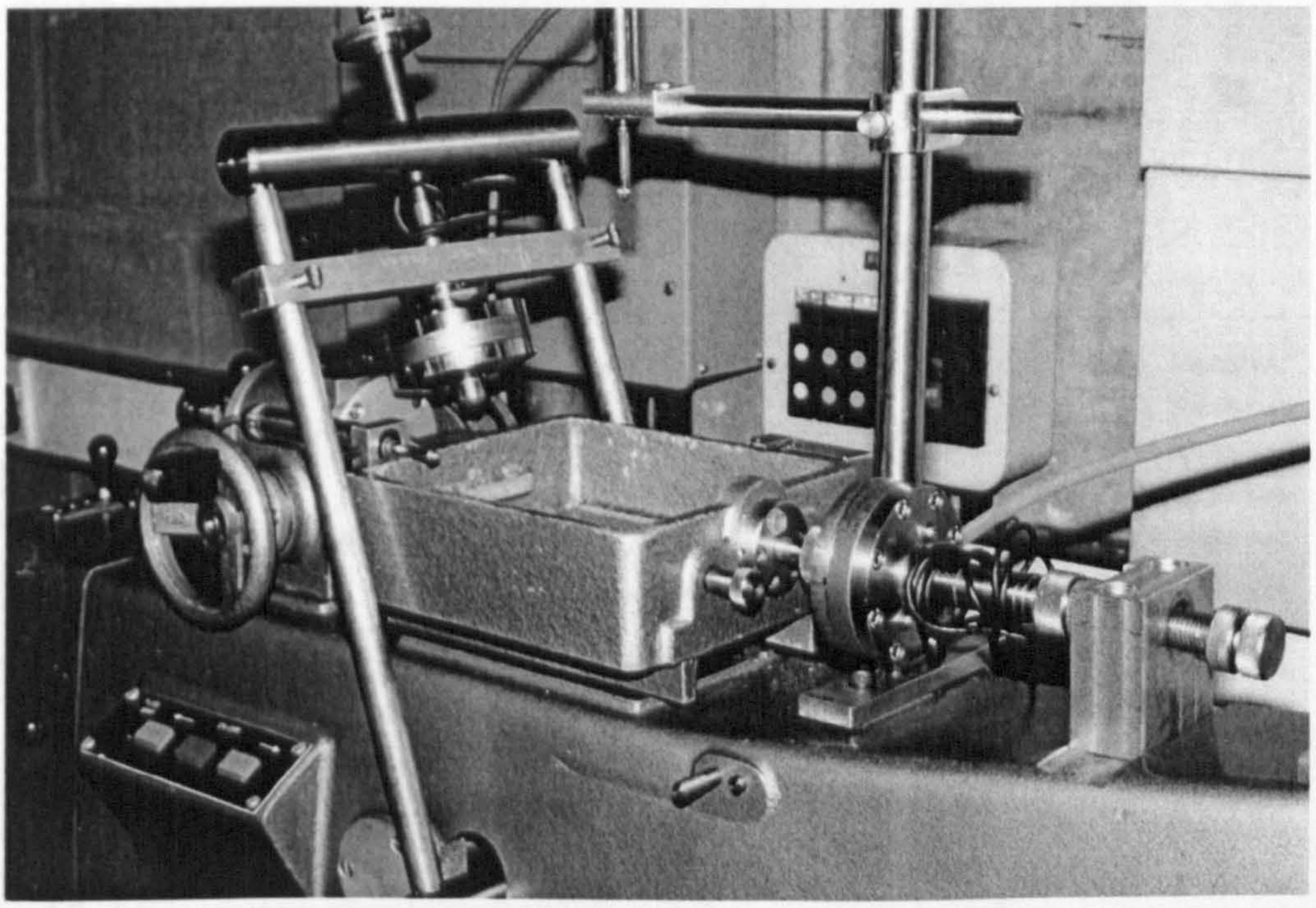

Figure 3-12: Computer controlled shear box used for the interface tests.

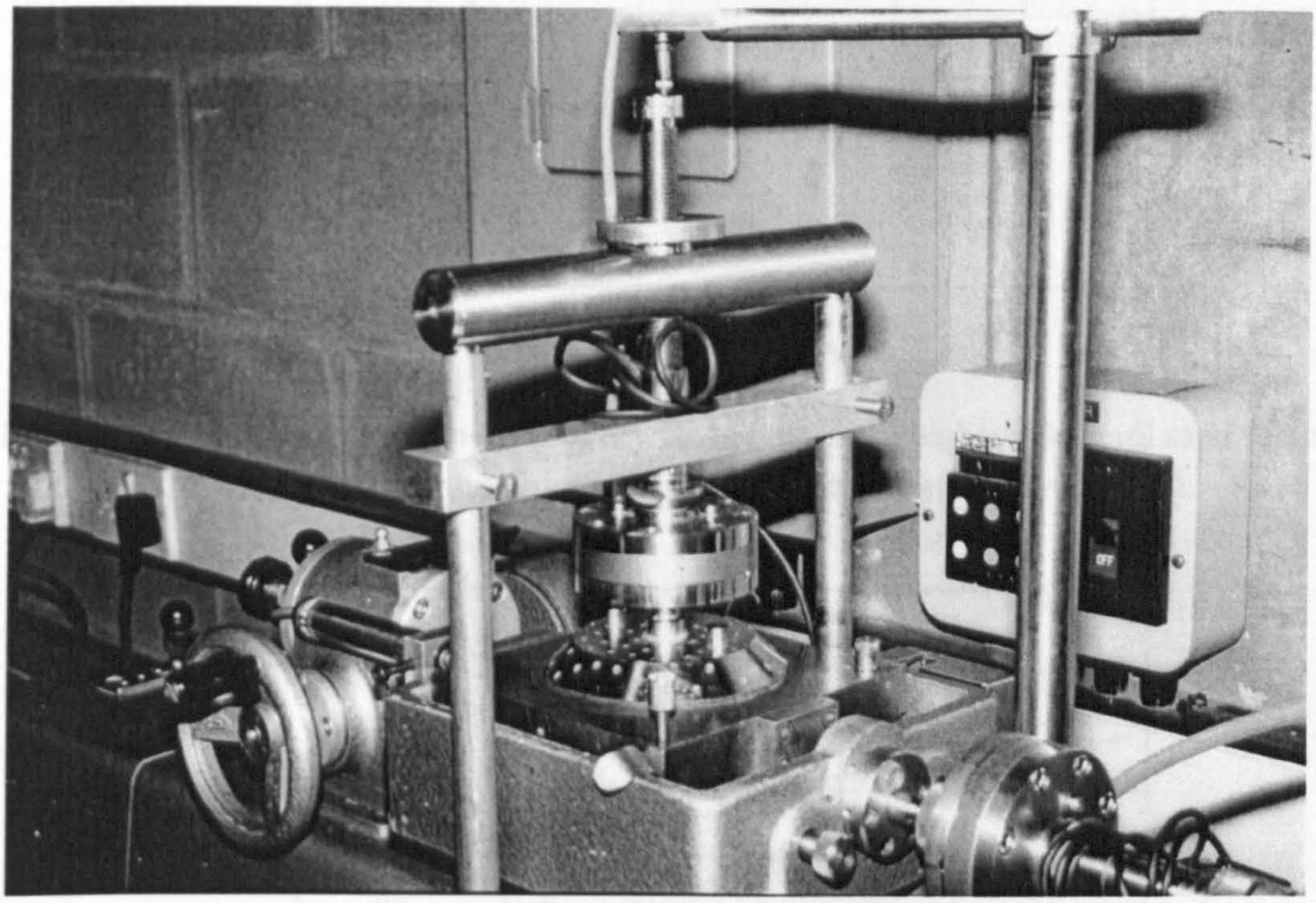

Figure 3-13: Set-up of shear box prior to testing.

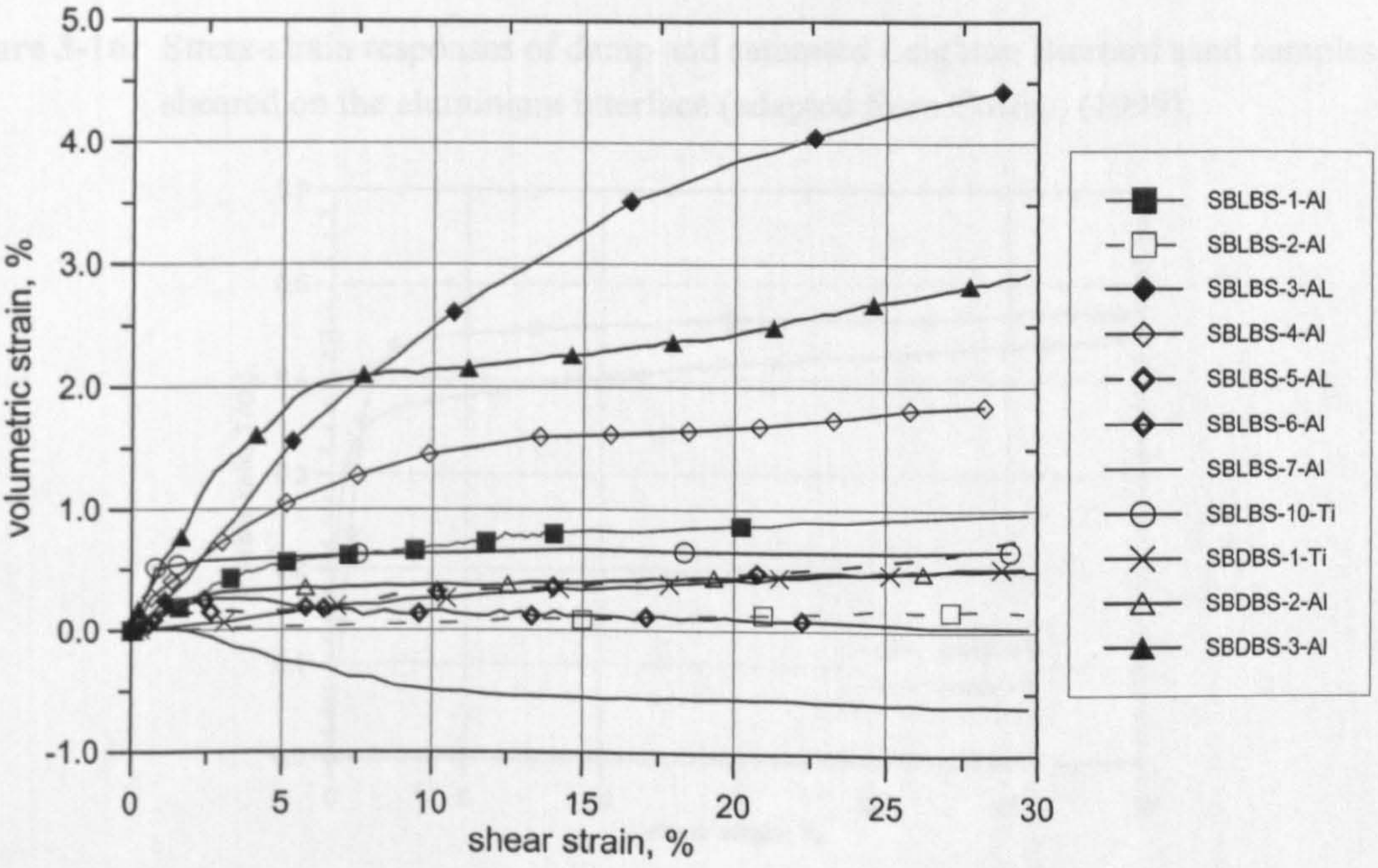

Figure 3-14: Strains during shearing in interface shear box tests (adapted from Coffey, (1999).

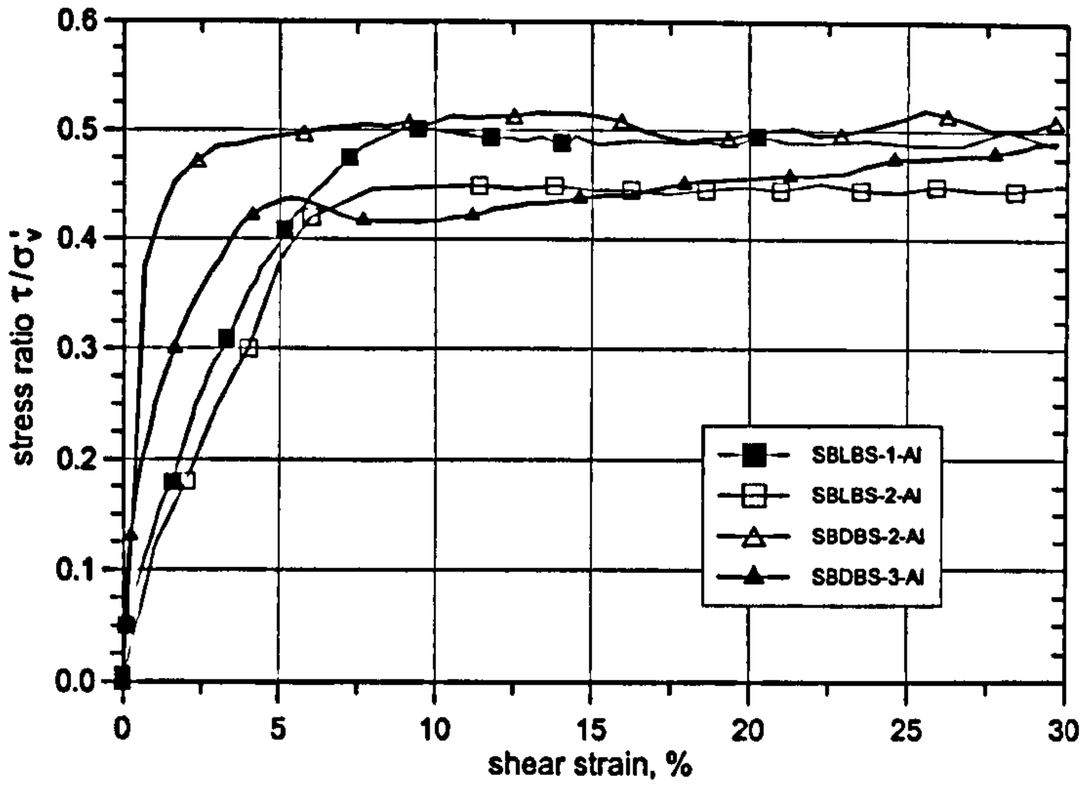

Figure 3-15 Stress-strain responses of dry Dogs Bay and Leighton Buzzard sand samples sheared on the aluminium interface (adapted from Coffey, (1999).

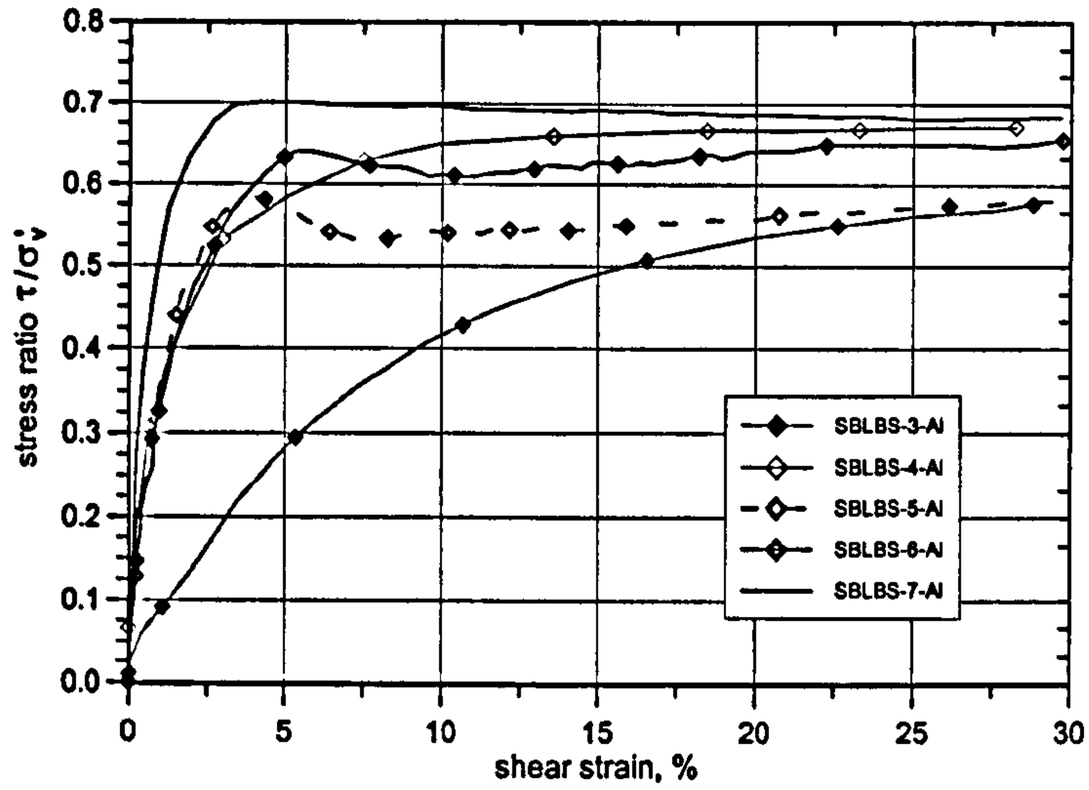

Figure 3-16: Stress-strain responses of damp and saturated Leighton Buzzard sand samples sheared on the aluminium interface (adapted from Coffey, (1999).

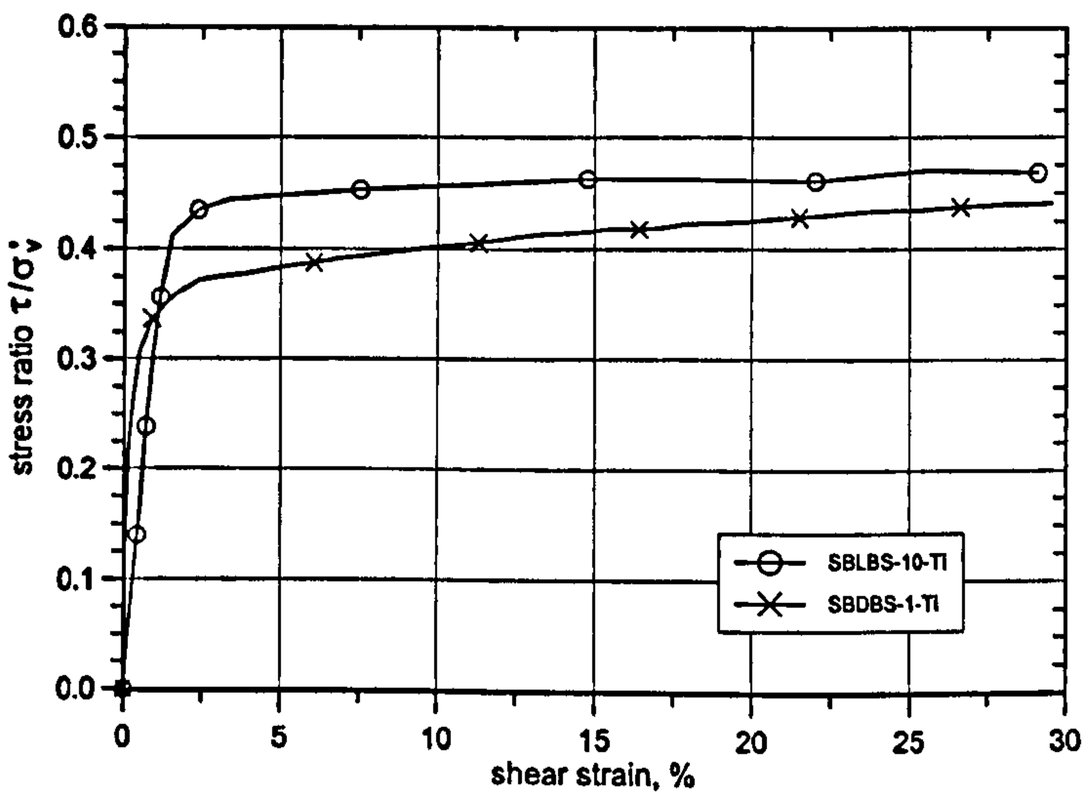

Figure 3-17: Stress-strain responses of dry Dogs Bay and Leighton Buzzard sand samples sheared on the titanium interface (adapted from Coffey, (1999).

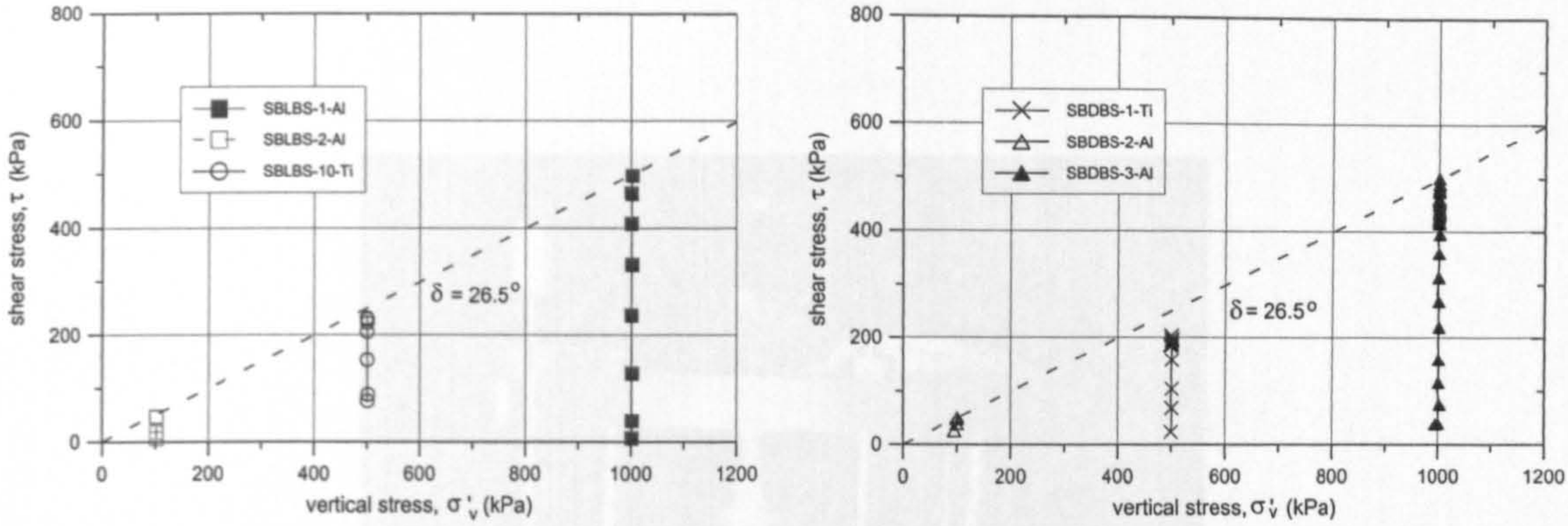

Figure 3-18: Stress paths for interface shear box tests a) dry Dogs Bay sand and b) dry Leighton Buzzard sand (adapted from Coffey, 1999).

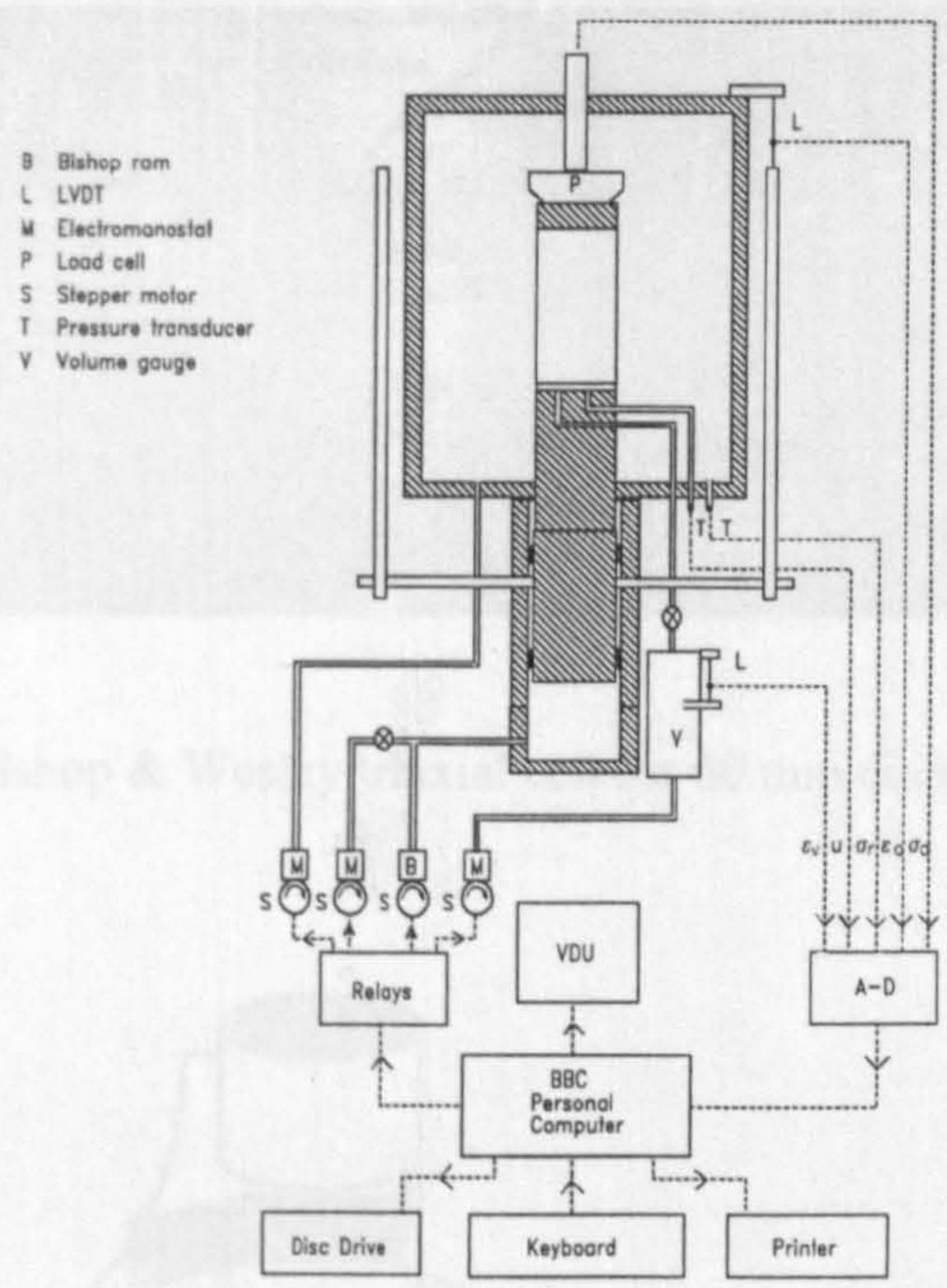

Figure 3-19: Schematic diagram of the BBC-system for the Bishop & Wesley stress path cell (after Stallebrass, 1990).

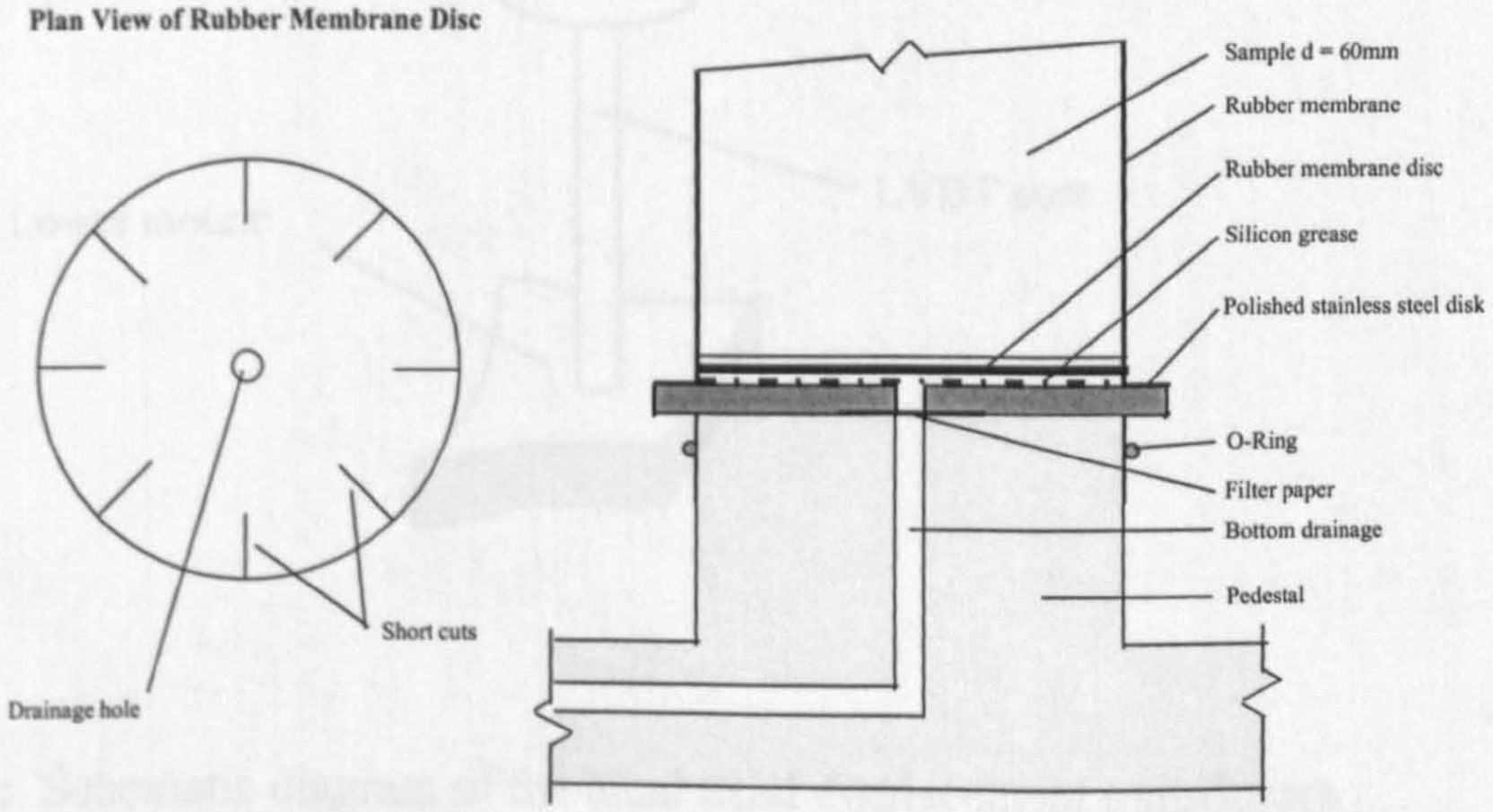

Figure 3-20: Details of the lubricated end platens (adapted from Head, 1985).

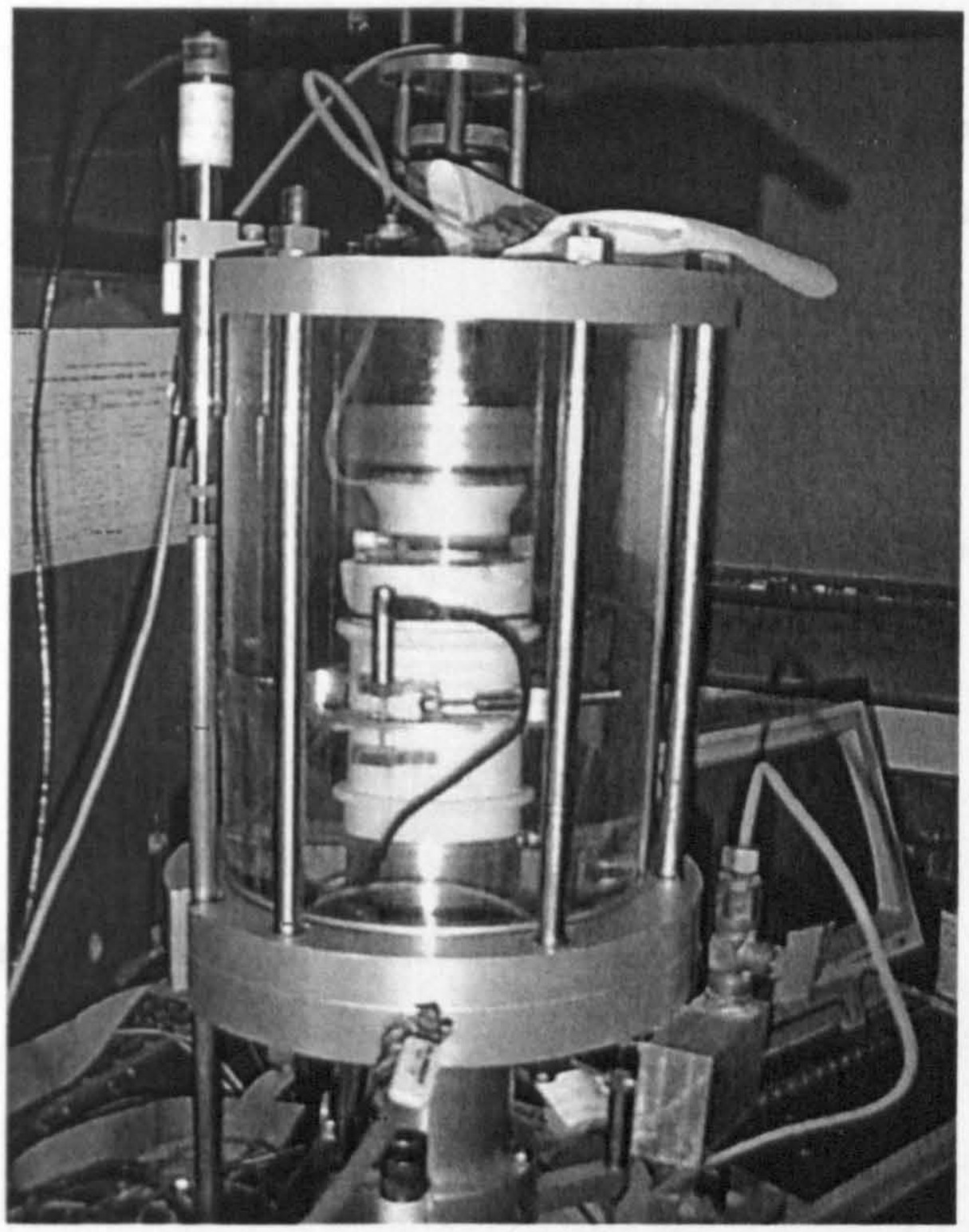

Figure 3-21: Modified Bishop & Wesley triaxial cell for 60 mm diameter samples.

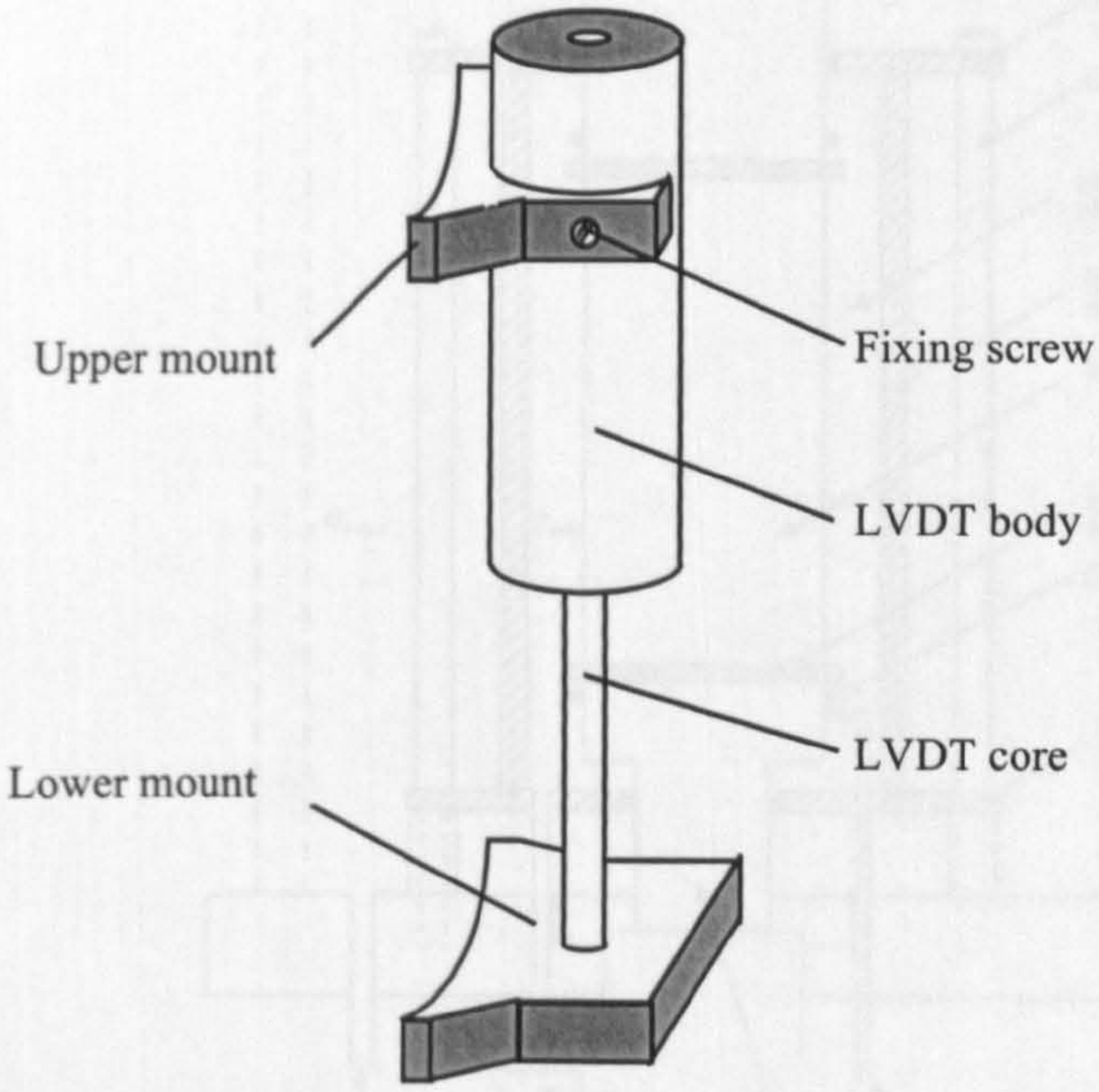

Figure 3-22: Schematic diagram of the local axial displacement transducers.

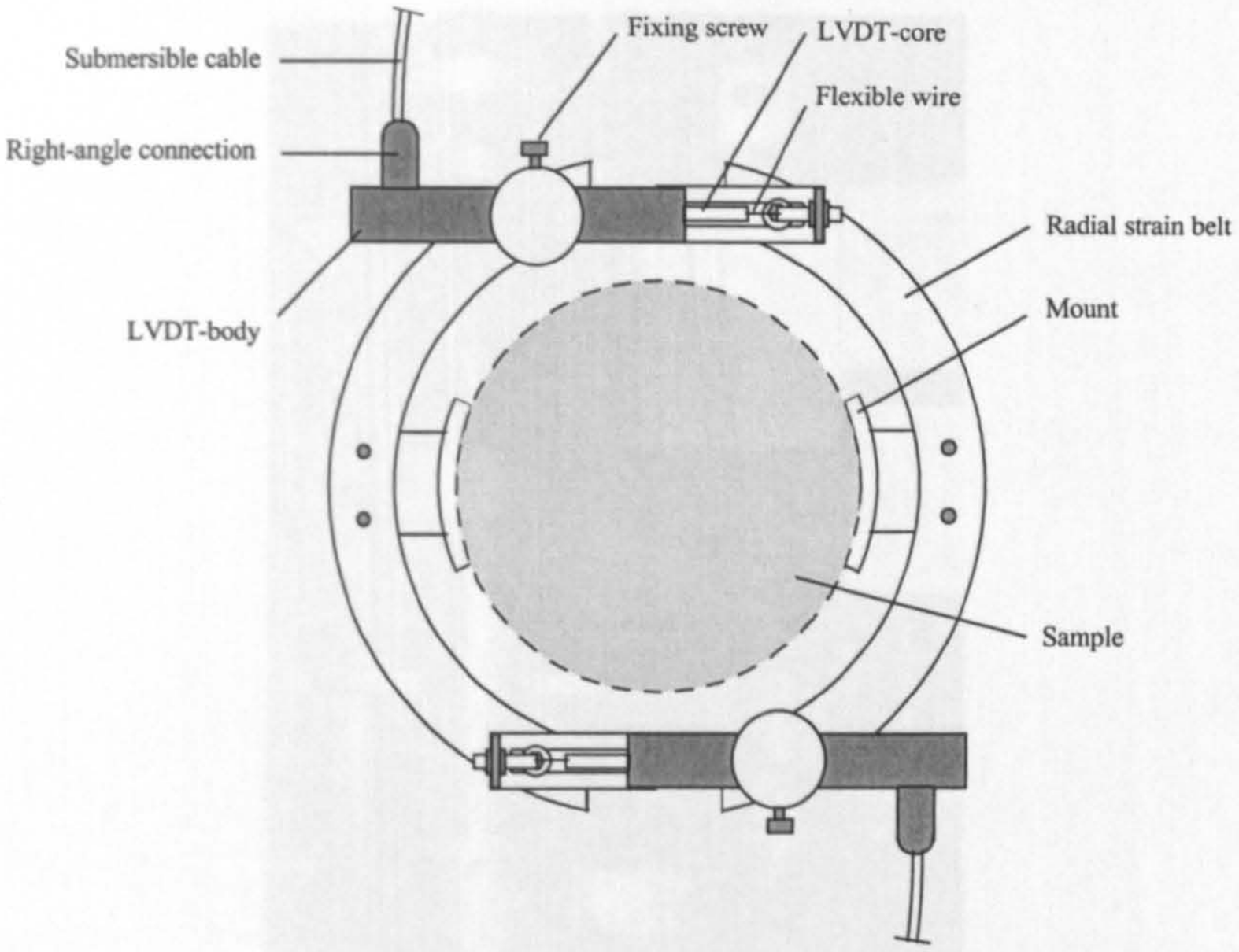

Figure 3-23: Schematic diagram of the radial strain belt.

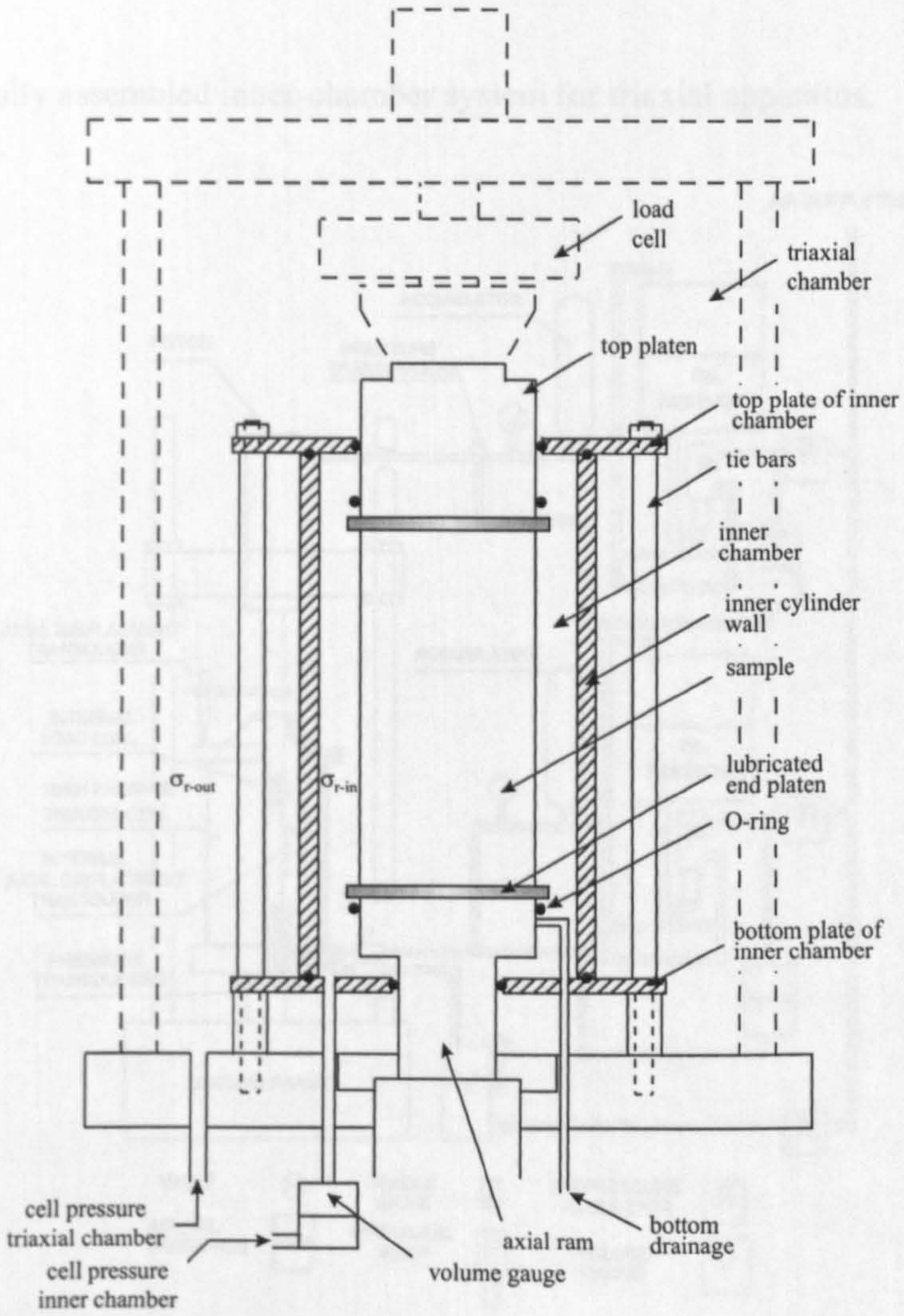

Figure 3-24: Schematic diagram of the inner-chamber system. ($\sigma'_{r\text{-}out}$ = pressure in outer-chamber, $\sigma'_{r\text{-}in}$ = pressure in inner-chamber)

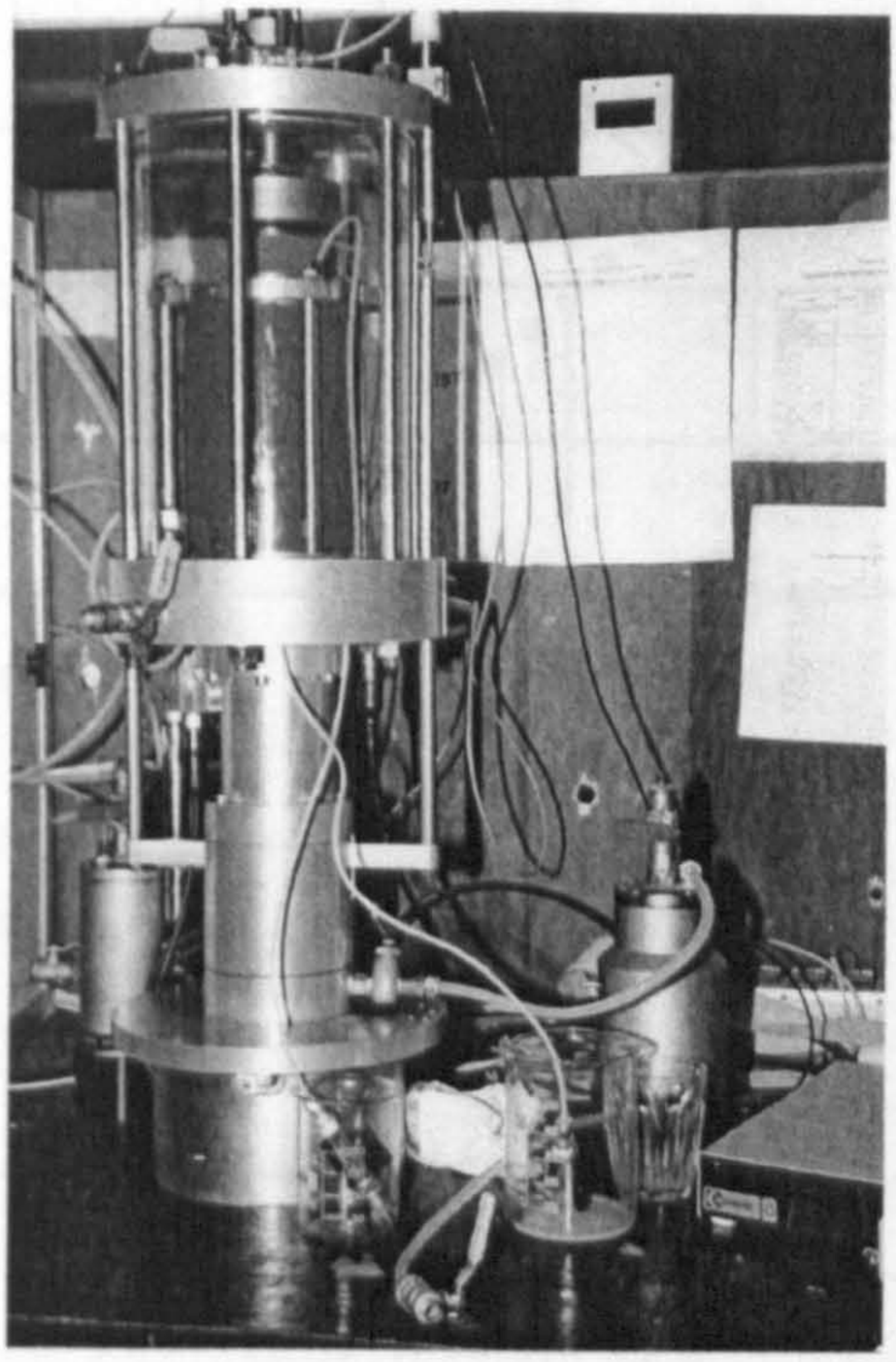

Figure 3-25: Fully assembled inner-chamber system for triaxial apparatus.

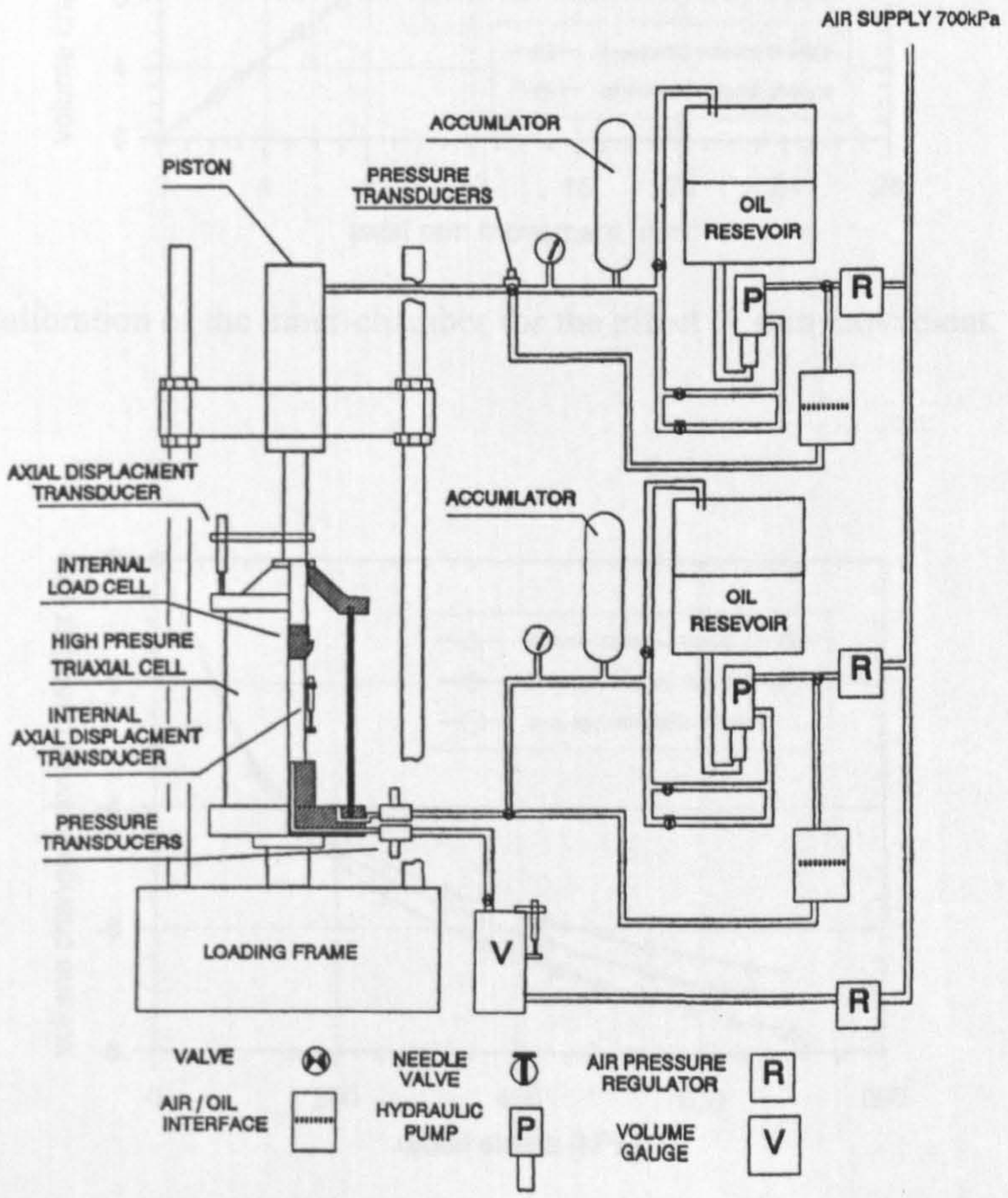

Figure 3-26: High pressure triaxial apparatus with a capacity of 10 MPa (after Cuccuvillo & Coop, 1999).

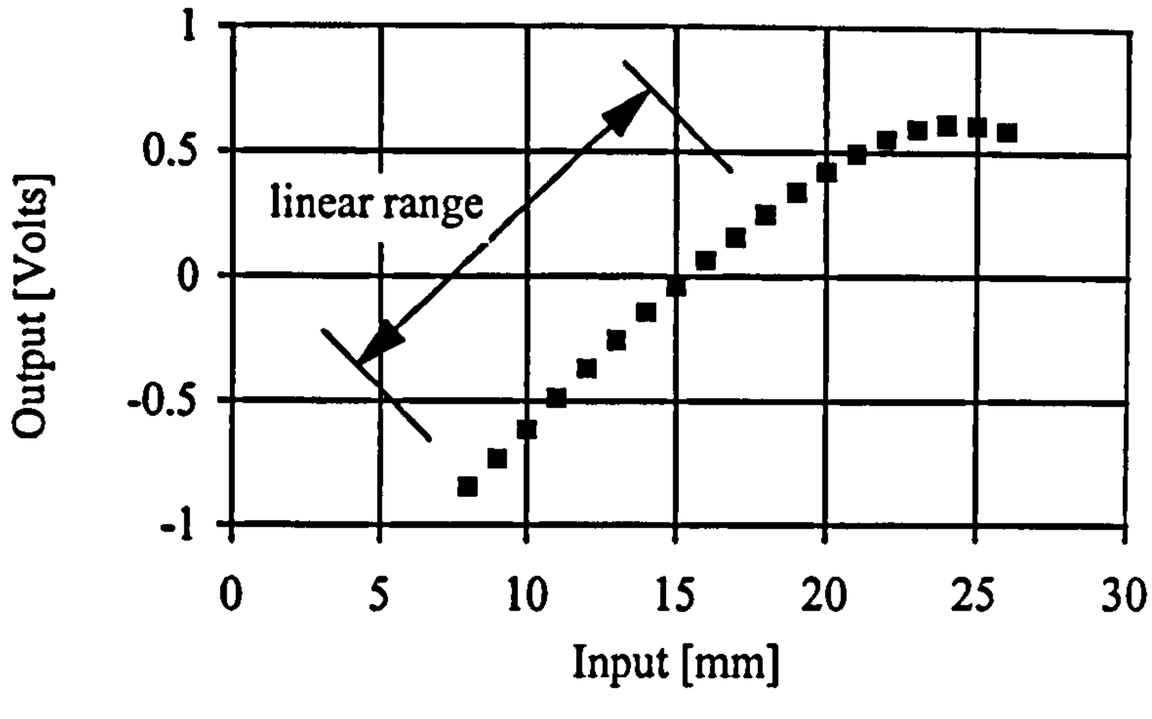

Figure 3-27: Typical calibration curve for local axial LVDT-2.

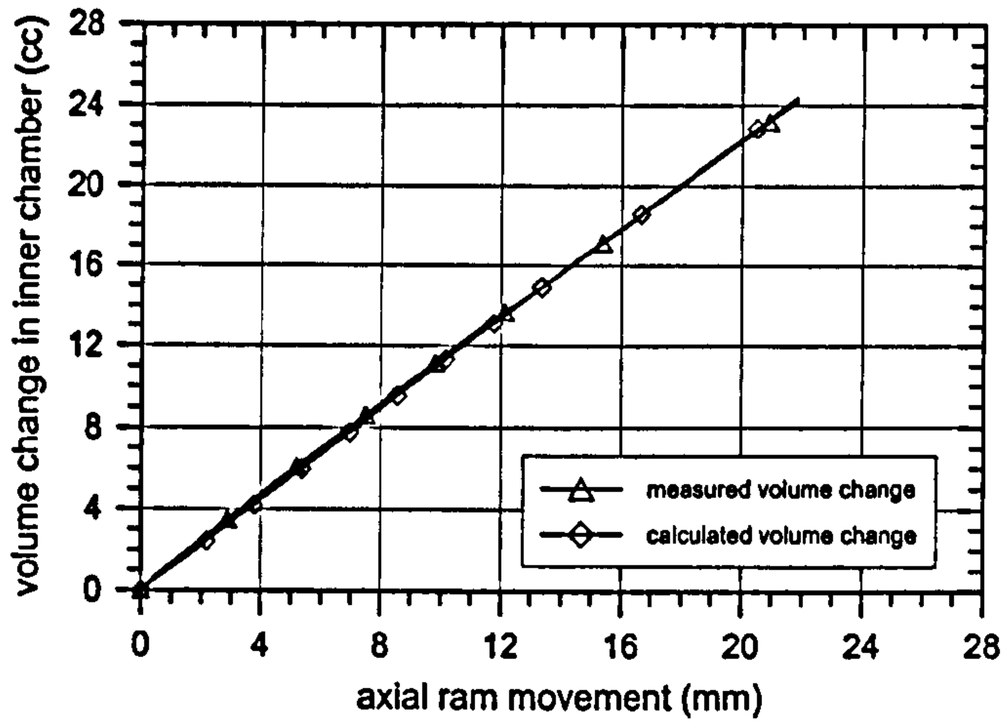

Figure 3-28: Calibration of the inner-chamber for the effect of ram movement.

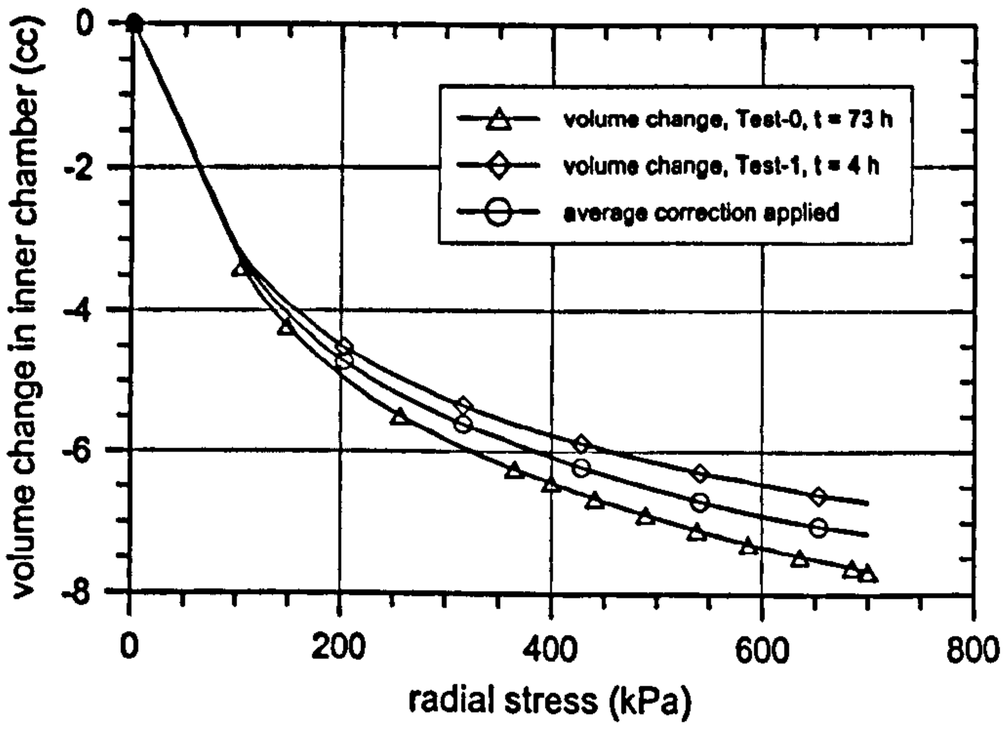

Figure 3-29: Calibration of the inner-chamber for the effect of changes in pressure.

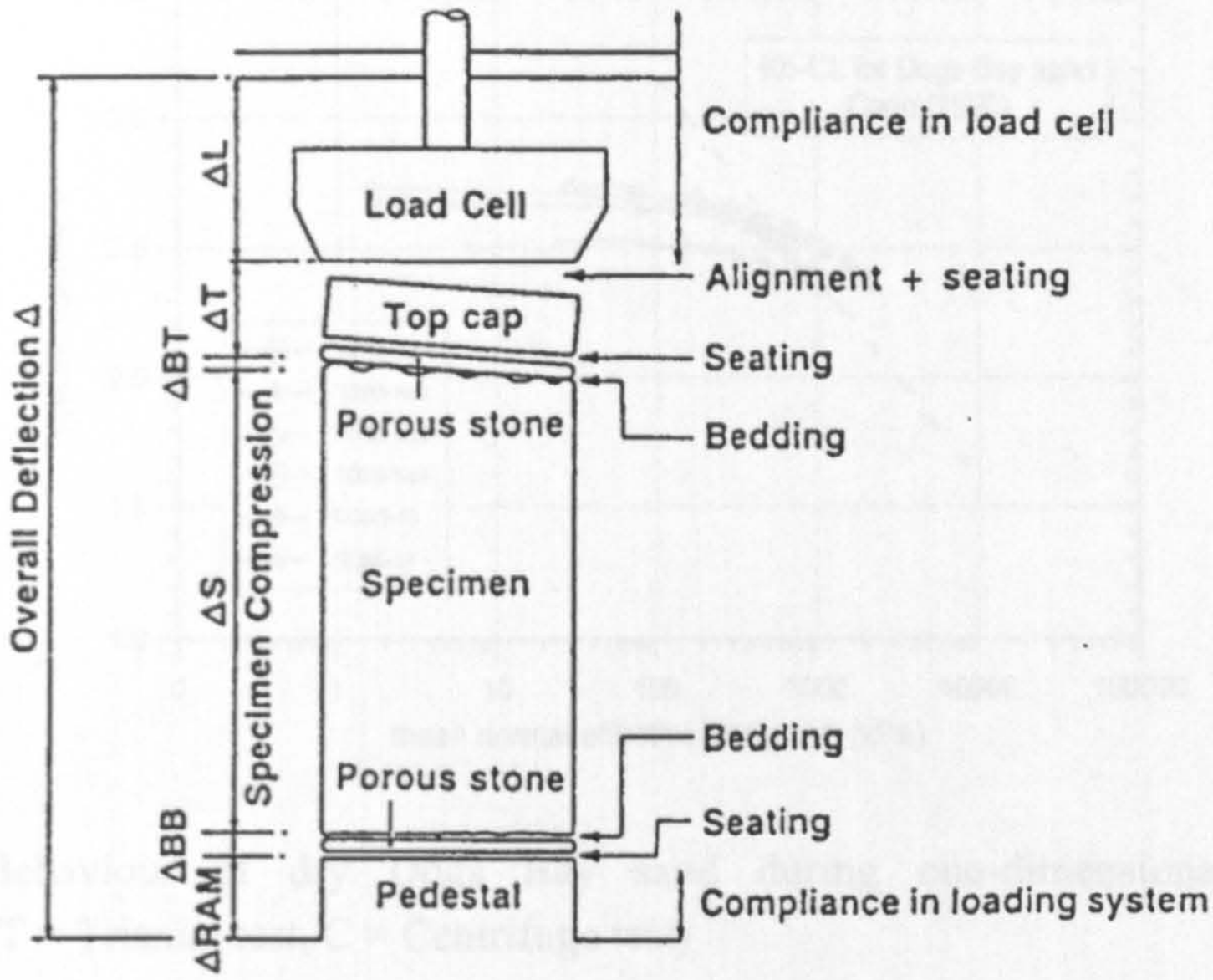

Figure 3-30: Sources of error in external axial deformation measurements (after Baldi et al., 1988).

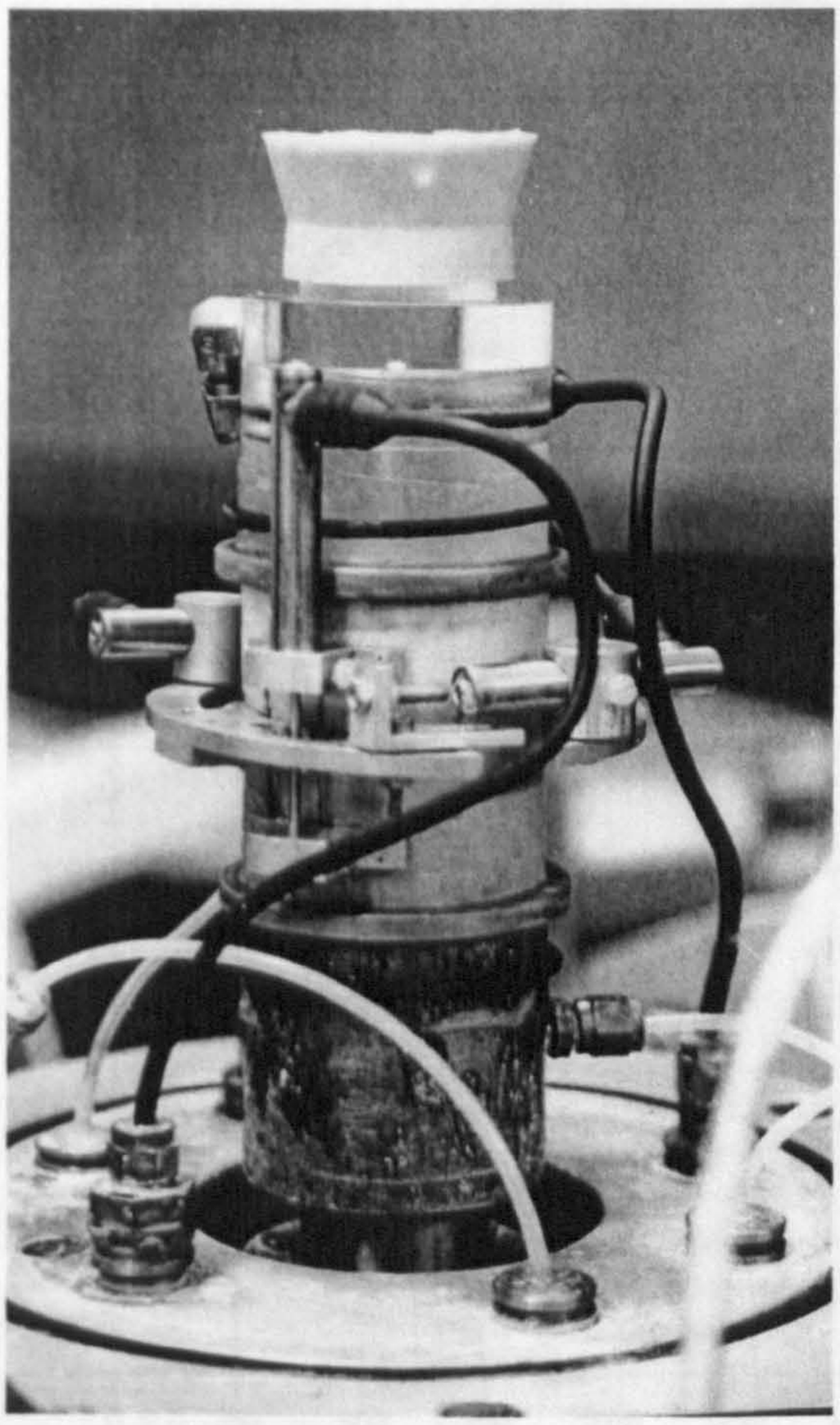

Figure 3-31: Set-up of a triaxial sample with local instrumentation.

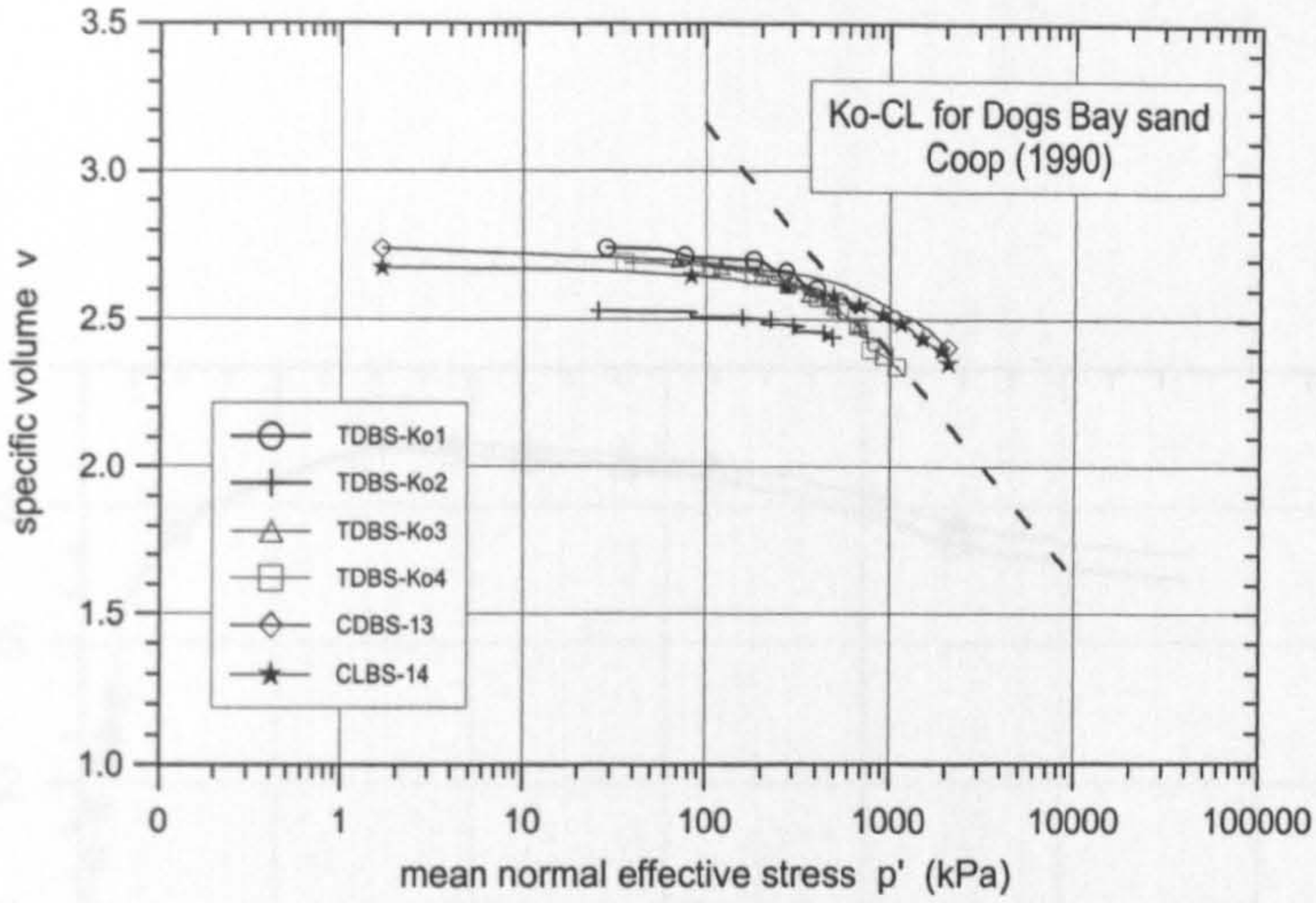

Figure 3-32: Behaviour of dry Dogs Bay sand during one-dimensional compression. (T = Triaxial test, C = Centrifuge test)

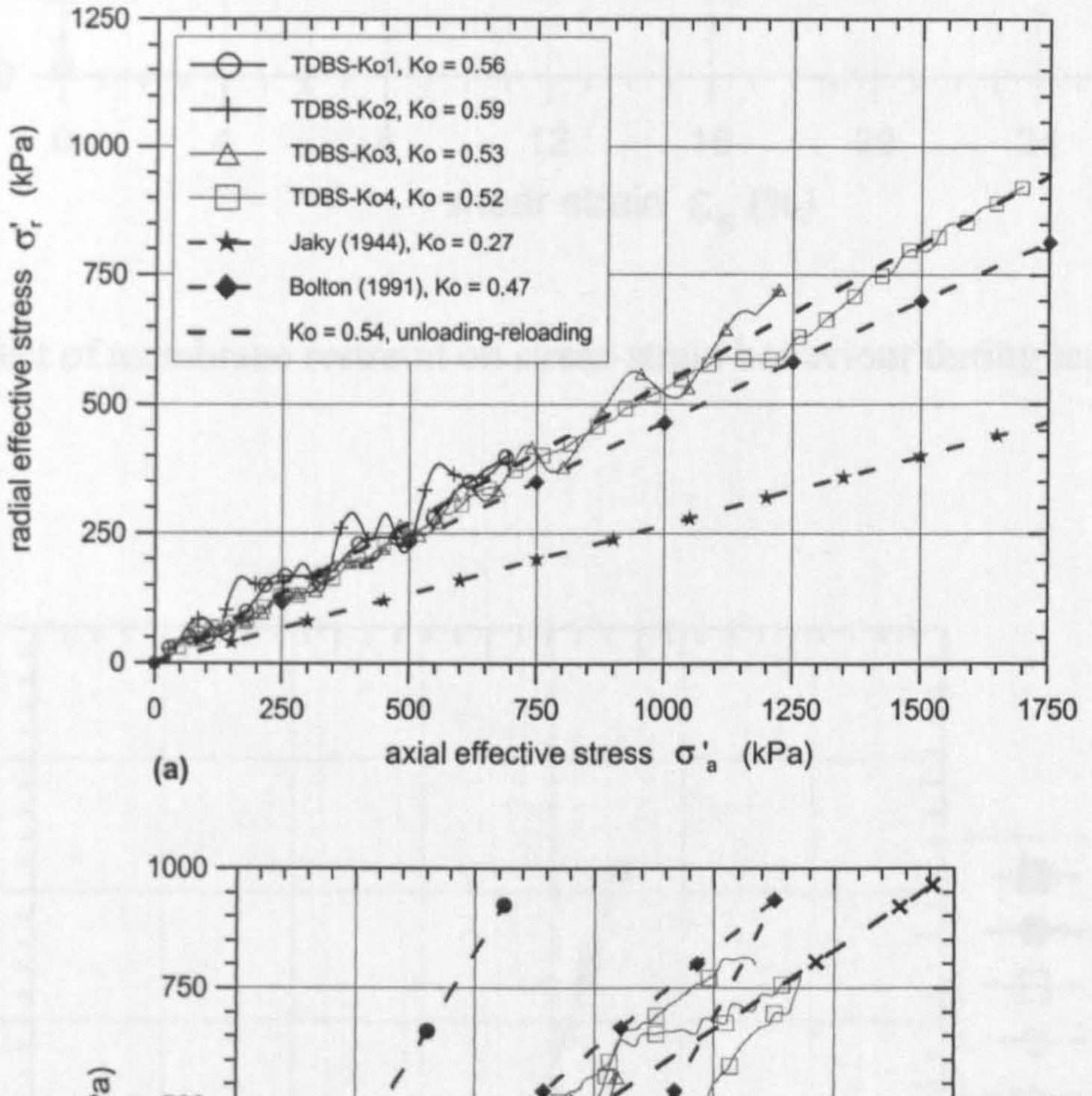

Figure 3-33: Measured and predicted K_o-values and stress paths for dry Dogs Bay sand during one-dimensional compression and unloading.

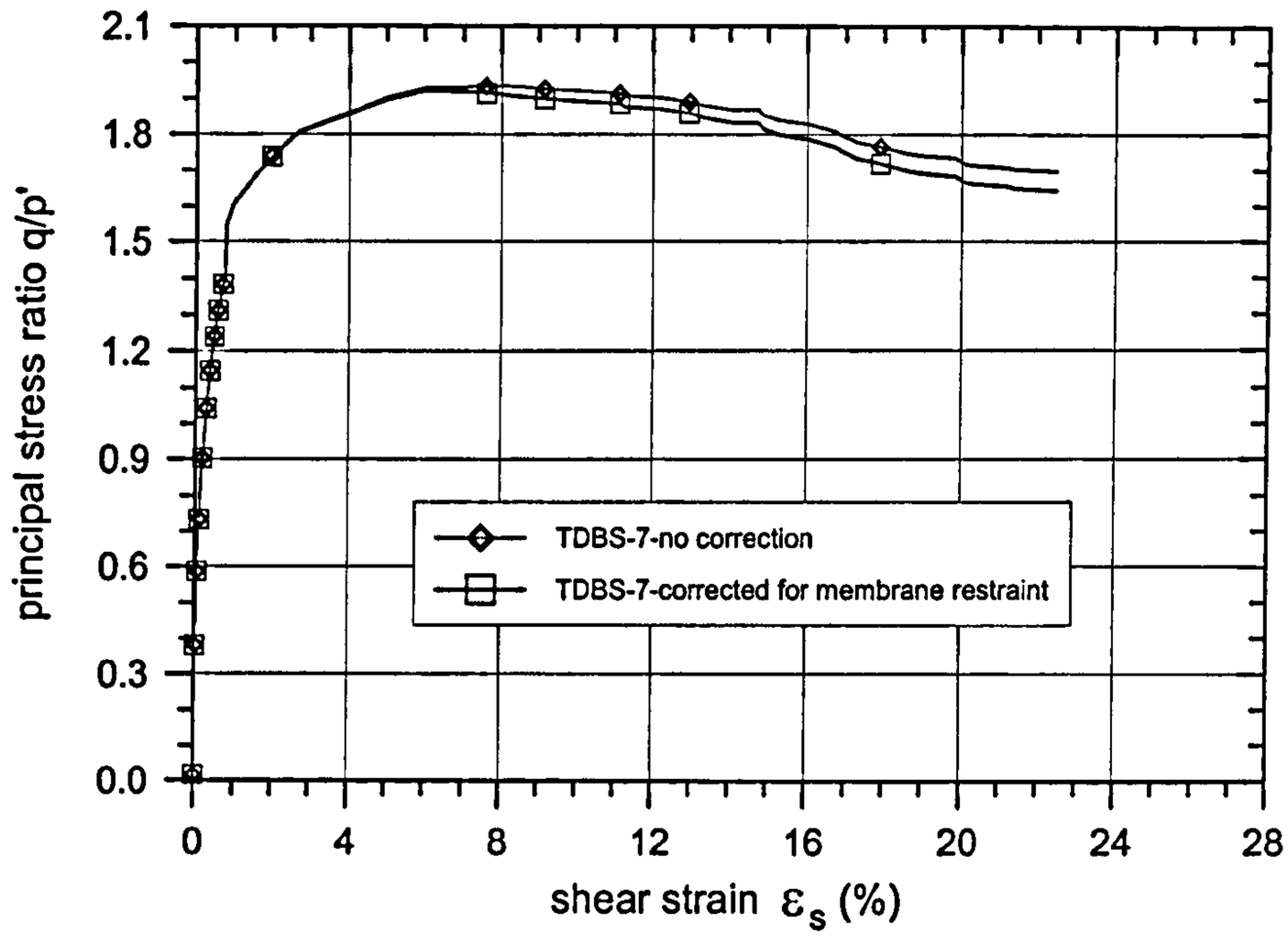

Figure 3-34: Effect of membrane restraint on stress-strain behaviour during test TDBS-7.

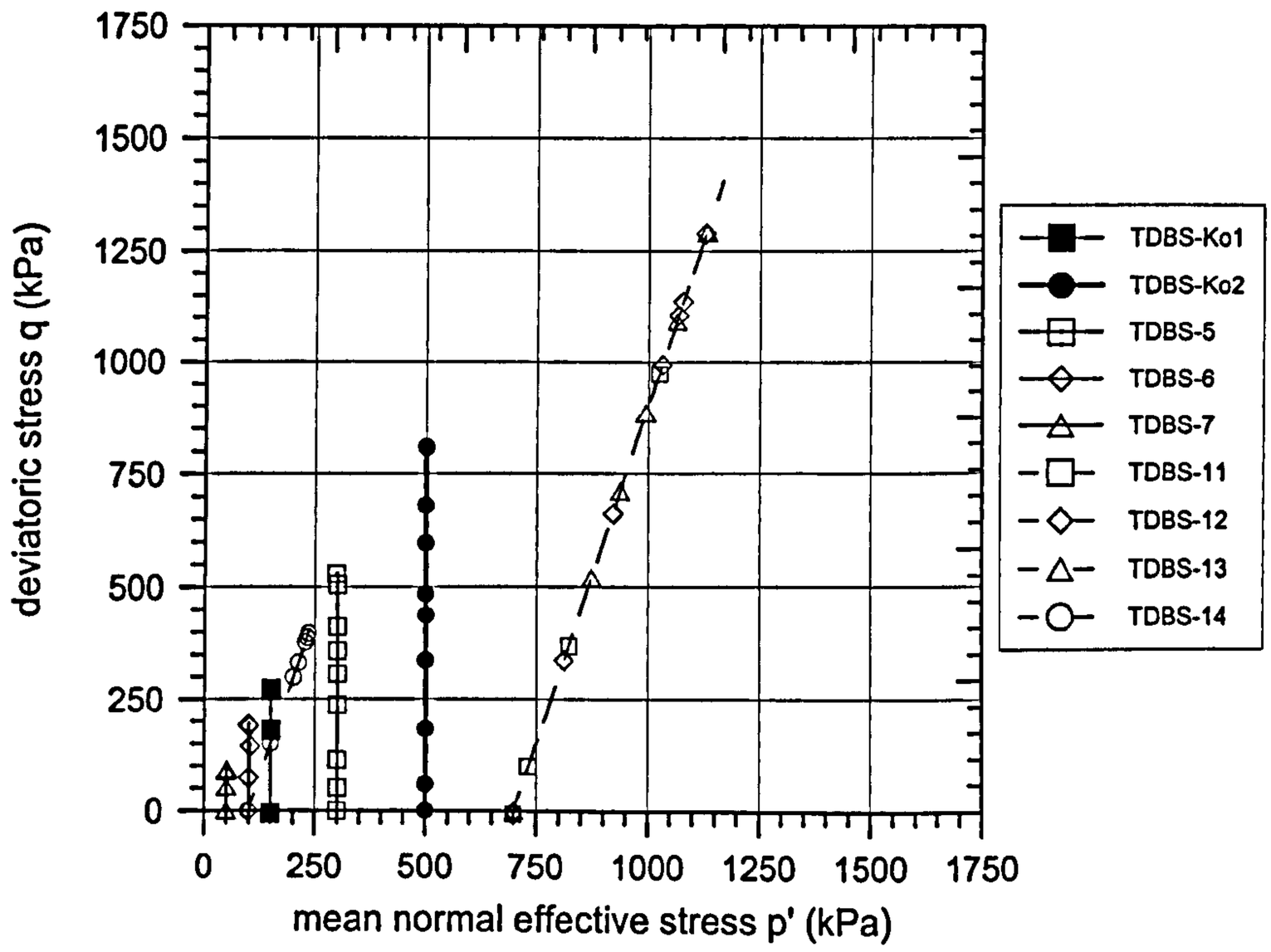

Figure 3-35: Stress paths during shearing of dry Dogs Bay sand.

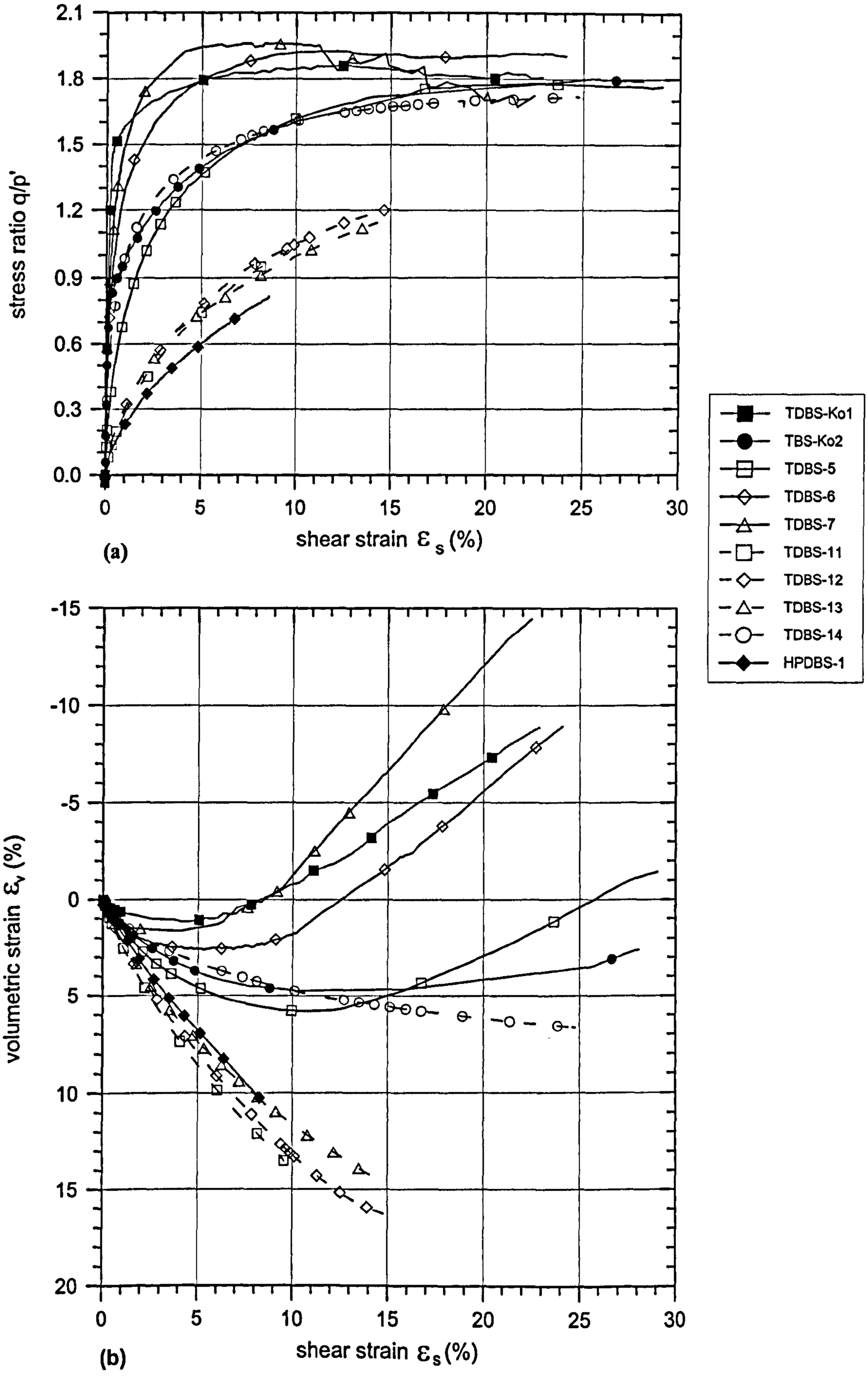

Figure 3-36: Stress-strain behaviour of dry Dogs Bay sand during shearing.

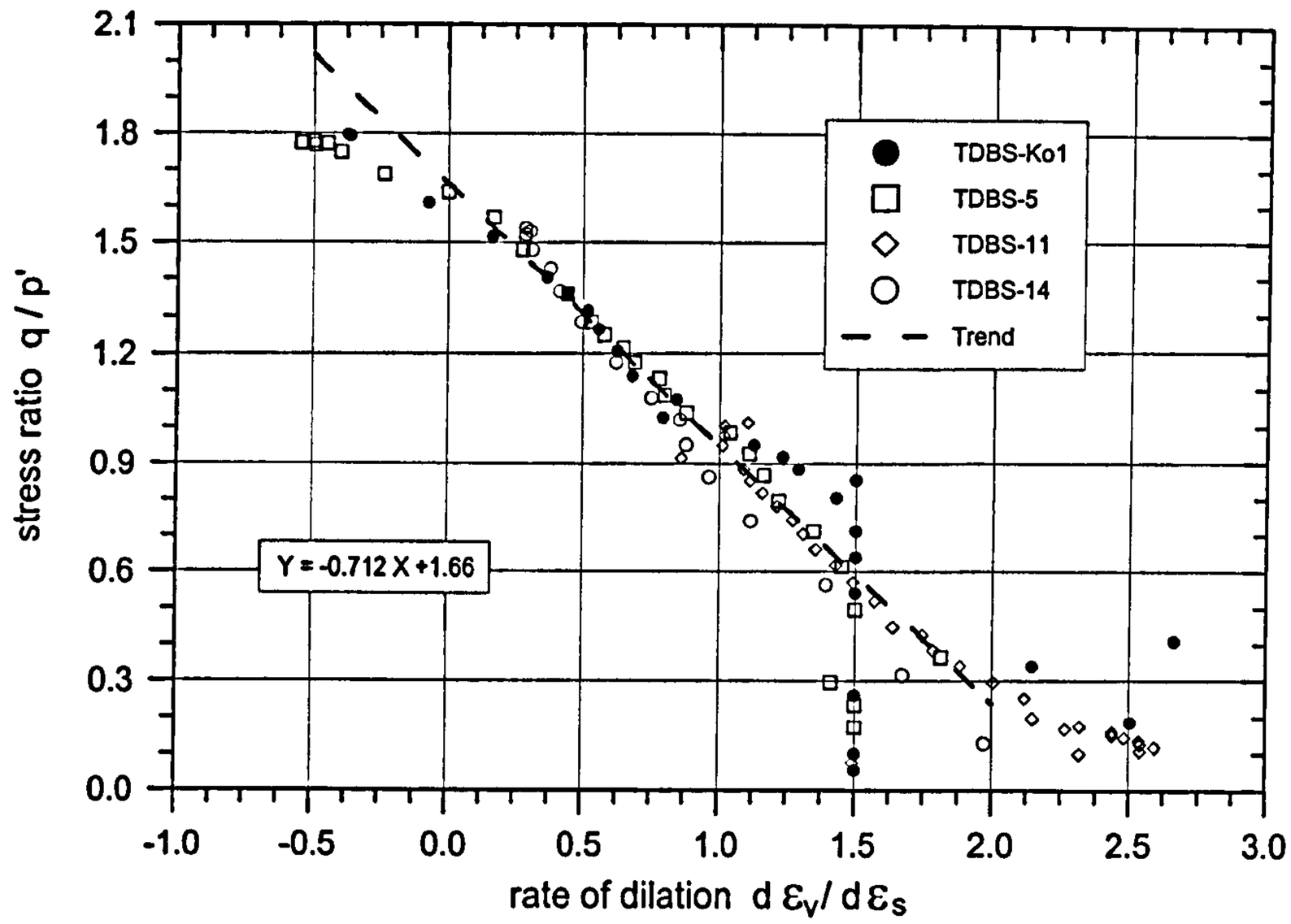

Figure 3-37: Typical stress-dilatancy relationship for Dogs Bay sand.

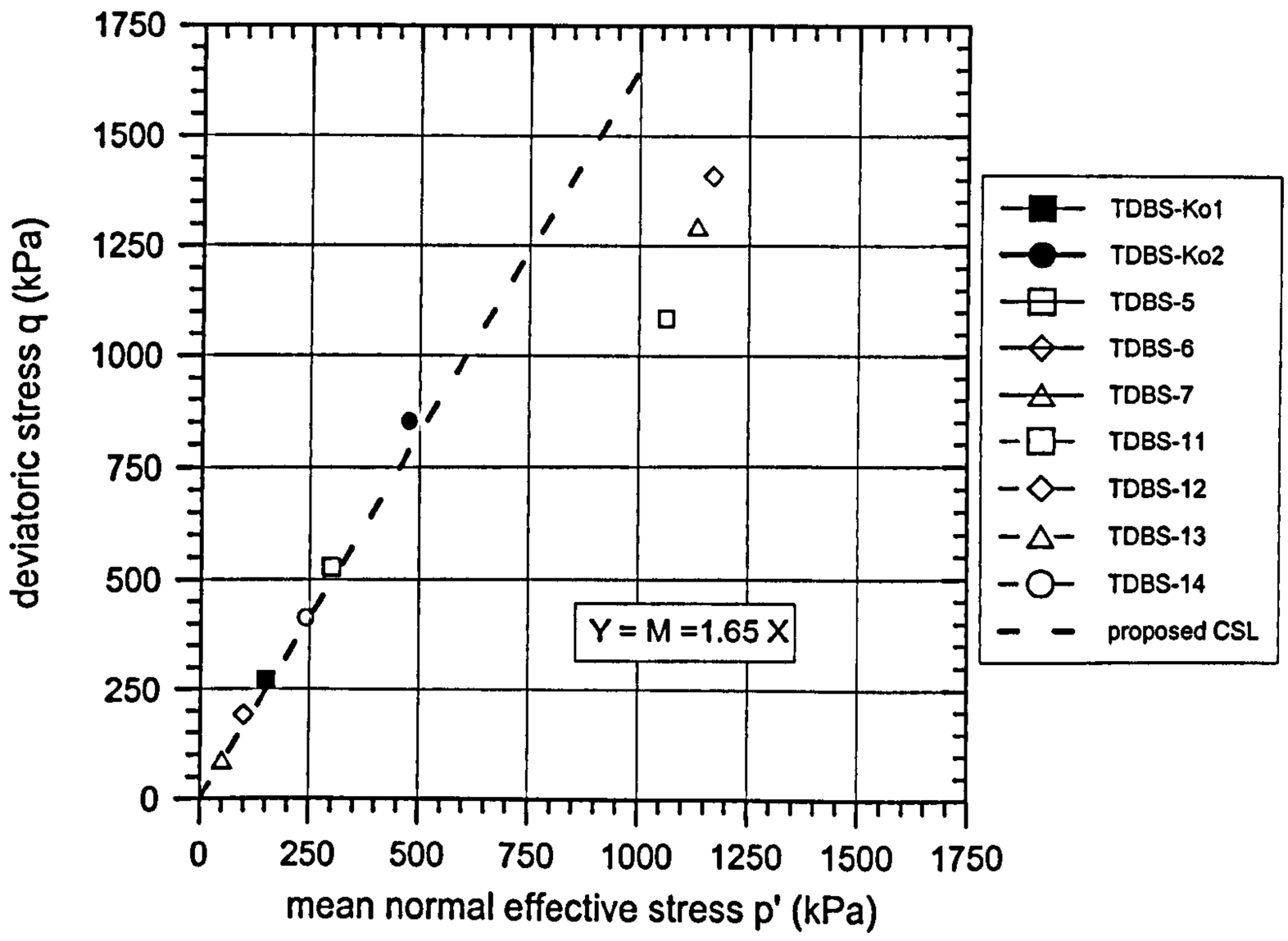

Figure 3-38: End of test states and the critical state line for Dogs Bay sand.

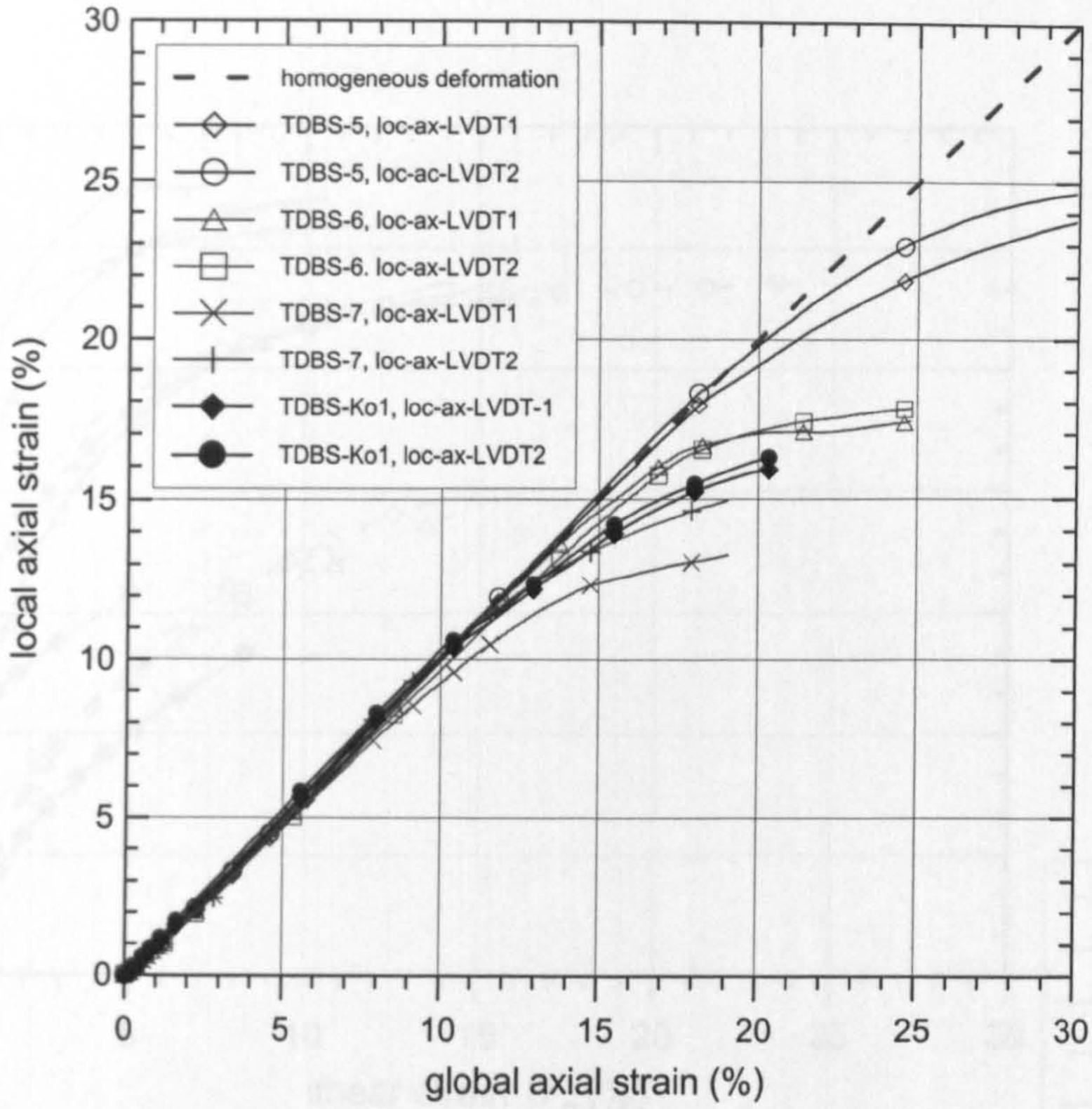

Figure 3-39: Non-homogeneous axial deformations during shearing of dry Dogs Bay sand.

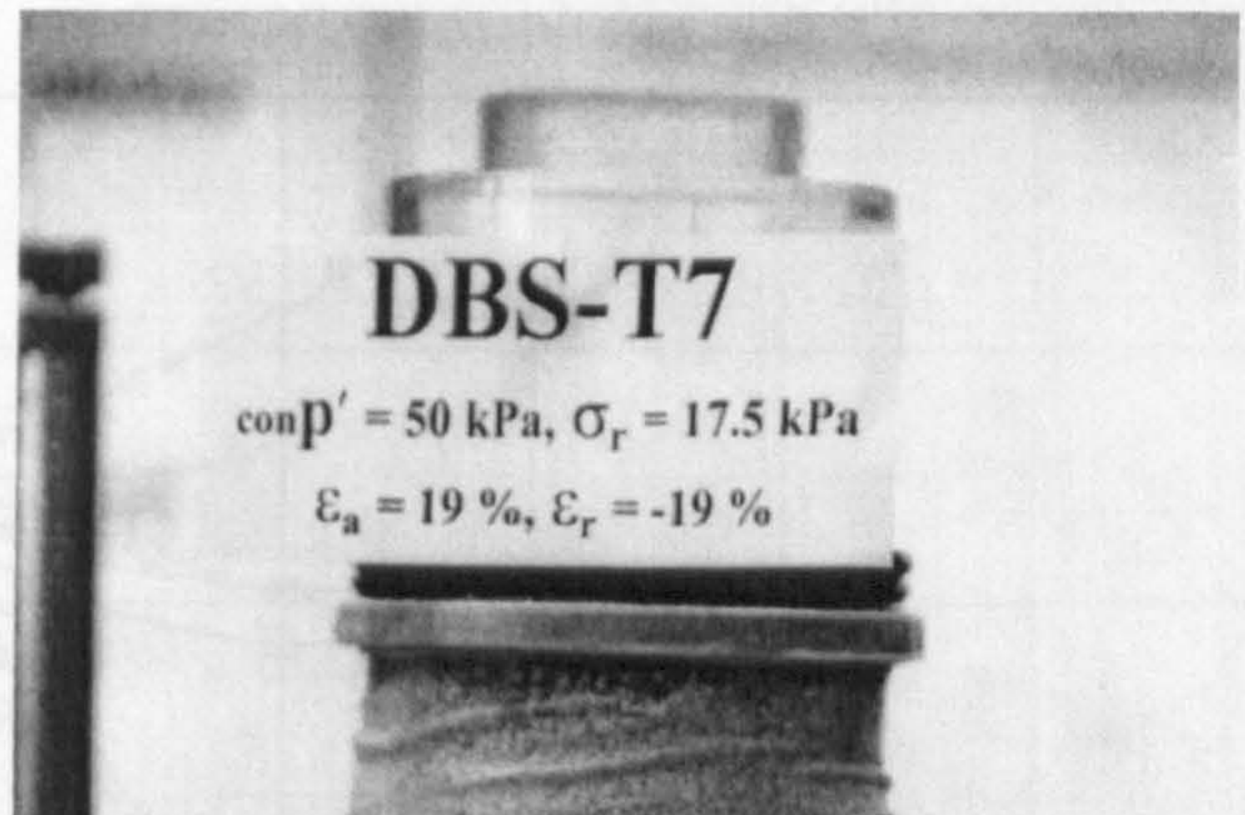

Figure 3-40: Final sample shape and shear bands at the end of shearing of sample TDBS-7. (local LVDTs removed for clarity)

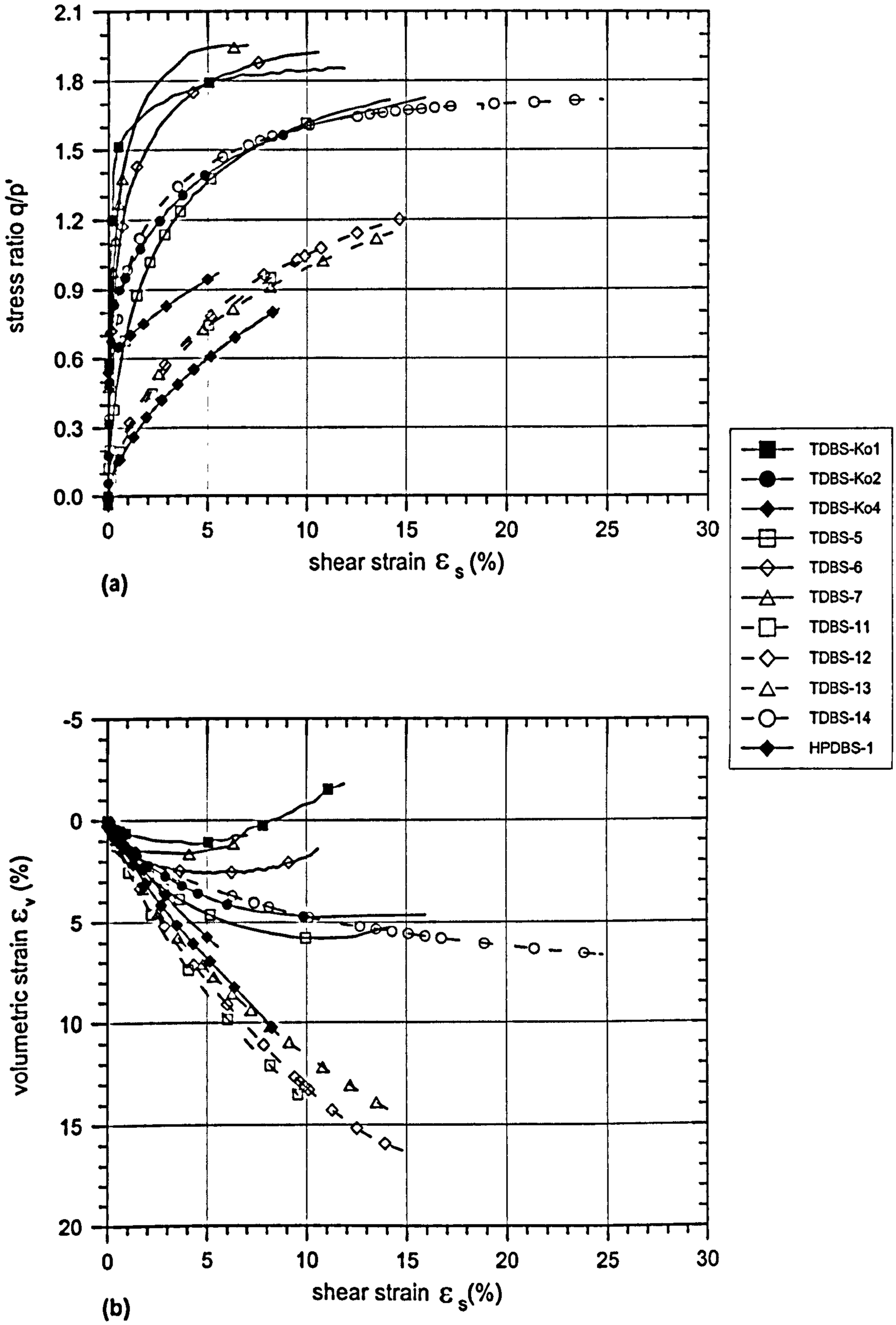

Figure 3-41: Stress-strain behaviour of dry Dogs Bay sand during shearing ignoring data in range of non-homogeneous deformations.

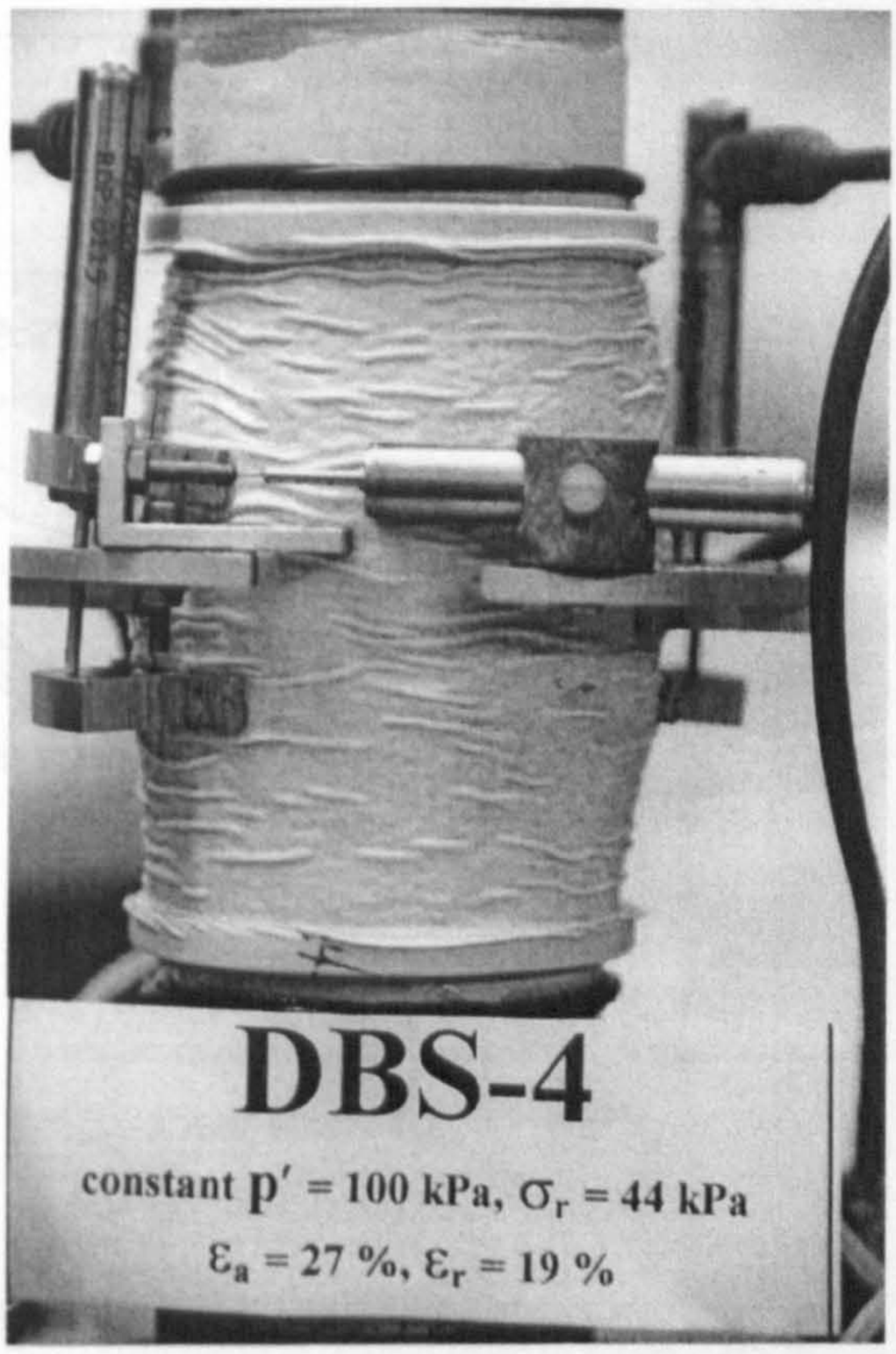

Figure 3-42: Sample TDBS-4 at the end of shearing showing shear bands and barrelled shape.

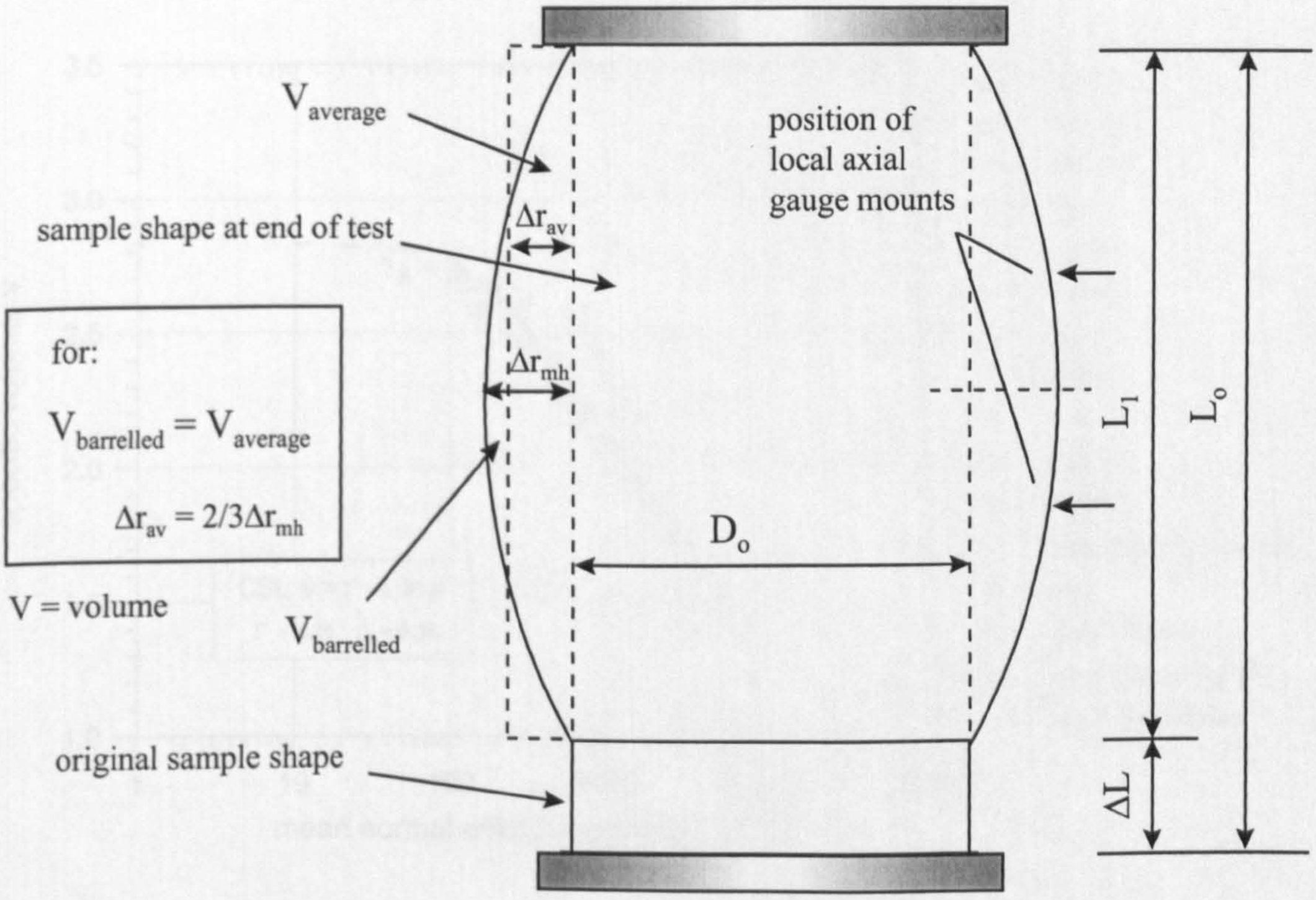

Figure 3-43: Procedure developed to account for the effect of barrelling.

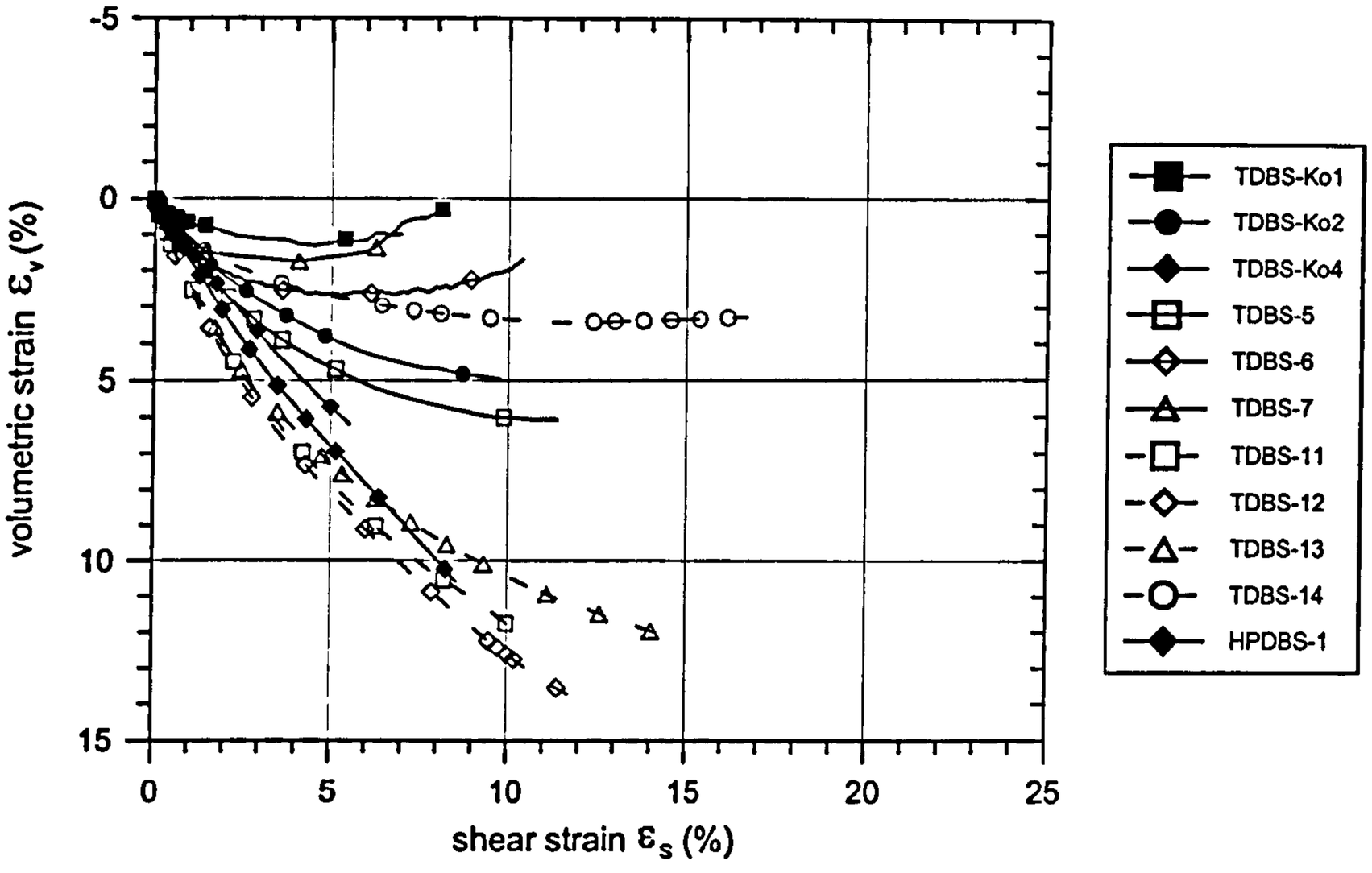

Figure 3-44: Corrected strain data for dry Dogs Bay sand during shearing taking account of barrelling effect.

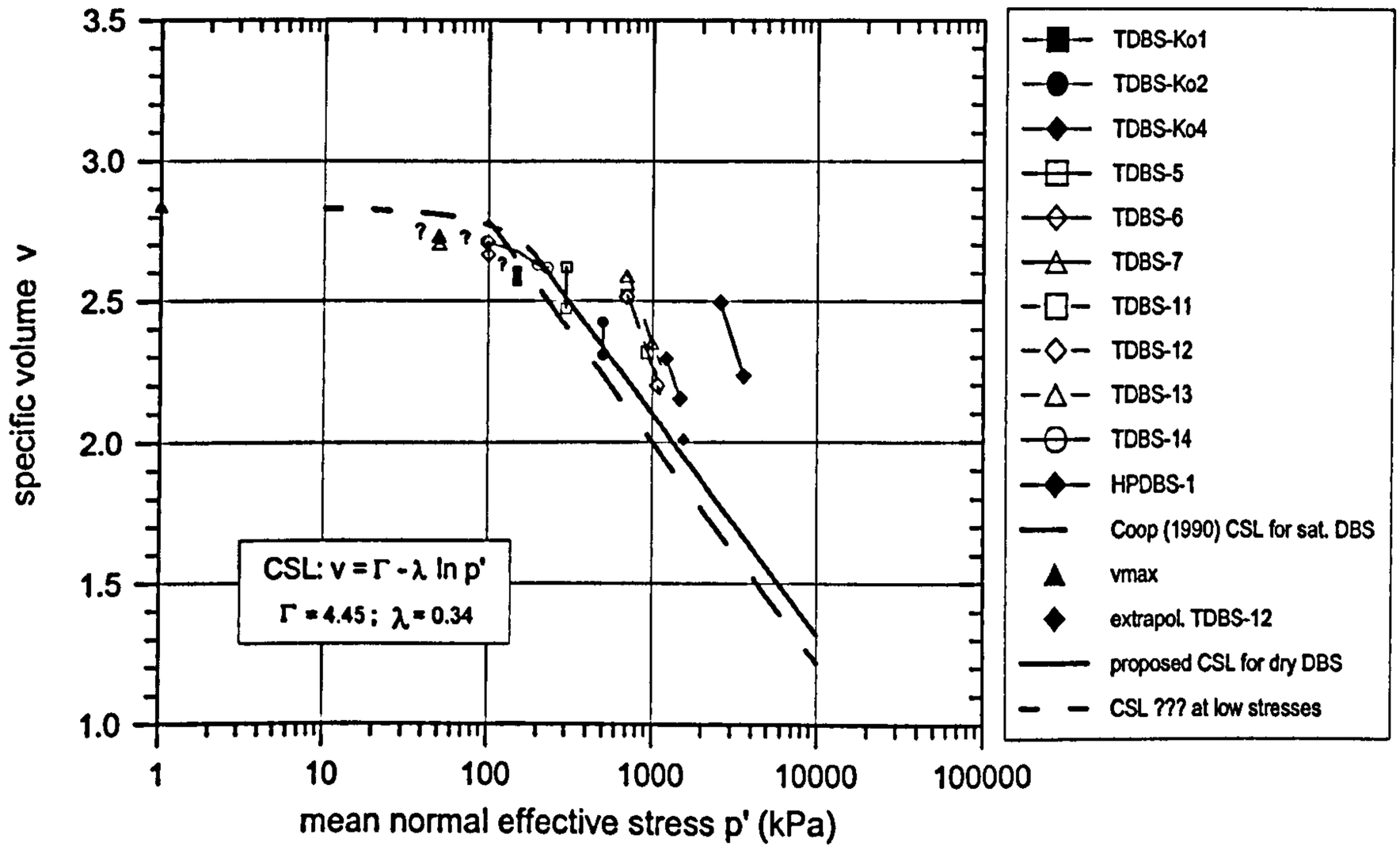

Figure 3-45: Proposed critical state line for dry Dogs Bay sand.

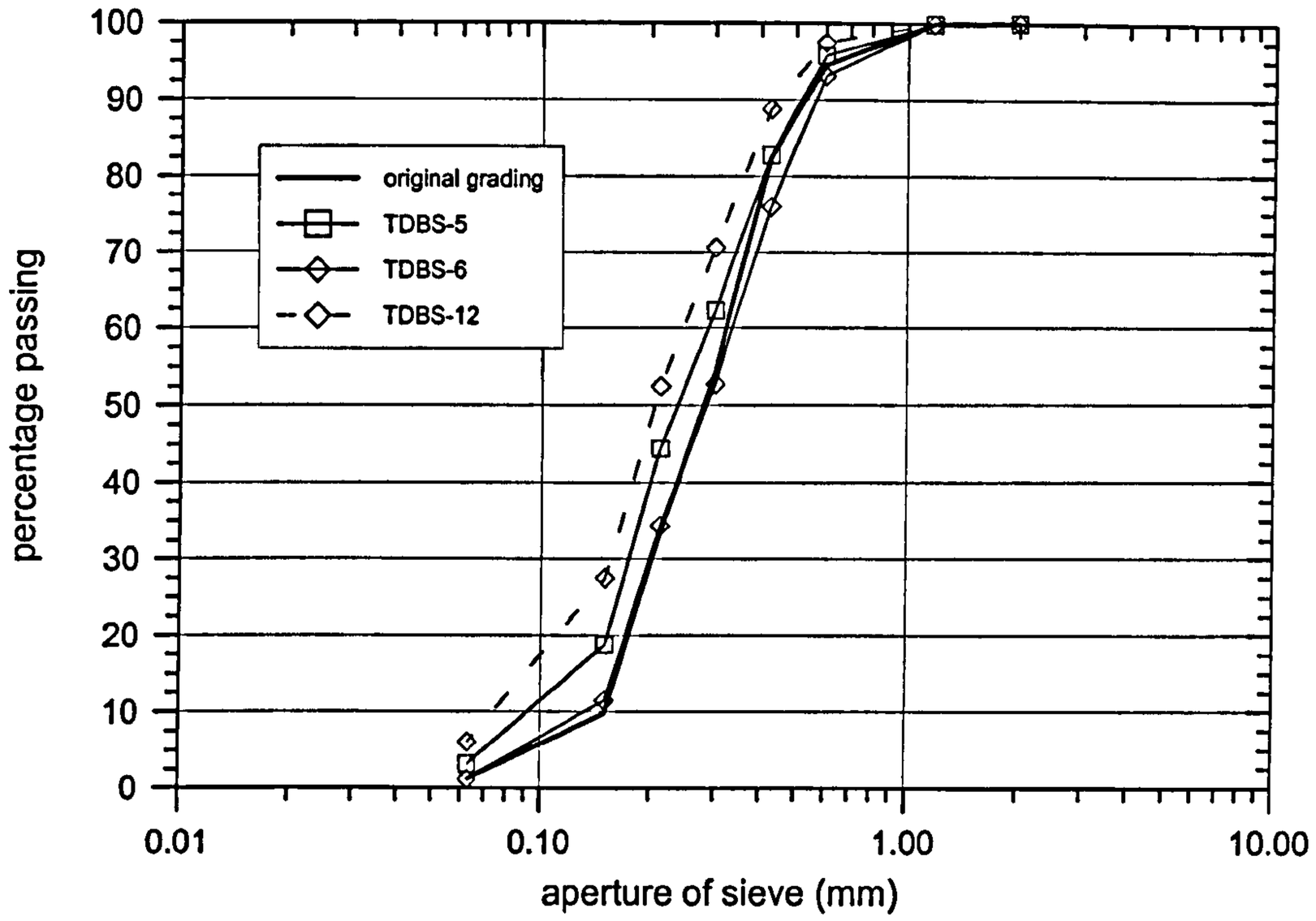

Figure 3-46: Grading curves before and after some typical triaxial tests on Dogs Bay sand.

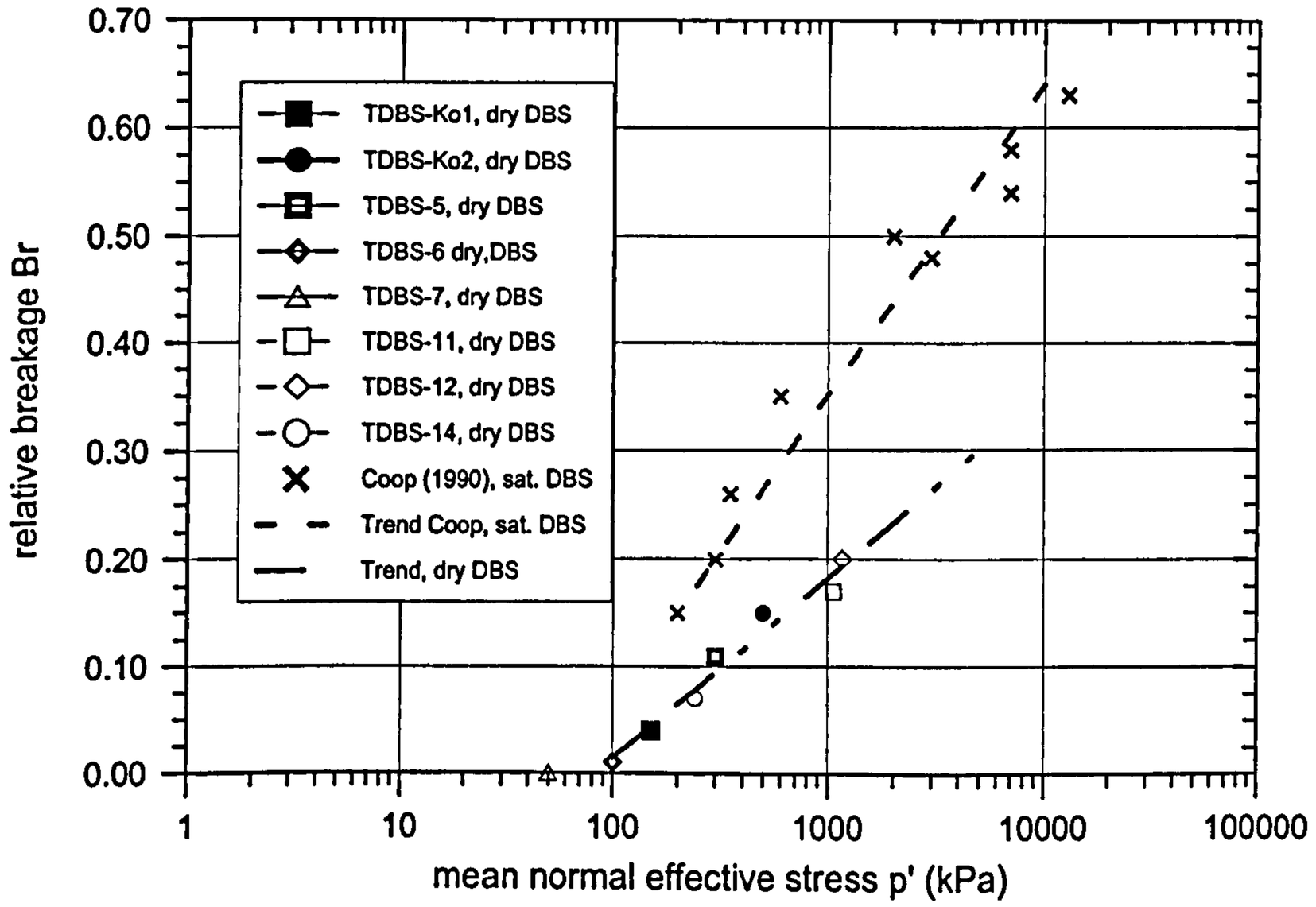

Figure 3-47: Particle breakage during shearing of dry and saturated samples of Dogs Bay sand.

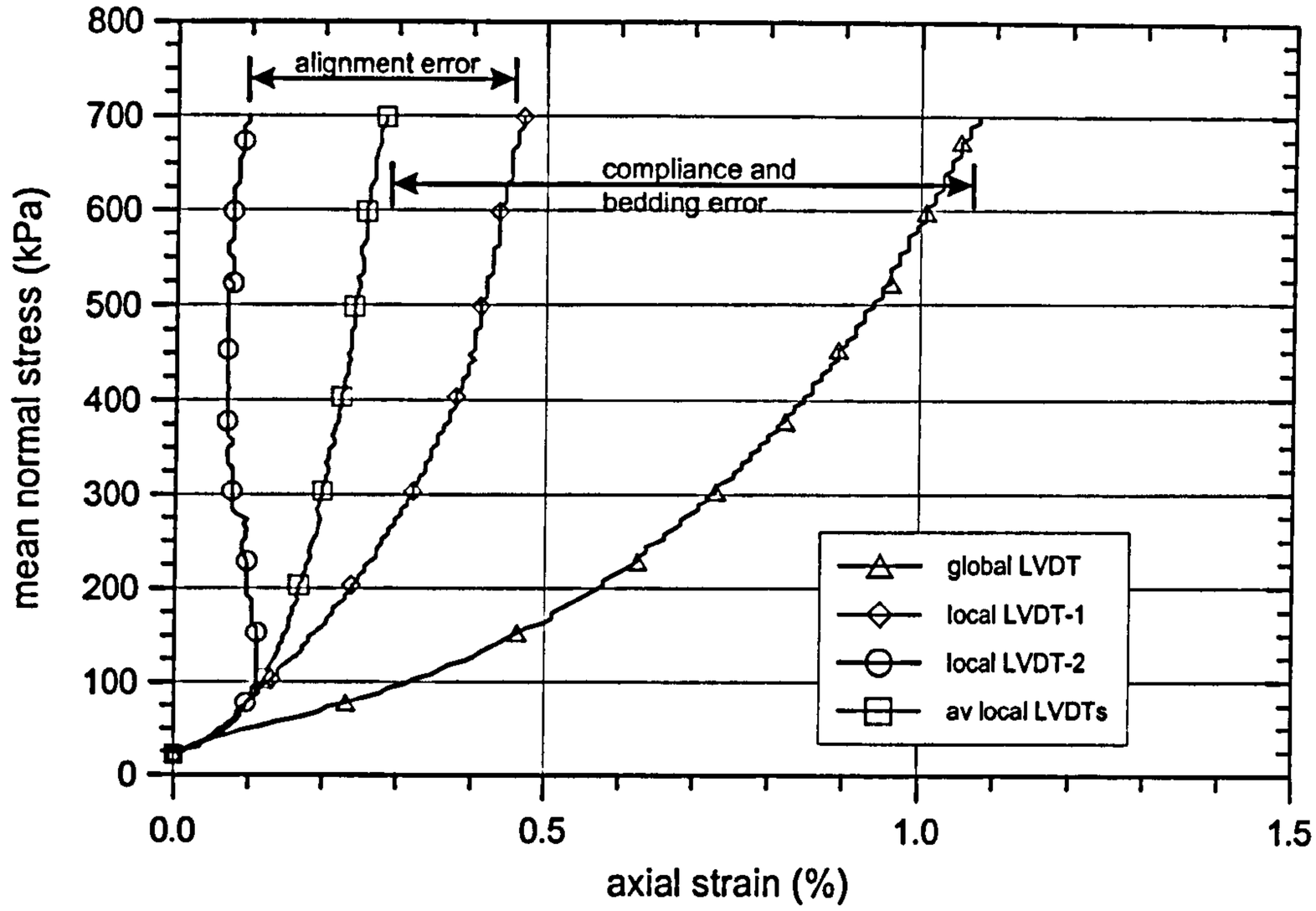

Figure 3-48: Effect of compliance, bedding error and compression of the grease layer on the axial strains.

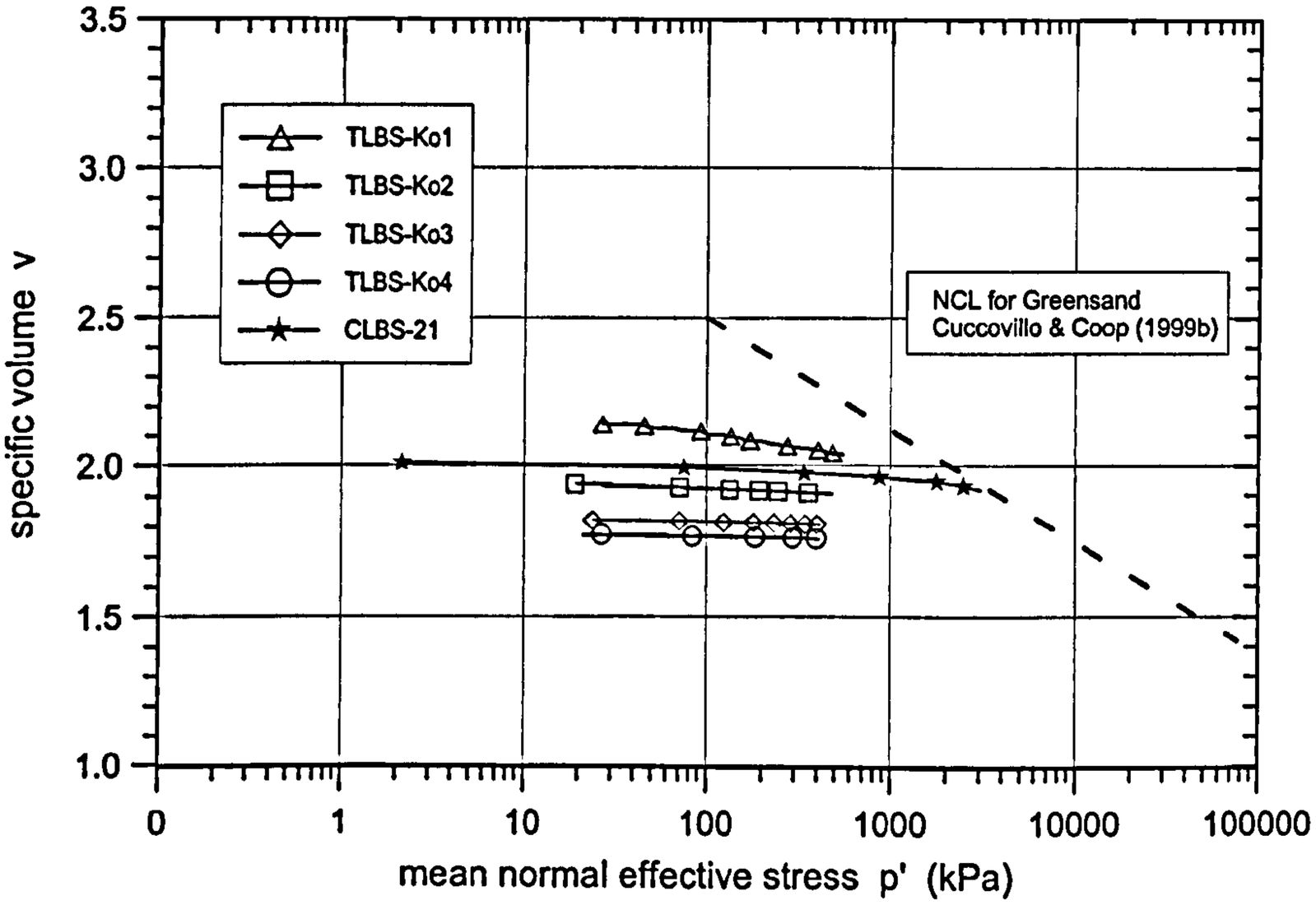

Figure 3-49: Behaviour of Leighton Buzzard sand during one-dimensional compression. (T = triaxial test, C = Centrifuge test)

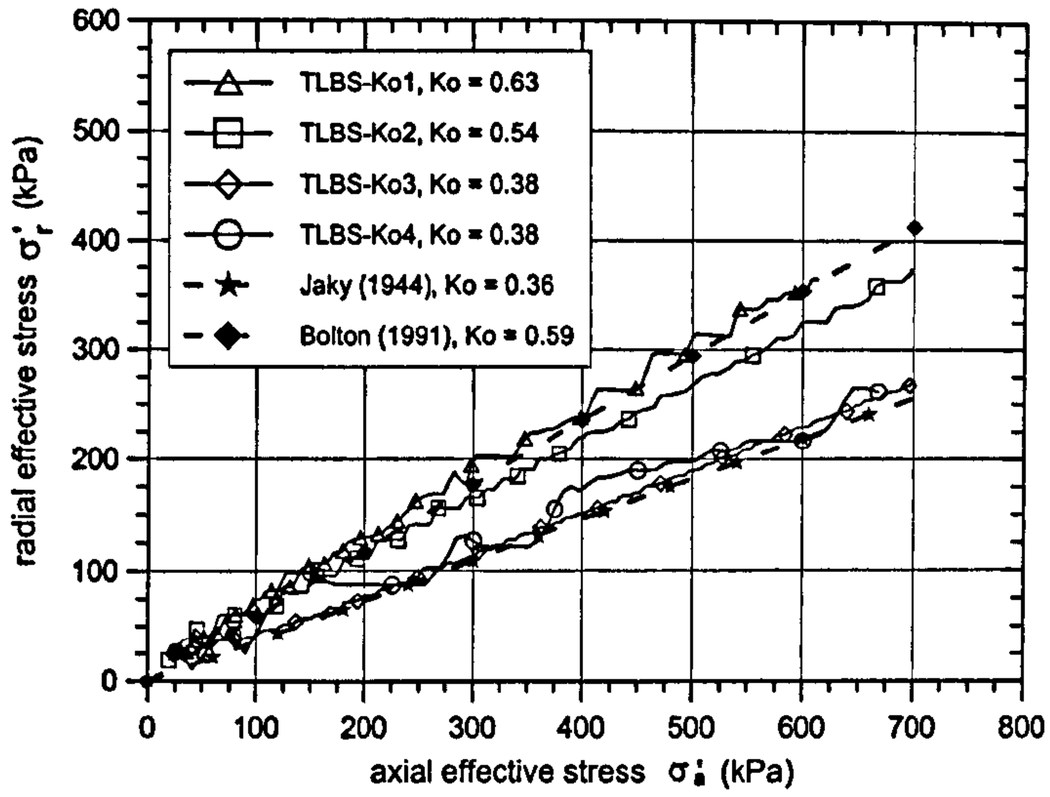

Figure 3-50: Measured and predicted K_o-values of Leighton Buzzard sand.

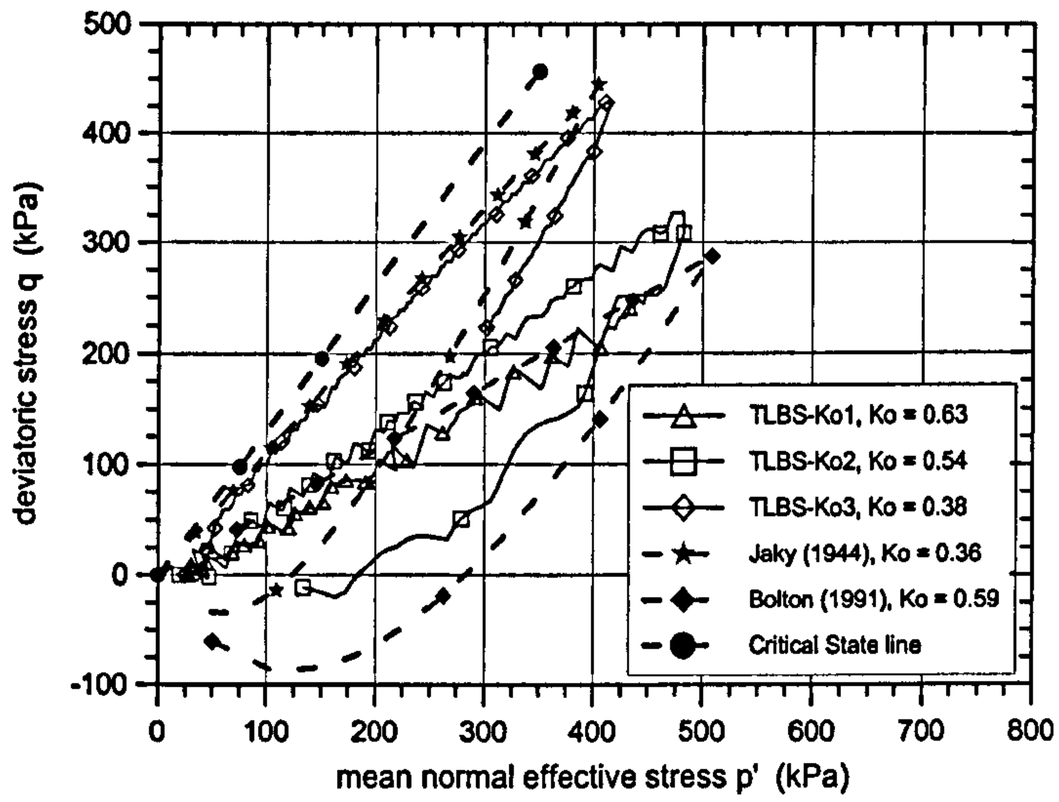

Figure 3-51: Measured and predicted stress paths for Leighton Buzzard sand during one-dimensional compression and unloading.

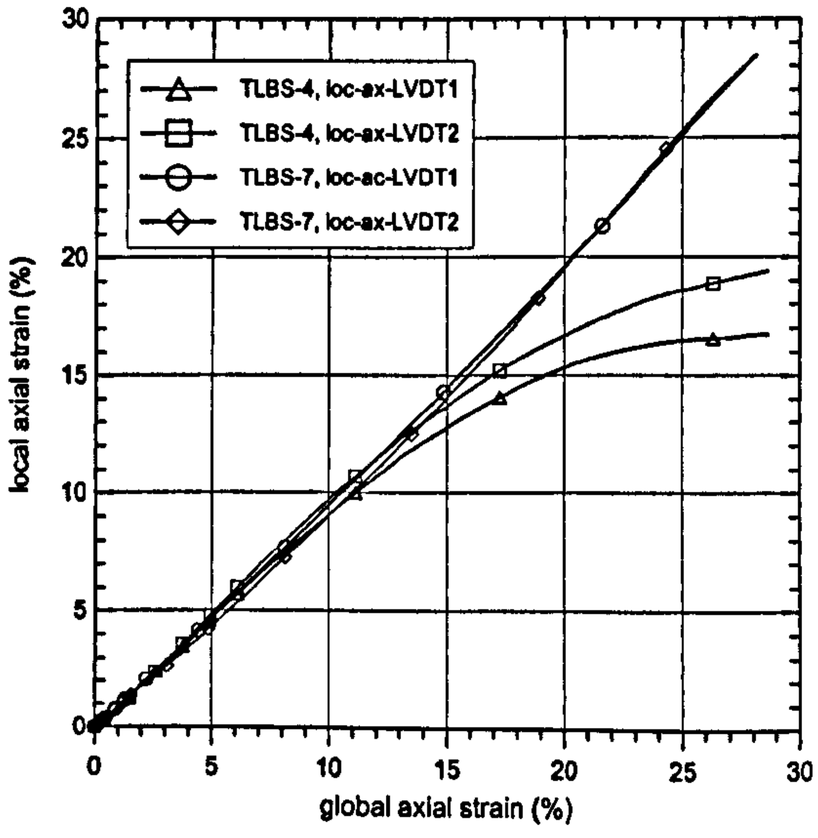

Figure 3-52: Non-homogeneous axial deformations during shearing of Leighton Buzzard sand.

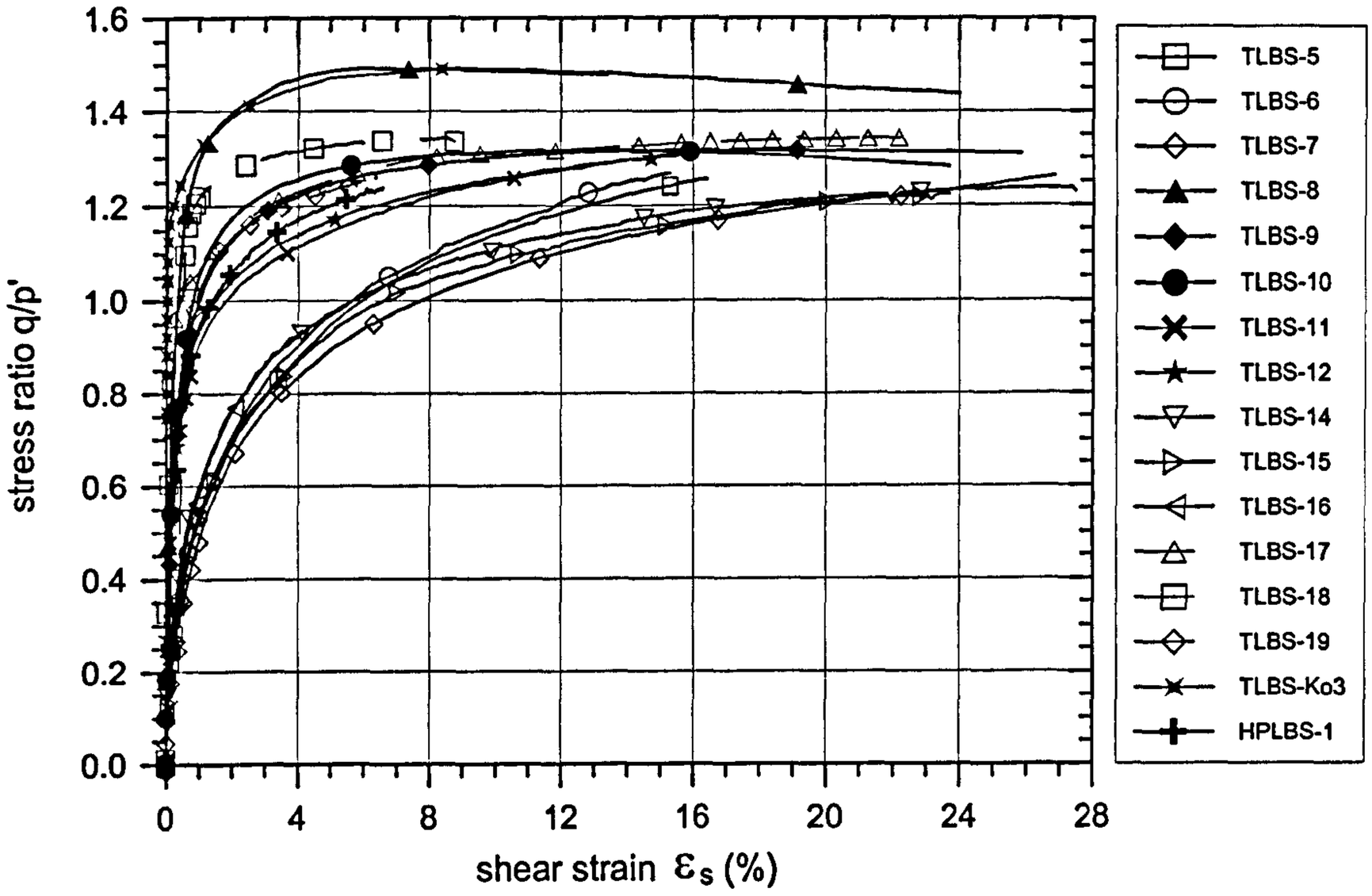

(a)

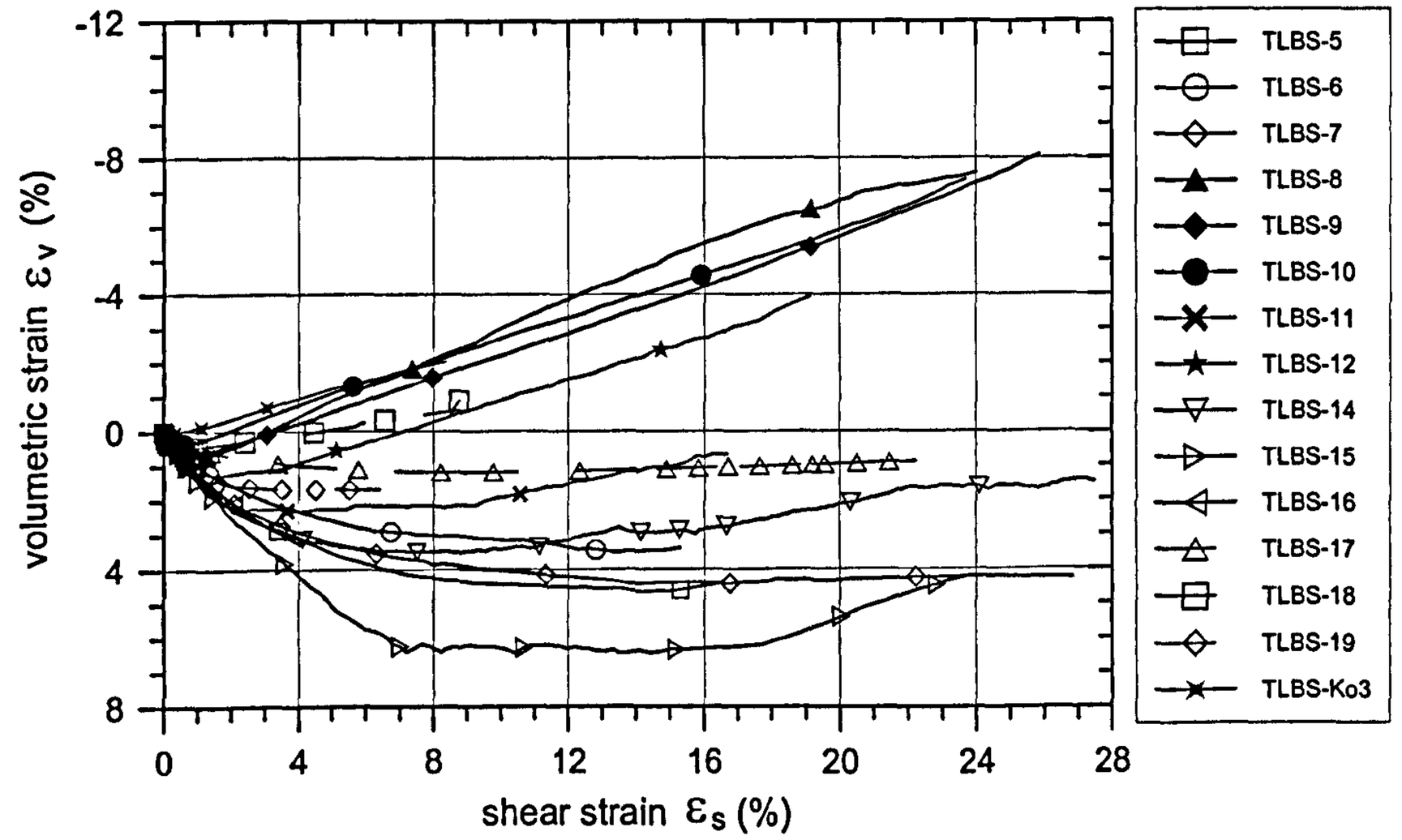

(b)

Figure 3-54: Stress-strain behaviour of Leighton Buzzard sand during shearing.

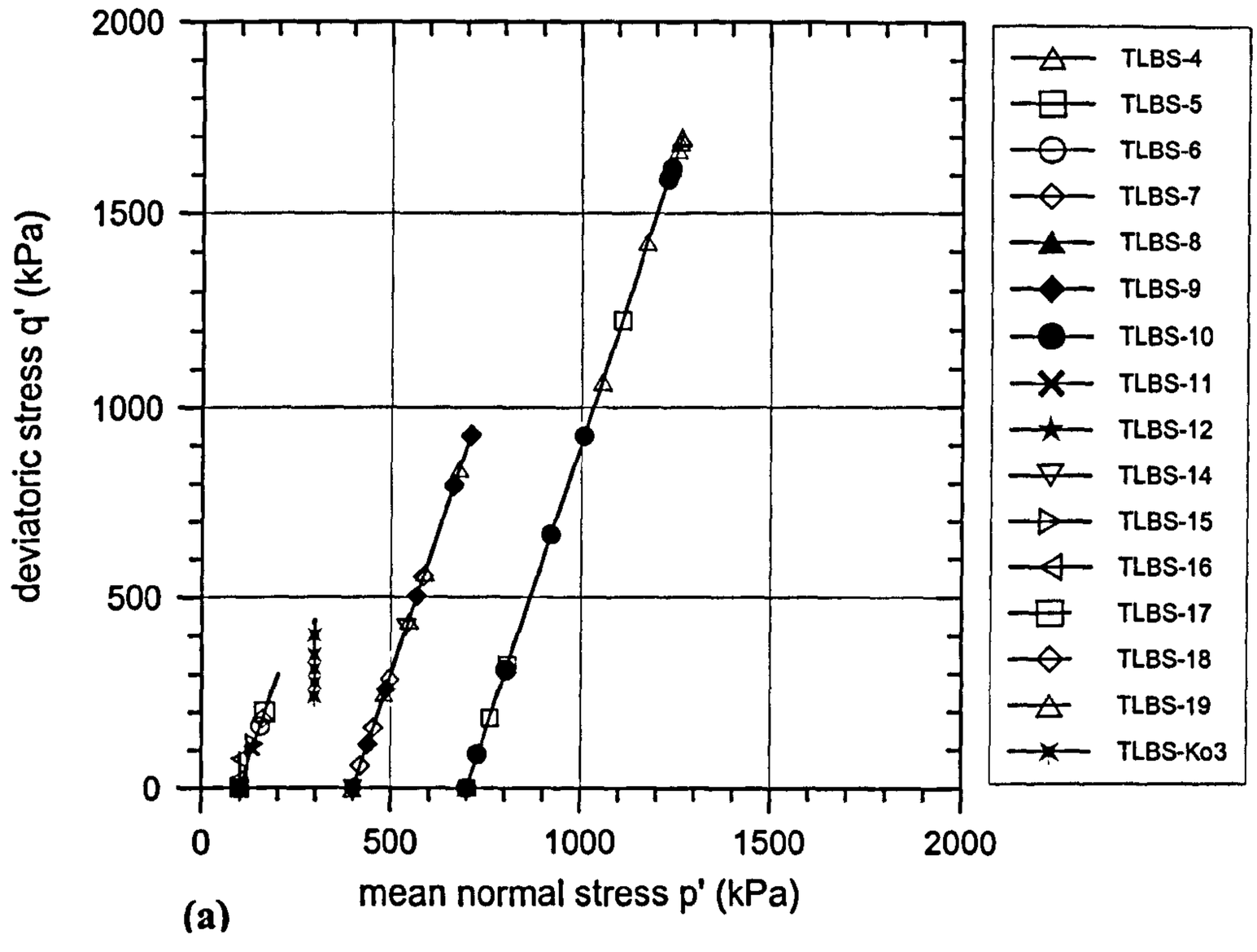

(a)

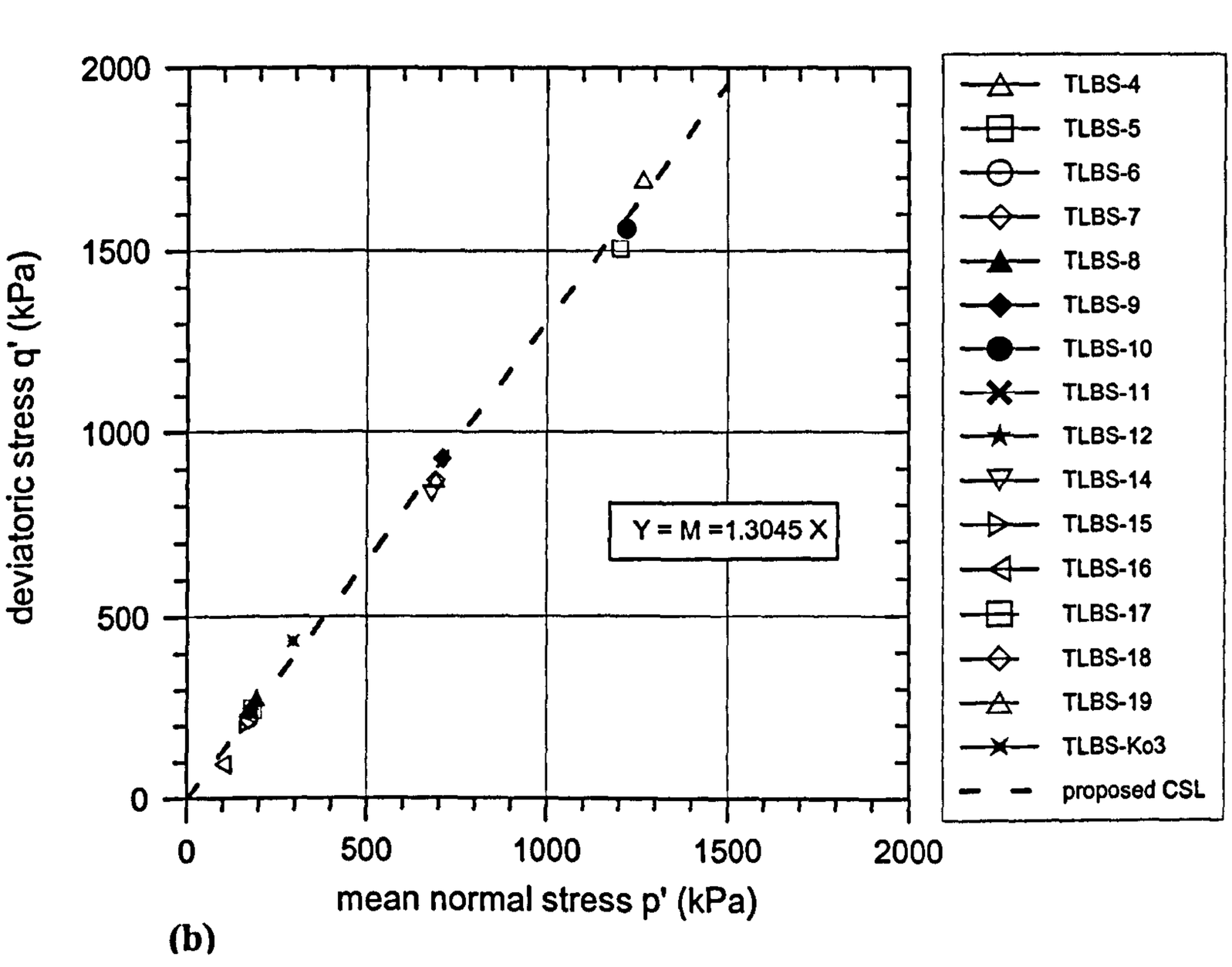

(b)

Figure 3-53: Stress paths (a) and end of test states and critical state line (b) for Leighton Buzzard sand.

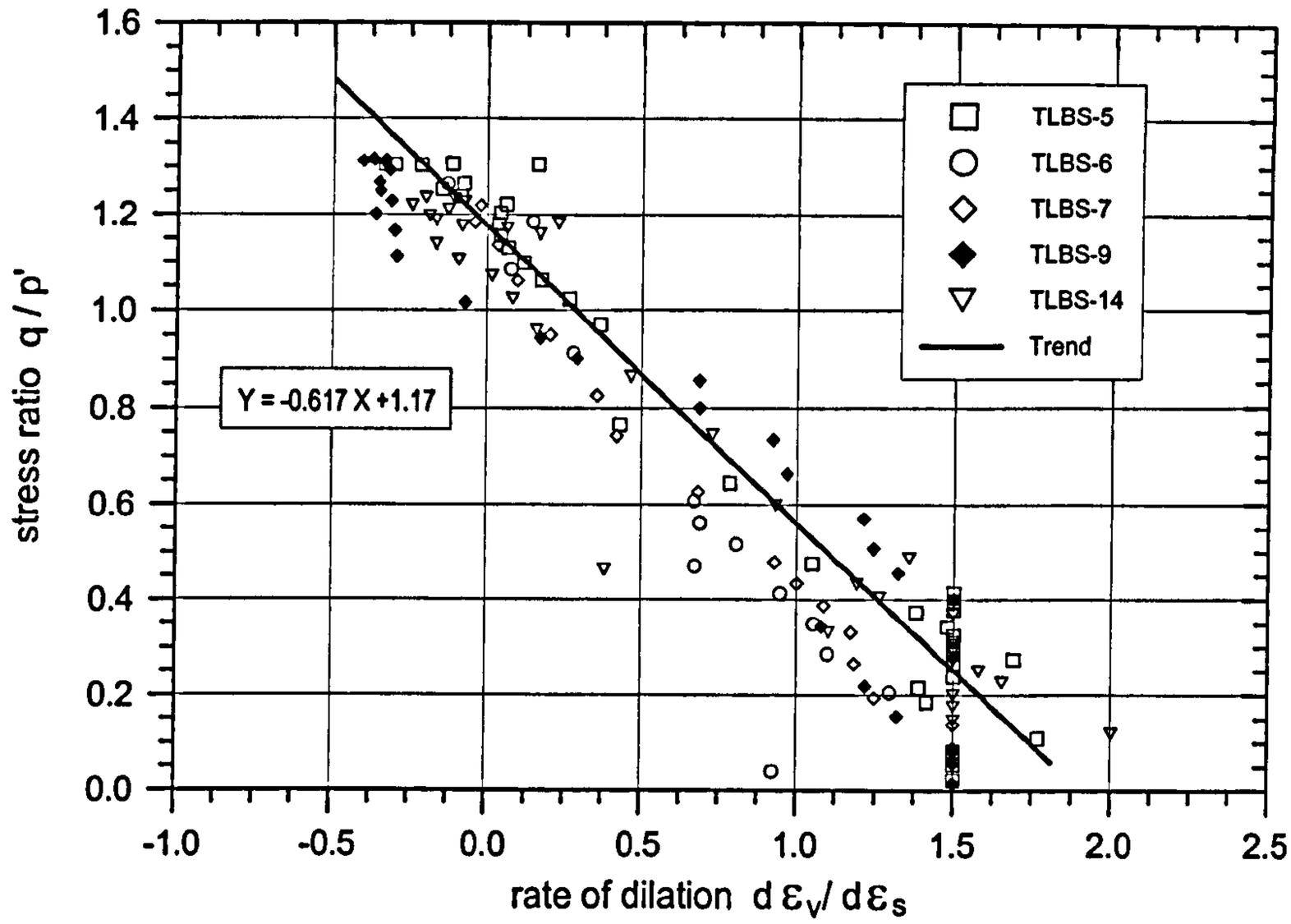

Figure 3-55: Typical stress-dilatancy relationship for Leighton Buzzard sand.

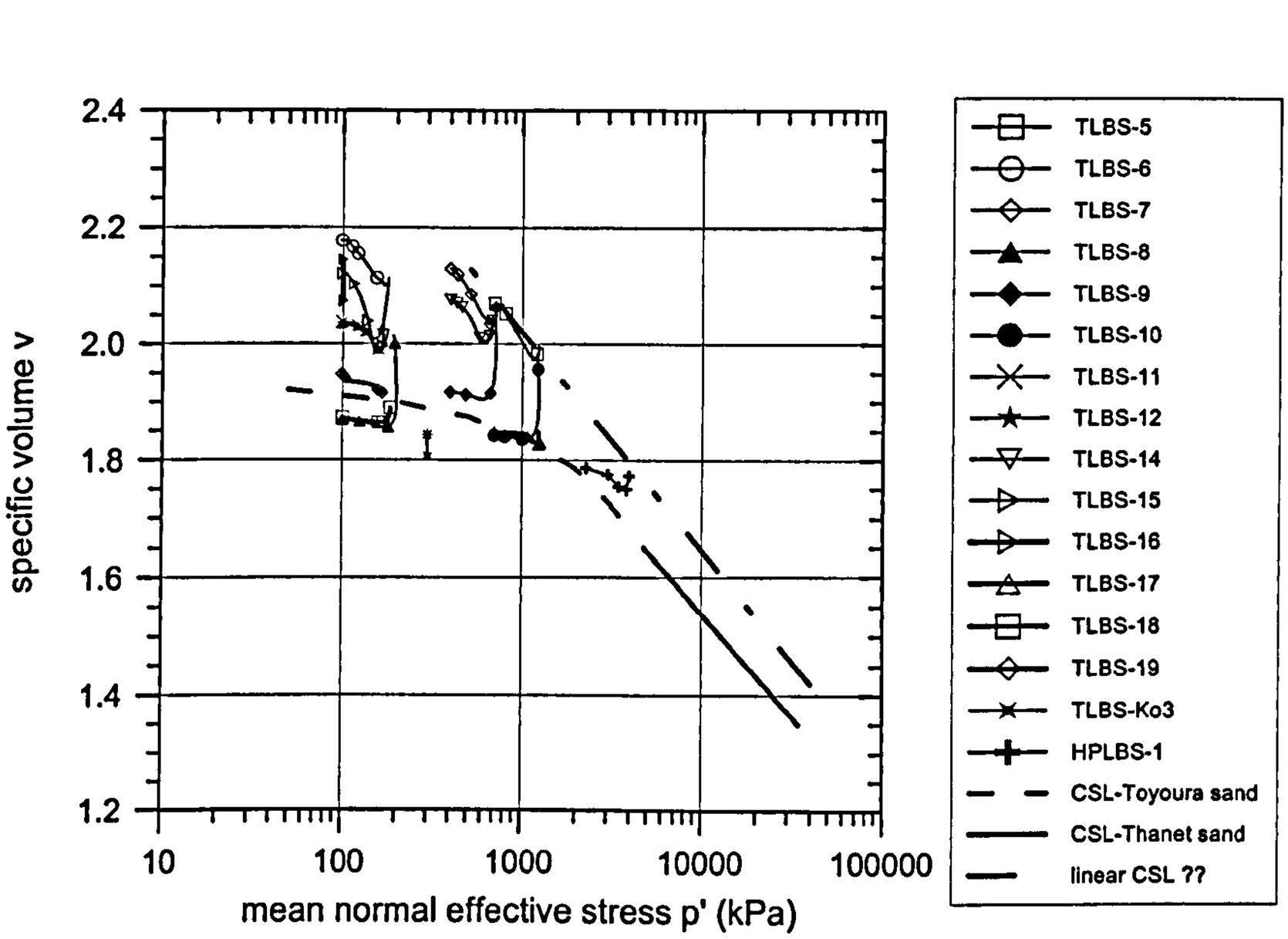

Figure 3-56: Stress-volume diagram for Leighton Buzzard sand during shearing.

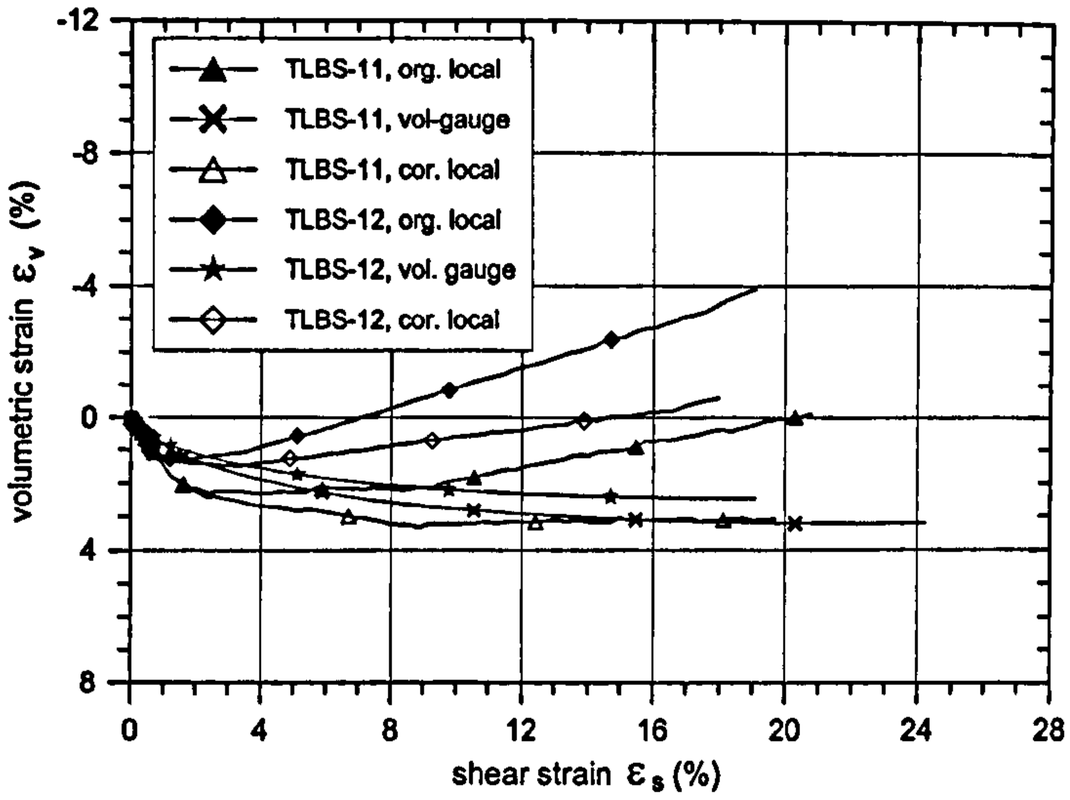

Figure 3-57: Difference between locally and globally measured strains during shearing of 1:1 samples of Leighton Buzzard sand. (org. = original, cor. = corrected)

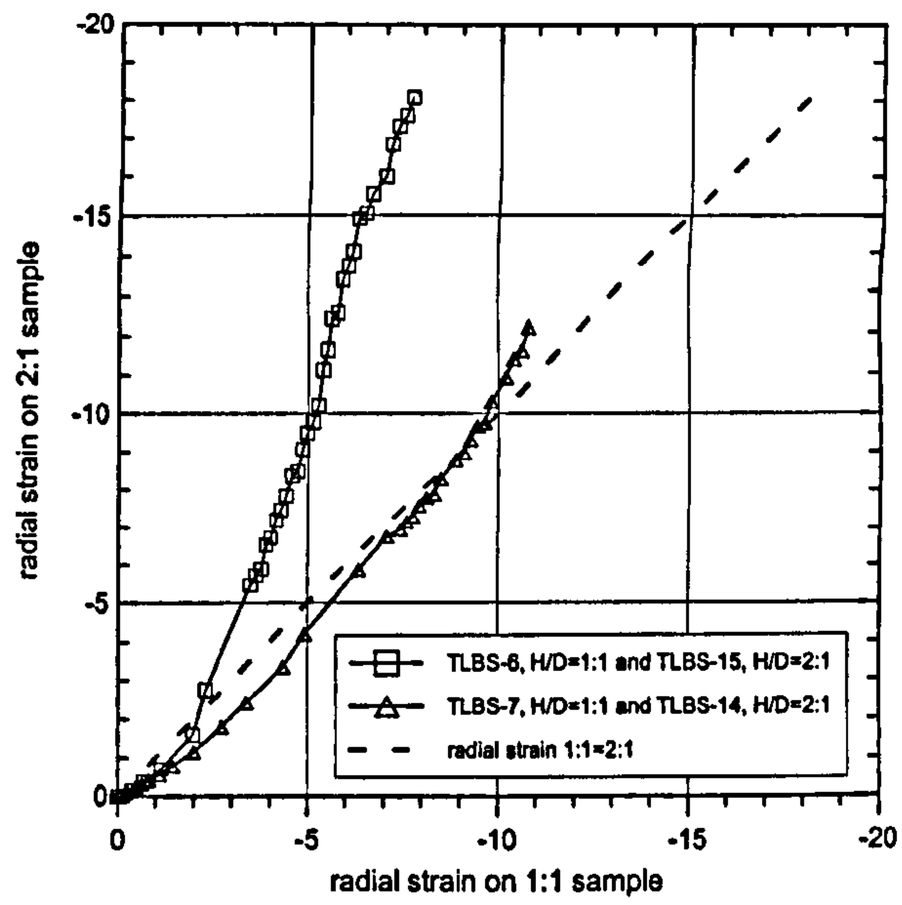

Figure 3-58: Effect of barrelling on measured local radial strains for samples of H/D = 1:1 and H/D = 2:1.

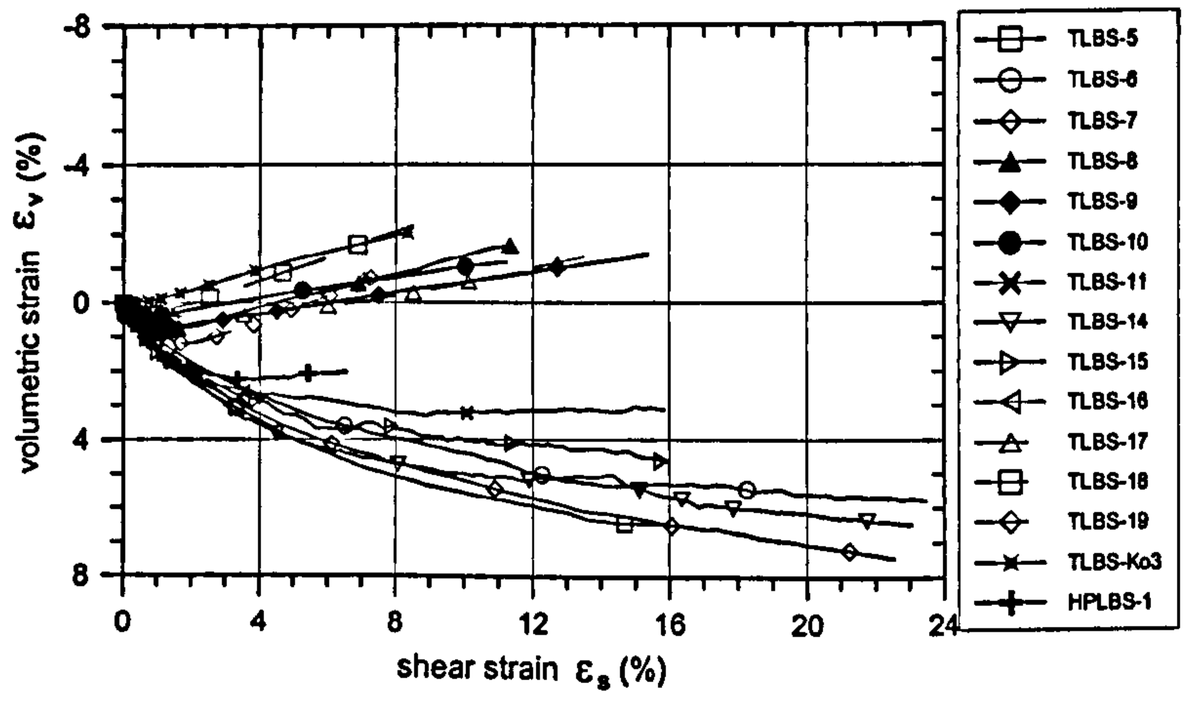

Figure 3-59: Corrected strain data during shearing taking account of barrelling effect, with estimated non-homogeneous strain regions deleted.

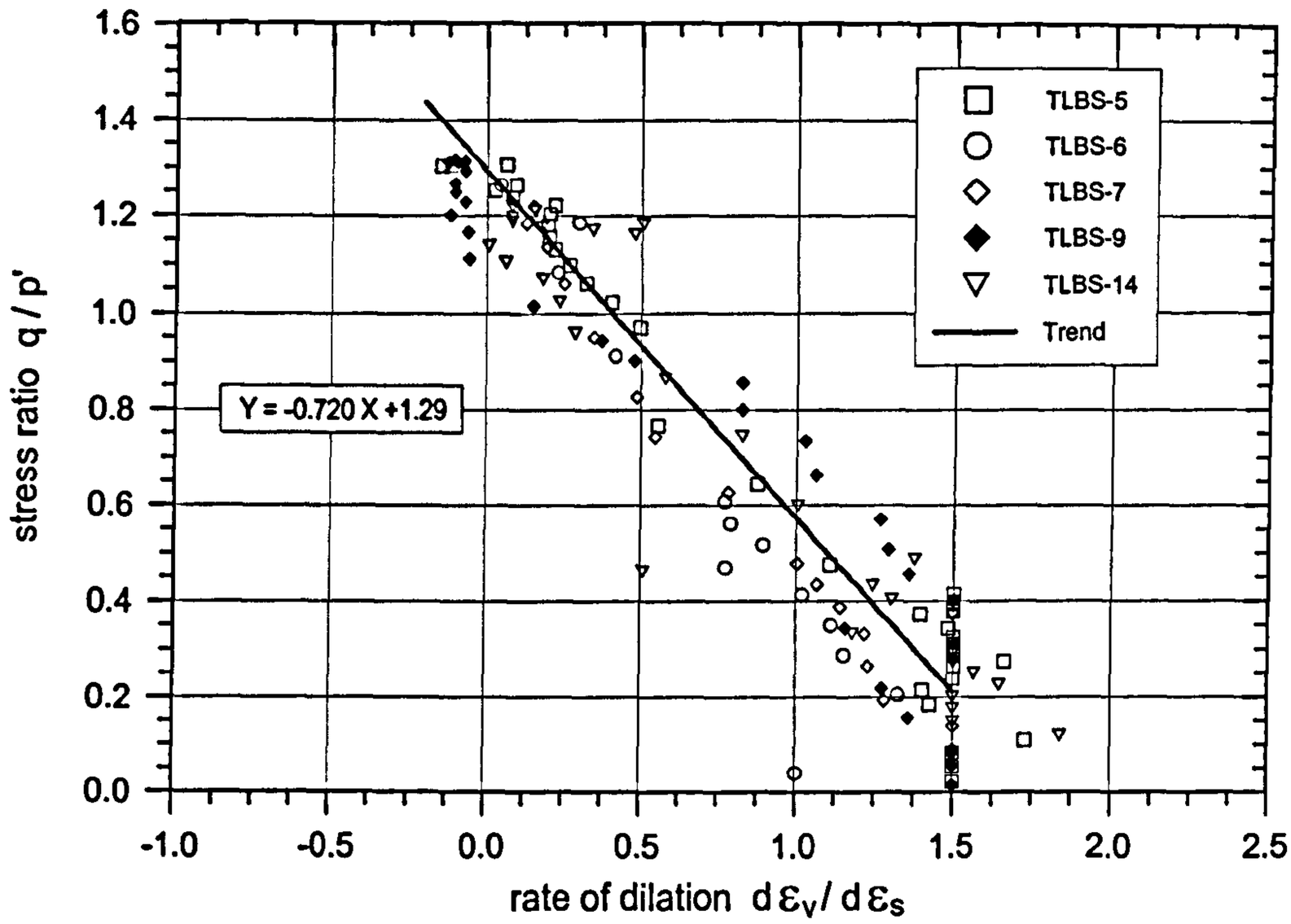

Figure 3-60: Final stress-dilatancy relationship for Leighton Buzzard sand.

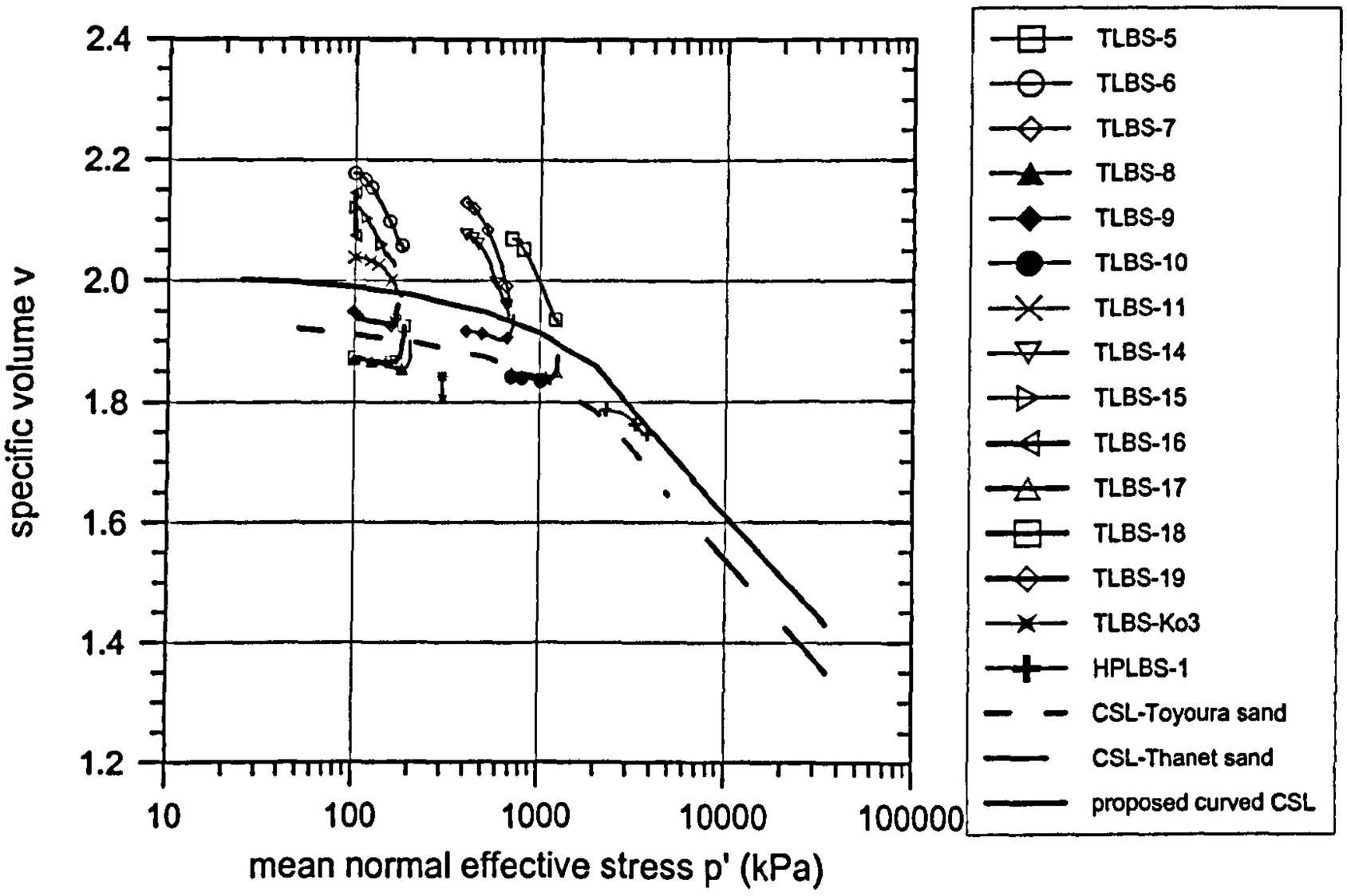

Figure 3-61: Final stress-volume diagram and proposed critical state line for Leighton Buzzard sand.

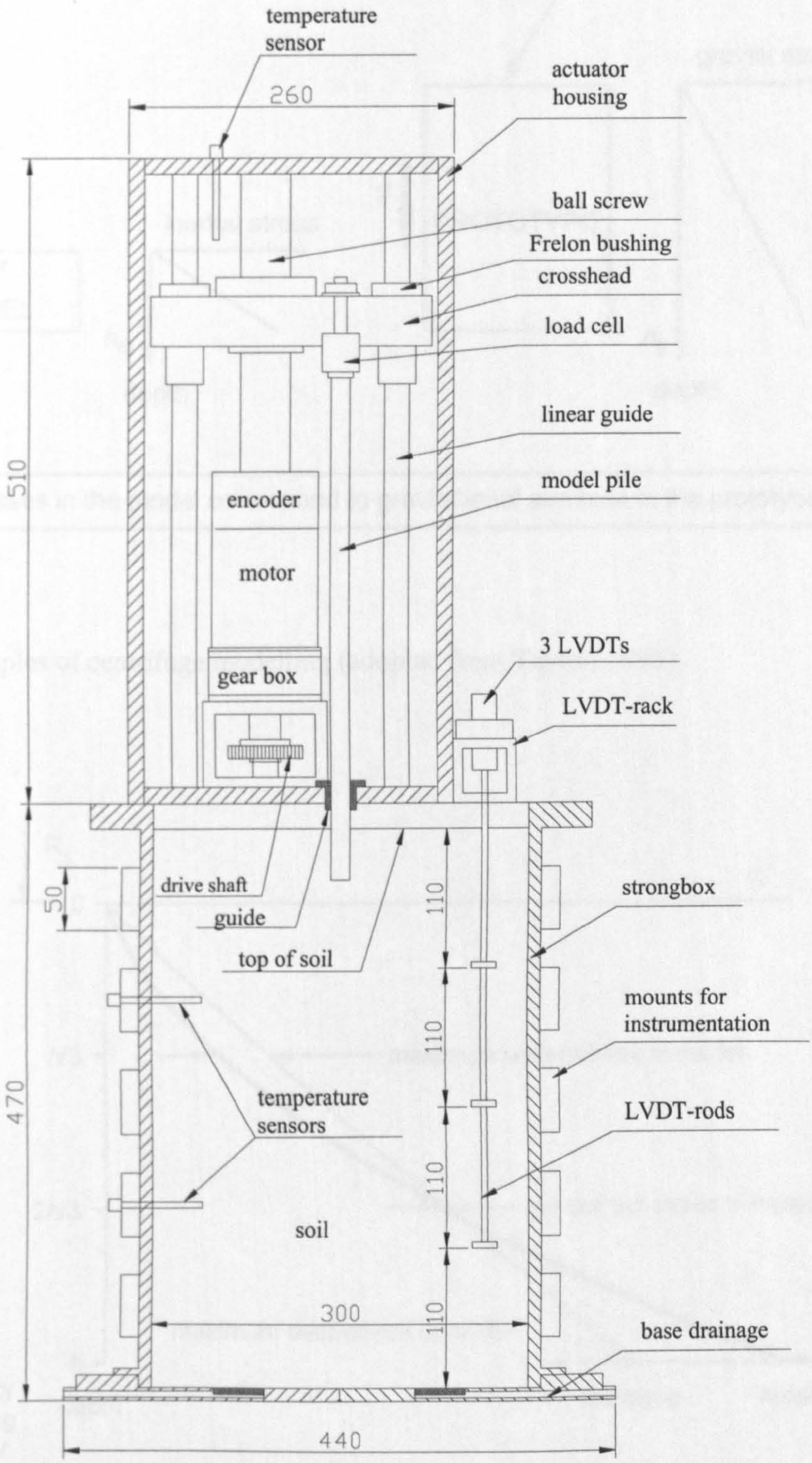

Figure 4-1: Actuator and strongbox assembly (all dimensions in mm).

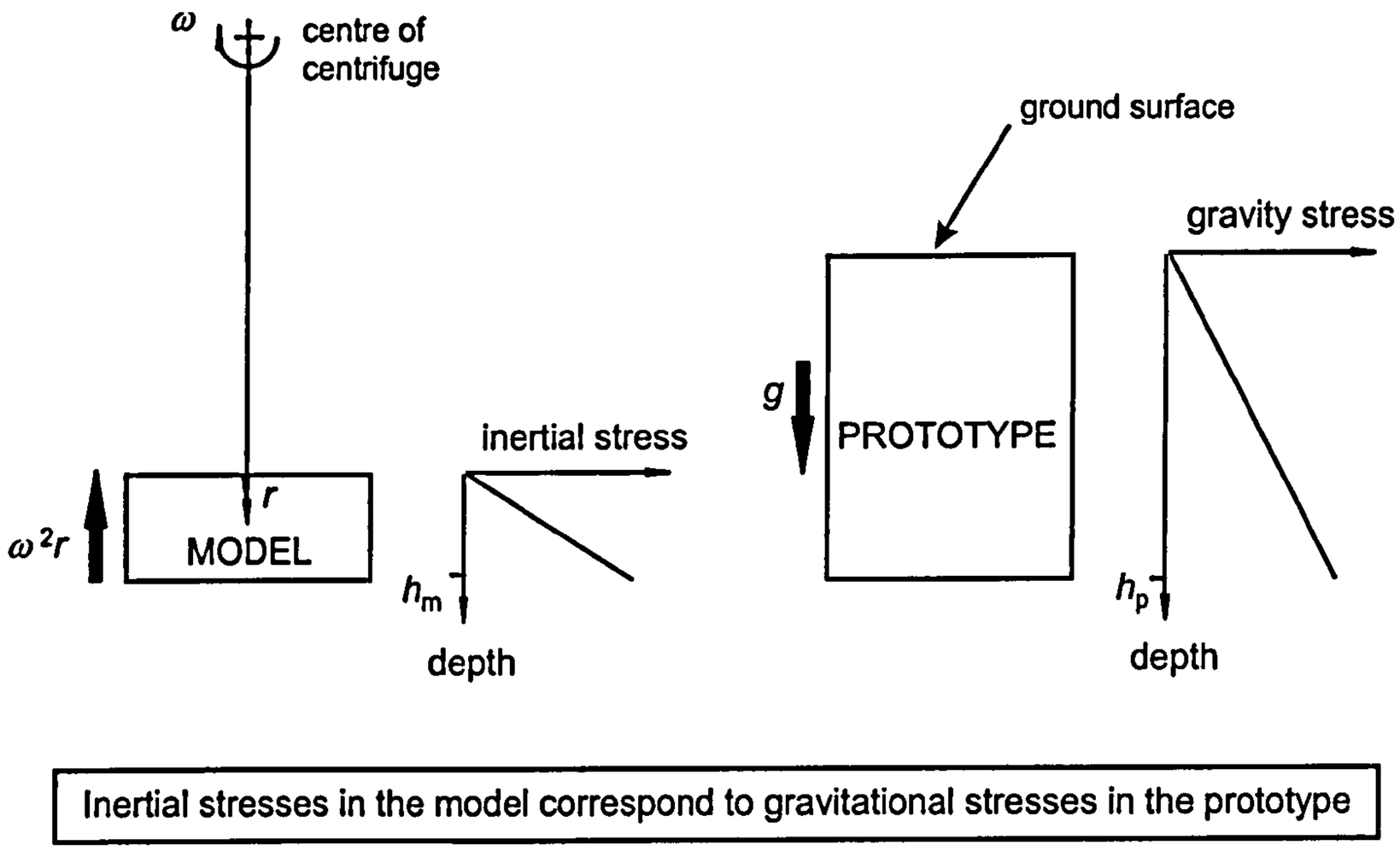

Figure 4-2: Principles of centrifuge modelling (adopted from Taylor, 1995).

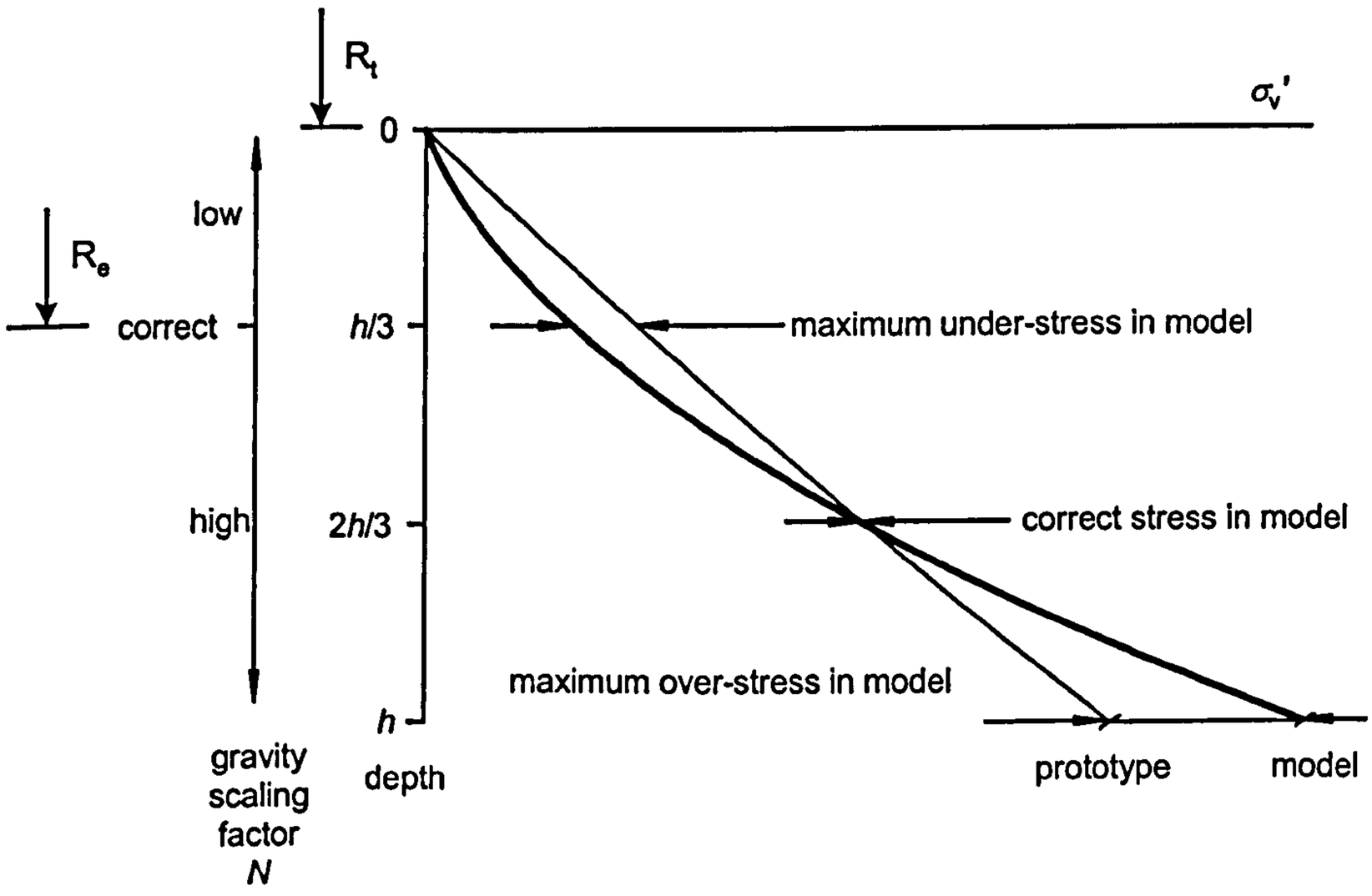

Figure 4-3: Comparison of stress variation with depth in a centrifuge model and its corresponding prototype (after Taylor, 1995).

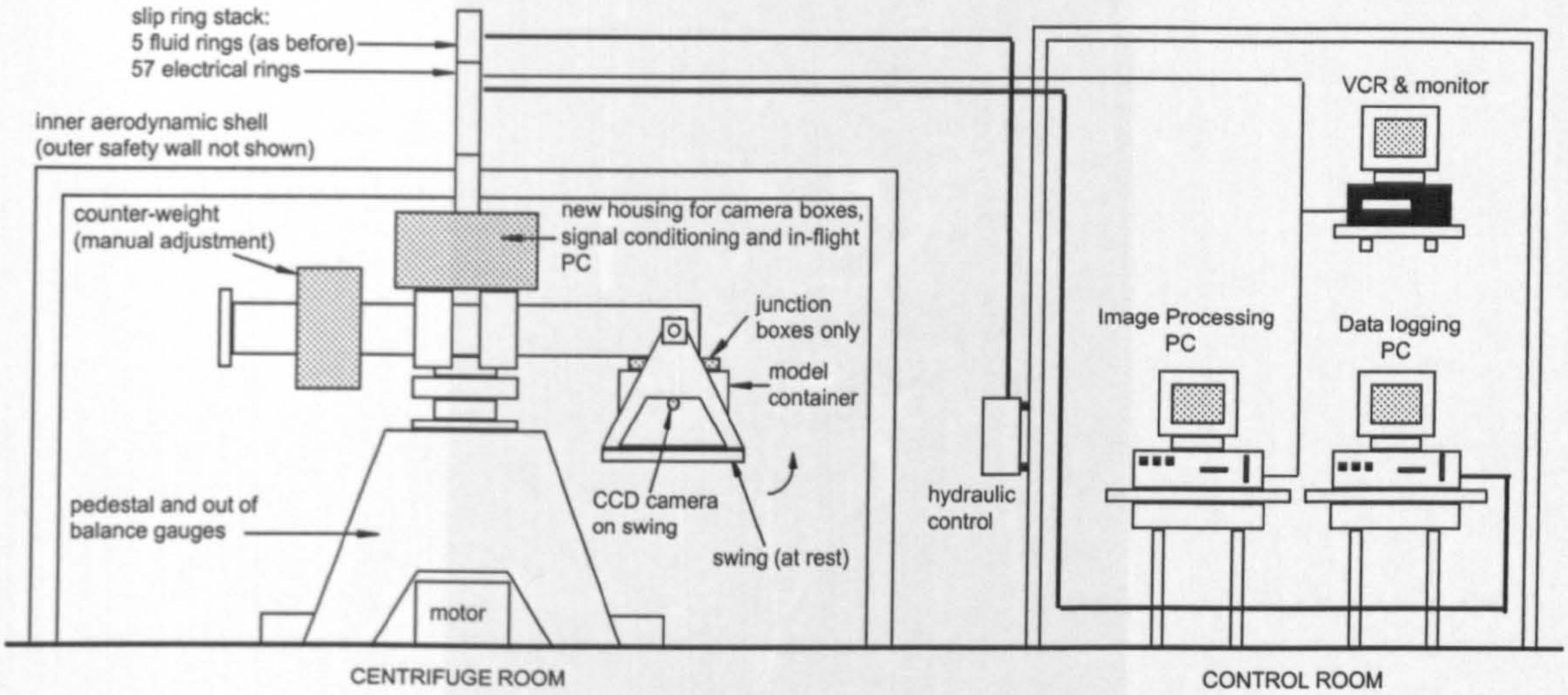

Figure 4-4: Schematic of City University centrifuge facility (after Grant, 1998).

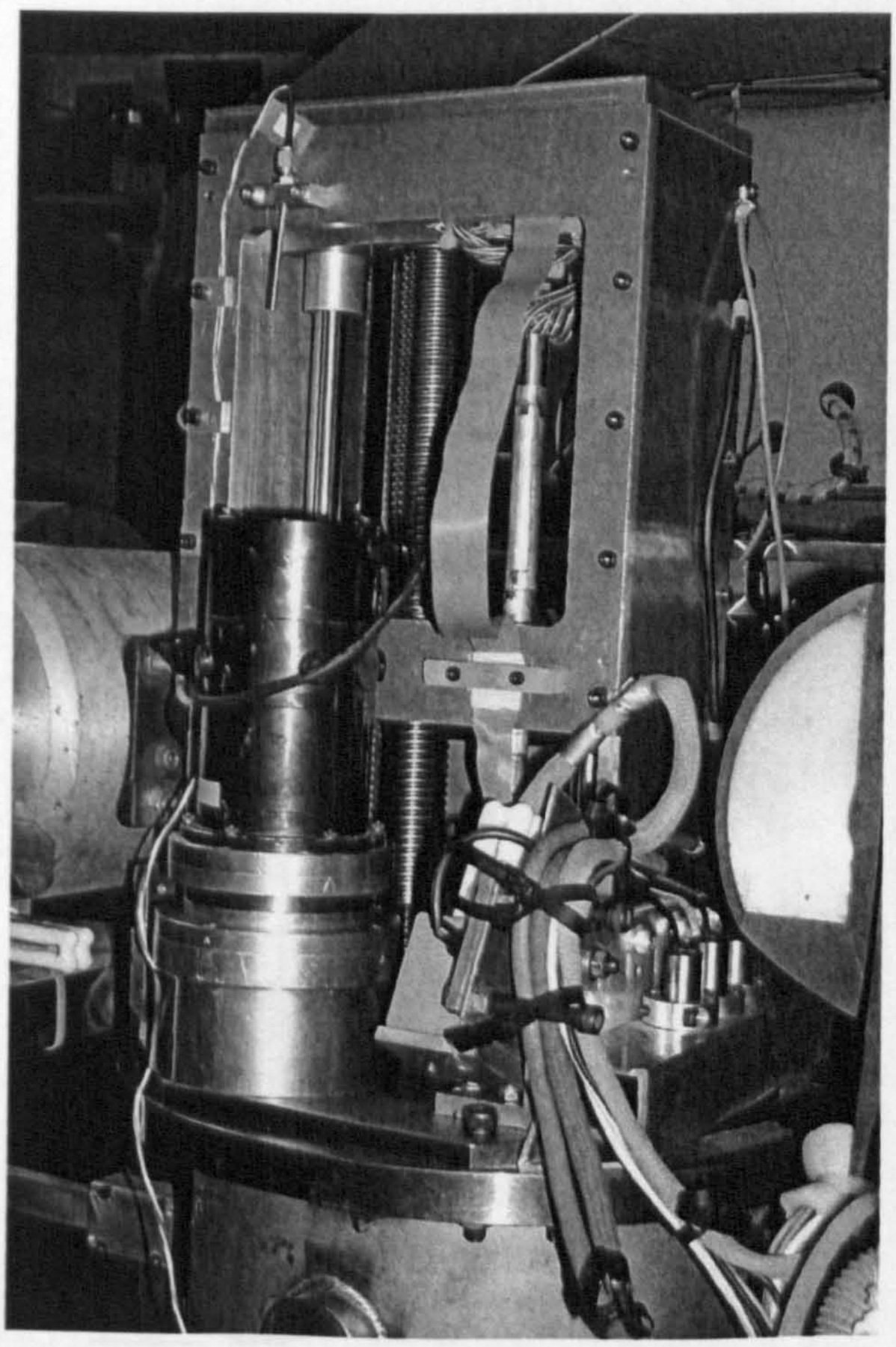

Figure 4-5: Fully assembled actuator on the centrifuge platform.

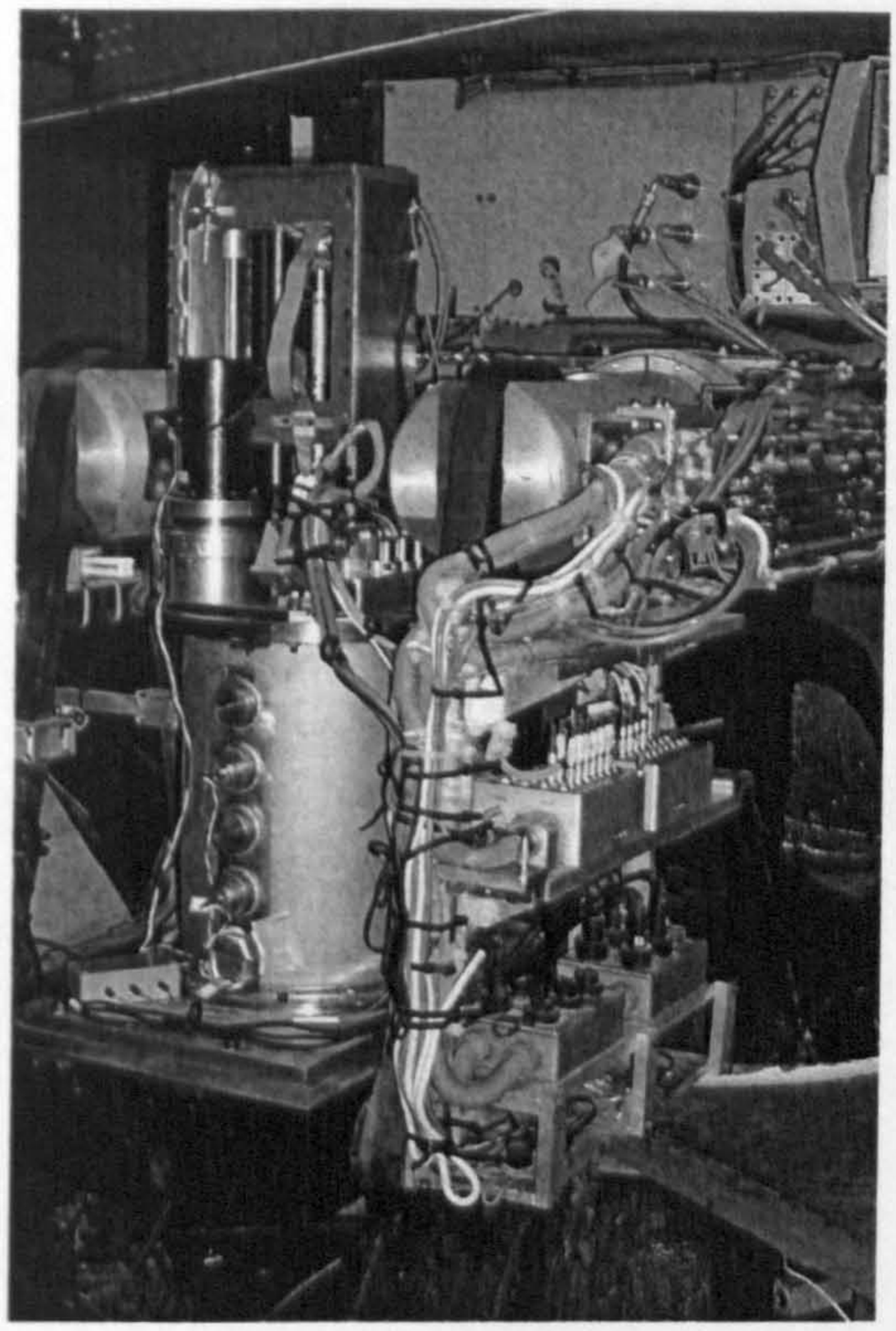

Figure 4-6: Fully assembled model on the centrifuge.

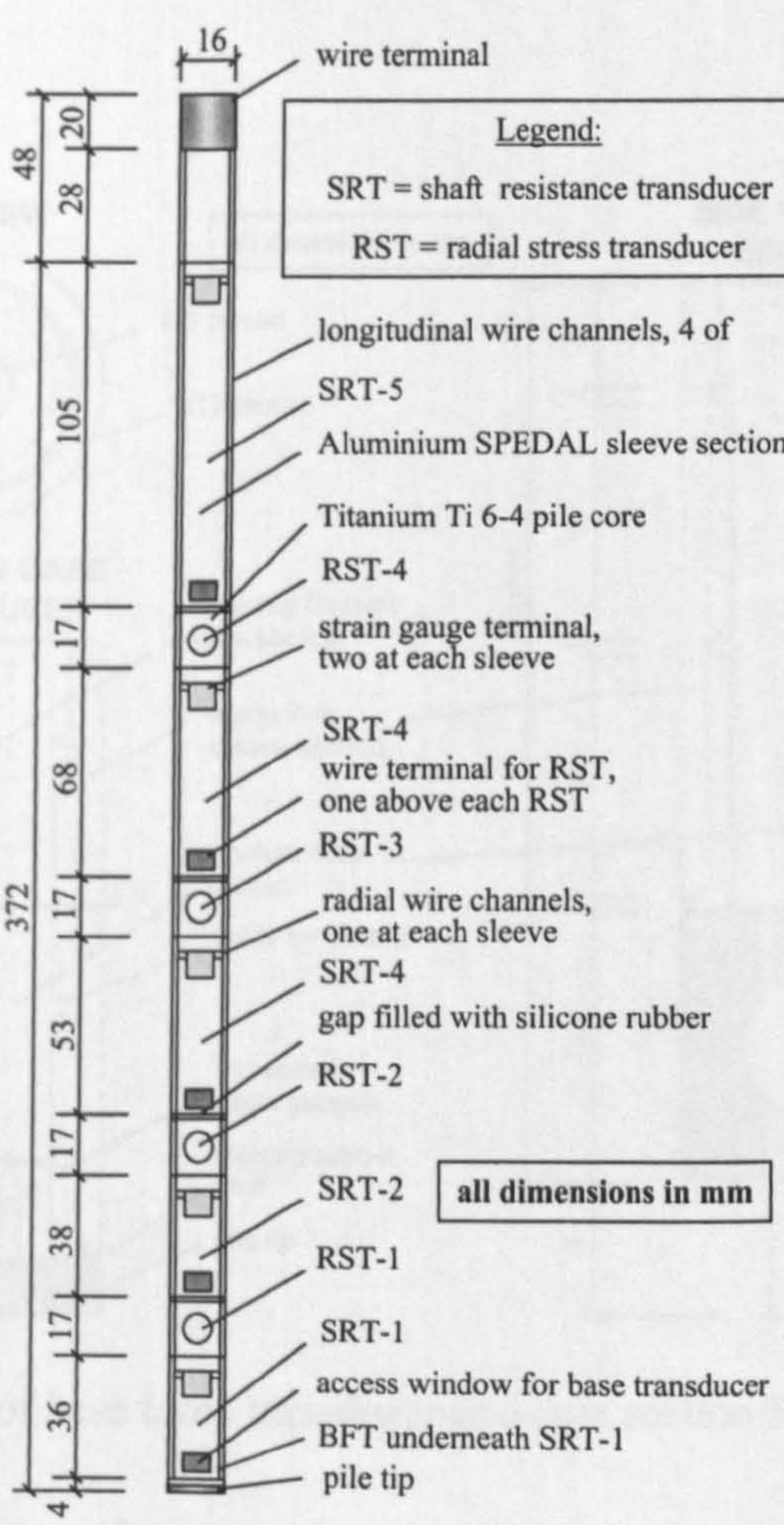

Figure 4-7: Schematic of the instrumented model piles CUIMP-2 to CUIMP-4.

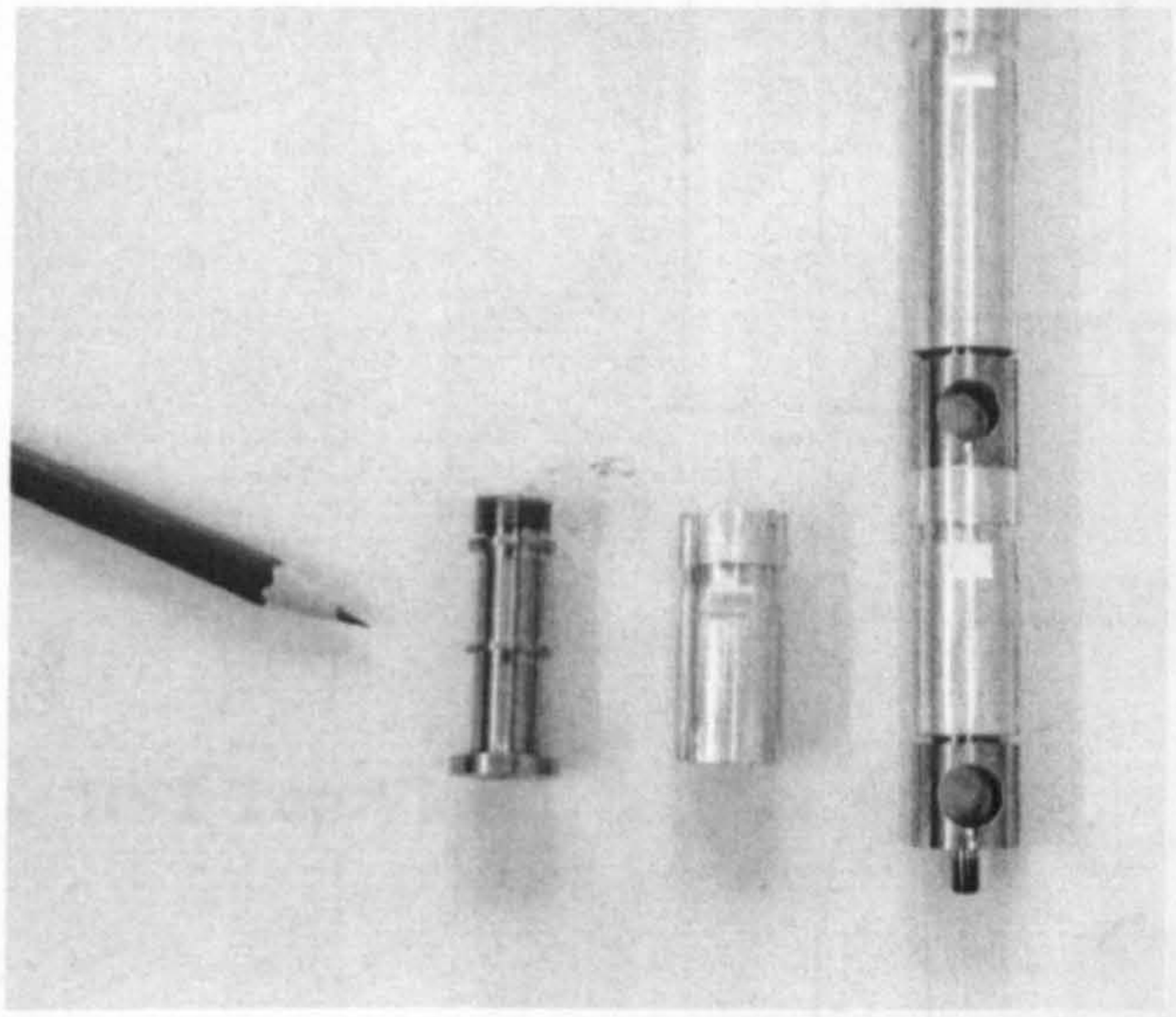

Segments of BFT and SRT-1 prior to pile assembly

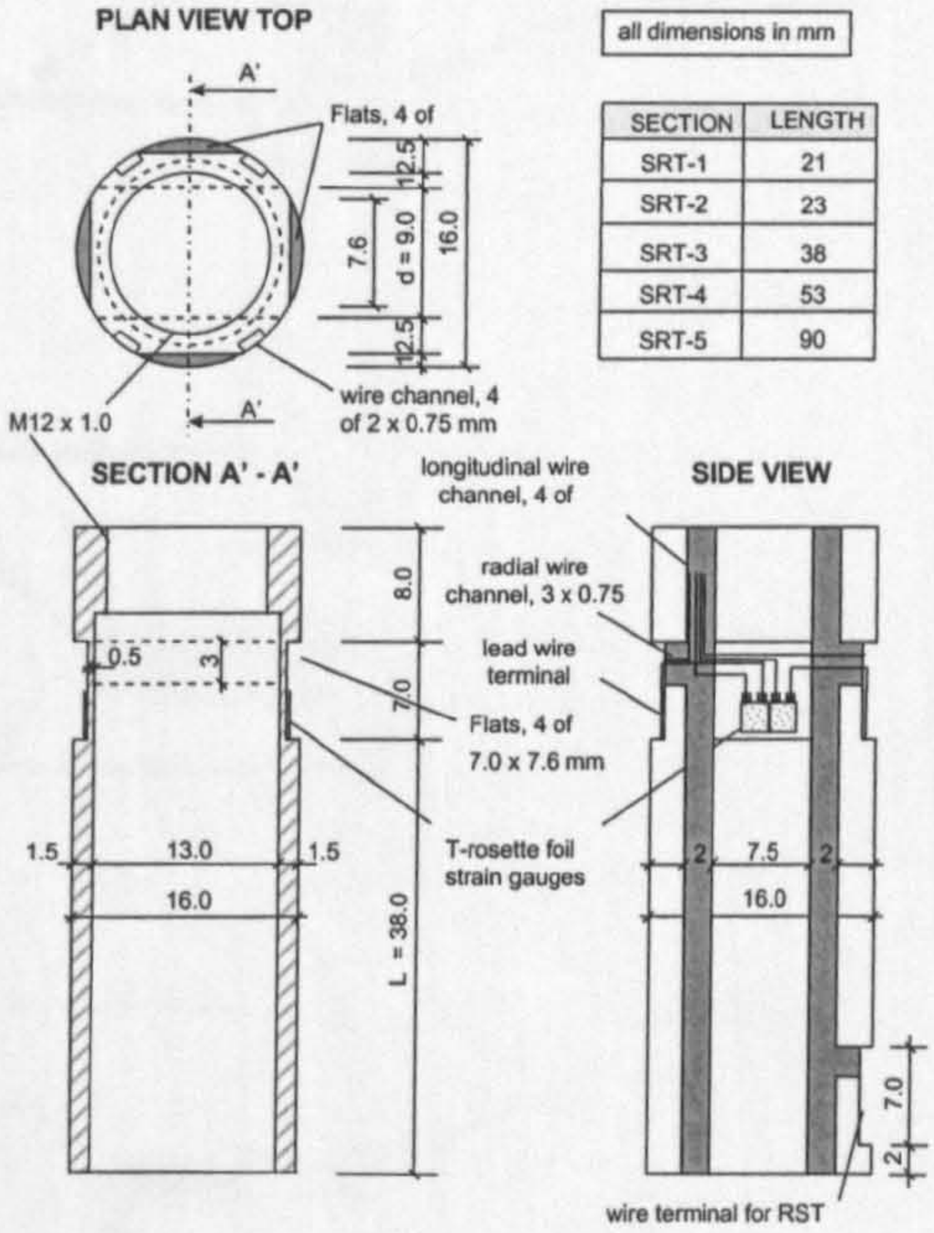

SECTION	LENGTH
SRT-1	21
SRT-2	23
SRT-3	38
SRT-4	53
SRT-5	90

Detail of friction sleeve

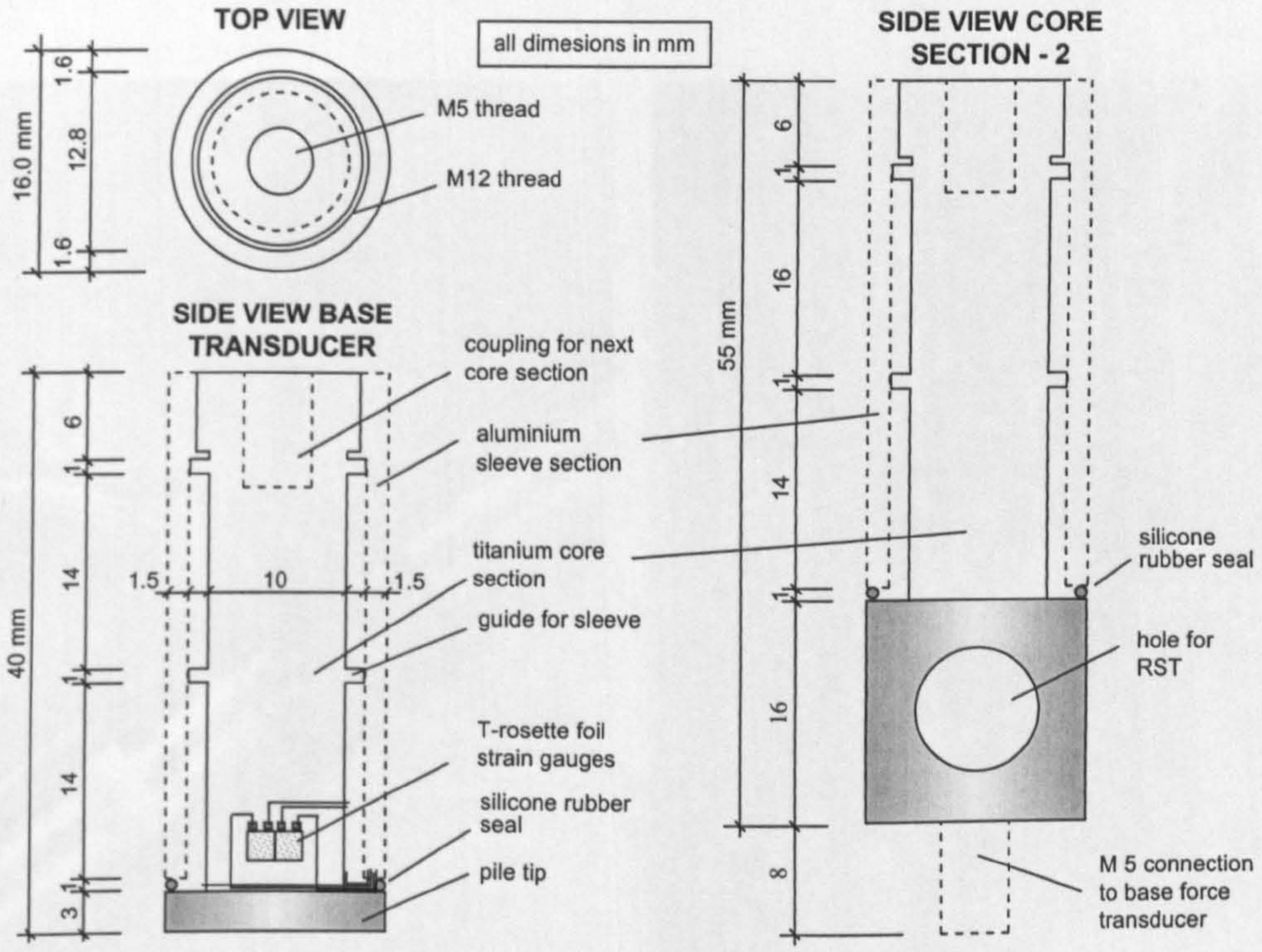

Detail of base force transducer and core section for SRT-2

Figure 4-8: Details of the base force transducer and friction sleeves of piles CUIMP- 2 to CUIMP-4.

RST Side View

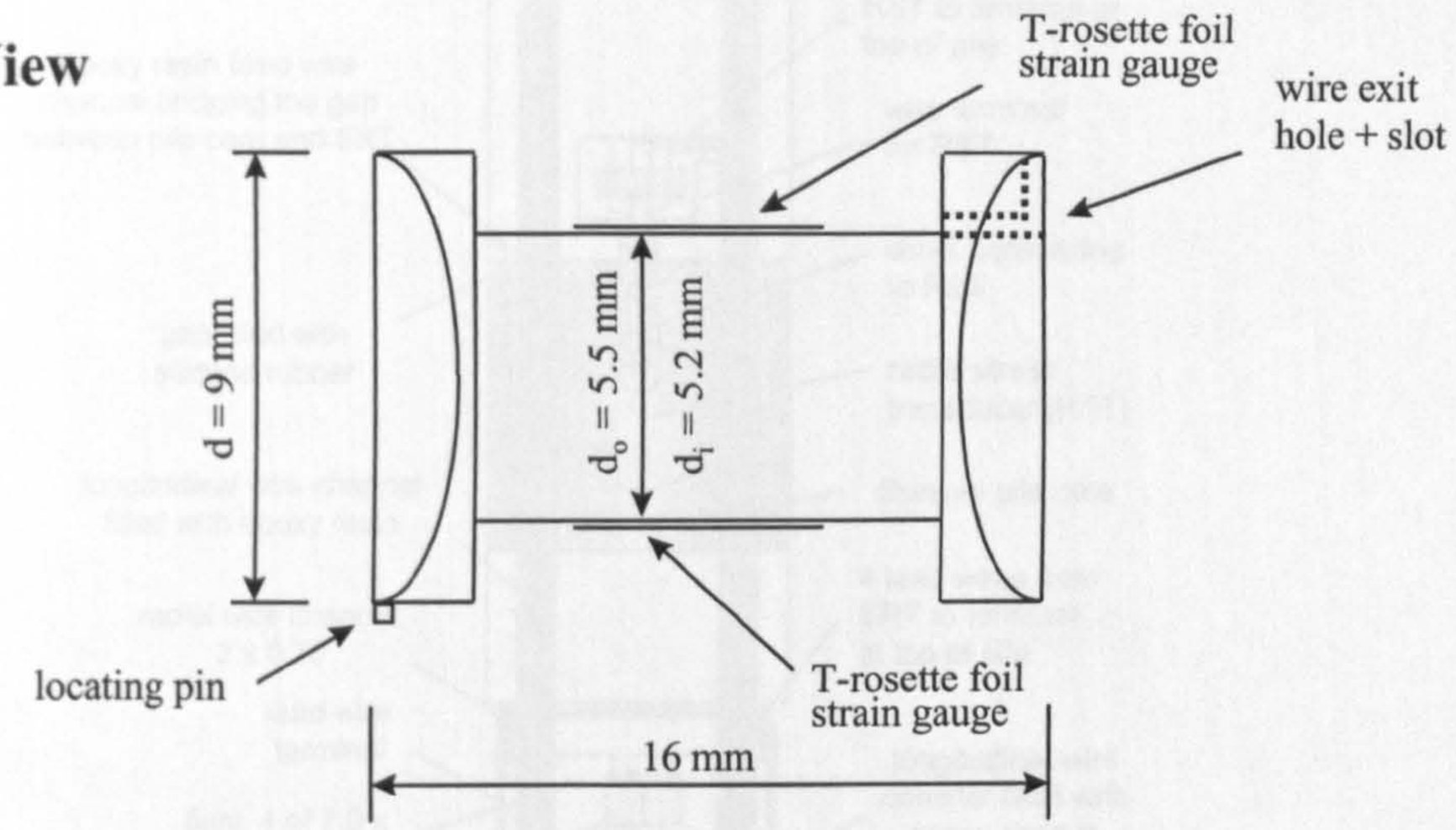

RST Top View

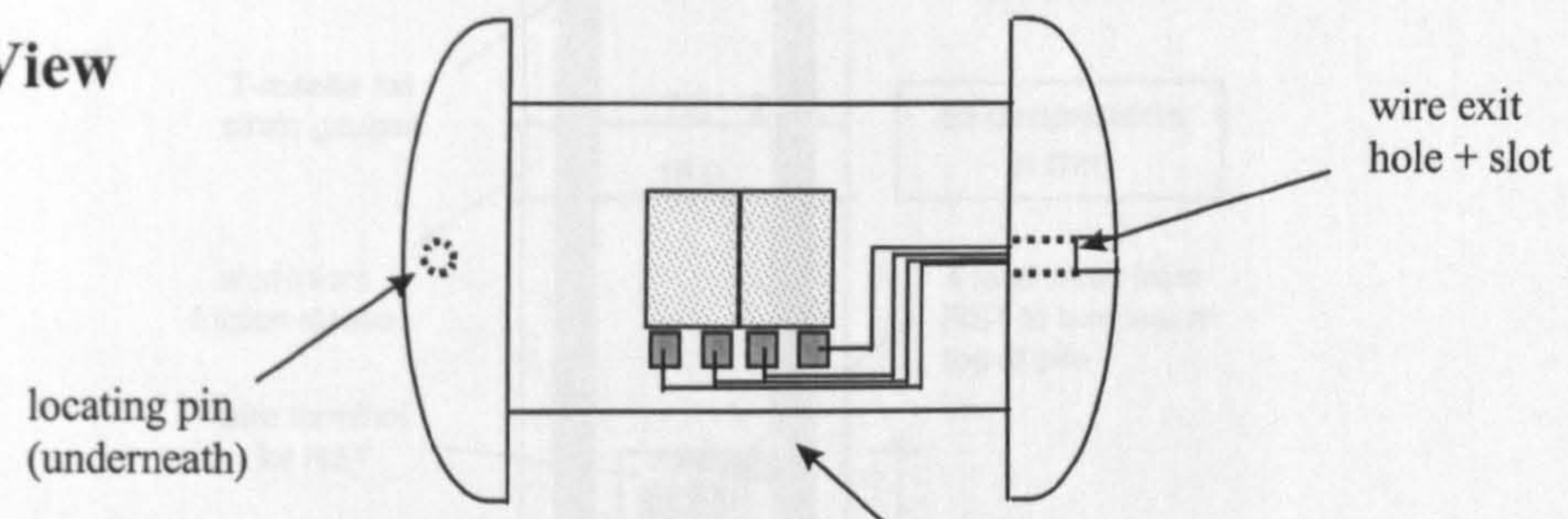

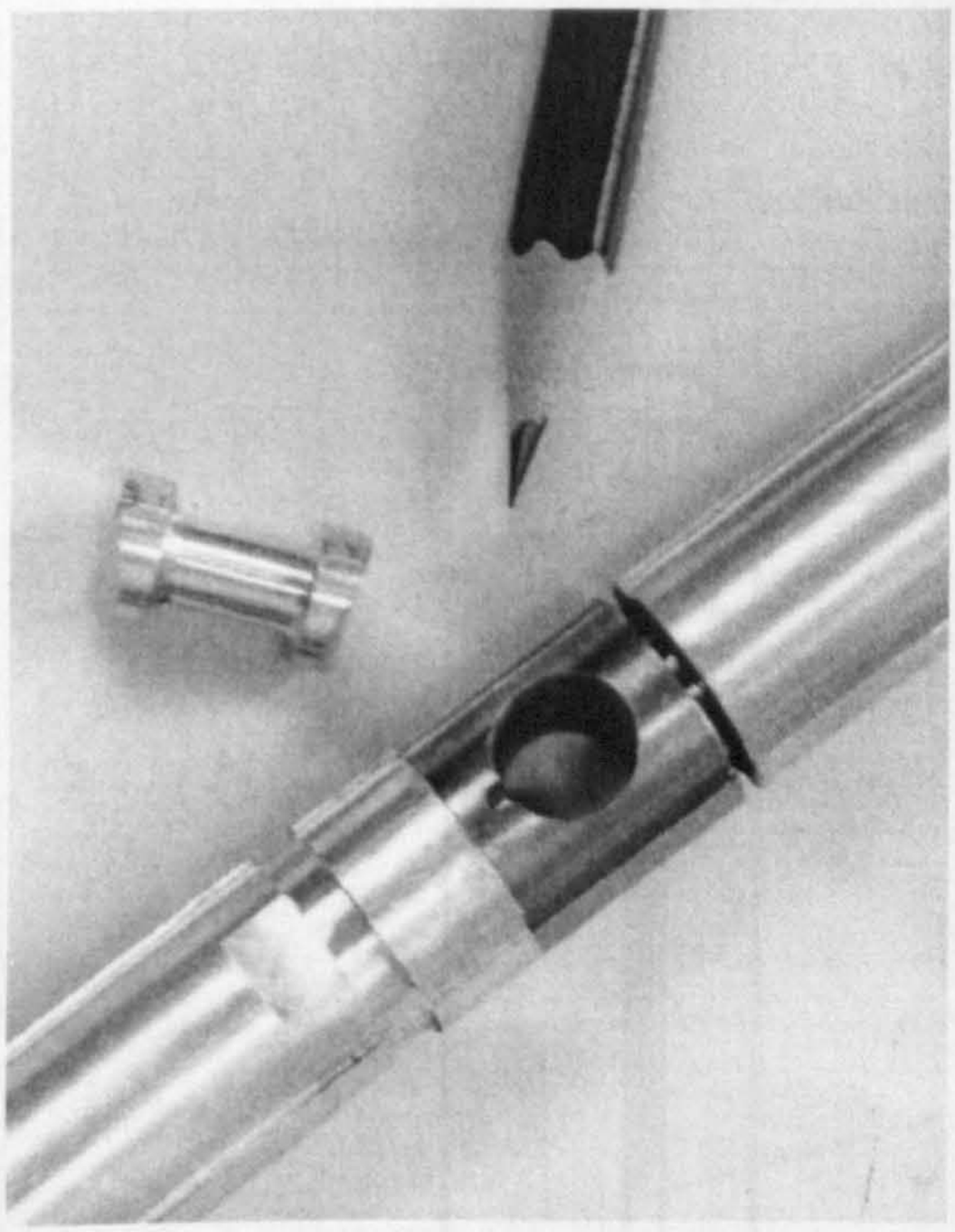

Dumb-bell prior to strain gauging

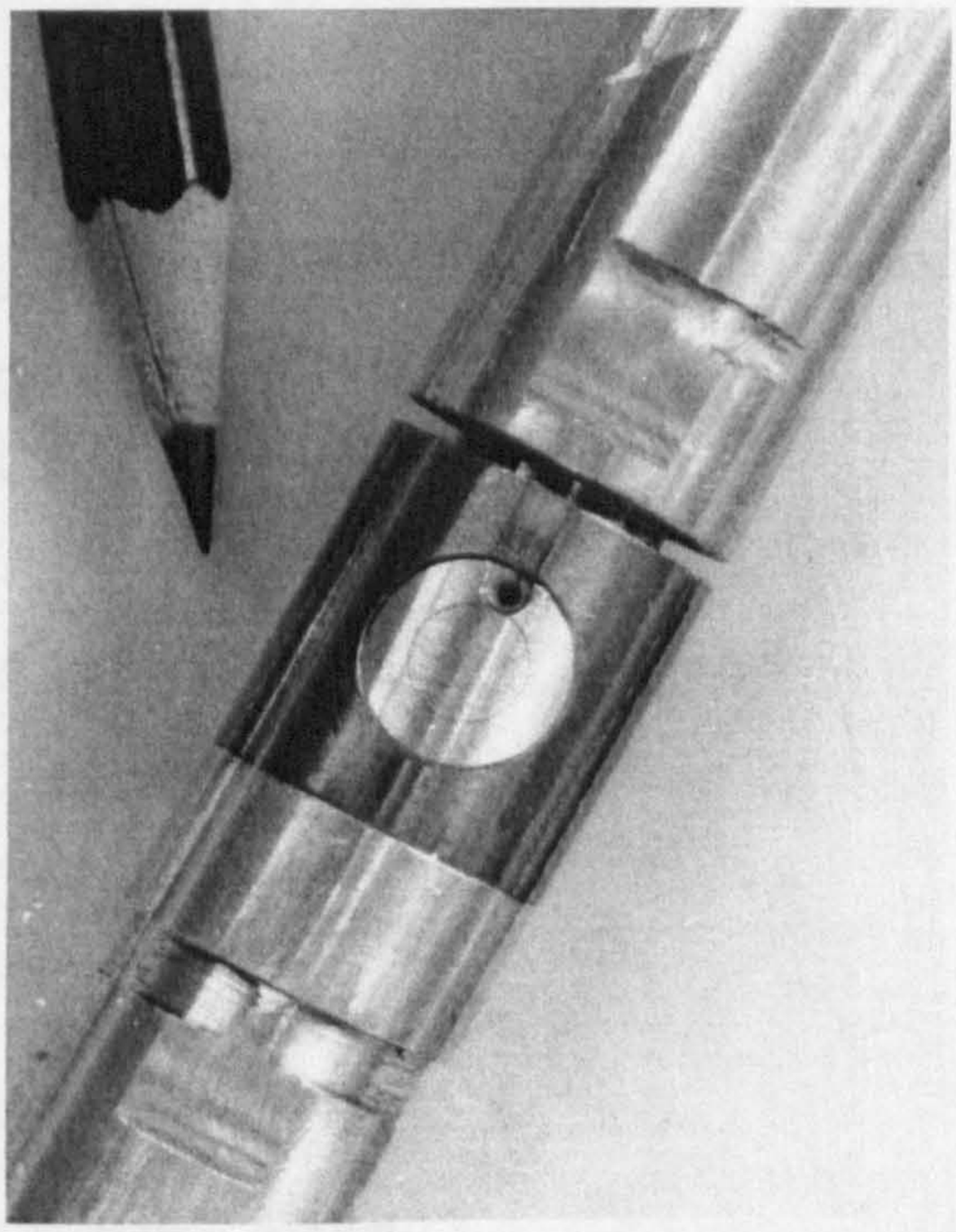

Dumb-bell inserted into the pile core

Figure 4-9: Detail of the radial stress transducer of piles CUIMP- 2 to CUIMP-4.

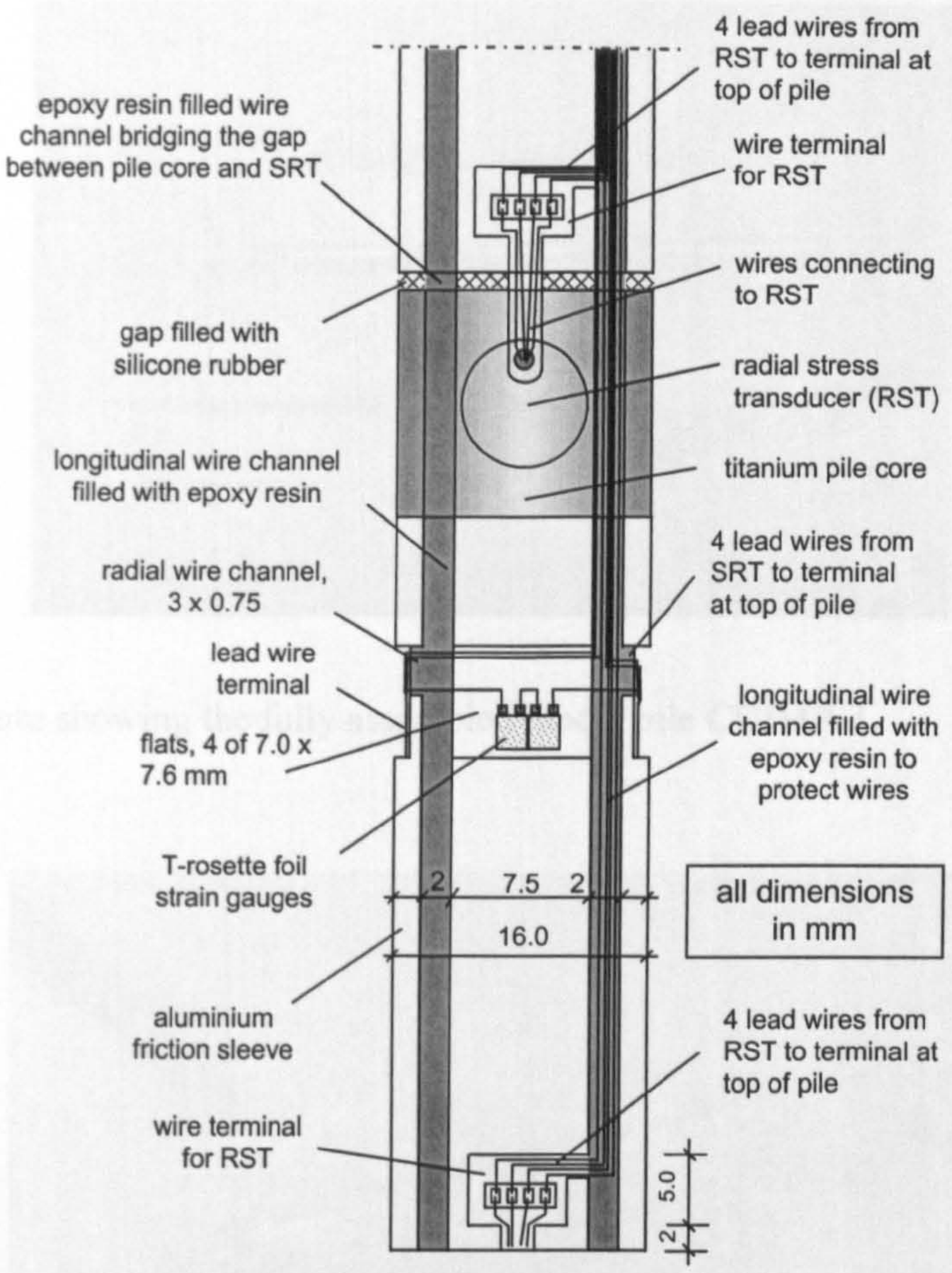

Figure 4-10: Detail of the wiring scheme on CUIMP-2 to CUIMP-4 (epoxy filling of radial wire channels and gauge and lead wires terminal flats is not shown).

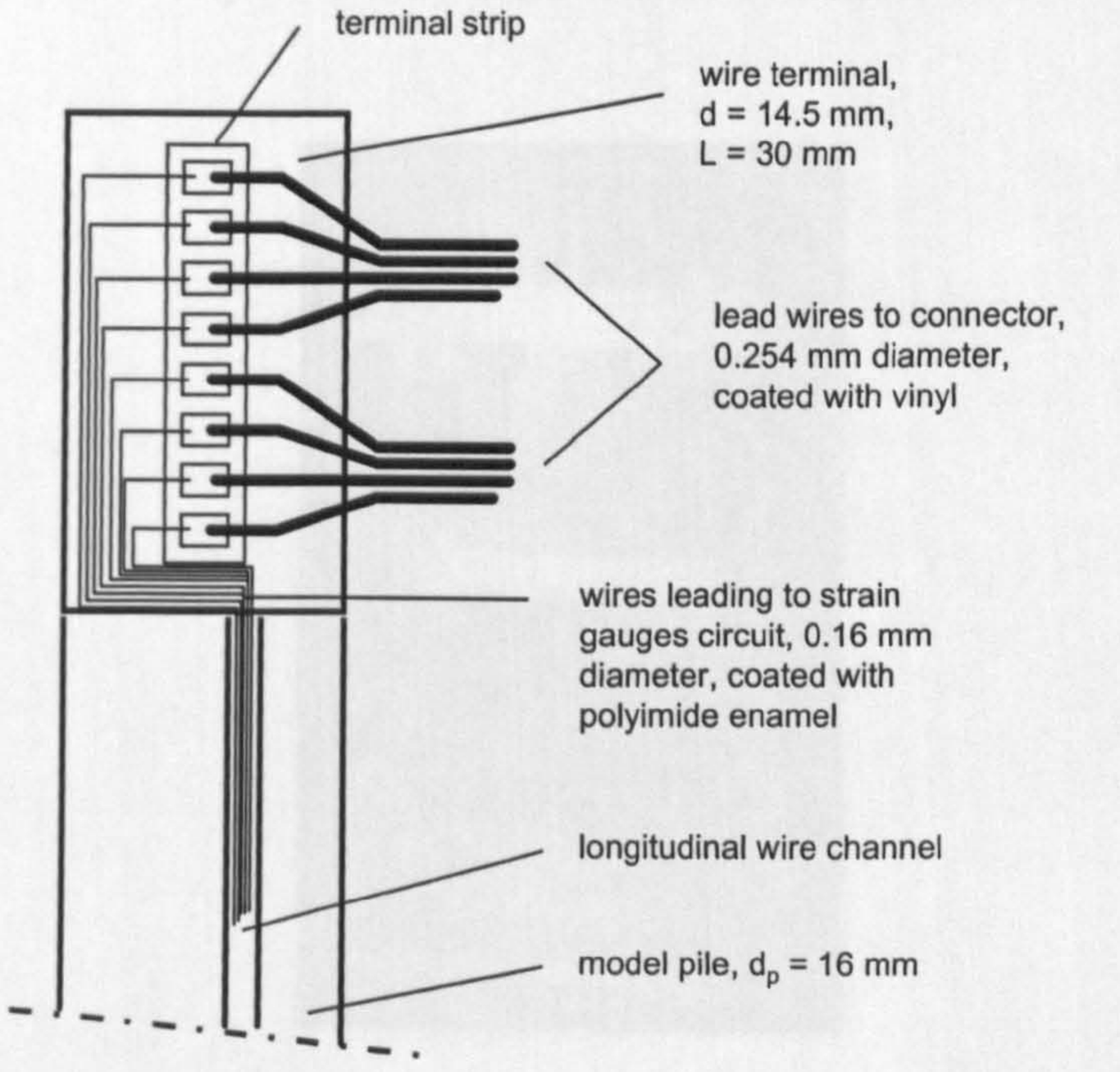

Figure 4-11: Detail of a typical wire terminal at the top of pile CUIMP-3.

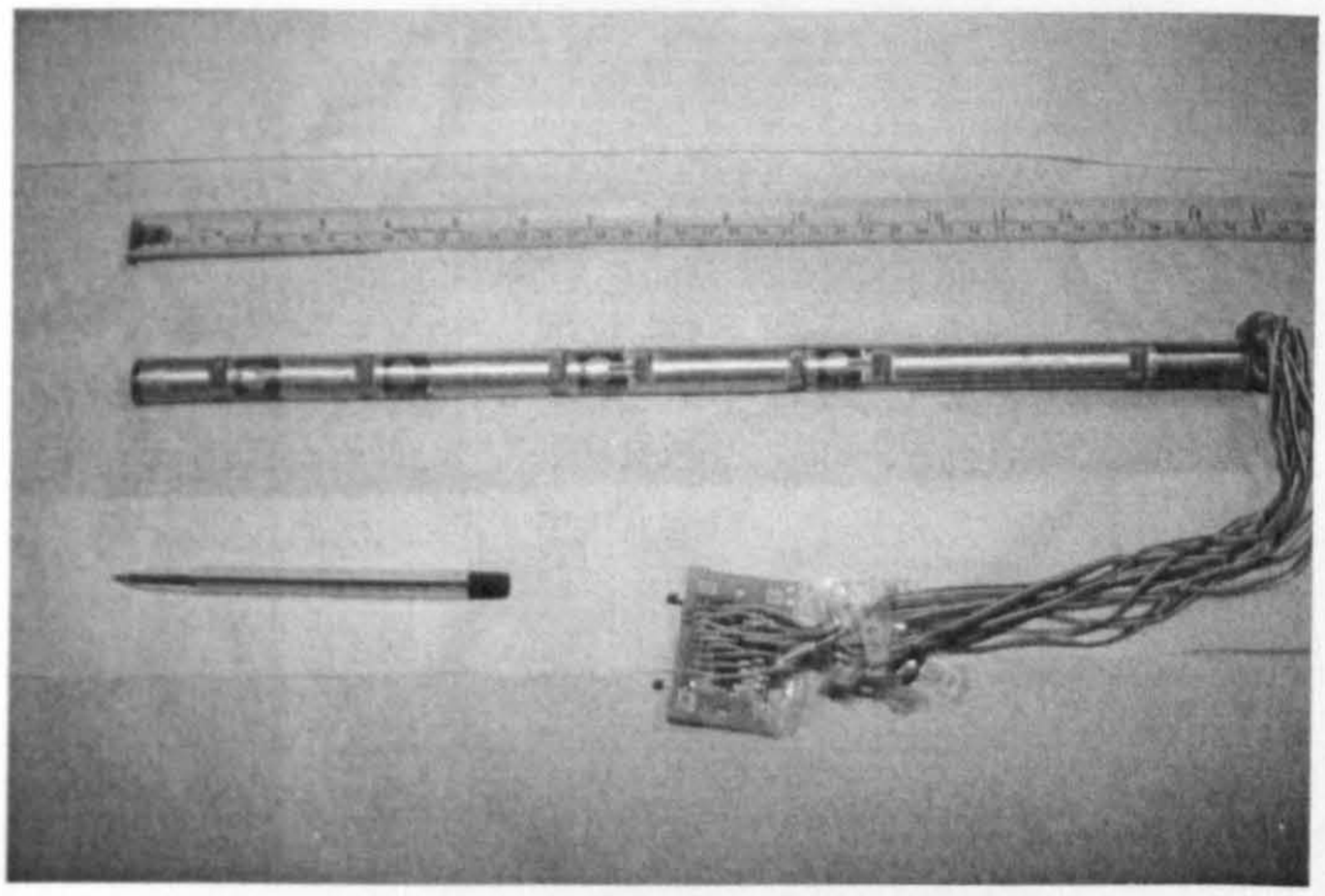

Figure 4-12: Picture showing the fully assembled model pile CUIMP-3.

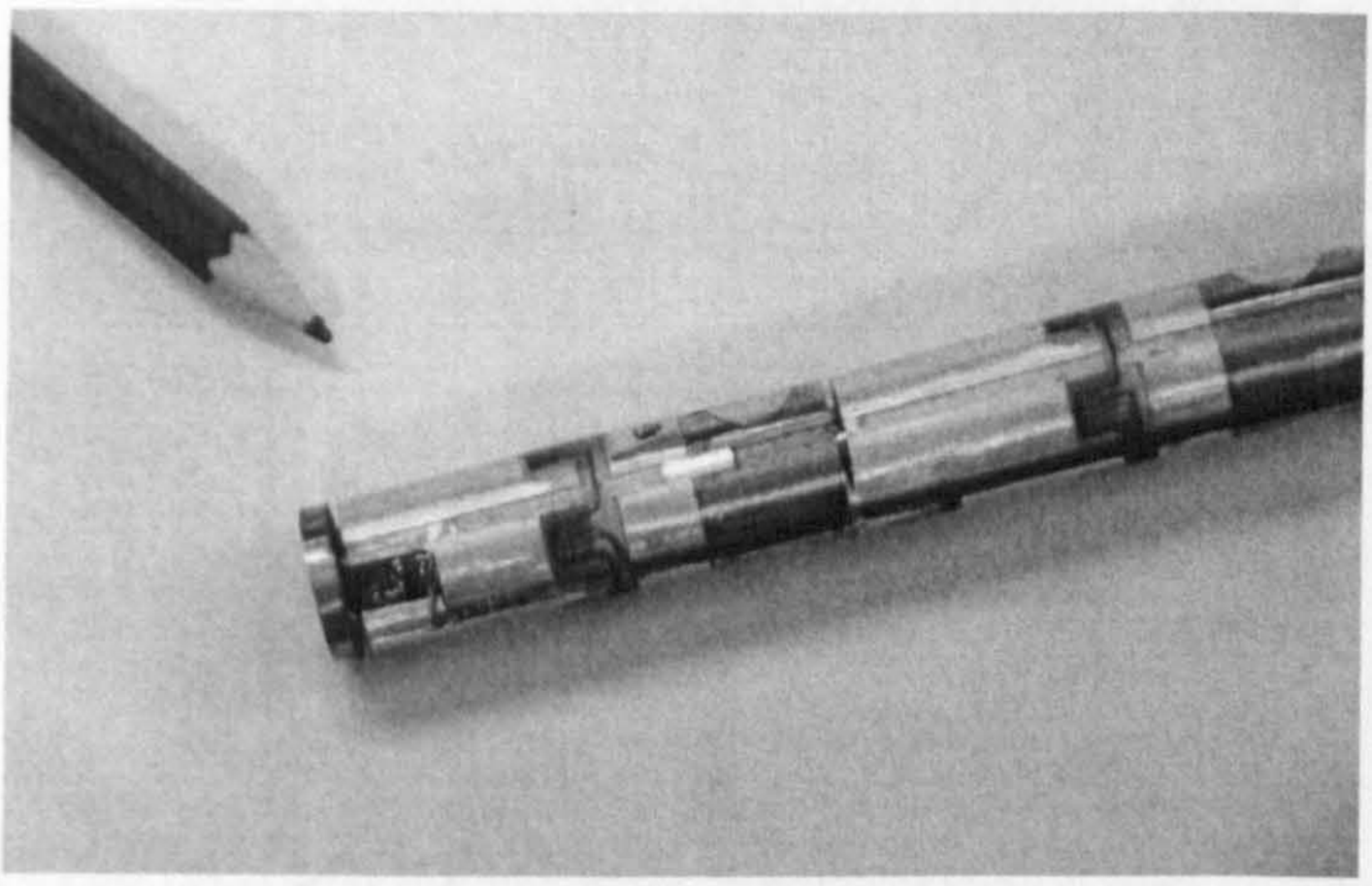

Figure 4-13: Detail of the improved connection of the base transducer.

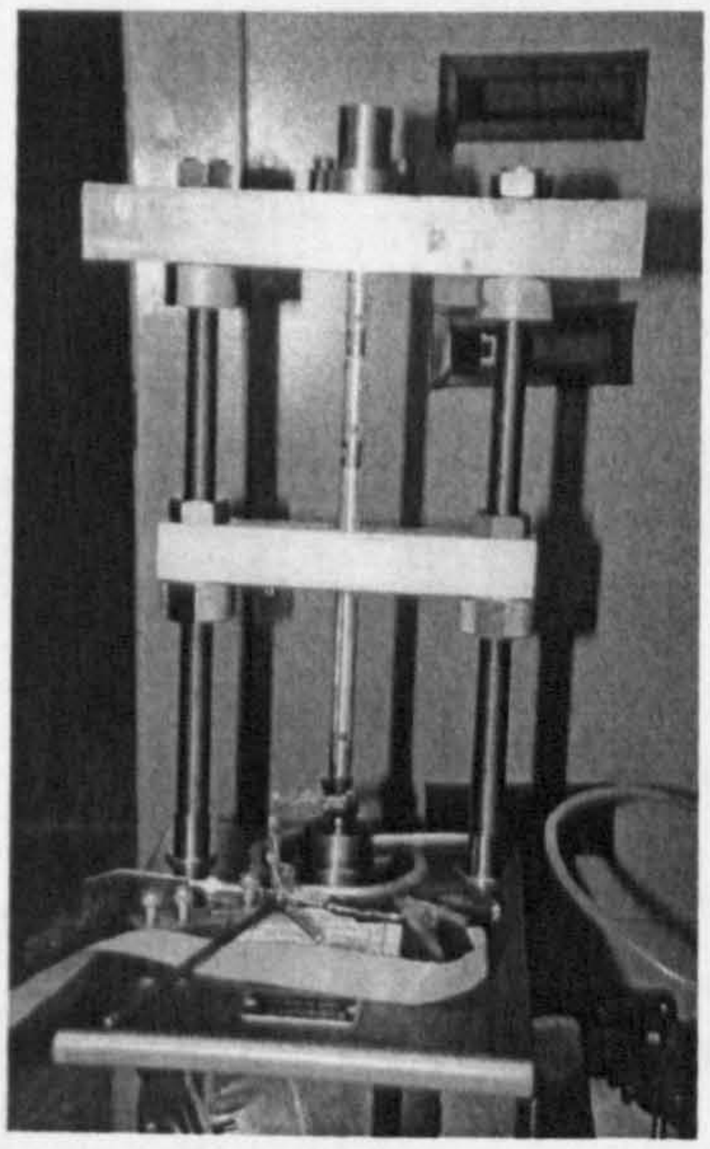

Figure 4-14: Calibration of the base transducer of CUIMP-3 using the Budenberg device.

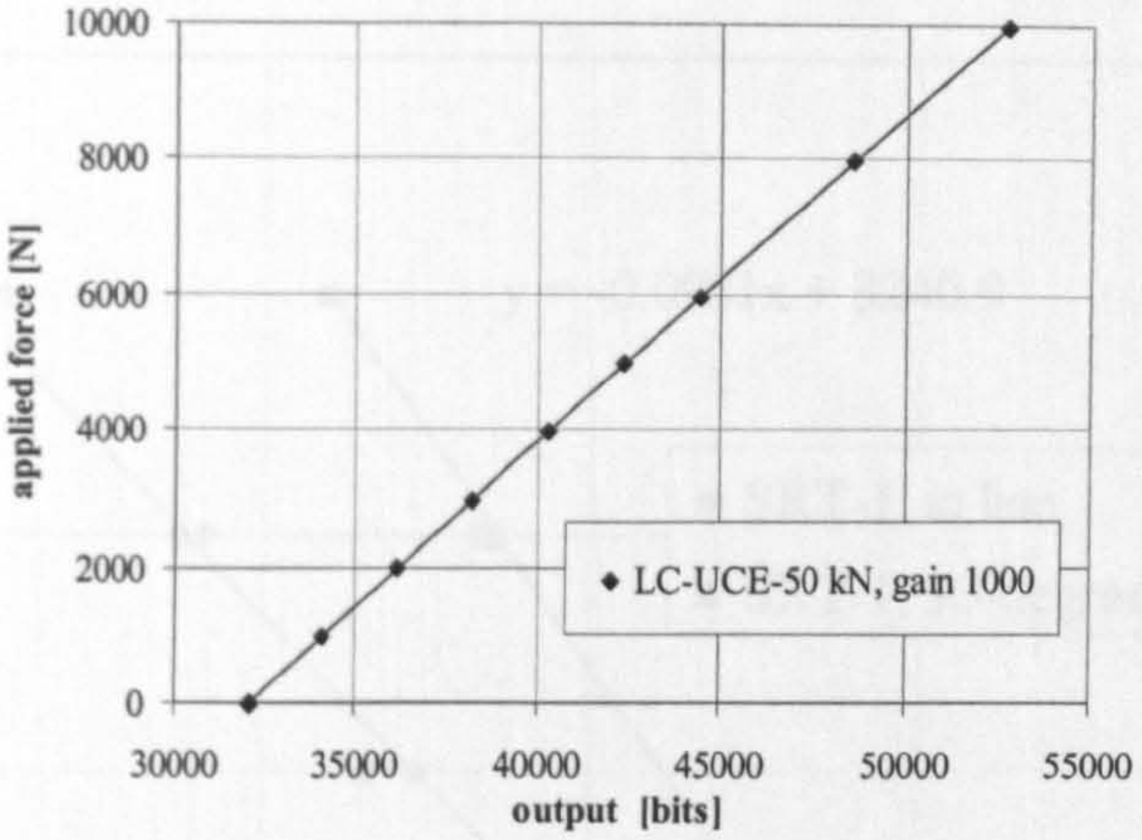

Figure 4-15: Typical calibration of the global compression-tension load cell.

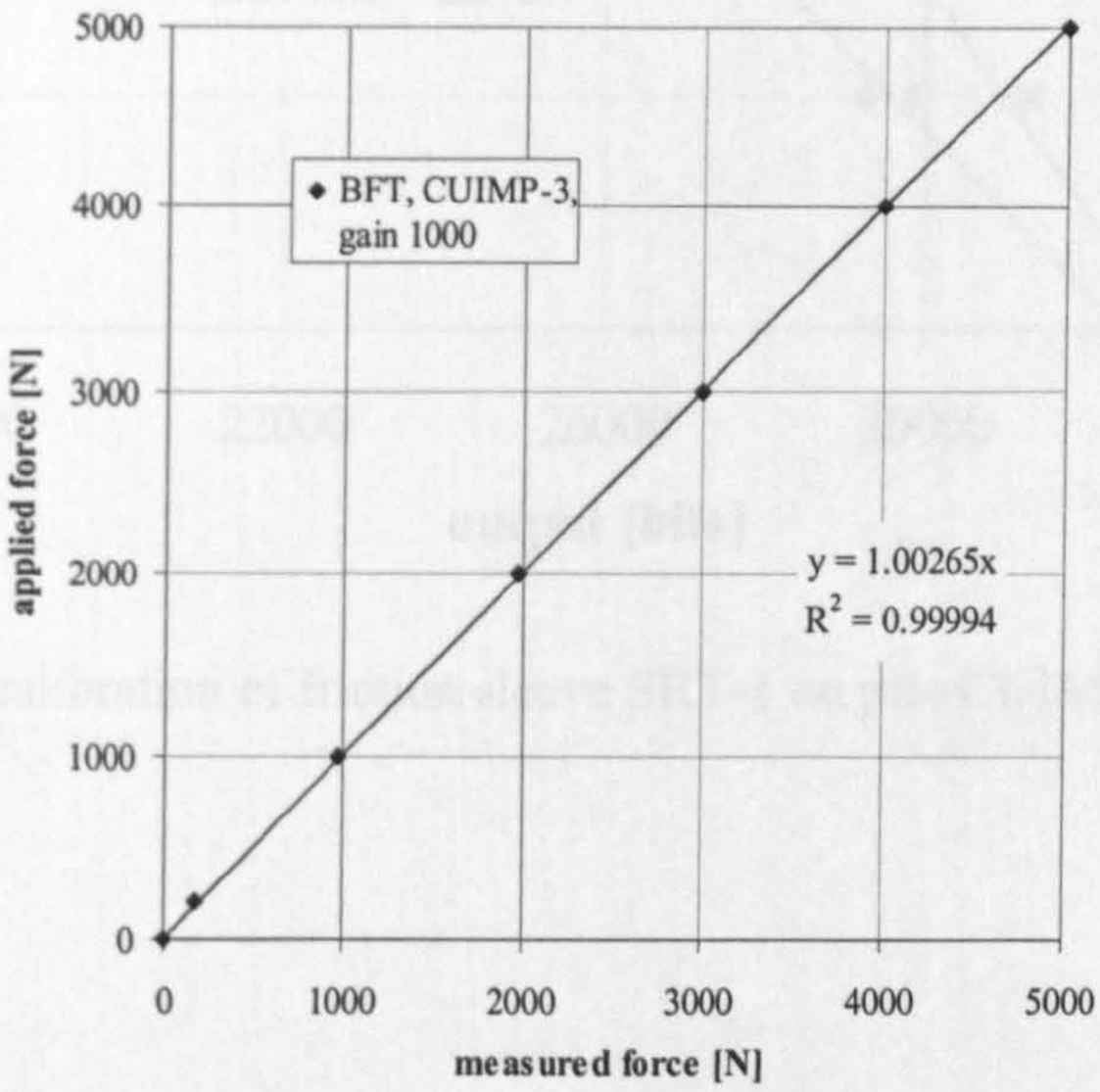

Figure 4-16: Typical calibration of the base force transducer.

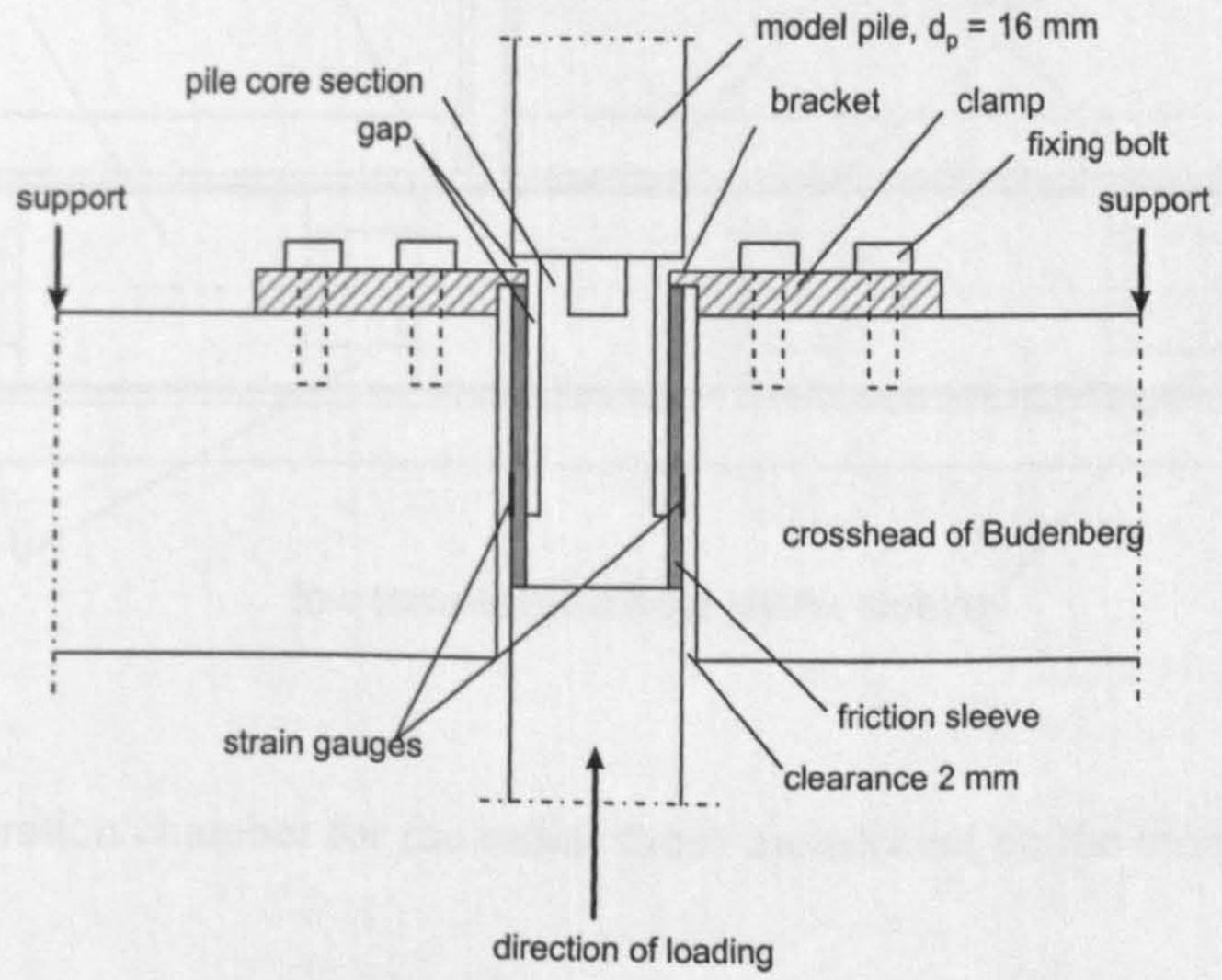

Figure 4-17: Connection of the friction sleeves to the Budenberg device during calibration.

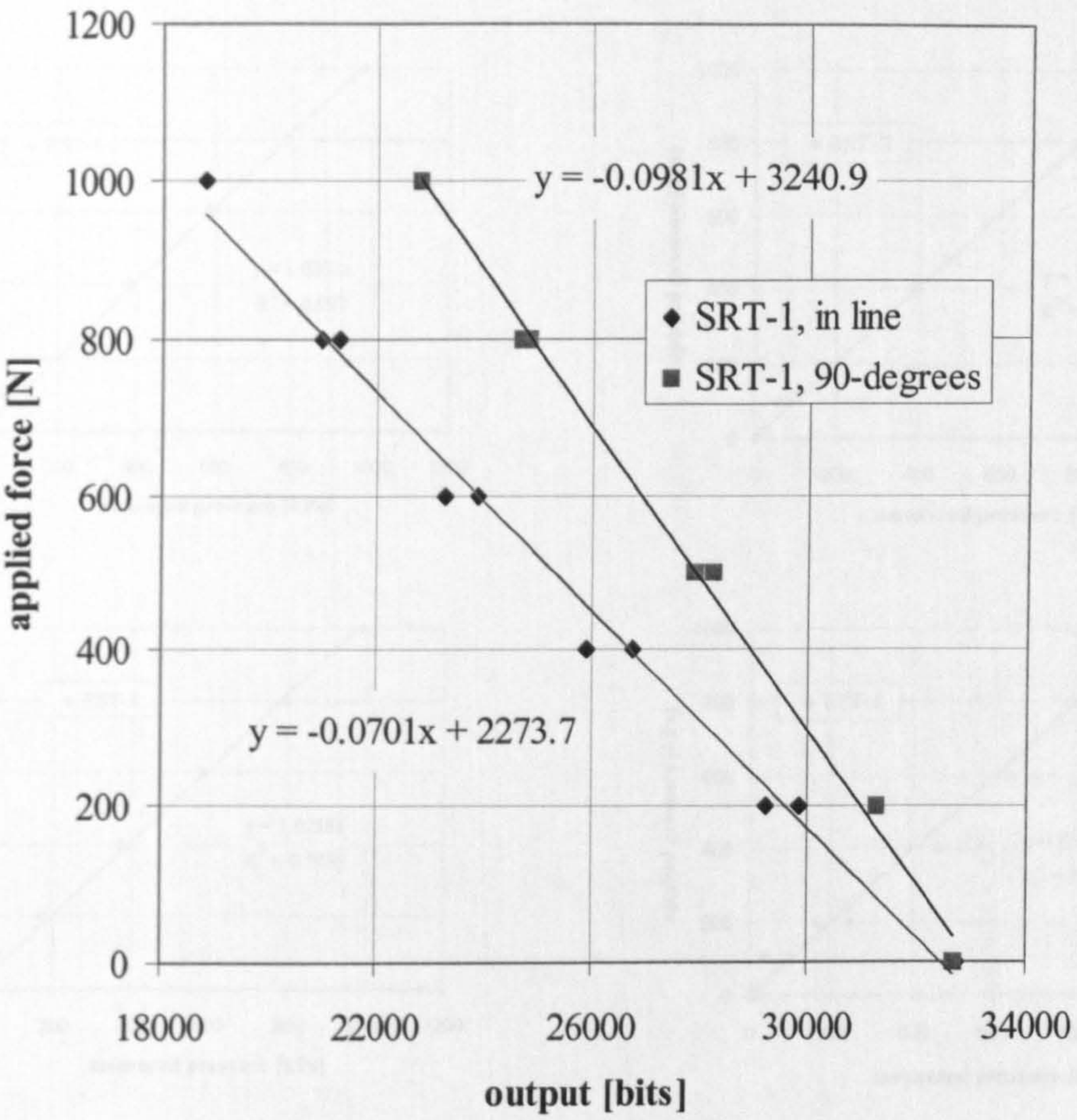

Figure 4-18: Typical calibration of friction sleeve SRT-1 on pile CUIMP-3.

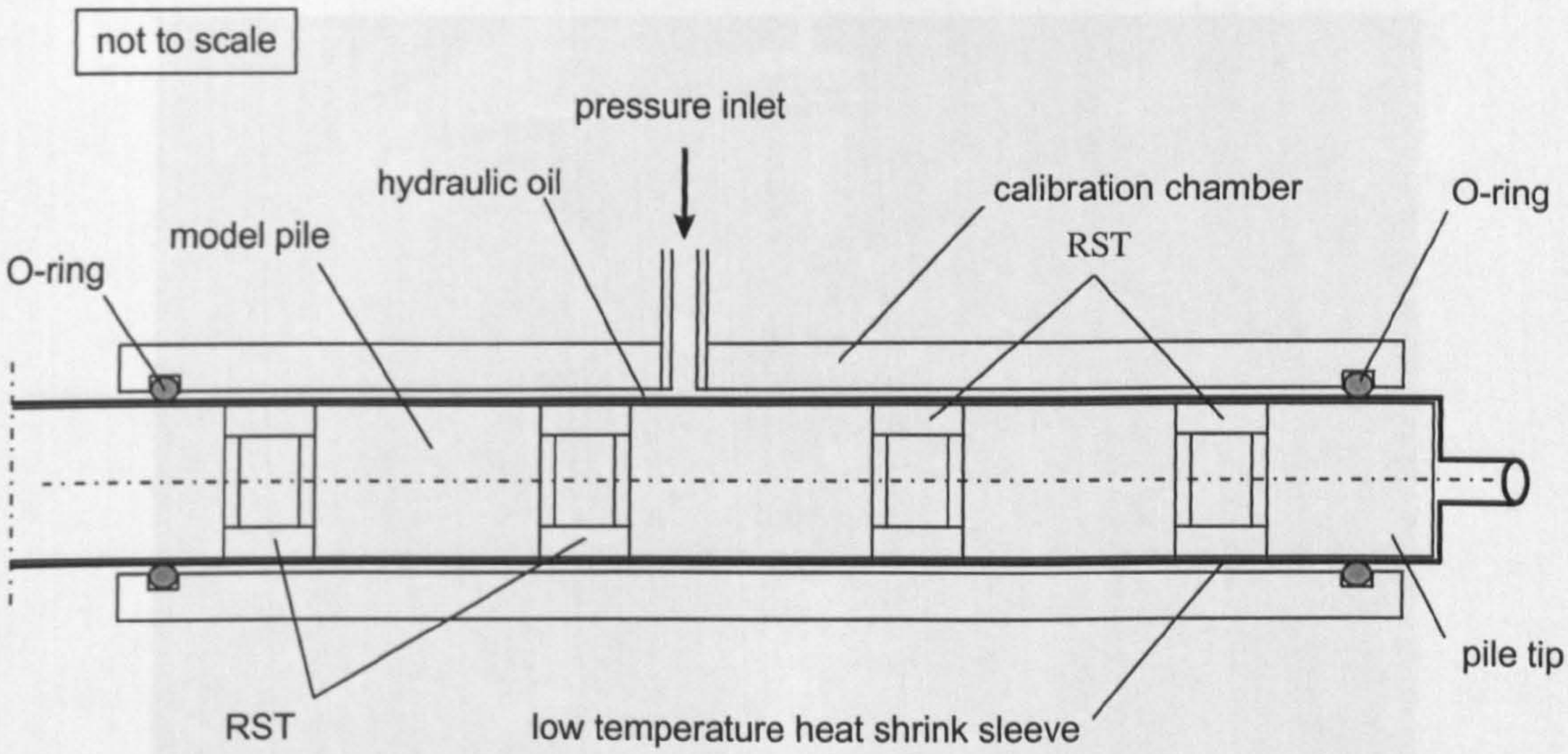

Figure 4-19: Calibration chamber for the radial stress transducers on the model piles.

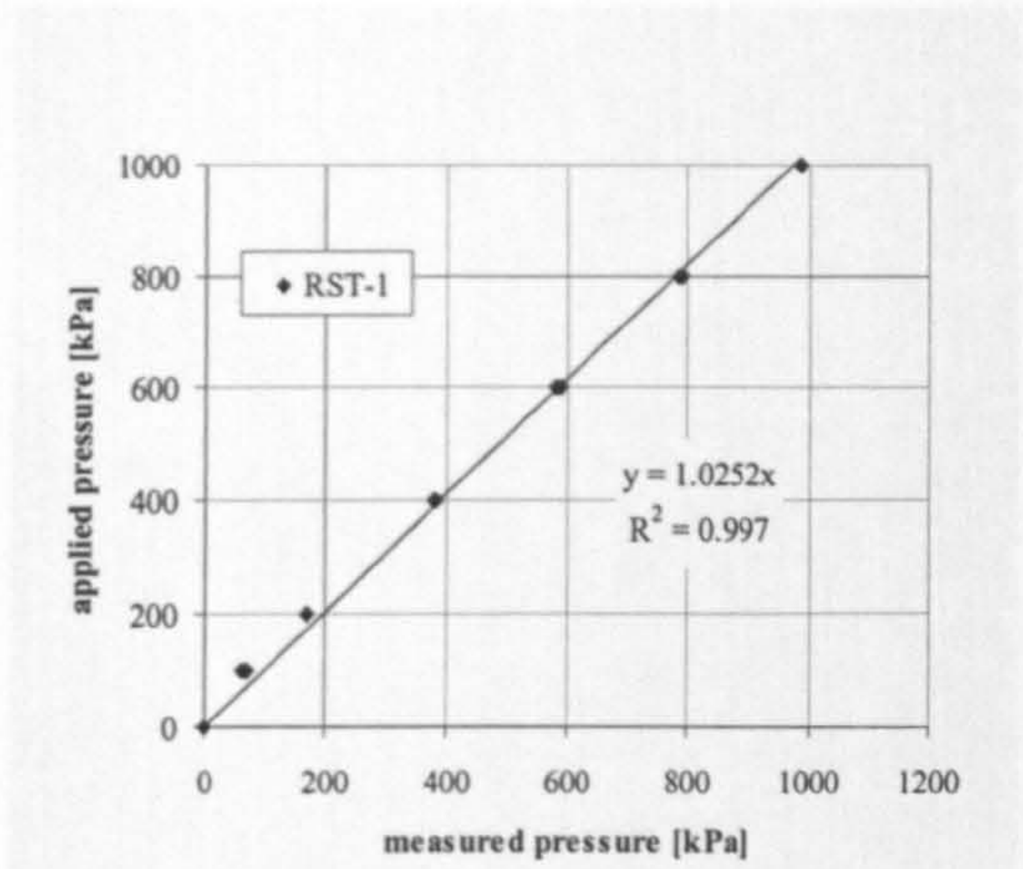

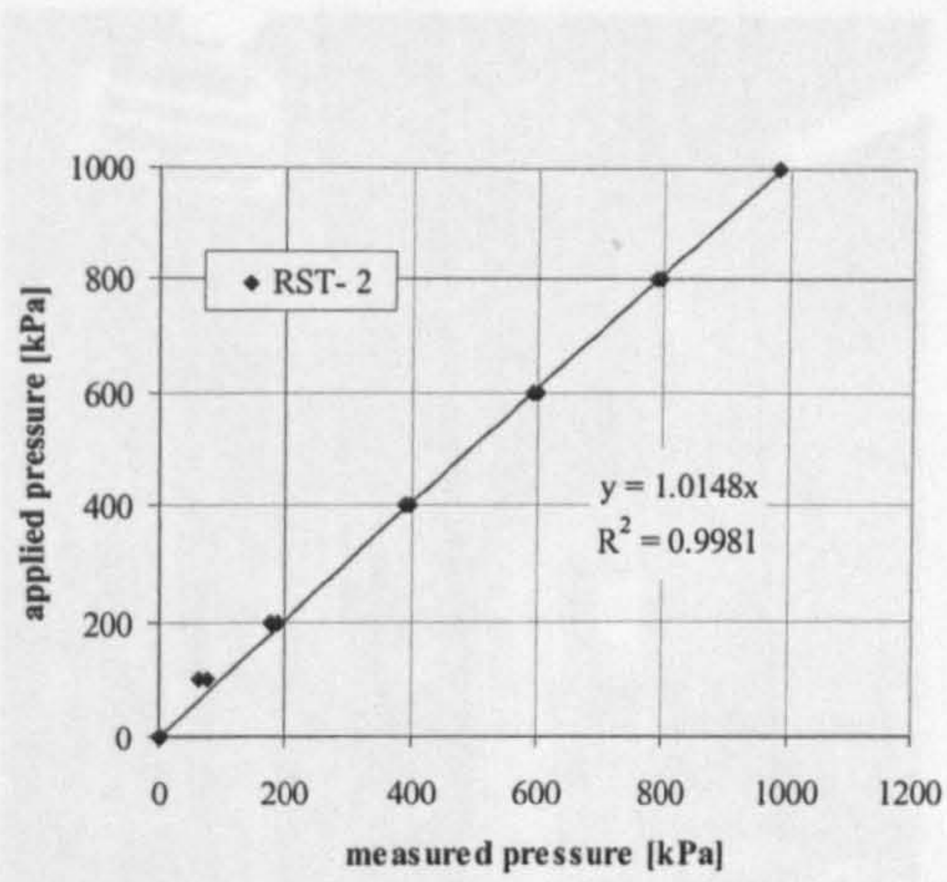

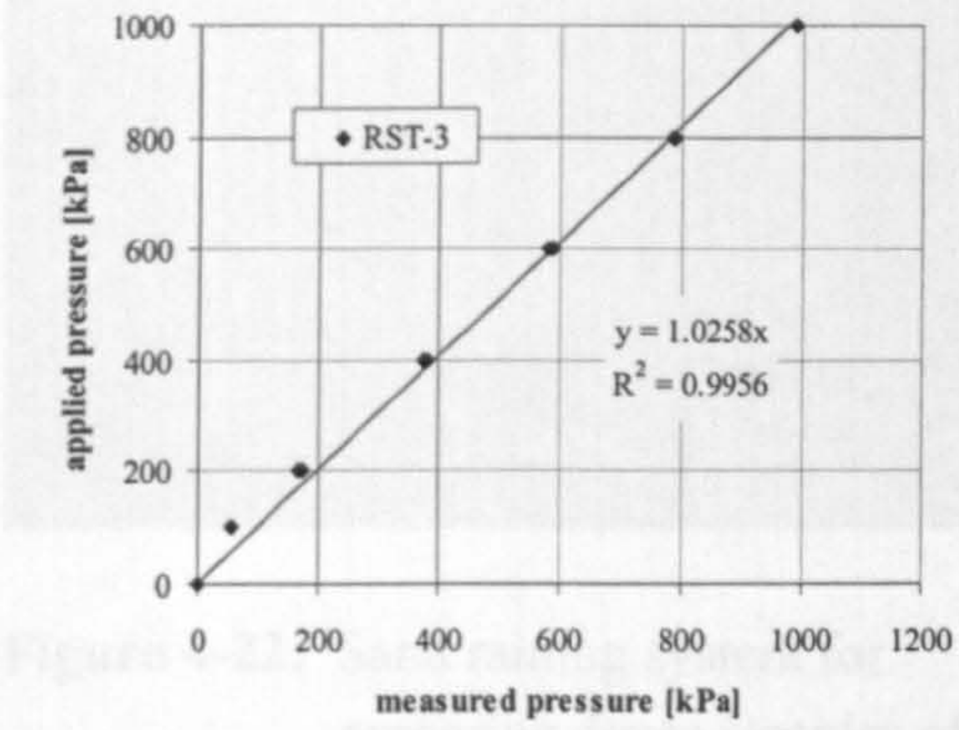

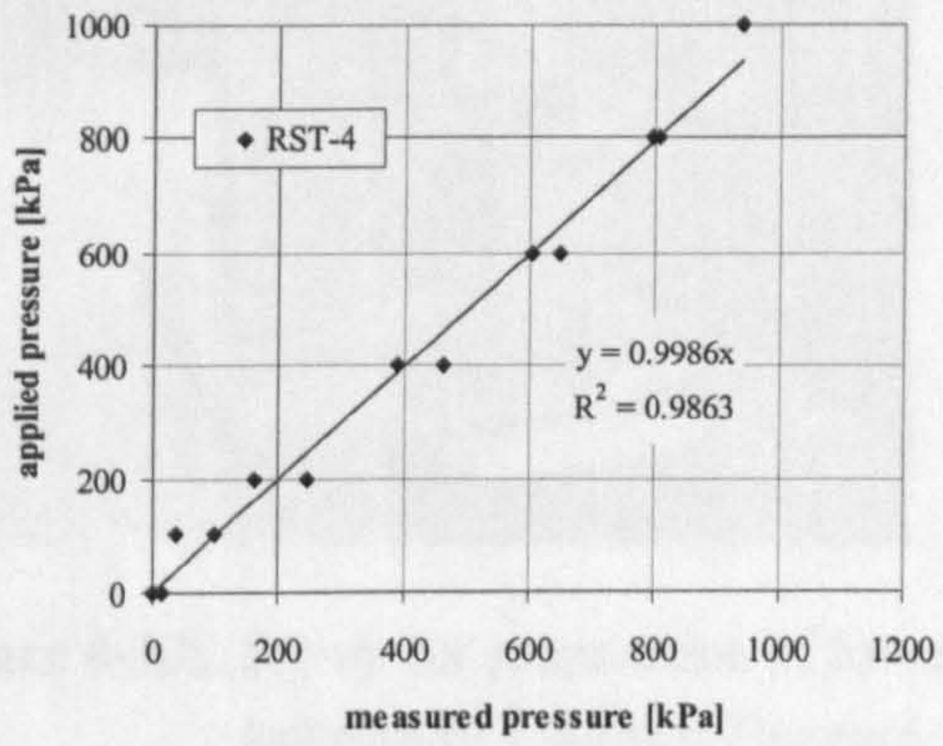

Figure 4-20: Typical calibration of radial stress transducers on pile CUIMP-3.

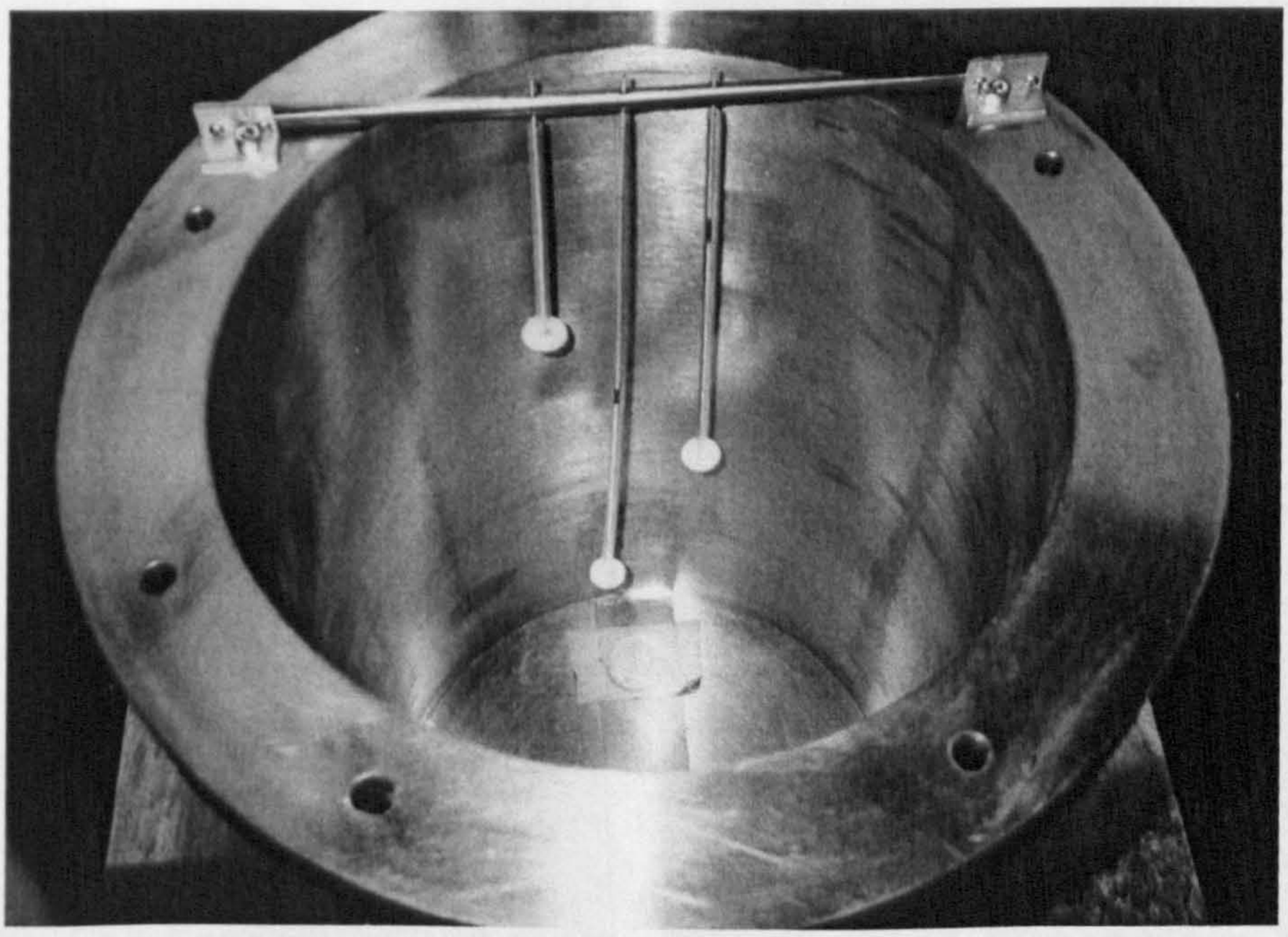

Figure 4-21: Set-up prior to placing the sand in the strongbox.

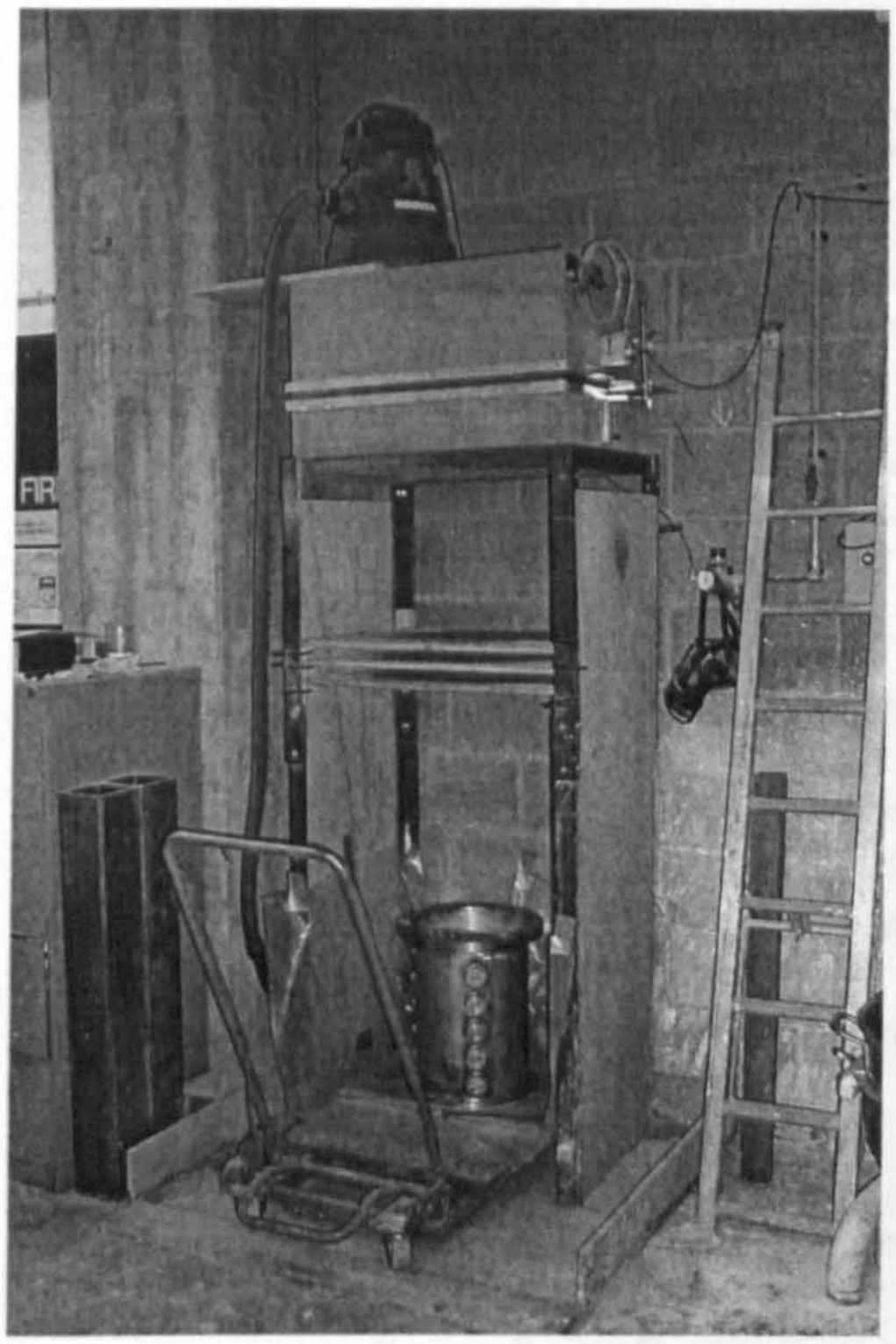

Figure 4-22: Sand raining system for preparing dense samples of Leighton Buzzard sand.

Figure 4-23: Set-up for preparation of loose samples of Leighton Buzzard sand.

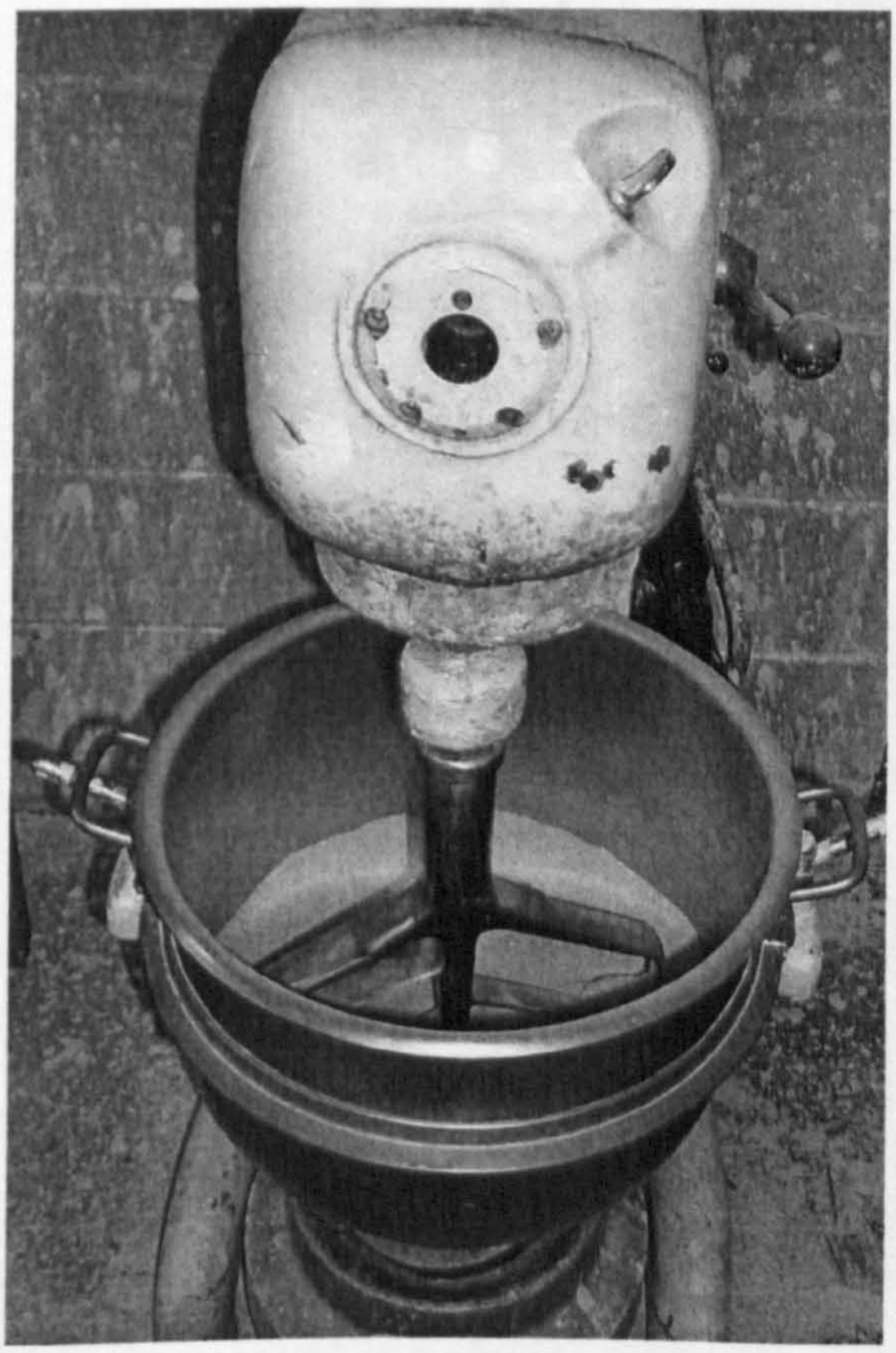

Figure 4-24: Mixing process prior to tests on Dogs Bay sand.

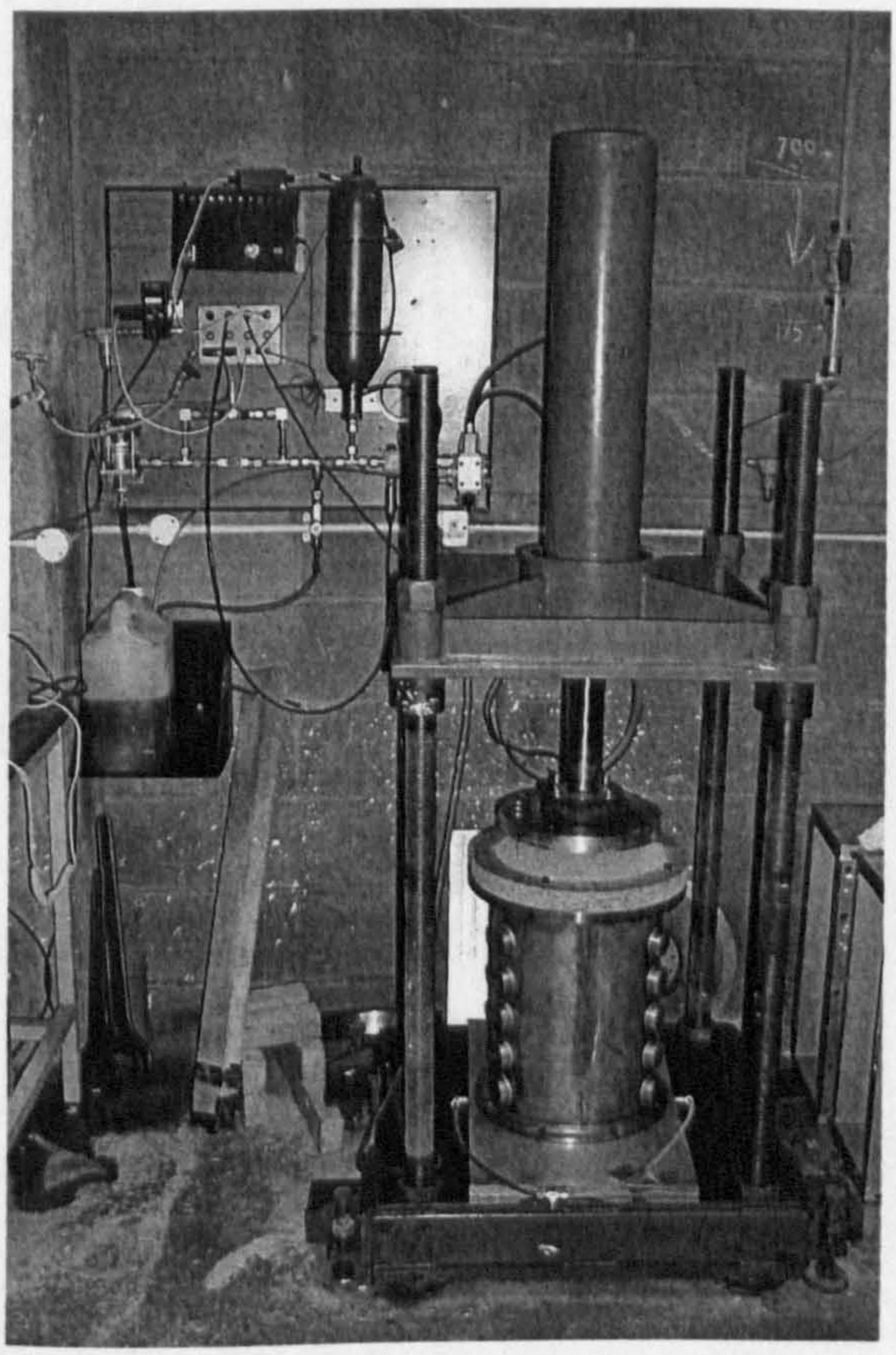

Figure 4-25: Set-up for compressing the overconsolidated samples.

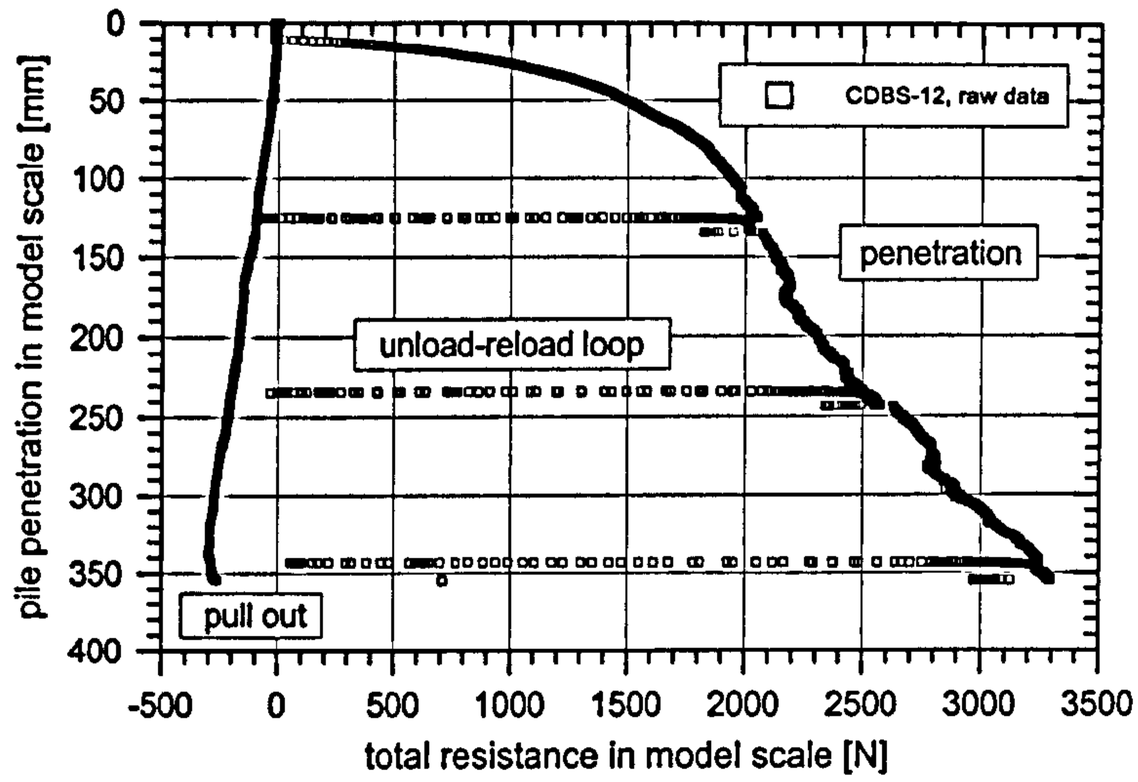

Figure 5-1: Typical raw test data for centrifuge test CDBS-12 on Leighton Buzzard sand.

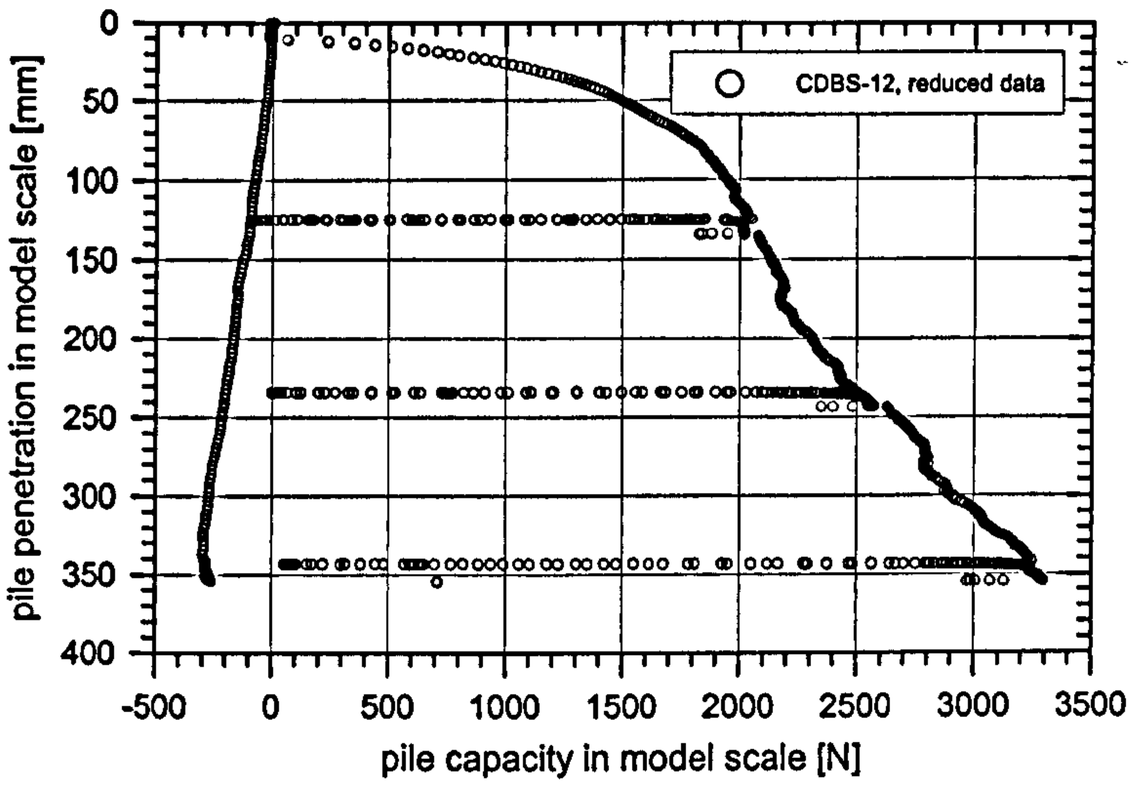

Figure 5-2: Reduced data set for global pile resistance during test CDBS-12.

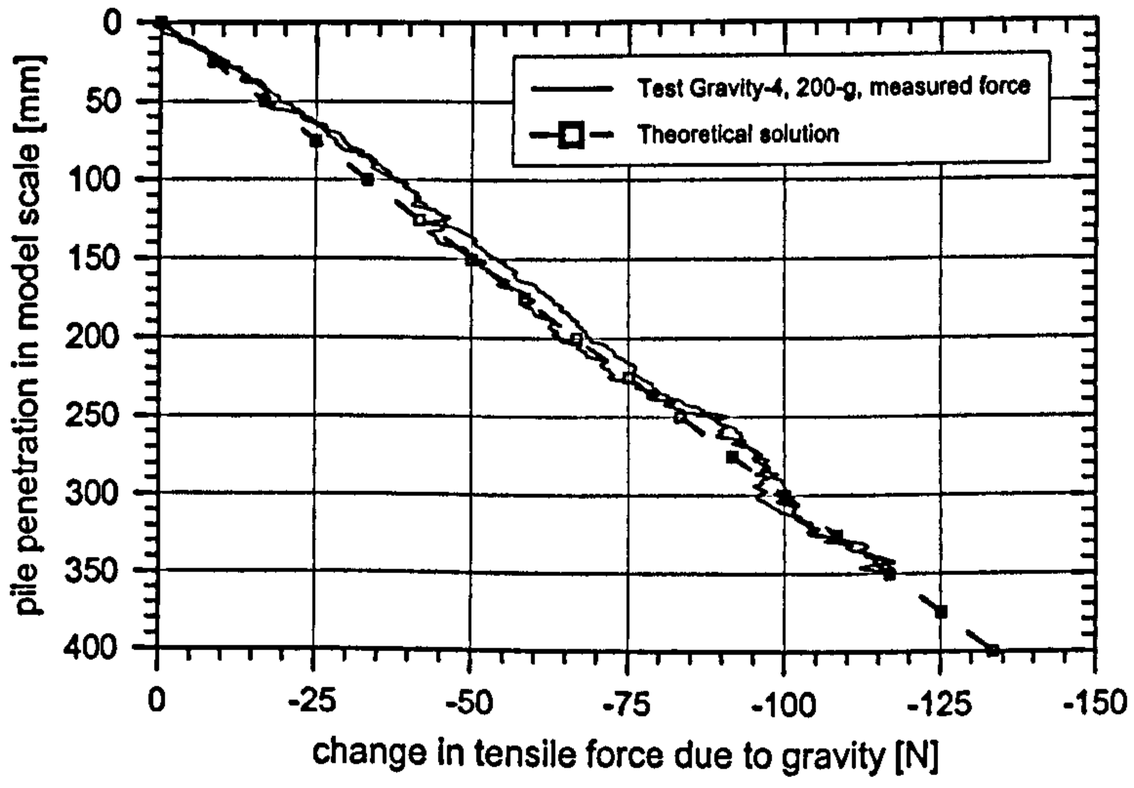

Figure 5-3 : Gravity effect on measured force of global load cell during pile installation.

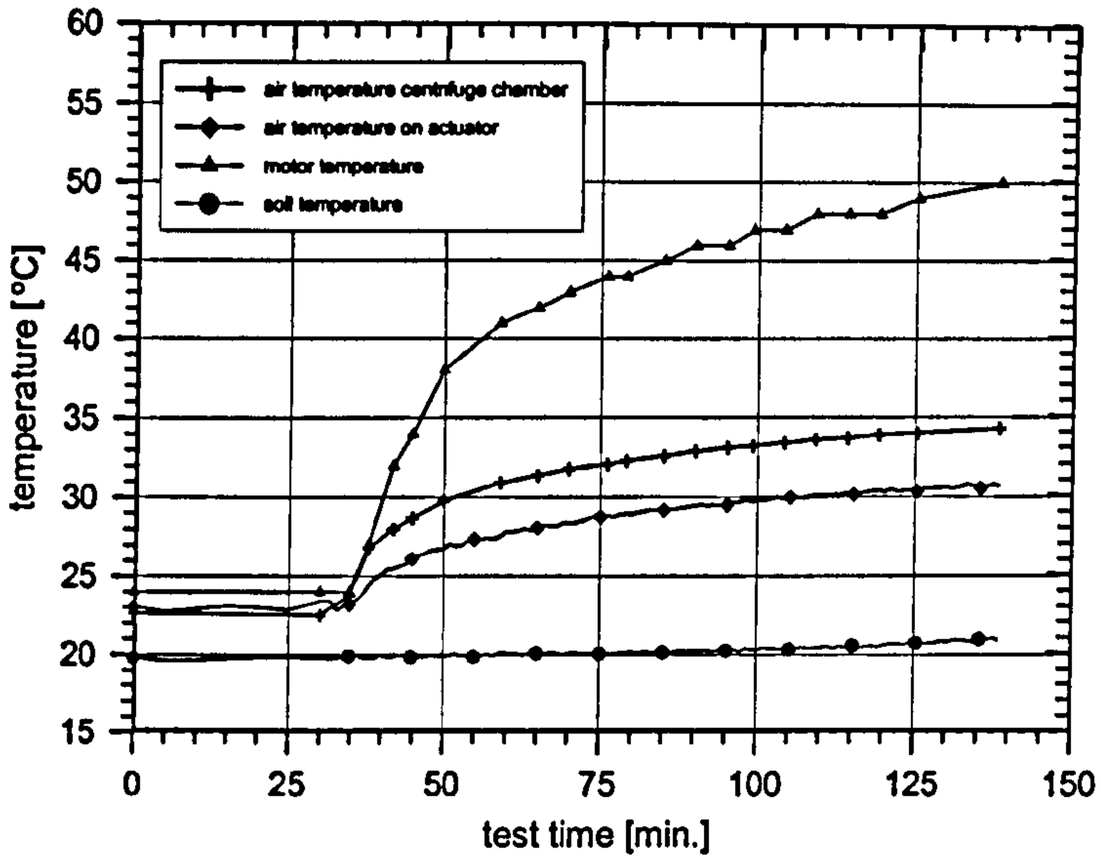

Figure 5-4: Natural temperature distribution during a 200-g centrifuge test.

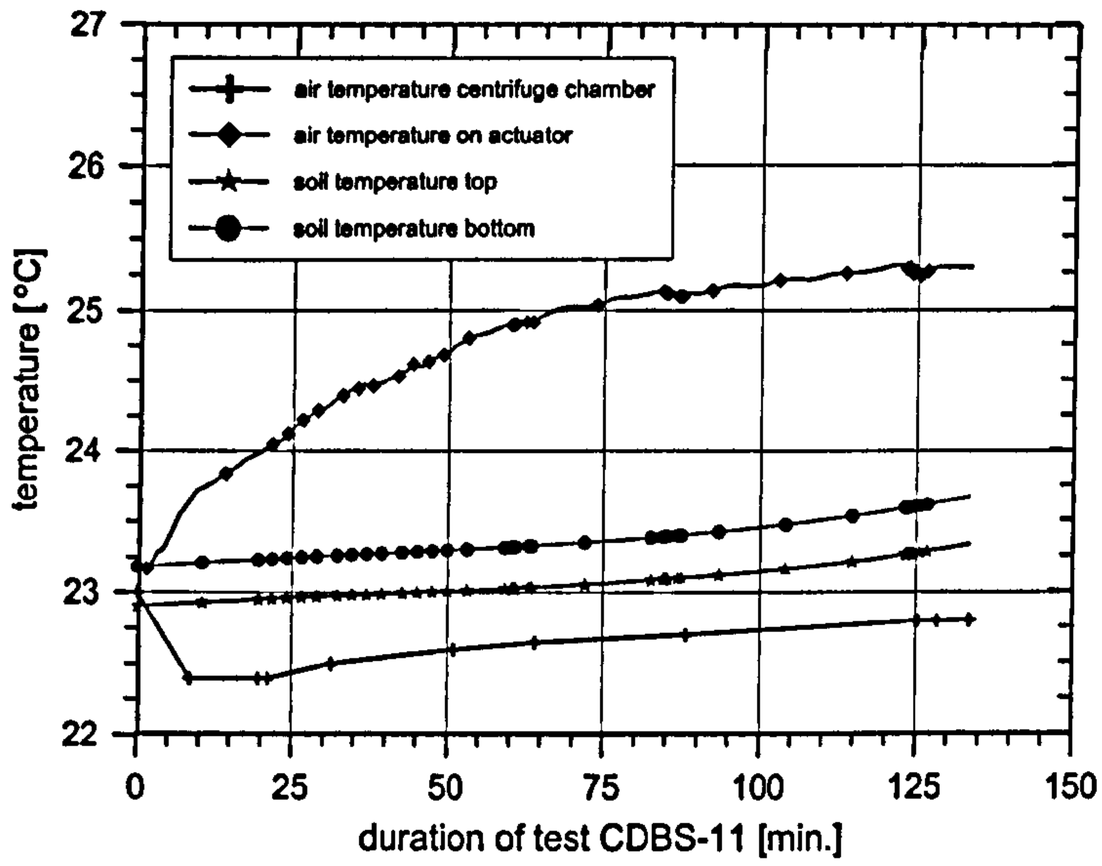

Figure 5-5: Temperature regime during the 200-g test CDBS-11 while evaporating water in the centrifuge chamber.

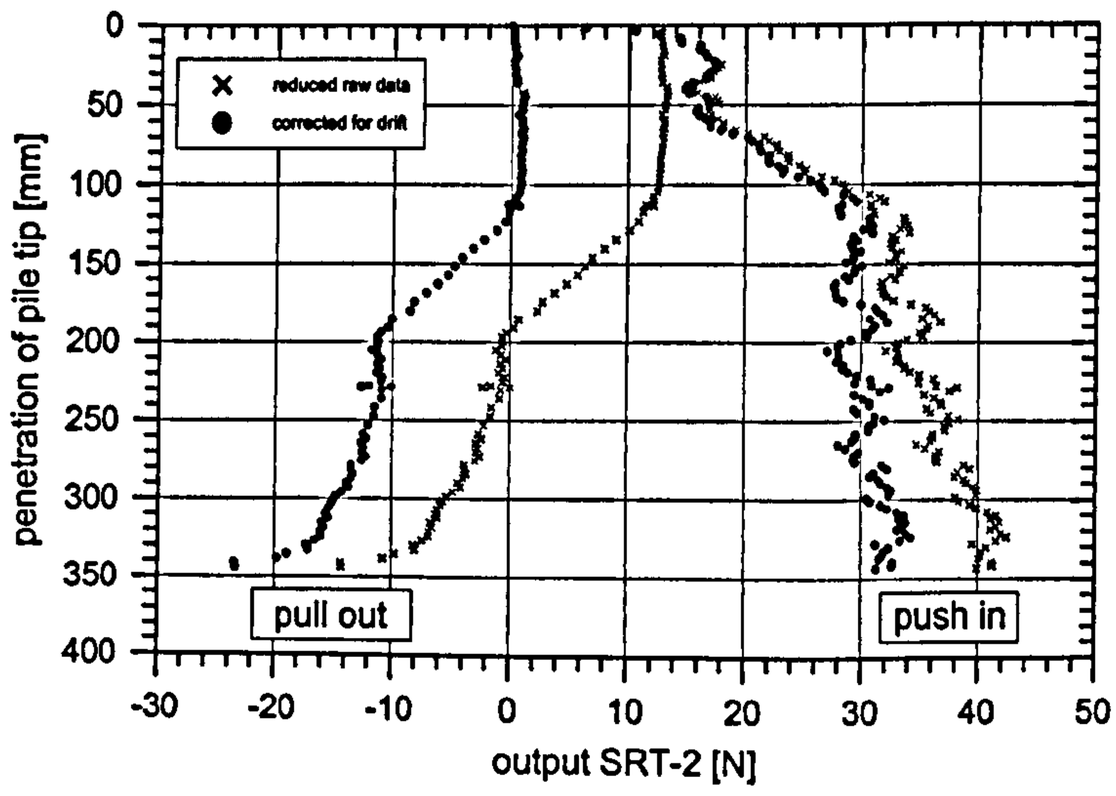

Figure 5-6: Drift correction for SRT-2 on CUIMP-4 during test CDBS-9.

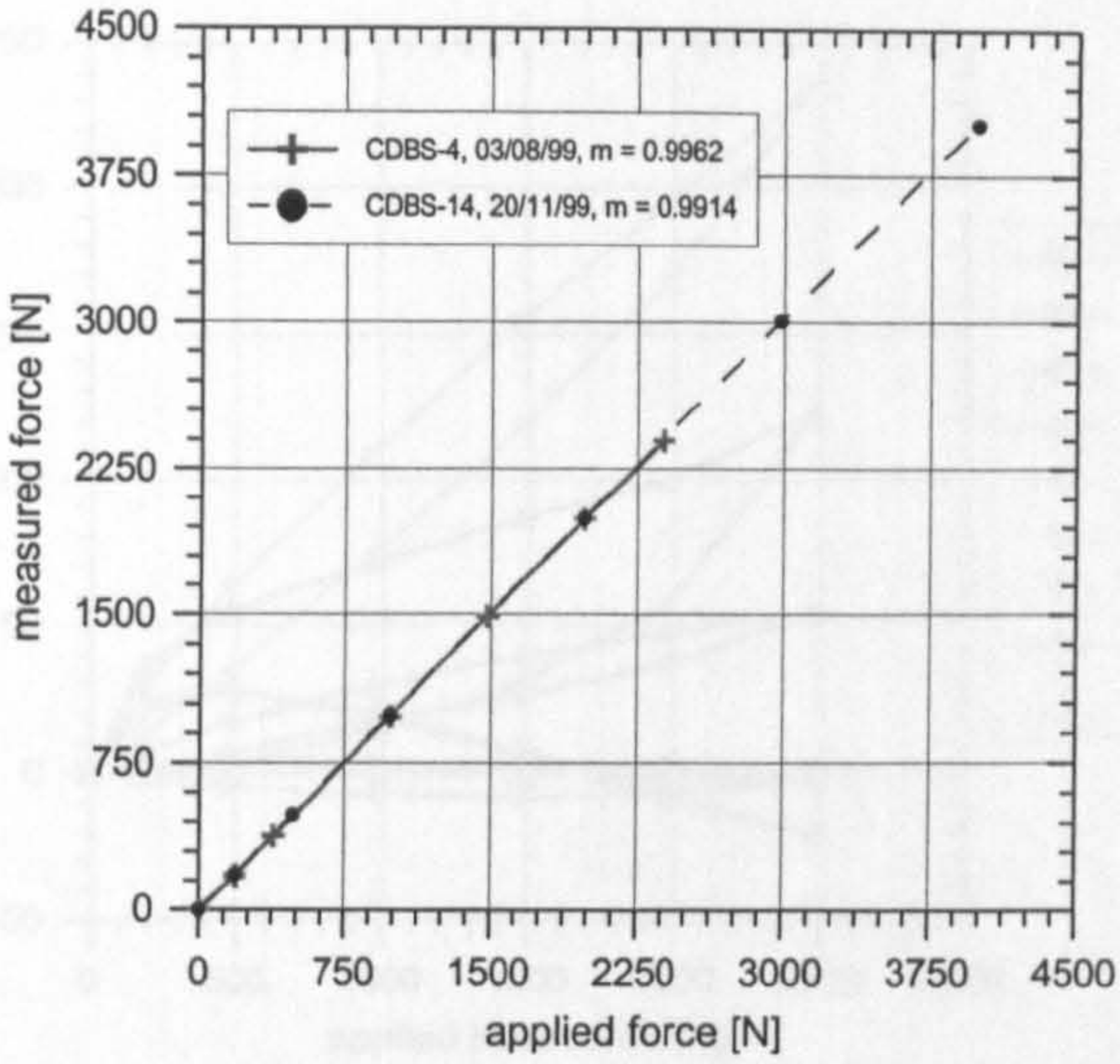

Figure 5-7: Repeatability of calibration of base transducer on CUIMP-4.

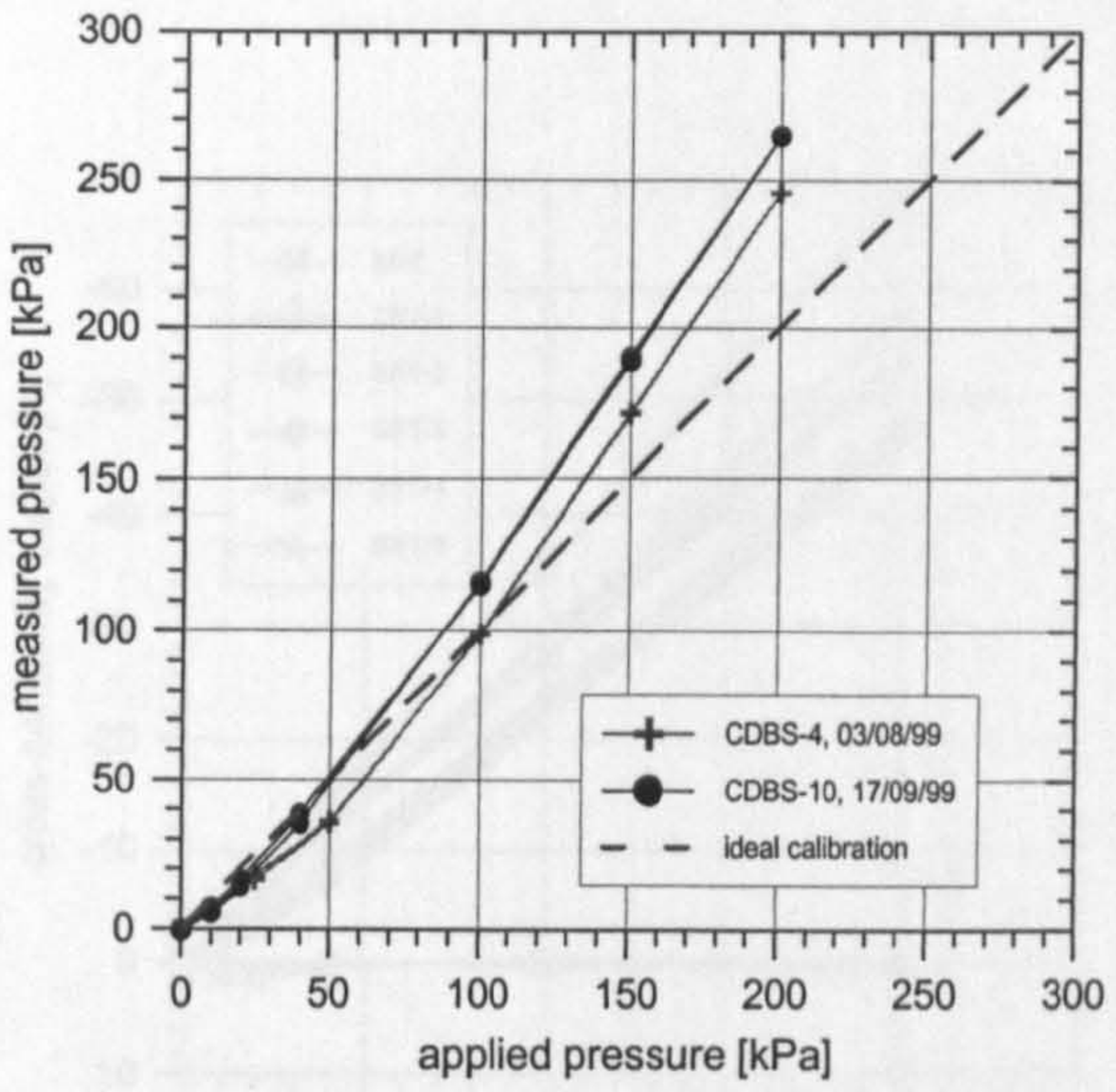

Figure 5-8: Change in calibration of RST-3 on CUIMP-4.

Figure 5-9: Typical non-linear output of RSTs on CUIMP-4.

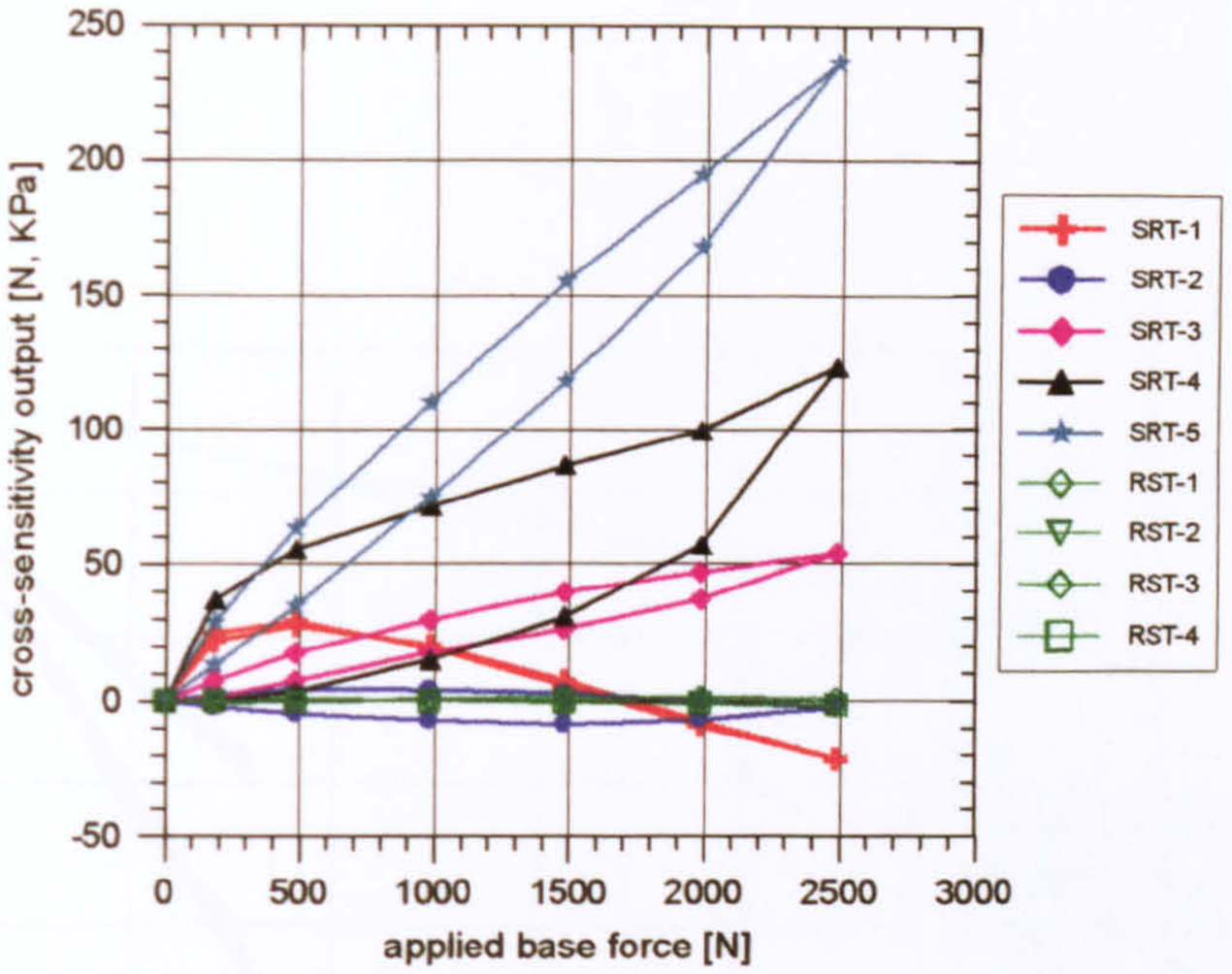

Figure 5-10: Cross-sensitivities of transducers on CUIMP-4 to base force after test CDBS-10.

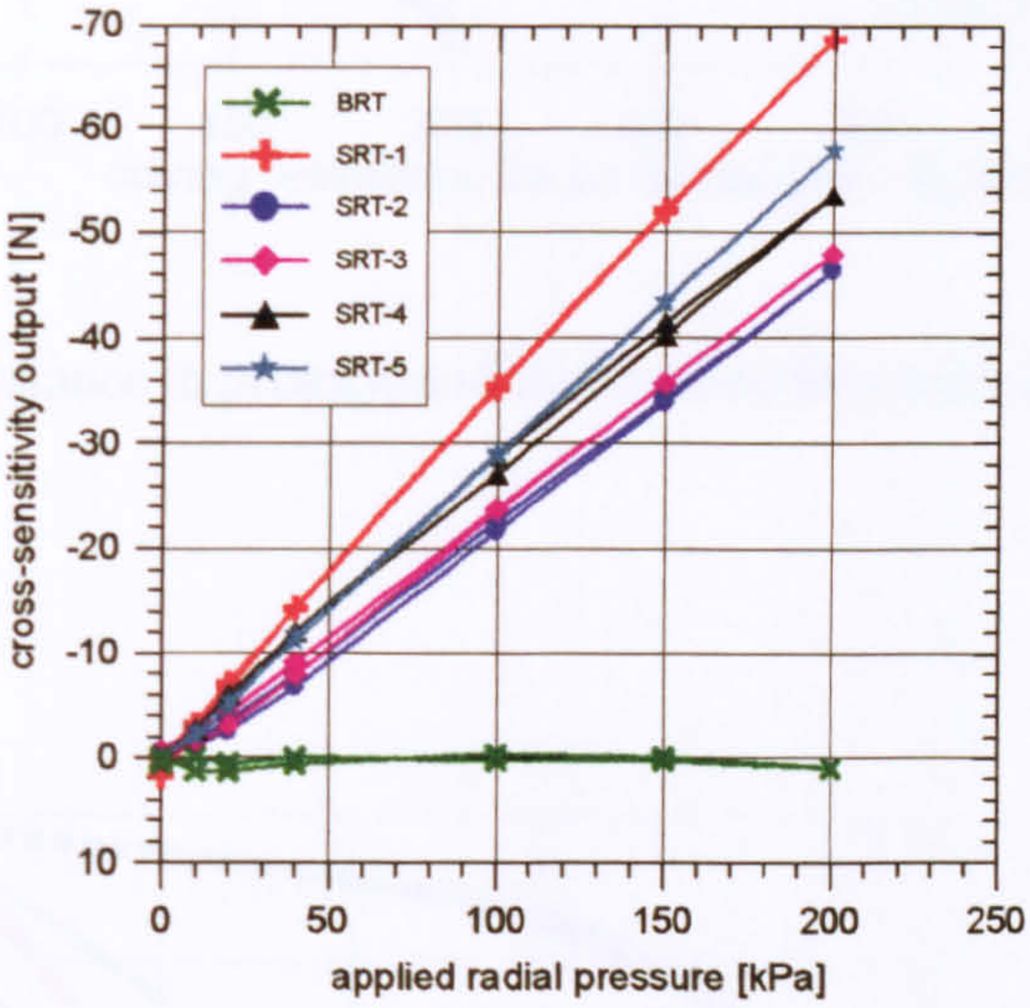

Figure 5-11: Cross-sensitivities of transducers on CUIMP-4 to radial stress after test CDBS-10.

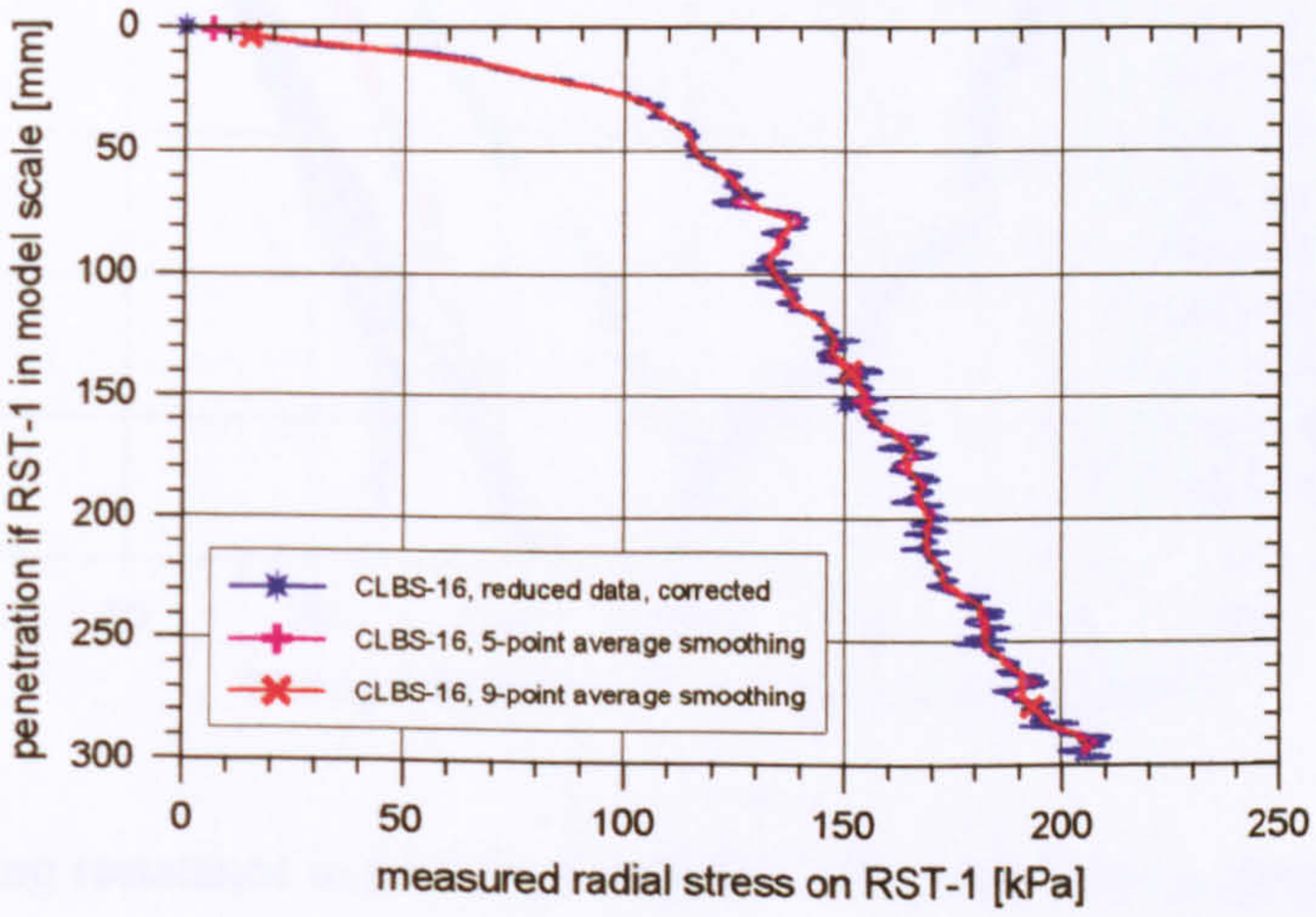

Figure 5-12: Comparison between 5 and 9 point smoothing procedure for RTS-1 during test CLBS-16.

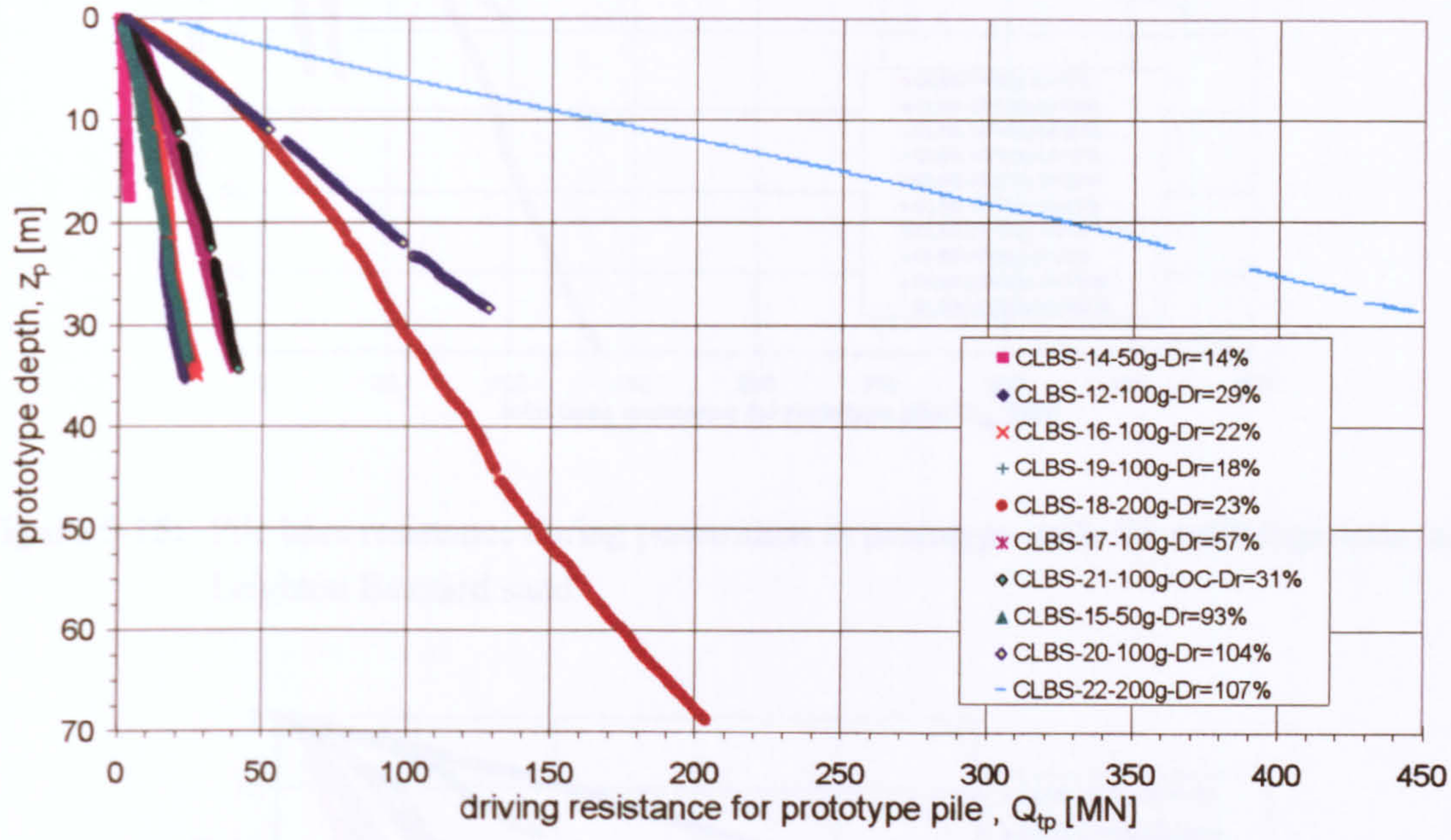

Figure 5-13: Driving resistance in prototype scale for centrifuge tests on Leighton Buzzard sand.

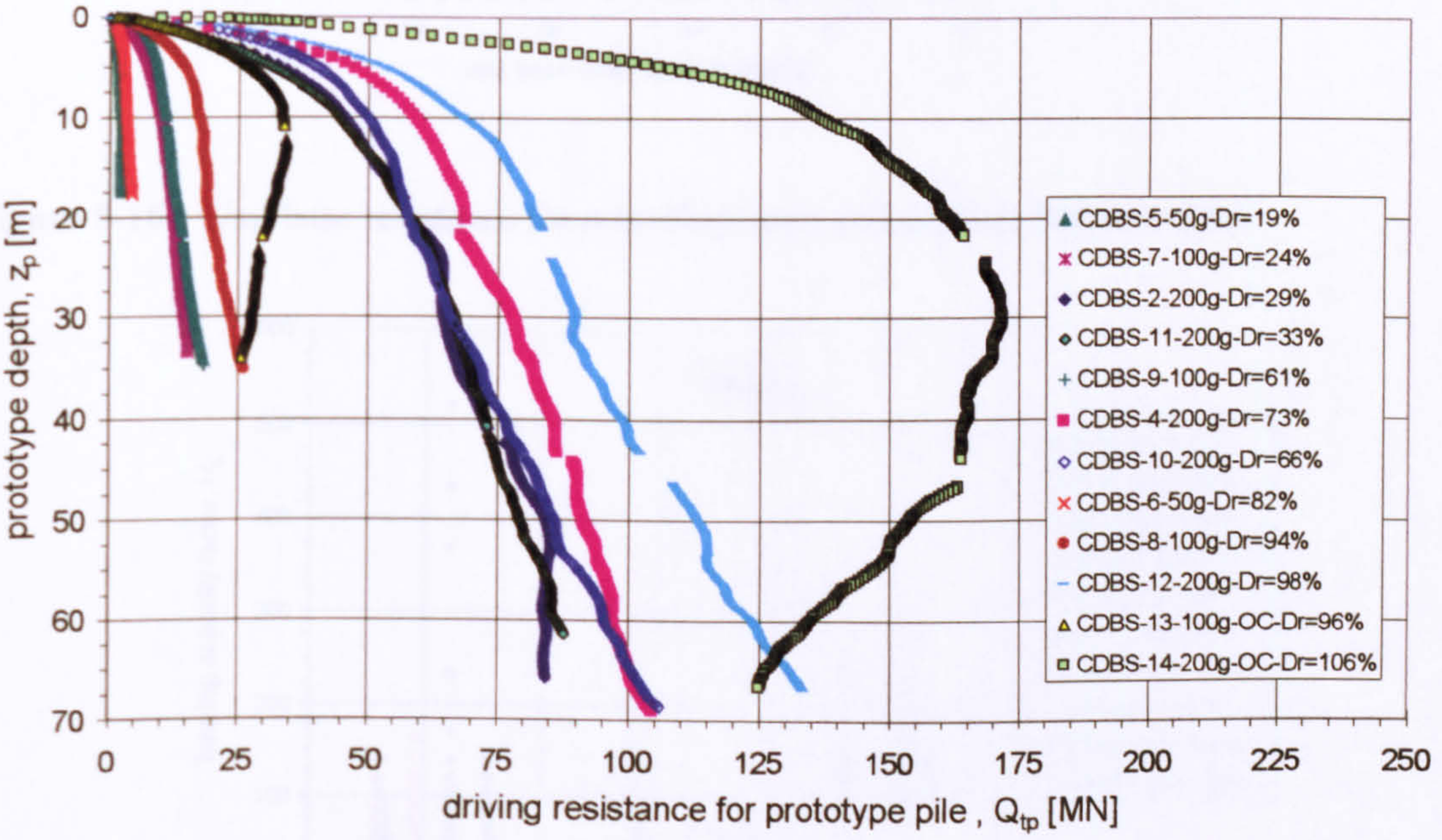

Figure 5-14: Driving resistance in prototype scale for centrifuge tests on Dogs Bay sand.

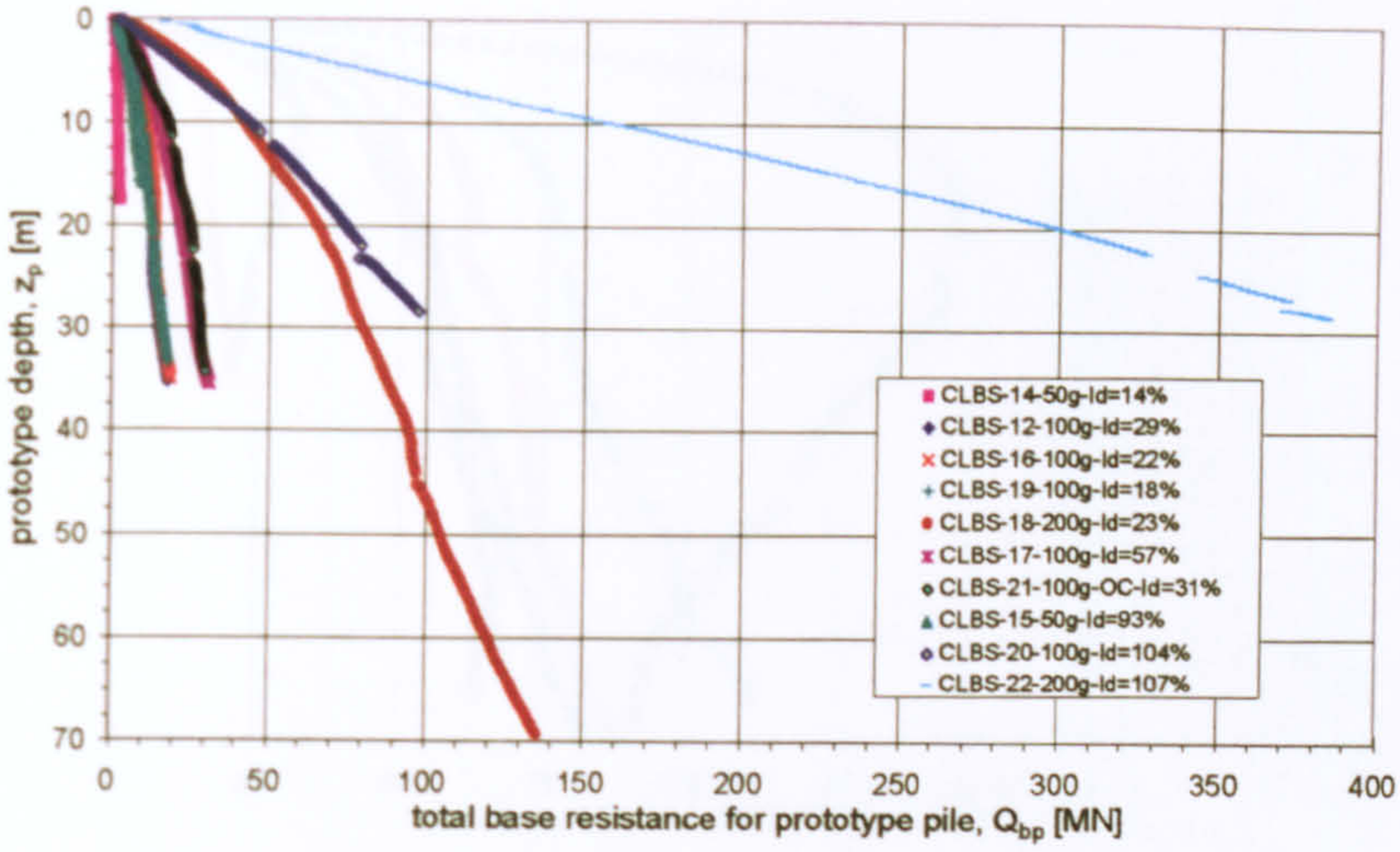

Figure 5-15: Pile base resistance during penetration in prototype scale for centrifuge tests on Leighton Buzzard sand.

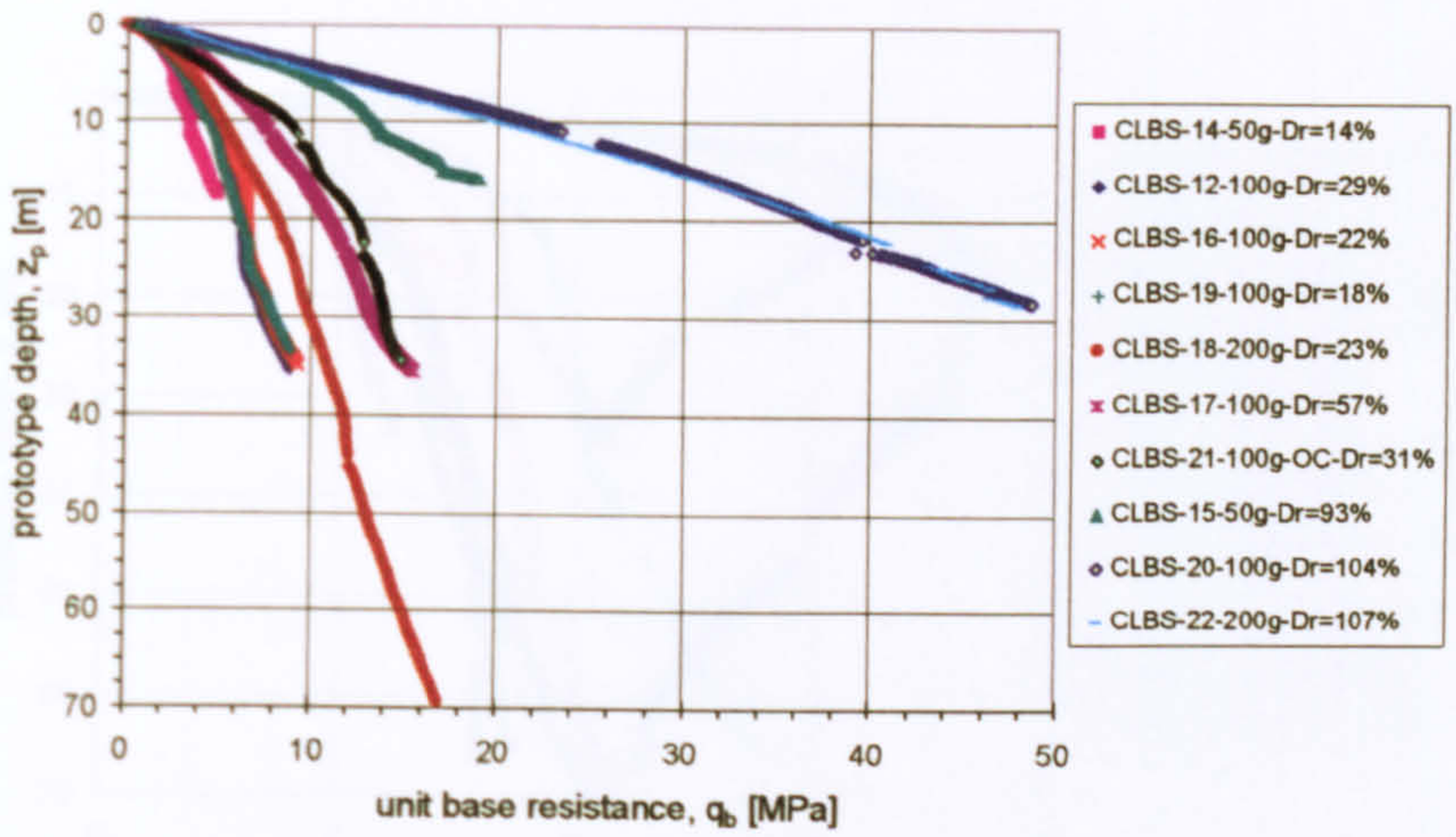

Figure 5-16: Unit base resistance for centrifuge tests on Leighton Buzzard sand.

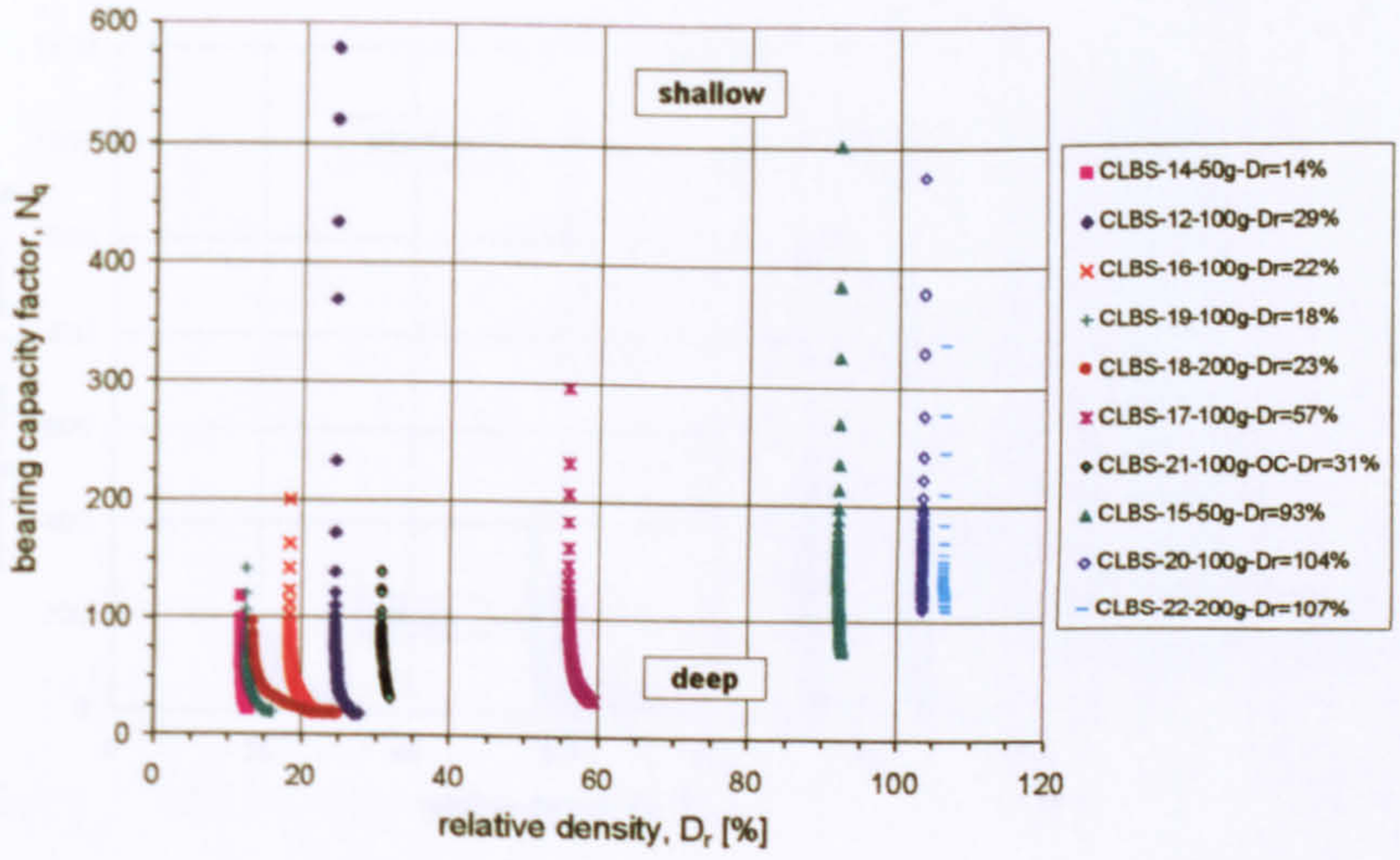

Figure 5-17: Correlation of bearing capacity factor with relative density for centrifuge tests on Leighton Buzzard sand.

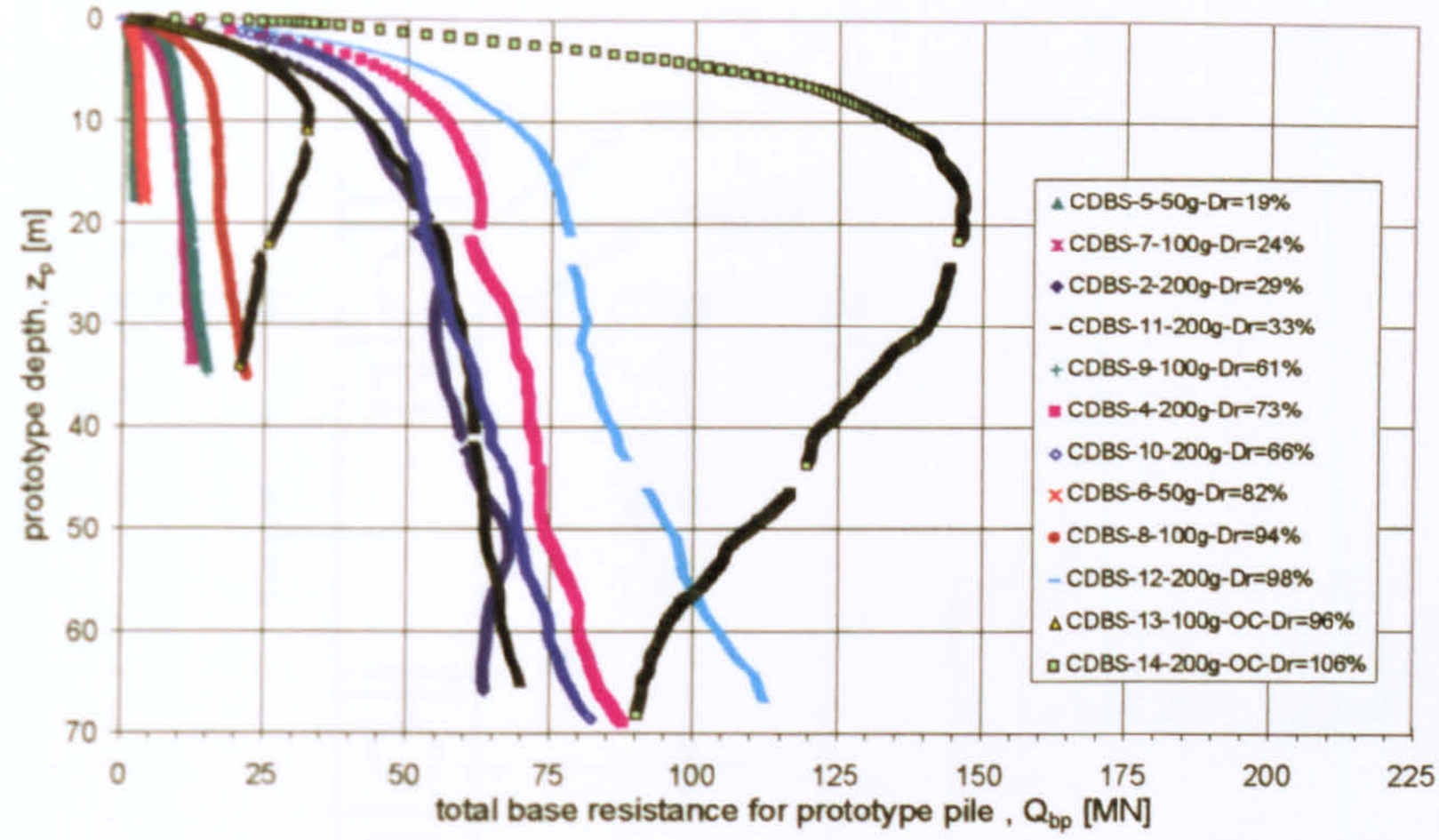

Figure 5-18: Pile base resistance during penetration in prototype scale for centrifuge tests on Dogs Bay sand.

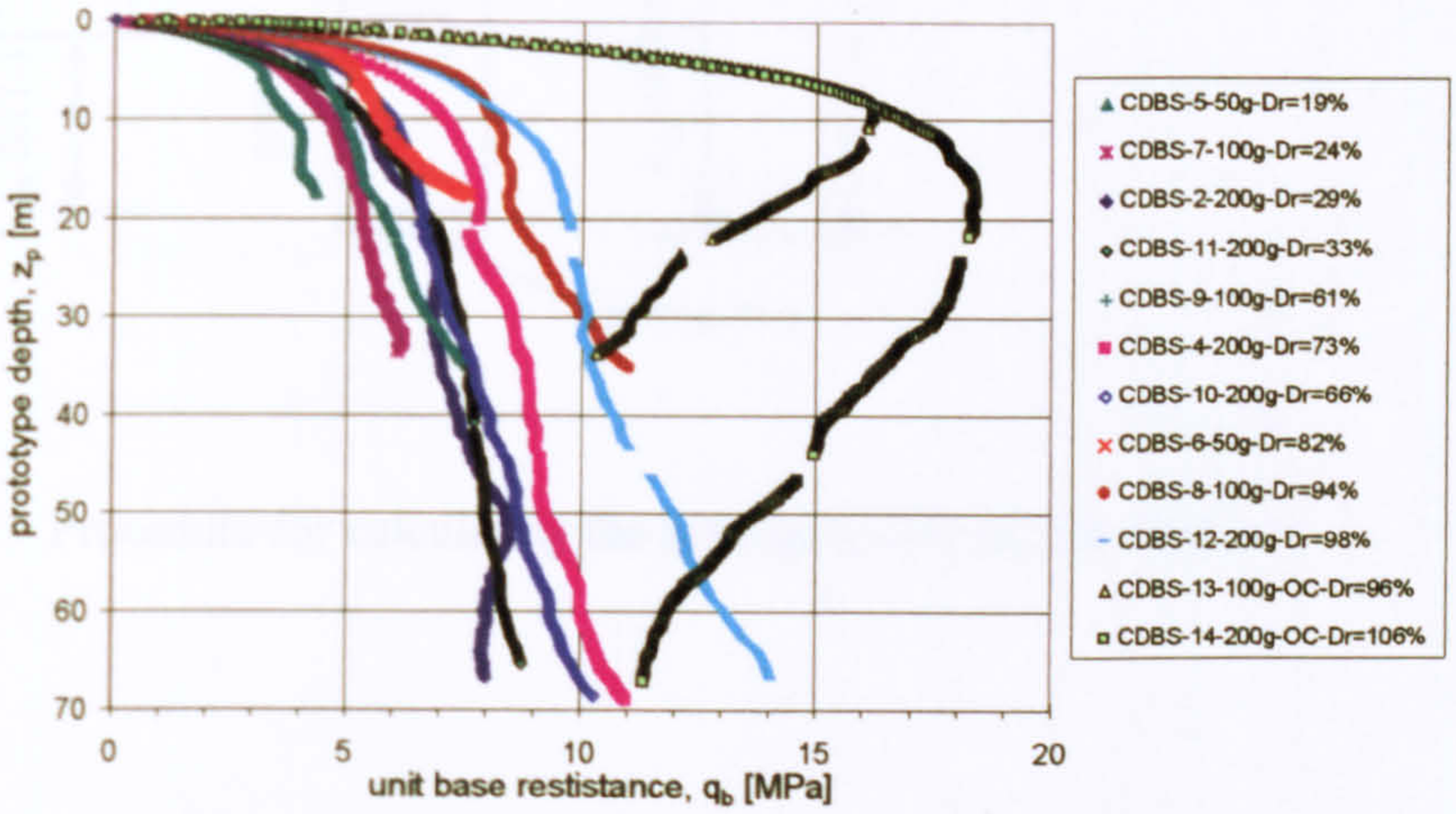

Figure 5-19: Unit base resistance for centrifuge tests on Dogs Bay sand.

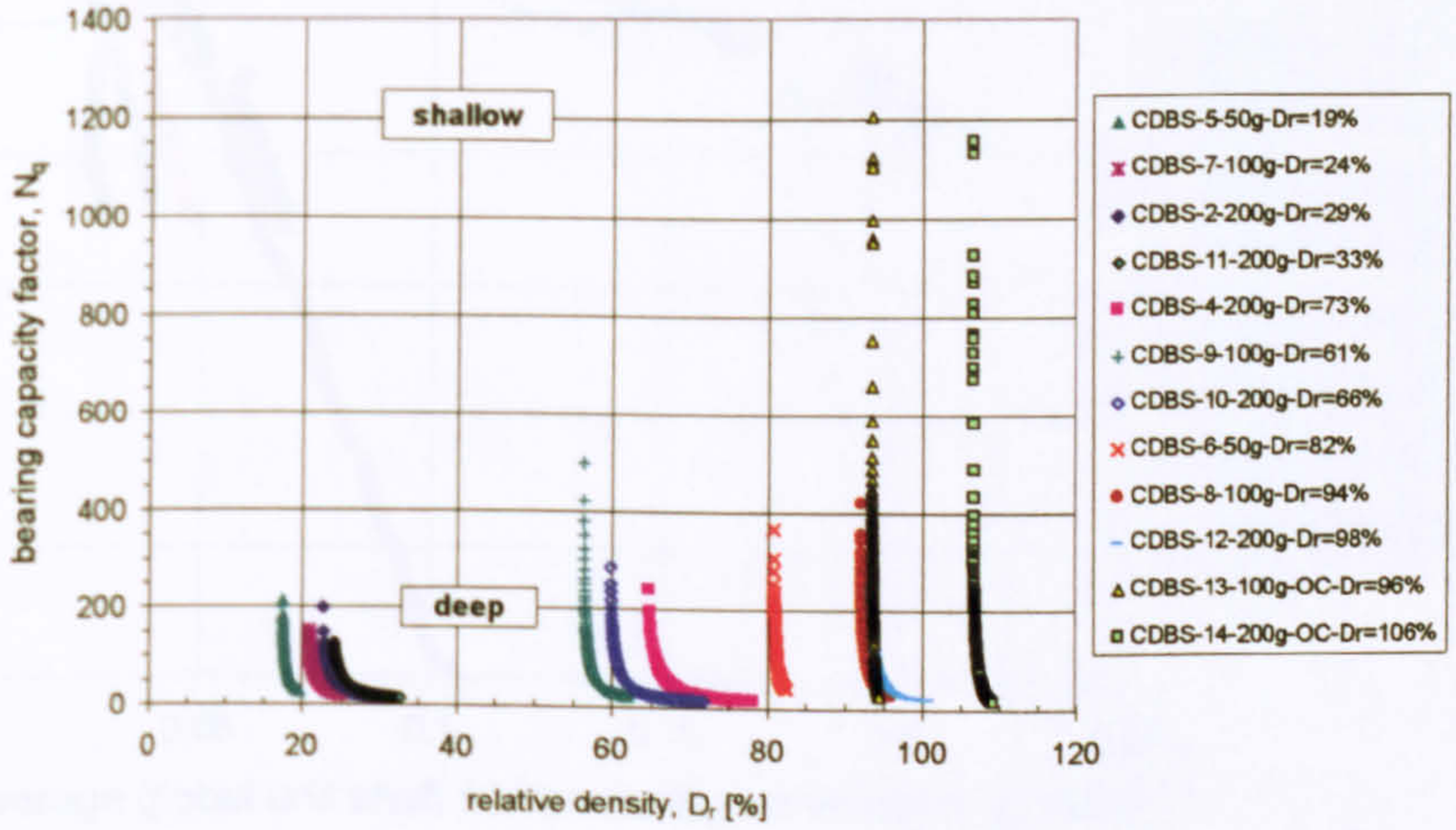

Figure 5-20: Correlation of bearing capacity factor with relative density for centrifuge tests on Dogs Bay sand.

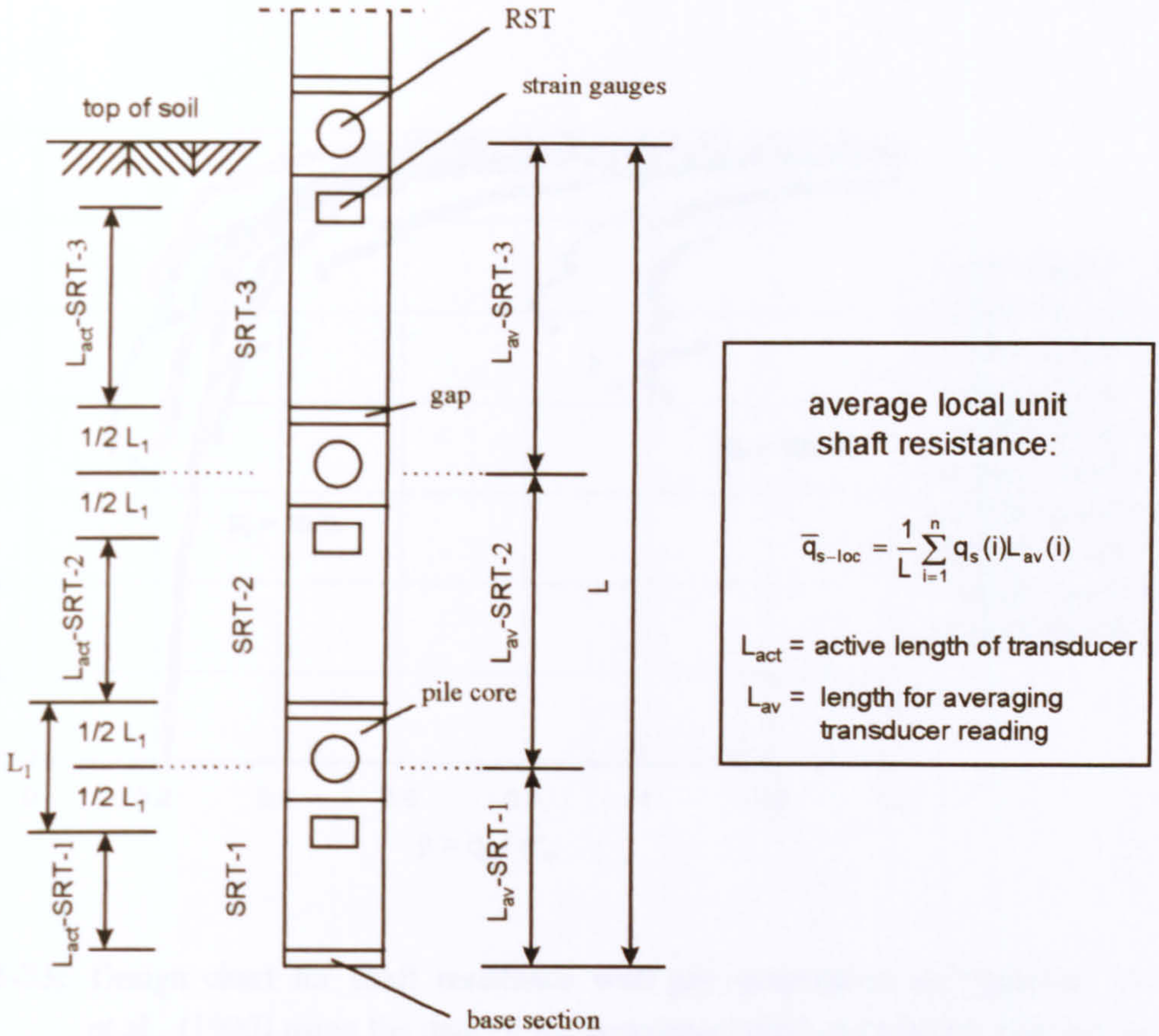

Figure 5-21: Procedure for calculating the average local unit shaft friction.

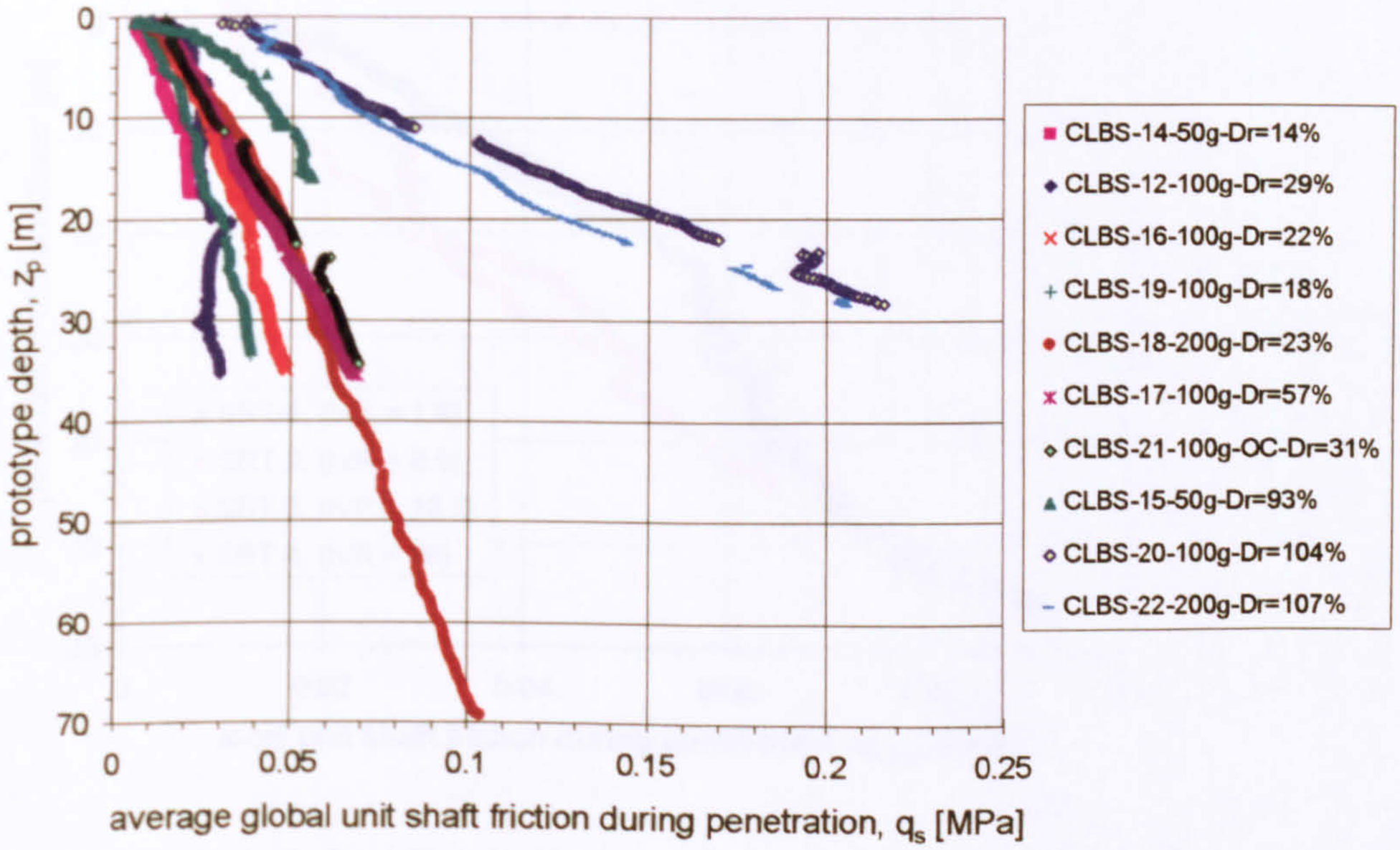

Figure 5-22: Average global unit shaft friction for centrifuge tests on Leighton Buzzard sand.

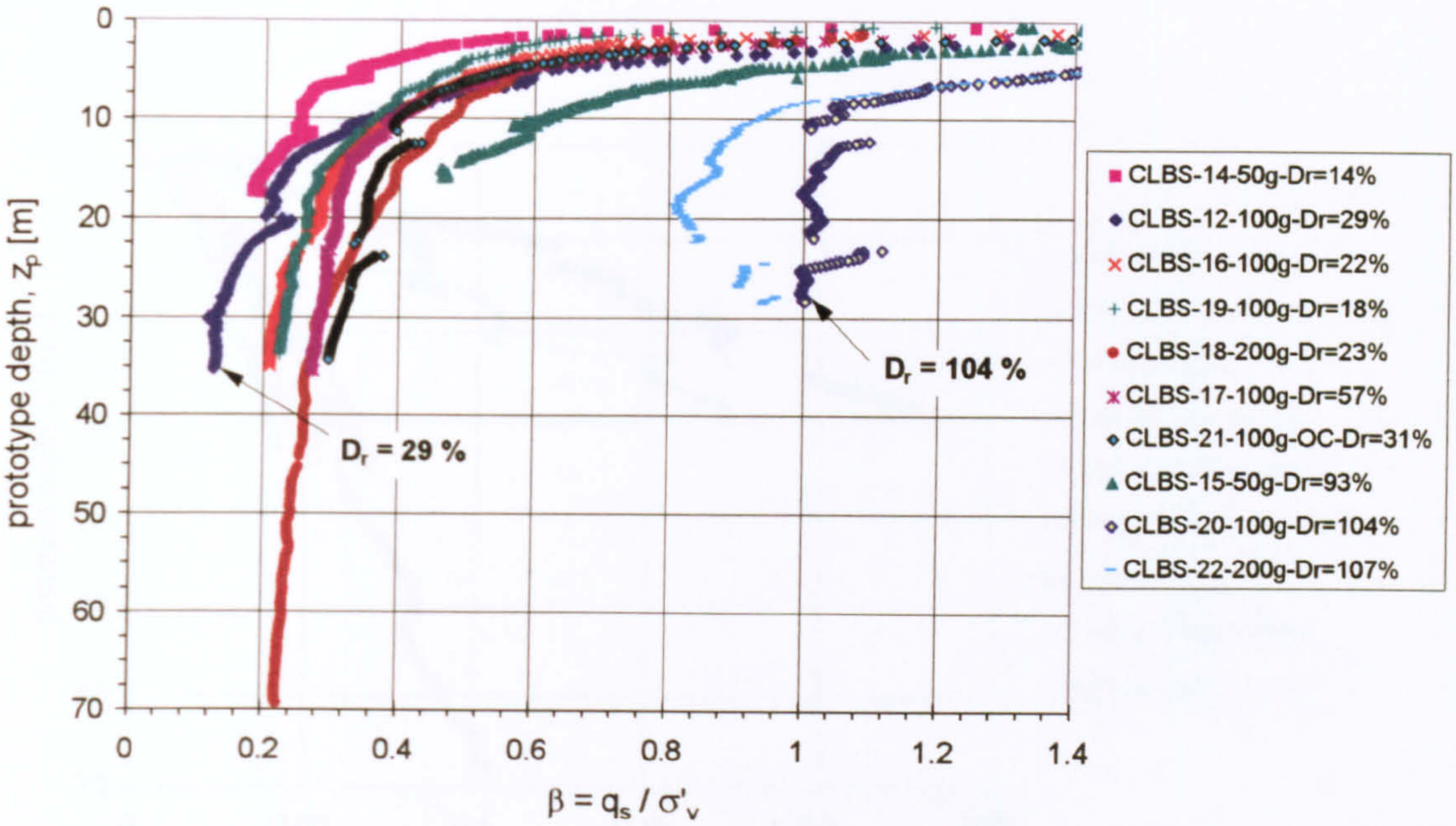

Figure 5-23: Design chart for shaft resistance with pile penetration as proposed by Toolan et al., (1990) using the data of the centrifuge tests on Leighton Buzzard sand (D_r-values represent average relative density at target g-level).

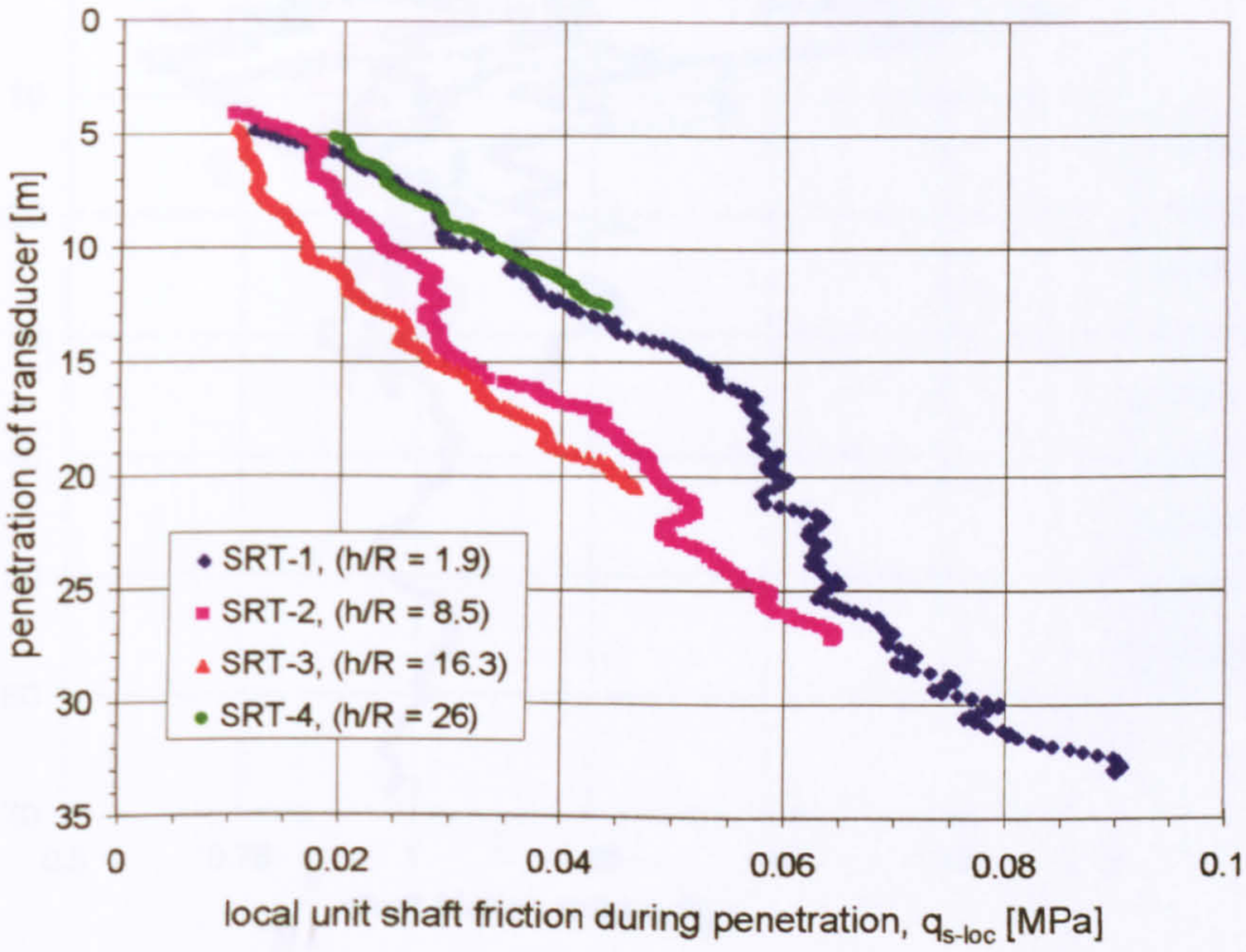

Figure 5-24: Typical plot of local unit shaft friction during penetration for Leighton Buzzard sand: test CLBS-16.

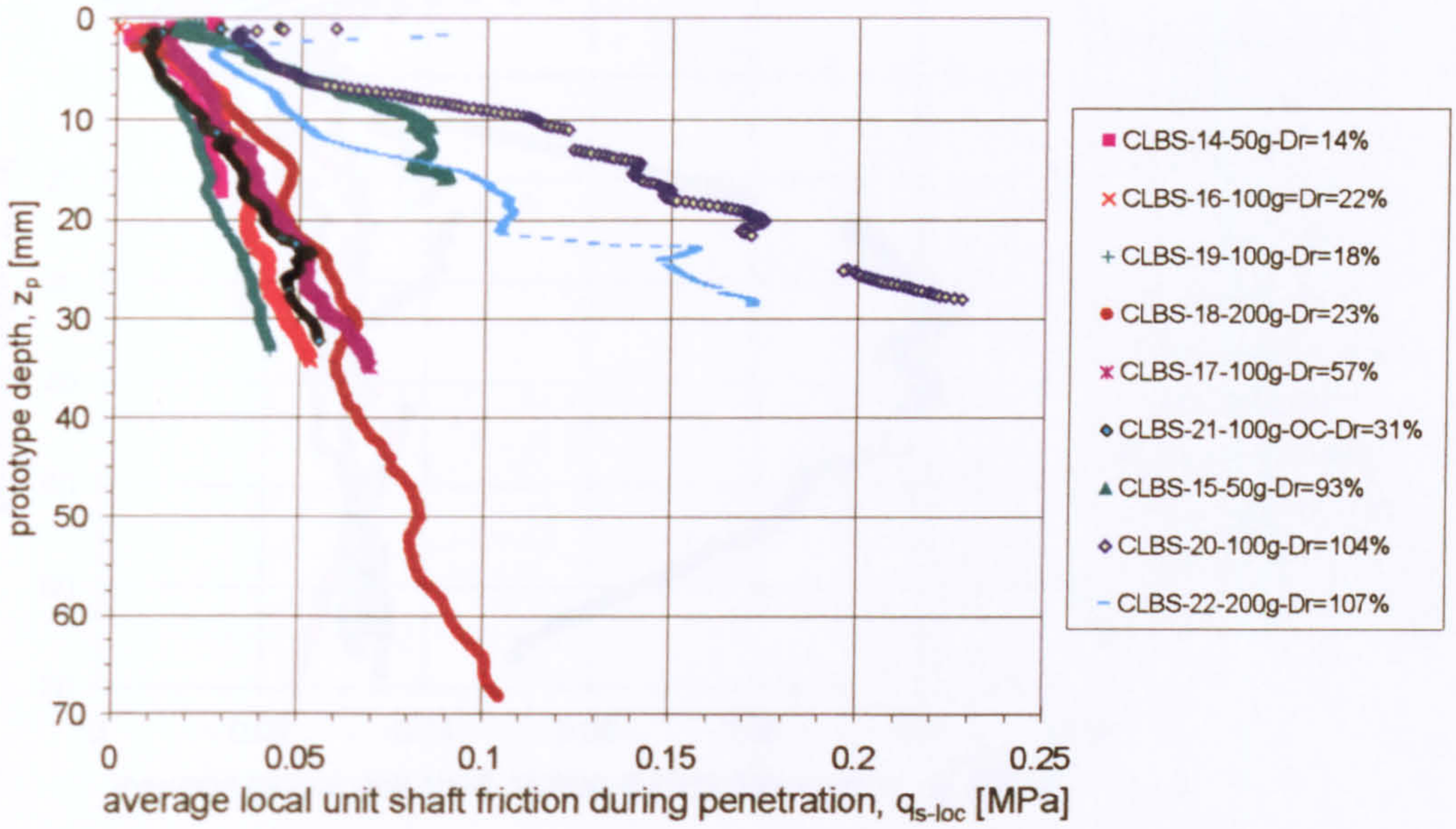

Figure 5-25a: Average local unit shaft friction for centrifuge tests on Leighton Buzzard sand.

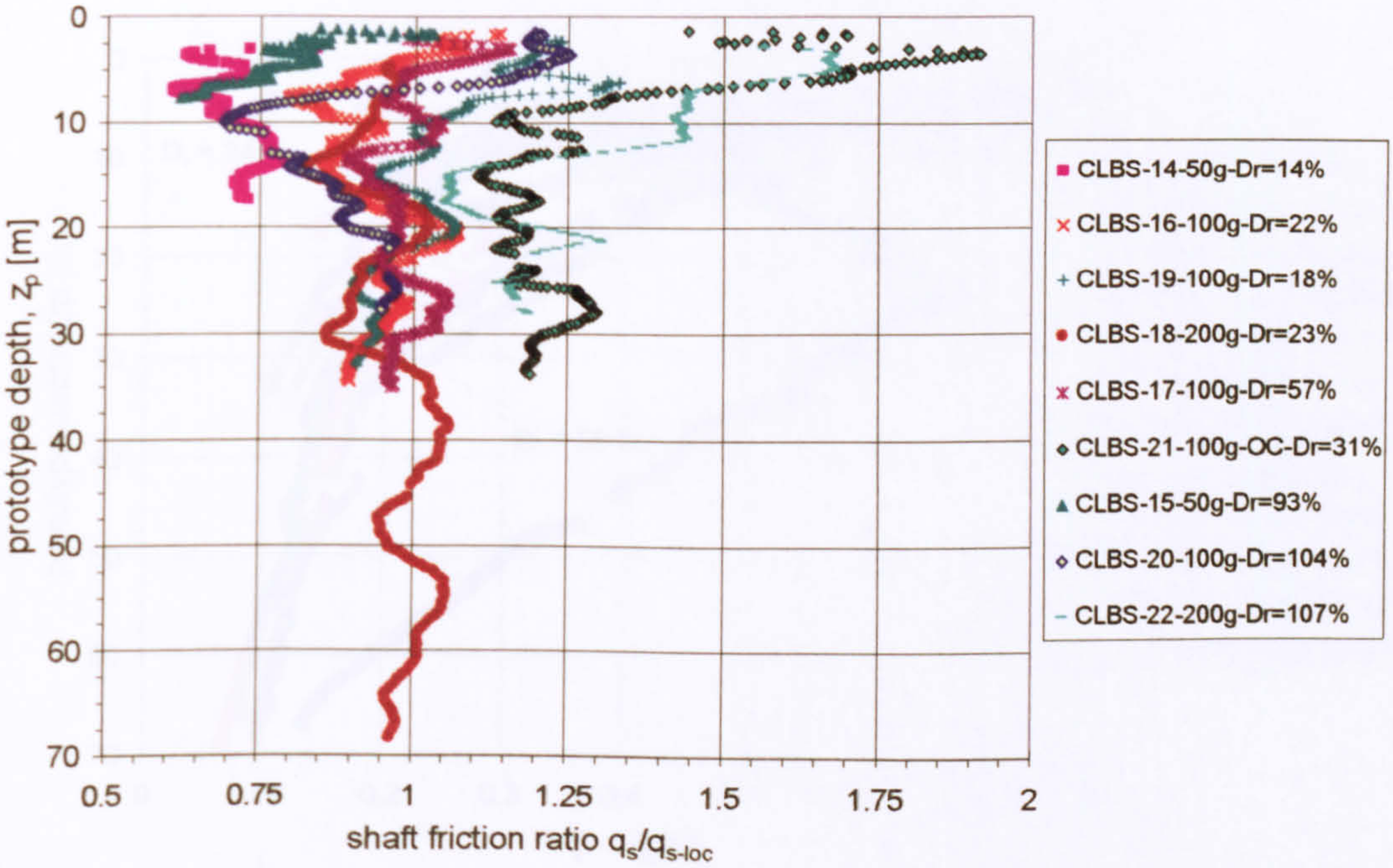

Figure 5-25b: Ratio of global to local unit shaft friction values for centrifuge tests on Leighton Buzzard sand.

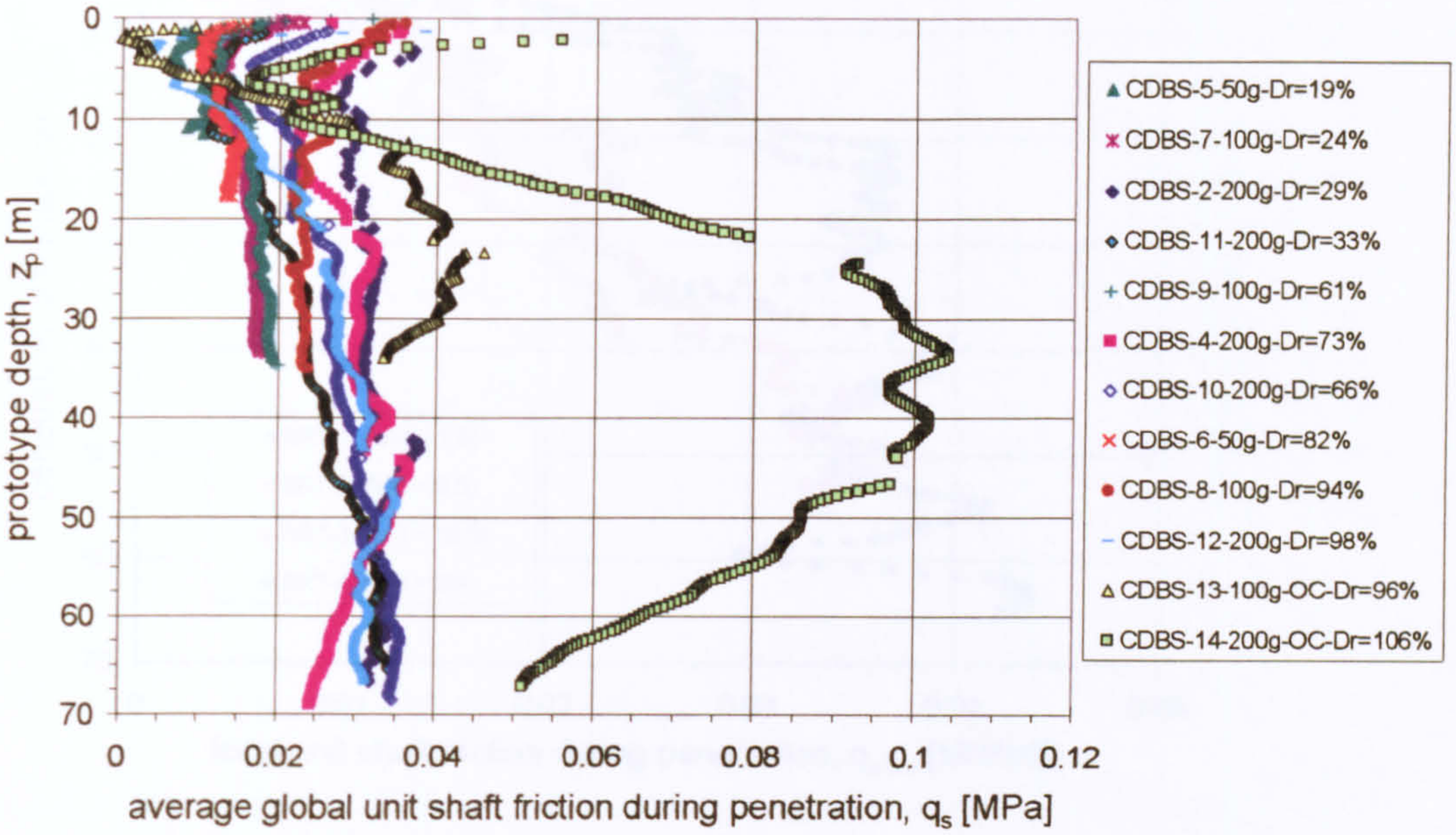

Figure 5-26: Average global unit shaft friction for centrifuge tests on Dogs Bay sand.

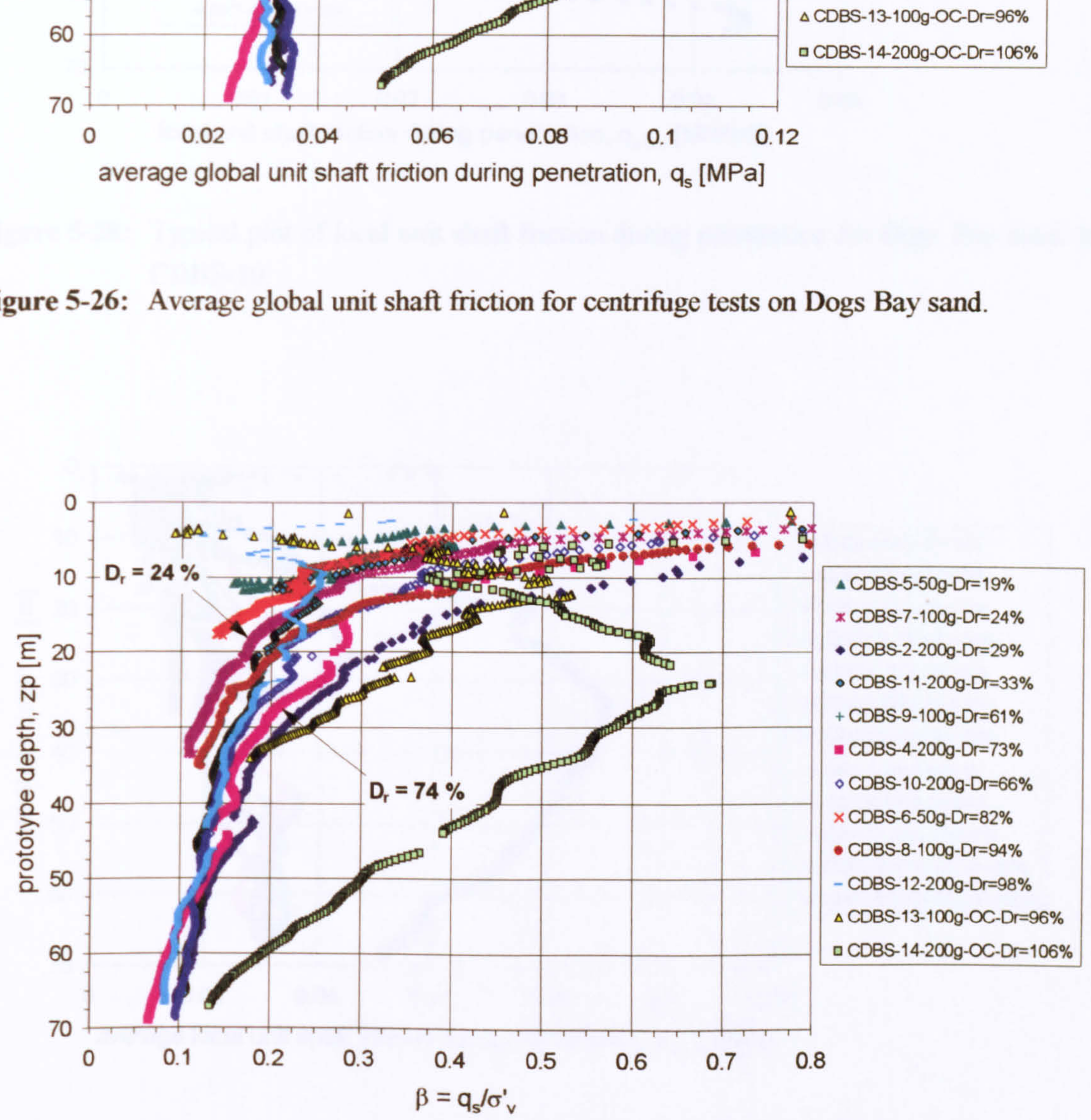

Figure 5-27: Design chart for shaft capacity with pile penetration as proposed by Toolan et al., (1990) using the data of the centrifuge tests on Dogs Bay sand (D_r-values represent average relative density at target g-level).

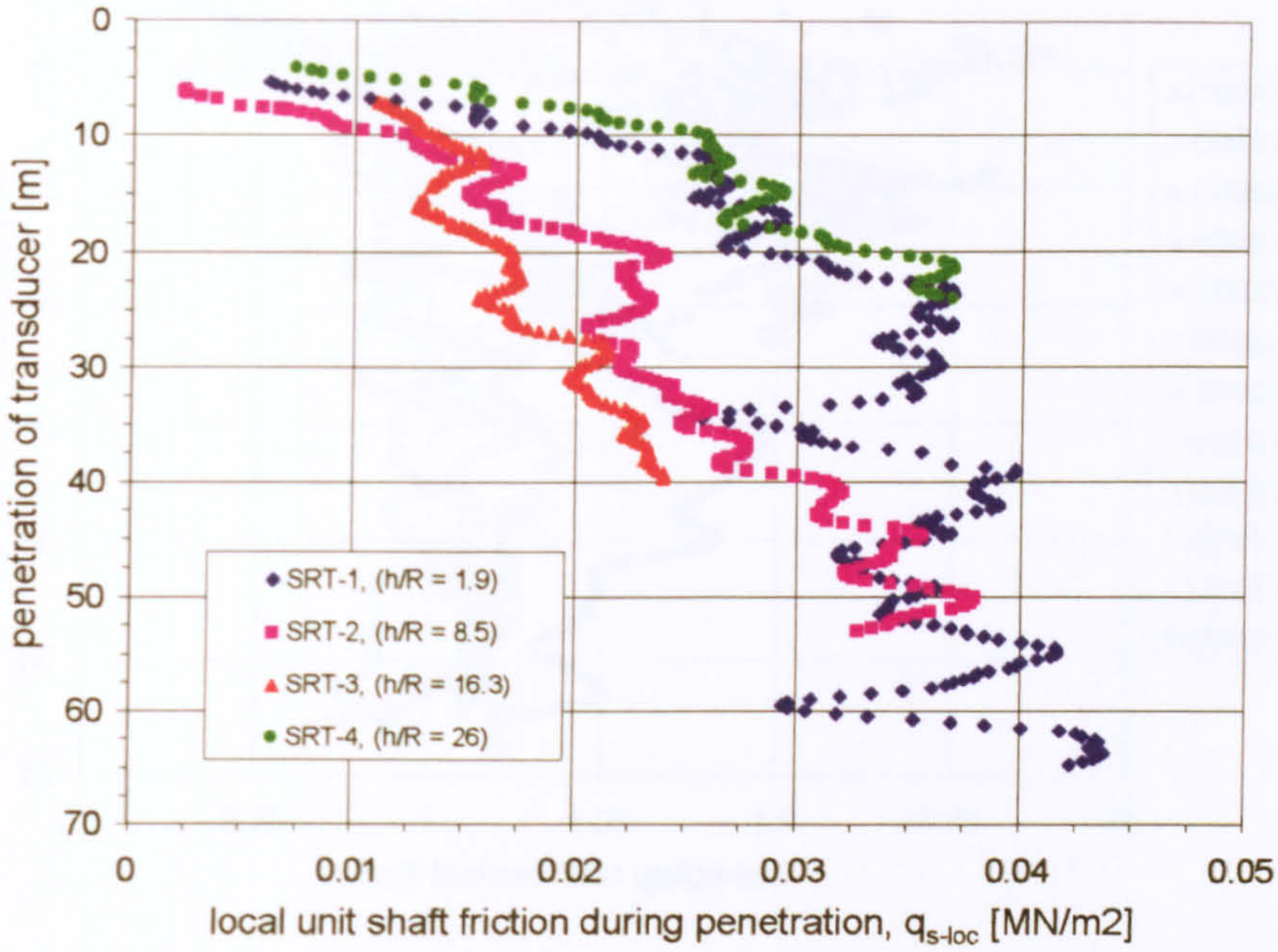

Figure 5-28: Typical plot of local unit shaft friction during penetration for Dogs Bay sand: test CDBS-10.

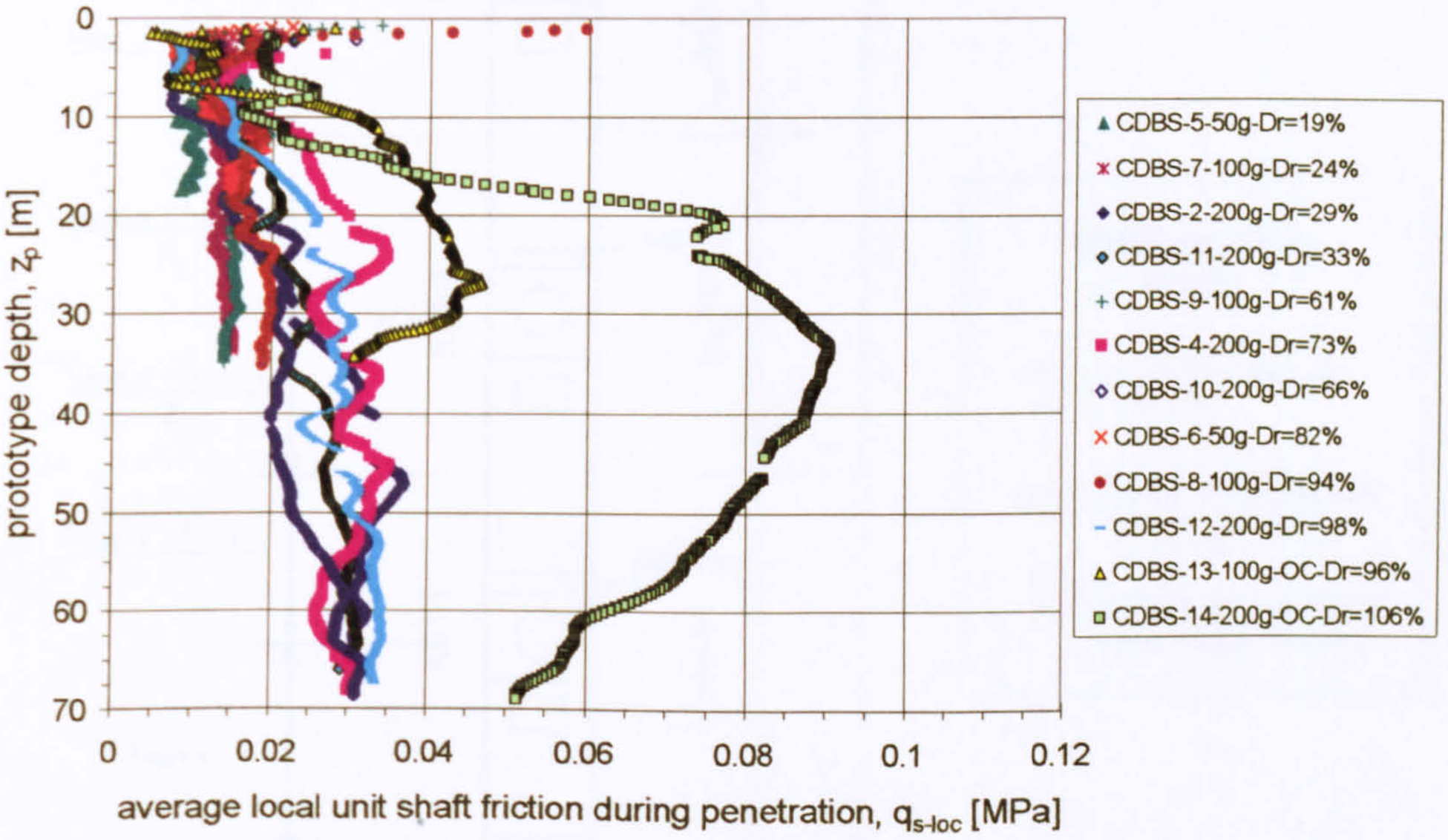

Figure 5-29a: Average local unit shaft friction for centrifuge tests on Dogs Bay sand.

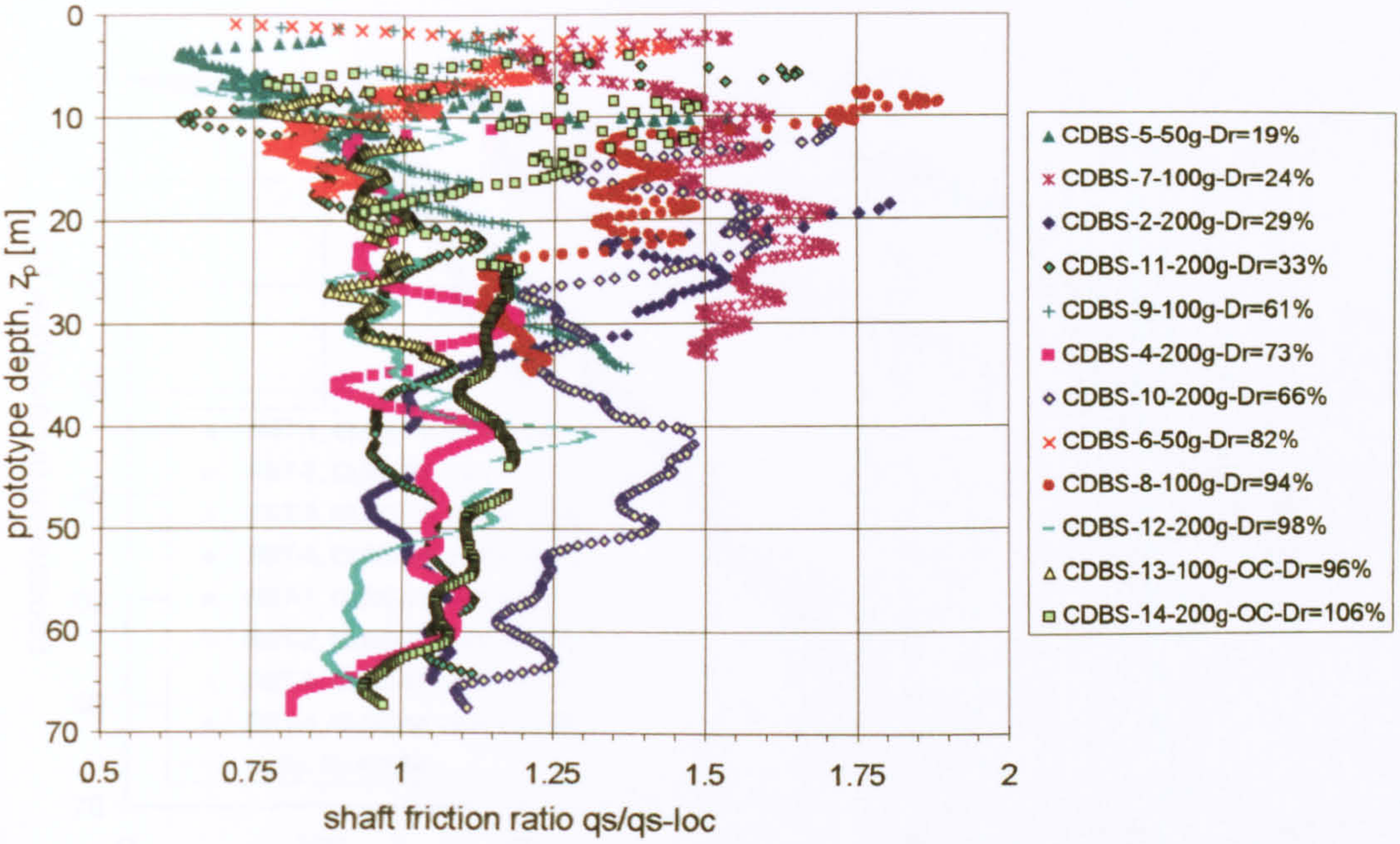

Figure 5-29b: Ratio of global to local unit shaft friction values for centrifuge tests on Dogs Bay sand.

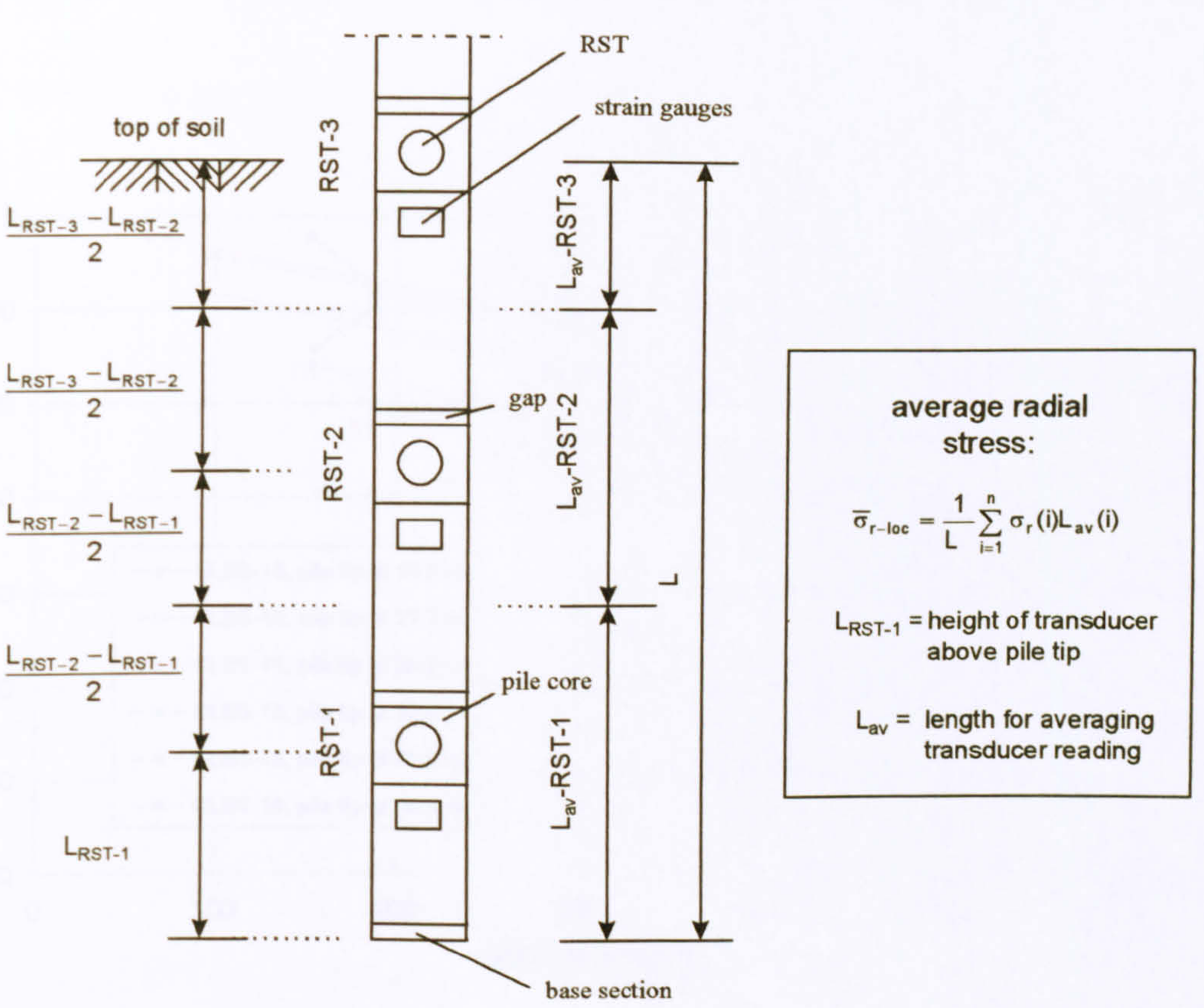

Figure 5-30: Procedure for calculating the average radial stress.

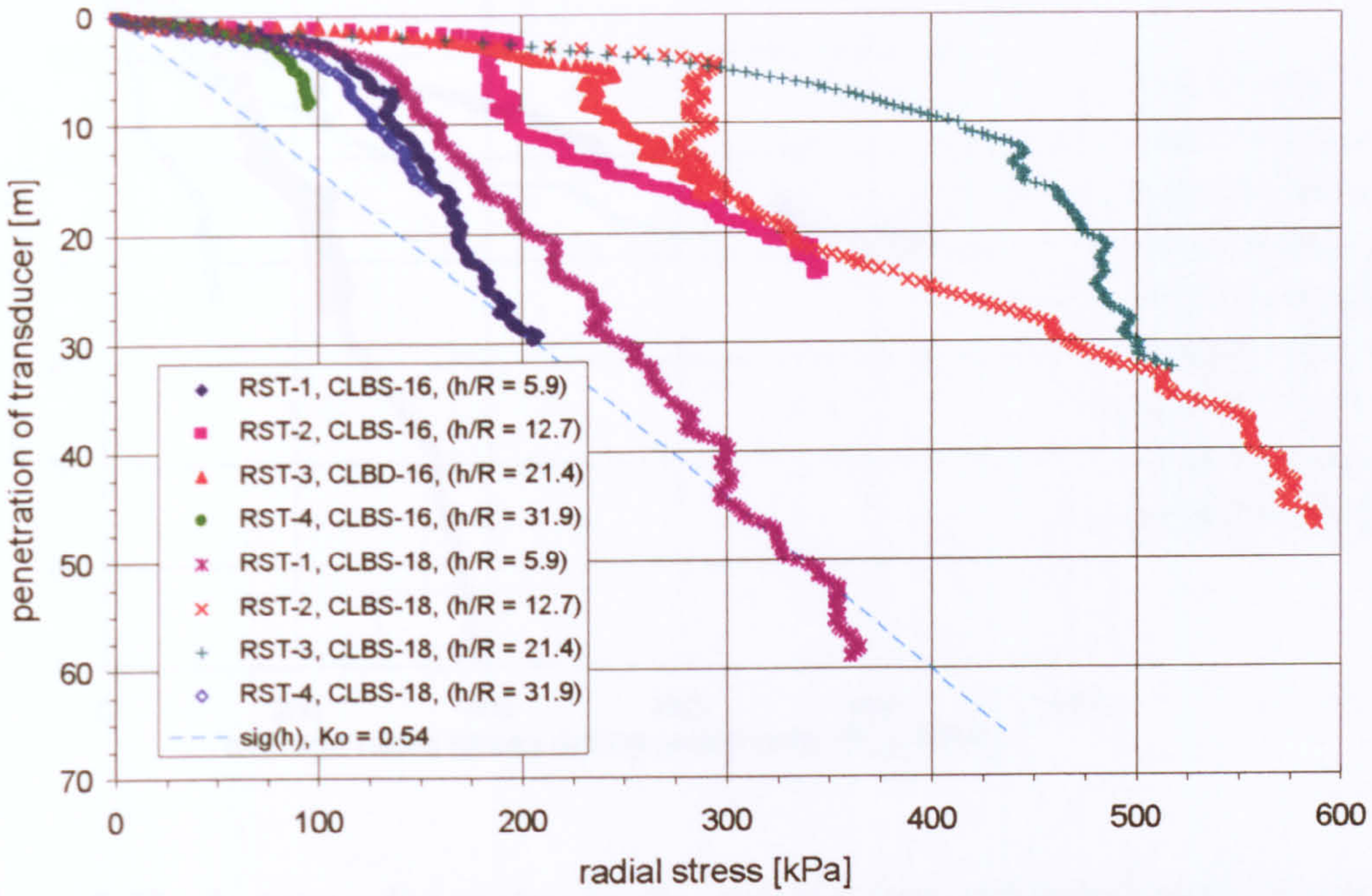

Figure 5-31: Radial stresses during installation of CUIMP-4 in tests CLBS-16 and CLBS-18.

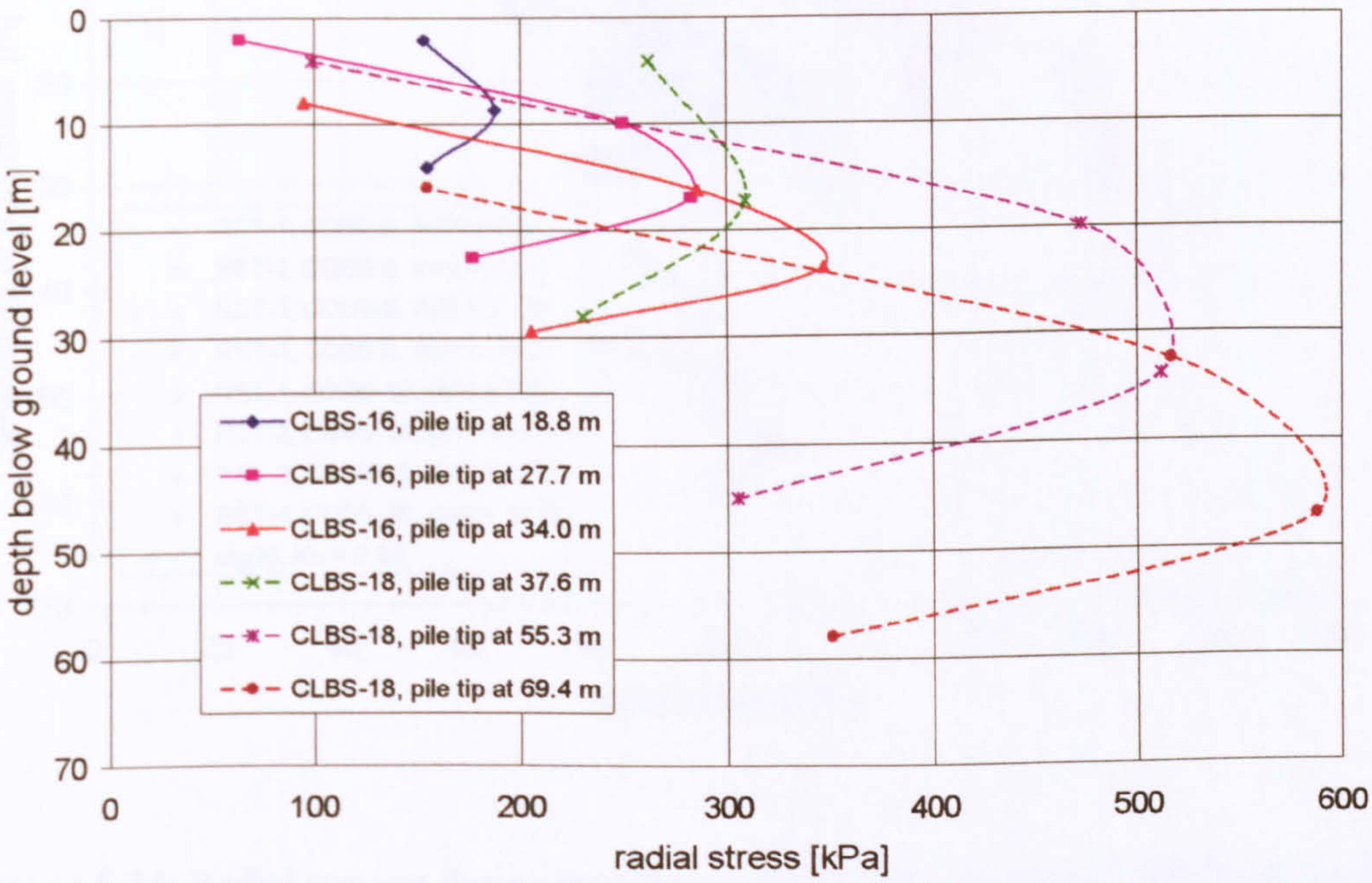

Figure 5-32: *h/R* effect on the radial stresses during installation of CUIMP-4 in tests CLBS-16 and CLBS-18.

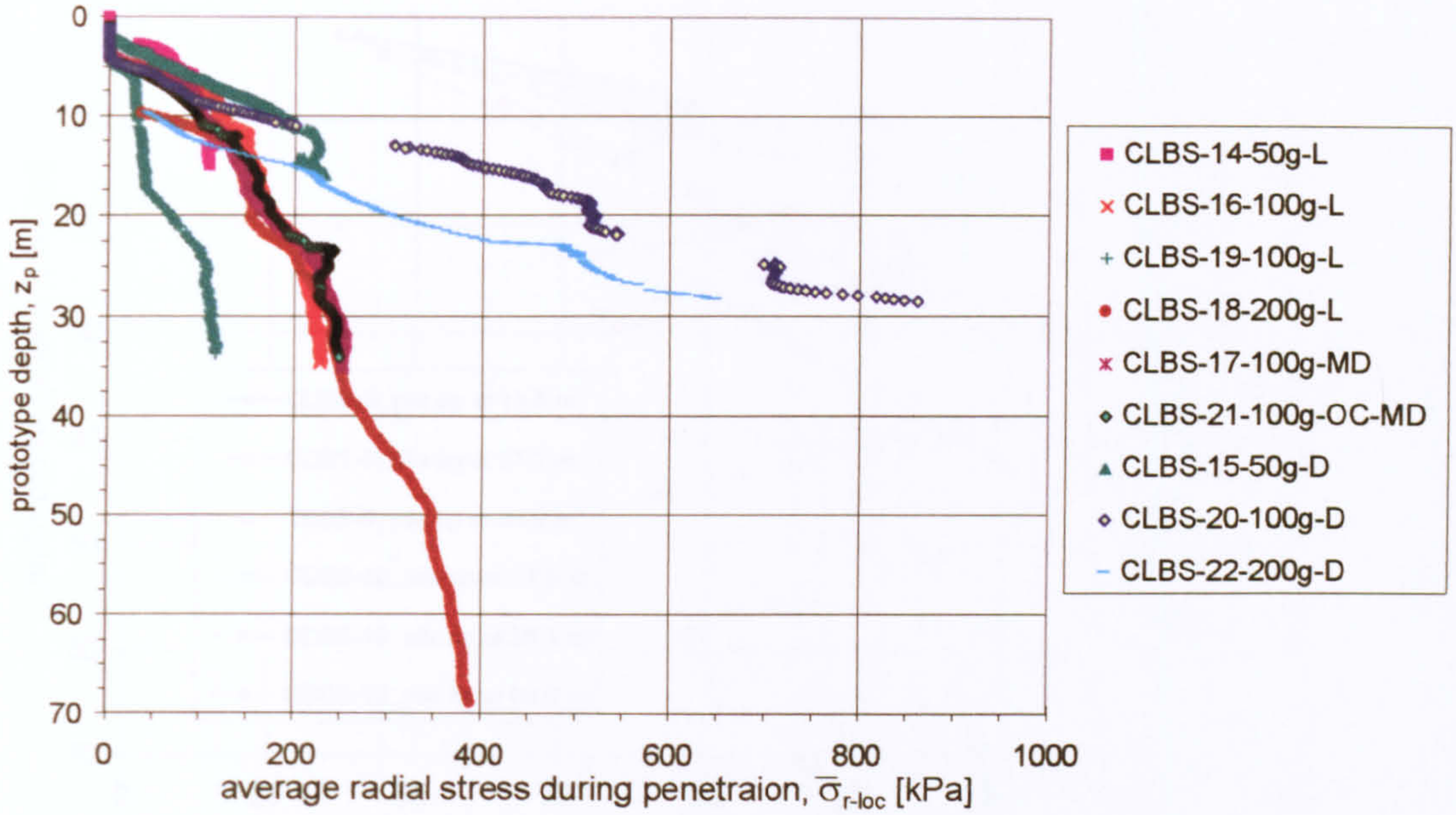

Figure 5-33: Average radial stresses for the centrifuge tests on Leighton Buzzard sand.

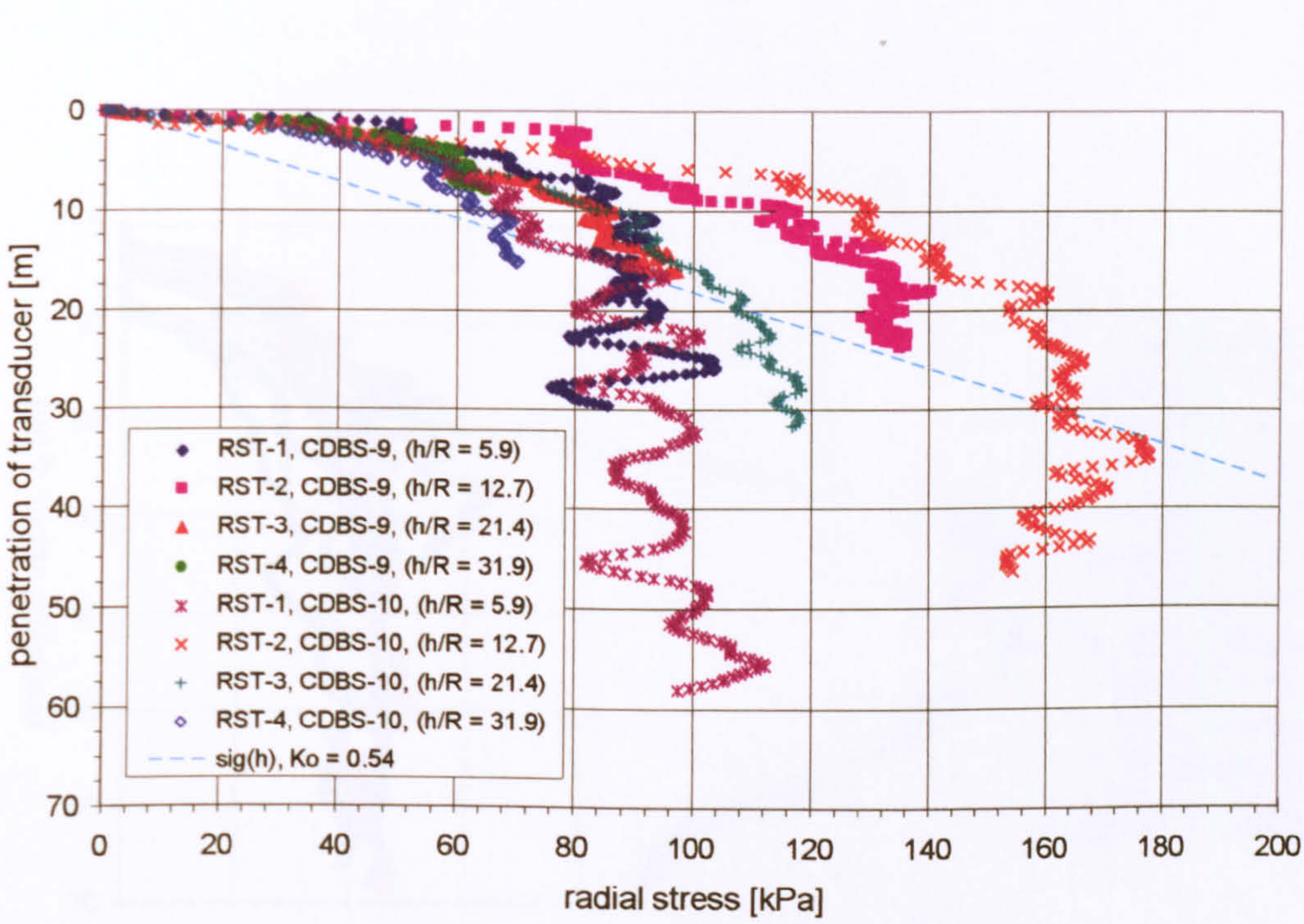

Figure 5-34: Radial stresses during installation of CUIMP-4 in tests CDBS-9 and CDBS-10.

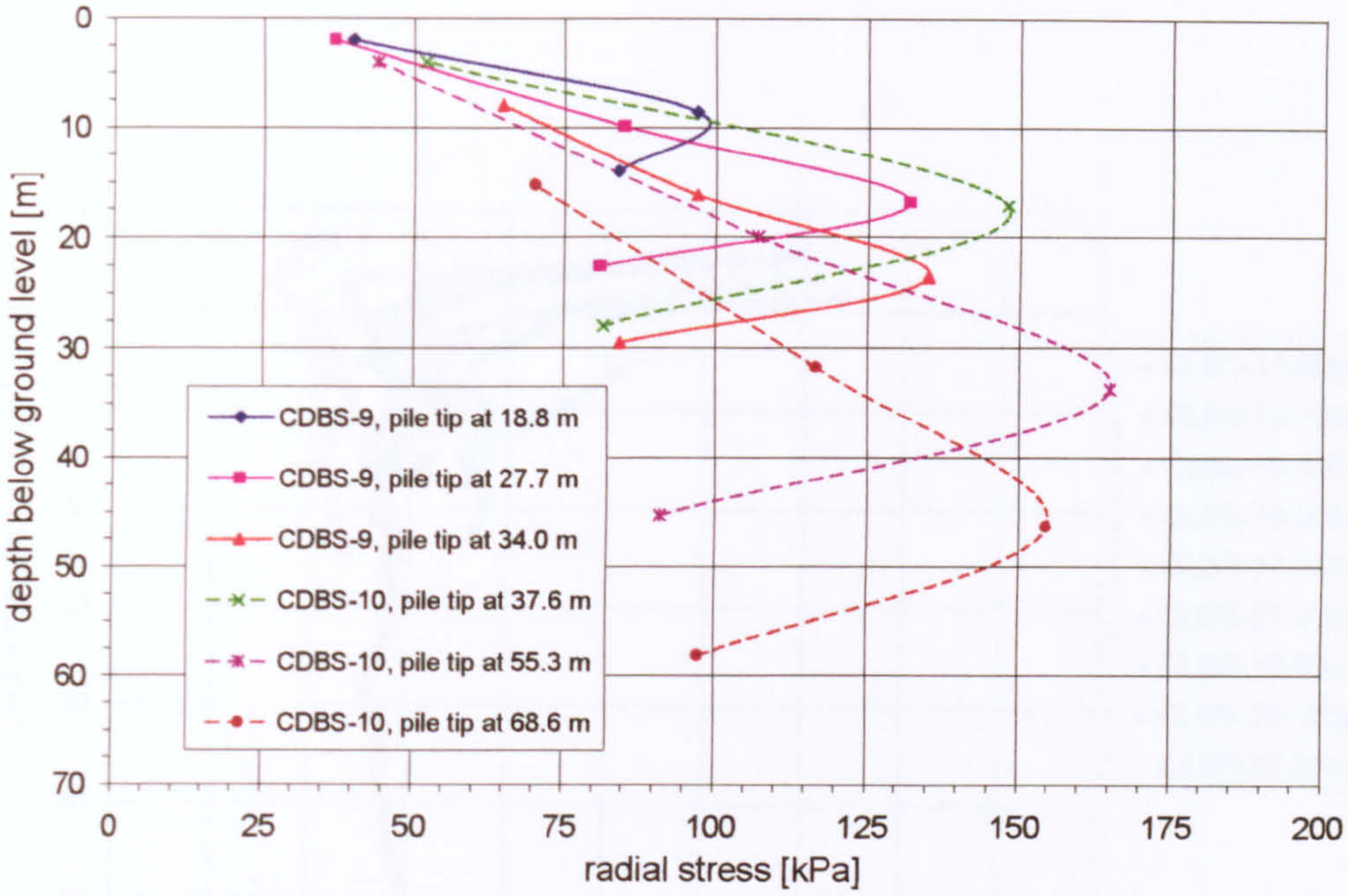

Figure 5-35: *h/R* effect on the radial stresses during installation of CUIMP-4 in tests CDBS-9 and CDBS-10.

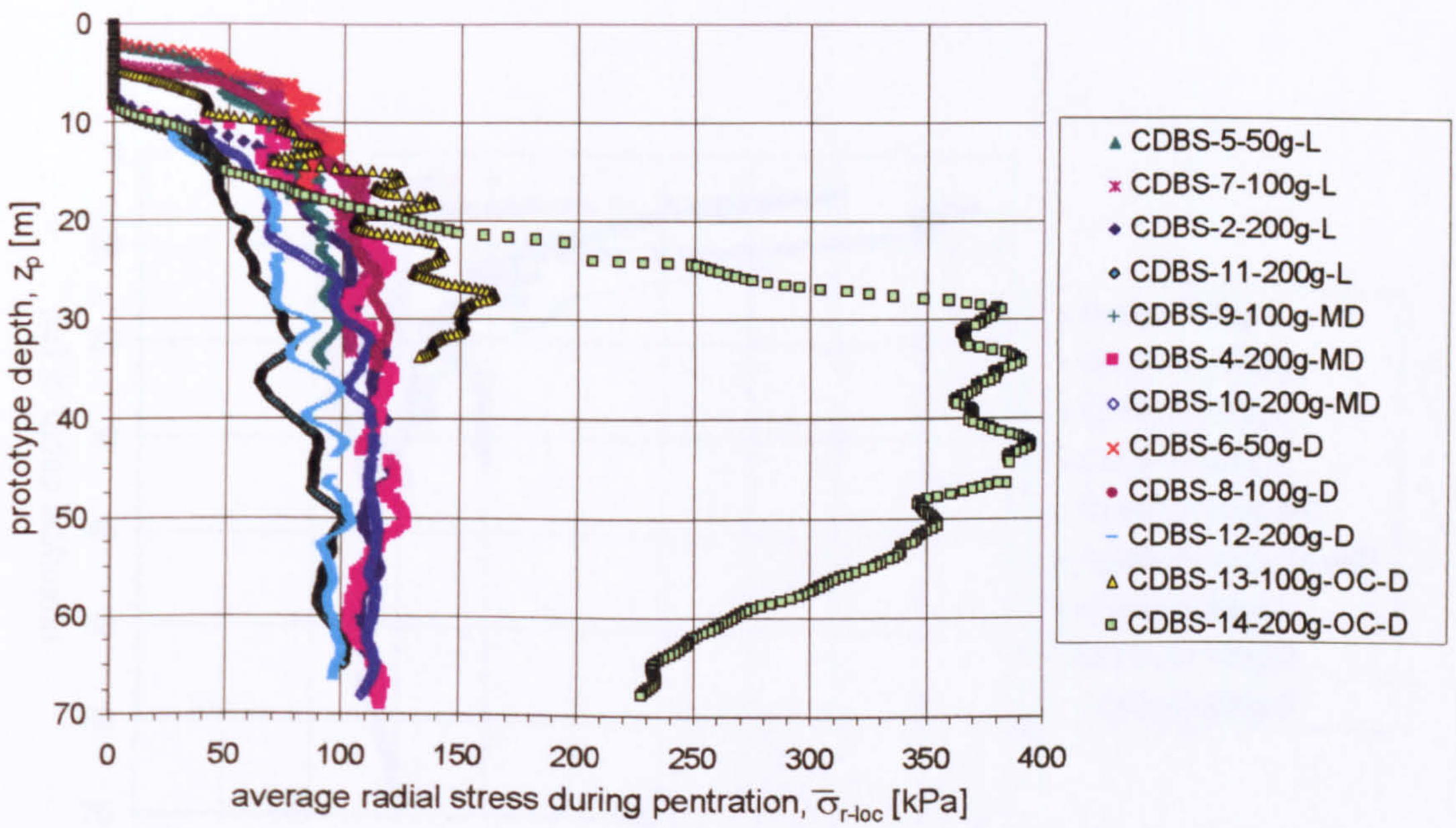

Figure 5-36: Average radial stresses for the centrifuge tests on Dogs Bay sand.

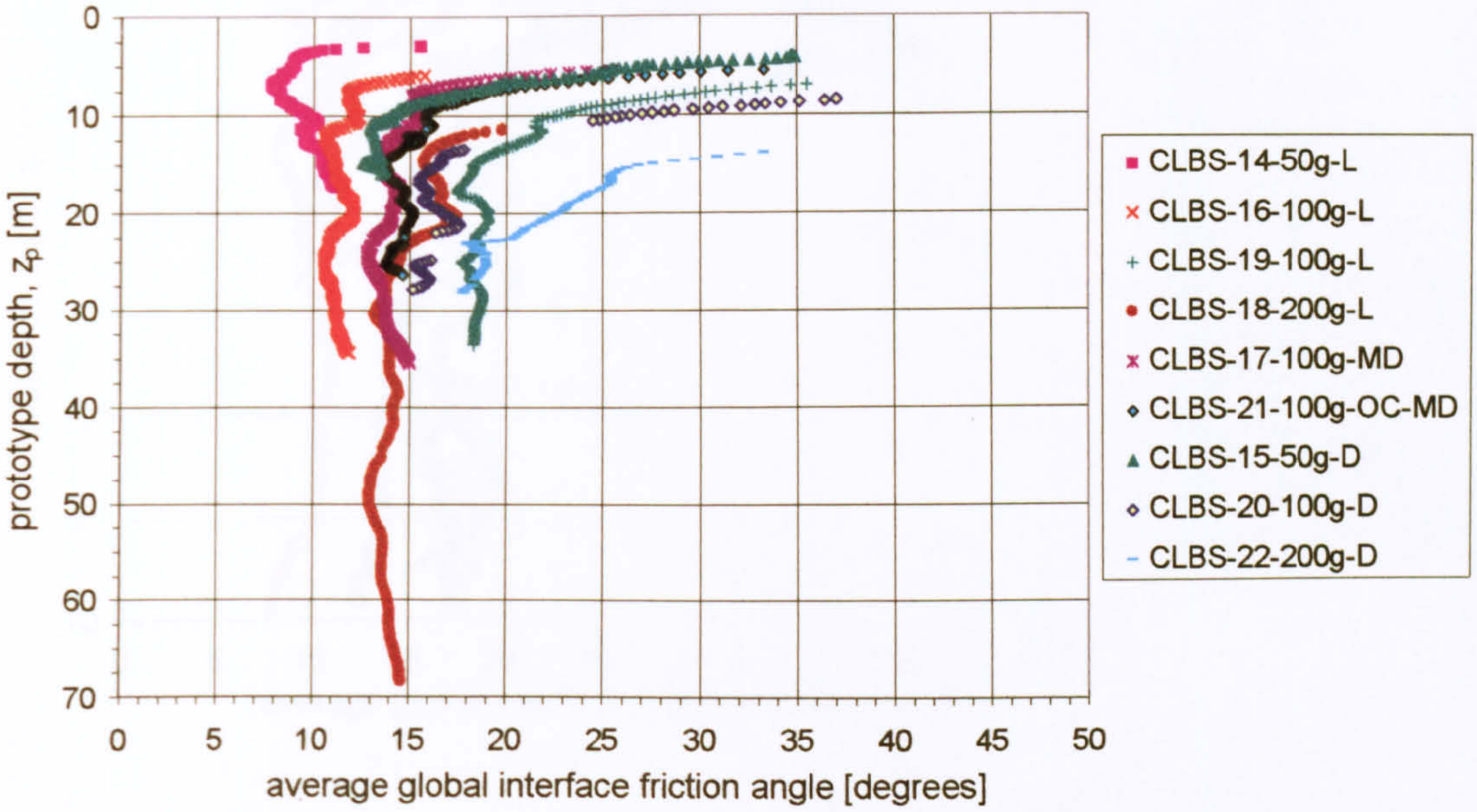

Figure 5-37: Interface friction angle given by average global unit shaft resistance and average radial stress for centrifuge tests on Leighton Buzzard sand.

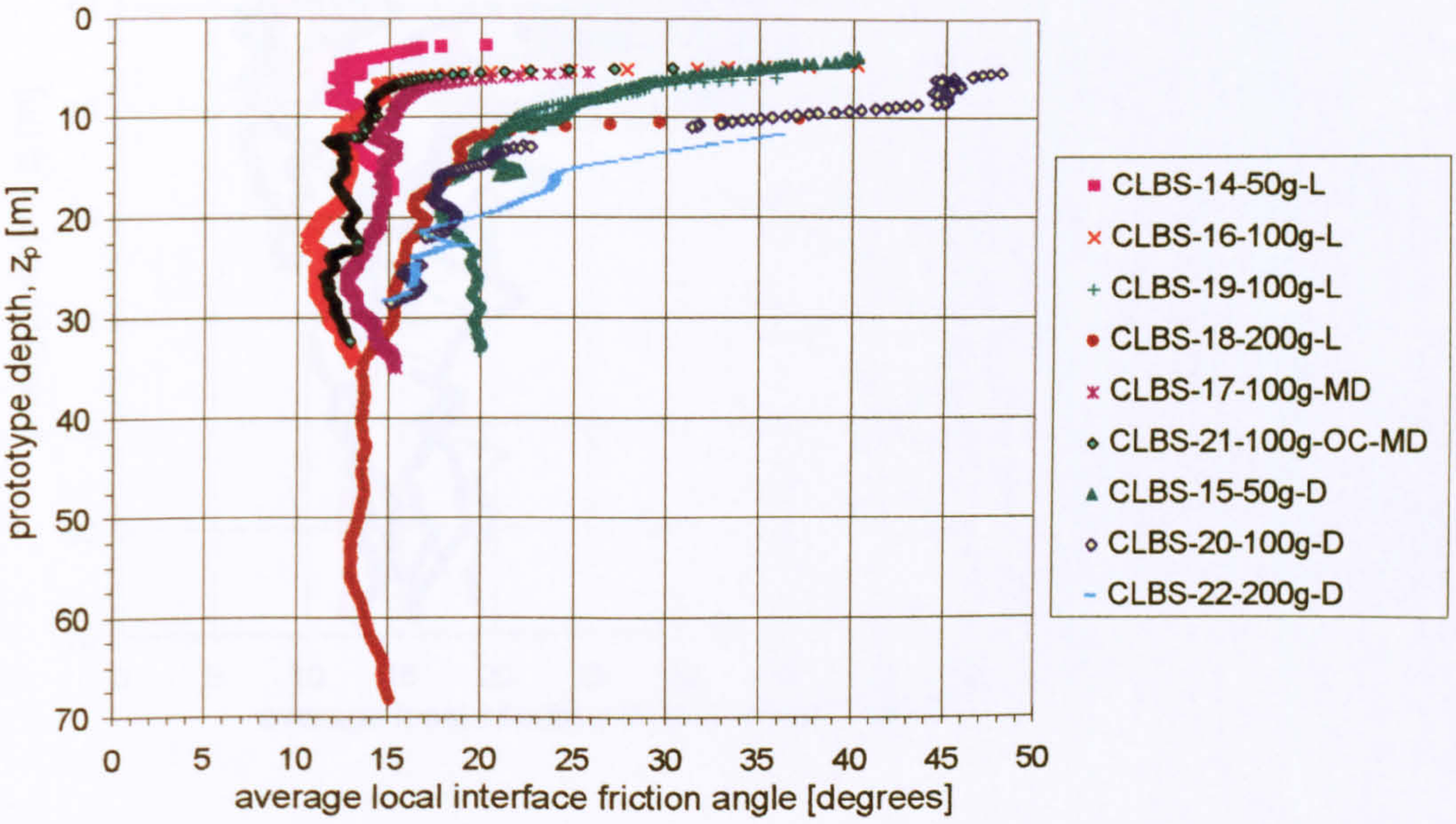

Figure 5-38: Interface friction angle given by average local unit shaft resistance and average radial stress for centrifuge tests on Leighton Buzzard sand.

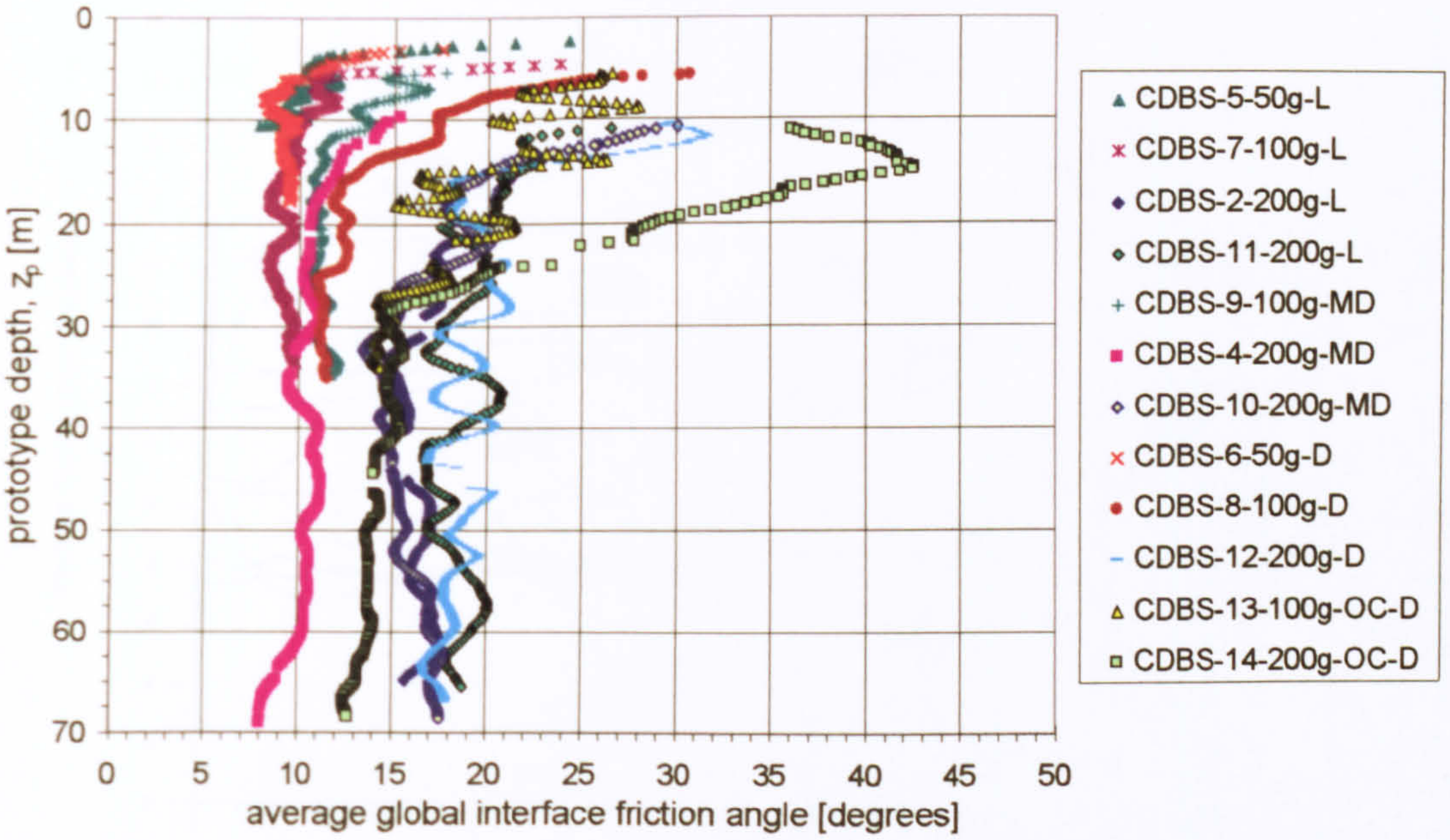

Figure 5-39: Interface friction angle given by average global unit shaft resistance and average radial stress for centrifuge tests on Dogs Bay sand.

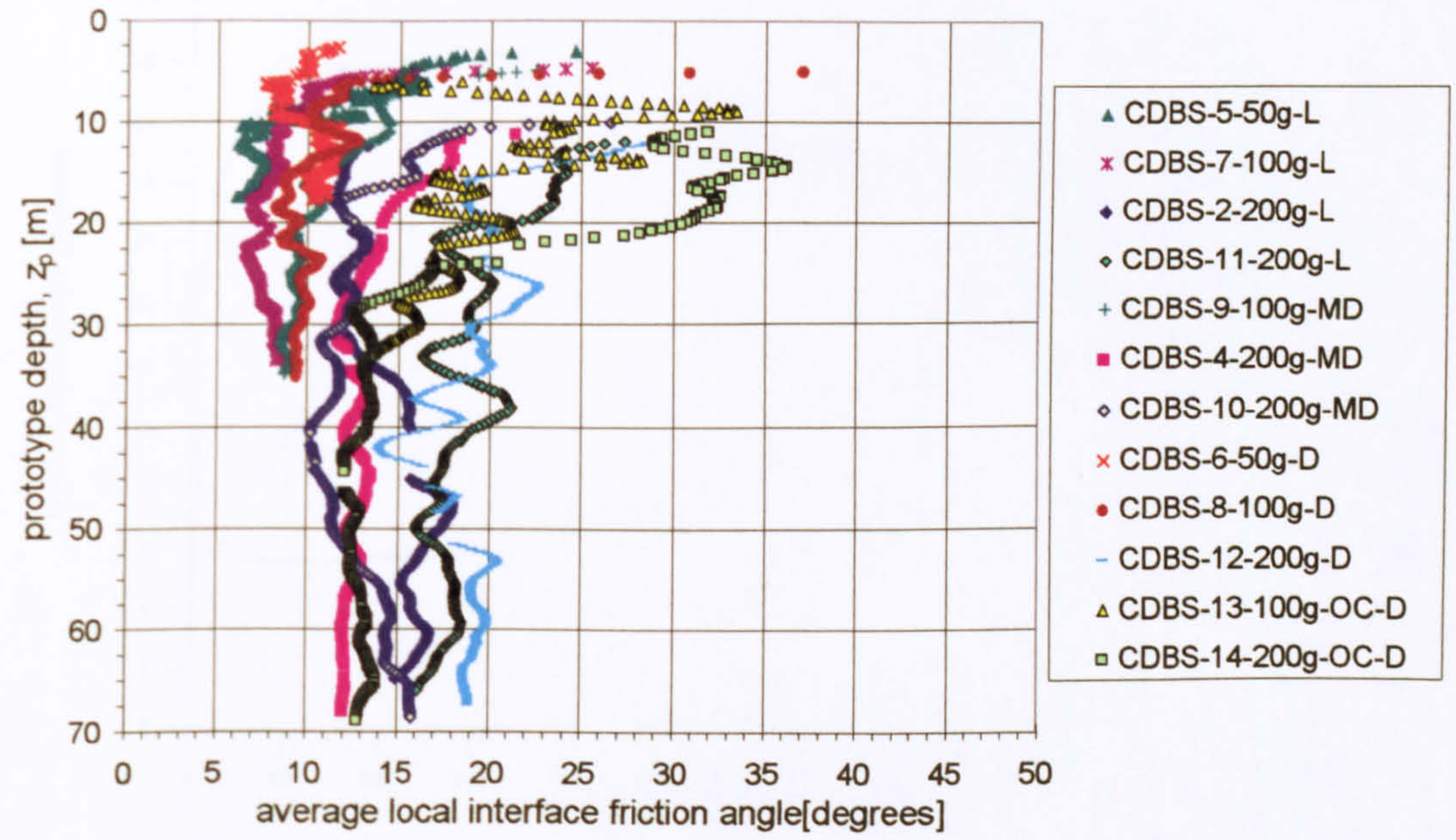

Figure 5-40: Interface friction angle given by average local unit shaft resistance and average radial stress for centrifuge tests on Dogs Bay sand.

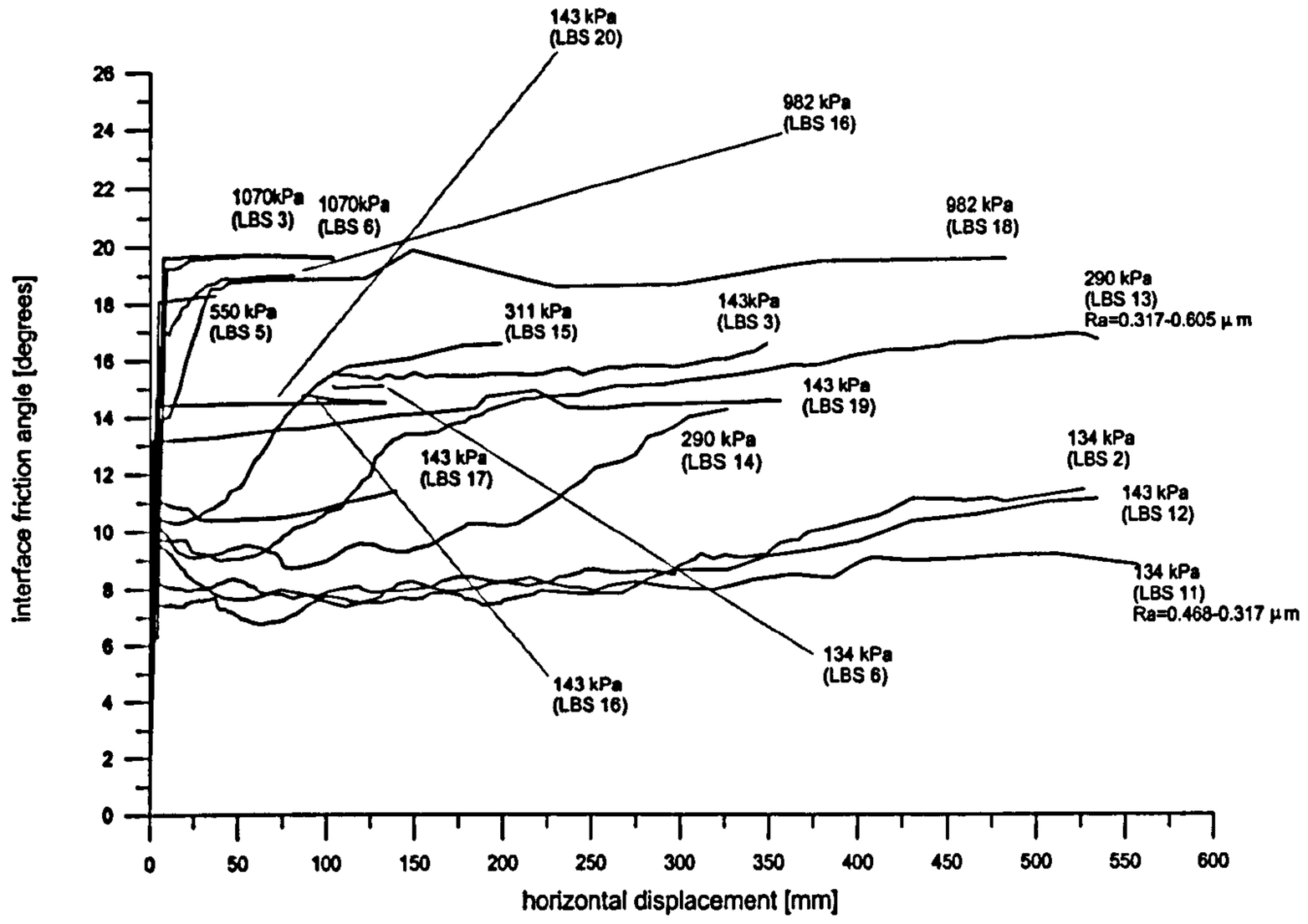

(a) Leighton Buzzard sand

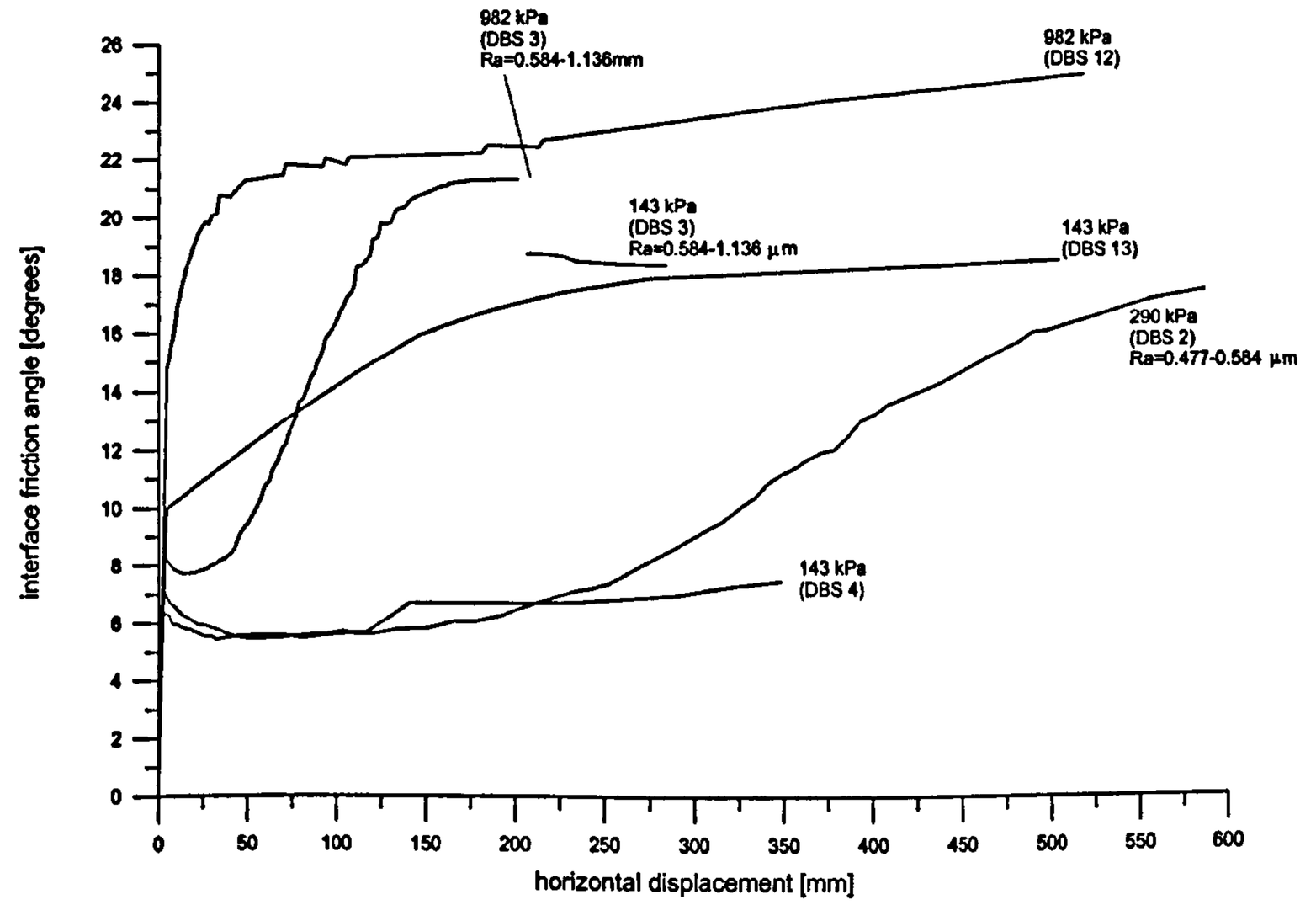

(b) Dogs Bay sand

Figure 5-41: Results of aluminium interface ring shear tests on Leighton Buzzard and Dogs Bay sand (after Cavalieri, 2000). (143 kPa refers to normal stress)

MEASUREMENT SETTINGS

Vv: 10000 **Vh**: 50 **Filter cut-off**: n/a **Date**: 4-1-1980

UNFILTERED PARAMETER RESULTS

Ra	0.536 μm	Rp	1.245 μm	Rv	4.102 μm
Rt	5.347 μm				

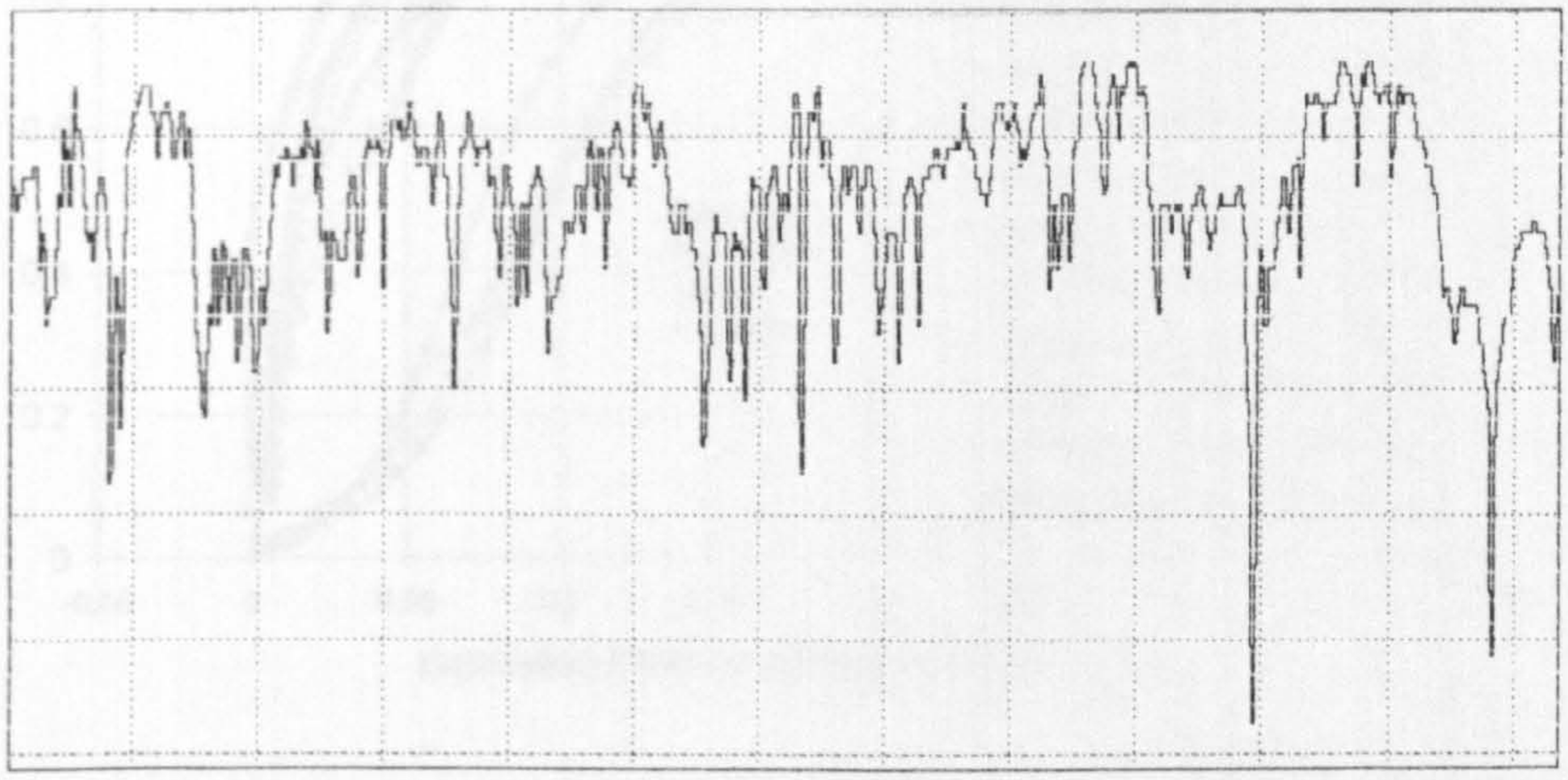

Vertical scale = 1.00 μm/div Horizontal scale = 0.20 mm/div

Figure 5-42: Roughness profile on aluminium section on CUIMP-3 at the end of the centrifuge test series.

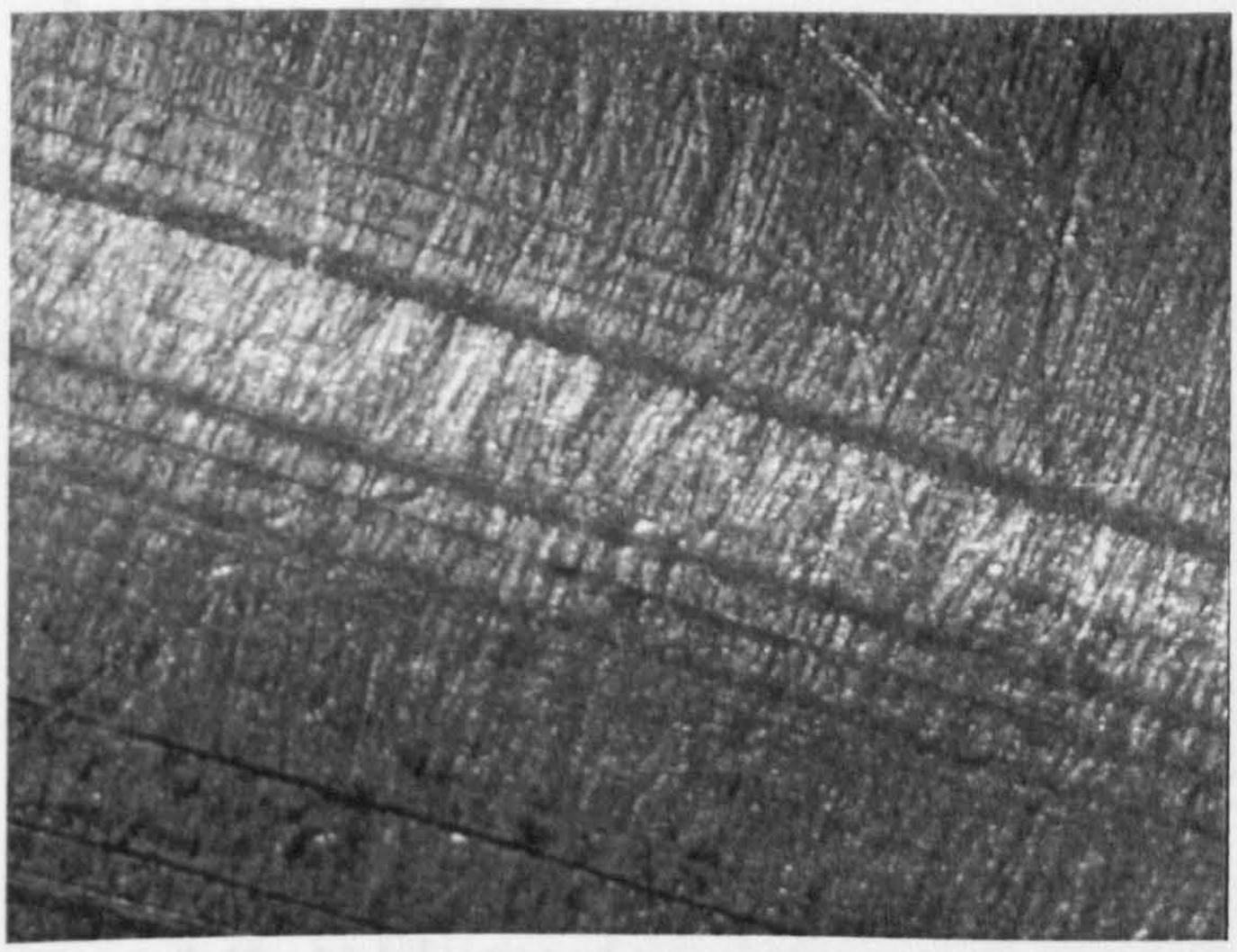

Figure 5-43: Magnified picture of the surface of an aluminium section on CUIMP-3 at the end of the centrifuge test series.

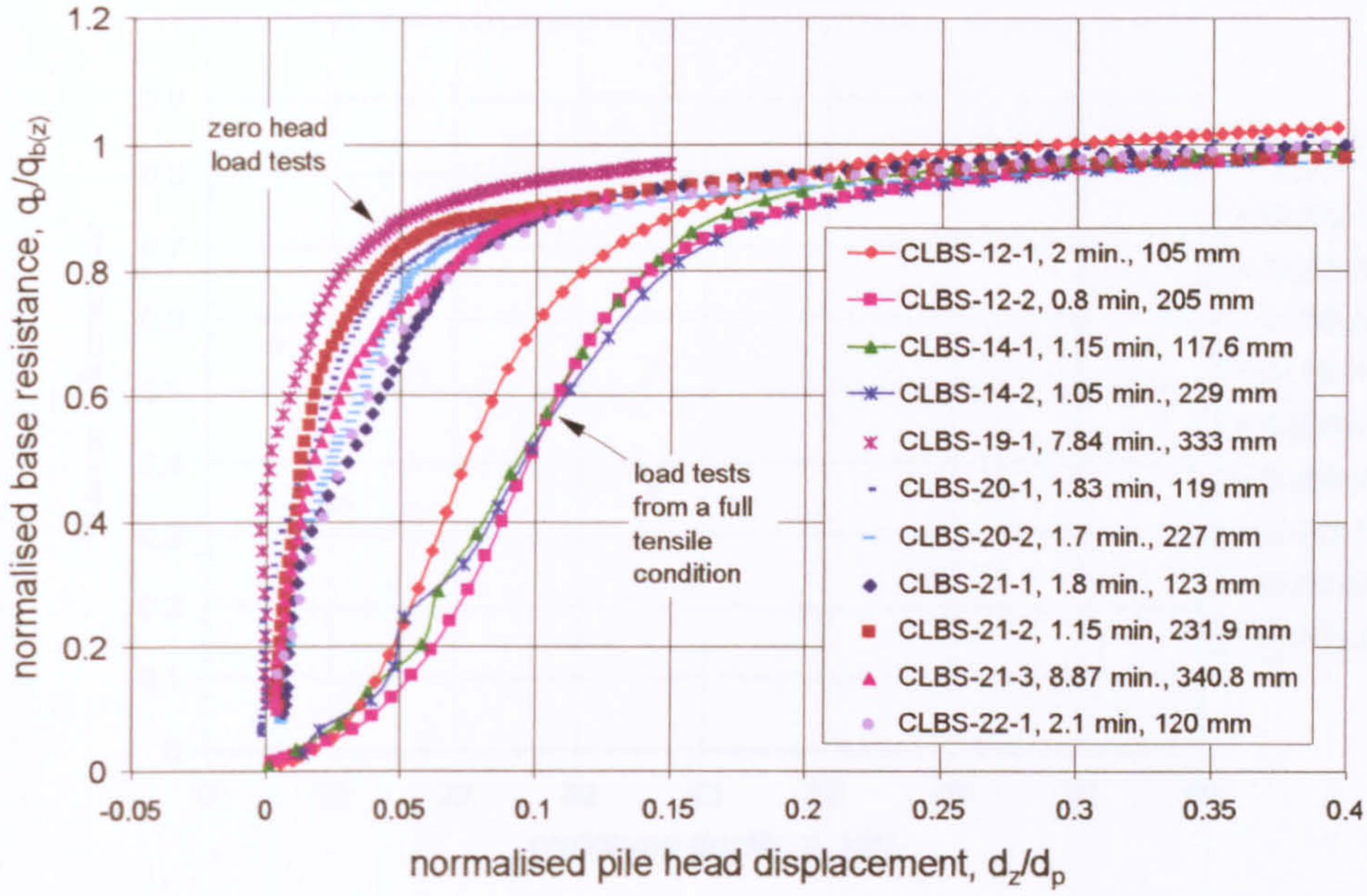

Figure 5-44: Mobilisation of unit end bearing during pile load tests in Leighton Buzzard sand.

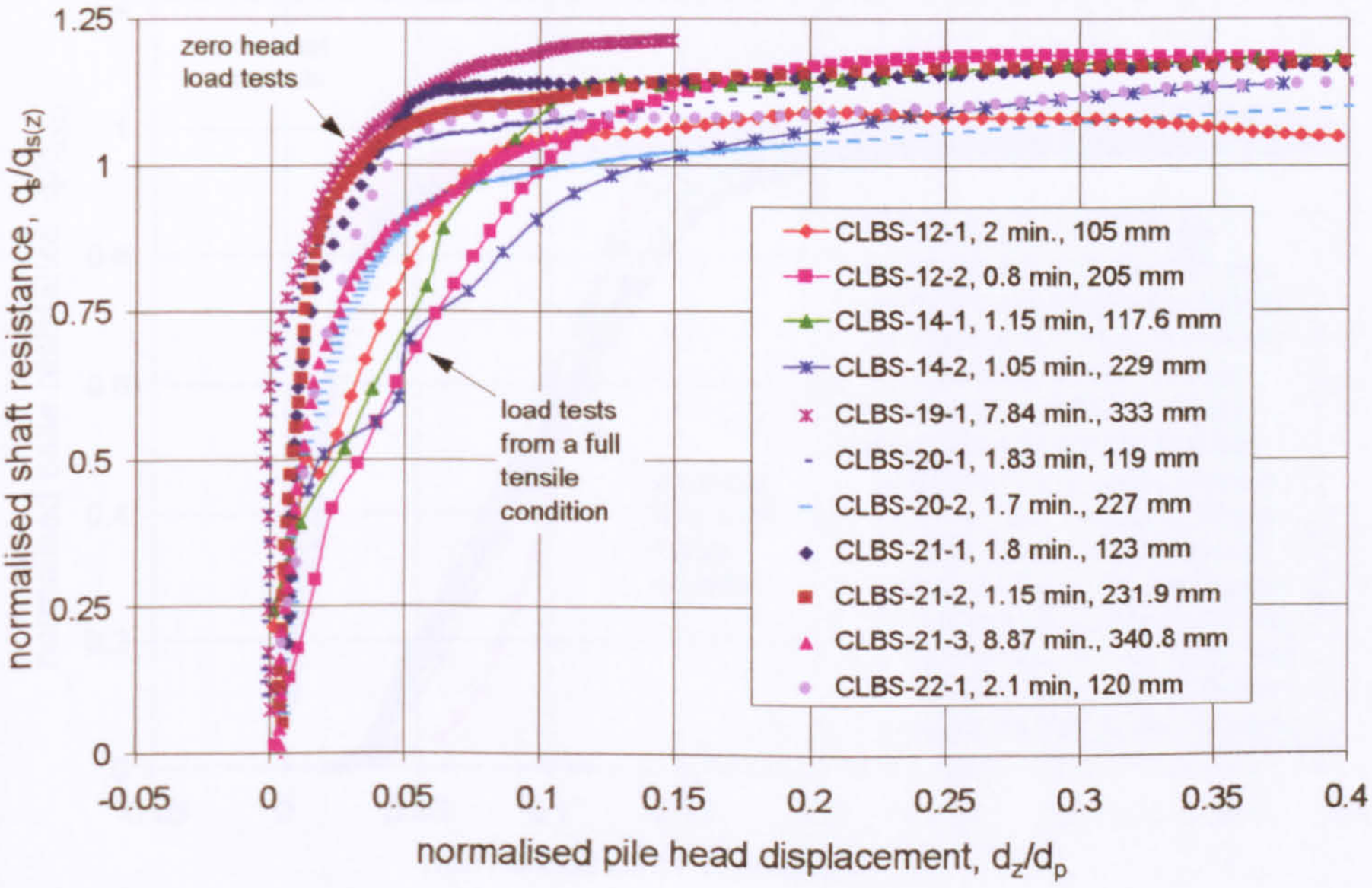

Figure 5-45: Mobilisation of unit shaft resistance during pile load tests in Leighton Buzzard sand.

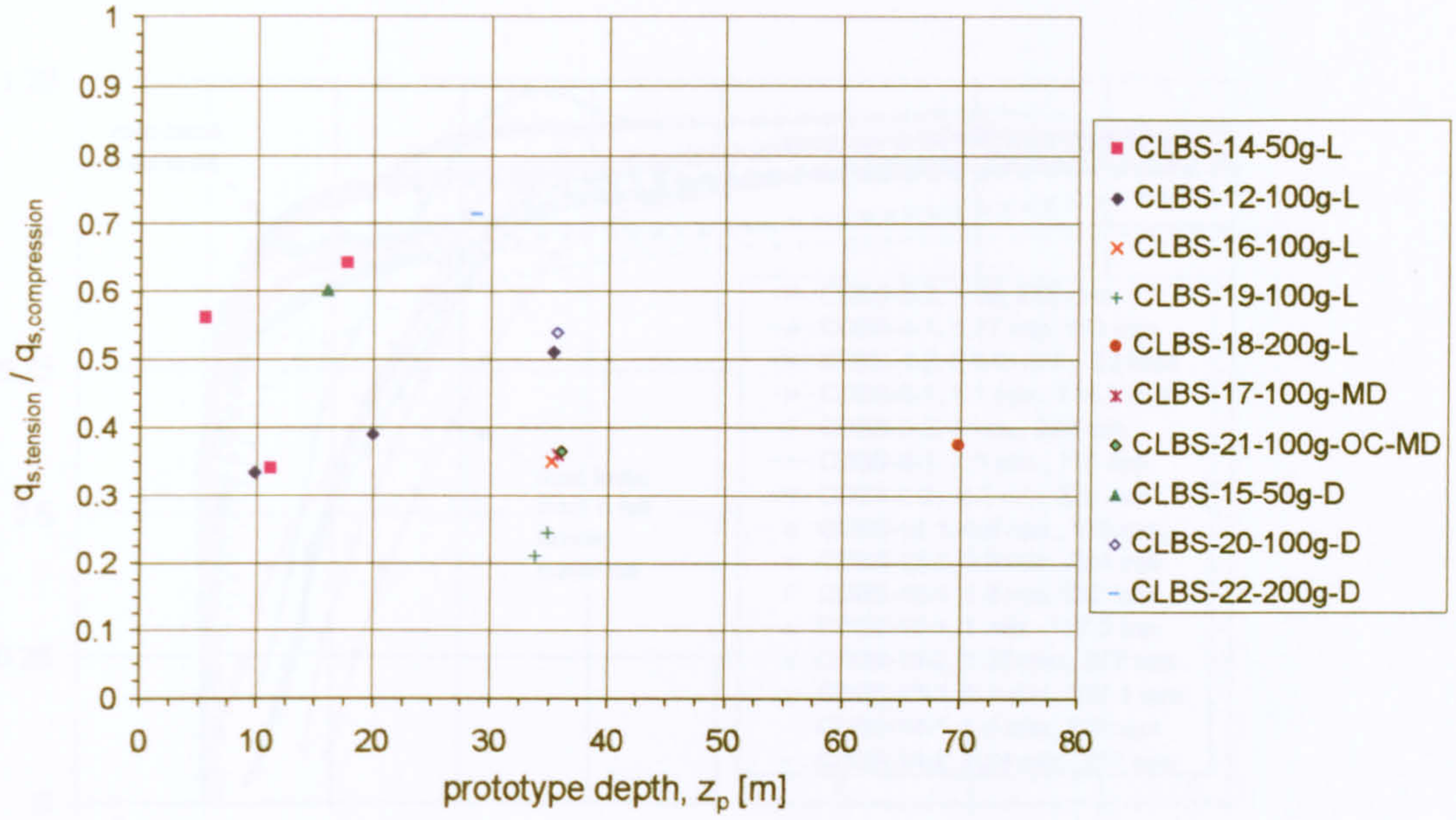

Figure 5-46: Comparison of tensile and compressive shaft capacities in Leighton Buzzard sand.

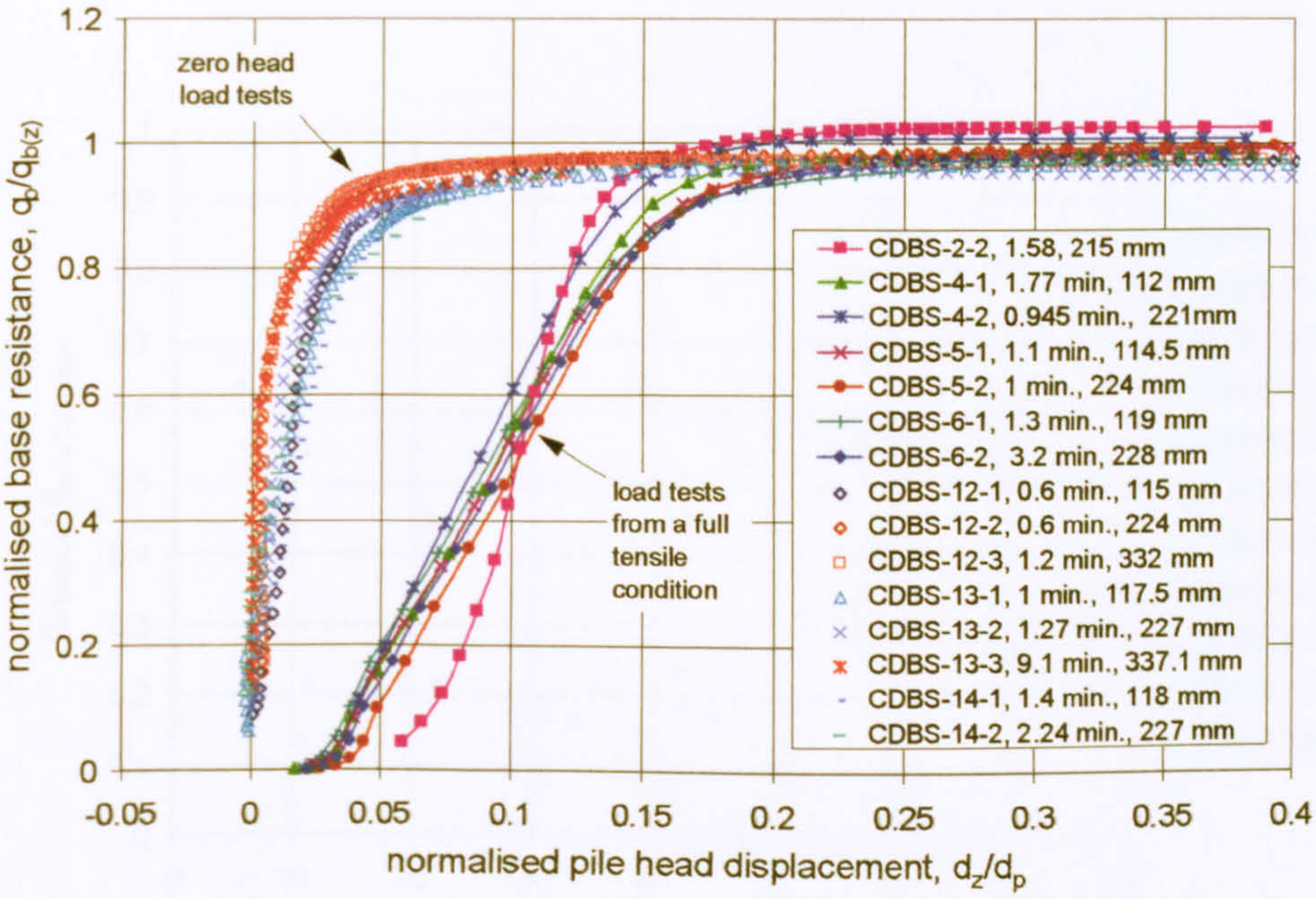

Figure 5-47: Mobilisation of unit end bearing during pile load tests in Dogs Bay sand.

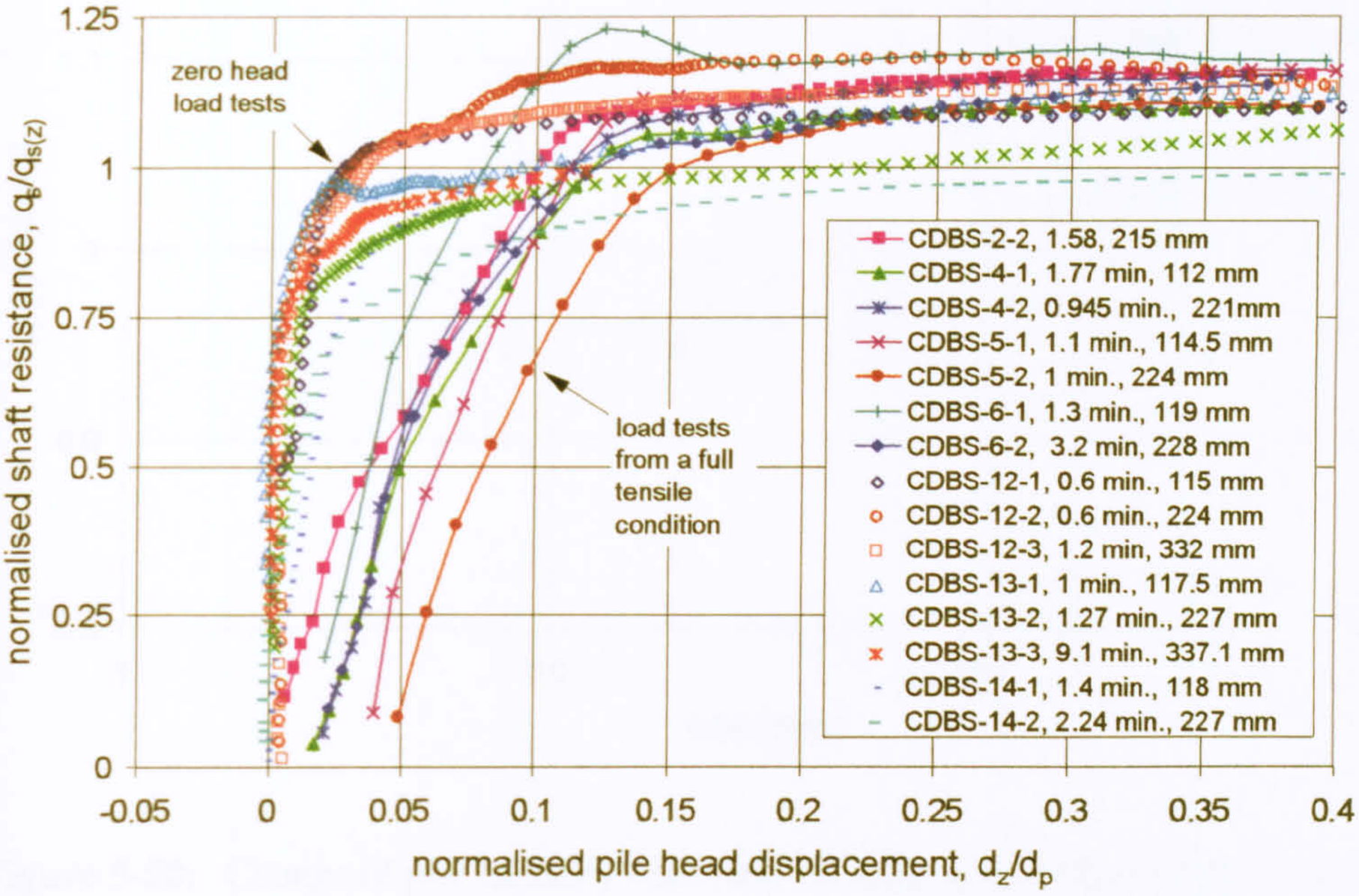

Figure 5-48: Mobilisation of unit shaft resistance during pile load tests in Dogs Bay sand.

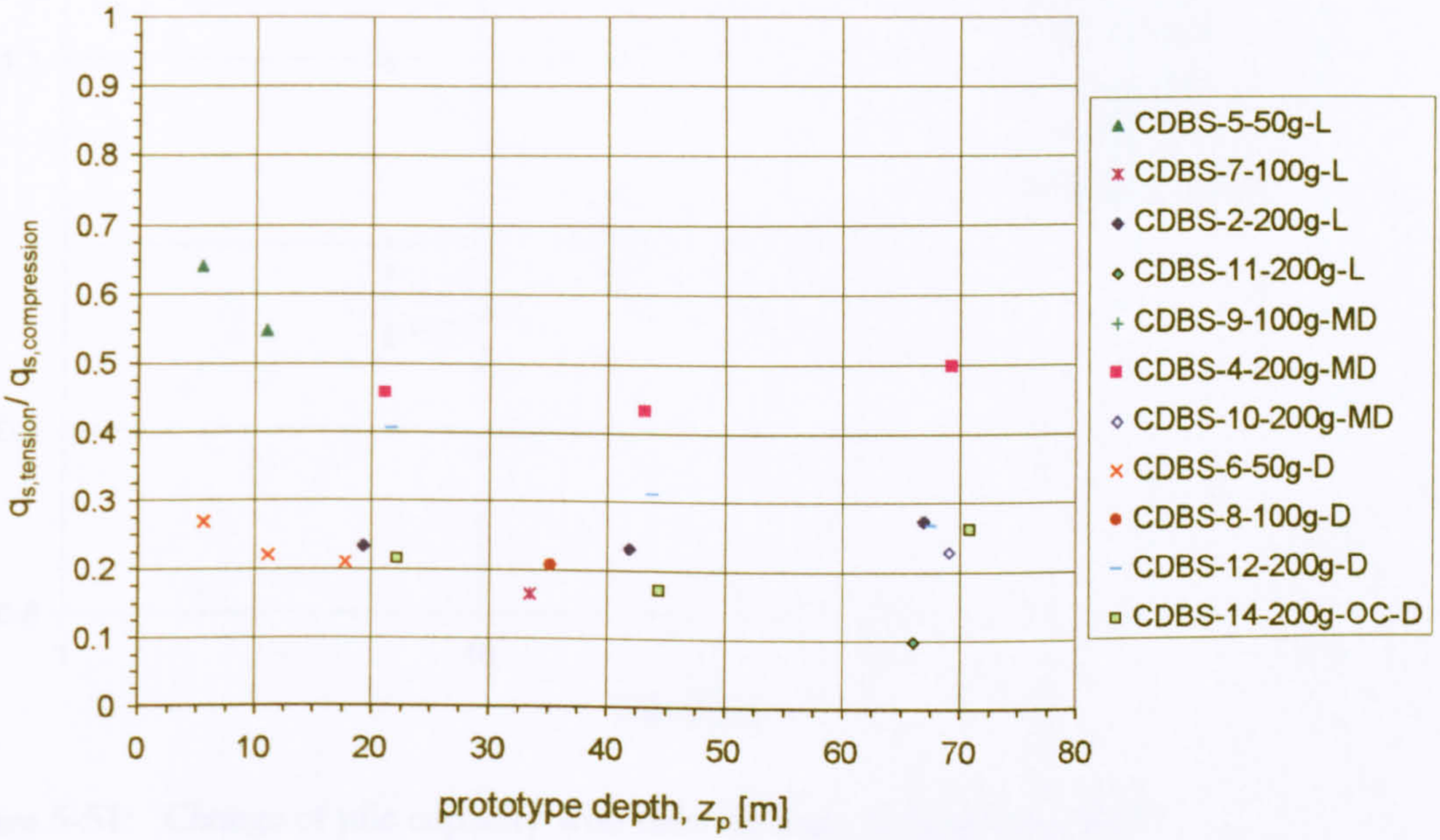

Figure 5-49: Comparison of tensile and compressive shaft capacities in Dogs Bay sand.

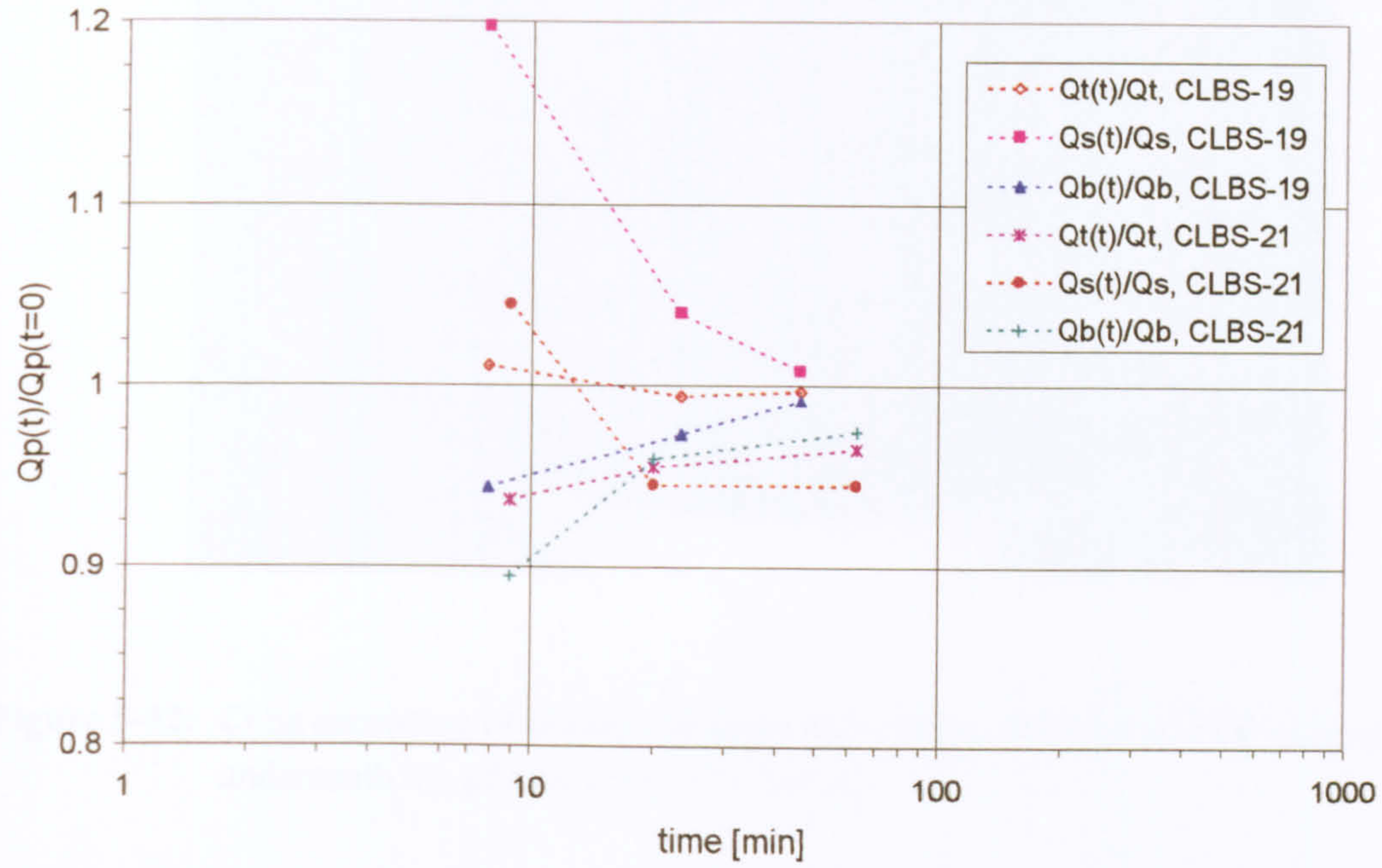

Figure 5-50: Change of pile capacity with time for tests in Leighton Buzzard sand.

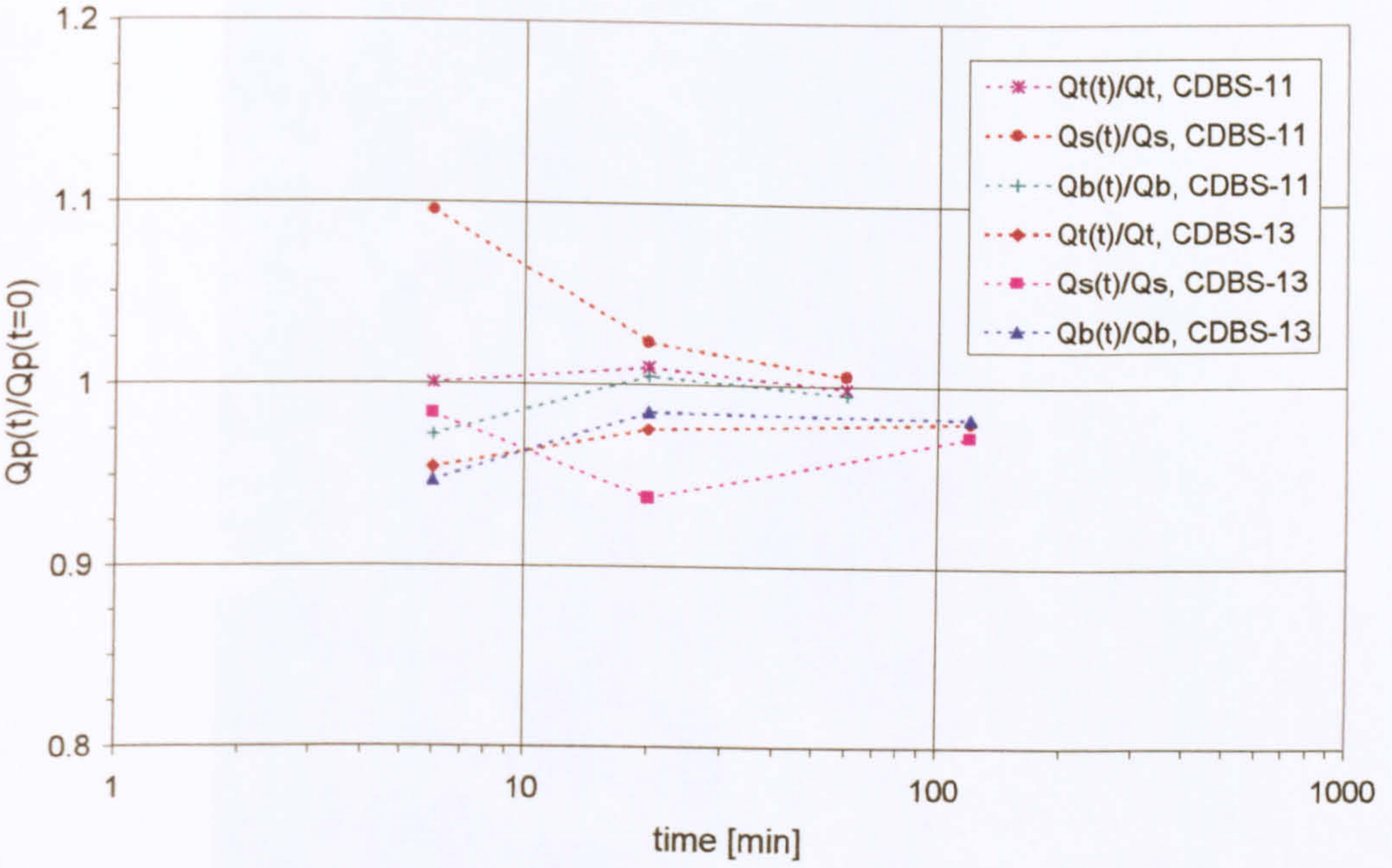

Figure 5-51: Change of pile capacity with time for tests in Dogs Bay sand.

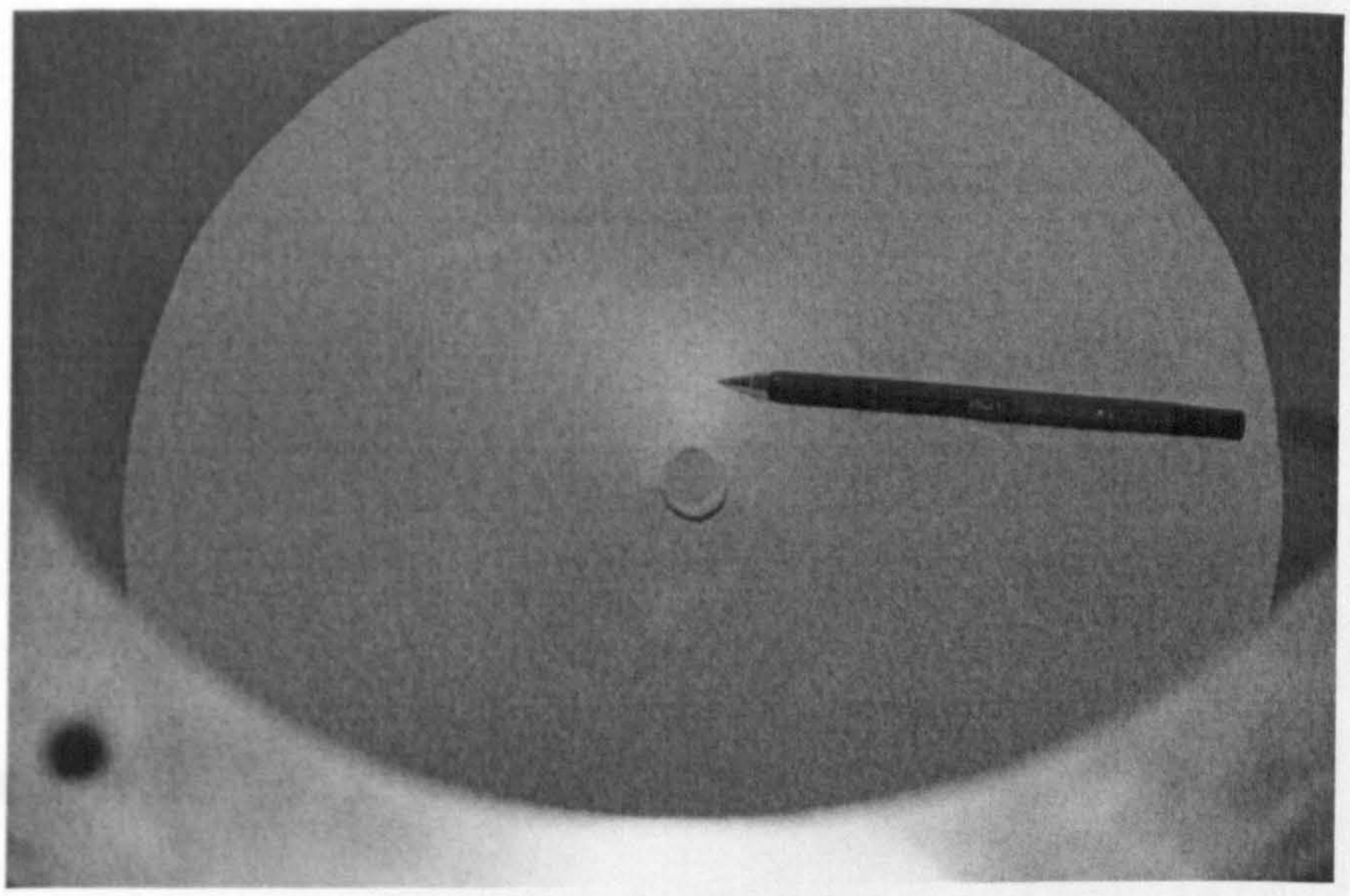

Figure 5-52: Cone consisting of crushed particles of Leighton Buzzard sand recovered underneath the pile tip after test CLBS-22.

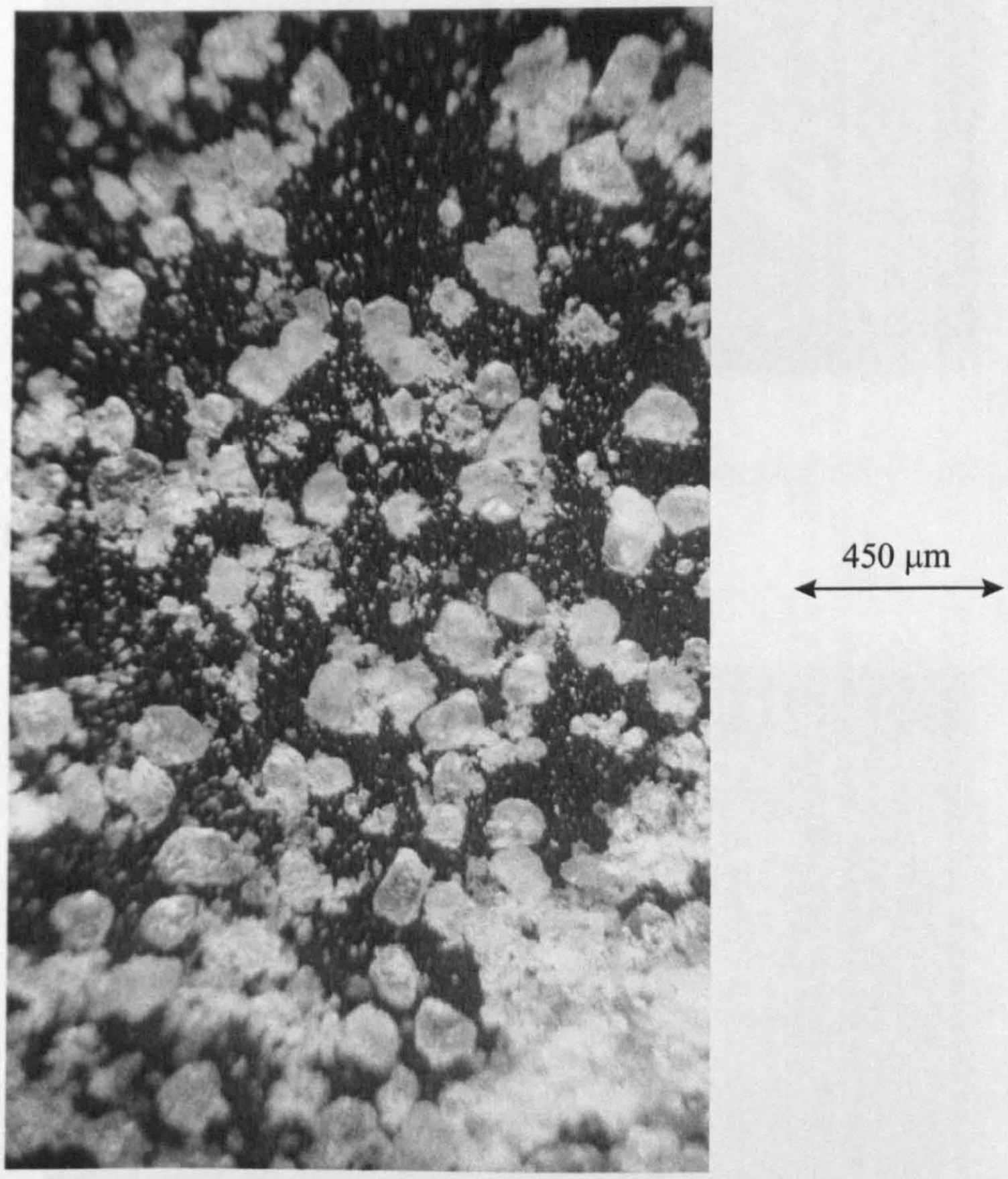

Figure 5-53: Microscopic view of Leighton Buzzard sand particles recovered in the vicinity of the pile tip after test CLBS-22.

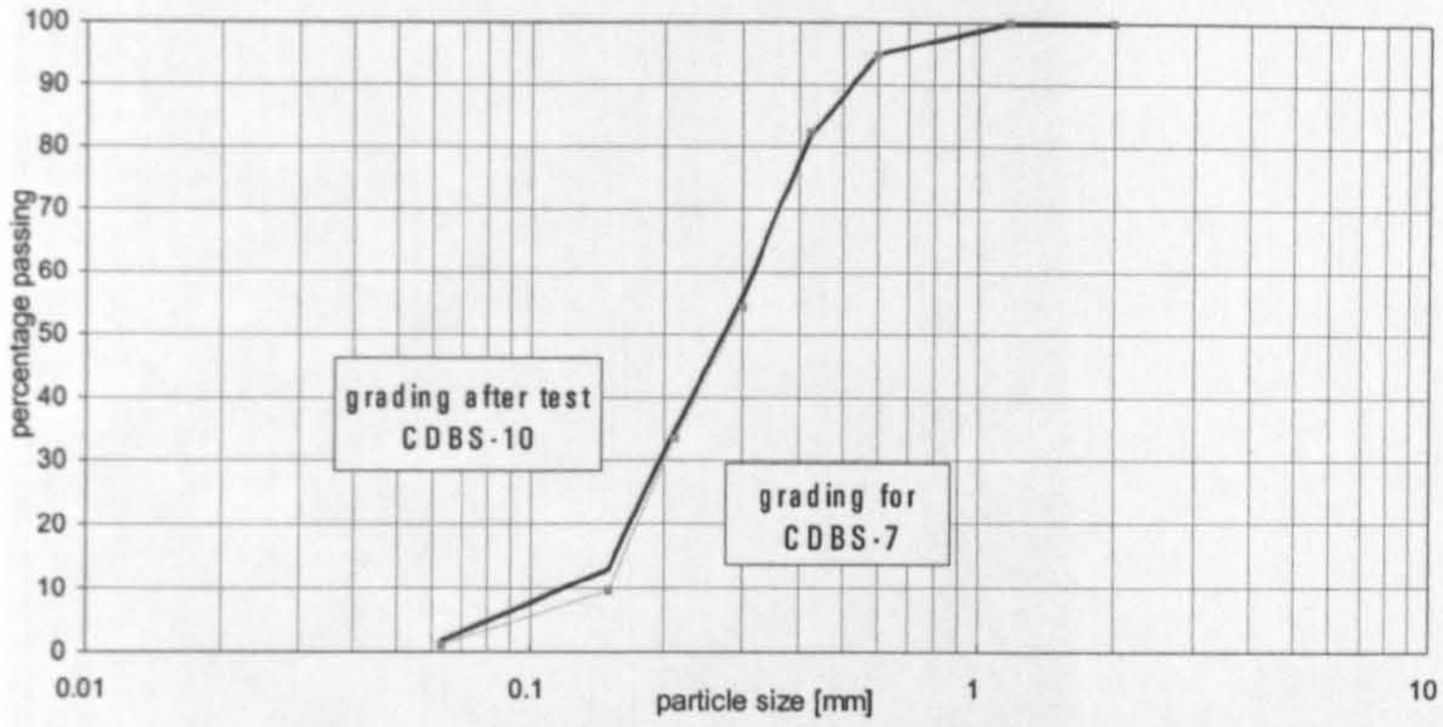

Figure 5-54: Change in grading between tests CDBS-7 and CDBS-10.

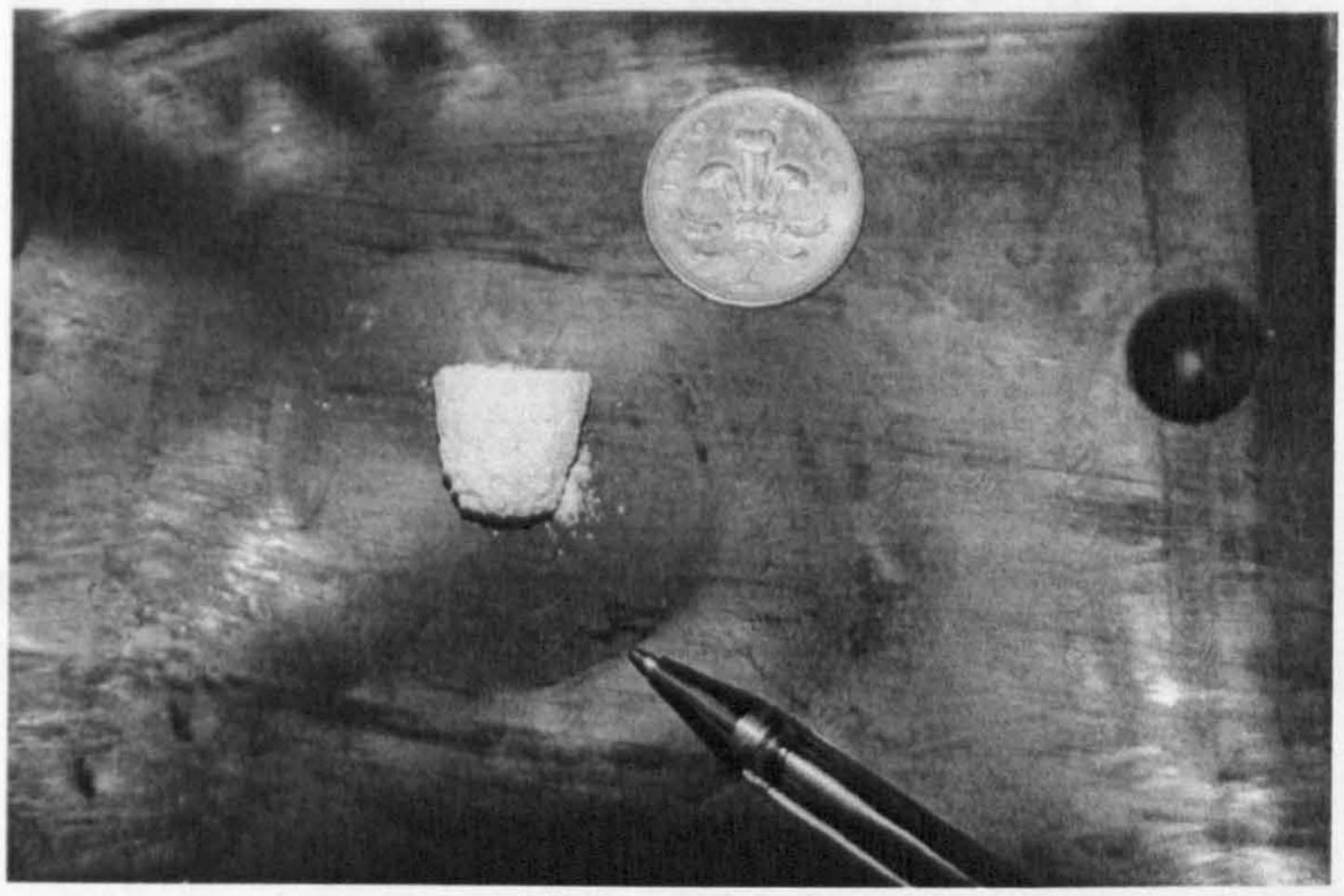

Figure 5-55: Cone consisting of crushed particles of Dogs Bay sand recovered underneath the pile tip after test CDBS-12.

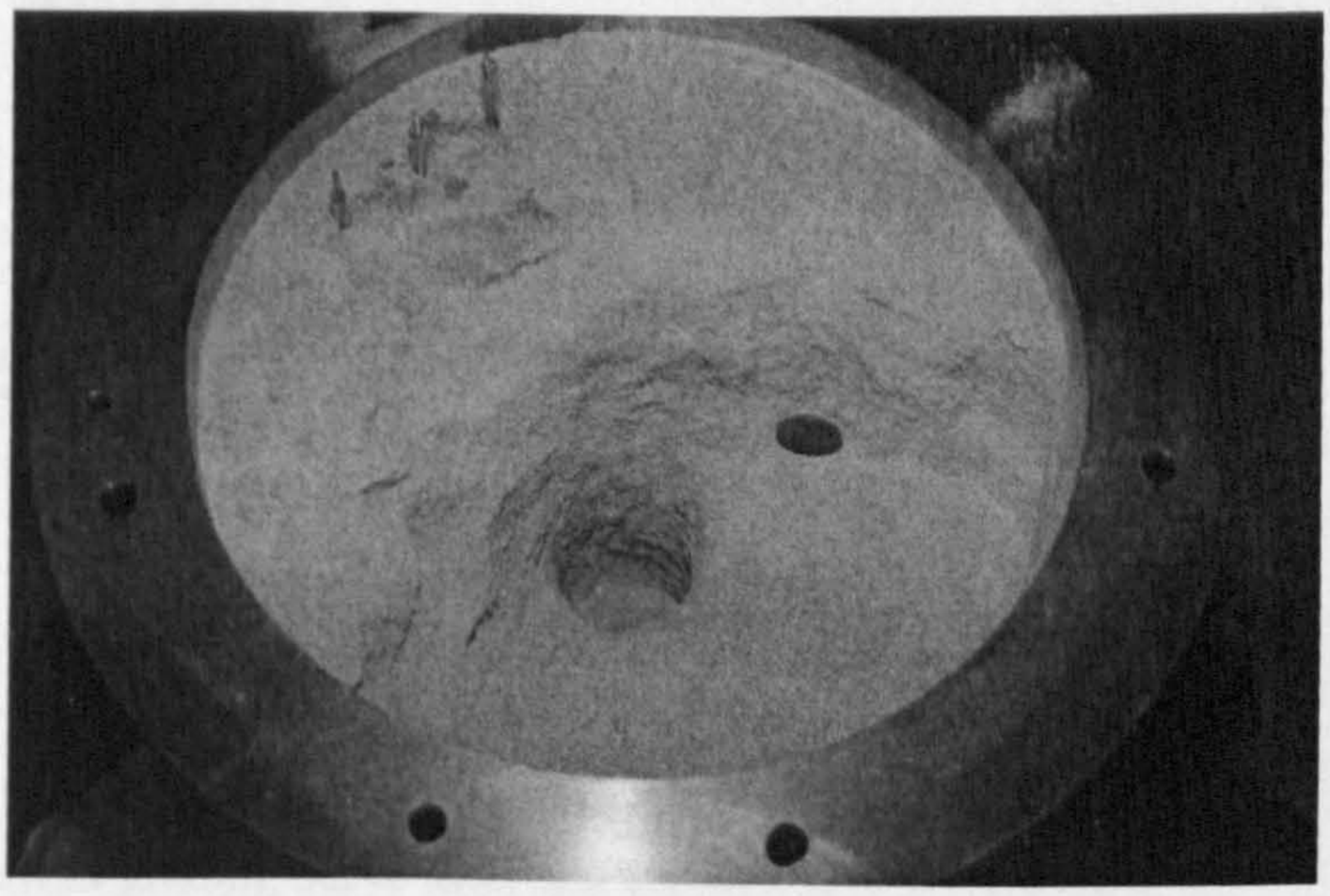

Figure 5-56: View inside the strongbox after test DBS-13 showing intact interlocked and re-moulded sand structure.

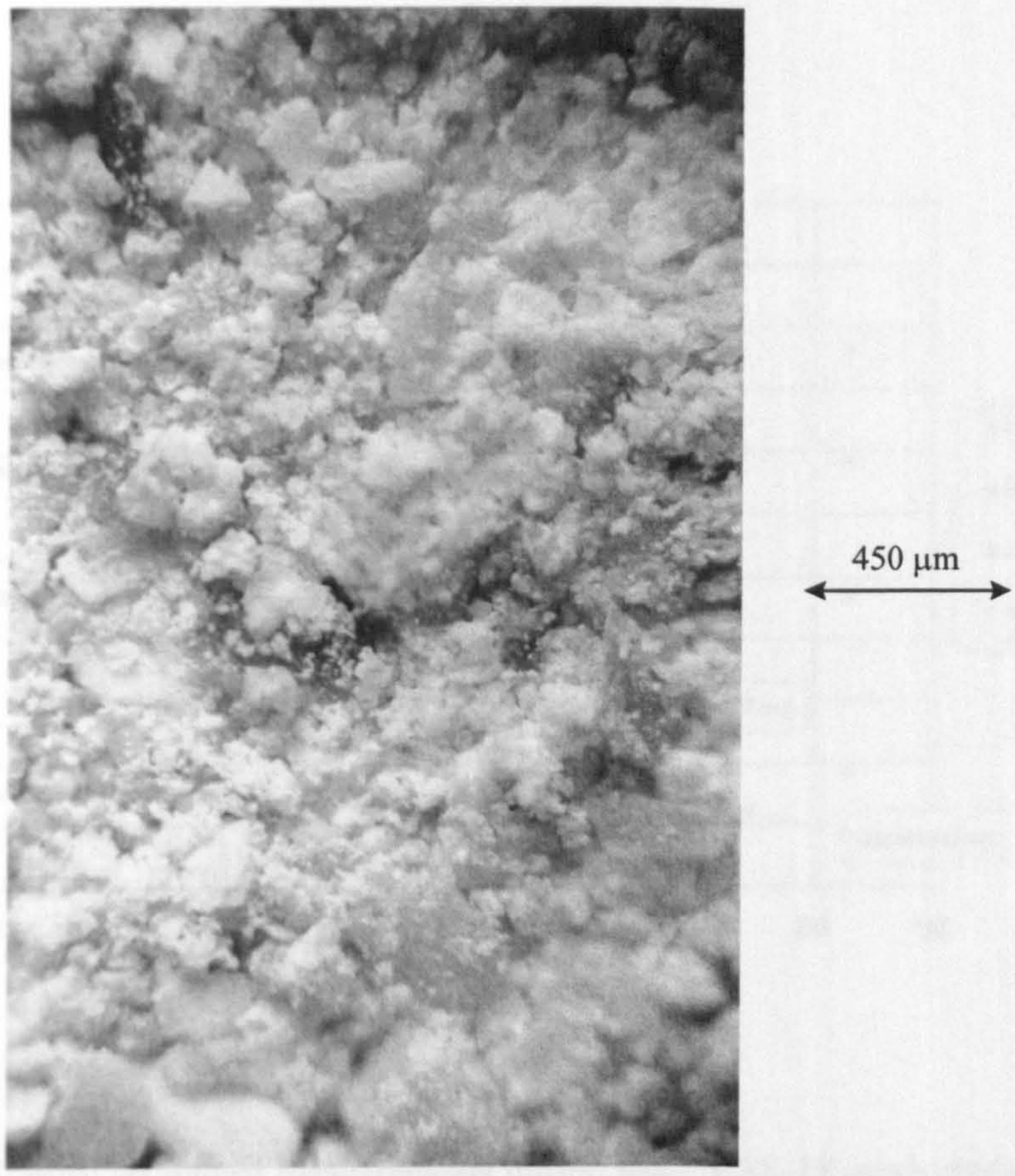

Figure 5-57: Microscopic view of Dogs Bay sand particles recovered in the vicinity of the pile after test CDBS-13.

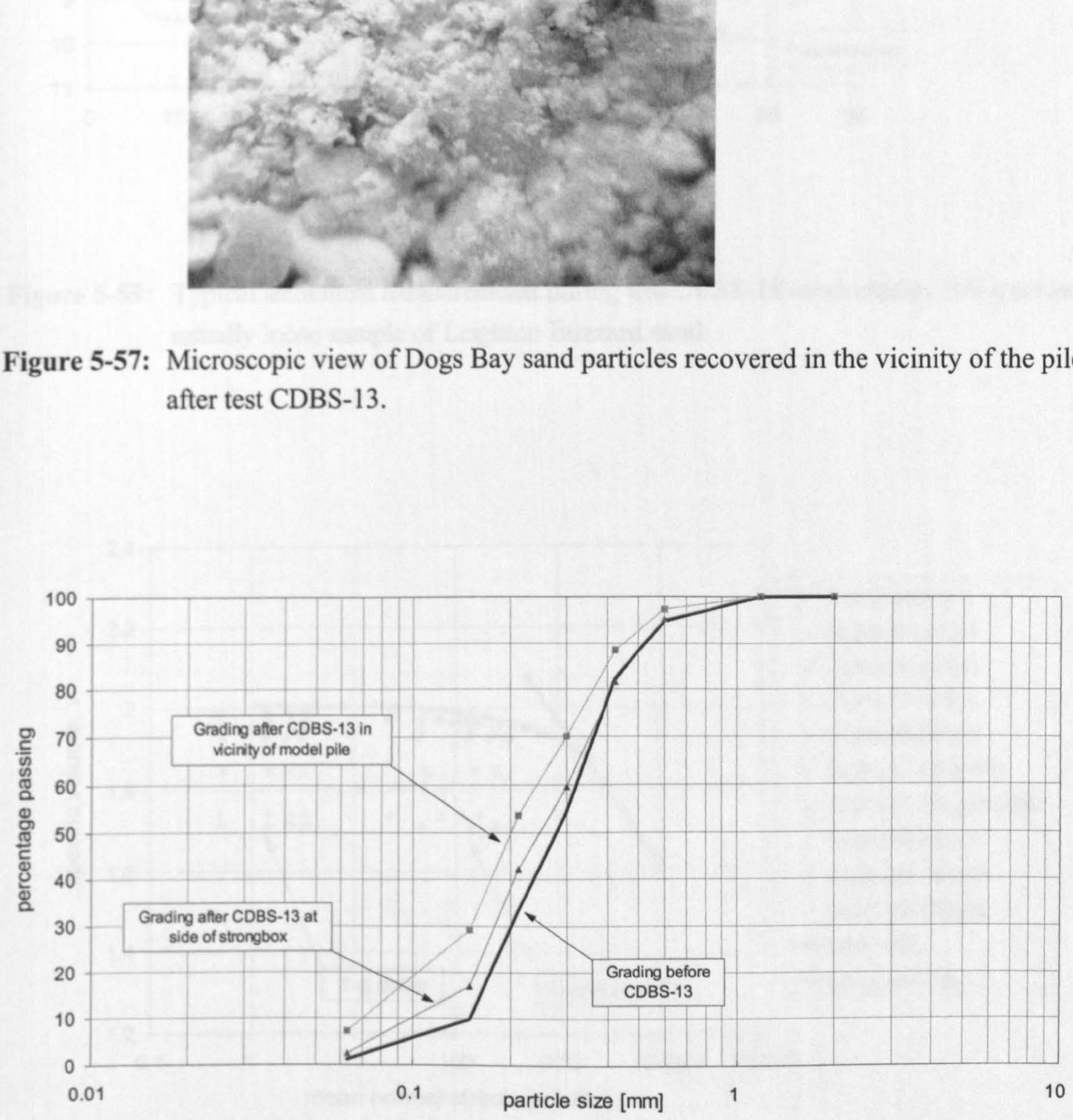

Figure 5-58: Shift in grading curve after test CDBS-13.

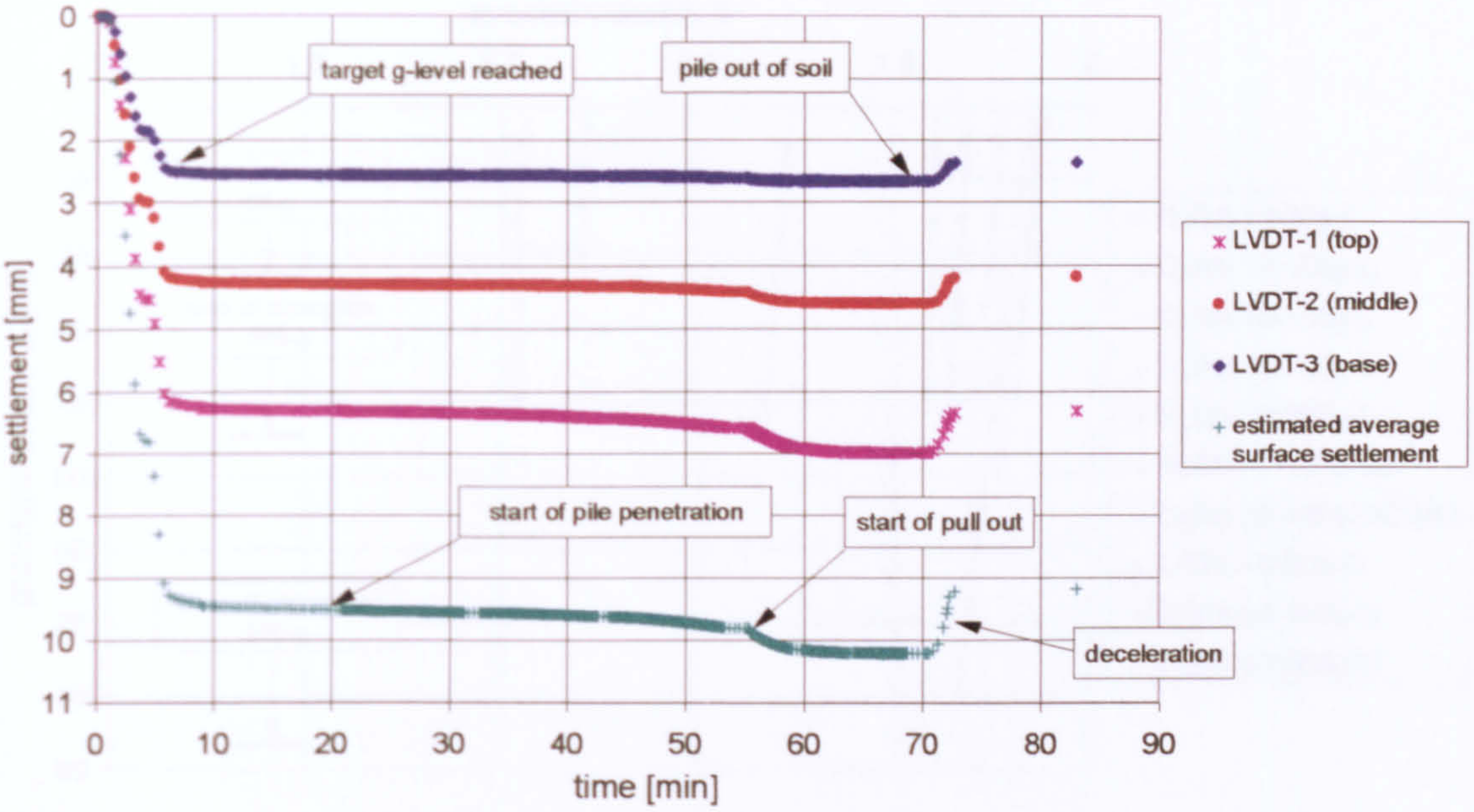

Figure 5-59: Typical settlement measurements during test CLBS-18 conducted at 200-g on an initially loose sample of Leighton Buzzard sand.

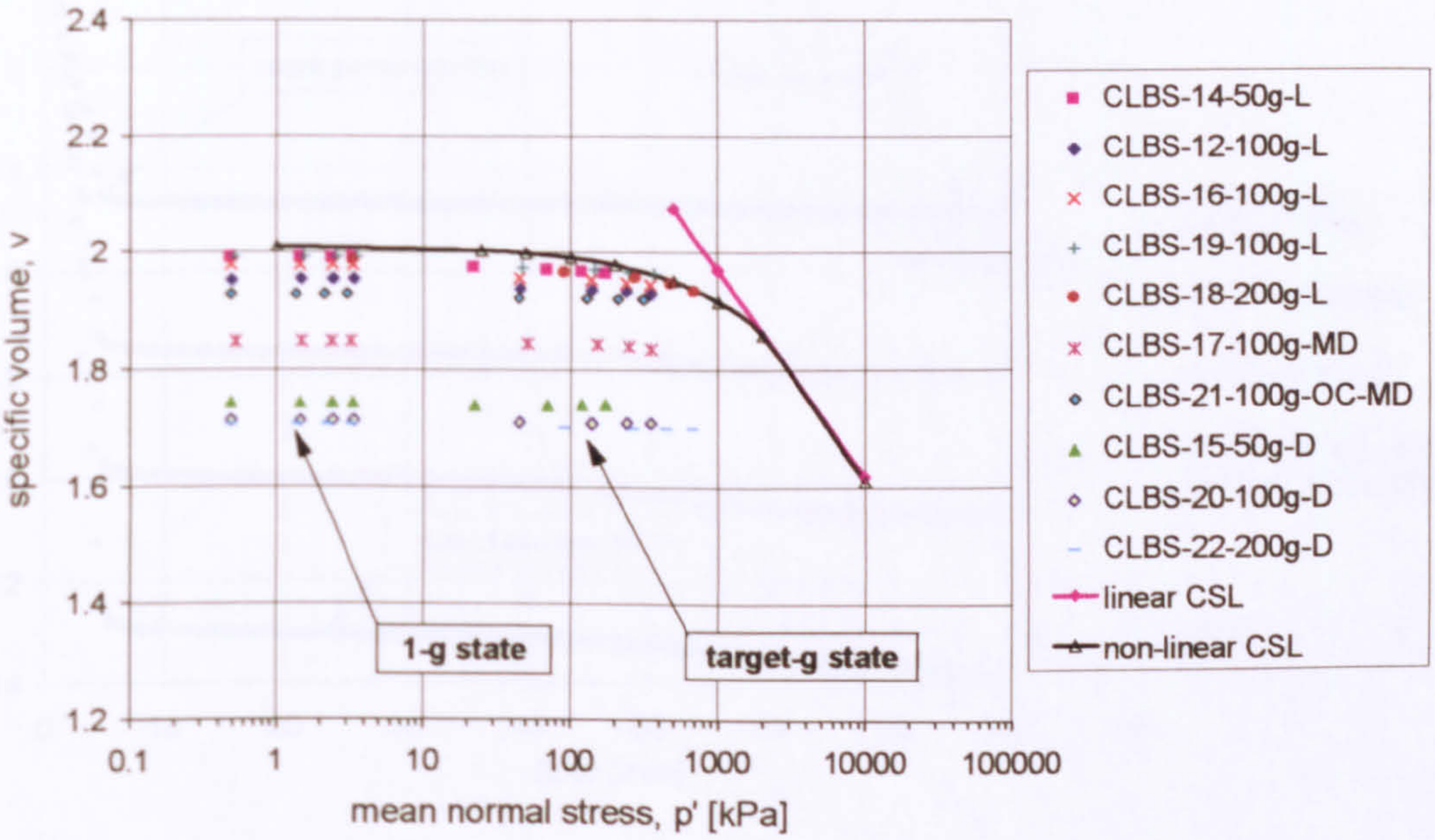

Figure 5-60: In situ states and critical state line for Leighton Buzzard sand.

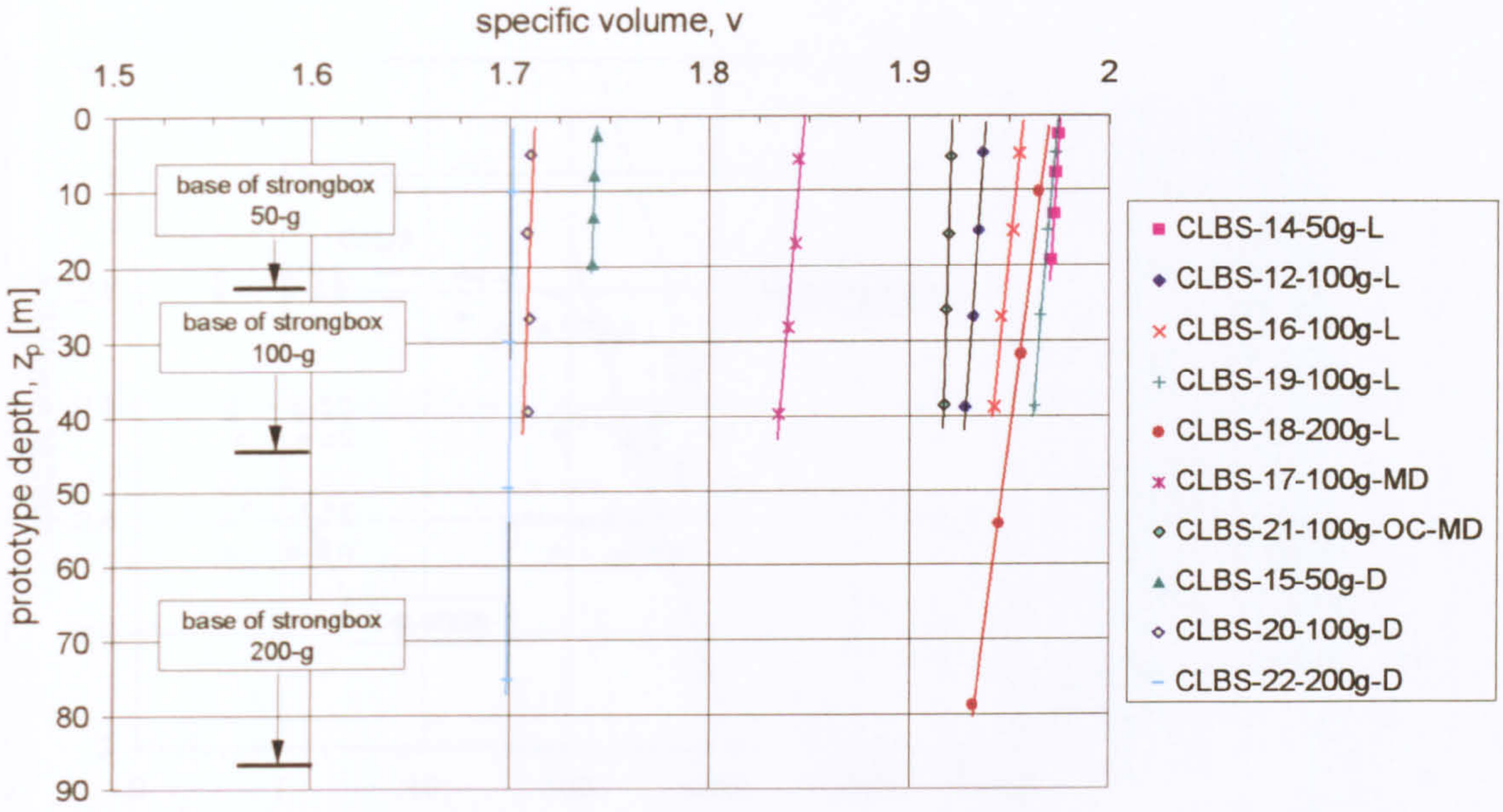

Figure 5-61: Measured in situ specific volume with depth profile for Leighton Buzzard sand.

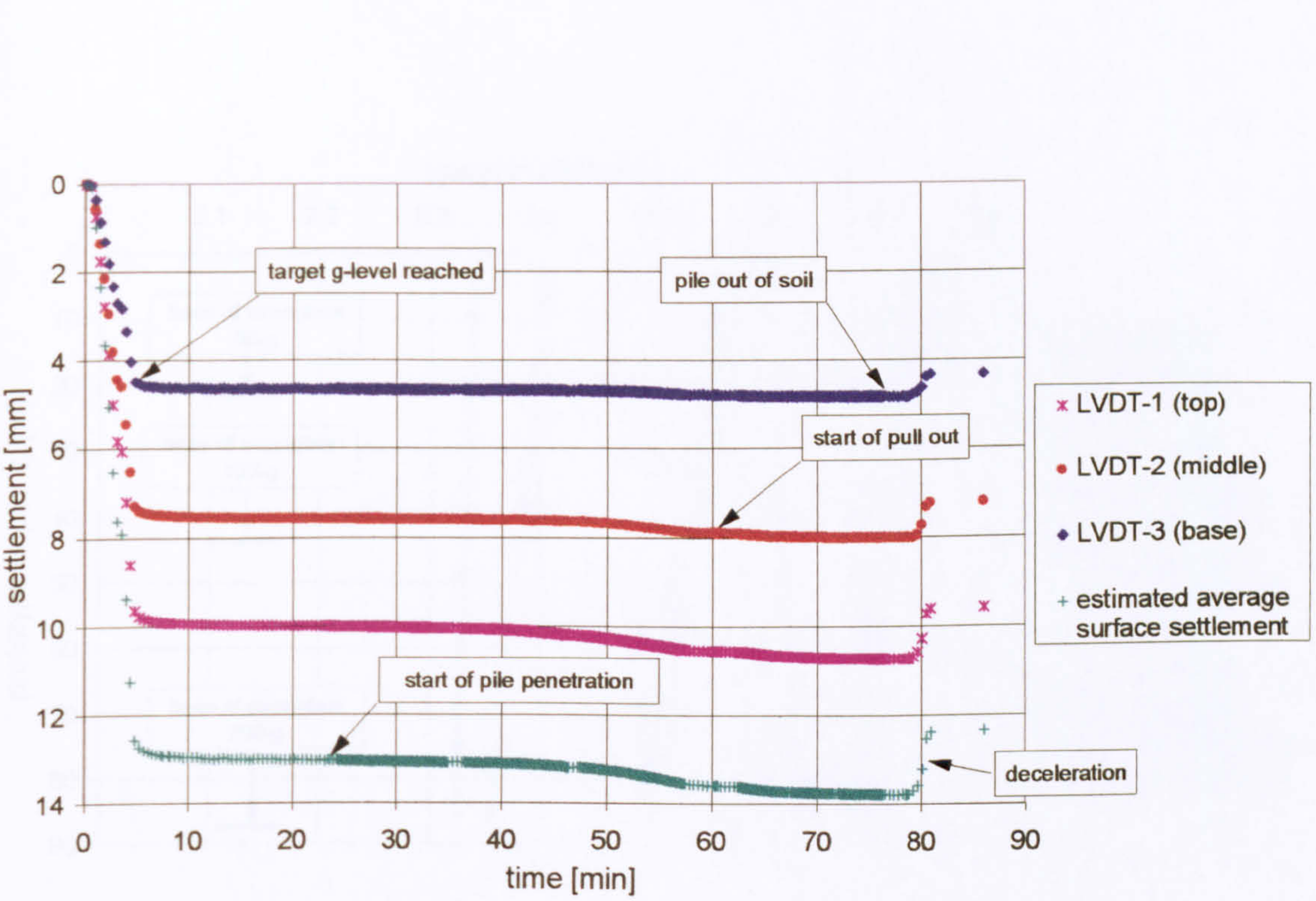

Figure 5-62: Typical settlement measurements during test CDBS-10 conducted at 200-g on an initially loose sample of Dogs Bay sand.

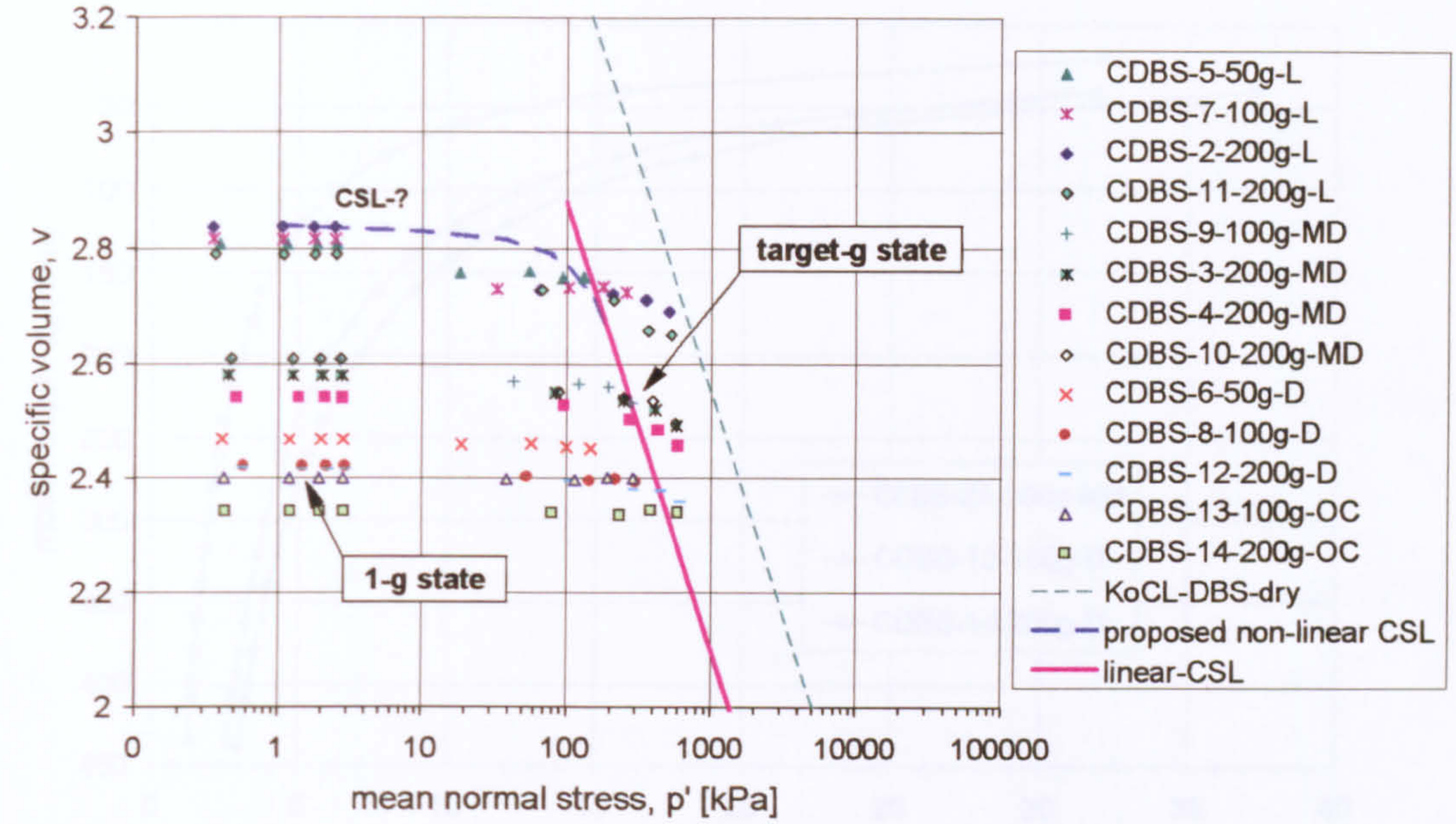

Figure 5-63: In situ states and critical state line for Dogs Bay sand.

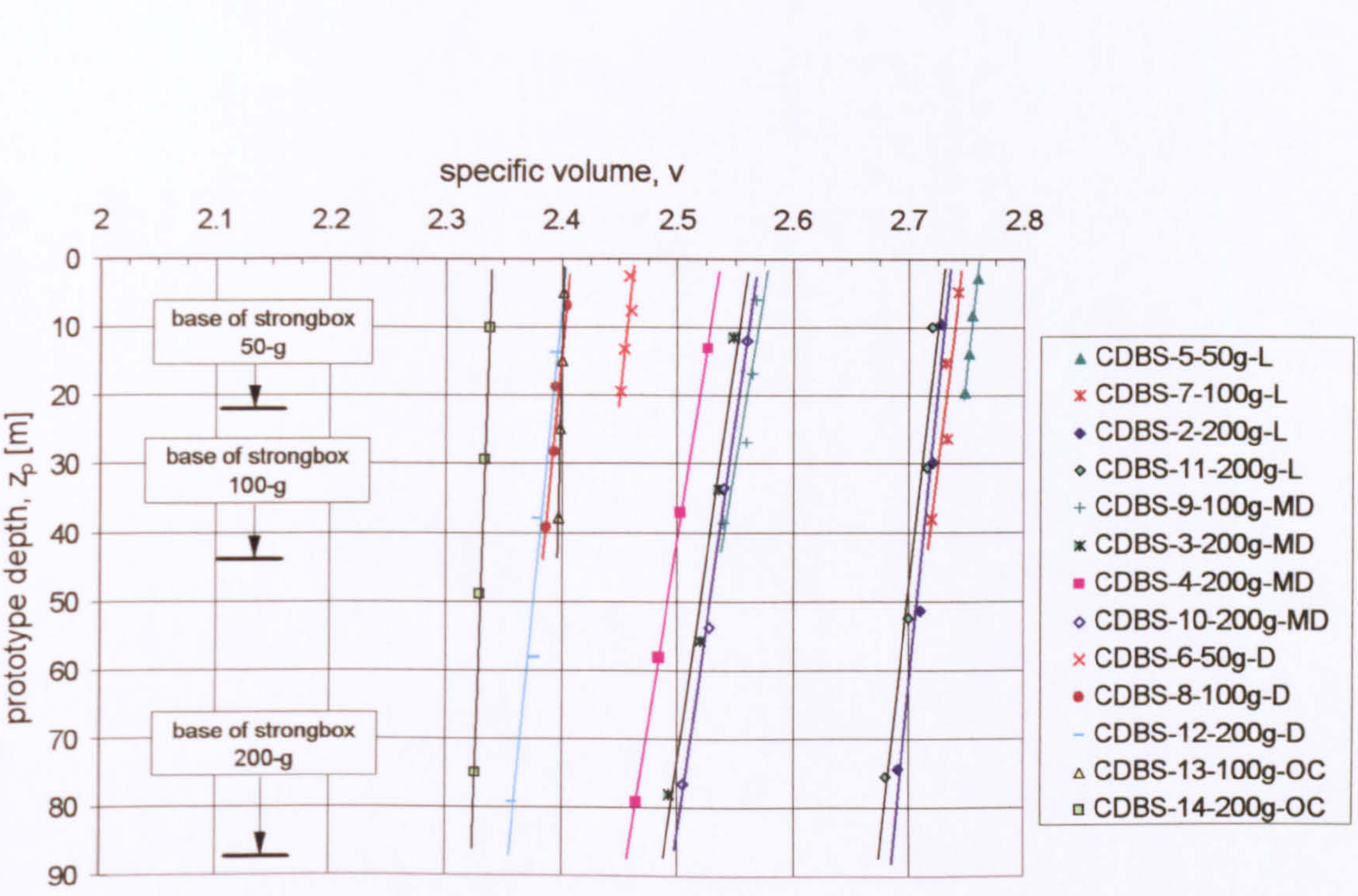

Figure 5-64: Measured in situ specific volume with depth profile for Dogs Bay sand.

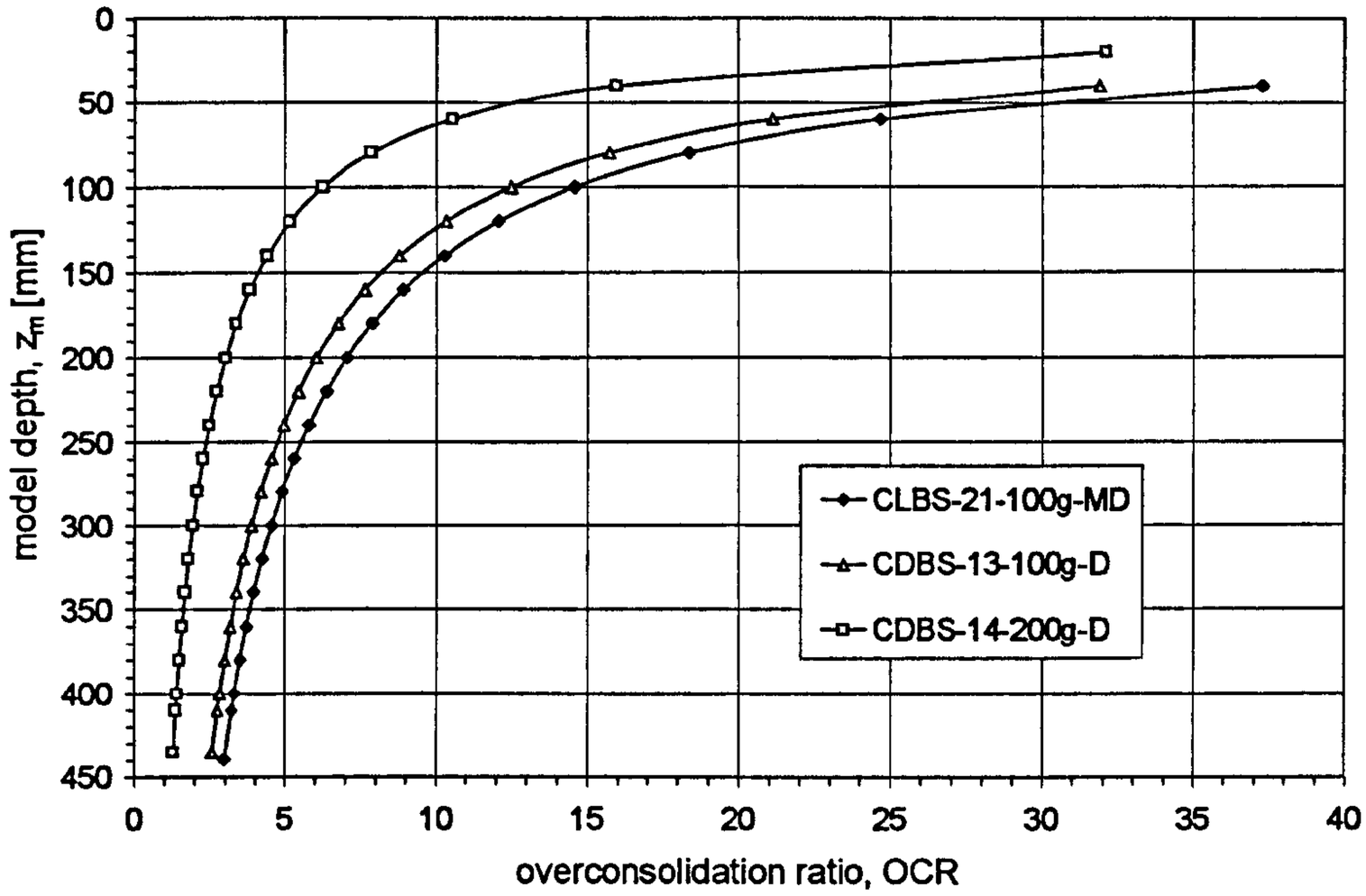

Figure 5-65: Profiles of overconsolidation ratio (OCR) with depth for centrifuge model tests on Leighton Buzzard and Dogs Bay sands.

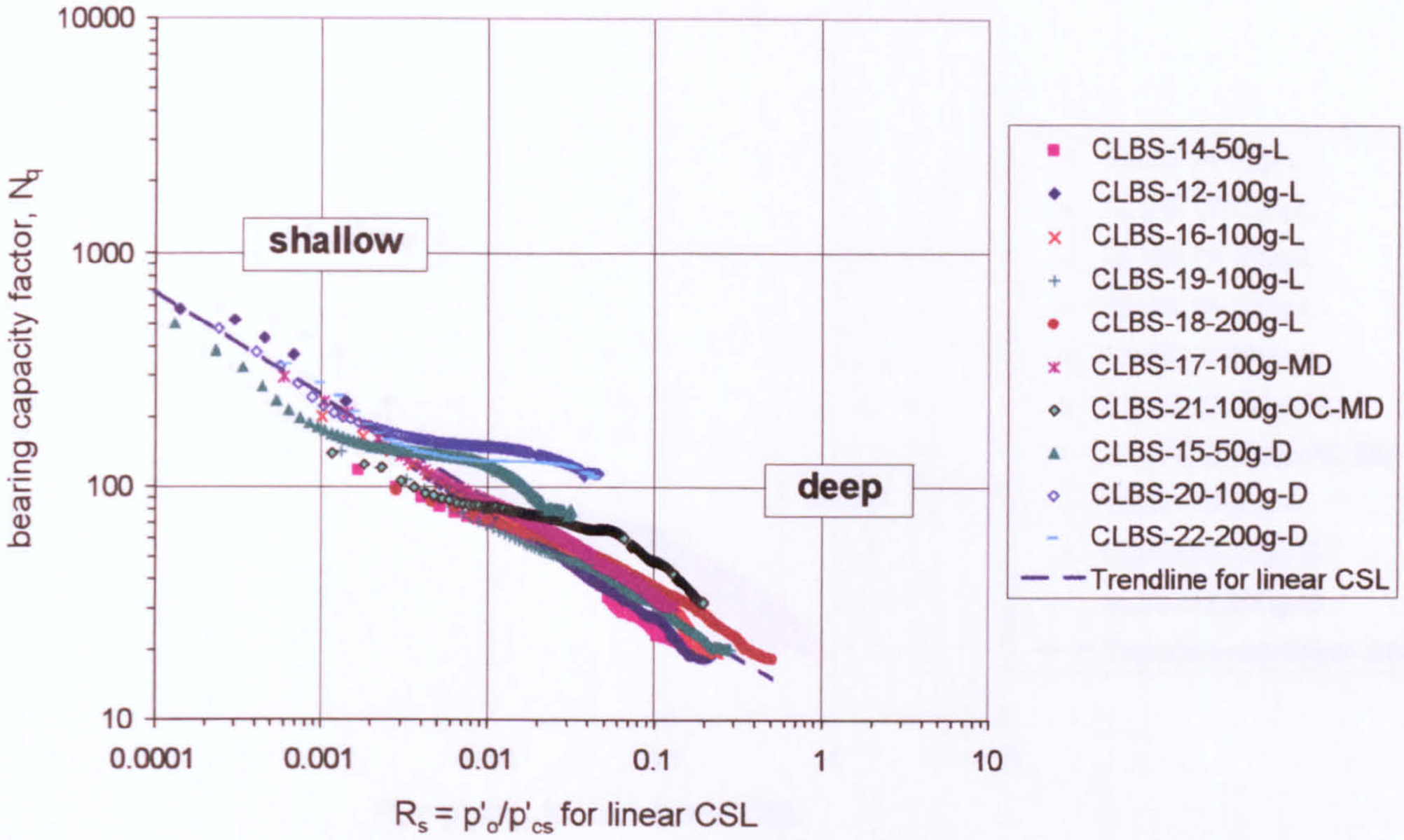

Figure 5-66: The influence of state on N_q during pile penetration based on a linear CSL for centrifuge tests on Leighton Buzzard sand.

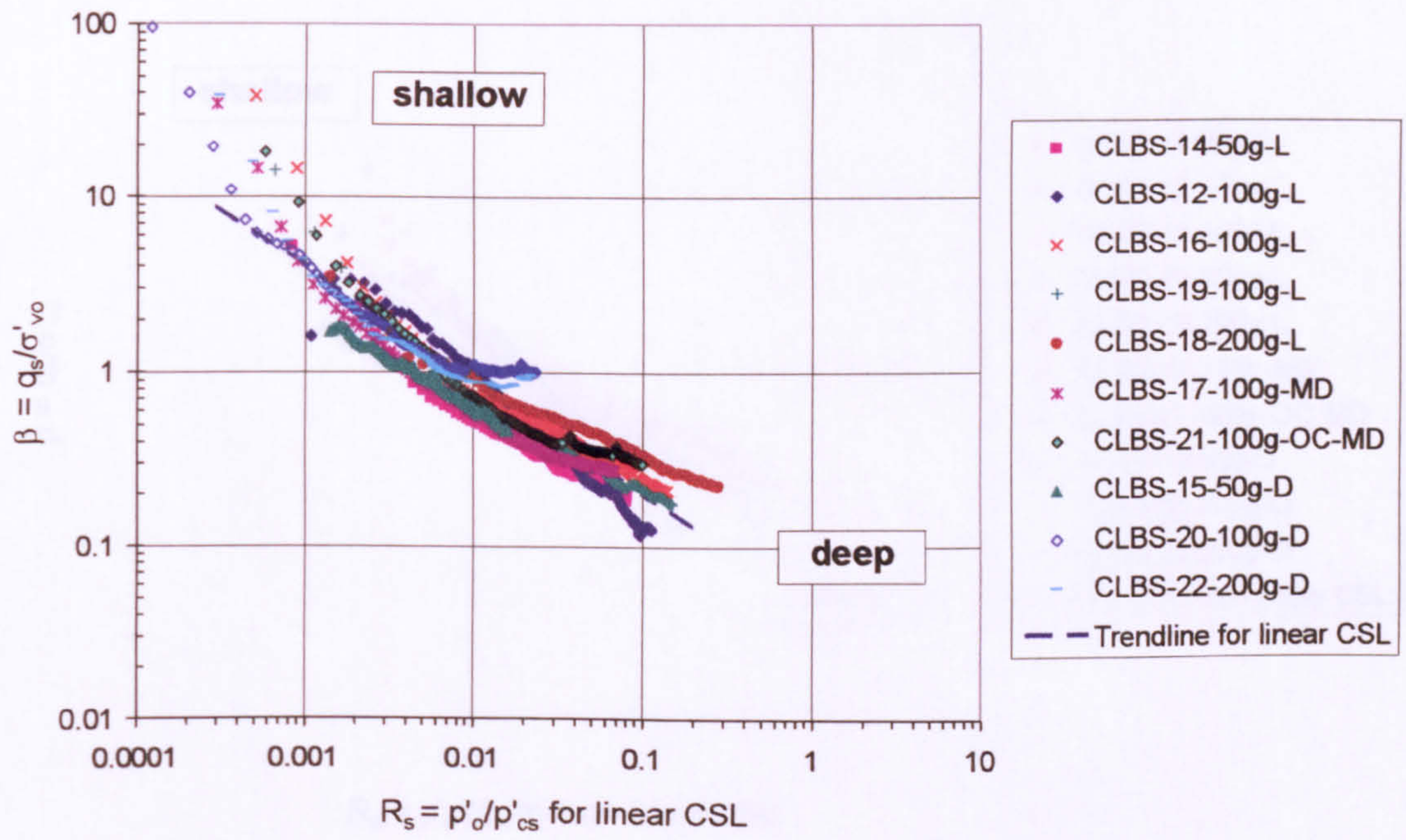

Figure 5-67: The influence of state on β during pile penetration based on a linear CSL for centrifuge tests on Leighton Buzzard sand.

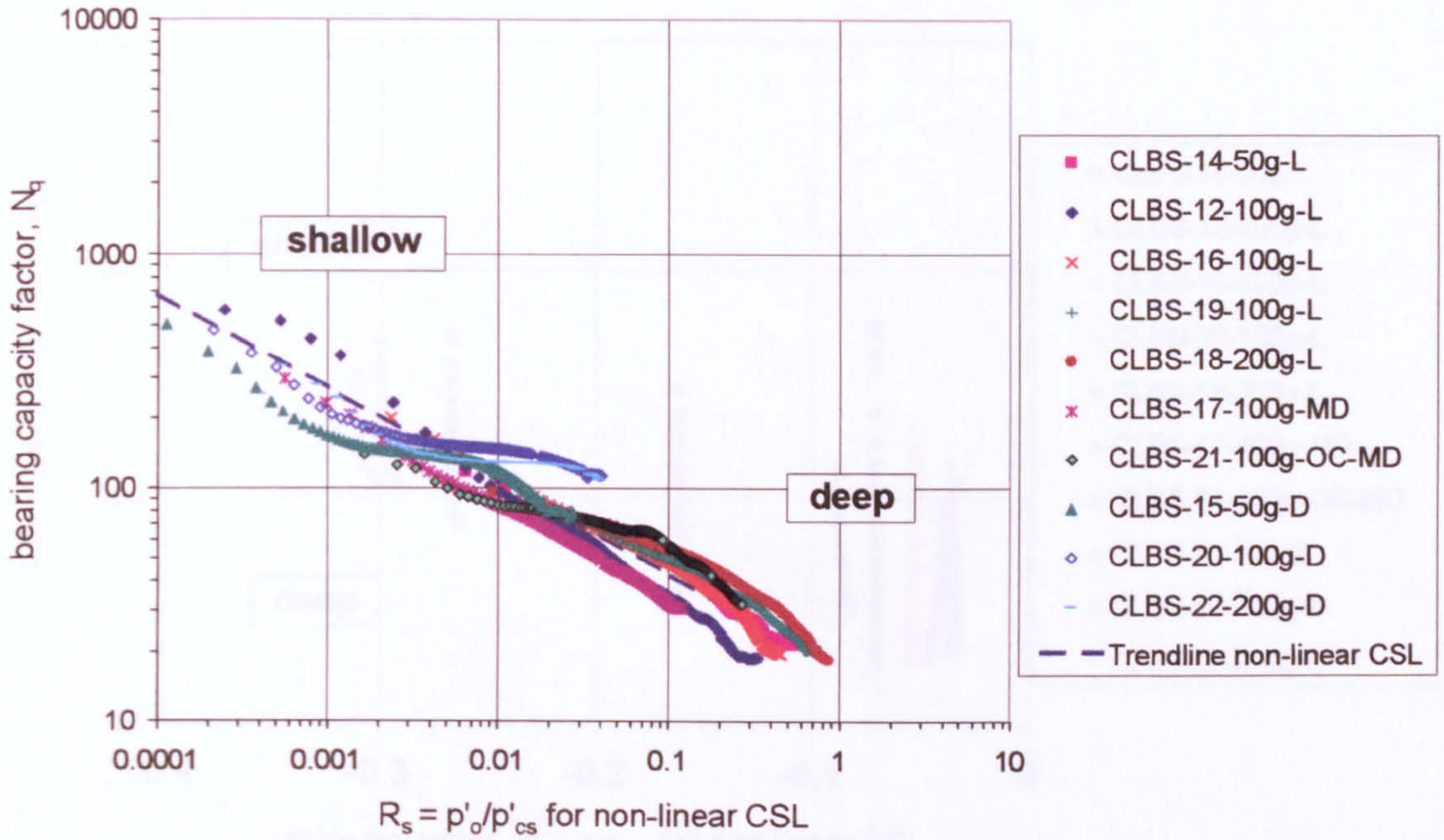

Figure 5-68: The influence of state on N_q during pile penetration based on a non-linear CSL for centrifuge tests on Leighton Buzzard sand.

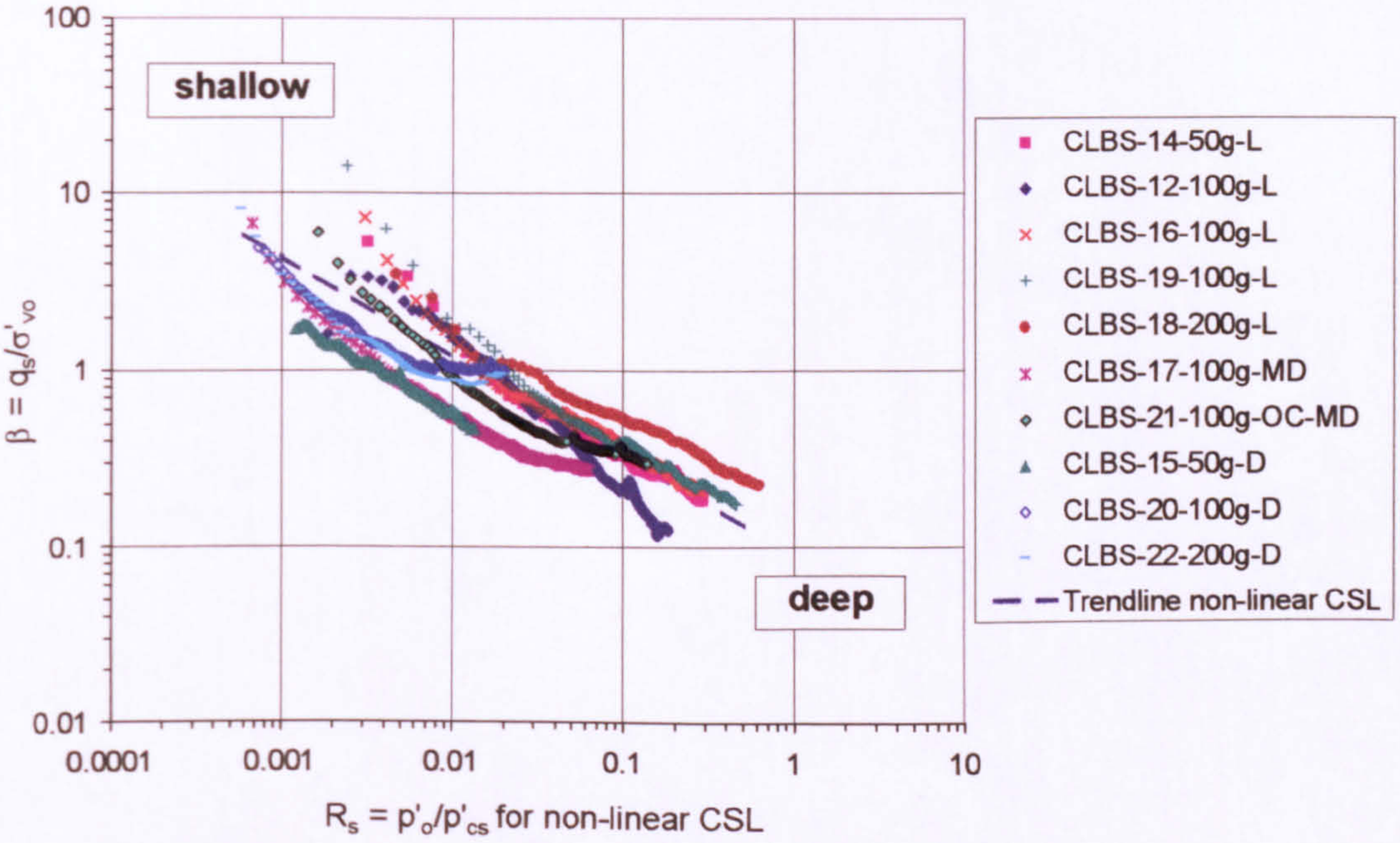

Figure 5-69: The influence of state on β during pile penetration based on a non-linear CSL for centrifuge tests on Leighton Buzzard sand.

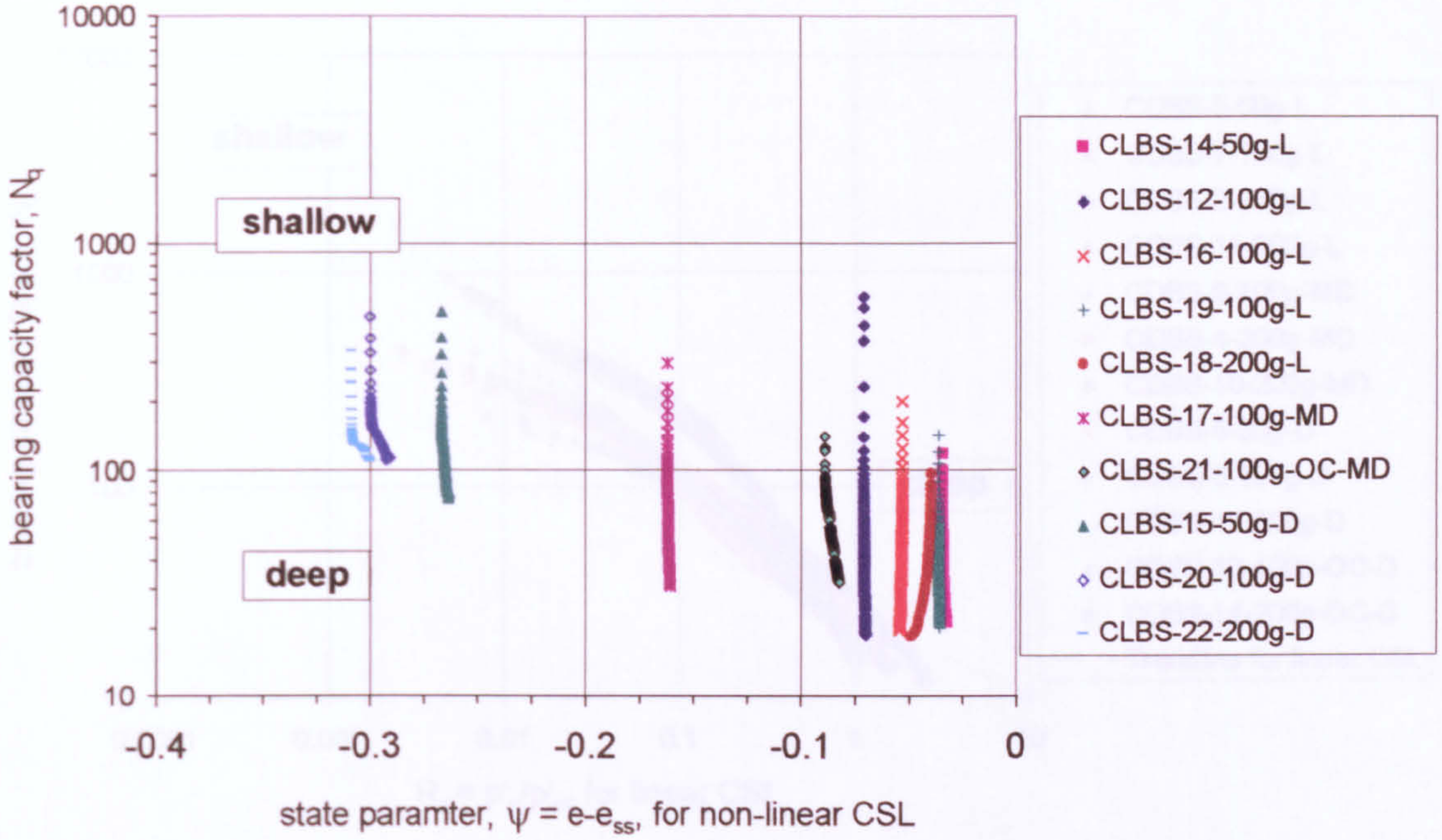

Figure 5-70: Normalisation of centrifuge tests on Leighton Buzzard sand (N_q-values) using the state paramter approach by Konrad (1988).

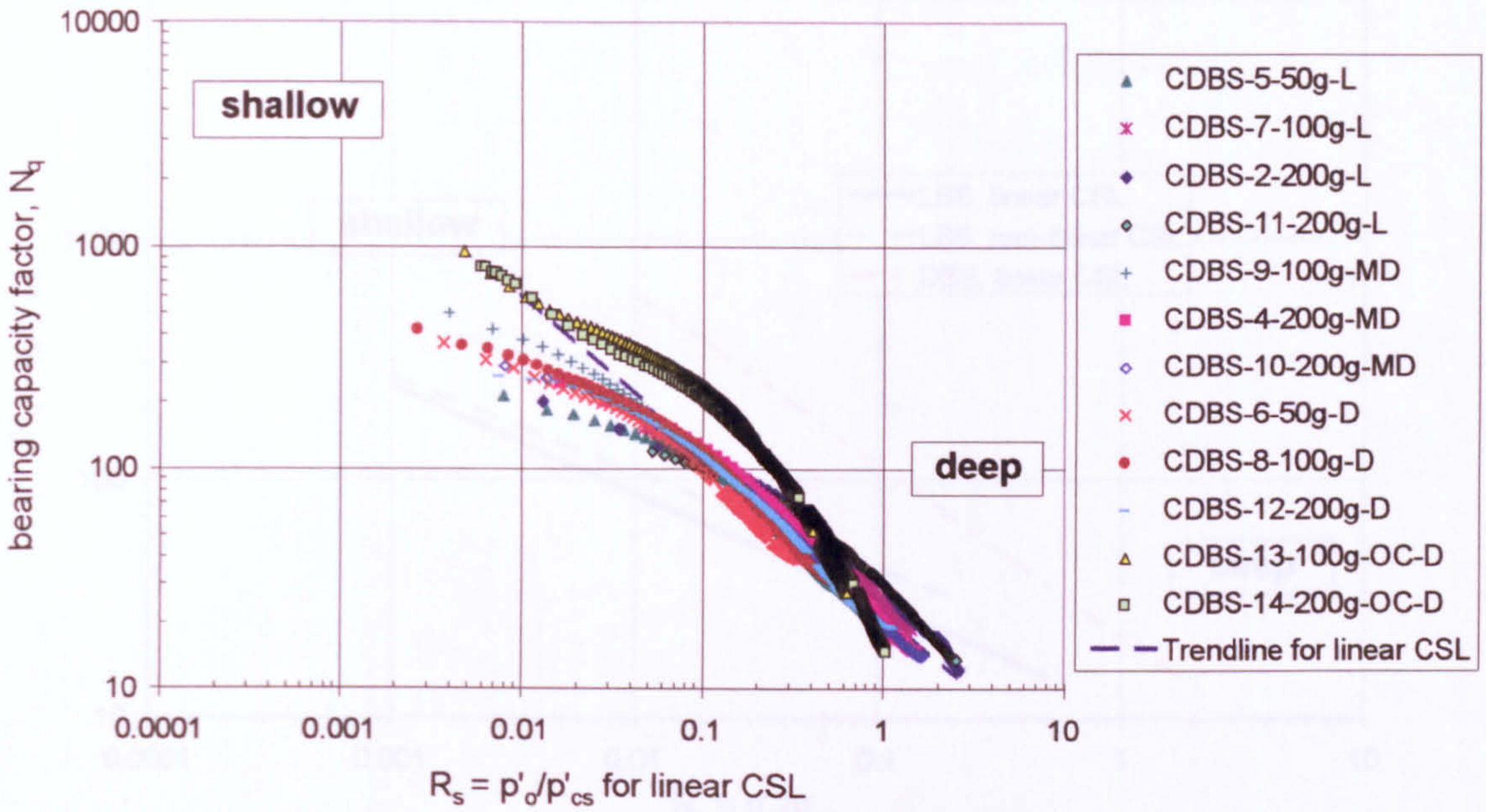

Figure 5-71: The influence of state on N_q during pile penetration based on a linear CSL for centrifuge tests on Dogs Bay sand.

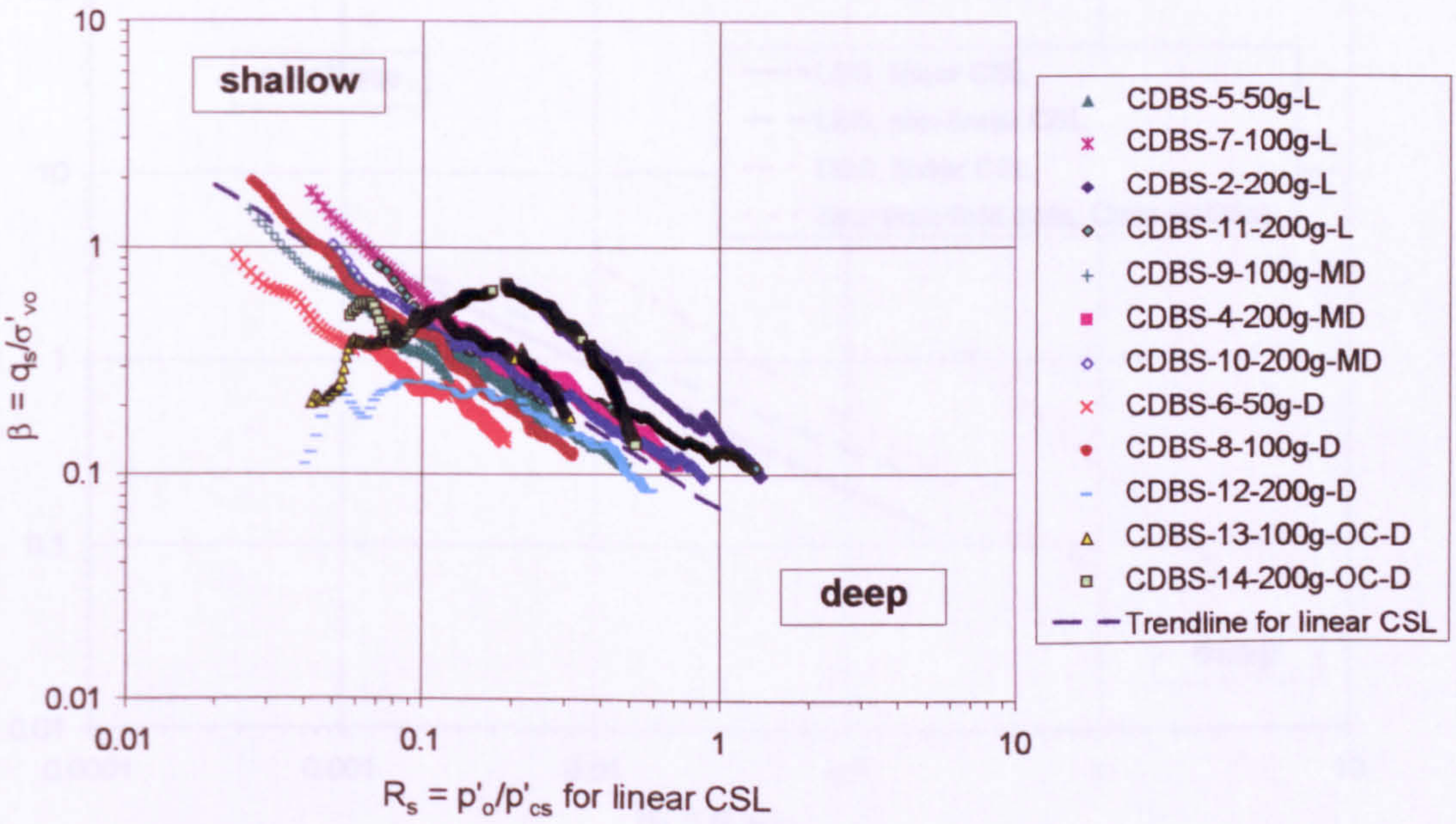

Figure 5-72: The influence of state on β during pile penetration based on a linear CSL for centrifuge tests on Dogs Bay sand.

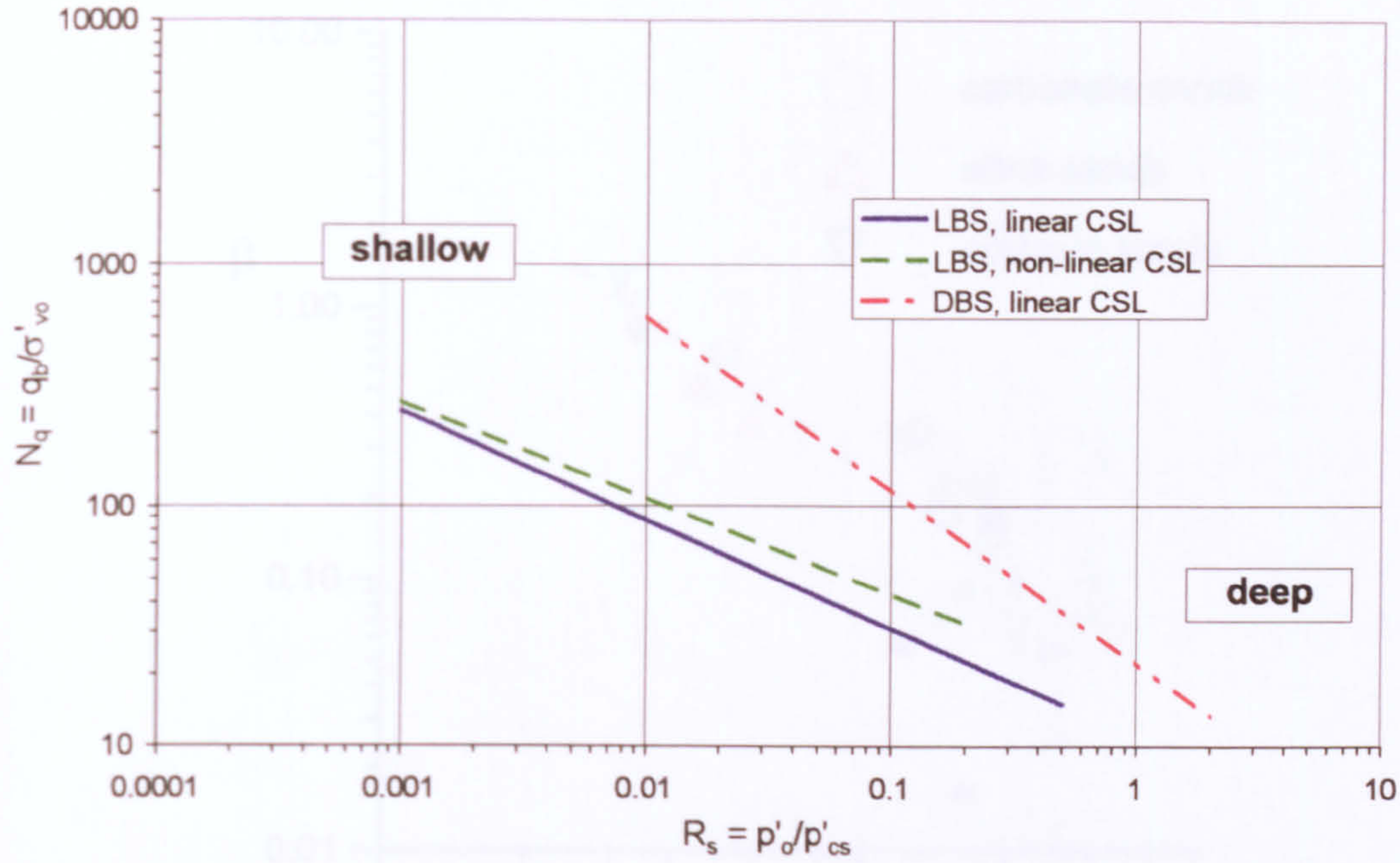

Figure 5-73: Comparison of trendlines for N_q as a function of state for centrifuge tests in Leighton Buzzard and Dogs Bay sands.

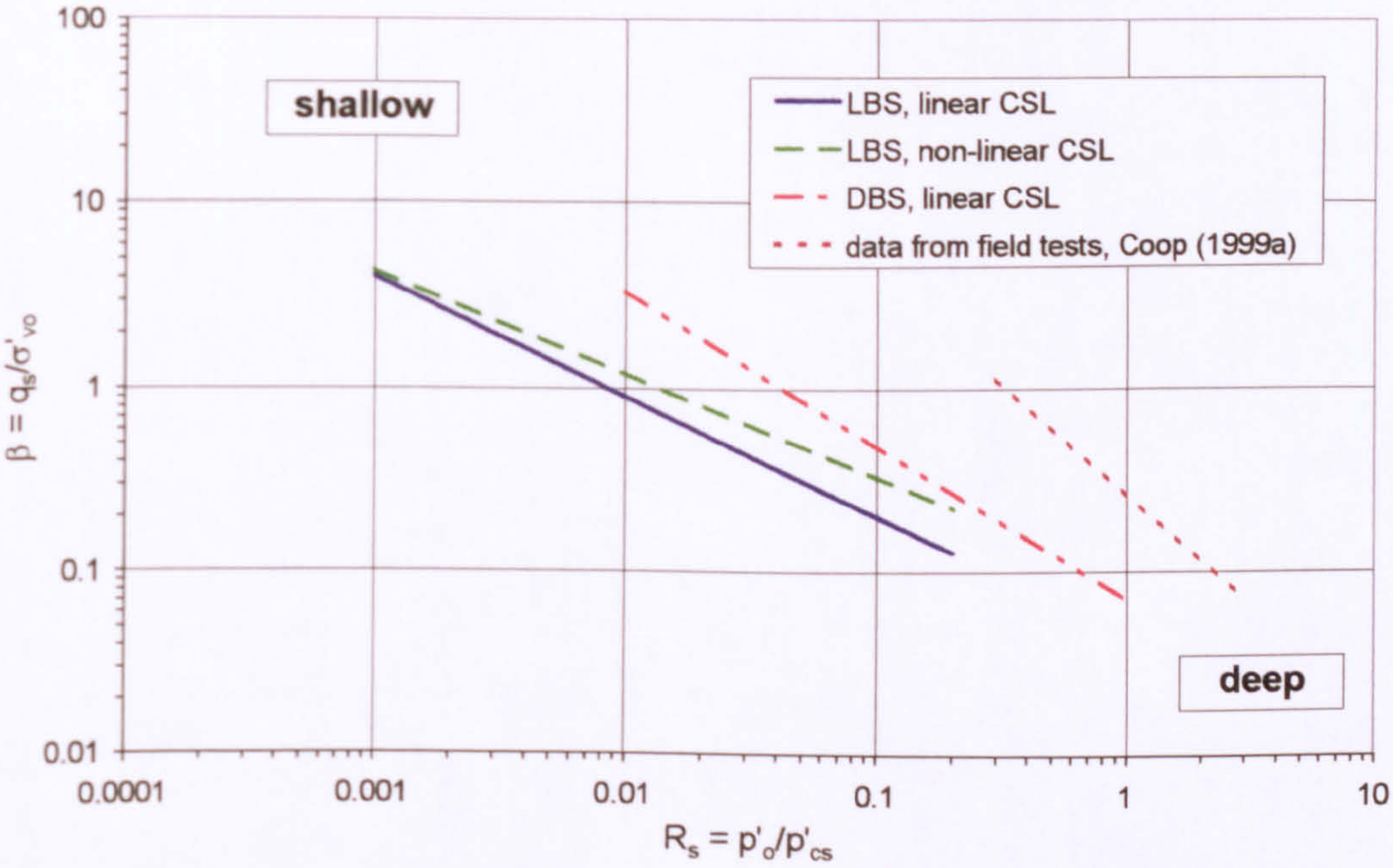

Figure 5-74: Comparison of trendlines for β as a function of state for centrifuge tests in Leighton Buzzard and Dogs Bay sands with data from pile tests in the field.

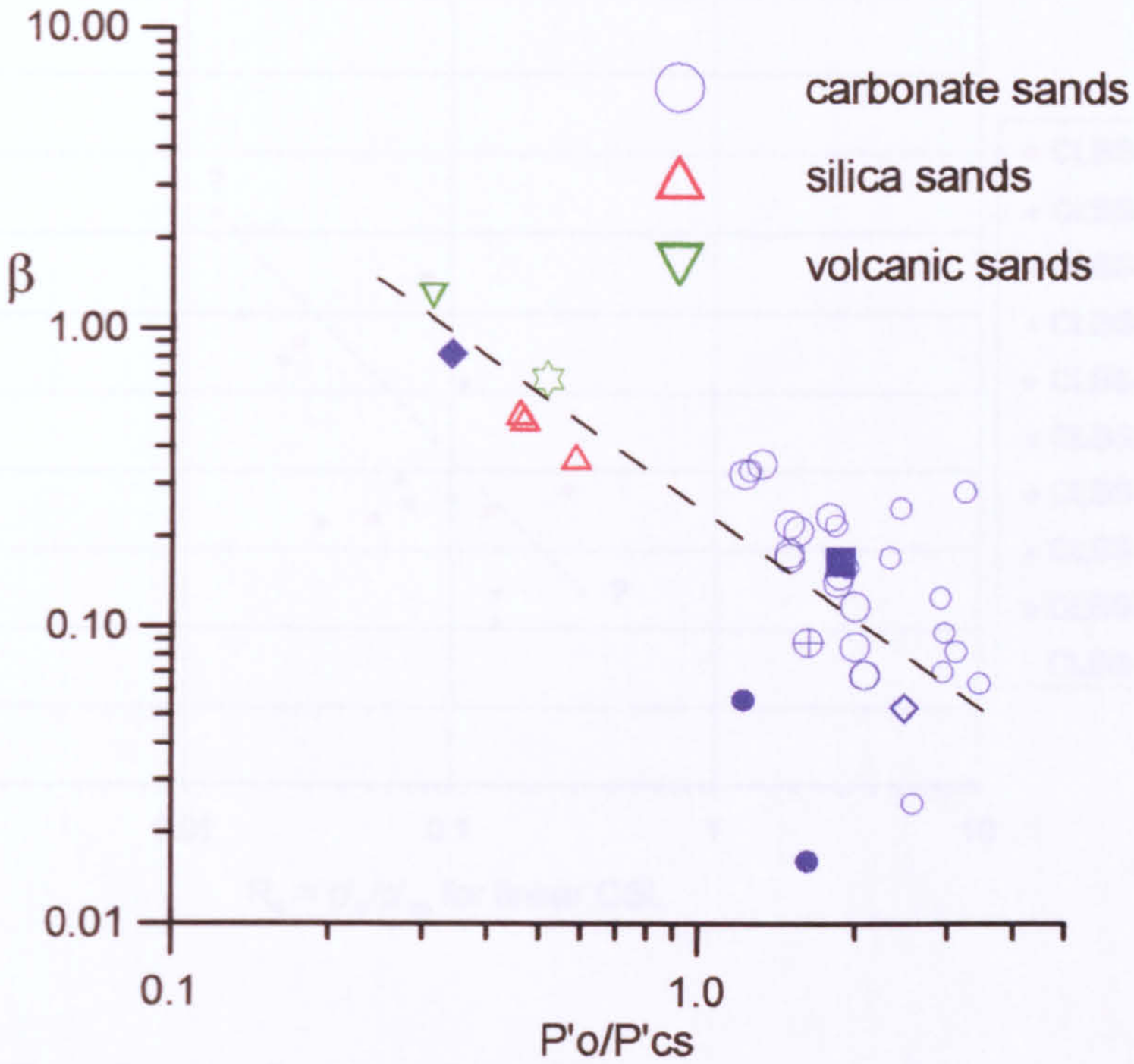

Figure 5-75: Re-interpreted data from pile load tests on a variety of sands(after Coop, 1999a).

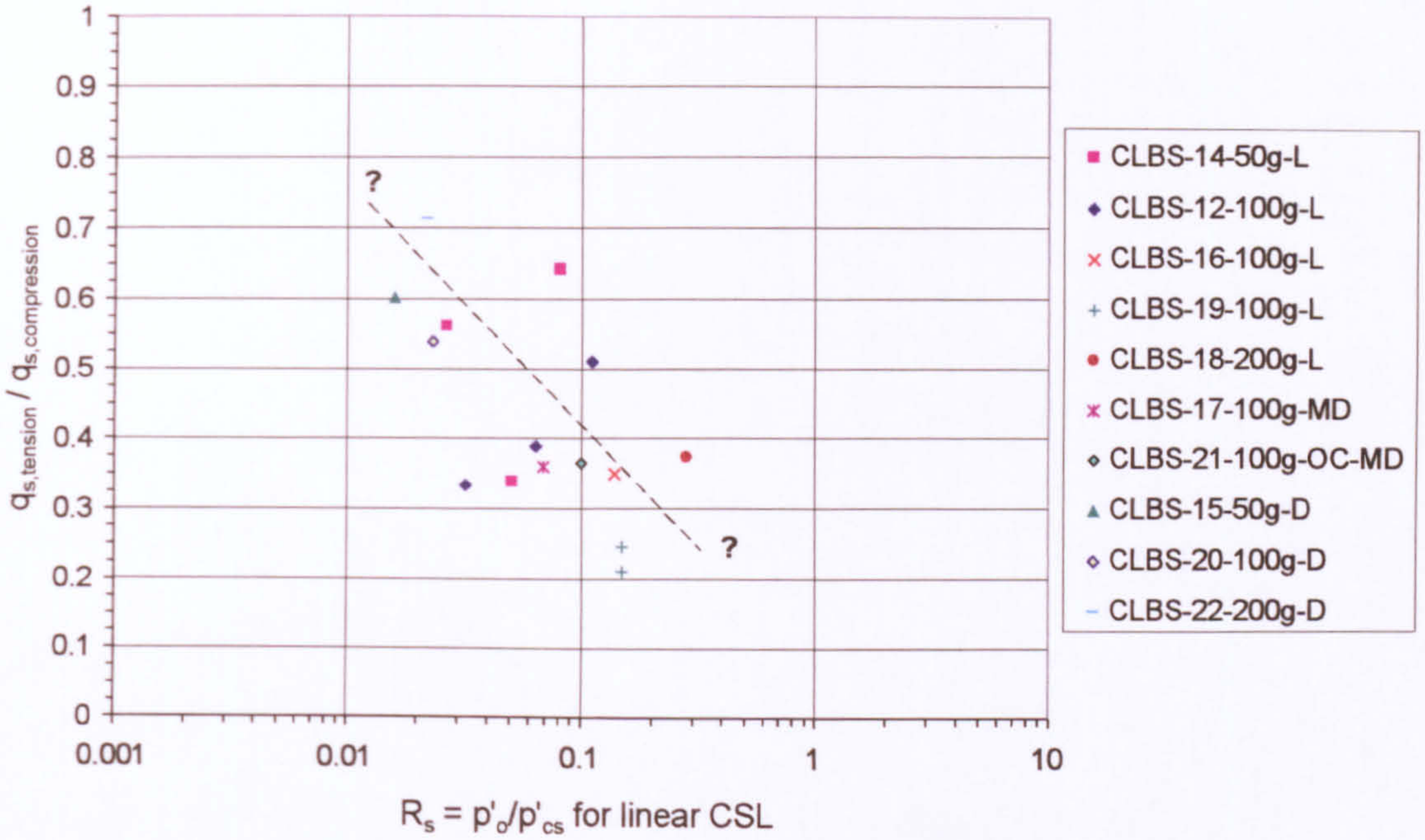

Figure 5-76: The influence of state on the mobilised tensile and compressive average global unit shaft friction based for centrifuge tests on Leighton Buzzard sand.

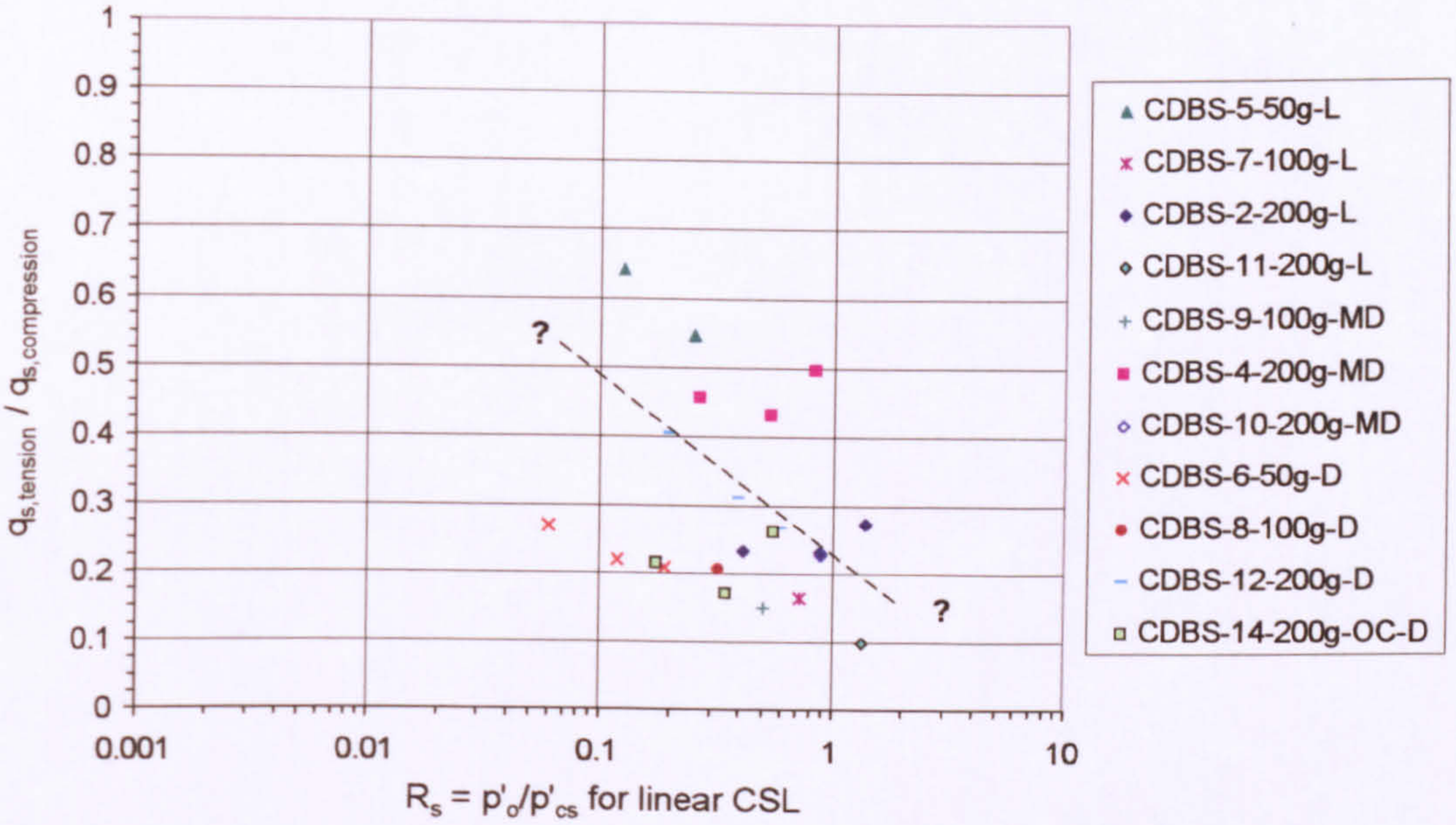

Figure 5-77: The influence of state on the mobilised tensile and compressive average global unit shaft friction for centrifuge tests on Dogs Bay sand.